UNIVERSITÉ DE STRASBOURG

ÉCOLE DOCTORALE DES SCIENCES DE LA VIE ET DE LA SANTE

INSERM UMR_S1109 – Tumor Biomechanics lab

Institut de Cancérologie Strasbourg-Europe

THÈSE

présentée par

Vincent MITTELHEISSER

Pour obtenir le grade de : **Docteur de l'Université de Strasbourg**

Discipline : Sciences de la Vie et de la Santé

Spécialité : Immunologie

Understanding the tumor immune microenvironment: bridging fundamental research and nanomedicine innovations

Soutenue publiquement le 7 Novembre 2024

THÈSE co-dirigée par :

Dr. Jacky GOETZ	Directeur de Recherche INSERM Centre de Recherche en Biomédecine de Strasbourg
Dr. Alexandre DETAPPE	Chercheur CLCC / Professeur conventionné Institut de Cancérologie Strasbourg-Europe

RAPPORTEURS :

Dr. Lucie SANCEY	Directrice de Recherche CNRS Institute for Advanced Biosciences, Université Grenoble-Alpes
Dr. Héctor PEINADO	Head of Microenvironment and Metastasis Group Centro Nacional de Investigaciones Oncológicas, Madrid

---

AUTRES MEMBRES DU JURY :

Pr. Sylvie FOURNEL	Professeure des Universités Centre de Recherche en Biomédecine de Strasbourg
Dr. Emmanuel DONNADIEU	Directeur de Recherche CNRS Institut Cochin, Paris

We must not forget that when radium was discovered no one knew that it would prove useful in hospitals. The work was **one of pure science**. And this is a proof that scientific work must not be considered from the point of view of the direct usefulness of it. It must be done for itself, for the beauty of science, and then there is always the chance that a scientific discovery may become like the radium a benefit for mankind.

Marie Curie

The Discovery of Radium

Lecture at Vassar College, 1921

The research described in this thesis was performed in the Tumor Biomechanics lab at the Institut National de la Santé et de la Recherche Médicale (UMR_S1109, Immuno-Rhumatologie moléculaire, Strasbourg France) and in the Nanotranslational lab at the Institut de Cancérologie Strasbourg-Europe; Strasbourg, France. The work described in this thesis was funded by a doctoral fellowship awarded by the French Ministery of Science (MSERI) and a 4th year fellowship from the Fondation ARC pour la recherche sur le cancer.

Remerciements

Tout d'abord, je souhaite remercier le ministère de l'Enseignement Supérieur, de la Recherche et de l'Innovation ainsi que la Fondation ARC pour la recherche sur le cancer sans qui cette thèse n'aurait pas été possible.

Merci à mes directeurs de thèse **Jacky Goetz** et **Alexandre Detappe** de m'avoir donné l'opportunité de rejoindre leurs équipes quand je n'étais qu'un étudiant en master au début de son chemin vers la thèse. Merci de m'avoir fait confiance sur ces nombreux projets et de m'avoir donné la possibilité d'explorer mes propres intérêts. Merci de votre soutien, vos conseils et de tous les efforts déployés pour faire de moi le scientifique que je suis aujourd'hui.

Merci à **Olivier Lefebvre** pour m'avoir appris de nombreuses ficelles du métier tout au long de ce périple. Merci pour ta bonne humeur, ton optimisme et ton soutien permanent.

Merci aux membres de mon jury de soutenance, **Lucie Sancey**, **Héctor Peinado**, **Emmanuel Donnadieu** et **Sylvie Fournel**, d'avoir accepté d'évaluer ce travail.

Merci aux membres de mon comité de suivi de thèse, **Aline Nonat, Alexandre Carisey** et **Sylvie Fournel** qui ont suivi l'évolution de ces projets. Merci pour vos conseils et nos discussions.

Le choix de faire une thèse est un long cheminement qui commence bien avant la décision en elle-même. Je souhaite remercier toutes les personnes qui ont participé à ce choix, à ma formation de scientifique et qui m'ont permis de grandir scientifiquement et humainement. Merci à **Catherine Helias** et **Antoine Ittel** d'avoir conforté mon choix de faire des études de pharmacie. Merci à **Laurent Miguet** de m'avoir permis de faire mon premier stage en laboratoire. Merci à **Peggy Kirstetter** de m'avoir fait confiance en M1 pour travailler (déjà) indirectement sur les plaquettes – et de m'avoir appris tout ce que je sais sur la cytométrie ! Merci à **Pauline Soulas-**

Sprauel de m'avoir transmis le goût de l'immunologie et d'avoir toujours su écouter et conseiller le jeune étudiant en pharma qui voulait faire de la recherche que j'étais !

Je souhaite également remercier toutes les personnes que j'ai rencontré au cours de mon master et ma thèse. Merci à **Nathalie** et **Cédric**. Merci aux « anciens » du CPS – **Marie-Charlotte**, **Éric** et **Chloé**, pour votre bonne humeur et votre soutien à différents moments de cette thèse. Merci aux membres de la grande communauté de l'immunologie strasbourgeoise pour notre marché parallèle d'anticorps, de réactifs et de cellules – merci notamment à **Léa**, **Karim** et **Alice**. Merci aux étudiants avec qui j'ai eu la chance de travailler et particulièrement merci à **Juliette** et **Diogo**. Merci à tous les étudiants en pharmacie que j'ai pu encadrer en TD et TP pour leur indulgence dans mes premières heures de l'autre côté du miroir. Merci aux masters d'immunologie et de biologie du développement avec qui j'ai pu partager mon engouement pour l'immunothérapie cellulaire. Merci à toutes les personnes avec qui j'ai eu la chance de collaborer sur différents projets. Merci à **Mark** et **Giovanni** ainsi qu'à **Mariel** et **Bruno**.

Merci à tous les membres du Goetz lab qui ont contribué à faire de cette équipe le super environnement de travail qu'il est : **Annabel**, **Laetitia**, **Vincent**, **Naël**, **Claire**, **Isabelle**, **Laurie**, **KJ**, **Jeanny**, **Guillaume**. Merci à **Florent** pour ta magie sur Word jusqu'aux derniers instants de cette thèse !

Une mention spéciale pour les personnes du laboratoire que j'ai le plus côtoyé au quotidien. Merci à mes très chers voisins de bureau, mon *Flematic core* sûr : **Valentin** et **Amandine**. Merci pour cette super ambiance, ces moments de décompression et votre aide/soutien. Sans vous cette thèse n'aurait définitivement pas eu la même saveur. Merci à **Zeynep** pour avoir permis la continuité dans cette ambiance après le départ de Valentin. Merci aux autres membres de *Flematic extended* : **Louis**, **Lucas** et **Marine**. Les cracks des EVs et de l'immunologie. Merci à la platelets team : **Cristina**, **Louis** et **Olivier** pour ces bons moments passés à l'animalerie, nos moments de solitude partagés et votre résilience sur certaines parties de ces projets !

I also want to particularly thank “my post-doc” team: **Cristina** and **Katka**. Thank you for your endless support, our scientific and other discussions, and your help in my quest for a great post-doc opportunity.

Une autre mention spéciale pour « ma deuxième maison ». Merci à tous les membres du PSG d’avoir grandement permis à la bonne réalisation de cette thèse par nos discussions café lors de mes visites impromptues pour décompresser et refaire le monde. Merci pour vos généreux prêts d’anticorps ! Merci à **Nadège**, **Stéphane**, **Yannick**, **Quentin**, **Julien**, **Elodie**, **Grégoire** et **Maud**. Merci particulièrement à **Sabine** pour tes murmures à l’oreille de l’Attune. Merci à **Julie**, ma binôme de quelques manip’ de fin de thèse, pour ton soutien dans nos moments de discussion et de doutes – et merci pour l’IL-18 ! Merci à **Damien** pour tous ces bons moments partagés de la fac de pharma à la thèse ! Merci à **Julie**, **Julien**, **Damien** et **Yannick** de m’avoir fait découvrir le ski !

En dehors du labo, merci à **Louisane** pour ton aide infaillible tout au long de ces années mais aussi pour les séances Starbucks/ciné qui nous ont sauvées plus d’une fois. Merci aux autres pharma, **Julie**, **Myriam**, **Gaëtan** et **Benjamin** pour votre amitié et vos soutiens sans faille depuis 10 ans.

Merci à **mes parents**, à **mon frère** et à **Marie**, à **mes grands-parents** pour leur soutien indéfectible et leur aide tout au long de ces années d’études (maintenant finies !!). Je vous en serai à jamais reconnaissant, plus que je ne pourrais jamais l’écrire dans ces remerciements. Merci !

Résumé français

INTRODUCTION

Les pathologies cancéreuses représentent un enjeu de santé publique majeur. Selon l'Organisation Mondiale de la Santé (OMS), 20 millions de nouveaux cas de cancer ont été diagnostiqués dans le monde en 2022. L'incidence des néo-diagnostics pourra même atteindre 29,5 millions de cas d'ici 2040 (Cancer Tomorrow).

Au cours de la progression cancéreuse, les cellules tumorales quittent la tumeur primaire et migrent via les vaisseaux lymphatiques ou sanguins jusqu'à un organe secondaire pour y former des métastases. Ces tumeurs secondaires sont responsables de la grande majorité des décès des patients atteints de cancer. Ainsi, comprendre les mécanismes contrôlant les différentes étapes de cette dissémination est essentiel afin de faire progresser les stratégies thérapeutiques. Lors de leur dissémination par la circulation sanguine, les cellules cancéreuses se lient à plusieurs types cellulaires, dont les plaquettes. Le rôle des plaquettes dans la phase intravasculaire de la progression métastatique est bien connu. Les plaquettes favorisent la survie des cellules tumorales circulantes (CTCs) en les protégeant de la destruction par les forces hémodynamiques et de la surveillance immunitaire. De plus, les plaquettes sont également connues pour promouvoir l'adhésion des CTCs à l'endothélium des organes cibles, soutenant ainsi l'établissement de métastases.

La formation de métastases implique la coévolution des cellules néoplasiques avec les cellules saines résidentes de l'organe cible. En effet, la croissance métastatique est soutenue par le dialogue entre les cellules tumorales et les cellules immunitaires et stromales composant le microenvironnement tumoral (TME). Les composants du TME et leurs interactions inter-cellulaires constituent autant de cibles thérapeutiques potentielles pour enrayer la croissance métastatique. Étonnamment, des analyses microscopiques ont montré que les plaquettes se retrouvaient également en nombre dans le TME. Ces observations suggèrent que les plaquettes pourraient également jouer un rôle à un stade plus tardif des atteintes cancéreuses, lorsque les métastases sont déjà établies. En revanche, la contribution des plaquettes post-extravasation reste encore peu étudiée. La compréhension de ces phénomènes permettrait, à terme, de développer de nouvelles approches thérapeutiques ciblant l'interaction plaquettes-cellules cancéreuses.

RESULTATS

Au cours de mon doctorat, j'ai d'abord consacré mon travail à déchiffrer la contribution des plaquettes aux étapes tardives de la cascade métastatique. Dans une première étude, nous avons induit une thrombocytopénie dans des modèles syngéniques murins à différentes étapes de la cascade métastatique (en amont ou après l'établissement de métastases) (Garcia-Leon et al., 2024). Nous avons ainsi observé que les plaquettes soutiennent la croissance des métastases établies en (*i*) favorisant la prolifération des cellules cancéreuses et (*ii*) en soutenant le caractère immunosuppresseur du TME. Nous avons démontré que cet effet était en partie dépendant de la glycoprotéine VI (GPVI), un récepteur uniquement exprimé par les plaquettes. En effet, la déplétion génétique de GPVI réduit efficacement la croissance des métastases établies. Ces contributions critiques des plaquettes à deux moments distincts de la cascade métastatique les établissent comme nouvelle cible thérapeutique intéressante pour limiter la formation de métastases. Cependant, les agents antiplaquettaires actuellement en clinique sont associés à un risque élevé de complications hémorragiques, les rendant inutilisables dans la prise en charge des pathologies cancéreuses. L'utilisation du glenzocimab, un anticorps ciblant GPVI utilisé en phase II dans le traitement des AVC ischémiques, apparaît comme un traitement prometteur et nous avons d'ailleurs pu efficacement réduire la croissance métastatique sans induire de perturbations hémostatiques collatérales par l'injection du glenzocimab dans notre modèle murin.

Lors de cette première étude, nous avons aussi mis en évidence que la liaison des plaquettes aux cellules tumorales métastatiques est hétérogène. En effet, certaines cellules cancéreuses se lient aux plaquettes plus efficacement que d'autres. En nous basant sur ces premiers résultats, nous avons, dans une deuxième étude, analysé des bases de données accessibles au public afin de trouver de nouveaux déterminants moléculaires impliqués dans cette différence de liaison (Mittelheisser et al., *In preparation*). Nous avons identifié CD24 comme un nouveau rhéostat des cellules tumorales régulant leur liaison avec les plaquettes et donc leur fonction pro-métastatique. En effet, nous avons démontré que l'expression membranaire de CD24 est positivement corrélée à la capacité de liaison plaquettaire des cellules tumorales. L'inhibition génétique de l'expression de CD24 dans les cellules tumorales a permis de réduire leur capacité à se lier aux plaquettes et a entravé la croissance des métastases pulmonaires dans un modèle syngénique murin. Une analyse détaillée des

foyers métastatiques a confirmé nos précédentes observations de la capacité des plaquettes à moduler le caractère immunosuppresseur du TME. En effet, lorsque les cellules tumorales se lient efficacement aux plaquettes, nous avons observé un enrichissement en neutrophiles pro-tumoraux dans leur TME. En revanche, l'absence de liaison aux plaquettes a entrainé une réorientation du microenvironnement immunitaire vers une réponse lymphoïde anti-tumorale, se traduisant par un enrichissement en lymphocytes T activés et en cellules NK. Les résultats de notre deuxième étude suggèrent que CD24 est, en partie, responsable de la liaison différentielle des plaquettes aux cellules tumorales et de leur fonction pro-métastatique subséquente. CD24 apparaît donc comme une cible thérapeutique potentielle pour contrecarrer l'interaction entre les plaquettes et les cellules tumorales ainsi que pour entraver la croissance métastatique.

Dans nos deux premières études, nous nous sommes principalement intéressés à l'impact des plaquettes sur les cellules tumorales et sur les cellules immunitaires composant le TME. Les plaquettes interagissent également avec d'autres cellules du TME, comme les fibroblastes. La liaison des plaquettes à ces derniers entraîne leur différenciation en fibroblastes associés au cancer (CAFs). Les CAFs produisent et sécrètent massivement des molécules de la matrice extra-cellulaire, entrainant une rigidification globale du TME. Ces modifications biomécaniques du TME sont perçues par les cellules immunitaires qui y répondent en modulant leur activation (nous avons d'ailleurs abordé en détail ces points de contrôles mécaniques de l'immunosurveillance dans une première revue) (Mittelheisser et al., 2024). Nous avons également souligné l'opportunité thérapeutique de moduler les propriétés biomécaniques du TME et identifié les nanoparticules (NPs) comme un moyen prometteur d'atteindre ce but.

La seconde partie de mon doctorat a donc été consacrée à développer de nouvelles stratégies nanothérapeutiques pour cibler les cellules cancéreuses ou réactiver les cellules immunitaires présentes dans le TME. A l'origine, la nanomédecine a été développée afin d'améliorer l'indice thérapeutique et le profil pharmacocinétique des molécules chimiothérapeutiques. Après leur administration, les NPs s'accumulent passivement dans la tumeur par l'effet de perméabilité et de rétention améliorées (EPR, *enhanced permeability and retention effect*). Plus récemment un mécanisme complémentaire de migration à travers les cellules endothéliales a été décrit. Cependant, ces processus varient considérablement entre

les patients et les types tumoraux, des différences pouvant même survenir au sein d'un même patient ou d'une tumeur au cours de sa progression. Cette forte variabilité rend le ciblage passif des NPs sous-optimal pour une bonne accumulation au sein des tumeurs et seule une quantité limitée de NPs (≈0,7% de la dose injectée) atteint la tumeur. Par conséquent, il reste essentiel d'améliorer le ciblage des cellules tumorales par les NPs. Ces techniques de ciblage reposent sur l'expression de certains antigènes tumoraux surfaciques par les cellules malignes. Conjuguer des NPs avec des anticorps monoclonaux dirigés contre ces antigènes tumoraux permettrait par conséquent un ciblage actif et sélectif des cellules cancéreuses. Ce nouveau type de « conjugués anticorps-NPs » représente une stratégie innovante pour augmenter l'accumulation des NPs au sein des tumeurs. Grâce à une méta-analyse des données issues de 161 études pré-cliniques publiées dans la littérature scientifique entre 2009 et 2021, nous avons pu confirmer que les conjugués anticorps-NPs permettaient une meilleure accumulation intra-tumorale (≈7,9% de la dose injectée par gramme de tumeur) (Mittelheisser et al., 2022). Au cours d'une troisième étude, nous avons développé, en collaboration avec l'équipe d'Andrey Klymchenko (UMR_7021 CNRS), des nanoémulsions lipidiques ciblées par des anticorps anti-HER2 (trastuzumab) ou anti-EGFR (cetuximab) (Fei, Mittelheisser et al., *In preparation*). Le ciblage des conjugués anticorps-NPs a été évalué *in vitro* par microscopie confocale et a montré que les NPs s'accumulaient sélectivement dans les cellules cancéreuses surexprimant les récepteurs ciblés.

Parallèlement, le développement de conjugués anticorps-NPs permet d'envisager le ciblage d'autres types cellulaires composant le TME, tel que les cellules immunitaires. Les cellules immunitaires infiltrées au sein des tumeurs sont confrontées à un TME globalement immunosuppresseur qui induit leur altération fonctionnelle. L'utilisation de conjugués anticorps-NPs dans le cadre de nanoimmunothérapies pourrait permettre de réactiver ces cellules immunitaires afin de promouvoir leurs fonctions. Ces approches de nanoimmunothérapies visant à délivrer des molécules immunostimulantes ont été largement évaluées dans plusieurs études précliniques que nous avons décrites dans une troisième revue (Mittelheisser et al., 2020). Cependant, l'impact du matériau des NPs sur les cellules immunitaires après leur internalisation reste inexploré. Étudier le devenir des NPs afin de pouvoir exploiter pleinement le potentiel des nanoimmunothérapies est essentiel. Dans une quatrième étude, nous avons caractérisé la réponse des cellules NK et des lymphocytes T à une

sélection de cinq nanomatériaux couramment utilisés dans les applications biomédicales (Mittelheisser et al., *In preparation*). Nous avons tout d'abord évalué l'impact des nanomatériaux sur la viabilité des cellules immunitaires et exclu les nanotubes de carbone ainsi que les nanomatériaux à base de terbium. Sur la base de cette présélection initiale, nous avons poursuivi notre étude sur les nanomatériaux composés de poly(acide lactique-*co*-glycolique) (PLGA) et de gadolinium chélaté dans une matrice de silice (Si-Gd). Via des approches de séquençage d'ARN et des études fonctionnelles, nous avons montré que les nanomatériaux à base de PLGA amélioraient les fonctions antitumorales des cellules NK dans un environnement immunosuppresseur dépourvu de cytokines. En revanche, notre analyse des lymphocytes T a mis en évidence que leur incubation avec des nanomatériaux composés de Si-Gd entravait leur activation ainsi que leurs réponses fonctionnelles à une stimulation antigénique polyclonale. Sur la base de ces résultats, nous avons identifié les NPs à base de PLGA comme des candidats potentiels pour le développement futur de conjugués anticorps-NPs visant à réactiver le système immunitaire des patients atteints de cancer.

CONCLUSION

Ma thèse a fait l'objet de plusieurs articles scientifiques et mis en évidence que :

1. Les plaquettes favorisent la croissance de métastases établies en soutenant le caractère immunosuppresseur du TME.
2. L'effet pro-métastatique des plaquettes repose, en partie, sur GPVI et CD24.
3. L'utilisation d'un anticorps anti-GPVI, tel que le glenzocimab, réduit la croissance métastatique sans impacter l'hémostase.
4. Conjuguer des NPs à des anticorps augmente leur accumulation intra-tumorale.
5. Les nanomatériaux à base de PLGA sont suffisants pour restaurer la fonction antitumorale des cellules NK en condition immunosuppressive.

English summary

INTRODUCTION

Metastasis is a multistep process characterized by the spread of malignant cells to distant organs. During cancer progression, tumor cells exit the primary tumor and migrate via lymphatic or blood vessels to a secondary organ, where they form metastases. These secondary tumors are responsible for the vast majority of deaths in cancer patients. Upon tumor cells dissemination, platelets act as the first responder and bind to them, thereby promoting their survival by protecting them from destruction by hemodynamic forces and immune surveillance. In addition, platelets also play a role in promoting the arrest of circulating tumor cells (CTCs) to the endothelium of metastatic sites, thus supporting the establishment of metastases.

While platelets contribution to the intravascular steps of the metastatic cascade has been known for decades, the impact of platelets on the metastatic microenvironment is still not well understood. Interestingly, microscopic analyses reveal that platelets massively populate the tumor microenvironment (TME). These observations indicate that platelets may also influence later stages of cancer progression, particularly after metastases have been established. However, their role in post-extravasation processes remains largely unexamined. Therefore, gaining a deeper understanding of the mechanisms controlling the different stages of cancer metastasis is essential to advancing therapeutic strategies and improving clinical outcomes.

RESULTS

During my PhD, I first dedicate my work to decipher platelets contribution to late steps of metastasis. In a first study, we subject experimental metastasis mouse models to several time-controlled thrombocytopenic regimens in order to longitudinally dissect the pro-metastatic role of platelets in lung metastasis (Garcia-Leon et al., 2024). We observe that platelets populate metastatic sites and support the metastatic outgrowth by *(i)* promoting cancer cells proliferation and *(ii)* rewiring the TME towards an immunosuppressive one. We further highlight that platelets favor the outgrowth established metastases in a glycoprotein VI (GPVI)-dependent manner. Indeed, genetic depletion of GPVI effectively reduces the growth of established metastases. Given the broad implications of platelets at each step of the cancer dissemination and

during later metastatic outgrowth, the use of anti-platelet strategies to hamper cancer progression seems an appealing approach. However, their use in routine oncologic care remains unexplored due to their high risk of bleeding complications. Yet, using glenzocimab, a humanized anti-GPVI antibody Fab fragment, we successfully impair metastasis growth without inducing collateral hemostatic perturbations.

Our first study addresses the unanswered question of whether CTCs interact equally with platelets. Some cancer cells bind to platelets more efficiently than others. Building on these initial findings, in a second study we analyze publicly available databases to find new molecular determinants involved in this difference in binding (Mittelheisser et al., *In preparation*). We identify CD24 as a novel rheostat of tumor cells regulating their binding to platelets and thus their pro-metastatic function. Indeed, we demonstrate that CD24 membrane expression positively correlates with the platelet-binding capacity of tumor cells. Genetic inhibition of CD24 expression in the triple negative breast cancer 4T1 cells significantly reduces the ability of tumor cells to bind to platelets and impedes the growth of lung metastases in a syngeneic mouse model. Furthermore, a detailed analysis of the metastatic foci confirmed our previous observations of the ability of platelets to modulate the TME immunosuppressive character. Indeed, when tumor cells effectively bound to platelets, we observe an enrichment of pro-tumor neutrophils in their TME. In contrast, the absence of platelet binding leads to a reorientation of the immune microenvironment towards an anti-tumoral lymphoid response, resulting in an enrichment of activated T lymphocytes and NK cells. Altogether the results of our second study suggest that CD24 is, in part, responsible for the differential binding of platelets to tumor cells and their subsequent pro-metastatic function. CD24 therefore appears to be a potential druggable target to hinder platelets-tumor cells interaction and metastatic progression, avoiding the collateral hemostatic perturbations of classical anti-platelet agents.

In our first two studies, we particularly investigate the impact of platelets on tumor cells and immune cells in the TME. Platelets also interact with other cells within the TME, such as fibroblasts. Platelet binding to the latter leads to their differentiation into cancer-associated fibroblasts (CAFs). CAFs produce and secrete extracellular matrix molecules on a massive scale, resulting in an overall stiffening of the TME. These biomechanical modifications of the TME are perceived by immune cells, which respond by modulating their activation (we have discussed these mechanical control points of immunosurveillance in detail in a first review) (Mittelheisser et al., 2024).

Throughout this review, we also emphasize that targeted nanoparticles (NPs) may be a promising method for modulating the biomechanical properties of tumors and TME.

A second part of my PhD work therefore aims to develop novel nanotherapeutic strategies to target the tumour cells and the TME. Nanomedicine originally aims to improve the therapeutic index and pharmacokinetic profile of chemotherapeutic molecules. After their administration, nanoparticles (NPs) passively accumulate in the tumor microenvironment through the enhanced permeability and retention effect (EPR). However, this passive targeting remains suboptimal, and only a limited amount of NPs (≈0.7% of the injected dose) reaches the tumor bed. Consequently, it remains essential to improve NPs targeting. An active, selective targeting of cancer cells could be achieved by coupling NPs with monoclonal antibodies directed against surface tumor associated antigens. This new type of “antibody-NPs conjugate” represents therefore an innovative strategy for increasing the accumulation of NPs within the tumor bed. Through a meta-analysis of literature data, we confirm that antibody targeted-NPs enabled better intra-tumoral accumulation (≈7.9% of the injected dose per gram of tumor) (Mittelheisser et al., 2022). In collaboration with Andrey Klymchenko's team (UMR_7021 CNRS), we further validate these observations by developing lipid nanoemulsions functionalized with anti-HER2 (trastuzumab) or anti-EGFR (cetuximab) antibodies (Fei, Mittelheisser et al., *In preparation*).

Additionally, the development of antibody-NPs conjugates creates opportunities to target other cell types within the tumor microenvironment (TME), including immune cells. Tumor-infiltrating immune cells often face a globally immunosuppressive TME, inducing their functional impairments. Nanoimmunotherapies utilizing antibody-NP conjugates hold the potential to reactivate these immune cells and restore their anti-tumoral function. These approaches, designed to deliver immunostimulatory molecules, have been extensively explored in several preclinical studies, as detailed in a third review (Mittelheisser et al., 2020). However, the impact of cargo-free NPs on the immune system after internalization remains largely unexamined. Understanding the fate of NP material is essential for unlocking the full potential of nanoimmunotherapies. To investigate the effect of NPs material, we characterize the response of primary NK- and pan T cells to a selection of five nanomaterials commonly used in biomedical applications (Mittelheisser et al., *In preparation*). We first assess the impact of nanomaterials on immune cell viability and exclude carbon nanotubes and terbium-based nanomaterials. Based on this initial pre-selection, we pursue our

study of nanomaterials composed of poly(lactic-*co*-glycolic acid) (PLGA) and gadolinium chelated in a silica matrix (Si-Gd). Using RNA-sequencing approaches and functional studies, we show that PLGA-based nanomaterials enhance the anti-tumor functions of NK cells in an immunosuppressive environment lacking cytokines. In contrast, our analysis of T cells reveals that their incubation with Si-Gd nanomaterials impairs their activation and functional responses to polyclonal antigenic stimulation. Based on these results, we identify PLGA-based NPs as potential candidates for developing antibody-NP conjugates aimed at reactivating the immune system of cancer patients.

Table of contents

TABLE OF CONTENTS **16**

TABLE OF FIGURES AND TABLES **19**

ABBREVIATIONS **20**

GENERAL INTRODUCTION **22**

1. CANCER INITIATION AND PROGRESSION **22**

1.1. CANCER ORIGINS AND MANIFESTATIONS 22

1.2. TUMOR CELLS HALLMARKS 23

1.2.1. Genomic instability and somatic mutations *23*

1.2.2. Sustained proliferation *24*

1.2.3. Replicative immortality *24*

1.2.4. Compressive stress *25*

1.3. TUMOR MICROENVIRONMENT AND BIOMECHANICAL CONSTRAINS 25

1.3.1. Vascular cells and increased interstitial pressure *26*

1.3.2. Immune cells *28*

1.3.3. Cancer-associated fibroblasts and ECM stiffening *29*

1.4. METASTATIC CASCADE 30

2. THESIS AIMS **33**

CHAPTER I PLATELETS FAVOR EACH STEP OF THE CANCER DISSEMINATION AND LATER METASTATIC OUTGROWTH **38**

1. PLATELET ROLE IN CANCER PROGRESSION **39**

1.1. TUMOR CELLS MODULATE PLATELET BIOLOGY 39

1.2. PLATELETS SHAPE THE PRIMARY TUMOR MICROENVIRONMENT 41

1.2.1. Platelets promote angiogenesis and vascular integrity *42*

1.2.2. Platelets induce primary tumor proliferation and invasiveness *43*

1.2.3. Platelets favor TME stiffening *44*

1.2.4. Platelets compromise anti-tumor immune response *45*

1.3. PLATELETS FAVOR TUMOR CELLS INTRAVASCULAR SURVIVAL AND EXTRAVASATION 47

1.3.1. CTCs bind and activate platelets *47*

1.3.2. Platelets favor CTCs intravascular survival *50*

1.3.3. Platelets facilitate CTCs adhesion to endothelium and support their metastatic seeding *52*

1.4. TEPS HELP ESTABLISHING THE METASTATIC MICROENVIRONMENT 54

2. PLATELETS FAVOR THE OUTGROWTH OF ESTABLISHED METASTASES 56

3. TUMORAL CD24 TUNES PLATELET BINDING AND SUPPORTS METASTASIS 76

CHAPTER II BIOMECHANICAL REGULATION OF CANCER IMMUNOSURVEILLANCE 113

CHAPTER III TUMOR TARGETING WITH ANTIBODY-NANOPARTICLES CONJUGATES 131

1. NANOPARTICLES IN ONCOLOGY 133

1.1. NANOPARTICLES DEFINITIONS 133

1.2. LIPOSOMES AND LIPID-BASED NANOPARTICLES 135

1.3. POLYMERIC NANOPARTICLES 135

1.4. CARBON-BASED NANOPARTICLES 137

1.5. THERANOSTIC NANOPARTICLES 138

2. ANTIBODIES CONJUGATION TO NANOPARTICLES 139

2.1. LYSINES 139

2.2. CYSTEINES 140

2.3. ASPARTIC AND GLUTAMIC ACIDS 142

2.4. BIOORTHOGONAL REACTIONS 142

3. OPTIMAL PHYSICOCHEMICAL PROPERTIES OF ANTIBODY-TARGETED NPS 144

4. GREEN CHEMISTRY-DRIVEN ANTIBODY-TARGETED NANOEMULSION DEVELOPMENT FOR CANCER THERAPY 156

CHAPTER IV LEVERAGING IMMUNOTHERAPIES WITH NANOMEDICINE 188

1. ANTI-TUMORAL IMMUNE RESPONSE 190

1.1. NK CELL-MEDIATED ANTI-TUMORAL RESPONSE 190

1.1.1. NK cells recognition of tumor cells and activation 191

1.1.2. NK cell-mediated tumor cells lysis 193

1.1.3. Orchestration of the adaptive immune response by NK cells 194

1.2. T CELL-MEDIATED ANTI-TUMORAL RESPONSE 195

1.2.1. Naïve T cells activation 196

1.2.2. Anti-tumoral response 199

1.3. CANCER IMMUNE ESCAPE 199

1.3.1. Reduced immunogenicity 200

1.3.2. Reduced immune cells co-activation 201

1.3.3. Immunosuppressive microenvironment 201

1.3.4. Resistance to apoptosis 202

2. LEVERAGING IMMUNOTHERAPY WITH NANOMEDICINE 203

3. NANOMATERIALS TRIGGER FUNCTIONAL RESPONSES IN PRIMARY HUMAN IMMUNE CELLS 220

DISCUSSION AND PERSPECTIVES 274

1. PLATELETS INFILTRATION IN METASTATIC FOCI 274

2. MOLECULAR CUES INVOLVED IN LATE METASTATIC OUTGROWTH 274

3. PLACE OF ANTIPLATELET AGENTS IN CANCER THERAPY 275

4. IMPROVING ANTIBODY-TARGETED NPS DESIGN 276

5. REACTIVATING NK CELLS WITH DRUG-FREE NANOMATERIALS 277

BIBLIOGRAPHY 279

ANNEXES 339

1. DEPLETION OF ALL PLATELET INTEGRINS IMPACTS HEMOSTASIS, THROMBOSIS AND TUMOR METASTASIS 340

2. ANTI-BCMA IMMUNO-NANOPET RADIOTRACERS FOR IMPROVED DETECTION OF MULTIPLE MYELOMA. 406

3. REINFORCED POLYMER-NPS HYDROGELS FOR SUBCUTANEOUS AND SUSTAINED DELIVERY OF TRASTUZUMAB 414

Table of figures and tables

Figure 1 – Hallmarks of cancer.....p.23
Figure 2 – Compressive stress.....p.25
Figure 3 – Tumor neovascularization.....p.28
Figure 4 – Tumor microenvironment stiffening.....p.30
Figure 5 – Metastatic cascade.....p.32
Figure 6 – Tumor cells alter platelet biology.....p.41
Figure 7 – Platelets functions in the primary tumor.....p.45
Figure 8 – Platelet-CTCs interactions promote platelet activation.....p.49
Figure 9 – Platelets foster CTCs survival in the circulation.....p.51
Figure 10 – Platelets facilitate CTCs arrest and extravasation.....p.53
Figure 11 – Nanoparticles delivery to tumors.....p.134
Figure 12 – Lysines amidation.....p.140
Figure 13 – Cysteine modification by Michael reaction.....p.141
Figure 14 – Conjugation to carboxylic acids.....p.142
Figure 15 – Bio-orthogonal chemical click reaction.....p.143
Figure 16 – Mechanisms of NK cells activation.....p.192
Figure 17 – NK cell-mediated tumor cell lysis.....p.194
Figure 18 – T cell-mediated anti-tumoral response.....p.196
Figure 19 – $CD4^+$ helper T cells activation by dendritic cells.....p.197
Figure 20 – $CD8^+$ T cells activation.....p.198
Figure 21 – Immuno-editing and immune escape.....p.200

Abbreviations

A

ADC – Antibody-drug conjugate

ADCC – Antibody-drug conjugate

ADP – Adenosine Diphosphate

AMP – Adenosine Monophosphate

APC – Antigen Presenting Cell

ATP – Adenosine Triphosphate

ATR – Active Transport and Retention

B

BM – Bone Marrow

C

CAF – Cancer-Associated Fibroblast

CCL – Chemokine (C-C motif) Ligand

CCR – Chemokine (C-C motif) Receptor

CD – Cluster of Differentiation

cDC – conventional Dendritic Cell

CNT – Carbon nanotube

CSF – Colony-Stimulating Factor

CTC – Circulating Tumor Cell

CTL – Cytotoxic T Lymphocyte

CXCL – Chemokine (C-X motif) Ligand

CXCR – Chemokine (C-X motif) Receptor

D

DAMP – Damage Associated Molecular Pattern

DC – Dendritic Cell

E

EC – Endothelial Cell

ECM – Extracellular Matrix

EGF – Epidermal Growth Factor

EGFR – Epidermal Growth Factor Receptor

EMA – European Medicines Agency

EMT – Epithelial-Mesenchymal Transition

EPR – Enhanced Permeability and Retention

F

Fab – Fragment antigen-binding region

FAK – Focal Adhesion Kinase

FDA – Food and Drug Administration

G

GARP – Glycoprotein A Repetitions Predominant

GM-CSF – Granulocyte-Macrophage CSF

GP – Glycoprotein

GPCRs – G Protein-Coupled Receptors

H

HER2 – Human Epidermal Growth Factor Receptor-2

HLA – Human Leukocyte Antigen

HMGB1 – High Mobility Group Box 1

I

ICAM – Intercellular Adhesion Molecule

IDO – Indoleamine-pyrrole 2,3-dioxygenase

IFN – Interferon

IFP – Interstitial Fluid Pressure

IgG – Immunoglobulin G

IL – Interleukin

IS – Immune Synapse

K

KIR – Killer-cell Immunoglobulin-like Receptor

L

LEC – Lymphatic Endothelial Cell

LFA – Lymphocyte Function-associated Antigen

LOX – Lysyl oxidase

LPA – Lysophosphatidic Acid

LTGFβ – Latent Transforming Growth Factor β

M

M-CSF – Macrophage CSF

MHC – Major Histocompatibility Complex

MICA/B - MHC class I polypeptide–related sequence A/B

MMP – Matrix Metalloproteinases

N

NCR – Natural Cytotoxicity Receptors

NE – Nanoemulsion

NET – Neutrophil Extracellular Trap

NK – Natural Killer

NP – Nanoparticle

O

OPN – Osteopontin

P

PEG – Polyethylene Glycol

PDGF – Platelet Derived Growth Factor

PDPN – Podoplanin

PF4 – Platelet Factor 4

PGE_2 – Prostaglandin E_2

PLGA – Poly(lactic-*co*-glycolic) Acid

PMN – Pre-metastatic Niche

S

SMAC – Supramolecular Activation Cluster

T

TAA – Tumor Associated Antigen

TBM – Tumor Mutational Burden

TC – Tumor Cell

TCIPA – Tumor Cell Induced Platelet Activation

TCR – T Cell Receptor

TME – Tumor Microenvironment

TEP – Tumor Educated Platelet

TGFβ – Transforming Growth Factor β

TNBC – Triple Negative Breast Cancer

TPO – Thrombopoietin

TRAIL – Tumor-necrosis-factor Related Apoptosis Inducing Ligand

U

ULBP – UL16-Binding Protein

UV – Ultra Violet

V

VCAM – Vascular Cell Adhesion Molecule

VEGF – Vascular Endothelial Growth Factor

VEGFR – VEGF Receptor

vWF – von Willebrand Factor

General introduction

Cancer is a major societal, public health and economic problem of the 21st century. Cancer killed 9.7 million patients in 2022, representing 30% of premature deaths from noncommunicable diseases worldwide (Bray et al., 2024). According to the World Health Organization (WHO), 1/5 person will develop a cancer in its lifetime and around 1/9 men and 1/12 women will die from it. Demographics-based predictions indicating that cancer incidence will reach 35 million by 2050 (Cancer Tomorrow). Better understanding cancer key risk factors, biology, spreading and resistance to therapy could avert millions of future cancer diagnoses and save many lives worldwide over the forthcoming decades.

1. Cancer initiation and progression

1.1. Cancer origins and manifestations

Cancer arises from genetic mutations in proto-oncogenes and tumor suppressor genes occurring during DNA replication and cell division (Martínez-Jiménez et al., 2020). Over the course of their lives, some individuals (5-10% of all cancer cases) will develop one of the more than fifty hereditary cancer syndromes (Garber and Offit, 2005). Among the prevalence of breast and colorectal cancers, the most widely recognized syndromes include the hereditary breast-ovarian cancer syndrome (*BRCA1* or *BRCA2* mutations) (Hall et al., 1990), the hereditary non-polyposis colon cancer (*MSH2*, *MLH1* and *MSH6* mutations) (Fishel et al., 1993) and the familial adenomatous polyposis (*APC* mutation) (Kinzler et al., 1991). Nevertheless, not all cancers are caused by familial syndromes. Most cancers arise from carcinogen-induced DNA damages, due to high-energy radiation (*e.g.*, UV light and X-ray irradiation) (El Ghissassi et al., 2009), various chemicals (*e.g.*, components of tobacco smoke, alcohol, and formaldehyde) (Yoshida et al., 2020), and oncogenic viruses (*e.g.*, human papillomavirus and hepatitis B virus) (Krump and You, 2018).

Depending on the cell of origin, cancer encompasses heterogeneous diseases manifestations. Hematological malignancies are characterized by permanent (leukemia) or transient (lymphoma in leukemic phase) circulation of tumoral cells throughout the body (Swerdlow et al., 2017). At the opposite, other cancers such

glioblastoma rarely spread (0.5%) outside their primary organs (here the brain) (Pasquier et al., 1980). The vast majority of cancers (>90%) are constituted by solid tumors, arising from epithelial cells (carcinoma – 98% of solid tumors) or from mesenchymal cells (sarcoma – 2% of solid tumors) (Bray et al., 2024). Following the formation of a primary mass, tumor cells (TCs) will eventually invade the surrounding stroma and potentially colonize a distant organ and give rise to secondary tumor foci (Valastyan and Weinberg, 2011).

1.2. Tumor cells hallmarks

Despite having diverse clinical manifestations, all cancers are characterized by anarchic proliferation of cells and other common features detailed below (Hanahan and Weinberg, 2011) (**Figure 1**).

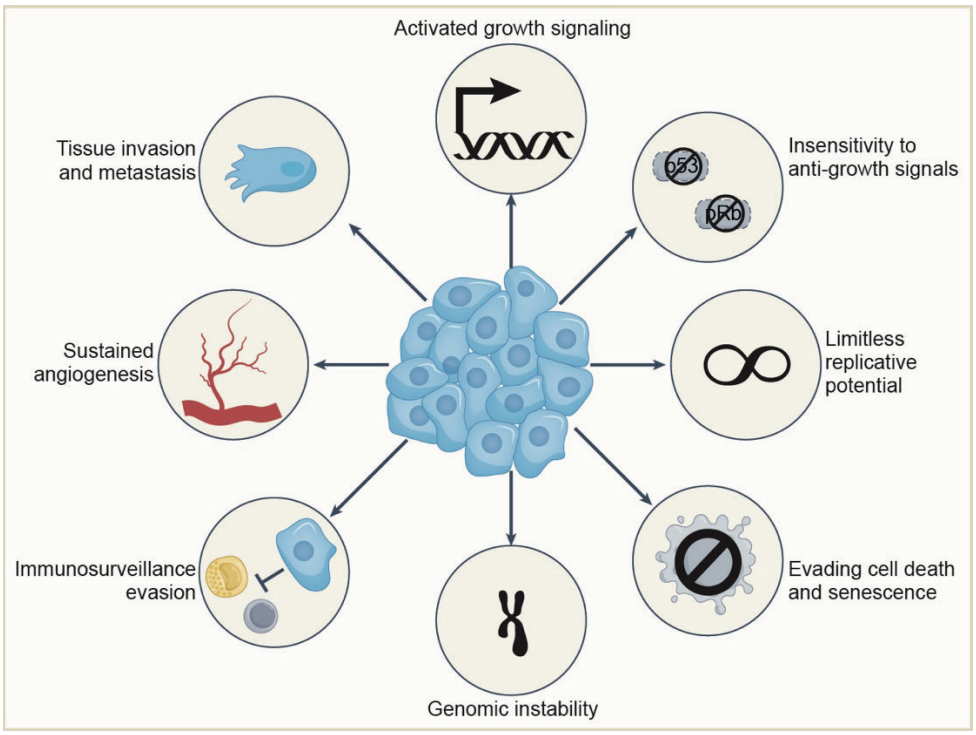

Figure 1 – Hallmarks of cancer.
Cancers are characterized by common hallmarks supporting their growth and progression. These hallmarks are not only tumor cells-intrinsic but also involves various contributions of the tumor microenvironment.

1.2.1. Genomic instability and somatic mutations

Abnormality in TCs genomes were first described more than a hundred years ago (Hansemann, 1890). Further genomic analyses revealed that most cancers originate from a single cell having selective growth advantage due to ≈2-8 mutations in tumorigenesis "driver" genes (*e.g.*, proto-oncogenes and tumor suppressor genes)

(Nowell, 1976). In addition to “driver” mutations, tumor initiating cells possess a “mutator” phenotype that leads to continuous somatic mutations acquisition (over 10,000) upon proliferation (Lengauer et al., 1998; Loeb, 1991; Vogelstein et al., 2013). Cancers evolve by an iterative process of clonal expansion, genetic diversification and clonal selection by microenvironment local pressures (Greaves and Maley, 2012). The acquisition and selection of mutations enable TCs to acquire other hallmarks such as sustained proliferation or pro-tumoral factors secretions.

1.2.2. Sustained proliferation

Healthy cells require mitogenic growth signals to enter an active proliferative state. Conversely, TCs acquire growth autonomy by (*i*) production and autocrine signaling of growth signals (Aaronson, 1991), (*ii*) hypersensitivity to growth signals through receptors (EGFR/*erbB*, HER-2/*neu*) overexpression (Slamon et al., 1987) and (*iii*) constitutive activation of growth signaling pathways by somatic mutations in oncogenes such as H-Ras (Kinzler and Vogelstein, 1996).

Tumor ability to expand is determined not only by the rate of cell proliferation but also by the rate of cell attrition. TCs can evade growth arrest by losing the expression of major cell cycle checkpoints such as the retinoblastoma protein (pRb) (Weinberg, 1995) or p53 protein (Symonds et al., 1994). Of note, losing p53 protein enables TCs to resist to apoptosis. Other than that, TCs can circumvent apoptosis by producing survival factors (Christofori et al., 1994), overexpressing anti-apoptotic oncogenes (Korsmeyer, 1992) or disrupting Fas death signaling circuit (Pitti et al., 1998).

1.2.3. Replicative immortality

Oncogenes sustained TCs proliferation and signals and escape from cell cycle control should induce an ever-increasing proliferation and tumor growth. This notion was undermined by the discovery that constitutive signaling by oncoproteins induces counteracting responses from TCs as induction of cellular senescence (Michaloglou et al., 2005; Serrano et al., 1997). Upon successive cell cycles, cells undergo progressive telomeres erosion (≈65 bp of telomeric DNA/cycle), eventually triggering either a non-proliferative state (*i.e.*, senescence) or a telomere crisis and subsequent apoptosis (Counter et al., 1992). To overcome this proliferating limitation, TCs upregulate the expression of the telomerase enzyme, which adds TTAGGG hexanucleotide repeats

onto the DNA telomeric ends (Bryan and Cech, 1999; Shay and Bacchetti, 1997). TCs are thereby acquiring a virtual “immortality” through unlimited cell proliferation cycles (Bodnar et al., 1998). In addition, loosing pRb and p53 proteins also allow cellular senescence avoidance (Wright et al., 1989).

1.2.4. Compressive stress

As TCs proliferate, the primary tumor volume expands in a mechanically confined environment leading to intratumoral solid stress (Nia et al., 2016; Stylianopoulos et al., 2012) (**Figure 2**). Although compressive stress onset reduces TCs proliferation (Cheng et al., 2009; Delarue et al., 2014), it significantly contributes to TCs invasion by fostering epithelial-to-mesenchymal transition (EMT) (Zulueta-Coarasa et al., 2022) and promoting TCs migration (Tse et al., 2012). Furthermore, TCs can mechanically adapt to the compressive stress and become softer, a feature that scales with their proliferation in confined TME (Matthews et al., 2020) and their metastatic potential (Guck et al., 2005; Swaminathan et al., 2011).

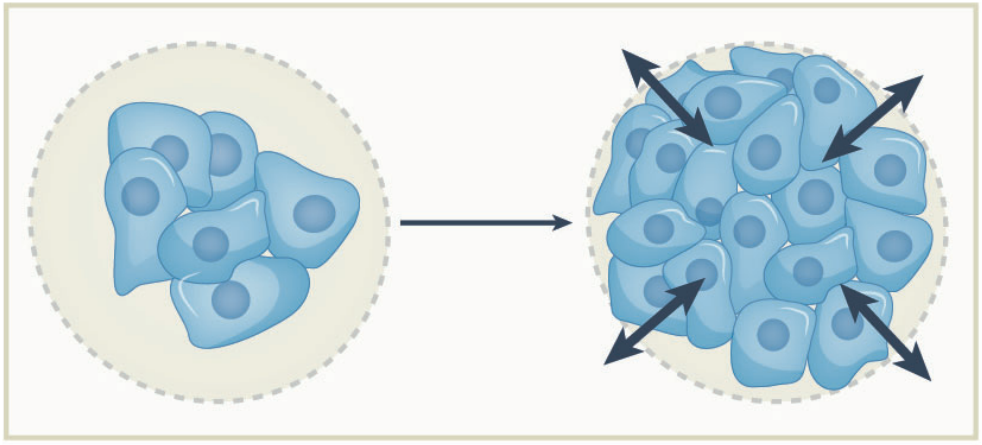

Figure 2 – Compressive stress.
Compressive forces (dark arrows) arise as tumor cells proliferate, leading to tumor volume expansion and mutual compression between the tumor and the elements of its microenvironment (dashed line).

1.3. Tumor microenvironment and biomechanical constrains

Tumor successful development requires TCs to orchestrate a supportive tumor microenvironment (TME) by recruiting and reprogramming non-malignant cells and by remodeling the vasculature and extracellular matrix (ECM). Tumors are hence composed of a highly structured ecosystem containing TCs surrounded by a rich diversity of immune cells, cancer-associated fibroblasts (CAFs), endothelial cells

(ECs), pericytes, collectively embedded in an altered, vascularized ECM. The reader should note that we will give here a global description of the TME components, but its composition and functional state greatly vary depending on the cancer type, disease stage (Klemm et al., 2020) as well as on the organ of origin (Lee and Ginhoux, 2022).

1.3.1. Vascular cells and increased interstitial pressure

Cellular functions and survival depend on O_2 and nutrients supplied by the vasculature, obligating virtually all cells in a tissue to reside within a 100µm distance from a capillary blood vessel (Alberts et al., 2022). At early stages (<1-2 mm^3), tumors typically display limited vascularization. Upon tumor growth (>1-2 mm^3), TCs must establish their own vascular supply of O_2 and nutrients and therefore induce an "angiogenic switch" (Hanahan and Folkman, 1996). Early tumor that failed to undergo this switch induce only microscopic tumoral lesions remaining in a dormant state (Naumov et al., 2009). Autopsies of patients deceased from non-cancer related causes revealed microscopic quiescent tumors in several organs, suggesting that only a small subset of tumors can trigger an efficient "angiogenic switch" (Black and Welch, 1993; Nielsen et al., 1987) (**Figure 3**).

Tumor "angiogenic switch" is mediated by a perturbation of the balance of angiogenesis inducers (*e.g.*, vascular endothelial growth factor A, VEGF-A) and countervailing endogenous inhibitors *e.g.*, thrombospondin-1) (Dameron et al., 1994; Volpert et al., 1997). Notably, TCs are a major source of pro-angiogenic factors, of which VEGF-A and its downstream signaling pathway are the predominant drivers (Volpert et al., 1997). VEGF-A engages its cognate receptor VEGFR-2 expressed on the ECs, leading to a tip cell selection and sprout extension towards the VEGF-A gradient (Hellström et al., 2007). Although TCs are an important source of VEGF-A, angiogenesis is a complex process involving extensive crosstalk between ECs, immune cells, and CAFs. CAFs are also a major source VEGF-A (Fukumura et al., 1998; Gerber et al., 2000) and of other pro-angiogenic factors (*e.g.*, platelet-derived growth factor-C, PDGF-C, basic fibroblast growth factor, bFGF or osteopontin, OPN) (Anderberg et al., 2009; Crawford et al., 2009). In addition to producing pro-angiogenic factors, CAFs also secrete myeloid cell chemoattractants. CAFs-derived CXCL14 recruit monocytes (Augsten et al., 2014) whose further differentiation in $Tie2^+$ tumor-associated macrophages in the perivascular niche promotes tumor angiogenesis (De Palma et al., 2005; Harney et al., 2015). CAFs-derived CXCL1, CXCL2 and IL8 recruit

neutrophils (Elyada et al., 2019) containing pro-angiogenic VEGF-A and BV8 rich granules (Gaudry et al., 1997; Shojaei et al., 2007). Pro-angiogenic neutrophils activity also relies on matrix metalloproteinases (MMPs) secretion which degrades sequestered pro-angiogenic molecules in the ECM, increasing their bioavailability for ECs (Bergers et al., 2000). Similarly, TCs and their associated TME also promote lymphangiogenesis through the secretion of VEGF-C and VEGF-D that stimulates lymphatic endothelial cells (LECs), particularly on the tumor periphery (Pathak et al., 2006).

Owing to ECs exposure to excessive and sustained pro-angiogenic cues, tumor-associated blood vessels typically acquire an aberrant morphology, characterized by excessive branching, discontinuous EC lining, with scant basement membrane and pericyte coverage (Baluk et al., 2005). Aberrant and permeable blood vessels in the TME result in continuous plasma deposition into the extracellular space (Hashizume et al., 2000), which cannot be cleared or drained owing to tumor growth-induced compressive stress of intra-tumoral lymphatic vessels, leading to high interstitial fluid pressure (IFP) within the tumor core (Padera et al., 2004; Stylianopoulos et al., 2012). IFP levels drop at the tumor periphery, thereby establishing interstitial fluid flow that drives interstitial fluid from the center to the tumor periphery (containing functional lymphatic vessels), facilitating its lymphatic drainage (Baxter and Jain, 1989). This convective interstitial fluid flow impairs drug distribution inside tumor (Heldin et al., 2004) and promotes TCs and pro-tumoral factors dissemination through vascular systems, potentially supporting cancer progression (Pereira et al., 2018).

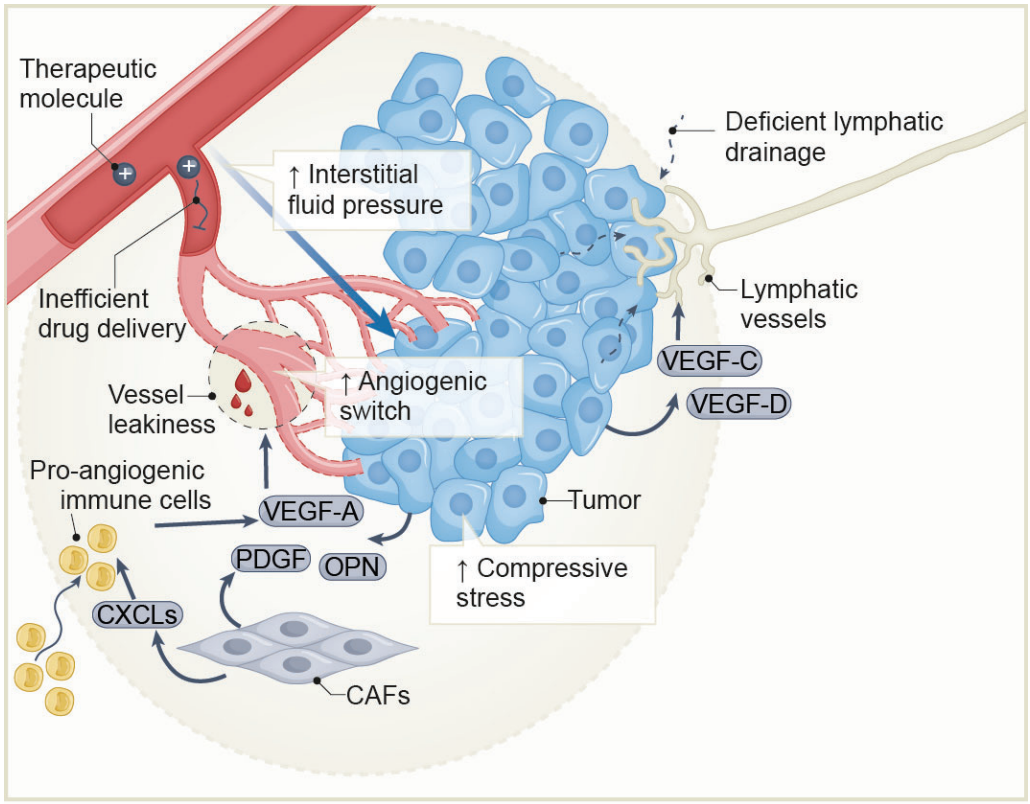

Figure 3 – Tumor neovascularization.
Tumors establish their own O_2 and nutrients supply by inducing an "angiogenic switch". Neoangiogenesis is a complex process involving extensive crosstalk between TCs, ECs, immune cells, and CAFs. TCs and CAFs secrete pro-angiogenic factors (*e.g.*, VEGF-A, PDGF or OPN) that induce ECs proliferation and sprouting. In addition, CAFs secrete chemoattractants (*e.g.*, CXCL14, CXCL1 or CXCL2) that recruit pro-angiogenic macrophages and neutrophils. Similarly, TCs secrete VEGF-C and VEGF-D that stimulates LECs. Owing to sustained pro-angiogenic cues, the neo-formed vascular and lymphatic systems are highly dysfunctional. Vessel leakiness coupled to inefficient lymphatic drainage induce fluid accumulation inside the tumor and increased interstitial fluid pressure.

1.3.2. Immune cells

Innate and adaptive immune cell types are found in the vicinity of TME, either inside the tumor mass, at its periphery or in draining lymph nodes. Single-cells technologies and multiplexed spatial analyses reveal that the immune compartment of the TME is highly dynamic and varies upon cancer progression (Rozenblatt-Rosen et al., 2020). Early tumors are characterized by an influx of immuno-stimulatory neutrophils and naive T cells, indicating that the innate and adaptive immune systems sense neoplastic transformation at its earliest stages (Gil Del Alcazar et al., 2017; Mascaux et al., 2019; Pylaeva et al., 2022). However, as the tumor grow, the co-evolving immune milieu undergoes profound changes and a transition toward an immunosuppressed TME ensues. The immunosuppression is characterized by a

progressive decrease in cytotoxic NK cells and T cells, less diverse TCR clonotypes and an increase in dysfunctional T cells skewed towards a pro-inflammatory phenotype. In parallel, myeloid cells are increasingly mobilized to the TME, where they polarize in immunosuppressive macrophages and neutrophils in response to local inflammatory cues (Bach et al., 2021; Mascaux et al., 2019).

Commonly accepted hypothesis indicates that changes in the immune TME are TC-driven. However, growing body of literature underscores the complementary role of tumor ECs. While immune cells are mainly pro-angiogenic, tumor ECs express low level of vascular adhesion molecules (*e.g.*, ICAM-1, VCAM-1, E-selectin, and P-selectin) which impairs immune cells trafficking into tumor and contributes to the TME immunosuppression. Additionally, tumor-associated ECs express increased levels of inhibitory immune checkpoint molecules (Lane et al., 2018; Rodig et al., 2003) and FasL (Motz et al., 2014), resulting in effector T cells suppression or apoptosis.

1.3.3. Cancer-associated fibroblasts and ECM stiffening

Along with immune cells, CAFs form a dominant component of the TME (Sahai et al., 2020). The majority of CAFs progenitors is constituted by tissue-resident fibroblasts that, under the strong transforming growth factor β (TGFβ) signaling found in the TME, acquire a myofibroblast phenotype (Massagué, 2008). However, various studies also indicated that CAFs might derived from different sources, spanning from resident fibroblasts, bone marrow-derived mesenchymal stem cells, and endothelial cells (Lavie et al., 2022).

CAFs myofibroblast phenotype is associated with traits of functional hyperactivation, including enhanced proliferation and motility, along with robust ECM biosynthesis and deposition capacity of fibrillar collagens, fibronectin isoforms, tenascin-C or OPN (Lu et al., 2012) (**Figure 4**). In addition to the overproduction of ECM components, CAFs can also modulate ECM mechanical properties by promoting fiber crosslinking. CAFs upregulate the lysyl oxidase (LOX) family of enzymes that mediate crosslinking of the ECM, in particular of fibrillar collagen (Levental et al., 2009) (**Figure 4**). Besides their role in matrix proteins deposition and crosslinking, CAFs induce force-dependent ECM stiffening by increasing their contractile activity (Choquet et al., 1997; Goetz et al., 2011; Han et al., 2018). Force-mediated ECM remodeling by CAFs also favors collagen (Provenzano et al., 2006) or fibronectin (Goetz et al., 2011) fibers alignment, which correlates with worst cancer outcomes. Of note, global matrix

stiffening further enhances YAP activation in CAFs, thus establishing a feed-forward self-reinforcing loop that sustains their pro-rigidification phenotype (Calvo et al., 2013).

In addition to providing a physical scaffold to TCs, ECM rigidification consequences are manifold. ECM stiffness promotes (*i*) EMT induction (Wei et al., 2015) ; (*ii*) angiogenesis (Bordeleau et al., 2017) ; (*iii*) TCs migration trails on aligned collagen fibers (Provenzano et al., 2006) and (*iv*) T cells exclusion (Salmon et al., 2012).

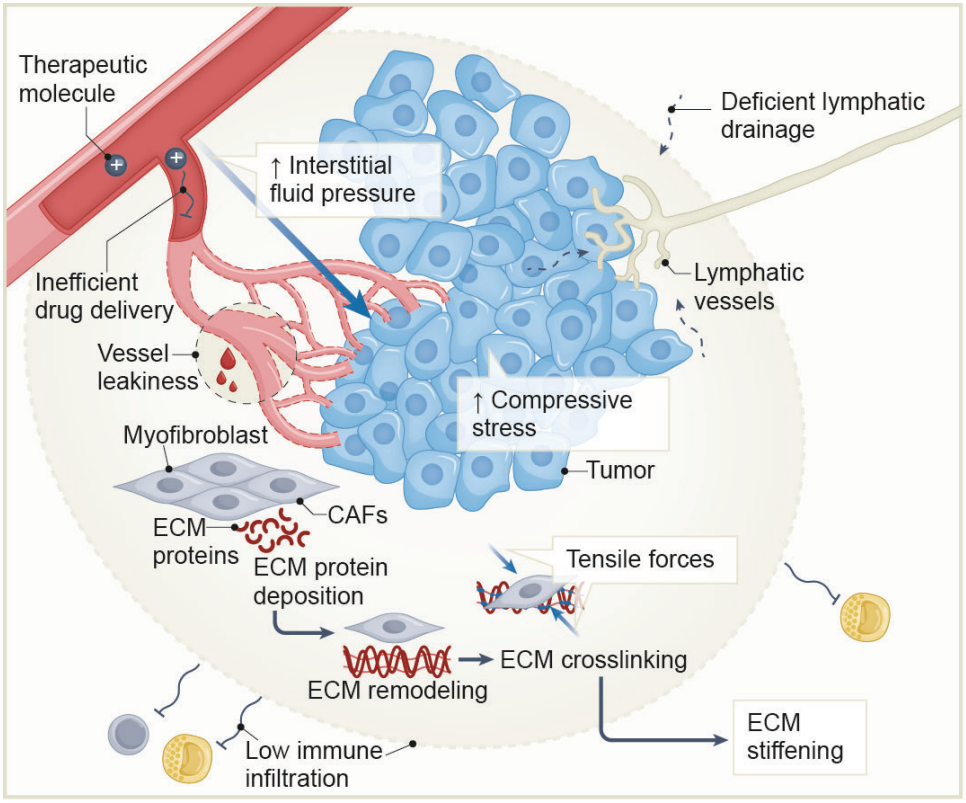

Figure 4 – Tumor microenvironment stiffening.
TGFβ signaling in the TME trigger fibroblasts transformation in CAFs. CAFs secrete, remodel and cross-link extracellular matrix (ECM) proteins, thereby inducing a global matrix rigidification. Together, TME biomechanical modifications (compressive stress, high IFP and ECM stiffening) acquired upon cancer progression limit the diffusion of therapeutic molecules and the infiltration of immune cells.

1.4. Metastatic cascade

Following the establishment of mutually reinforcing connections, primary tumor masses generate pioneer TCs that move out, invade adjacent tissues, and thence travel to distant sites where they may establish new colonies (**Figure 5**).

Tumor cells invasion | The invasion process begins when TCs detach from their neighboring cancer cells by losing the expression of E-cadherin in favor of N-cadherin

(Dongre and Weinberg, 2019). During the EMT, TCs lose epithelial features and gain mesenchymal traits that facilitate their migration, notably through the expression of a new integrin repertoire and of MMPs (Dongre and Weinberg, 2019). After detaching from each other, TCs start to invade the surrounding stroma (Clark and Vignjevic, 2015) as single cells or collectively in strands or clusters (Aceto et al., 2014) and gain access to lymphatic or blood vessels, where they can intravasate.

Tumor cells intravasation | The aberrant and highly permeable vasculature of the TME facilitates TCs intravasation. Furthermore, TCs intravasation might be fostered by $Tie2^{+}$ tumor-associated macrophages in the perivascular niche (Arwert et al., 2018; Harney et al., 2015). As they travel through the bloodstream, circulating TCs (CTCs) face severe stresses including hemodynamic shear forces, loss of adhesion to the ECM and patrolling immune cells (Strilic and Offermanns, 2017). Thus, among all the CTCs, many will undergo apoptosis and only a few cells will be able to extravasate and form metastases.

Tumor cells extravasation | The circulation step often comes to an end when CTCs encounter vessels in which moderate blood flow speeds enable CTC-endothelium interactions that favor stable cell arrest (Follain et al., 2018; Osmani et al., 2019) or when CTCs occlude topographically disordered and/or narrow vessels (Paul et al., 2019).

Of note, CTCs arrest is a complex chain of events that not only single CTCs but also homoclusters of CTCs (Allen et al., 2019) and heteroclusters formed with platelets (Labelle et al., 2014) or immune cells (*e.g.*, neutrophils and monocytes) (Bekes et al., 2011; Labelle et al., 2014; Qian et al., 2011). Arrested CTCs then extravasate by diapedesis or endothelial remodeling (Follain et al., 2018; Karreman et al., 2023) and invade the perivascular stroma where they may encounter a permissive and supportive microenvironment and proliferate to give rise to metastases (Peinado et al., 2017). Conversely, CTCs facing a microenvironment lacking supportive cues enter dormancy (Luzzi et al., 1998) and wait for a more opportune moment to multiply (Borriello et al., 2022; Di Martino et al., 2021; Harper et al., 2016).

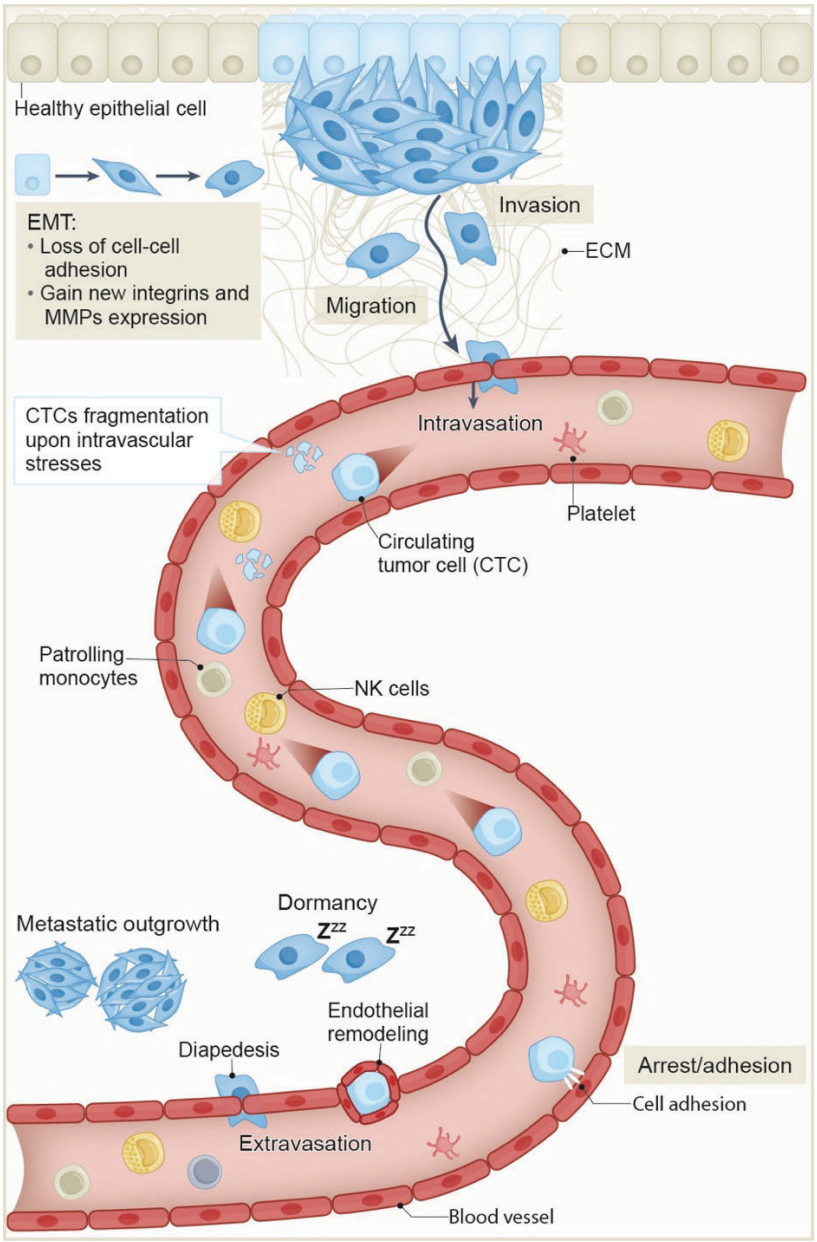

Figure 5 – Metastatic cascade.
Malignant cells invade their stroma and gain access to lymphatic or blood vessels, into which they intravasate. As they travel through the bloodstream, CTCs face severe stresses (*e.g.*, shear stress, anoikis and patrolling immune cells) that may trigger their death. CTCs circulation often stops when they adhere to the endothelium or mechanically arrest due to vessels architecture. Arrested CTCs extravasate by endothelial remodeling or diapedesis and invade the perivascular stroma where they may enter dormancy or proliferate to form metastases.

Importantly, one should note that TCs dissemination does not lead to the random appearance of metastasis with an even distribution throughout the body. Clinical data obtained during autopsies of cancer patients indeed demonstrate that different primary tumor types led to different organ-specific metastases (Gao et al., 2019). This organotropism was first explained by the “seed-and-soil” hypothesis

(Paget, 1889). In this hypothesis, Stephen Paget stipulated that the “seeds” (*i.e.*, TCs) evenly spread throughout the body, but give rise to metastases only in sites where the “soil” (*i.e.*, the microenvironment) is favorable. Twenty years later, James Ewing proposed that metastatic dissemination occurs by purely mechanical factors that are determined by the anatomical structure of the vascular system (Ewing, 1928). Recent efforts in understanding metastasis formation highlight the complementarity of Paget’s and Ewing’s hypotheses. Paget’s “seed-and-soil” hypothesis was further confirmed by the description of TCs ability to remotely prepare the microenvironment for the future arrival of disseminated TCs by establishing pre-metastatic niches (Peinado et al., 2017). Ewing’s biomechanical hypothesis was validated by several observations from the Tumor Biomechanics lab and other illustrating that the vascular system architecture (Paul et al., 2019) and the hemodynamics characteristics (Follain et al., 2018) initially determine permissive adhesion and arrest spots for TCs, even before the compatibility between TCs and their environment comes into play.

2. Thesis aims

Metastatic disease accounts for the majority of cancer-related deaths (Dillekås et al., 2019; Steeg, 2006). Understanding a deeper understanding of the mechanisms controlling cancer metastasis is therefore essential to advance therapeutic strategies and improve clinical outcomes. Upon their dissemination, tumour cells bind to several blood cells, including platelets. While platelets play a role in shielding CTCs and promoting their arrest, the impact of platelets on the metastatic microenvironment is still not well understood.

We first aim to decipher platelets contribution to late steps of metastasis. In a first study (*Chapter I*), we demonstrate that platelets populate metastatic sites and influence metastatic outgrowth by *(i)* promoting TCs proliferation and *(ii)* rewiring the immune TME towards an immunosuppressive one. Besides describing platelets roles in the metastatic sites, we also establish that platelets binding to metastatic TCs is heterogenous. In a second study (*Chapter I*), we screen platelets ligands expressed by different metastatic TCs and identified CD24 as a player implicated in platelets binding to TCs. Genetic knock-down of CD24 expression in TCs reduce their platelets-binding abilities and impair lung metastasis outgrowth. We will discuss the platelets roles in shaping metastatic foci in a review in preparation.

In addition to biochemical immunosuppressive cues, metastasis-infiltrating immune cells also encounter a globally stiffened microenvironment that modulate their functions. We discussed these mechanical regulations of immunosurveillance in a first review (*Chapter II*). Throughout this review, we also highlight that tumour-targeted nanoparticles (NPs) might provide a promising means of delivering agents that modulate the biomechanical properties of tumours. We then aim to develop novel nanotherapeutic strategies to target TCs and their TME. Through a meta-analysis of literature data (*Chapter III*), we confirmed that targeted-NPs with antibody against tumor associated antigens leads to significantly greater tumor uptake than that of naked NPs. We further validate these observations by developing anti-HER2 targeted lipid nanoemulsions by green chemistry (*Chapter III*). In parallel to the development of targeted-NPs, leveraging NPs to deliver immunostimulatory molecules to immune cells emerge as a novel therapeutic concept (*Chapter IV*). However, the impact of cargo-free NPs on the immune system after internalization remains unknown. To investigate the effect of cargo-free NPs, we characterize (*Chapter IV*) the response of primary NK- and pan T cells to a selection of five NPs commonly used in biomedical applications. We identify that PLGA NPs were able to prime both NK- and T cells activation and antitumoral functions, making them suitable candidates for further targeting approaches aiming to reactivate the immune system of cancer patients.

General introduction

List of scientific papers

*shared first authorship.

This thesis is based on the following publications and manuscripts:

1. Garcia-Leon MJ*, Liboni C*, **Mittelheisser V***, Bochler L, Follain G, Mouriaux C, Busnelli I, Larnicol A, Colin F, Peralta M, Osmani N, Gensbittel V, Bourdon C, Samaniego R, Pichot A, Paul N, Molitor A, Carapito R, Jandrot-Perrus M, Lefebvre O, Mangin PH#, Goetz JG#. "***Platelets favor the outgrowth of established metastases.***"
   Nature Communications 15:3297 (2024) – Highlighted in Unistra, INSERM and national media (Radio France, Sciences et Avenir) press releases.

This project, in collaboration with the laboratory of Pierre Mangin (INSERM UMR_S1255, Etablissement Français du Sang-Alsace), aims to decipher platelets contribution to late steps of metastasis. For this study, I performed the experiments assessing platelet binding to tumor cells. I also performed the immunophenotyping of lung metastases and analyzed the RNASeq data.

2. **Mittelheisser V***, Liboni C*, Mouriaux C, Grazia Trivigno SM, Louis Bochler L, Garcia-Leon MJ, Larnicol A, Paulen L, Stemmelen T, Mangin PH, Lefebvre O and Goetz JG. "***Tumoral CD24 tunes platelet binding and supports metastasis.***"
   In preparation.

This project aims to identify new molecular determinants contributing to the heterogeneous binding between platelets and tumor cells. I designed the study, conducted the majority of the experiments and analyses, and wrote and edited the manuscript.

3. **Mittelheisser V***, Gensbittel V*, Bonati L*, Li W*, Tang L#, Goetz JG#. "***Evidence and therapeutic implications of biomechanically regulated immunosurveillance in cancer and other diseases.***"
   Nature Nanotechnology 19:281–297 (2024)

This review, in collaboration with the laboratory of Li Tang (Biomaterials for Immunoengineering Laboratory, Institute of Bioengineering, EPFL), highlights how mechanosensitive properties of immune cells influence their responses in various diseases and how targeting the biomechanical features of the disease milieu or immune cells is a promising strategy for manipulating therapeutic outcomes.

4. **Mittelheisser V**, Coliat P, Moeglin E, Goepp L, Goetz JG, Charbonnière LJ, Pivot X, Detappe A. "***Optimal Physicochemical Properties of Antibody-Nanoparticle Conjugates for Improved Tumor Targeting.***"
   Advanced Materials 34:2110305 (2022) – Highlighted in a Unistra/CRBS and CNRS press releases.

This meta-analysis performed for my PharmD confirmes that targeted-NPs with antibody against tumor associated antigens leads to significantly greater tumor uptake than that of naked NPs. For this study, I reviewed the literature between 2009 and 2021, extracted the biodistribution and pharmacokinetics data and performed the analyses, and wrote and edited the manuscript.

5. Boide Trujillo V-J*, **Mittelheisser V***, Liu F*, Lefebvre O, Andreiuk B, Yudhistira T, Anton N, Goetz JG [#] and Klymchenko AS[#]. "***Functionalization of lipid nanoemulsions with humanized antibodies using plug-and-play cholesterol anchor for targeting cancer cells***"
   In preparation.

This project, in collaboration with the laboratory of Andrey Klymchenko (UMR_7021 CNRS), aims to validate the targeting abilities of lipid nanoemulsions functionalized with anti-HER2 (trastuzumab) antibodies. For this study, I designed the biological validation of the trastuzumab-target nanoemulsion, conducted the experiments and analyses, and wrote and edited the manuscript.

6. **Mittelheisser V**, Banerjee M, Pivot X, Charbonnière LJ, Goetz JG, Detappe A. "***Leveraging immunotherapy with nanomedicine.***"
   Advanced Therapeutics 3:2000134 (2020)

This review details the use of immune cells-targeted NPs designed to deliver immunostimulatory molecules to reactivate these immune cells and restore their anti-tumoral function.

7. **Mittelheisser V**, Lefebvre O, Banerjee M, Soltani R, Ghosh S, Dupas A, Diringer MC, Blumberger J, Bochler L, Harlepp S, Larnicol A, Pichot A, Stemmelen T, Molitor A, Rompai M, Carapito C, Carapito R, Ménard-Moyon C, Bianco A, Charbonnière LJ, Lux F, Tillement O, JG[*] and Detappe A[*]
   "***Nanomaterials trigger functional responses in primary human immune cells***"
   In revision

This project aims to investigate the effect of NPs material on primary human immune cells in order to provide rationale for developing antibody-NP conjugates aimed at reactivating the immune system of cancer patients. I designed this study and carried out the majority of the experiments and analyses, and wrote and edited the manuscript.

Chapter I

Platelets favor each step of the cancer dissemination and later metastatic outgrowth

Besides platelets function in hemostasis, experimental evidences define them as active players in all the steps of cancer progression. In this Chapter I, we will summarize platelets role on primary tumor growth, TCs vascular dissemination and metastatic foci establishment. While platelets are known to infiltrate primary tumors, no evidence proves that this phenomenon occurs in metastases.

In this Chapter, we will also present our results documenting that platelets populate metastatic foci and favor the outgrowth of established metastases via an immunosuppression of the metastatic TME. Furthermore, we also demonstrate that TCs have unequal platelets binding capacities. Our additional investigations highlight that CD24 expression on TCs tunes platelets binding and pro-metastatic functions.

Publications associated to this chapter:

Garcia-Leon MJ*, Liboni C*, **Mittelheisser V***, Bochler L, Follain G, Mouriaux C, Busnelli I, Larnicol A, Colin F, Peralta M, Osmani N, Gensbittel V, Bourdon C, Samaniego R, Pichot A, Paul N, Molitor A, Carapito R, Jandrot-Perrus M, Lefebvre O, Mangin PH#, Goetz JG#. "***Platelets favor the outgrowth of established metastases.***"
Nature Communications 15:3297 (2024) – doi:10.1038/s41467-024-47516-w

Mittelheisser V*, Liboni C*, Mouriaux C, Grazia Trivigno SM, Louis Bochler L, Garcia-Leon MJ, Larnicol A, Paulen L, Stemmelen T, Mangin PH#, Lefebvre O# and Goetz JG#. "***Tumoral CD24 tunes platelet binding and supports metastasis.***"
In preparation.

1. Platelet role in cancer progression

Platelets involvement in cancer growth and metastasis is an established concept that initially emerged even before platelets were first described in 1882 by the Italian pathologist Giulio Bizzozero (Bizzozero, 1882). In pioneering observations, the French clinician Armand Trousseau diagnosed himself and his patients in 1865 with migratory thrombophlebitis, which was later determined as caused by late-stage occult carcinomas (Trousseau, 1872). The link between TCs and thrombus formation was later confirmed in 1877 by Theodor Billroth who noted, during autopsies, that tumor metastasis were often accompanied by “thrombi filled with specific tumor elements” (Billroth, 1877). At the same time, Leopold Riess first described the association between thrombocytosis and solid tumors (Riess, 1872). By the time these observations were made (around a century ago), numerous clinical reports associated paraneoplastic thrombocytosis (*i.e.*, >450.10^9 platelets/L) and Trousseau’s syndrome (hypercoagulability, microangiopathy) with occult malignancies (Bailey et al., 2017; Levin, 1964; Sack et al., 1977) and poor prognosis in ovarian (Stone et al., 2012), lung (Pedersen and Milman, 1996), colorectal (Sasaki et al., 2012), gastric (Ikeda et al., 2002), and breast cancers (Taucher et al., 2003).

Nevertheless, the first experimental evidence of this mechanism was provided only in 1968 by Gasic and collaborators (Gasic et al., 1968). After treating mice with neuraminidase to induce a thrombocytopenia, they observed a marked reduction in lung metastasis which correlated with the decreased platelet count. Further evidence derived from the transfusion of platelet-rich plasma (PRP) which restored metastatic potential in thrombocytopenic mice (Gasic et al., 1968). Over time, the employment of transgenic mice models deficient in key platelet molecules (such as NFE2, GPVI or the $\alpha_{IIb}\beta_3$ and $\alpha_6\beta_1$ integrins) (Bakewell et al., 2003; Camerer et al., 2004; Jain et al., 2009; Mammadova-Bach et al., 2016) provide additional elements to refine platelets crucial roles in tumor metastasis, and define them as important components of the microenvironment.

1.1. Tumor cells modulate platelet biology

Paraneoplastic thrombocytosis is caused by a paracrine circuit of thrombopoietic factors released from the primary tumor. A first study conduct on

ovarian cancer patients identify interleukin 6 (IL-6) as a key player in cancer-induced platelets production (Kaser et al., 2001; Stone et al., 2012). Ovarian cancer cells promote directly and indirectly (through IL-6) the secretion of thrombopoietin (TPO) (Ryu et al., 2003; Sasaki et al., 2012) (**Figure 6**). By binding its cognate c-Mpl receptor on bone marrow (BM) megakaryocytes, TPO stimulates their growth and maturation (Kaushansky, 1995). Upon terminal differentiation, megakaryocytes produce proplatelets (*i.e.*, pseudopodial elongations) that extend into BM sinusoidal blood vessels and fragment under blood shear, releasing platelets from their tips (Brown, 1913; Italiano et al., 1999). Of note, paraneoplastic thrombocytosis is also observed in other malignancies such as breast cancer (Harano et al., 2017) and colitis-associated colorectal cancer (Grivennikov et al., 2009), but is not associated with an increase in TPO levels. Tumors secrete cytokines known to directly promote megakaryopoiesis, such as the chemokine ligand 5 (CCL5) (Machlus et al., 2016), the granulocyte-macrophage colony-stimulating factor (GM-CSF) (Suzuki et al., 1992) and the platelet factor 4 (PF4) (Pucci et al., 2016) (**Figure 6**). However, further investigations are necessary to determine their role in thrombocytosis arising from malignancies. Recent findings indicate that colon and breast cancers also produce kynurenine, which steers megakaryocytic-erythroid progenitor cells differentiation towards megakaryocytes by activating the aryl hydrocarbon receptor-Runt-related transcription factor 1 (AhR–RUNX1) axis (Zhou et al., 2023).

TCs do not only modify platelets number, but also induce qualitative changes in their content, forming tumor-educated platelets (TEPs) (**Figure 6**). Recent investigation using a spontaneous murine model of breast cancer (MMTV-PyMT mice) highlights a breast cancer-induced pro-inflammatory phenotype in the megakaryocytic lineage. This phenotype is characterized by a disrupted polyploidization and an increased lipocalin-2 and S100A8/A9 proteins levels in the platelets. These findings suggest that tumor-driven alterations of megakaryocytes are passed onto their platelet progeny, promoting lungs colonization by TCs (Roweth et al., 2022). TEPs also present an altered structure. Electron cryotomography analysis of platelets obtained from ovarian cancer patients reveal disintegrated microtubules and elevated mitochondria numbers (Wang et al., 2015). Combination of megakaryocytic inflammatory phenotype and increased platelets mitochondrial mass is associated with platelet hyperactivity, underlying Trousseau's syndrome (Davizon-Castillo et al., 2019). Hyperactive platelets

present a lowered activation threshold in response to TC-secreted weak platelets agonists, such as adenosine diphosphate (ADP) (Egan et al., 2011) or IgG (Miao et al., 2019) (**Figure 6**). This notion is corroborated in cancer patient plasma by the presence of platelet activation markers, such as soluble CD40 ligand (sCD40L) (Huang et al., 2012), soluble P-selectin (Ay et al., 2008) and higher aggregation *ex vivo* in response to ADP, adrenaline and collagen activation (Cooke et al., 2013).

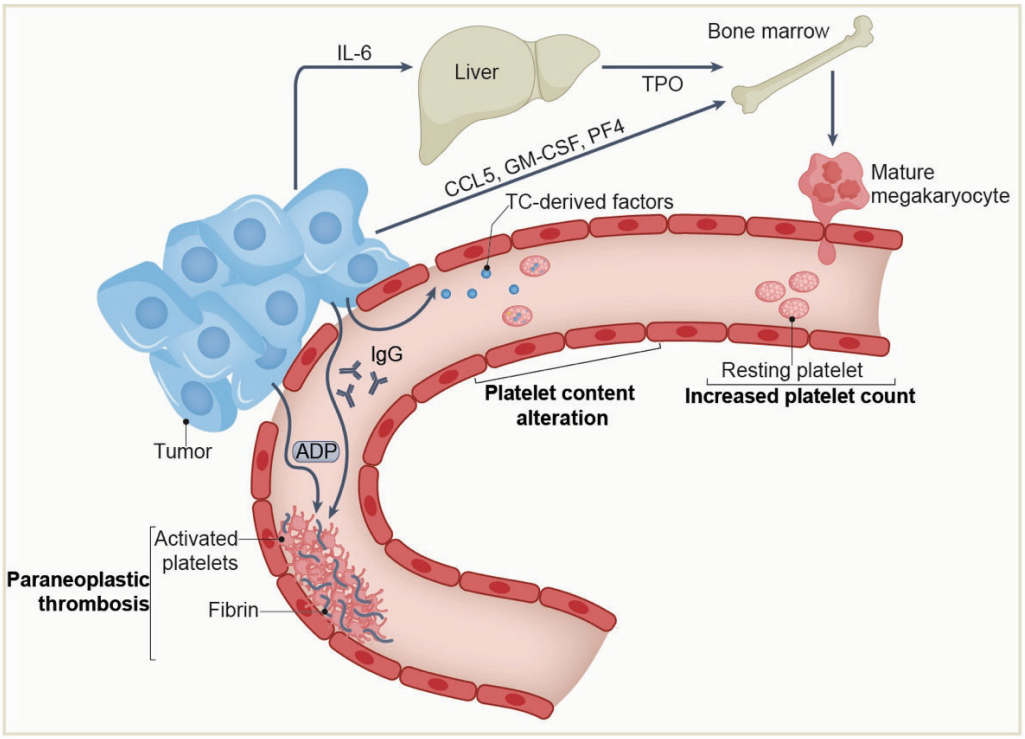

Figure 6 – Tumor cells alter platelet biology.
Tumors stimulate megakaryocyte maturation through hepatic production of TPO or directly by secreting CCL5, GM-CSF and PF4. Mature megakaryocytes produce resting platelets. Tumor also secrete soluble factors, which can be taken up by circulating platelets, thus altering platelet RNA and protein profiles and forming tumor-educated platelets (TEPs). TEPs are hyperactive and more sensitive to activation by tumor-derived weak platelet agonists, eventually leading to cancer-associated thrombosis formation.

1.2. Platelets shape the primary tumor microenvironment

Solid tumors that have grown beyond the critical size of 1-2 mm^3 require increased vascularization to meet their oxygen and nutrient requirements. To that end, TCs release pro-angiogenic factors such as the VEGF that activate ECs and stimulate their sprouting and proliferation (Hellström et al., 2007). Interestingly, activated endothelia upregulate the expression of von Willebrand Factor (VWF) (Kalagara et al., 2018), P-selectin (McEver et al., 1989), $\alpha_V\beta_3$ integrins (Brooks et al., 1994) and tissue

factor (Contrino et al., 1996), which bind to platelets, thus promoting their local recruitment to the tumor site.

1.2.1. Platelets promote angiogenesis and vascular integrity

Platelets α-granules contain stored pools of pro-angiogenic factors such as VEGF (Möhle et al., 1997), PDGF (Heldin et al., 1981) and stromal cell-derived factor-1 (SDF-1, also known as CXCL12) (Massberg et al., 2006) that can be released upon platelet local activation within the VEGF-stimulated tumor vasculature (Verheul et al., 2000). Remarkably, intravital microscopy show platelets rolling along the endothelium, but no firm adhesion nor thrombus formation within the tumor microcirculation (Ho-Tin-Noé et al., 2008; Manegold et al., 2003). Due to the lack of adherent platelets and thrombi formation, it is speculated that the mechanisms involved in platelet pro-angiogenic functions at the tumor site differ from those involved in primary hemostasis.

The reduction of the blood flow within tumor microvessels may allow the localized release of platelet pro-angiogenic and pro-lymphangiogenic factors. This local secretion stimulates angiogenesis through ECs proliferation (Jiang et al., 2017; Li et al., 2014) (**Figure 7**) and pericytes recruitment (Li et al., 2014; Stone et al., 2012; Zhang et al., 2020). Additionally, platelet-derived factors recruit hematopoietic progenitors (Jin et al., 2006; Stellos et al., 2008) and BM-derived cells (Feng et al., 2011) to the primary tumors, later triggering their differentiation into mature ECs. Platelets also intervene in lymphangiogenesis by stimulating lymphatic growth via the secretion of PDGF (Cao et al., 2004) or VEGF-C (Lim et al., 2019) (**Figure 7**) and by preventing the mixing of lymphatic and blood circulations through the engagement of platelet C-type lectin-like receptor-2 (CLEC-2) receptor by podoplanin (PDPN) on lymphatic ECs (Haining et al., 2021). Because of these effects on angiogenesis and lymphangiogenesis, platelets foster primary TCs early dissemination through the blood vasculature and the lymphatic circulation (Wong and Hynes, 2006).

Furthermore, one should note that platelets also continuously prevent intratumoral hemorrhage by promoting neovascular integrity (Ho-Tin-Noé et al., 2008; Kisucka et al., 2006). Indeed, platelets α-granules also contain anti-angiogenic factors such as angiopoietin-1 and serotonin, which stabilize the tumor vasculature by promoting mural cell coating, basement membrane deposition and by counteracting VEGF effect (Ho-Tin-Noé et al., 2008). Moreover, platelets prevent potential

neutrophil-mediated vascular damages through the secretion of anti-inflammatory factors (Ho-Tin-Noé et al., 2009; Volz et al., 2019). Interestingly, pro-angiogenic and anti-angiogenic factors are sorted in distinct subpopulations of α-granules, which are differentially released depending on the stimuli. Granules loaded with VEGF are selectively released after ligation of protease-activated receptor 1 (PAR1), whereas granules containing anti-angiogenic factors are released upon PAR4 activation (Italiano et al., 2008; Ma et al., 2005). This suggests that TCs could hijack platelets to balance the angiogenic milieu.

1.2.2. Platelets induce primary tumor proliferation and invasiveness

Recruited platelets extravasate from adjacent vessels and infiltrate the primary tumor stroma (Le Chapelain et al., 2024; Yap et al., 2017), notably via pathways mediated by the focal adhesion kinase (FAK) (Haemmerle et al., 2016), the CX3C chemokine receptor 1 (CX3CR1) (Miao et al., 2020) or the G protein-coupled receptors (GPCRs) Gαi and Gα13 (Cho et al., 2021). Once infiltrated inside the TME, platelets bind to TCs mainly through their surface receptors P-selectin (Qi et al., 2015) and CLEC-2 (Costa et al., 2019). Recently, we have demonstrated using a new transgenic mice model ($PF4^{Cre}$-$\beta1^{-/-}$/$\beta3^{-/-}$) that platelets adhesion and activation through β1 integrins ($\alpha_2\beta_1$, $\alpha_5\beta_1$ and $\alpha_6\beta_1$) as well as their aggregation via β3 integrins ($\alpha_{IIb}\beta_3$) are actively participating to primary tumor growth by remodeling the TME (**Annex 1**). Integrins effect on primary tumor progression is likely to be synergistic as no effects were observed using single deficient transgenic mice models (Mammadova-Bach et al., 2016).

TCs bound platelets release growth factors, including epidermal growth factor (EGF) (Chen et al., 2018), TGFβ (Hu et al., 2017) and androgens (Zaslavsky et al., 2015) upon activation (**Figure 7**). Interestingly, platelets express glycoprotein A repetitions predominant (GARP) protein at their membrane, which capture latent TGFβ (LTGFβ) secreted from other stromal cells. Active TGFβ liberation occurs by the cleavage of the LTGFβ-GARP complex by thrombin generated in the TME. Hence, platelets directly produce TGFβ or act as a reservoir (Metelli et al., 2020). In addition to inducing primary tumor proliferation in a paracrine manner through their releasates, platelets transfer their mitochondria to TCs by direct interactions, inducing their reprogrammation to a pro-metastatic state (Cereceda et al., 2024; Zhang et al., 2023).

Besides, PDGF and TGFβ secreted by degranulating platelets work in synergy with integrin $\alpha_2\beta_1$-mediated signaling that activates the downstream Wnt–β-catenin and NF-κB pathways in TCs, endowing them with an EMT phenotype (Labelle et al., 2011; Zhang et al., 2019; Zuo et al., 2019). Platelets-mediated EMT induction is also induced via direct transfer of platelets content (*e.g.*, RNA, proteins, lipids) to TCs (Rodriguez-Martinez et al., 2022). A key characteristic of the EMT program is the ability to confer to primary TCs properties essential metastatic dissemination; among them: increased motility, invasiveness, and the ability to degrade components of the ECM (Kalluri and Weinberg, 2009). Of note, EMT transcriptional programs induction is more pronounced in highly vascularized tumor areas, where platelets are initially recruited (Puram et al., 2017). In addition, EMT transcriptional programs positively correlate with platelets activation (Miyashita et al., 2015). Primary tumor invasion is also promoted by platelet-induced secretion of MMPs that degrade the ECM allowing TCs to leave the primary site and invade the peripheral blood circulation (Dilly et al., 2013; Fishman et al., 2001; Saito et al., 2021).

1.2.3. Platelets favor TME stiffening

Intratumoral platelets collaborate with non-neoplastic cells present in the TME to promote a permissive and supportive microenvironment for TCs. Among the non-neoplastic cells, infiltrated platelets can interact through CLEC-2 with PDPN-expressing fibroblasts (Miyashita et al., 2019). Upon this interplay, platelets secrete TGFβ (De Wever et al., 2004) and PDGF (Anderberg et al., 2009) that act on fibroblasts, driving their differentiation into CAFs, resulting in excessive ECM deposition (Zhang et al., 2022). Furthermore, platelets stimulate LOXs expression in TCs (Qi et al., 2016), inducing the reticulation of collagen fibers that stiffen the matrix (Levental et al., 2009) (**Figure 7**). Besides, platelets are capable of direct ECM reorganization by driving fibronectin fibrillogenesis *in vitro* via $\alpha_{IIb}\beta_3$ integrin (Lickert et al., 2022). Platelets sense the stiffness of their microenvironment and become activated (Qiu et al., 2014), further fueling and exacerbating the global TME stiffening. Additionally, platelet-derived PDGF secretion in the TME is also associated with an increased interstitial fluid pressure (Pietras et al., 2001).

Overall, platelet-driven TME modifications impair diffusion of chemotherapeutic drugs in the tumor bed (Salnikov et al., 2003) and imped intra-tumoral infiltration of immune cells (Li et al., 2019).

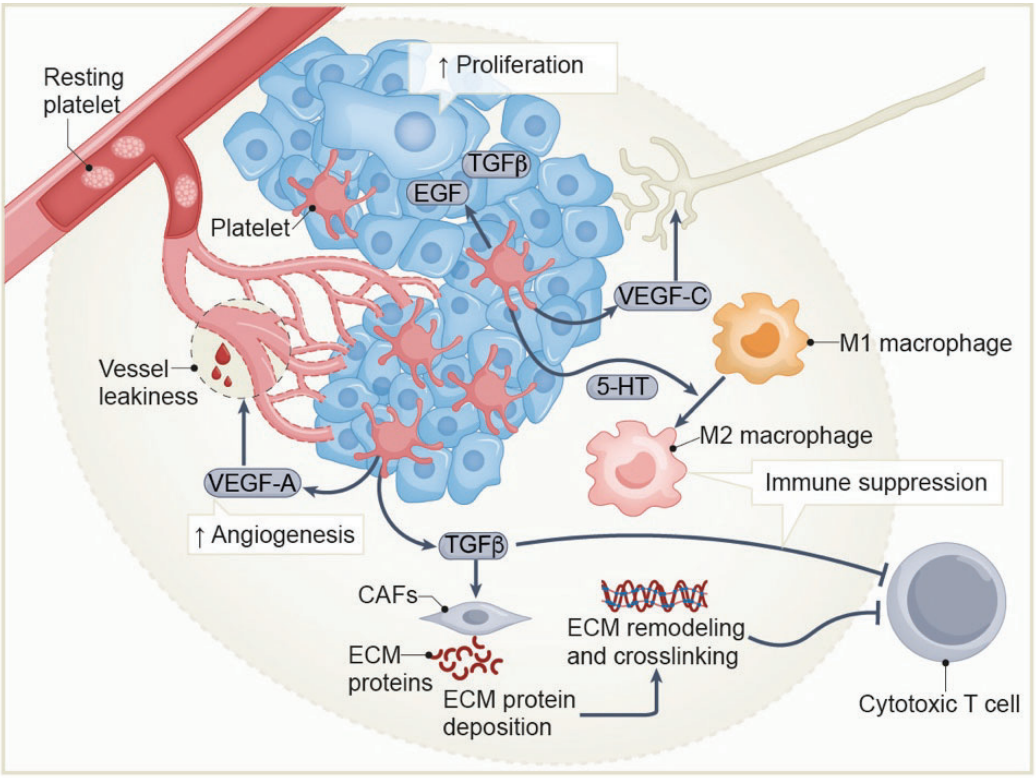

Figure 7 – Platelets functions in the primary tumor.
Within the primary tumor, platelets sustain TCs proliferation through the secretion of growth factors such as EGF or TGFβ. Platelets also promote angiogenesis through VEGF-A and lymphangiogenesis by VEGF-C secretion. Besides, platelet-derived TGFβ recruits cancer-associated fibroblasts, promotes excessive deposition of ECM by CAFs, which can impede the intratumoral infiltration of immune cells. Furthermore, platelet-derived TGFβ and serotonin (5-HT) contribute to an immunosuppressive microenvironment by respectively hindering T cells function and promoting the transition of M1 macrophages to the M2 phenotype.

1.2.4. Platelets compromise anti-tumor immune response

Platelets can also suppress directly the immune response. Their binding to antigen presenting cells (APCs) induces a skewed maturation resulting in functionally deficient dendritic cells (DCs). Deficient DCs are incapable of antigen cross-presentation and subsequent naive T cell activation (Hilf et al., 2002; Kissel et al., 2006; Singh et al., 2021). Platelets also promote myeloid cells polarization towards pro-tumoral phenotypes in a paracrine manner. Indeed, platelet-derived factors such as TGFβ, prostaglandin E_2 (PGE_2) or sCD40L foster neutrophils (Fridlender et al., 2009)

and macrophages (Prima et al., 2017) anti-tumoricidal activities as well as dendritic cells dysfunctions in orchestrating T cell responses (Bayerl et al., 2023) (**Figure 7**).

Platelets can also directly bind to T cells, impairing T cell receptor (TCR)-triggered activation and proliferation (Zamora et al., 2017). In addition to direct effects, platelets secretion of TGFβ and lactate provokes strong constrains in T cells functions (Rachidi et al., 2017) and spoil bispecific antibodies-mediated T cells anti-tumoral responses (Lutz et al., 2022). Platelets can also weaken T cells responses by inducing programmed death-ligand 1 (PD-L1) upregulation on cancer cells, notably through growth factors (Asgari et al., 2021; Guo et al., 2022) or serotonin (Schneider et al., 2021) secretion. Upon contact with platelets, tumors can transfer them PD-L1 protein in a fibronectin-integrin $\alpha_5\beta_1$-GPIbα-dependent manner (Hinterleitner et al., 2021). Platelet expressing PD-L1 hinder T cells infiltration and induce cytotoxic $CD8^+$ T cell exhaustion (Hinterleitner et al., 2021; Rolfes et al., 2018). Interestingly, platelet PD-L1 expression was superior in predicting the response towards immune checkpoint inhibitors as compared to standard histological PD-L1 quantification on tumor biopsies. This observation is strengthened by clinical reports suggesting that PD-L1 expression on intra-tumoral platelets contributes to the pharmacological activity of anti-PD-L1 atezolizumab (Colarusso et al., 2023; Rolfes et al., 2018). Besides, platelets induce others immune checkpoint molecules on TCs. Among them, ectonucleoside triphosphate diphosphohydrolase-1 (ENTPD1, CD39) expression is promoted in TCs upon direct binding with platelets (Ning et al., 2024). CD39 hydrolyzes extracellular adenosine triphosphate (ATP) and adenosine diphosphate (ADP) to adenosine monophosphate (AMP) in concert with CD73 which further catalyzes the hydrolysis of AMP to adenosine, a potent immunosuppressive molecule (Bastid et al., 2015).

Nevertheless, other studies using mice model of hepatocellular carcinoma reported that platelets suppressed liver tumor growth via activating $CD8^+$ T cells through CD40L-induced dendritic cells maturation (Elzey et al., 2003), P_2Y_{12}-dependent CD40L release (Ma et al., 2022) or β3 integrins transfer to T cells (Zhou et al., 2024). Furthermore, a secretome library identifies PDGF-DD as a ligand for the NK cells activating NKp44 receptor, thereby leading to interferon-γ (IFNγ) release and TCs cell cycle arrest (Barrow et al., 2018). Additional work further validates differences in platelets-driven immune response modulation between triple negative breast cancer (TNBC) and melanoma (Le Chapelain et al., 2024), thereby suggesting that platelets

impact on the primary TME might be cancer type-dependent and warrants further investigation.

1.3. Platelets favor tumor cells intravascular survival and extravasation

When leaving the primary tumor and upon intravasation, TCs leave the supportive TME and experience the hostile blood flow high shear stress, that can disrupt their membranes (Headley et al., 2016). CTCs also encounter patrolling immune cells (Adams et al., 2014; Szczerba et al., 2019), that detect them and kill them. While CTCs are rapidly destroyed after entering the bloodstream when exposed to these hostile cues, they may also bind and activate circulating platelets within 1 minute leading to microaggregates formation (Labelle et al., 2014; Yu et al., 2013), a phenomenon known as tumor cell-induced platelet aggregation (TCIPA). TCIPA and TCs-platelets interactions are warranted for successful hematogenous metastatic dissemination.

1.3.1. CTCs bind and activate platelets

Platelets bind to TCs through receptors containing an immunoreceptors tyrosine-based activation motif (ITAM), such as glycoprotein VI (GPVI) (Mammadova-Bach et al., 2020), CLEC-2 (Suzuki-Inoue et al., 2007) and FcγRIIa (Miao et al., 2019; Mitrugno et al., 2014) (**Figure 8**). The respective binding of GPVI and CLEC-2 with their tumoral ligands, galectin-3 and PDPN triggers ITAM-based signaling. TCs also induce TCIPA by releasing high-mobility group box 1 protein (HMGB1) that interacts with platelets Toll-like receptor 4 (TLR4), initiating a myeloid differentiation factor 88 (MyD88)-dependent signaling (Yu et al., 2014). Activation of ITAM and MyD88 pathways in platelets result in granule release, P-selectin expression and inside-out integrins activation, including $\alpha_{IIb}\beta_3$ (Rayes et al., 2019; Zhang et al., 2009). P-selectin and $\alpha_{IIb}\beta_3$ surface expression guarantees stable TCs-platelets binding (Lonsdorf et al., 2012). P-selectin recognizes ligands containing a terminal Sialyl Lewis^X (SLe^X), such as P-selectin glycoprotein ligand-1 (PSGL-1), CD24 and CD44 expressed by different tumor cell types (Aigner et al., 1997; Alves et al., 2008; Dimitroff et al., 2005) (**Figure 8**). Integrin $\alpha_{IIb}\beta_3$ binds to tumor $\alpha_V\beta_3$ integrin via their ligands (*e.g.*, fibrinogen, fibronectin, von Willebrand factor) acting as bridging molecules between TCs and platelets (Dardik et al., 1997; Lonsdorf et al., 2012) (**Figure 8**). Platelet integrins inside-

out activation also allow additional interactions between TCs and platelets, such as the platelets $\alpha_6\beta_1$ and tumoral ADAM-9 binding (Mammadova-Bach et al., 2016) (**Figure 8**).

Of note, following TC-induced activation of ITAM-based signaling, platelets undergo a shape change and release ADP, which further enforces activation in an autocrine manner (Kahner et al., 2006) (**Figure 8**). Platelets activation by TCs can also be triggered in a paracrine manner as TCs secrete platelets weak (*e.g.*, ADP, MMP-2) (Haemmerle et al., 2016; Jurasz et al., 2001) and potent (*e.g.*, thromboxane A_2, thrombin) agonists (De Leval et al., 2003; Liu et al., 2011). The complex two-way communication pathway between leading to TCIPA demand further investigation to be fully characterized.

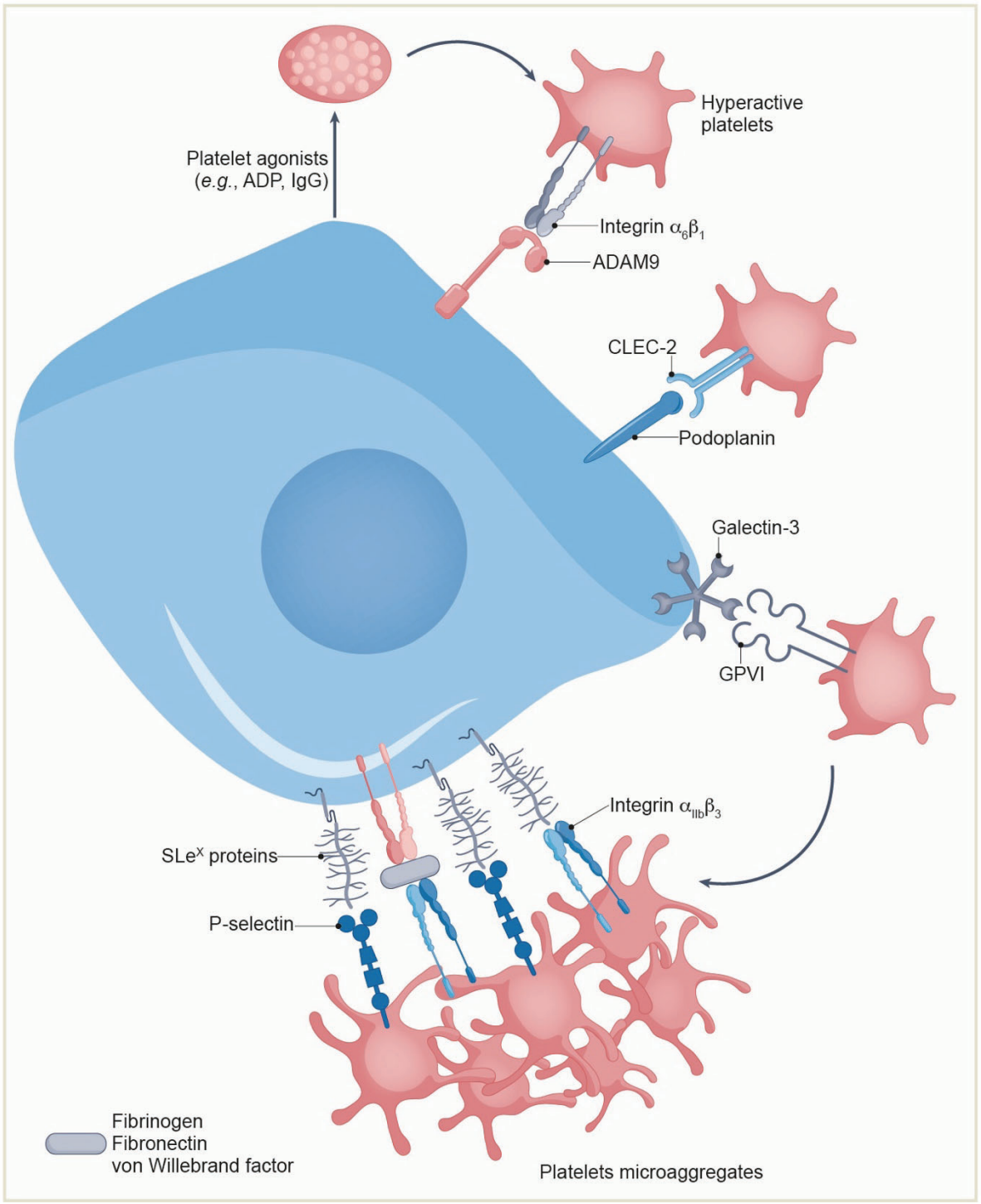

Figure 8 – Platelet-CTCs interactions promote platelet activation.
Interactions between platelets and CTCs occur preferentially with hyperactivated platelets through binding to multiple activation-associated receptors of the platelets, including integrins, CLEC2, GPVI and P-selectin. Direct contact between platelets and CTCs further activates the platelets, enhancing their adhesive properties and consequently resulting in the formation of platelet microaggregates around CTCs.

1.3.2. Platelets favor CTCs intravascular survival

Platelets act as the first responder after CTCs intravasation and are vital to maintain their survival and to promote efficient metastasis. First, activated platelets protect TCs from the deleterious effects of shear stress (Egan et al., 2014). Besides, CTCs also endure anoikis (*i.e.*, apoptosis upon the loss of attachment to ECM) (Strilic and Offermanns, 2017). Platelets binding to CTCs reduce their susceptibility to anoikis. Indeed, the direct binding of platelets to CTCs inhibit anoikis through the activation of RhoA-mediated Yes-associated protein 1 (YAP1) dephosphorylation, thereby promoting its nuclear translocation and the expression of pro-survival genes in ovarian ascites (Haemmerle et al., 2017) (**Figure 9**). Furthermore, upon TCIPA, platelets release brain-derived neurotrophic factor (BDNF) that activates the tropomyosin-related kinase B (TrkB) receptor expressed on colorectal CTCs (Geiger and Peeper, 2007; Tanaka et al., 2014).

Moreover, platelets can protect CTCs from immune recognition notably by forming a cloak around them, physically shielding them from tumor necrosis factor α (TNF-α) (Philippe et al., 1993) and natural killer (NK) cells (Nieswandt et al., 1999; Palumbo et al., 2005) (**Figure 9**). Platelets binding to CTCs mediates the shedding of NKG2D ligands, in particular MICA and MICB, from the surface of TCs, consequently impairing NK cells anti-tumoral immune surveillance (Maurer et al., 2018). Besides hiding CTCs from immune cell, platelets also enable the cells to successfully undergo immune escape by transferring MHC class I molecules onto the surface of TCs (**Figure 9**). MHC-I pseudo-expressed by TCs binds NK cells Killer Ig-like (KIRs) inhibitory receptors, thus suppressing NK cells-mediated cytotoxicity and IFNγ production (Placke et al., 2012a). Additionally, the transfer of another platelet-derived protein, the regulator of G protein signaling 18 (RGS18) into pancreatic CTCs upregulate the expression of the immune-checkpoint molecule human leukocyte antigen E (HLA-E). HLA-E binds to NKG2A on NK cells and inhibits their anti-tumoral functions (Liu et al., 2023). Furthermore, TCIPA stimulate rapid upregulation of immune modulators such as glucocorticoid-induced TNFR-related ligand (GITRL) at the platelets surface. Hence, CTCs pseudo-express GITRL, which interacts with its receptor GITR expressed by NK cells, leading to a reduction in their anti-tumor activity and response to IL-15 activation (Placke et al., 2012b). In addition, platelets activation upon CTCs binding also induces the release of TGF-β, which inhibits the NK cells anti-tumor

reactivity by downregulating their activating receptors NKG2D and CD226 expressions (Cluxton et al., 2019; Kopp et al., 2009; Lee et al., 2004).

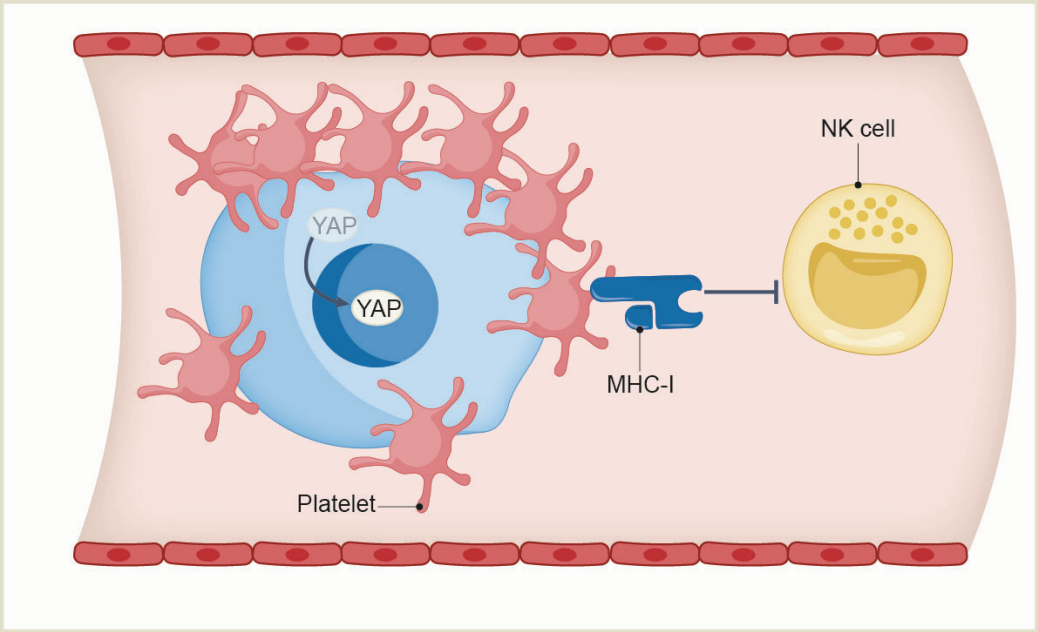

Figure 9 – Platelets foster CTCs survival in the circulation.
In the circulation, platelet microaggregates coat CTCs and protect them from shear stress and anoikis by promoting YAP1 nuclear translocation. In addition, platelets also shield CTCs against NK cell-mediated immune surveillance by transferring MHC class I molecules onto the surface of CTCs.

Furthermore, platelets-CTCs clusters interact with neutrophils. Platelets P-selectin can bind to its receptor PSGL-1 expressed by neutrophils, inducing their activation and the formation of neutrophil extracellular traps (NETs), which are web-like structures composed of extracellular DNA adorned with histones (Etulain et al., 2015; Hidari et al., 1997). NETs synergize with TCIPA by presenting histones to platelets TLR4, inducing their activation and further promoting a positive feedback loop between platelets and NETs (Ren et al., 2021; Semeraro et al., 2011). This complex neutrophils-platelets crosstalk leads to NETs entrapment of CTCs, thus enhancing their proliferative and metastatic capacities (Cools-Lartigue et al., 2013; Szczerba et al., 2019), as well as further suppressing intravascular NK cells-mediated immune surveillance (Spiegel et al., 2016).

1.3.3. Platelets facilitate CTCs adhesion to endothelium and support their metastatic seeding

Besides protecting CTCs within the bloodstream, platelets also actively support their seeding in distant metastatic organs. First, platelets foster CTCs rolling along the endothelium via their P-selectin expression (Kim et al., 1998; McCarty et al., 2000). Interestingly, platelet-expressed P-selectin promote melanoma metastasis to the lungs but not to liver, suggesting that platelets may promote organ-specific arrest (Coupland et al., 2012) (**Figure 10**). After this initial phase, platelet integrins mediate the transition from selectin-dependent CTCs rolling to stable arrest. Indeed, CTCs hijack platelet endothelial adhesion receptors, such as, $\alpha_{IIb}\beta_3$ integrin (Rayes et al., 2019), β_3 integrin (Rodriguez-Martinez et al., 2022) and the GPIbα-IX-V complex (Jain et al., 2007; Martins Castanheira et al., 2022; Rodriguez-Martinez et al., 2022). In addition to adhesions to the endothelium, heterotypic clusters arrest by occluding the vessel. CTCs express EMT-associated heat shock protein 47 (Zhu et al., 2015), which facilitates collagen secretion and deposition by TCs (Xiong et al., 2020). Then, collagen at the CTCs surface is recognized by platelets GPVI, inducing a micro-thrombi formation (Feitsma et al., 2022) that facilitates CTCs arrest by embolization, spreading in the vasculature (Im et al., 2004) and ECs activation (Ferjančič et al., 2013). Another study further suggests that TC-derived tissue factor promotes thrombin-induced clot formation upon platelets binding which plays a key role for as the starting point of brain metastasis (Feinauer et al., 2021).

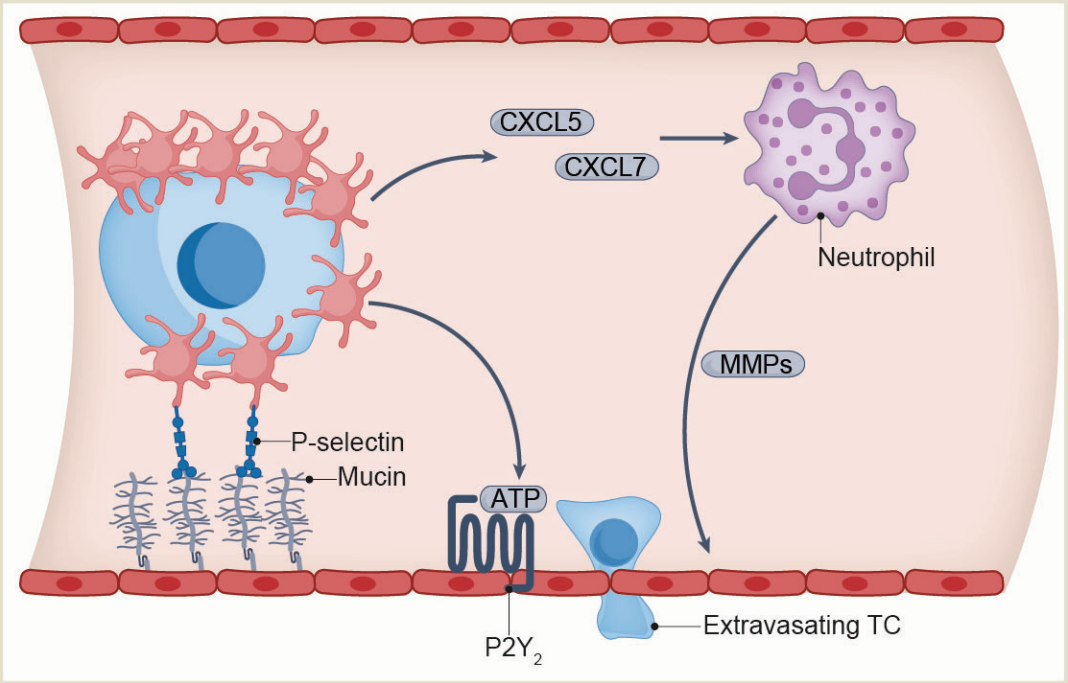

Figure 10 – Platelets facilitate CTCs arrest and extravasation.
At distant metastatic sites, platelets promote TCs adhesion to the endothelium and assist in transendothelial extravasation to form solid metastatic foci. Surface adhesion molecules, such as P-selectin, on the platelets bind mucins present on endothelial cells, facilitating the arrest of TCs at the vascular endothelium. ATP released from the platelets then interacts with $P2Y_2$ receptors on endothelial cells to augment the endothelial gaps, promoting the extravasation of CTCs. In addition, platelet-derived CXCL5 and CXCL7 recruits neutrophils which further sustain CTCs extravasation.

Following firm adhesion, CTCs cross the endothelial barrier. Extravasation requires first the increase of vascular permeability, to which platelets contribute (Reymond et al., 2013). Upon TCIPA, platelets release permeability-increasing molecules, such as VEGF (Martín-Granado et al., 2017), sphingosine 1-phosphate (S1P) (Weigel et al., 2023) and lysophosphatidic acid (LPA) (Boucharaba et al., 2004), that weaken the ECs barrier. The activation of platelets by CTCs expressing CD97 (Ward et al., 2018) or galectin-3 (Mammadova-Bach et al., 2020), induces the secretion of ATP from their dense granules. In turn, platelets-derived ATP triggers $P2Y_2$ signaling in ECs, which disrupts their tight junctions and facilitates CTCs transmigration (Schumacher et al., 2013). CD97-initiated platelet activation also induces localized LPA secretion, which stimulates RHO signaling through CD97-LPAR heterodimers, coupling the invasive phenotype of CTCs to vascular permeability (Ward et al., 2018). While CTCs-expressed galectin-3 is known to bind to platelets GPVI

(Mammadova-Bach et al., 2020), CD97 counter-receptor on platelets is still unknown, thus confirming the need for additional studies to decipher TCIPA mechanisms.

Then, to efficiently cross the vascular basement membrane, CTCs should be able to degrade the ECM underlying the endothelium (Reymond et al., 2013). Basement membrane crossing can be directly promoted by activated platelets secretion of MMPs (Labelle et al., 2014; Rolli et al., 2003), hyaluronidase-2 (Albeiroti et al., 2015), and heparanase (Vlodavsky et al., 1992), that can degrade collagen-rich ECM. Platelets also act indirectly in concert with myeloid cells. Indeed, activated platelets release CXCL5 and CXCL7, which recruit rapidly (<2h post-arrest) neutrophils to the early metastatic niche (Labelle et al., 2014). In response to platelet-CTCs aggregates, neutrophils become activated and secrete MMP-9, which degrades the ECM and facilitates CTCs extravasation (Bekes et al., 2011). Additionally, monocytes are recruited to the early metastatic niche directly by CTCs secreting CCL2 (Qian et al., 2011) or indirectly by the locally platelets-activated endothelium that releases CCL5 (Läubli et al., 2009) and express the vascular cell adhesion molecule-1 (VCAM-1) and the vascular adhesion protein-1 (VAP-1) (Ferjančič et al., 2013). Recruited monocytes promotes CTCs transendothelial migration through VEGF (Qian et al., 2011) and E-selectin (Häuselmann et al., 2016) dependent endothelial retractions.

1.4. TEPs help establishing the metastatic microenvironment

After their extravasation, CTCs need a permissive and supportive microenvironment to efficiently colonize the organ, to grow and divide and foster an overt metastatic disease. For their progeny to be successful, the primary tumors secrete factors (*e.g.*, growth factors, cytokines, hormones) and extracellular vesicles that prepare the future metastatic organ microenvironment, leading to the formation of a pre-metastatic niche (PMN) (Peinado et al., 2017). The PMN formation is initiated by a local alteration of the microenvironment that promotes the recruitment of metastasis-supporting BM-derived cells (Erler et al., 2009; Kaplan et al., 2005) and granulocytes (Kowanetz et al., 2010). Besides TC-derived factors, TEPs induce bone remodeling to facilitate the PMN establishment by conveying TGFβ and MMP1 from primary melanoma and prostate to their bone metastatic site (Kerr et al., 2013).

Conversely, TCs colonizing unprepared metastatic microenvironment lack supportive cues and often fail metastatic colonization. These TCs are either eliminated from the tissue parenchyma or enter dormancy (Luzzi et al., 1998). TEPs also support metastasis in inhospitable environment by delivering proangiogenic cytokines derived from aggressively growing primary breast tumors to indolent TCs at distant sites. TEPs release their pro-tumoral content in response to exposed collagen IV and CD24 expressed on metastasized TCs, thereby supporting indolent TCs through neovascularization and later outgrowth to form overt metastasis (Kuznetsov et al., 2012).

Complementary to their intravascular CTCs support, platelets favor early metastatic colonization by participating to the PMN formation or by helping indolent TCs to grow. Paget's “seed and soil” theory could therefore be slightly modified to include “seed, soil and fertilizer”, in which platelets would play the crucial role of “fertilizer”.

2. Platelets favor the outgrowth of established metastases

In the introductory material of this Chapter I, we described several pro-tumoral roles of platelets in (*i*) promoting primary tumor growth and invasion, (*ii*) protecting CTCs during their intravascular journey, (*iii*) helping CTCs to extravasate and (*iv*) favoring early metastatic colonization. However, whether platelets are capable of tuning late metastatic steps remain unknown and unexplored.

To longitudinally dissect the pro-metastatic role of platelets in lung metastasis and identify the best target to impair their involvement, we subject experimental metastasis mouse models to several time-controlled thrombocytopenic regimens. We highlight that platelets favor the outgrowth of established metastases in a GPVI-dependent manner. To counteract GPVI function, we use the glenzocimab, a humanized anti-GPVI antibody Fab fragment, and successfully impair metastasis growth without inducing collateral hemostatic perturbations.

Altogether, our results demonstrate for the first time platelets late contribution on tumor metastasis by massively infiltrating metastatic foci.

nature communications

Article

https://doi.org/10.1038/s41467-024-47516-w

Platelets favor the outgrowth of established metastases

Received: 22 September 2023

Accepted: 26 March 2024

Published online: 13 May 2024

Check for updates

Maria J. Garcia-Leon[1,2,3,4,10,12] ✉, Cristina Liboni[1,2,3,4,12], Vincent Mittelheisser[1,2,3,4,12], Louis Bochler[1,2,3,4], Gautier Follain[1,2,3,4,11], Clarisse Mouriaux[5], Ignacio Busnelli[1,2,3,4], Annabel Larnicol[1,2,3,4], Florent Colin[1,2,3,4], Marina Peralta[1,2,3,4], Naël Osmani[1,2,3,4], Valentin Gensbittel[1,2,3,4], Catherine Bourdon[5], Rafael Samaniego[6], Angélique Pichot[2,3,7], Nicodème Paul[2,3,7], Anne Molitor[2,3,7], Raphaël Carapito[2,3,7,8], Martine Jandrot-Perrus[9], Olivier Lefebvre[1,2,3,4], Pierre H. Mangin[5] ✉ & Jacky G. Goetz[1,2,3,4] ✉

Despite abundant evidence demonstrating that platelets foster metastasis, anti-platelet agents have low therapeutic potential due to the risk of hemorrhages. In addition, whether platelets can regulate metastasis at the late stages of the disease remains unknown. In this study, we subject syngeneic models of metastasis to various thrombocytopenic regimes to show that platelets provide a biphasic contribution to metastasis. While potent intravascular binding of platelets to tumor cells efficiently promotes metastasis, platelets further support the outgrowth of established metastases via immune suppression. Genetic depletion and pharmacological targeting of the glycoprotein VI (GPVI) platelet-specific receptor in humanized mouse models efficiently reduce the growth of established metastases, independently of active platelet binding to tumor cells in the bloodstream. Our study demonstrates therapeutic efficacy when targeting animals bearing growing metastases. It further identifies GPVI as a molecular target whose inhibition can impair metastasis without inducing collateral hemostatic perturbations.

Metastasis is a pathological process during which tumor cells (TCs) use the bloodstream to colonize distant organs. Yet, the fundamental mechanisms driving metastasis remain poorly understood, limiting the development of efficient therapeutic schemes. When disseminating, circulating TCs (CTCs) face several hostile forces that are detrimental to their survival[1]. Yet, they can exploit hemodynamics to arrest and successfully grow upon extravasation[2–4]. In addition, CTCs efficiently partner with the

[1]Tumor Biomechanics, INSERM UMR_S1109, Strasbourg, France. [2]Université de Strasbourg, Strasbourg, France. [3]Fédération de Médecine Translationnelle de Strasbourg (FMTS), Strasbourg, France. [4]Equipe Labellisée Ligue Contre le Cancer, Paris, France. [5]UMR_S 1255, INSERM, Etablissement Français du Sang-Alsace, Université de Strasbourg, F-67000 Strasbourg, France. [6]Instituto de Investigación Sanitaria Gregorio Marañón (IISGM), Unidad de Microscopía Confocal, Madrid, Spain. [7]Laboratoire d'ImmunoRhumatologie Moléculaire, Plateforme GENOMAX, Institut national de la santé et de la recherche médicale (INSERM) UMR_S 1109, Institut thématique interdisciplinaire (ITI) de Médecine de Précision de Strasbourg Transplantex NG, Faculté de Médecine, France. [8]Service d'Immunologie Biologique, Plateau Technique de Biologie, Pôle de Biologie, Nouvel Hôpital Civil, Hôpitaux Universitaires de Strasbourg, 1 Place de l'Hôpital, 67091 Strasbourg, France. [9]UMR_S 1148, INSERM, Université Paris-Cité, Paris, France. [10]Present address: Domain therapeutics, Parc d'Innovation – 220 Boulevard Gonthier D'Andernach, 67400 Strasbourg – Illkirch, France. [11]Present address: Turku Bioscience Centre, University of Turku and Åbo Akademi University, Turku, Finland. [12]These authors contributed equally: Maria J. Garcia-Leon, Cristina Liboni, Vincent Mittelheisser.
✉e-mail: mgarcialeon@domaintherapeutics.com; Pierre.Mangin@efs.sante.fr; jacky.goetz@inserm.fr

bloodstream ecosystem and interact with blood components on their way to metastasis[5–8].

Among these, platelets are perfect allies: they promote metastatic progression[9] by protecting CTCs from destruction by shear forces, mediate immune evasion, favor adhesion and extravasation at distant sites, facilitate neo-angiogenesis, and sustain a tumor-prone inflammation[10]. Although recent work suggests that platelets can also hamper tumor initiation and growth, as shown in hepatic[11–13] and ovarian[11] tumors, they have mostly been shown to promote TC metastasis. A seminal study documented the inhibition of metastasis by platelet depletion, which can be rescued by platelets transfusion[14]. The depletion of platelet receptors, such as the vWF receptor GPIb, and the collagen receptor GPVI, results in the inhibition of lung metastasis of melanoma and lung carcinoma cells, respectively[15–17].

Anti-platelet strategies became inevitably obvious candidates for impairing metastasis. First, in the bloodstream, CTCs rapidly bind, activate, and aggregate circulating platelets. This provides a physical shield to CTCs and favors intravascular arrest and survival[18,19], as well as successful extravasation and metastatic outgrowth[20–22]. While it is thus tempting to target the intravascular CTCs-platelet interaction with anti-platelet therapies for impairing metastasis, whether this is a universal feature of cancers remains unexplored. It is thus likely that platelets' contributions may differ depending on cancer types[23,24], leading to an unclear outcome when using anti-platelet drugs in oncologic patients[25], in addition to the fact that they cause bleeding. Second, our current knowledge of the pro-metastatic function of platelets focuses on their contribution to the intravascular behavior of CTCs, which subsequently impacts metastatic fitness[10,20,21]. Whether platelets are capable of tuning extravascular and late metastatic steps remain unknown and unexplored. Yet, they could offer additional means for targeting platelets during metastasis. Finally, the development of efficient anti-platelet strategies to fight metastasis faces major pitfalls inherent to the properties of platelets[26,27]. The majority the current of anti-platelet strategies are accompanied by increased bleeding risk[28] and fail when used against metastasis. As this remains a major concern, the use of anti-platelet therapies remains unexplored in the clinic.

Building on such limitations, we designed a study aiming at interrogating which steps of the metastasis cascade are controlled by platelets and whether this is impacted by platelet binding. We first demonstrated that such binding is heterogenous among metastatic TCs. We selected two mouse TCs lines and subjected them to several thrombocytopenic (TCP) regimes in syngeneic mouse models to interrogate the timings at which platelets mostly contribute to metastatic outgrowth. We show that platelets are crucial for the adhesion, clustering, and survival of TCs within the vasculature and we provide further evidence that platelets support their long-term metastatic potential in vivo. We observed that platelets efficiently colonize metastatic foci, in both murine and human samples. Depletion of platelets in animals carrying growing metastases was sufficient to reduce metastatic outgrowth, demonstrating that platelets favor metastasis independently of platelet-TC interaction in the bloodstream and mostly via immune suppression, which could be targeted with new treatment strategies. We focused our attention on the platelet receptor GPVI, which is exclusively expressed at the surface of platelets and whose targeting inhibits platelet function with no impact on bleeding. Genetic depletion and pharmacological targeting of the platelet-specific receptor GPVI in humanized mouse models efficiently reduced the growth of established metastases, independently of active platelet binding to TCs in the bloodstream. Our findings highlight, distinctly from previous studies, that interfering with GPVI can impair metastatic outgrowth of already-established metastases. We believe that such discovery paves the way for establishing successful therapeutic intervention in patients where the primary tumor has already generated one or several metastatic sites.

Results

TCs bind and activate platelets in vitro with different efficiencies

Platelets have been reported to bind CTCs[9] but whether this applies to every cell type remains unknown. We first checked in vitro the efficiency of human platelets to interact with various human and mouse TC lines, either from breast cancer (epithelium-derived) or melanoma, using scanning electron microscopy (SEM). We found out that platelets do not equally bind TCs (Fig. 1A, B). While some cells, such as 4T1 or MCF7, efficiently bind platelets, others, such as B16F10 or MDA-MB-231, cannot bind more platelets than passive beads (Fig. 1A, B and supplementary Fig. 1A). As platelets' shape provides information on their potential to be activated by TCs, we assessed their morphology (Fig. 1C, D) and observed that TCs behave as weak platelet agonists. We probed their activation through their ability to promote tumor-induced platelets activation (TCIPA) (Fig. 1E, F), which correlated with platelet binding. We further observed that TCs fail to promote aggregation (supplementary Fig. 1B, D) although they bind platelets also in the absence of plasma proteins (supplementary Fig. 1E, F) or activate them (supplementary Fig. 1G, H), altogether indicating that TCs do not equally bind and activate platelets, questioning how and when platelets impact the metastatic properties of TCs. To do so, we selected two mouse TC lines known for their high metastatic properties (4T1 vs B16F10) and that are compatible with experimental metastasis approaches in a syngeneic background where platelet counts can be easily manipulated.

Platelets may orchestrate the intravascular behavior of CTCs and may control lung seeding in vivo

It is well-established that the early seeding of TCs shapes their metastatic potential[29]. Thus, we next interrogated whether differential platelet binding may influence metastasis in vivo. We designed an experimental lung metastasis assay that allows us to probe the behavior of TCs at very early and sequential steps, including late ones, of the metastatic cascade (Fig. 2A). We depleted platelets using an α-GPIb treatment that proved to be equivalently efficient in both animal models (BALB/c and C57BL6/J, Fig. 2B) and assessed TCs initial lung seeding by sequential in vivo imaging of 4T1 or B16F10 luciferase-expressing cells, starting from 15 minutes post injection (mpi) up to 24 hours post injection (hpi) (Fig. 2A). 4T1 cells reached and efficiently seeded control lungs from 15mpi to 24hpi (33-fold), as shown previously for metastatic cells[29]. However, when 4T1 cells were injected in TCP mice, lung seeding was drastically reduced by 10-fold when compared to control conditions. In contrast, the lung seeding potential of B16F10 cells was independent of the presence of platelets (Fig. 2C, D). These data suggest that lung seeding of known metastatic TCs does not necessarily depend on platelets and their platelet binding potential.

To provide a live and quantitative description of this platelet-dependent intravascular arrest of TCs, we next used our previously established experimental metastasis model in the zebrafish embryo[2]. Fluorescently-labeled TCs and human citrated platelet-rich plasma (cPRP) were co-injected in the duct of Cuvier of *Tg(Fli1a:GFP)* embryos at 2 days post-fertilization (dpf) and live-monitored during 4 mpi (Fig. 2E). Careful live tracking of TCs[2] showed that platelets favor the stable arrest of 4T1 in the caudal plexus (Fig. 2F, supplementary Fig. 2A) thus reducing their circulation time (supplementary Fig. 2A). In contrast, platelets did not affect the circulation and arrest patterns of B16F10 (Fig. 2G, supplementary Fig. 2B). A heatmapping analysis, allowing quantitative location of the hotspot of arrested TCs, revealed that platelets favored the stable arrest of 4T1 cells in high shear arterial vessels (DA, dorsal aorta; CV, caudal vein) without impacting the entry of TCs into small sized vessels (ISV, intersegmental vessels, supplementary Fig. 2A, C, D) where arrest is mostly imposed by physical constraints. Interestingly, although platelets did not affect the number of B16F10 stable arrest events in non-constraining arterial vessels, they

https://doi.org/10.1038/s41467-024-47516-w

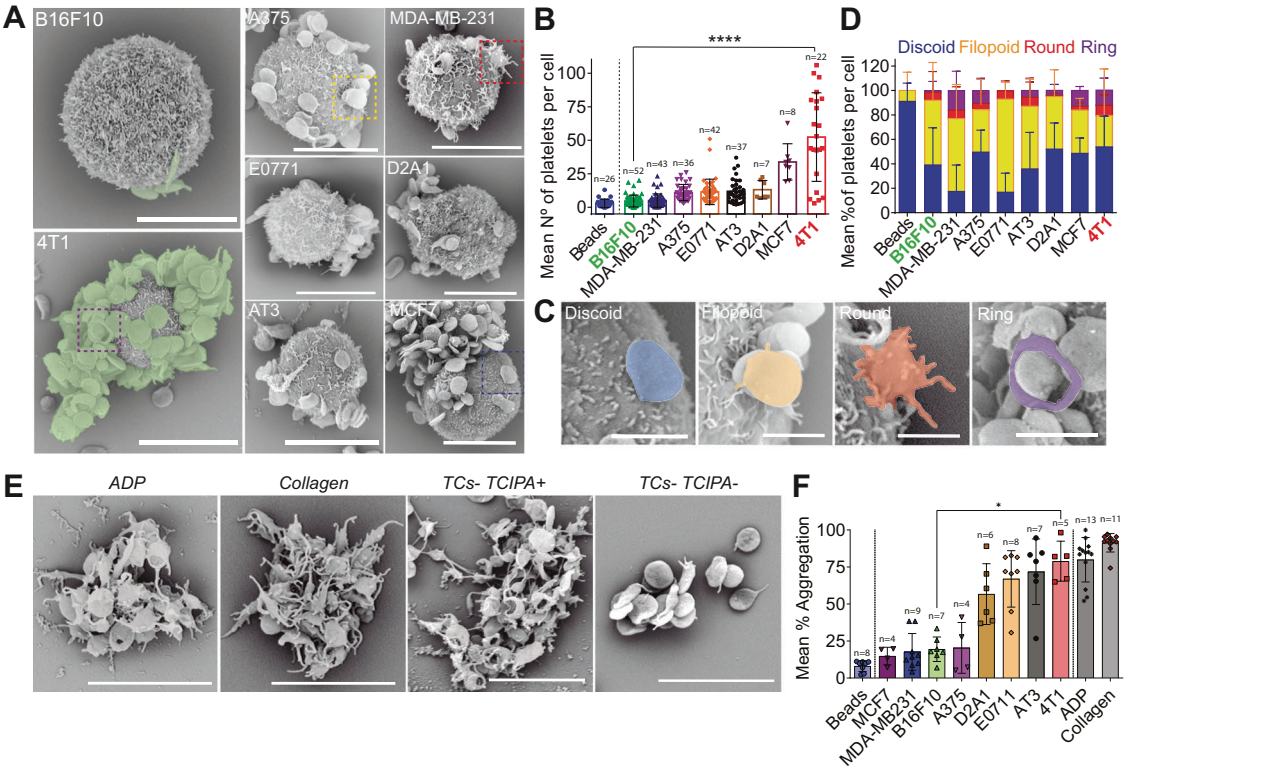

Fig. 1 | TCs bind and aggregate blood platelets with different efficiencies. A SEM images of TCs interacting with mouse platelets contained within mouse citrated platelet-rich plasma (cPRP). Mouse breast carcinoma (4T1) and mouse melanoma (B16F10) cells are highlighted. Scale bar: 10 µm. **B** Platelet binding profiles quantification graph of **A**. Number of platelets per cell for *n* cells (the number of cells per cell line analyzed are displayed above the histogram) are shown as mean ± SD and analyzed using Kruskal–Wallis with False discovery rate post-test (1 experiment was performed for MDA-MB-231, E0771 and D2A1, 2 for MCF7 and A375, and 3 for AT3 and B16F10), $q < 0.0001$. **C** SEM images of TC-bound platelets at different activation states including discoid (resting), filopodia (low activation), round (full activation) and ring-shaped platelets (unknown function). Scale bar: 2 µm. **D** Platelet shape profiles quantification graph of **C**. Relative amount platelet shape per TCs for *n* cells or beads (beads $n = 22$, B16F10 $n = 48$, MDA-MB-231 $n = 38$, A375 $n = 36$, E0771 $n = 42$, AT3 $n = 37$, D2A1 $n = 8$, MCF7 $n = 8$, 4T1 $n = 21$) are shown as mean ± SD (2 and 6 independent experiments were performed for 4T1 and B16F10, respectively); activation stages are color-coded. **E** SEM images of mouse platelet aggregates after platelet aggregation assay using cPRP with ADP and collagen as classic agonists, and 4T1 and B16F10 TCs TCIPA+ or TCIPA− cells. Scale bar: 8 µm. **F** Platelet aggregation quantification graph of **E**. Relative human cPRP platelet aggregation for *n* aggregation curves (the number of aggregation curves per cell line analyzed are displayed above the histogram) are shown as mean ± SD and analyzed using Kruskal–Wallis with False discovery rate post-test, four independent aggregation experiments were performed, $q = 0.014$. Source data are provided as a Source Data file.

favored their entry and arrest into ISV (supplementary Fig. 2B–D). We next probed arrest events at the nanoscale using correlative light electron microscopy (CLEM)[2,30] and observed that stably arrested 4T1 cells efficiently interacted with platelets with an activated morphology (filopodia, Fig. 2H) and endothelial cells. Altogether, this provides the innovative in vivo demonstration that platelet binding favors the intravascular arrest and adhesion of CTCs to the endothelial wall, which can be probed at nanoscale (CLEM).

We next analyzed TC-platelet binding in mouse lung sections containing early-seeded (15mpi and 2hpi) 4T1 or B16F10 TCs (supplementary Fig. 3A). While imaging at 15mpi allows catching the very initial in vivo behavior of TCs, around 50% of the input cells are already cleared from the lungs after 2hpi in the absence of platelets (Fig. 2C, D), thus identifying a critical platelet-dependent step. 3D high-resolution imaging at 15mpi revealed that 4T1 cells significantly bind, recruit and aggregate platelets in vivo (Fig. 2I), validating our initial in vitro observations. As expected, the size (volume) and number of platelet aggregates were also significantly lower in TCP animals (supplementary Fig. 3B). While they are initially low as observed in vitro, the number of platelets found near B16F10 cells increased significantly at 2hpi (Fig. 2J) suggesting that platelets are passively recruited in vivo to arrest sites, either by blood flow clogging, TCs cytoplasmic release of platelet aggregation inducers, or other mechanisms. When probing cell survival using cell morphometrics at 2hpi, we observed increased nuclear fragmented (non-viable) 4T1 cells in α-GPIb-treated animals (supplementary Fig. 3A, C, D) suggesting that platelets favor intravascular survival of 4T1 cells, as previously reported[18]. Interestingly, nuclear fragmentation levels of B16F10 were unperturbed upon thrombocytopenia. Because platelets can passively be recruited at TCs 2hpi (supplementary Fig. 3E) upon flow clogging, they are likely to favor the intravascular survival of neighboring viable arrested cells, as previously observed[31]. We further probed the ability of platelets to promote the clustering of CTCs, which is known to favor seeding and metastatic potential[5]. In vitro, platelets favor the clustering of 4T1 cells but not B16F10 cells (supplementary Fig. 3F, G), in line with their ability to bind platelets (supplementary Fig. 3G and Fig. 1A, B). Of note, 4T1 cells form more and bigger clusters than B16F10 cells, whether alone or when bound to platelets (supplementary Fig. 3G, H), with a direct impact on cell survival (supplementary Fig. 3I) as observed in vivo (supplementary Fig. 3E). In conclusion, using a novel in vivo analysis of early lung metastatic seeding in mice and zebrafish embryos, we show that platelet counts do not equally impact the lung seeding of metastatic TCs although they strongly orchestrate their clustering potential and early intravascular survival.

Platelets control metastatic fitness at early stages

We next wondered whether a positive impact of platelets on lung seeding would translate into efficient metastatic outgrowth. We longitudinally tracked metastatic burden over time in control and TCP mice after a single treatment with α-GPIb antibody prior TCs injection

https://doi.org/10.1038/s41467-024-47516-w

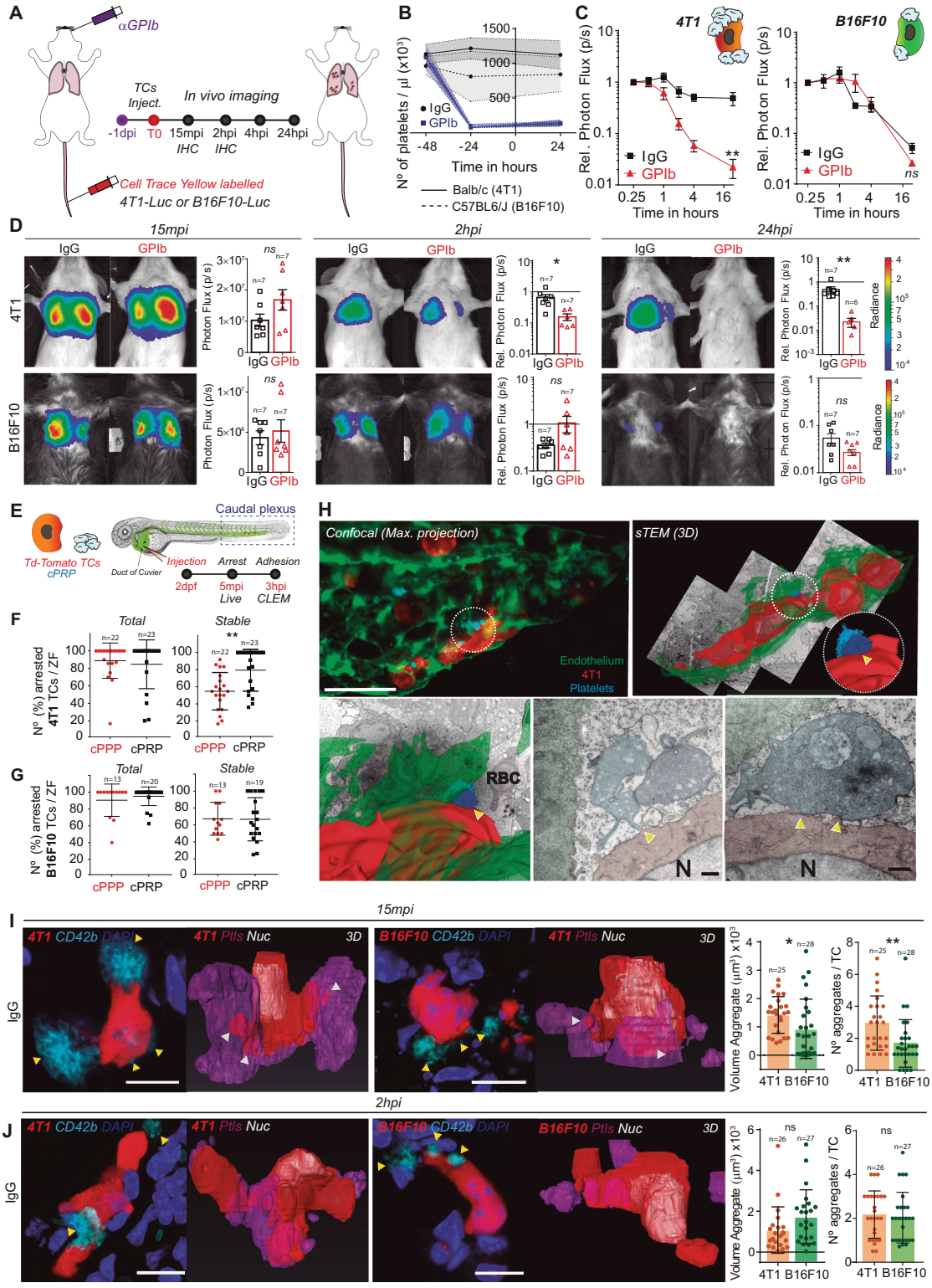

(14 days, Fig. 3A). This model, where platelet counts quickly recovered and reached approximately 50% of the normal numbers at day 7 (Fig. 3B), was referred as short-term thrombocytopenia (shortTCP).

Metastatic outgrowth (day 14) was significantly reduced by shortTCP (Fig. 3C). Interestingly, shortTCP impacted the growth of B16F10 metastases only after lung seeding. Indeed, although B16F10 lung seeding was equivalent at 24hpi (Figs. 2C, D, 3C, D), the metastatic burden was significantly reduced by shortTCP (14dpi, Fig. 3C, D). While we cannot exclude that metastatic outgrowth is impacted by the quick recovery of the platelet counts (Fig. 3B), these data demonstrate that platelets are likely to control initial events of metastatic seeding (day 1 post injection) that later translate into a significant reduction of metastatic outgrowth (day 14). Yet, these data also hint toward a secondary effect of platelets at later stages of metastasis, as observed in

Fig. 2 | In vivo lung seeding of 4T1 or B16F10 TCs is differentially influenced by platelets. A Infographics showing the experimental setting. **B** Graph showing platelet counts on IgG- and GPIb-treated BALB/c and C57BL6/J animals, as mean ± SD ($n = 7$ mice per group, 2 independent experiments were performed). **C** Relative bioluminescence kinetics of 4T1-Luc and B16F10-RedLuc TCs lung seeding during 24 hours in normal and TCP mice ($n = 7$ mice per group) are shown as mean ± SEM and analyzed using two-way ANOVA with False discovery rate post-test (2 independent experiments were performed), $q = 0.0028$. **D** Representative images and timepoint comparisons of relative lung bioluminescence in control versus TCP animals in 4T1 (up) and B16F10 (down) TCs models. Lung bioluminescence quantifications of n mice (the number of mice analyzed is displayed above the histogram) are shown as mean ± SEM and analyzed using two-sided Mann–Whitney test (two independent experiments were performed), 4T1 2hpi $p = 0.0047$, 24hpi $p = 0.0012$. **E** Infographics showing the experimental setting to study the early steps of the metastatic cascade in vivo in the ZF embryo. **F**, **G** Quantification of total and stable arrest of 4T1 (**F**) and B16F10 (**G**) cells in the caudal plexus of the ZF embryo during 5 minutes of live video microscopy. Arrested TCs of n ZF embryos (the number of ZF embryos analyzed are displayed above the dot plots) are shown as mean ± SD and analyzed using two-sided Mann–Whitney test (4 independent experiments were performed), $p = 0.0034$. **H** Representative confocal and CLEM images of 4T1 cells arrested intravascularly in the caudal plexus of the ZF embryo after 3hpi. Arrowheads indicate contact between platelets and TCs. Scale: 50 µm (confocal); 500 nm (CLEM). **I**, **J** Representative confocal images of single 4T1 or B16F10 cells arrested in mouse lungs at 15mpi (**I**) and 2hpi (**J**). Arrowheads show the interaction of single platelets and platelet aggregates with the TCs. Scale bar: 10 µm. On the right, the volume and number of platelet aggregates around the arrested TCs is shown. Platelet and TCs volumes were calculated upon segmentation of TCs (n values are displayed above the histograms) and platelets using the AMIRA software and are shown as mean ± SD and analyzed using two-sided Mann–Whitney test (1 experiment with 3 mice was performed for each timepoint), (**I**) $p = 0.034$ and $p = 0.002$. Source data are provided as a Source Data file.

the B16F10 model, where thrombocytopenia significantly diminishes metastatic burden at day 14 with, however, no impact on lung seeding (day 1).

To explore the mechanisms that may underpin this effect occurring after seeding, metastatic lungs were surgically resected on day 14. Macroscopic inspection of B16F10 metastatic foci revealed, as expected, that shortTCP significantly reduced their numbers (Fig. 3E, supplementary Fig. 4A), in agreement with the lower bioluminescent signal observed at day 14 (Fig. 3C, D). While the size of the B16F10 foci appeared similar (Fig. 3E), these lesions displayed a significant decrease in Ki67-positive cells, indicating that their proliferation index was impacted by platelet depletion (Ki67, Fig. 3G, H), although the latter had no effect on seeding. Interestingly, such an effect was not observed in 4T1 foci (Ki67, Fig. 3F, H, supplementary Fig. 4A), suggesting that platelets may tune the proliferation of B16F10 during the growth of already-established metastatic foci. While platelets were shown to promote the recruitment of a pro-inflammatory microenvironment favoring the proliferation of TCs[32], shortTCP did not affect immune cell recruitment in any of the two cell models (Fig. 3I–K). These results further demonstrate the versatility of the pro-metastatic effects of platelets and their ability to support metastatic outgrowth at timings (early seeding vs late outgrowth) that might differ depending on the TCs. Platelets were proven to colonize and support primary tumors[11,32,33]. Yet, whether they also populate and support metastatic foci remains to be demonstrated. We assessed the number of single (≤3 platelets) or aggregated (>3 platelets) intra-metastatic platelets and observed that total platelet numbers and aggregates were diminished upon shortTCP in both models (supplementary Fig. 4B), despite the recovery in platelet counts (Fig. 3B). Importantly, while platelet numbers within control 4T1 and B16F10 metastases were equivalent (supplementary Fig. 4B), the number of aggregates within B16F10 metastases was significantly higher than in 4T1 metastases, hinting toward the idea that B16F10 cells are likely to better recruit, activate and aggregate platelets within metastatic foci (supplementary Fig. 4B, C). Altogether, these results demonstrate that while transient thrombocytopenia does not equally impact seeding over two cancer models (Fig. 2), it significantly perturbs their subsequent outgrowth. Because platelet aggregates populate metastatic foci and shape their proliferation index, it is tempting to speculate that they can shape late stages of metastasis.

Platelets control late steps of metastatic outgrowth

Since platelets populate metastatic foci (supplementary Fig. 4B, C), where, as demonstrated, they are able to release important pro-metastatic molecules[34,35] and to circumvent the limitations of the yet classically used shortTCP model, we designed a long-term thrombocytopenia model (longTCP) by the sequential injection of α-GPIb mAb every three to four days, starting 24 h before TCs injection (Fig. 4A). Doing so, we could maintain platelet counts low up to day 10 post injection (Fig. 4B) and therefore fully impair platelets interactions during the initial growth phase of micro-metastatic foci. A metastatic outgrowth of 4T1 cells was similarly reduced in longTCP (Fig. 4C, D) compared to shortTCP (Fig. 3C, D), confirming that platelets can strongly contribute to the early steps of the metastasis cascade. We further confirmed that such a platelet-dependent effect was not limited to lung metastasis and performed a pan-organ experimental metastasis assay where mice, under longTCP regimen, were subjected to arterial (intracardiac) injection of TCs (supplementary Fig. 5A, B). In the same way as what was observed for lung metastasis, longTCP significantly reduced metastatic outgrowth in several organs in 4T1-injected BALB/c mice (lungs, intestine, ovary, spleen, liver, kidney, brain, and the bone marrow; supplementary Fig. 5C, D). Interestingly, longTCP massively declined lung metastatic outgrowth of B16F10 (Fig. 4C, D) (45-fold), compared to shortTCP (3-fold), further emphasizing the additive effect of depleting platelets at late stages of metastasis. While lungs were equally seeded in the presence and absence of platelets (Fig. 4C, D, 15mpi and Fig. 2), longTCP completely abrogated the growth of B16F10 cells resulting in metastases-free lungs at 14dpi (Fig. 4C–F). Overall, together with the observation that platelets are passively recruited by B16F10 cells at 2hpi (Fig. 2) and that they massively populate metastatic foci at 14dpi (Fig. 3G, J), these results suggest that platelets may tune metastatic outgrowth independently of the early intravascular interaction with TCs.

To assess the role of platelets at later stages of metastatic outgrowth, we depleted platelets only once TCs had efficiently seeded the lungs and initiated metastatic growth. We decreased platelet counts from 3dpi with three successive injections of α-GPIb mAb until 10 dpi (Fig. 5A), naming this novel approach as lateTCP and thus interrogating a different contribution of platelets to metastasis (Fig. 5B). LateTCP significantly reduced B16F10 metastatic outgrowth from day 7 (Fig. 5C, D), further substantiating that platelets can control the growth of already-established and growing metastatic foci. While the number of foci in control and α-GPIb-treated mice was similar, their size was significantly reduced (Fig. 5E, F), which was related to a decline in Ki67-positive proliferating cells (Fig. 5G). As expected, we again observed that the number of intra-metastatic platelets was significantly diminished in lateTCP (Fig. 5H), suggesting that recruitment and density of platelets within metastatic foci are crucial for their outgrowth. Interestingly, the number of intra-metastatic, but not extra-metastatic, CD45-positive immune cell infiltrates were significantly reduced in TCP animals, suggesting a role of platelets in modifying the immune tumor microenvironment (TiME) towards immunosuppression (Fig. 5I), as previously shown[36]. Prompted by these observations, we performed bulk RNASeq on formalin-fixed paraffine-embedded (FFPE) samples. Transcripts related to melanoma progression and poor prognosis (*Sox6*, *Sox11*, *Tfap2a*, *Myo7a*) were upregulated in IgG-treated animals (Fig. 5J). This was counteracted by a positive regulation of immune cell-related genes (*Thy1*, *Trbc2*, *Cd79b*, *Ighg2b*, *Bank1*, *Wdfy4*) in α-GPIb-

https://doi.org/10.1038/s41467-024-47516-w

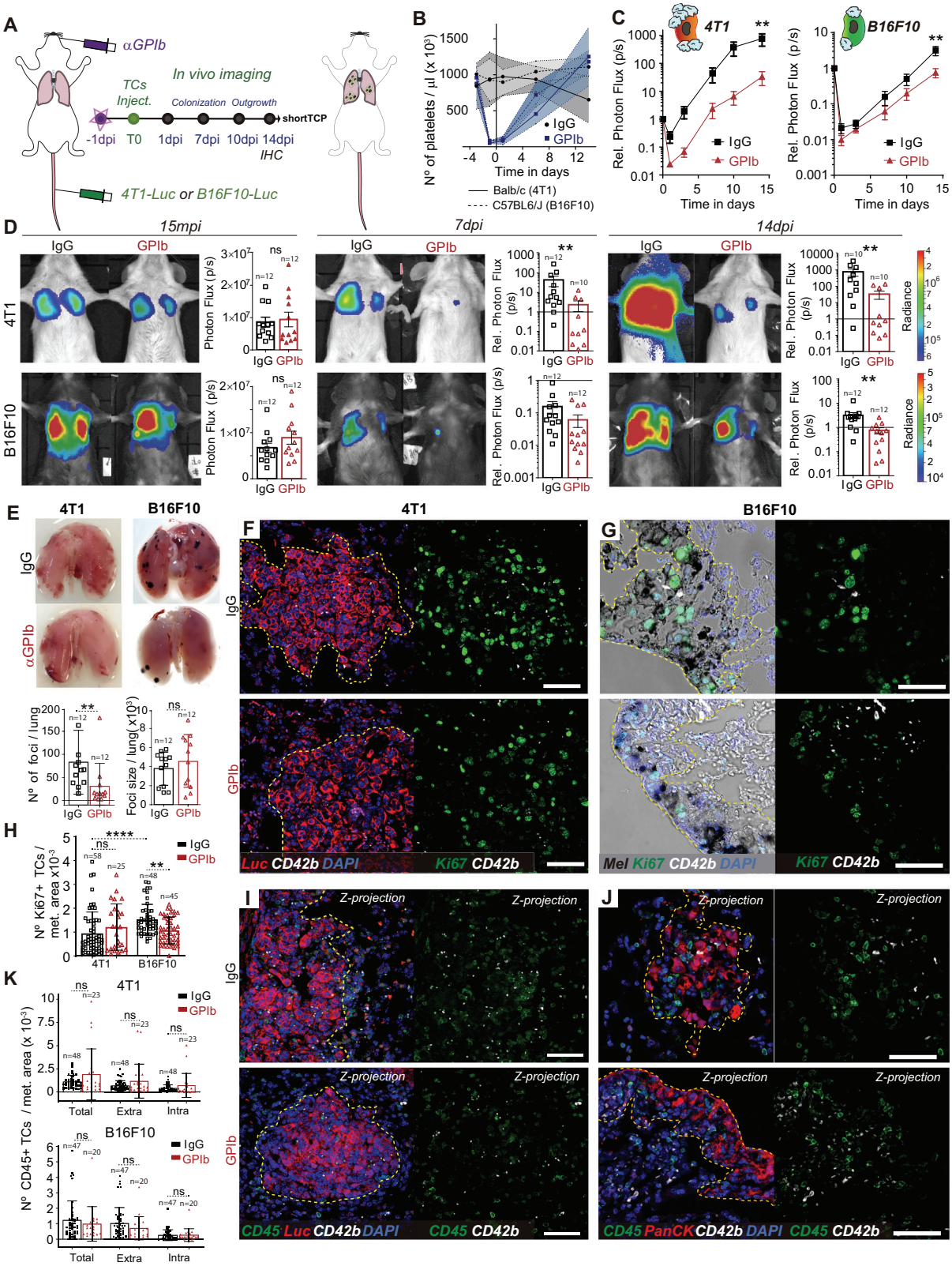

treated lungs (Fig. 5J). α-GPIb treatment also led to overexpression of genes associated with T cell co-stimulation, such as *Cd28*, *Cd55,* and *Nsg2*. Further analysis of upregulated genes in α-GPIb samples highlighted GO terms associated with negative regulation of IL-6 production, immune system process, and locomotion but a positive upregulation of muscle system process, myofibril assembly, and blood circulation (Fig. 5J). These results substantiate the in vivo data (Fig. 5C–I) and show that platelets may favor transcriptional programs involved in proliferative metastatic outgrowth by controlling the immune system.

Platelets control late steps of metastasis via GPVI

The late contribution of platelets to metastatic outgrowth opens a promising therapeutic window that could circumvent the current

Fig. 3 | Long-term TCs metastatic potential is defined by the early TC-Platelet interplay. A Infographics showing the experimental setting. **B** Graph showing platelet counts on IgG- and α-GPIb-treated BALB/c and C57BL6/J animals shown as mean ± SD. **C** Relative bioluminescent kinetics of 4T1-Luc and B16F10-RedLuc TCs lung seeding and outgrowth in IgG and shortTCP mice ($n = 12$ mice per groups) are shown as mean ± SEM and analyzed using two-way ANOVA with False discovery rate post-test (2 independent experiments were performed), 4T1 $q = 0.0022$, B16F10 $q = 0.0041$. **D** Representative images and timepoint (15mpi, 7dpi, and 14dpi) comparisons of total lung bioluminescence in IgG versus shortTCP animals in 4T1 (up) and B16F10 (down) TCs models. Lung bioluminescence quantifications of n mice (the number of mice analyzed is displayed above the histogram) are shown as mean ± SEM and analyzed using two-sided Mann–Whitney test (2 independent experiments were performed), 4T1 7dpi $p = 0.0071$, 14dpi $p = 0.00889$, B16F10 14dpi $p = 0.0011$. **E** Macroscopic analysis of mice lungs at 14dpi. Images show IgG and α-GPIb-treated lungs with 4T1 or B16F10 metastatic foci. B16F10 foci number (left) and size (right) quantifications of n mice ($n = 12$ per group, also displayed above the histogram) are shown as mean ± SD and analyzed using two-sided Mann–Whitney test (2 independent experiments were performed), $p = 0.0017$. **F**, **G** Representative images from paraffine-stained IgG and shortTCP BALB/c-4T1 lungs (F) and C57BL6/J-B16F10 (**G**) at 14dpi probed against the proliferation marker Ki67 (green) and the platelet receptor CD42b (white). Scale bar: 50 µm. **H** Number of $Ki67^+$ cells (number of images analyzed are displayed above the histogram) per metastatic area defined by α-pan-cytokeratin (4T1, **F**) staining or intrinsic melanin expression (B16F10, **G**) are shown as mean ± SD and analyzed using Kruskal–Wallis with False discovery rate post-test (two independent experiments were performed), $q = 0.0001$ and $q = 0.0095$. **I**, **J** Representative images from paraffin-stained IgG and shortTCP BALB/c-4T1 (**I**) and C57BL6/J-B16F10 (**J**) lungs at 14dpi probed against the hematopoietic lineage marker CD45 (green) and the platelet receptor CD42b antibodies (white). Scale bar: 50 µm. **K** Total, intra-metastatic, and extra-metastatic number of $CD45^+$ cells (number of images analyzed are displayed above the histogram) per metastatic area defined by α-Luc (4T1, **I**) or α-pan-cytokeratin staining (B16F10, **J**) are shown as mean ± SD and analyzed using Mann–Whitney test (2 independent experiments were performed). Source data are provided as a Source Data file.

limitations in impairing metastatic extravasation or in detecting early metastatic foci that often occur even before cancer diagnosis[37,38]. Yet, one needs to identify the molecular targets involved and design a strategy that would avoid deleterious TCP effects while impairing the outgrowth of established metastases. To do so, we first exploited *in-house* genetic models that allow us to test the contribution of a specific platelet receptor, namely the collagen and fibrin receptor GPVI. GPVI is an immunoglobulin (Ig)–like glycoprotein that binds to many different adhesive proteins and stimulates platelet activation resulting in GPIIb/IIIa integrin activation[39]. Recent studies placed it as an attractive candidate in the promotion of platelet-dependent metastasis[40–42], mostly for the minimal impact on hemostasis. Whether it also tunes late steps of metastasis remains to be demonstrated.

To allow for syngeneicity in the $GPVI^{-/-}$ mouse model and the use of two models (Fig. 6A), we engineered the mouse breast cancer AT3[41] cell line for stable luciferase expression to mirror the previously used 4T1 model (Fig. 1A) and allowed its use in a fully immunocompetent model. Interestingly, the metastatic outgrowth of AT3 cells remained unaltered in the absence of GPVI (Fig. 6B, C). Similarly, when platelets-depleting GPVI with an anti-GPVI antibody (supplementary Fig. 6B–F) that maintains a normal platelet count (supplementary Fig. 6C), lung seeding (1dpi) and metastatic outgrowth (14dpi) of 4T1 cells remained unaffected (supplementary 6C–F) suggesting that removing GPVI might be inefficient for TCs whose metastatic behavior is shaped by early intravascular platelet-TCs interactions. In contrast, the metastatic progression of B16F10 was significantly reduced in the absence of GPVI (Fig. 6B, C). While B16F10 seeding appeared unaffected (1dpi) as observed previously (Fig. 2), metastatic outgrowth was progressively impaired over time, starting from 7dpi (Fig. 6B, C), as we observed in the longTCP model (Fig. 5G, H). Macroscopic analysis of lungs revealed again that the number of foci was similar in both conditions, while their size (and proliferation index) was significantly reduced in the absence of GPVI (Fig. 6D, E). In addition, the number of intra-metastatic platelets was significantly reduced in $GPVI^{-/-}$ mice (Fig. 6F). Interestingly, their activation ability, evaluated by the number of aggregates, was not affected (Fig. 6F). When probing transcriptional programs of growing metastases and surrounding stroma in both conditions, we observed, as expected, an overexpression of genes linked to pigmentation, melanin biosynthesis and cell cycle progression (DNA unwinding and mitotic spindle assembly) in WT samples, while lung metastases of $GPVI^{-/-}$ presented an increase in terms associated with Ca^{2+} signaling pathway, blood circulation, monoatomic ion transportation, myofibril assembly and muscle system process (Fig. 6G). GPVI-expressing mice presented a positive z-scoring for genes related with melanoma progression and detrimental prognosis (*Mlana*, *Mc1r*, *Rab38*, *Cd63*, *Mlph*, *Pmel*, *Myo7a*, *Satb2*), immune checkpoint proteins (ICP) (*Cd276*, *Sirpa*, *Lgals3*) and cell cycle progression (*Cdk1*, *Ccnb1*, *Cdca2*, *Ccda8*, *Cdc20*, *Cdc25a*, *Mcm2*, *Mcm3*, *Mcm5*, *Top2a*, *Birc5*). On the other hand, $GPVI^{-/-}$ mice display a positive z-score for immune cells-related genes (*Cd3g*, *Ebf1*, *Fcamr*, *Irf4*, *Ly6D*, *Nos1*, *H2-Q10*), suggesting a rewiring of the immune microenvironment at the metastatic site (Fig. 6G). Overall, these results converge with our observations in the context of lateTCP (Fig. 5J). They suggest that platelets, via GPVI, favor major colonization and metastatic outgrowth of B16F10 cells via immune suppression, as testified by the significant increase in selected immune-related genes, such as *Cd3g*, *Nos1*, *Nos3*. Also, genes related to T cells activation (*Sell*) and protection from activation-induced cell death (*Cd5*), as well as genes associated with pro-inflammatory macrophages (*Nos1*, *Muc5b*) and neutrophils activation (*H2-Q10, S1pr4*) were further activated in the absence of GPVI. In addition, genes related to endothelial activation (*Nos3*) and extravasation of neutrophils, macrophages, and lymphocytes to sites of inflammation (*Aoc3*) were also upregulated in $GPVI^{-/-}$ samples. Altogether, this further suggests a rewiring towards a pro-inflammatory immune microenvironment at the metastatic site.

Notably, the upregulation of immune checkpoint inhibitor genes in the WT samples raises the possibility that TCs may not only proliferate faster but also manage to evade the immune system, hence leading to more efficient metastatic outgrowth. Prompted by these intriguing suggestions, we further characterize the immune microenvironment employing an ex vivo multiparametric flow cytometry approach (Fig. 6H, supplementary Fig. 7). While no difference in proportion of total $CD45^+$ cells was observed (Fig. 6H), neutrophils' proportion was higher in $GPVI^{-/-}$ mice (at 14dpi, Fig. 6H, and 29dpi, supplementary Fig. 6A). $GPVI^{-/-}$ mice also presented a recruitment of interstitial macrophages (IM) from the bone marrow at 14dpi (Fig. 6H). Expression of *Nos1* and *Muc5b* underlined by tissue-wide RNASeq suggested that recruited IM possessed a pro-inflammatory phenotype[43,44]. Interstitial macrophage recruitment was accompanied by a decrease in lung resident alveolar macrophage proportions (Fig. 6H), whose essential role in lung metastasis has recently been highlighted[45]. B and T cell populations did not seem significantly perturbed at 14dpi while they were significantly reduced in a later timepoint (29dpi) (Fig. 6H and supplementary Fig. 6A). Altogether, these results point to an early immune response mediated by innate populations, which transitions to a preponderant effect on T and B cells at later timepoints. In addition, these data support the role of GPVI platelets' receptor in shaping metastatic outgrowth of TCs via immune suppression at the metastatic site and further emphasizes the need to consider the heterogeneity of TCs-platelet binding and molecular targets when designing platelet-targeted anti-metastatic strategies. Furthermore, they allow us to validate GPVI as an ideal target, thanks to its minimal effect on bleeding and its contribution to late steps of tumor metastasis, which makes it an appealing candidate for testing its anti-metastatic potential in a human-relevant context.

https://doi.org/10.1038/s41467-024-47516-w

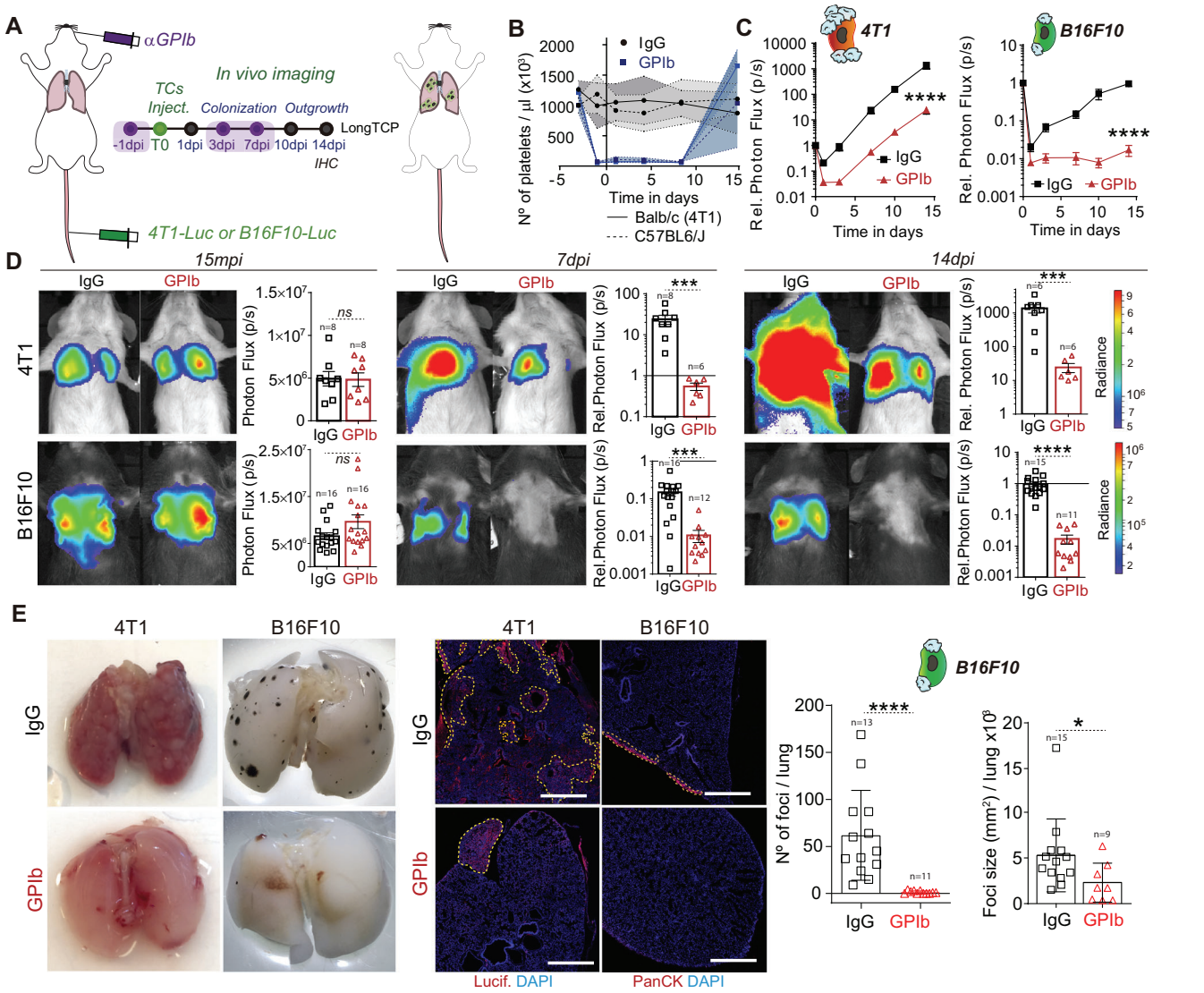

Fig. 4 | Platelets contributes to metastatic outgrowth of already formed 4T1 and B16F10 metastatic foci. A Infographics showing the experimental setting. **B** Graph showing platelet counts on IgG- and α-GPIb-treated BALB/c and C57BL6/J animals shown as mean ± SD. **C** Relative bioluminescence kinetics of 4T1-Luc and B16F10-RedLuc TCs lung seeding and outgrowth in IgG and long TCP mice ($n = 8$ mice per group for 4T1-Luc experiments, $n = 16$ per group for B16F10-RedLuc experiments) are shown as mean ± SEM and analyzed using two-way ANOVA with False discovery rate post-test (1 and 2 independent experiments were performed for 4T1 and B16F10 respectively), 4T1 $q = 0.0001$, B16F10 $q = 0.0001$. **D** Representative images and timepoint quantifications (15mpi, 7dpi, and 14dpi) of total lung bioluminescence in control versus long TCP animals in 4T1 (up) and B16F10 (down) TCs models. Lung bioluminescence quantifications of n mice (the number of mice analyzed is displayed above the histograms) are shown as mean ± SEM and analyzed using two-sided Mann–Whitney test (2 independent experiments were performed), 4T1 7dpi $p = 0.0007$, 14dpi $p = 0.0007$; B16F10 7dpi $p = 0.0001$, 14dpi $p = 0.0001$. **E** Macroscopic analysis of mice lungs at 14dpi (left) and low magnification confocal images of lung metastases defined by luciferase (4T1) or pan-cytokeratin (B16F10) staining at 14dpi (center). Scale bar: 500 µm. B16F10 foci number and size (number of mice analyzed per group are displayed above the histogram) are shown as mean ± SD (right panel) and analyzed using two-sided Mann–Whitney test (2 independent experiments were performed), foci number $p = 0.0001$, foci size $p = 0.029$. Source data are provided as a Source Data file.

Targeting the human GPVI receptor with a humanized antibody impairs metastasis

While this study and others[40] confirm that GPVI is a promising target for impairing metastasis, its relevance to human pathology is missing. Therefore, better preclinical models and humanized therapeutic tools, with ideally no TCP effects, are needed. We first interrogated whether platelets would also populate human metastatic foci. With that aim, we analyzed human lung metastasis biopsies from metastatic melanoma patients and found detectable intra-metastatic platelets (Fig. 7A), providing the prime evidence that platelets can populate human metastatic foci and further suggesting that they may control metastasis at the late stages of their progression. We then exploited our previously established genetically modified mouse strain human GPVI (hGPVI)[42], which bears a knock-in copy version of human GPVI without presenting any viability or hematological defects, making it the best candidate to test α-GPVI compounds. To counteract GPVI function, we exploited glenzocimab (ACT017, Acticor Biotech)[46], a humanized antibody fragment (Fab) that has recently completed a phase II trial in stroke patients and is currently examined in a phase II/III trial (ACTISAVE, ClinicalTrials.gov Identifier: NCT05070260). This compound binds to hGPVI to block ligand binding, without causing thrombocytopenia or GPVI membrane depletion, and it is not associated with bleeding events[47].

https://doi.org/10.1038/s41467-024-47516-w

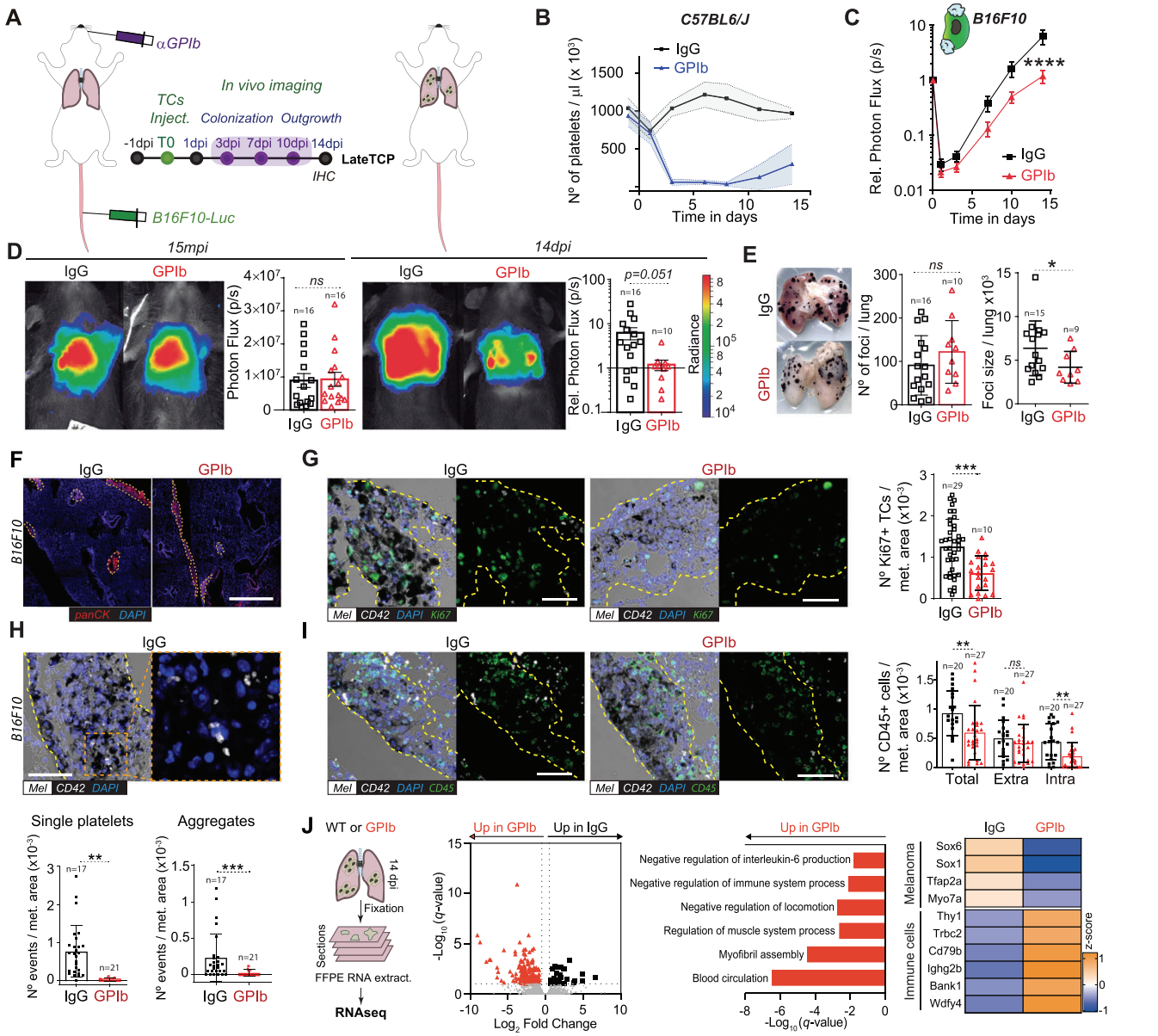

Fig. 5 | Platelets significantly influence the late outgrowth of B16F10 metastatic foci but not 4T1 ones. A Infographics of the experimental scheme. **B** Graph of platelet counts of IgG- and α-GPIb-treated animals are shown as mean ± SD. **C** Relative bioluminescence kinetics of B16F10-RedLuc TCs lung seeding and outgrowth in IgG and late TCP mice ($n = 16$ per group) are shown as mean ± SEM and analyzed using two-way ANOVA with False discovery rate post-test (2 independent experiments were performed), $p = 0.0001$. **D** Representative images and timepoint comparisons (15mpi and 14dpi) of total lung bioluminescence in control versus late TCP animals in B16F10 TCs models. Lung bioluminescence quantifications of n mice (the number of mice analyzed is displayed above the histogram) are shown as mean ± SD and analyzed using two-sided Mann–Whitney test (2 independent experiments were performed), 14dpi $p = 0.0513$. **E** Macroscopic analysis of mice lungs at 14dpi. Images show IgG- and α-GPIb-treated lungs with B16F10 metastatic foci (number of mice analyzed per group are displayed above the histogram). B16F10 foci number and mean foci size are presented as mean ± SD and analyzed using two-sided Mann–Whitney test (2 independent experiment were performed), foci size $p = 0.0401$. **F** Low magnification confocal images of lung metastases defined by pan-cytokeratin staining at day 14 post injection. Scale bar: 500 µm. **G–I** Immunohistochemical analysis of IgG and late TCP mice lungs at 14dpi. **G** Representative images of lung sections from IgG and late TCP B16F10 probed against the proliferation marker Ki67 (green), the platelet receptor CD42b (white) and intrinsic melanin expression (black). Scale bar: 50 µm. Total number of images analyzed are displayed above the histogram. Number of Ki67⁺ cells per metastatic area are shown as mean ± SD and analyzed using two-sided Mann–Whitney test (2 independent experiments were performed), $p = 0.0097$. **H** Representative images of lung sections from IgG and late TCP B16F10 probed against the platelet receptor CD42b (white). Scale bar: 50 µm. Total number of images analyzed are displayed above the histograms. Single platelet (≤3) and platelet aggregates (>3) per metastatic area are shown as mean ± SD and analyzed using two-sided Mann–Whitney test (2 independent experiments were performed), single $p = 0.0065$, aggregates $p = 0.0002$. **I** Representative images of lung sections from IgG and late TCP B16F10 probed against the hematopoietic lineage marker CD45 (green), the platelet receptor CD42b (white), and intrinsic melanin expression (black). Scale bar: 50 µm. Total number of images analyzed are displayed above the histogram. Total, intra-metastatic, and extra-metastatic number of CD45⁺ cells per metastatic area defined by melanin are shown as mean ± SD and analyzed using Mann–Whitney analysis (2 independent experiments were performed), total $p = 0.0016$, intra $p = 0.0058$. **J** FFPE-RNASeq analysis. From the left: representative infographics of the experimental scheme; volcano plot of genes differentially regulated in IgG and α-GPIb-treated mice; GO terms assignment of α-GPIb-derived samples upregulated genes; z scoring comparing IgG and α-GPIb samples for selected genes. Data are representative of three mice per group from two independent experiments. Source data are provided as a Source Data file.

https://doi.org/10.1038/s41467-024-47516-w

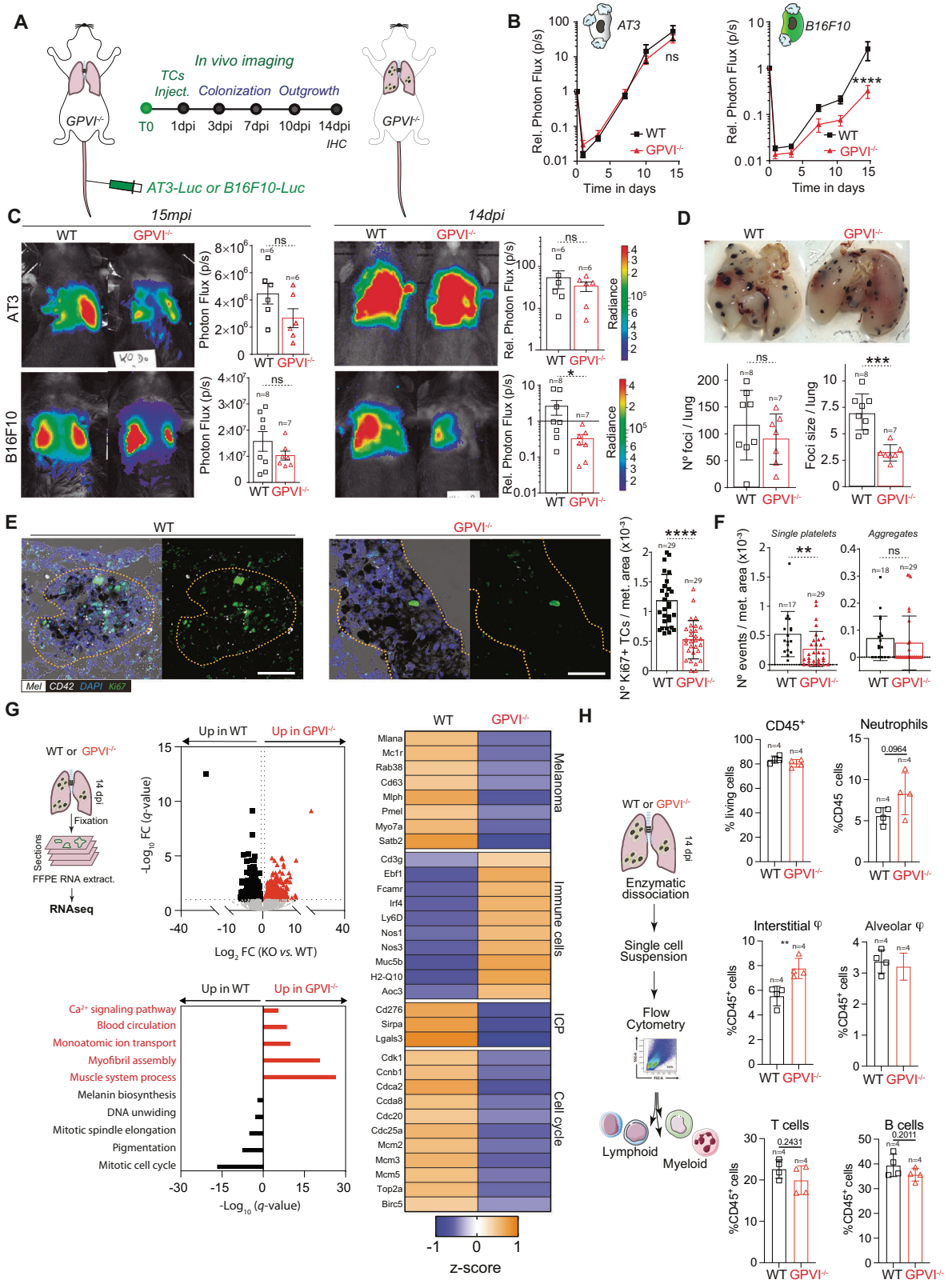

Building on the exciting observation that lateTCP could reduce the growth of established metastases (Fig. 5), we subjected hGPVI mice to an experimental metastasis protocol targeting the growth of already formed metastases (mimicking lateTCP, Fig. 5G). The half-life of glenzocimab in mice is rather short when compared to humans[47]. We thus administrated glenzocimab progressively using osmotic pumps that were implanted subcutaneously (Fig. 7B). We confirmed that glenzocimab did not affect platelet counts (Fig. 7C) and was found to be successfully bound to mouse platelets (Fig. 7D) fourteen days after pump implantation. Longitudinal imaging of B16F10 lung metastasis revealed that the metastatic burden of glenzocimab-treated hGPVI mice was significantly reduced starting from 4 days after the implantation of the pump (Fig. 7E, F), reaching a four-fold decrease at 14dpi (Fig. 7E). Macroscopic inspection of the lungs manifested that

https://doi.org/10.1038/s41467-024-47516-w

Fig. 6 | GPVI receptor-mediated platelets' metastatic outgrowth effect. **A** Infographics showing the experimental setting. **B** Relative bioluminescence kinetics of AT3-RedFluc-L2 and B16F10-RedLuc TCs lung seeding and outgrowth in WT and GPVI$^{-/-}$ mice ($n = 6$ mice per group for AT3, $n = 7$ or 8 respectively for WT or GPVI$^{-/-}$ group for B16F10) are shown as mean ± SEM and analyzed using two-way ANOVA with False discovery rate post-test (1 experiment was performed), B16F10 $q = 0.0001$. **C** Representative images and timepoint comparisons (15mpi, left; 14dpi, right) of total lung bioluminescence in WT versus GPVI$^{-/-}$ depleted animals in AT3 (up) and B16F10 (down) TCs models. Lung bioluminescence quantifications of n mice (the number of mice analyzed is displayed above the histogram) are shown as mean ± SD and analyzed using two-sided Mann–Whitney test (1 experiment was performed), B16F10 14dpi $p = 0.0289$. **D** Macroscopic analysis of mice lungs injected with B16F10 cells at 14dpi. Pictures of WT (left) and GPVI$^{-/-}$ (right) lungs are show. B16F10 foci number and size are shown as mean ± SD and analyzed using two-sided Mann–Whitney test (1 experiment was performed, number of mice analyzed per group are displayed above the histogram), foci size $p = 0.003$. **E** Representative zoomed images of the immunohistochemical analysis of lung tissue sections of WT and GPVI$^{-/-}$ mice probed against the proliferation marker Ki67 (green), the platelet receptor CD42b (white), and intrinsic melanin expression (black). Scale bar: 50 µm. Total number of lung sections analyzed is displayed above the histogram. Number of Ki67^{+} cells per metastatic area are shown as mean ± SD and analyzed using two-sided Mann–Whitney test (1 experiment was performed), $p = 0.0001$. **F** Number of intra-metastatic platelets (from **E**, total number of lung sections analyzed are displayed above the histogram) per metastatic area in WT and GPVI$^{-/-}$ animals are shown as mean ± SD and analyzed using two-sided Mann–Whitney test (1 experiment was performed), $p = 0.0045$. **G** FFPE RNASeq analysis. From the left: representative infographics of the experimental scheme; volcano plot of genes differentially regulated in WT and GPVI$^{-/-}$; GO terms assignment of WT and GPVI$^{-/-}$ upregulated genes; z-scoring comparing WT and GPVI$^{-/-}$ samples for selected genes. Data are representative of 3 mice per group from 2 independent experiments. **H** Ex vivo lungs immunophenotyping. Left: Infographics describing the experimental scheme. Right: percentage of relative immune cells populations as assessed by flow cytometry analysis 14dpi. Data are represented as mean ± SD and analyzed using two-sided Student test ($n = 4$ mice per group, 1 experiment was performed, interstitial macrophage $p = 0.0078$). Source data are provided as a Source Data file.

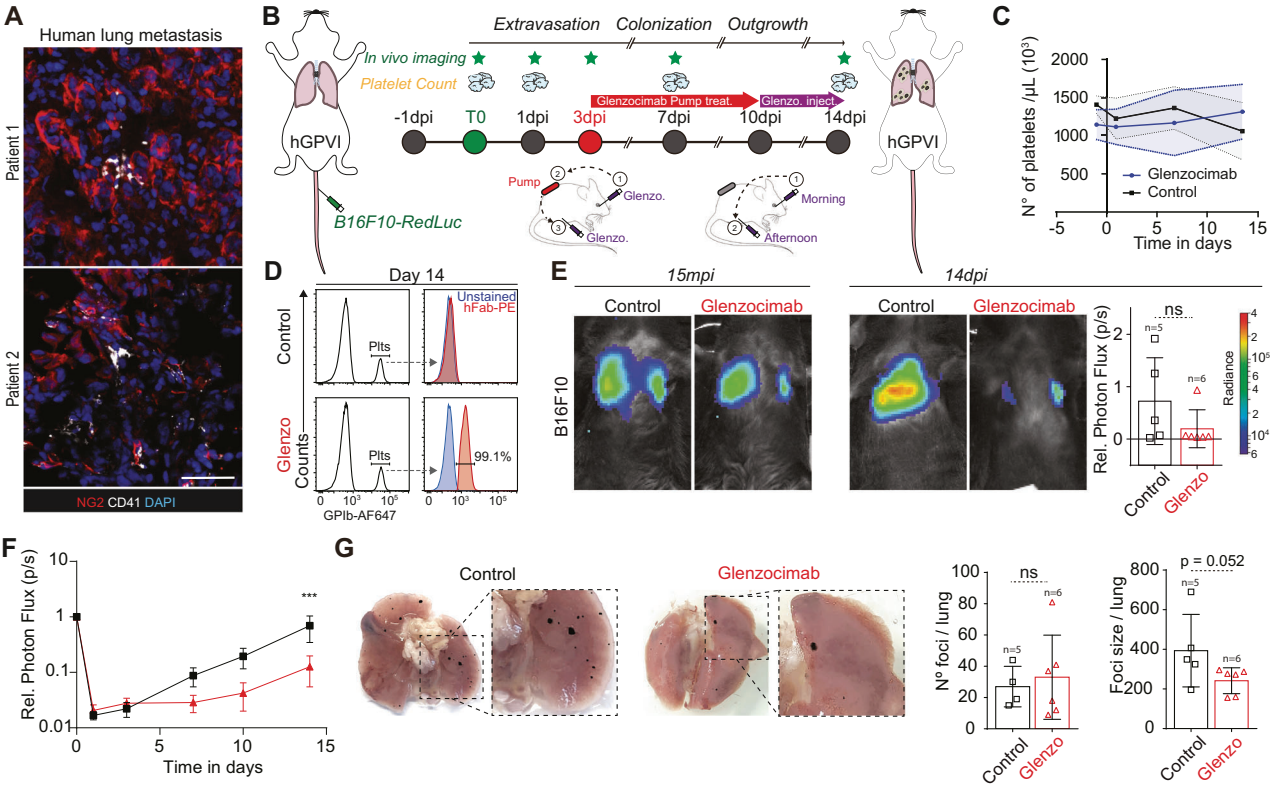

Fig. 7 | Therapeutic targeting of the human GPVI receptor impairs metastatic outgrowth of established foci. **A** Representative confocal images of human biopsies from melanoma metastases (patient1 and patient2) probed against the melanoma marker NG2 (red) and the platelet marker CD41 (white). Scale bar: 50 µm. **B** Infographics showing the experimental setting. Glenzocimab administration is performed via subcutaneous osmotic pumps from 3dpi to 10 dpi (red arrow) then continued by morning retro-orbital (1) and afternoon intra-peritoneal (2) injection until 14dpi. **C** Graph showing platelet counts in control and Glenzocimab-treated animals ($n = 5$ mice in the control group, $n = 6$ in the Glenzocimab group) and shown as mean ± SD. **D** Flow cytometry analysis of mouse platelets labeled ex vivo. Left: electronic gating strategy on platelets labeled with α-GPIb-647. Right: ex vivo platelets staining with anti-human (Fab)–PE-labeled antibody at 14dpi. **E** Representative images and timepoint (15mpi and 14dpi) comparisons of total lung bioluminescence in control versus Glenzocimab-treated animals. Day 14 lung bioluminescence quantifications of n mice (the number of mice analyzed are displayed above the histogram) are shown as mean ± SD and analyzed using two-sided Mann–Whitney test (2 independent experiments were performed). **F** Relative bioluminescence kinetics of B16F10-RedLuc TCs lung seeding and outgrowth in isotype or glenzocimab-treated mice ($n = 5$ mice in the control group, $n = 6$ in the Glenzocimab group) are shown as mean ± SEM and analyzed using two-way ANOVA with False discovery rate post-test (2 independent experiments were performed), $q = 0.0007$. **G** Macroscopic analysis of lungs from mice injected with B16F10 cells at 14dpi. Pictures of control (left) and glenzocimab-treated (right) lungs are shown. B16F10 foci number and size are shown as mean ± SD and analyzed using two-sided Mann–Whitney test (2 independent experiments were performed, number of mice analyzed per group is displayed above the histogram). Source data are provided as a Source Data file.

glenzocimab had, as expected since the treatment started after seeding, no effect on the number of metastatic foci, but reduced their size (Fig. 7G). Altogether, these results identify, distinctly, an α-GPVI compound able to target human GPVI and impair metastatic progression without side effects (thrombocytopenia, bleeding). Considering the very positive safety profile of glenzocimab and its efficiency in repressing growing metastasis, we provide evidence for the repositioning of this therapeutic agent with previously unmet clinical potential.

Discussion

This manuscript reports a pioneering longitudinal analysis of the pro-metastatic role of platelets in lung metastasis by subjecting in parallel two complementary TCs models to experimental metastasis assays in the zebrafish embryo and mice. The two TCs were tested in six mouse models of time-controlled thrombocytopenia and by the genetic and pharmacological blocking of the platelet receptor GPVI. We report that different TCs interact with platelets differently, and confirmed that such ability can, in part, shape intravascular arrest and metastatic fitness of TCs. Importantly, we provide an original study demonstrating that platelets contribute to late steps of metastasis and document the therapeutic efficacy of targeting GPVI in animals carrying growing metastases, an experimental approach never tested before. Altogether, our data identify GPVI as the main molecular target whose inhibition can impair metastasis without inducing collateral hemostatic perturbations.

The established mechanisms proposed for the pro-metastatic role of platelets (including platelet binding, activation, and aggregation by TCs) have been traditionally insufficient in providing momentum for the development and establishment of anti-platelet drugs in routine oncologic care. Options for therapeutic intervention are limited by the narrow and early window within the metastatic process where platelets interact with CTCs. Surprisingly, one assumes that all cancers interact equivalently with platelets, leading to controversial results in different cancer models[23,24] and unclear outcomes when using anti-platelet drugs in oncologic patients[25,48]. Indeed, while CTCs are widely considered to be covered by platelets when entering the blood[18], whether this applies to all cancer types remains to be demonstrated. Here, we show that TCs do not all bind platelets equally (Fig. 1) and, importantly, that TCIPA seems to occur only at high concentrations of TCs in vitro, which is an unlikely scenario in vivo[26,49,50]. In this regard, thrombocytosis has been documented as a poor prognosis factor, reflecting an aggressive tumor phenotype in cervical, colon, and non-small cell lung cancer patients[51,52]. On the contrary, in pancreatic cancer, thrombocytopenia was associated with a worse prognosis, thus indicating the varied influence of platelets depending on the type of cancer[53,54]. All these issues have left anti-platelet drugs out of the standard cancer treatments and/or prophylaxis. In order to provide further insights into platelets' pro-metastatic role also in the late stages of the disease, we developed in this study a novel experimental approach merging the single cell analysis of in vivo arrested TCs combined with in vivo bioluminescence longitudinal analysis of micro- and macro-metastases in mouse models of time-controlled thrombocytopenia. Thanks to this, we were able to identify GPVI platelet receptor as a mediator of this platelets' function, and we probed the feasibility of its targeting with a therapeutic antibody.

We first explored the pro-metastatic effect of platelets at early stages and found that platelets favor the survival of intravascularly arrested TCs by direct binding to the surface of viable cells or by passive recruitment around non-viable cells. This passive recruitment may occur by vessel occlusion or release of platelet-activating cytoplasmic content such as tissue factor (TF)[20,55]. While direct binding significantly supports long-term metastatic fitness (Fig. 3), passive recruitment of platelets by flow clogging further supports metastasis by impacting late outgrowth behavior (14dpi). Previous work has suggested a key role for thrombin and clot formation as the starting point of brain metastasis[20], however, not all metastatic cell lines express TF. Considering that metastasis is a very inefficient process, and that intravascular cell death is a well-known cause of TF release and thrombin production, the co-option of viable with non-viable cells may help the viable cell to successfully metastasize, as previously observed[56]. Such ability of platelets to be passively recruited to metastatic cells may be capital for designing anti-platelet drugs for treating different cancer types.

While previous reports have found evidence of platelets inside primary tumors[11,32,33], no evidence proves that this could apply to metastasis. We have now documented that metastatic sites are populated by platelets suggesting that they might be able to extravasate with or independently from TCs, as reported previously[57]. Platelets have been shown to migrate within tissues[58], suggesting that they could actively populate growing metastases, but whether they require extravasation to seed metastases remains to be demonstrated, as they might just interact and imprint TCs in circulation. For example, while TCs interact with platelets, fibrin, or fibrinogen from 0 to 6 h post injection, platelets are not found at intravascular arresting sites from 6 to 24hpi[54], meaning that early intravascular interactions are frugal. In this sense, the GPVI receptor may tune metastasis by passive and intermittent interaction with TCs at the arrest sites[59], similar to what is shown by our genetic and pharmacological loss-of-function models at late steps of the cascade. Furthermore, the observation that platelets' number but not their aggregation capacity is affected in GPVI-KO animals could hint towards migration deficiencies in this model and open new areas of investigation.

Platelets are known to release significant amounts of bioactive material within releasates[60] that shape, for example, their invasion abilities. In addition, they also secrete microparticles and extracellular vesicles, with angiogenic[61], immunosuppressive[10], and pro-survival abilities[62] capacity, as hinted in this study (increased proliferative index in the presence of platelets in our short and lateTCP models). These observations were further validated by RNASeq on FFPE lung sample where genes associated with melanoma progression and proliferation were overexpressed in IgG-treated animals (Fig. 5J) or repressed in our in-house GPVI$^{-/-}$ model (Fig. 6G).

Besides the early shielding, and protecting CTCs from immune cells during circulation, platelets profoundly impact the TiME. Indeed, we demonstrated here that platelets massively infiltrate lung metastatic lesions and are activated by B16F10 TCs (Fig. 3G, F and supplementary Fig. 4B, C). Upon activation, platelets release large quantities of immunomodulatory molecules (TGFβ, PGE2, maresin-1, etc.) whose roles in T cells polarization modulation, anti-inflammatory macrophages induction, myeloid-derived suppressor cells (MDSCs), N2 neutrophils and/or tolerogenic dendritic cells recruitment has been previously demonstrated[63,64]. Moreover, platelets express class I MHC conferring a "pseudonormal" phenotype to cancer cells and subverting NK cells anti-tumoral functions[65]. They are also able to convert ATP in adenosine, a potent immunosuppressive molecule, through membrane expression of the ectonucleotidases CD39 and CD73[66]. Platelet's role in pro-tumoral, immunosuppressive TiME promotion was also confirmed in our models. Indeed, RNASeq of α-GPIb-treated lungs highlighted an increase in immune cell-related transcripts (Fig. 5J). Furthermore, our data suggest that platelets-driven immune suppression is in part mediated by GPVI as demonstrated by RNASeq and ex vivo lung immunophenotyping of our in-house GPVI$^{-/-}$ mouse model. In this study, we underlined that GPVI deletion was associated with higher immune cell transcript expression (Fig. 6G) and recruitment of bone marrow-derived interstitial macrophages (IM) presenting a pro-inflammatory gene signature (Fig. 6G, H). On the other hand, mice expressing GPVI showed increased expression of immune checkpoint inhibitor genes (*Cd279*, *Sirpa*). Overexpression of galectin-3 (*Lgals3*), a known GPVI ligand[59], in metastatic lungs further supports

the implication of GPVI in the TiME remodeling. In addition, recent meta-analyses underpinned the association of high platelets to lymphocytes ratio (PLR) with dismal response to chemotherapy and poor overall survival in clinical settings[67,68]. Based on these pieces of evidence, we might speculate that platelets influence metastatic outgrowth by (i) promoting cancer cell proliferation and (ii) rewiring the TiME towards an immunosuppressive one. Nonetheless, additional investigations are needed to deepen our observations, notably on the cellular functions of the metastatic TiME, their associated transcriptional program, and local cytokines secretion. Given these exciting indications, reduction of platelets' count seems an appealing approach to hamper metastatic burden. Nevertheless, the augmented risk of bleeding due to their depletion makes this approach not feasible, instead boosting the targeting of platelets' receptors to circumvent this issue. In this line, our study shows that depletion or targeting of platelets' GPVI successfully impairs the proliferation rate within B16F10 metastatic foci with no collateral damage. These data reinforce the potential of targeting GPVI in cancer as shown in previous studies where it already leads to decreased intratumor hemorrhage and improved intra-tumoral administration of chemotherapeutic agents[17]. Overall, this points toward GPVI as a promising candidate for the development of new anti-metastatic drugs able to address cancer once the metastatic spread is already initiated, which accounts for most of the cases in clinical practice. Such achievement is of utmost importance considering that we also inform here on how a pharmacologic blockade of GPVI with glenzocimab (Acticor Biotech), an anti-GPVI F(ab) fragment evaluated in phase I clinical trials to prevent ischemic stroke, efficiently reduces experimental metastasis. As most of the compounds available in the market are associated with increased risk of hemorrhage in clinical settings or limited efficacy against metastasis, with the exception of aspirin[69], this finding results particularly promising as glenzocimab presents an anti-thrombotic effect without inducing any bleeding in healthy volunteers and in patients[70]. Altogether, our work demonstrates that targeting platelets in a progressively metastatic animal model can impair their growth, and it further identifies GPVI as the key molecular target whose inhibition can hamper metastasis without inducing collateral hemostatic perturbations.

Methods

Cell lines

The mouse breast cancer cell lines 4T1, E0771, AT3, and D2A1, and the mouse melanoma cell line B16F10, were cultured under standard conditions (37 °C, 5% CO_2) using RPMI-1640 or DMEM, respectively, supplemented with 10% FBS and 1% penicillin-streptomycin solution. The human breast cancers MDA-MB-231, MCF7, and melanoma cell lines A375, we cultured under the same conditions (DMEM). Their viabilities in vitro were assayed before aggregation and SEM assays and in vivo experimental metastasis experiments by an ADAM-MC Automated cell counter (ThermoFisher).

Cell line engineering

For in vivo imaging on zebrafish embryos, 4T1 and B16F10 cells were engineered to express a Lifeactin-tdTomato fusion protein. Briefly, the Life-tdTomato DNA fragment from the Addgene plasmid tdTomato-Lifeact-7 (number 54528) was inserted in the pLSFFV-Ires-Puromycin or pLenti-CMV-mPGK-Puromycin lentiviral vectors to generate the pLSFFV-LifeActin-tdTomato-Ires-Puro and the pCMV-LifeActin-tdTomato-mPGK-Puro lentivirus lentiviral vectors used to transduce 4T1 and B16F10, respectively. Lentivirus particle production and transduction procedures have been previously described[30]. For confocal imaging of single arrested TCs in mice lungs, luciferase-expressing 4T1 or B16F10 cells were labeled in vitro with CellTrace Yellow (Thermo Fischer) according to manufacturer's instructions.

For in vivo imaging in mice, regular firefly luciferase (*Photinus pyralis*) (4T1-Luc, a kind gift from Corinne Laplace-Builhé, Institut Gustave Roussy Paris) or red-shifted firefly luciferase (Bioware® Brite B16F10-RedFLuc, PerkinElmer) was used. A luciferase-expressing breast cancer AT3 cell line[41] was engineered in-house with RediFect RedFluc Lentiviral Particles (PerkinElmer). To avoid immune rejection in immunocompetent C57BL6/J recipients, an in vivo-derived AT3 cell line was established from murine lung metastases. Briefly, mouse lungs containing AT3-RedFLuc metastasis were collected on day 18 post injection (dpi) from tail vein injected animals. Tissue was chopped into 1 mm^3 pieces with a scalpel, resuspended in 4000 μL of dissociation buffer (Miltenyi Biotech Neural Tissue Dissociation Kit (P) 130-092-628) and mild enzymatically digested with 2.5 mg/ml collagenase solution (Sigma-Aldrich C9891) and 400 μg/mL DNaseI under gentle mixing at 37 °C for 10 min. Enzyme P (50 μL) and enzyme A (60 μL) were sequentially added and incubated 5 minutes each. The cell suspension was filtered through a 40 μm cell strainer (Corning, 431750) before centrifugation for 5 min, 400 × *g* at room temperature (RT). The cell-containing pellet was plated in DMEM medium + 10% FCS + 1% PS + 1% Gentamicin + 5 μg/ml Fungizone + 1 μg/ml puromycin in a T75 flask. After a few days of puromycin selection, the cell line was considered established (AT3-RedFluc-LM1). To ensure the absence of immune rejection on immunocompetent recipients a second round of in vivo derivation was performed, thus generating the AT3-RedFluc-LM2 cell line, further used in our experiments.

Platelets' isolation

Human citrated platelet-rich plasma (cPRP) was obtained from supernatant derived from citrate buffer (3.8%) collected blood centrifuged 250 × *g* for 16 min at room temperature. Washed human platelets suspensions were obtained under informed consent from healthy donors not undergoing any platelets-affecting drug treatment for the previous 10 days. Blood was collected in the presence of 1/7 volume of citric acid-citrate-dextrose (ACD) pH 6.5, and washed platelets were prepared as described previously[71]. The quality of preparations was routinely screened in a light aggregometry assay with ADP 5 μM as aggregation inductor in the presence of fibrinogen (for washed platelets) or in its absence (for cPRP).

Murine citrated platelet-rich plasma (cPRP) blood was collected by aortic puncture in citrate buffer 0.315% following centrifugation of the whole blood in microtubes during 1 min at 1900 × *g* at RT. Murine washed platelet suspensions were obtained from aortic puncture in anesthetized mice (intra-peritoneal, i.p., ketamine 100 mg/kg, xylazine 20 mg/kg). Blood (700–800 μL) was collected in an ACD-preloaded syringe by puncture at the level of the separation of the aortic artery into the two iliac arteries. Mice were sacrificed by cervical dislocation at the end of the procedure.

Clusters formation and anoikis resistance assay

2×10^6 4T1 or B16F10 cells in suspension were co-incubated with 2×10^7 murine cPRP for 2 hours at 37 °C 5%CO_2 on a tilting tray. Cells were then washed with serum-free medium, and clusters were imaged on an inverted microscope. Macroscopic RGB images with identical zooming were loaded on ImageJ, and clusters' area was measured after polygon selection definition.

Response to anoikis was determined in clustered cells plated at 500,000 cells/mL in sixwell ultra-low adherence plate in complete culture medium for 24 h or 48 h later. At the end of the incubation, cells were harvested and stained with Zombie NIR (Biolegend, Cat.423105) (1:1000) for 15 minutes at RT in the dark, prior to wash and signals' acquisition on an Attune NxT (Invitrogen) flow cytometer (20,000 events/conditions). Data were analyzed using FlowJo™ v10 Software (TreeStar).

Zebrafish handling and intravascular injection of TCs

Tg(fli1a:eGFP) Zebrafish (*Danio rerio*) embryos from a Tubingen background were kindly provided by the group of F. Peri from EMBL (Heidelberg, Germany) and further grown and bred in our in-house zebrafish facility. Embryos were maintained in Danieau 0.3× medium (17.4 mM NaCl, 0.2 mM KCl, 0.1 mM MgSO4, 0.2 mM Ca(NO3)2) buffered with HEPES 0.15 mM (pH = 7.6), supplemented with 200 µM of 1-Phenyl-2-thiourea (Sigma-Aldrich) to inhibit the melanogenesis, as in[72]. Forty-eight-hour post-fertilization (48hpf) embryos were mounted in a 0.8% low melting point agarose pad under 650 µM tricaine (ethyl-3-aminobenzoatemethanesulfonate) anesthesia. LifeAct-TdTomato TCs were injected with a Nanoject microinjector 2 (Drummond) and micro-forged glass capillaries (25–30 µm inner diameter) filled with mineral oil (Sigma). For the intravascular injection of TCs, 100×10^6 TCs/mL 4T1 or B16F10 were washed (EDTA 0.48 mM, Versene, Gibco) and gently detached (Trypsin solution 0.125% diluted in Versene 1×, Gibco), then resuspended in serum-free RPMI-1640 or DMEM medium and maintained in ice until injection. Prior injection, 50 µL TCs:50 µL human cPRP (350-450,000 platelets/µL (1/4 ratio approx.)) were mixed and incubated at 37 °C for 2-3 minutes. Human citrated platelet poor plasma (cPPP) was used as a negative control. Finally, 23 nL of the TCs-platelets mix was injected in the duct of Cuvier under the M205 FA stereomicroscope (Leica), as in ref. 73.

Mice

8–16 weeks male WT C57BL6/J immunocompetent mice were used for the B16F10 melanoma cell model, while female WT immunocompetent BALB/c mice were used for the 4T1 breast cancer model. All mice were purchased from Charles River Labs. C57BL6/J mice deficient for the platelet receptor GPVI ($GPVI^{-/-}$), and the humanized GPVI model (hGPVI) were generated as previously described[42]; males and females were used for both models. Animals were housed in pathogen-free conditions with food and water *ad libitum* and appropriate enrichment (sterile pulp paper and coarsely litter). Mice were monitored daily, and terminally sick animals were euthanized under an approved protocol. All animal procedures were performed in accordance with institutional guidelines and approval, under the APAFIS authorization 14741-2018041816337540.

Experimental pulmonary metastasis assay and bioluminescent imaging

Subconfluent 4T1-Luc or B16F10-RedFluc were washed with EDTA 0.48 mM Versene, Gibco), gently detached using a 0.25% trypsin-0.02% EDTA solution (Gibco), washed in media containing 10% FBS, resuspended at 1.5×10^6 TCs/mL in serum-free media, filtered through a 40 µm mesh (Falcon) and kept on ice until injection. Viability (>85% prior injection) was determined by trypan blue exclusion. TCs (100 µL) were injected through the lateral tail vein (intra-venously, i.v.) with a 25-gauge needle. In vivo imaging was performed shortly after to establish initial lung seeding (15mpi) by i.p. injection of D-luciferin solution (150 mg/kg) and subsequent (5 minutes later) signal acquisition of mice (isofluorane-anesthetized - Isoflo, Zeotis) ventral view with an IVIS Lumina III (PerkinElmer) imaging system. The rate of total light emission of the lung metastatic area was analyzed using the Living Image software (PerkinElmer) and expressed as numbers of photons emitted per second (p/s). Subsequent imaging points at 0.5, 1, 2, 4, and 24 h (initial homing) and 1, 3, 7, 10, and 14 days (outgrowth) after TCs injection were monitored. Dynamics of homing and extravasation appeared similar (around 24hpi) when the outgrowth of the two cell lines was assessed. For later timepoints (1, 3, 7, 10, 14 days), the relative total light emission of the lung metastatic area compared to day 0 was calculated and represented.

Intracardiac cells injection

5×10^6 4T1-Luc/mL suspension in PBS was prepared as aforementioned. 500,000 cells were injected in the left ventricle with a 25-gauge needle in anesthetized mice placed in ventral position. In vivo imaging and analysis were performed as before. At the time of the sacrifice, ex vivo signal was measured from harvested organs (lungs, intestine, ovary, spleen, liver, kidney, brain, bone marrow), and the rate of total light emission was analyzed and expressed as numbers of photons emitted per second (p/s).

Platelet and GPVI receptor depletion and pharmacological blockage

Severe thrombocytopenia was induced by i.v. injection of 2 mg/kg of in-house-produced α-GPIb antibody (RAM.6)[74] or IgG isotype control per mouse. Injections were set according to the experimental scheme: −1dpi TCs for shortTCP; -1/3/7dpi TCs for LongTCP; 3/7/10 dpi TCs for LateTCP. Murine GPVI platelets' receptor was antagonized by 50 µg of JAQ1 mAb (1 mg/mL, Emfret) or rat IgG isotype control (Emfret) subcutaneously (s.c.) injected per mouse. Anti-human GPVI antibody Glenzocimab (ACT017, Acticor Biotech[46]) was delivered through an Azlet osmotic pump (model 2001) implanted s.c. on mouse's dorsal side (APAFIS authorization 37433-2022052016445806). Pump delivery was maintained for 7 days at 1 µl/hour with a concentration of 20 mg/ml. After, the treatment was continued for an additional 3 days with 10 mg/mL/serum physiological retro-orbitally injected per mouse in the morning and 120 µL/mouse i.p. injected in the afternoon.

Platelet counts

Murine whole blood was collected into EDTA (6 mM) after severing the mouse tail. The platelet count and size were determined in a Scil Vet abc automatic cell counter (Scil Animal Care Company, Holtzheim, France). The platelet count on human platelet suspensions (cPRP and/or washed platelets) was assessed in an automatic platelet counter (XN-1000, Sysmex).

Ex vivo flow cytometry

Single-cell suspension was obtained from freshly harvested left lung lobes. Tissue was cut into approximately $2mm^3$ pieces using a scalpel, then enzymatically digested with Tumor Dissociation kit, mouse (Miltenyi, 130-096-730) at 37 °C for 42 minutes using the gentleMACS Octo Dissociator (Miltenyi, 130-096-427) according to manufacturer's protocol. Cell suspension was filtered through a 50 µm mesh and red blood cells were lysed in ACK Buffer [150 mM NH_4Cl, 10 mM $KHCO_3$, 0.1 mM Na_2EDTA]. Non-viable cells were stained with Fixable Viability Dye-eFluor™780 (eBioscience™, 65-0865-14) for 15 minutes at room temperature in the dark. Aspecific antibodies' binding was minimized with anti-CD32/CD16 blocking antibody (TruStain FcX™ 1:50, Biolegend, Cat.101320 for 20 minutes at 4 °C). Primary conjugated (Table S1) were incubated for 15 minutes at 4 °C. Samples were acquired with Attune NxT (Invitrogen) flow cytometer and data were analyzed using FlowJo™ v10 Software (ThreeStar).

Light transmission aggregometry (LTA)

TC-induced platelet aggregation (TCIPA) was analyzed by Light Transmission Aggregometry (LTA), equivalent for human and mouse. Aggregations were initiated in aggregation vials adding 600×10^5/200 µL of washed platelets or non-diluted cPRP. Next, 50 µL of TCs (or control beads) in TA buffer or serum-free culture media were added at up to 3×10^6/mL final concentration. Platelets' suspensions were stirred at 1100 rpm. Control samples were activated with 5 µM ADP in presence or absence of human fibrinogen (320 µg/mL, in-house generated[71]) or native equine tendon collagen Type 1 (2.5 µg/mL, Collagen Reagens HORM® Suspension, Takeda) in 300 µL final volume.

Prior to aggregation, TCs were washed and gently detached by non-enzymatic means (EDTA 0.48 mM, Versene 1×, Gibco), washed twice in RPMI-1640 or DMEM medium without serum + 0.1% BSA + 2 mM $CaCl_2$ + 1 mM $MgCl_2$, or in TA buffer. Platelets' aggregation was measured at 37 °C by a standard turbidimetric method in an APACT 4004 aggregometer (ELITech Group, Puteaux, France). Serum-free media or TA buffer were used as control together with PEG-treated 10 µm polystyrene beads (Phosphorex). Amplitudes of the aggregation curves generated with APACT LPC software were compared. The initial drop in light scattering due TCs addition to running aggregation vials was subtracted in Microsoft Excel, providing adjusted and comparable aggregation curves.

Scanning electron microscopy

Gently detached TCs (EDTA 0.48 mM, Versene, Gibco), pre-washed in serum-free media (for cPRP) or TA buffer (for washed platelets), were incubated with platelet suspensions at the previously indicated concentrations. PEG (Polyethylene glycol) blocked beads were used as a control. LTA assay-derived TCs and platelet mixes were fixed 1:1 v/v in 2× fixative solution (4% paraformaldehyde, 5% glutaraldehyde in standard 0.1 M Sodium Cacodylate buffer, NaCac) and sedimented O/N at 4 °C. Then, pellets only were gently resuspended in NaCac Buffer and seeded on poly-L-lysine pre-coated (Sigma) glass coverslips in a 24-wells plate for 30 minutes at RT. Supernatants were removed, and coverslips were fully dried in an oven at 60 °C for 1 h. Following this, coverslips were washed with 0.2 µm-filtered NaCac buffer and dH_2O. Next, they were dehydrated with an increasing ethanol series (1 × 70%, 1 × 80%, 1 × 95% 5 min each and 2 × 100% 30 minutes each) and a 1,1,1,3,3,3-hexamethyldizilazane (HDMS, Merck, Millipore) graded series (25%, 50%, 75% and 100%, 5 min each). Cells were mounted onto 12 mm EM Aluminum Mounts for AMRAY (EMS, Hatfield) employing Leit-C conductive carbon cement (CCC, Plano GmbH, Germany). Samples were platinum metallized under vacuum using a Cressington Sputter Coater 208HR coupled to a Pfeiffer Vacuum (Germany). Image acquisition was performed at high resolution (10–15 kV) and ×6000–10,000 magnification on a PhenomWorld SEM desktop microscope (Phenom-World B.V, The Netherlands).

CLEM sample preparation and image acquisition

Correlative light and electron microscopy (CLEM) was performed as previously described[72]. Briefly, ZF embryos were chemically fixed with 2.5% glutaraldehyde and 2% paraformaldehyde in 0.1 M NaCac buffer (pH 7.4) for 48 hr at 4 °C, then 3× washed with 0.1 M NaCac buffer, pH 7.4, and fixed again with 0,05% malachite green, 2.5% glutaraldehyde in 0.1 M NaCac buffer, pH 7.4 for 25 min in ice bath. Samples were post-fixed for 45 min in 1% OsO_4 in 0.1 M NaCac buffer, pH 7.4 in a fume hood in ice bath then 2× washed in 0.1 M NaCac buffer (ice-cold to avoid thermal changes). Next, specimens were incubated in 1% aqueous tannic acid solution for 25 min in ice bath and 5× washed with distilled water (DW). Dehydration was performed with an ethanol's series (25%, 50%, 70%, 95%, and 100%) and acetone-dry at RT for 10 min. Then samples underwent a series of resin-acetone solution bath (1:3; 1:1; 3:1) finishing in 100% Epon resin for 3 × 1h at RT. Polymerization was performed in an oven at 60 °C for 48 h. The resin block was trimmed by ultramicrotomy. After targeting region of interest (ROI), 90 nm thin sections were collected and placed in slot Formvar cupper grids. The TEM data set was acquired with a Hitachi 7500 TEM, with 80 kV beam voltage, and the 8-bit images were obtained with a Hamamatsu camera C4742-51-12NR. The images were segmented using an open-source software ImageJ; AMIRA and IMARIS as follows: a) single images were stitched in a bigger composed image and combined into a 3D-stack; b) The combined 3D-stack was aligned and the contrast adjusted, by ImageJ. C) The segmentation of objects of interest, (arrested TCs, platelets) and 3D Volume reconstruction, by AMIRA and IMARIS.

Tissue histology and immunohistochemistry

Human melanoma samples from lung metastases were obtained, processed, and stained as previously described[75]. Lungs harvested from mice sacrificed under isoflurane anesthesia and lidocaine analgesia (5 mg/kg) were washed and fixed O/N in 4% paraformaldehyde/phosphate-buffered saline (PBS) solution (EMS). Left lobes were treated for paraffine inclusion, while right ones for Optimal Cutting Temperature (OCT) inclusion (Tissue freezing media, Leica). Prior to paraffine embedding, O/N fixed lungs were 2× PBS, 2× ethanol 50% washed for 45 minutes then dehydrated O/N in 70% Ethanol. Tissues were processed in an automated Leica inclusion machine: 2 × 70%, 1 × 80%, 1 × 95% and 2 × 100% for 1 hour each, 2 × 45 min xylene/toluene each, and paraffin-embedded for 2 hours. Cryosections of 20 µm (for single cell analyses and segmentation) or 10 µm (for regular IF analyses) paraffin sections were mounted on poly-lysine-coated slides (SuperFrost UltraPlus, Thermo Fisher Scientific). Following a reverse dehydration scale, tissue antigens in paraffine-embedded specimens were retrieved by boiling in sodium citrate solution (10 mM, pH 6.0, Sigma). Unspecific antibody binding was blocked for 1 h in blocking solution (3% bovine serum albumin-BSA, 20 mM $MgCl_2$, 0.3% Tween 20, 5% FBS in PBS). Background and nonspecific staining controls were used. Primary antibodies (Table S1) were incubated O/N followed by secondary antibodies (Table S1) for 1 h room temperature prior to nuclei staining (DAPI-Thermo Fisher Scientific) and slides mounting (FluoromountG-SouthernBiotech). For biotinylated antibodies, tissue endogenous biotin was quenched with Avidin/Biotin blocking solution (Vector Laboratories) before secondary antibody. Antibody signal was developed after 1 h incubation with the Avidin/Biotin-HRP complex (Elite Vectastain ABComplex Kit, Vector Laboratories) and 1 h incubation with Streptavidin-647 (BioLegend).

FFPE RNA tissue extraction and bulk RNA sequencing

Total RNA was isolated from 10×10 µm thin slides of paraffine-embedded lungs stocked at room temperature. NucleoSpin total RNA FFPE XS Micro kit (Cat. 740969.50, Macherey-Nagel) was used according to manufacturer's instruction, and RNA was eluted in 30 µL final volume. RNA concentration was assessed after extraction at the NanoPhotometer® N60 (Implen). RNA integrity (>50% DV200) was assessed by Bioanalyzer (total RNA Pico Kit and RNA 6000 Nano Kit, 2100 Instrument, Agilent Technologies, Paolo Alto, CA, USA). Sequencing libraries were prepared using "NEBNext Ultra II Directional RNA Library Prep Kit for Illumina "combined with "NEBNext rRNA Depletion Kit v2" for ribosomal RNA depletion (New England Biolabs, Ipswich, MA). Libraries were pooled and sequenced (paired-end, 2 × 100bp) on a NextSeq2000 according to the manufacturer's instructions (Illumina Inc., San Diego, CA, USA).

Analysis of RNA-sequence reads: Identification of differentially expressed genes

For each sample, quality control was carried out and assessed with the NGS Core Tools FastQC[76] and QualiMap[77]. Sequence reads (minimum 88 million per sample) were mapped to *Mus musculus* mm10 using STAR[78] to obtain a BAM (Binary Alignment Map) file. An abundance matrix was generated after quantification with salmon[79] using default parameters. At last, differential expression analyses were performed using the DEseq2[80] package of the Bioconductor framework for RNA-Seq data[81]. Volcano plots were constructed based on $\log_2$ fold change (≥ or ≤0.5) and $-\log_{10}$ adjusted p value (<1). Enrichment analysis of Gene Ontology (GO) terms was conducted using Metascape

(http://metascape.org)[82]. Gene selectively associated with immune cells were curated using ImmGen (https://www.immgen.org).

Laser scanning confocal microscopy (LSCP)

For immunohistochemical analyses, images were acquired using a Leica TCS SP8 laser scan confocal microscope using a ×20/1.0 W-Plan-Apochromat objective (oil (NA 0.75) and a ×63 Plan-Apochromat [oil (NA 1.4)] magnification. For 3D segmentation of cells and platelet aggregates, no less than 10 z-stacks (1 AU) of single cells or clusters were acquired in 12-bit color depth and non-saturating settings.

For in vivo zebrafish imaging of TCs circulation and arrest, a Leica TCS SP8 microscope equipped using an M205 FA stereomicroscope (Leica) and a ×20/1.0 W-Plan-Apochromat objective (oil (NA 0.75)) on an SP8 confocal microscope (Leica) were used.

Image processing and analysis

For metastatic foci number and size, macroscopic 8-bit lung (B16F10-seeded) images (MacOS 15.4, iPhone8) with identical zooming and size (100 × 100 px) were automatically thresholded on ImageJ. Binary masks obtained were analyzed by the "analyze particles" plugin with circularity set between 0.2–1.0 to exclude lung edge shadows and pixel size below 15 px considered as noise. Platelet aggregates and cell volumes of TCs intravascularly arrested in mice lungs were obtained after segmentation in AMIRA Visage 6 from the confocal acquisition of Z-stacks covering the whole cell-aggregate volume. For immunofluorescence images, brightness and contrast were equally adjusted in control and treated samples on ImageJ and/or Adobe Photoshop CS4 software.

Statistics

Statistical analysis was performed with GraphPad Prism 9.4. The normal distribution of the data sets was assessed by the Shapiro–Wilk normality test. According to the number of data sets compared, the Mann–Whitney test or Kruskal–Wallis test followed by the original FDR method of Benjamini and Hochberg post-test were applied. In kinetics experiments, a two-way ANOVA followed by the original FDR method of Benjamini and Hochberg post test was used ($^{*}p < 0.05$; $^{**}p < 0.01$, $^{***}p < 0.001$, $^{****}p < 0.0001$). In all cases, the α-level was set at 0.05. All the data in graphs were presented as mean ± Standard Deviation (SD), except for the kinetics where mean ± SEM was used.

Ethics statement

Human studies were performed according to the Helsinki declaration and regulations provided by the Ethics Committee from Hospital Gregorio Maranon, Madrid, Spain, Protocol Version 05/Junio 2018. Control human blood samples were obtained from volunteer blood donors who gave written informed consent recruited by the blood transfusion center where the research was performed (Etablissement Français du Sang, Grand Est). All procedures were registered and approved by the French Ministry of Higher Education and Research. The donors gave their approval in the CODHECO number AC- 2008 - 562 consent form for the samples to be used for research purposes. Immunocompetent and genetically modified mice used in this study were housed under pathogen-free conditions, and all procedures were performed in accordance with the European Union Guideline 2010/63/EU. The study was approved by the Regional Ethical Committee for Animal Experimentation of Strasbourg, CREMEAS (CEEA 35) under the APAFIS authorization 14741-2018041816337540 and 37433-2022052016445806. According to the ethical committee and approved experimental protocol, the signal of luminescence relative to D0 was considered as an indicator of tumor burden. The limit was set to a signal not superior at 10,000 times the input signal in the lungs. This value was never overcome in our experimental setting. Other parameters (Grimance pain scale and signs of suffering) were daily evaluated to ensure the well-being of the animals. Animals in conditions of suffering or presenting an excessive tumor burden were euthanized according to the scoring scale of the ethical approval protocol.

Reporting summary

Further information on research design is available in the Nature Portfolio Reporting Summary linked to this article.

Data availability

FFPE RNA sequencing data are publicly available in ArrayExpress accession E-MTAB-13864 at the following address: "www.ebi.ac.uk/biostudies/arrayexpress/studies/E-MTAB-13864". All the other data are available within the article and its Supplementary Information. Source data are provided with this paper.

Code availability

MatLab scripts used for the heat mapping analysis in zebrafish (supplementary Fig. 2) are available here[2].

References

1. Follain, G. et al. Fluids and their mechanics in tumour transit: shaping metastasis. *Nat. Rev. Cancer* **20**, 107–124 (2020).
2. Follain, G. et al. Hemodynamic forces tune the arrest, adhesion, and extravasation of circulating tumor cells. *Dev. Cell* **45**, 33–52.e12 (2018).
3. Osmani, N. et al. Metastatic tumor cells exploit their adhesion repertoire to counteract shear forces during intravascular arrest. *Cell Rep.* **28**, 2491–2500.e5 (2019).
4. Osmani, N. et al. Probing intravascular adhesion and extravasation of tumor cells with microfluidics. *Methods Mol. Biol.* **2294**, 111–132 (2021).
5. Aceto, N. et al. Circulating tumor cell clusters are oligoclonal precursors of breast cancer metastasis. *Cell* **158**, 1110–1122 (2014).
6. Peralta, M., Osmani, N. & Goetz, J. G. Circulating tumor cells: towards mechanical phenotyping of metastasis. *iScience* **25**, 103969 (2022).
7. Gkountela, S. et al. Circulating tumor cell clustering shapes DNA methylation to enable metastasis seeding. *Cell* **176**, 98–112.e14 (2019).
8. Szczerba, B. M. et al. Neutrophils escort circulating tumour cells to enable cell cycle progression. *Nature* **566**, 553–557 (2019).
9. Labelle, M., Begum, S. & Hynes, R. O. Platelets guide the formation of early metastatic niches. *Proc. Natl Acad. Sci.* **111**, E3053–E3061 (2014).
10. Haemmerle, M., Stone, R. L., Menter, D. G., Afshar-Kharghan, V. & Sood, A. K. The platelet lifeline to cancer: challenges and opportunities. *Cancer Cell* **33**, 965–983 (2018).
11. Stone, R. L. et al. Paraneoplastic thrombocytosis in ovarian cancer. *N. Engl. J. Med.* **366**, 610–618 (2012).
12. Ma, C. et al. Platelets control liver tumor growth through P2Y12-dependent CD40L release in NAFLD. *Cancer Cell* **40**, 986–998.e5 (2022).
13. Senft, D. Platelets limit liver tumours. *Nat. Rev. Cancer* **22**, 608–608 (2022).
14. Gasic, G. J., Gasic, T. B. & Stewart, C. C. Antimetastatic effects associated with platelet reduction. *Proc. Natl Acad. Sci.* **61**, 46–52 (1968).
15. Jain, S., Russell, S. & Ware, J. Platelet glycoprotein VI facilitates experimental lung metastasis in syngenic mouse models. *J. Thromb. Haemost.* **7**, 1713–1717 (2009).
16. Jain, S. et al. Platelet glycoprotein Ibα supports experimental lung metastasis. *Proc. Natl Acad. Sci.* **104**, 9024–9028 (2007).

17. Volz, J. et al. Inhibition of platelet GPVI induces intratumor hemorrhage and increases efficacy of chemotherapy in mice. *Blood* **133**, 2696–2706 (2019).
18. Labelle, M. & Hynes, R. O. The initial hours of metastasis: the importance of cooperative host–tumor cell interactions during hematogenous dissemination. *Cancer Discov.* **2**, 1091–1099 (2012).
19. Nieswandt, B., Hafner, M., Echtenacher, B. & Männel, D. N. Lysis of tumor cells by natural killer cells in mice is impeded by platelets. *Cancer Res.* **59**, 1295–1300 (1999).
20. Feinauer, M. J. et al. Local blood coagulation drives cancer cell arrest and brain metastasis in a mouse model. *Blood* **137**, 1219–1232 (2021).
21. Schumacher, D., Strilic, B., Sivaraj, K. K., Wettschureck, N. & Offermanns, S. Platelet-derived nucleotides promote tumor-cell transendothelial migration and metastasis via P2Y2 receptor. *Cancer Cell* **24**, 130–137 (2013).
22. Mehta, P., Lawson, D., Ward, M. B., Kimura, A. & Gee, A. Effect of human tumor cells on platelet aggregation: potential relevance to pattern of metastasis. *Cancer Res.* **47**, 3115–3117 (1987).
23. Erpenbeck, L., Nieswandt, B., Schön, M., Pozgajova, M. & Schön, M. P. Inhibition of platelet GPIbα and promotion of melanoma metastasis. *J. Invest. Dermatol.* **130**, 576–586 (2010).
24. Echtler, K. et al. Platelet GPIIb supports initial pulmonary retention but inhibits subsequent proliferation of melanoma cells during hematogenic metastasis. *PLoS One* **12**, e0172788 (2017).
25. Lucotti, S. & Muschel, R. J. Platelets and metastasis: new implications of an old interplay. *Front. Oncol.* **10**, 1350 (2020).
26. Jurasz, P., Alonso-Escolano, D. & Radomski, M. W. Platelet-cancer interactions: mechanisms and pharmacology of tumour cell-induced platelet aggregation. *Br. J. Pharmacol.* **143**, 819–826 (2004).
27. McFadyen, J. D. & Kaplan, Z. S. Platelets are not just for clots. *Transfus. Med. Rev.* **29**, 110–119 (2015).
28. Falanga, A. et al. EHA guidelines on management of antithrombotic treatments in thrombocytopenic patients with cancer. *HemaSphere* **6**, e750 (2022).
29. Headley, M. B. et al. Visualization of immediate immune responses to pioneer metastatic cells in the lung. *Nature* **531**, 513–517 (2016).
30. Hyenne, V. et al. Studying the fate of tumor extracellular vesicles at high spatiotemporal resolution using the zebrafish embryo. *Dev. Cell* **48**, 554–572.e7 (2019).
31. Liotta, L. A., Saidel, M. G. & Kleinerman, J. The significance of hematogenous tumor cell clumps in the metastatic process. *Cancer Res.* **36**, 889–894 (1976).
32. Haemmerle, M. et al. FAK regulates platelet extravasation and tumor growth after antiangiogenic therapy withdrawal. *J. Clin. Invest.* **126**, 1885–1896 (2016).
33. Li, R. et al. Presence of intratumoral platelets is associated with tumor vessel structure and metastasis. *BMC Cancer* **14**, 167 (2014).
34. Labelle, M., Begum, S. & Hynes, R. O. Direct signaling between platelets and cancer cells induces an epithelial-mesenchymal-like transition and promotes metastasis. *Cancer Cell* **20**, 576–590 (2011).
35. Johnson, K. E. et al. Aspirin inhibits platelets from reprogramming breast tumor cells and promoting metastasis. *Blood Adv.* **3**, 198–211 (2019).
36. Schmied, L., Höglund, P. & Meinke, S. Platelet-mediated protection of cancer cells from immune surveillance - possible implications for cancer immunotherapy. *Front. Immunol.* **12**, 640578 (2021).
37. Hüsemann, Y. et al. Systemic spread is an early step in breast cancer. *Cancer Cell* **13**, 58–68 (2008).
38. Hu, Z. et al. Quantitative evidence for early metastatic seeding in colorectal cancer. *Nat. Genet.* **51**, 1113–1122 (2019).
39. Jandrot-Perrus, M. et al. Cloning, characterization, and functional studies of human and mouse glycoprotein VI: a platelet-specific collagen receptor from the immunoglobulin superfamily. *Blood* **96**, 1798–1807 (2000).
40. Tesfamariam, B. & Wood, S. C. Targeting glycoprotein VI to disrupt platelet-mediated tumor cell extravasation. *Pharmacol. Res.* **182**, 106301 (2022).
41. Stewart, T. J. & Abrams, S. I. Altered immune function during long-term host-tumor interactions can be modulated to retard autochthonous neoplastic growth. *J. Immunol.* **179**, 2851–2859 (2007).
42. Mangin et al. A humanized glycoprotein VI (GPVI) mouse model to assess the antithrombotic efficacies of anti-GPVI agents. *J. Pharmacol. Exp. Ther.* **341**, 156–163 (2012).
43. Baig, M. S. et al. NOS1-derived nitric oxide promotes NF-κB transcriptional activity through inhibition of suppressor of cytokine signaling-1. *J. Exp. Med.* **212**, 1725–1738 (2015).
44. Roy, M. G. et al. Muc5b is required for airway defence. *Nature* **505**, 412–416 (2014).
45. Kramer, E. D. et al. β-Catenin signaling in alveolar macrophages enhances lung metastasis through a TNF-dependent mechanism. *JCI Insight.* **8**, e160978 (2023).
46. Lebozec, K., Jandrot-Perrus, M., Avenard, G., Favre-Bulle, O. & Billiald, P. Design, development and characterization of ACT017, a humanized Fab that blocks platelet's glycoprotein VI function without causing bleeding risks. *MAbs* **9**, 945–958 (2017).
47. Jadoui, S. et al. Glenzocimab does not impact glycoprotein VI-dependent inflammatory haemostasis. *Haematologica* **106**, 2000–2003 (2021).
48. Serebruany, V. L., Cherepanov, V., Cabrera-Fuentes, H. A. & Kim, M. H. Solid cancers after antiplatelet therapy: confirmations, controversies, and challenges. *Thromb. Haemost.* **114**, 1104–1112 (2015).
49. Alonso-Escolano, D., Strongin, A. Y., Chung, A. W., Deryugina, E. I. & Radomski, M. W. Membrane type-1 matrix metalloproteinase stimulates tumour cell-induced platelet aggregation: role of receptor glycoproteins. *Br. J. Pharmacol.* **141**, 241–252 (2004).
50. Katagiri, Y. et al. Characterization of platelet aggregation induced by the human melanoma cell line HMV-I: roles of heparin, plasma adhesive proteins, and tumor cell membrane proteins. *Cancer Res.* **51**, 1286–1293 (1991).
51. Gao, L., Zhang, H., Zhang, B., Zhang, L. & Wang, C. Prognostic value of combination of preoperative platelet count and mean platelet volume in patients with resectable non-small cell lung cancer. *Oncotarget* **8**, 15632–15641 (2017).
52. Wang, Y.-H. et al. The pretreatment thrombocytosis may predict prognosis of patients with colorectal cancer: a systematic review and meta-analysis. *Biomark. Med.* **11**, 195–210 (2017).
53. Schwarz, R. E. Platelet counts and prognosis of pancreatic cancer. *Lancet* **353**, 2158–2159 (1999).
54. Wojtukiewicz, M. Z., Sierko, E., Hempel, D., Tucker, S. C. & Honn, K. V. Platelets and cancer angiogenesis nexus. *Cancer Metastasis Rev.* **36**, 249–262 (2017).
55. Monroe, D. M. & Key, N. S. The tissue factor-factor VIIa complex: procoagulant activity, regulation, and multitasking. *J. Thromb. Haemost.* **5**, 1097–1105 (2007).
56. Allen, J. E. et al. Apoptotic circulating tumor cells (CTCs) in the peripheral blood of metastatic colorectal cancer patients are associated with liver metastasis but not CTCs. *Oncotarget* **5**, 1753–1760 (2014).
57. Sood, A. K. et al. Stress hormone–mediated invasion of ovarian cancer cells. *Clin. Cancer Res.* **12**, 369–375 (2006).
58. Gaertner, F. et al. Migrating platelets are mechano-scavengers that collect and bundle bacteria. *Cell* **171**, 1368–1382.e23 (2017).
59. Mammadova-Bach, E. et al. Platelet glycoprotein VI promotes metastasis through interaction with cancer cell-derived Galectin-3. *Blood* **135**, 1146–1160 (2020).
60. Lazar, S. & Goldfinger, L. E. Platelets and extracellular vesicles and their cross talk with cancer. *Blood* **137**, 3192–3200 (2021).

61. Italiano, J. E. et al. Angiogenesis is regulated by a novel mechanism: pro- and antiangiogenic proteins are organized into separate platelet α granules and differentially released. *Blood* **111**, 1227–1233 (2008).
62. Vismara, M. et al. Platelet-derived extracellular vesicles regulate cell cycle progression and cell migration in breast cancer cells. *Biochim. Biophys. Acta Mol. Cell Res.* **1868**, 118886 (2021).
63. Munn, D. H. & Bronte, V. Immune suppressive mechanisms in the tumor microenvironment. *Curr. Opin. Immunol.* **39**, 1–6 (2016).
64. Rachidi, S. et al. Platelets subvert T cell immunity against cancer via GARP-TGFβ axis. *Sci. Immunol.* **2**, eaai7911 (2017).
65. Placke, T. et al. Platelet-derived MHC class I confers a pseudo-normal phenotype to cancer cells that subverts the antitumor reactivity of natural killer immune cells. *Cancer Res.* **72**, 440–448 (2012).
66. Chaurasia, S. N., Kushwaha, G., Pandey, A. & Dash, D. Human platelets express functional ectonucleotidases that restrict platelet activation signaling. *Biochem. Biophys. Res. Commun.* **527**, 104–109 (2020).
67. Templeton, A. J. et al. Prognostic role of platelet to lymphocyte ratio in solid tumors: a systematic review and meta-analysis. *Cancer Epidemiol. Biomark. Prev.* **23**, 1204–1212 (2014).
68. Qi, X. et al. Prognostic significance of platelet-to-lymphocyte ratio (PLR) in patients with breast cancer treated with neoadjuvant chemotherapy: a meta-analysis. *BMJ Open* **13**, e074874 (2023).
69. Tao, D. L., Tassi Yunga, S., Williams, C. D. & McCarty, O. J. T. Aspirin and antiplatelet treatments in cancer. *Blood* **137**, 3201–3211 (2021).
70. Voors-Pette, C. et al. Safety and tolerability, pharmacokinetics, and pharmacodynamics of ACT017, an antiplatelet GPVI (Glycoprotein VI) fab. *Arterioscler. Thromb. Vasc. Biol.* **39**, 956–964 (2019).
71. Cazenave, J.-P. et al. Preparation of washed platelet suspensions from human and rodent blood. *Methods Mol. Biol.* **272**, 13–28 (2004).
72. Goetz, J. G. et al. Endothelial cilia mediate low flow sensing during zebrafish vascular development. *Cell Rep.* **6**, 799–808 (2014).
73. Stoletov, K. et al. Visualizing extravasation dynamics of metastatic tumor cells. *J. Cell Sci.* **123**, 2332–2341 (2010).
74. Strassel, C. et al. Synthesis of GPIb beta with novel transmembrane and cytoplasmic sequences in a Bernard-Soulier patient resulting in GPIb-defective signaling in CHO cells. *J. Thromb. Haemost.* **4**, 217–228 (2006).
75. Samaniego, R. et al. Mesenchymal contribution to recruitment, infiltration, and positioning of leukocytes in human melanoma tissues. *J. Invest. Dermatol.* **133**, 2255–2264 (2013).
76. Andrews, S. FastQC: a quality control tool for high throughput sequence data. *Web Serv.* available http//www.bioinformatics.babraham.ac.uk/projects/fastqc (2010).
77. Okonechnikov, K., Conesa, A. & García-Alcalde, F. Qualimap 2: advanced multi-sample quality control for high-throughput sequencing data. *Bioinformatics* **32**, 292–294 (2016).
78. Dobin, A. et al. STAR: ultrafast universal RNA-seq aligner. *Bioinformatics* **29**, 15–21 (2013).
79. Patro, R., Duggal, G., Love, M. I., Irizarry, R. A. & Kingsford, C. Salmon provides fast and bias-aware quantification of transcript expression. *Nat. Methods* **14**, 417–419 (2017).
80. Love, M. I., Huber, W. & Anders, S. Moderated estimation of fold change and dispersion for RNA-seq data with DESeq2. *Genome Biol.* **15**, 550 (2014).
81. Gentleman, R. C. et al. Bioconductor: open software development for computational biology and bioinformatics. *Genome Biol.* **5**, 1–16 (2004).
82. Zhou, Y. et al. Metascape provides a biologist-oriented resource for the analysis of systems-level datasets. *Nat. Commun.* **10**, 1523 (2019).

Acknowledgements

We thank all members of JGG's team (past and present) for their constant discussions and help on this particular topic. J.G.G. is the coordinator of the NANOTUMOR Consortium, a program from ITMO Cancer of AVIESAN (Alliance Nationale pour les Sciences de la Vie et de la Santé, National Alliance for Life Sciences & Health) within the framework of the Cancer Plan (France). Work and people in the lab of J.G.G. are mostly supported by the INCa (Institut National Du Cancer, French National Cancer Institute), charities (La Ligue contre le Cancer, ARC (Association pour la Recherche contre le Cancer), FRM (Fondation pour la Recherche Médicale), the National Plan Cancer initiative, the Region Grand Est, INSERM and the University of Strasbourg. This work has been directly funded by the INCa grant (PLBIO 2016-164) and by the support of the Ligue contre le Cancer (labelisation), the Association Ruban Rose, and the SATT Conectus (Strasbourg). M.G.L. has been funded by the University of Strasbourg (IdeX, investissements d'Avenir), the INCa and the SATT Conectus (Strasbourg). M.P. and C.L. are supported by INCa, F.C. by NANOTUMOR, and V.M. by a Ph.D. fellowship from the French Ministry of Science (MESRI) and by the Foundation ARC (Association pour la recherche contre le Cancer grant number ARCDOC420230100060005). G.F. was supported by La Ligue contre le Cancer. L.B. is supported by FRM (Fondation pour la Recherche Médicale - ECO202206015567). We acknowledge PIC-STRA (imaging platform of the CRBS) for the support in image acquisition. We are grateful to Acticor for providing the Glenzocimab antibody and to François Bertucci for providing human samples. We are also thankful to recent donators (Rohan Athlétisme Saverne, Traileurs de la Rose) to support our work. Parts of the figure were drawn by using pictures from Servier Medical Art. Servier Medical Art by Servier is licensed under a Creative Commons Attribution 3.0 Unported License (https://creativecommons.org/licenses/by/3.0/).

Author contributions

M.G.L. designed and conceived the project and performed most of the experiments, analyzed the data and wrote the manuscript; C.L. performed part of the mouse experiments, analyzed the data, wrote the manuscript and provided technical support during the revision; V.M. performed part of the mouse experiments, in vitro platelets-TCs interaction experiments, RNASeq data analysis, analyzed the data, wrote the manuscript and provided technical support during the revision process; L.B. performed lung immunophenotyping experiments, analyzed the data, and provided technical support during the revision process; G.F. performed zebrafish experiments and analyzed the data; C.M. performed platelets experiments and analyzed the data; I.B. performed CLEM experiments in zebrafish and analyzed the data; A.L. performed FFPE RNA extraction and provided technical support through all the project; F.C. provided technical support, revised the manuscript and prepared the figures; M.P. provided technical support with the zebrafish experiments; N.O. provided technical support during the revision and designed platelets-TCs interaction experiments; V.G. provided technical support with the zebrafish experiments; C.B. provided technical support; R.F. provided and stained human melanoma samples; A.P., N.P., A.M., R.C. performed RNASeq experiments, generated the libraries and analyzed the data; M.J.P. provided critical discussion through the project; O.L. contributed to design the project, performed part of the mouse experiments, provided technical support analyzed the data and wrote the manuscript; P.H.M. and J.G.G. designed, conceived and supervised the project, provided financial support and wrote the manuscript.

Competing interests

M.P.J. is a scientific co-founder of Acticor Biotech and a scientific adviser. All other authors declare no competing interests.

Additional information

Supplementary information The online version contains supplementary material available at https://doi.org/10.1038/s41467-024-47516-w.

Correspondence and requests for materials should be addressed to Maria J. Garcia-Leon, Pierre H. Mangin or Jacky G. Goetz.

Peer review information *Nature Communications* thanks Richard Hynes and the other, anonymous, reviewer(s) for their contribution to the peer review of this work. A peer review file is available.

Reprints and permissions information is available at http://www.nature.com/reprints

Publisher's note Springer Nature remains neutral with regard to jurisdictional claims in published maps and institutional affiliations.

Open Access This article is licensed under a Creative Commons Attribution 4.0 International License, which permits use, sharing, adaptation, distribution and reproduction in any medium or format, as long as you give appropriate credit to the original author(s) and the source, provide a link to the Creative Commons licence, and indicate if changes were made. The images or other third party material in this article are included in the article's Creative Commons licence, unless indicated otherwise in a credit line to the material. If material is not included in the article's Creative Commons licence and your intended use is not permitted by statutory regulation or exceeds the permitted use, you will need to obtain permission directly from the copyright holder. To view a copy of this licence, visit http://creativecommons.org/licenses/by/4.0/.

© The Author(s) 2024

3. Tumoral CD24 tunes platelet binding and supports metastasis

Platelets quickly cover CTCs after they enter the bloodstream. The current assumption that all CTCs interact equally with platelets may account for the unclear outcomes associated with the use of anti-platelet drugs in cancer patients. In the previous study, we reported that different TC types interact with platelets differently. This result suggests that platelets binding efficiency might, in part, shape intravascular arrest and metastatic fitness of TCs. Hence, one major question arises from this previous work: what is driving the heterogeneous platelets binding to TCs?

In our follow-up study, we screen publicly available databases and identify CD24 as a new TC rheostat regulating platelet binding and their subsequent pro-metastatic function. We describe that TCs CD24 surface expression positively correlates to TC-platelets binding and pro-metastatic clustering potential *in vitro*. Next, in a syngeneic mouse model of experimental metastasis, we highlight that CD24 knock-down in the triple negative breast cancer 4T1 cells significantly the number of lungs metastatic foci in a platelet-dependent manner. Furthermore, we observe that CD24 knock-down induces the rewiring of the immune TME towards an anti-tumoral lymphoid response.

Altogether, our results suggest that tumoral CD24 tunes platelets binding and support metastasis by notably inducing a supportive TME. Therefore, these findings identify CD24 as a potential druggable target to counteract platelets-TCs interaction and metastatic progression, avoiding the collateral hemostatic perturbations of classical anti-platelet agents.

Tumoral CD24 tunes platelets binding and pro-metastatic functions

Vincent Mittelheisser[1-5,*#], Cristina Liboni[1-5,*], Clarisse Mouriaux[3,6], Silvia Maria Grazia Trivigno[3,6], Louis Bochler[1-5], Maria J. Garcia-Leon[1-5,#], Annabel Larnicol[1-5], Laetitia Paulen[1-5], Tristan Stemmelen[2-4,7], Pierre H. Mangin[3,6,*], Olivier Lefebvre[1-5,*] and Jacky G. Goetz[1-5,§]

[1]Tumor Biomechanics lab.
[2]INSERM UMR_S1109, Strasbourg, France.
[3] Université de Strasbourg, Strasbourg, France.
[4] Fédération de Médecine Translationnelle de Strasbourg (FMTS), Strasbourg, France.
[5] Equipe Labellisée Ligue Contre le Cancer.
[6] UMR_S1255, INSERM, Etablissement Français du Sang-Alsace, Strasbourg, France.
[7] Plateforme GENOMAX, Institut thématique interdisciplinaire (ITI) de Médecine de Précision de Strasbourg Transplantex NG, Faculté de Médecine, Strasbourg, France.

*** Equal contribution:**
VM and CL have contributed equally.
PM and OL have contributed equally.

 # Current address:
VM: Institut Curie, INSERM U392, Integrative analysis of T cells activation team, Paris, France.
MGL: Domain therapeutics, Illkirch, France.

§ Correspondence:
Jacky G. Goetz, jacky.goetz@inserm.fr
INSERM UMR_S1109, Centre de Recherche en Biomédecine de Strasbourg (CRBS), Fédération de Médecine Translationnelle de Strasbourg (FMTS), Strasbourg, France.
Web: www.goetzlab.fr

Abstract

One of the earliest steps of breast cancer metastasis occurs when tumor cells (TCs) disseminate through the bloodstream. There, they interact with several blood components. Among them, platelet favor TC survival and metastatic spread. While the binding of platelet to TC is highly variable, its molecular controls and downstream consequences remain unidentified. Here, we first document that high CD24 expression correlates with increased platelet binding and poorer survival in breast cancer. We further demonstrate that CD24-mediated platelet binding regulates TC cluster formation and resistance to anoikis *in vitro*. Depleting CD24 expression significantly reduces TC metastatic potential by rewiring the metastatic tumor microenvironment (mTME), affecting immune compartments and secreted factors. Overall, our work identifies CD24 as a molecular cue controlling TC-platelet interaction, dictating their metastatic potential. As such, it represents a druggable target to counteract platelet-TC collaboration in metastasis.

Keywords: platelets, CD24, metastasis

Introduction

Upon cancer progression, tumor cells (TC) disseminate through the bloodstream to colonize distant organs and form life-threatening metastases. During their intravascular journey, circulating TC (CTC) face several hostile forces that are detrimental to their survival (1). Once their entered the bloodstream, CTC rapidly bind, activate and aggregate circulating platelets (2,3). Platelets provide a physical shield to CTC protecting them from destruction by shear forces (4) and by patrolling immune cells (5). In addition, this interaction favors the subsequent TC adhesion and extravasation at distant sites (6,7), facilitating metastatic foci formation. Interestingly, we recently demonstrate that TC interact with platelet in phenotypically distinct ways, which is variable across cellular models and cancer types (8). By inducing a transient thrombocytopenia at the time of TC tail vein injection, we next reveal that high-binding TC rely on interactions with platelet to achieve successful early lung seeding, whereas low-binding TC seeding is independent of the presence of platelet (8). Yet, the molecular determinants of differential platelet binding abilities by TC remain largely unknown.

Building on such limitations, we designed a study aiming at interrogating which molecular cues are responsible for the high *versus* low platelets binding phenotype of TC. Through the examination of publicly available datasets, we found that CD24 expression was significantly increased in TC that highly bind platelets. This is in line with several studies that have reported CD24 as broadly overexpressed in numerous human malignancies, both solid and hematological (9). Interestingly, its expression varies upon cancer progression and is usually tied with a more aggressive course of the disease and poorer survival rate (10,11). Mechanistically, CD24 is a glycosylphosphatidylinositol-anchored membrane protein functioning as an adhesion molecule for P-selectin expressed both on the endothelium and on activated platelets (12,13). Its expression on TC correlates with higher P-selectin-dependent arrest in the lung (14,15) and, via binding to tumor-educated platelets, induces tumor vascularization and growth (16). Yet, the role of TC-expressed CD24 on platelet binding and subsequent metastatic fitness remains unexplored.

In this study, we genetically depleted CD24 expression in breast cancer TC with a shRNA approach and first demonstrated that CD24, in part, tunes TC abilities to bind platelet. We also showed that CD24-mediated platelet binding was crucial for TC pro-metastatic clustering and resistance to anoikis. *In vivo*, shCD24 cells demonstrated a

reduced metastatic burden compared to parental cells together with a profound rewiring of the tumor immune microenvironment (TiME). As the relative contribution of endothelial *versus* platelet P-selectin to TC arrest in the lung still remains unclear (14,15), we subjected mice to a short thrombocytopenia prior TC injection. Platelet-depleted mice presented an additional reduction of metastatic burden, corroborating the concept according to which CD24-mediated TC binding to platelet underlies TC seeding and subsequent metastatic outgrowth. Altogether, our study demonstrates that CD24 is a druggable target for preventing metastatic progression as, among others, it favors the binding and function of pro-metastatic platelet.

Results

Platelet binding to TC scales with poor prognosis CD24 expression levels.

To dissect the molecular clutch controlling platelets binding to TC in the context of BCa, we screened publicly available databases of RNA-sequencing and assess the expression of known receptors involved in TC binding to platelet (12,17–22) (**Fig.1A**). Based on the findings of our previous work, we selected the murine metastatic triple negative breast cancer (TNBC) 4T1 cells as high platelets binding phenotype and compared them to B16F10 (murine melanoma) cells that we previously demonstrated as low platelets binders (8). Besides, to investigate the expression of platelet receptors during metastatic progression, we further evaluated the 67NR cells, which are the non-metastatic isogenic counterpart of 4T1 (23) (**Fig.1A**). By analyzing the differential expression of the identified platelet receptors genes, we observed that P-selectin ligands *CD24* and *Podocalyxin* (PODXL) were solely overexpressed in 4T1 cells compared to 67NR cells and B16F10 cells, suggesting their implication in both high-platelet biding phenotype and metastatic progression (**Fig.1B**). To confirm the relevance of *CD24* or *PODXL* in human breast cancer, we examined their expression in breast cancer patients by exploring RNA-sequencing data from The Cancer Genome Atlas (TCGA) BRCA dataset (**Fig.1C**). Interestingly, *CD24* expression was significantly increased in human breast cancer tissues compared to healthy breast tissues (**Fig.S1A**). Furthermore, in depth analysis of breast cancer PAM50 subtypes revealed that *CD24* expression was mostly increased in TNBC and HER2-amplified patients (**Fig.S1A**). Yet, when stratified, only TNBC patients presenting high *CD24* expression level had a significantly poorer overall survival (**Fig.S1B**). More particularly, *CD24* expression was increased in TNBC patients (Miller cohort) during local lymph node

(LN) invasion when compared to their primary tumor (**Fig.S1C**), underscoring its role in breast cancer cells metastatic abilities. When patients were stratified in the TCGA BRCA dataset based on their LN invasion (LN^{neg} vs LN^{pos}), we further highlighted that high *CD24* expression led to poorer overall survival in patients presenting lymph node invasion as compared to those without (**Fig.S1D**). In line with these results, high *CD24* level and lymph node infiltration led to a higher risk of disease recurrence (**Fig.S1E**). Conversely, *PODXL* expression was significantly decreased in human breast cancer cells compared to healthy tissue and widespread in several other clusters within the tumor microenvironment (TME) (**Fig.S1F-G**). Moreover, *PODXL* expression had no impact on patients' overall survival (**Fig.S1H**). Together, these results suggested that *CD24* expression correlated with *i*) high platelet-binding to TC and *ii*) with breast cancer cells metastatic abilities and overall survival. Hence, we decided to further evaluate CD24 role in platelets binding to TCs.

Building on these observations, we next thoroughly investigated *CD24* expression within the TME cell populations analyzing single-cell RNA-sequencing data from 5 primary TNBC samples (24). Tumor cells exhibited robust expression of *CD24*, whereas its expression was weak in all other main TME cell clusters, thus illustrating the potential of CD24 as a tumor-specific target (**Fig.1D**). Since CD24 is associated with lymph node invasion, we further investigated the cellular heterogeneity between the primary TNBC TME and its matched metastatic TME. Focusing on lung metastases, a major site of TNBC spread (25), we performed xCell analysis on primary TNBC and matched lung metastatic lesions (**Fig.1C**) from the Stavanger (3 primary-metastasis pairs) (26) and the University of North Carolina Rapid Autopsy Program (RAP) (4 primary-metastasis pairs) (27) cohorts (**Table S1**). Interestingly, although immune and stromal scores were similar between primary TNBC and their matched lung metastases, we observed a notable increase in platelet infiltration in lung metastatic nodules compared to primary tumors (**Fig.1E**). This platelet infiltration (assessed by *GP6* expression which is restricted to megakaryocytic lineage (28)) within the TME significantly positively correlated with *CD24* expression, but not with other platelet receptors like, *CD44*, *SELPLG*, *PODXL*, *PDPN*, *ITGAV*, *ITGB3* or *CD97* with the exception of galectin-3 (*LGALS3*), the prototypical GPVI receptor (**Fig.1F**).To further validate the translatability of our transcriptomic observations at the protein level, we conducted flow cytometry analyses, which confirmed, in agreement with the *in-silico* analysis, robust CD24 protein expression in 4T1 cells and minimal expression at

the surface of 67NR and B16F10 cells (**Fig.1G**). We further extended our investigations by probing CD24 expression in the additional low-platelets binding AT3 cell line (8). As expected, CD24 presented a significantly lower expression at their surface compared to high platelets binding 4T1 cells (**Fig.1G**). Building on our previous study (8), we highlighted a significant positive correlation (R^2 = 0.99) between CD24 surface expression levels on murine tumor cells (**Fig.S1I**) and the number of platelets bound per cell as seen by scanning electron microscopy. In addition, a second 2D model of platelets binding to tumor cells confirmed the significant correlation (R^2 = 0.98) between the CD24 surface expression levels and the number of platelets bound per cells as observed by immunofluorescence (**Fig.1H**). Altogether, these results identified CD24 as a new TCs specific rheostat regulating platelet binding and thus pro-metastatic functions.

CD24 controls the binding of platelet impacting survival and clustering potential of TC

To functionally investigate the role of CD24-mediated platelet binding in cancer progression, we reduced CD24 expression via a shRNA approach in the 4T1 cell line (**Fig.2A**). We first validated the successful knock-down of CD24 at the genomic (RT-qPCR) and protein level (flow cytometry) in the 4T1 shCD24 cells compared to their control counterpart (4T1 shScramble) (**Fig.2B-C**). Of note, CD24 expression levels were similar between 4T1 shScramble and their native counterparts (**Fig.S2A**). These same cell lines were assessed for their ability to bind platelets *in vitro*. In this setting, we observed that 4T1 shCD24 displayed significantly reduced ability to bind platelets (**Fig.2D**), reaching levels similar to “low- binding” cells (**Fig.S2B**). As platelet activation is deeply linked to loss of circular shape (29), we next assessed platelet morphology. In addition, to their increased number, platelets showed a decrease in circularity index when bound to 4T1 shScramble cells compared to 4T1 shCD24 cells (**Fig.2D**) or to $CD24^{neg}$ 67NR, B16F10 and AT3 cells (**Fig.S2C**), suggesting that CD24 expression by TC promoted the binding of activated platelet. We next assessed the ability of platelet to promote the clustering of TC (**Fig.2E**), a step known to promote seeding and metastases formation (30). We previously showed that platelets favored the clustering of 4T1 cells but not of B16F10 cells, in line with their platelet binding profile (8). In agreement with this, CD24 knock-down significantly reduced 4T1 cells clustering number and size (**Fig.2E**). Pro-metastatic clustering impairment was also associated

with a reduction of resistance of 4T1 shCD24 cells to anoikis (**Fig.2F**). Overall, these results show that CD24 tunes platelet binding to TC and likely contributing to the pro-metastatic function of platelet, affecting TC clustering and fitness.

CD24-mediated platelet binding controls lung seeding and colonization and subsequent metastatic outgrowth.

Owing to these *in vitro* results, we probed the metastatic potential of 4T1 shScramble and 4T1 shCD24 cells *in vivo*. Building on our previously published results showing that platelet-binding levels differently impact TC lung seeding (8), we first decided to demonstrate that CD24 pro-metastatic function is indeed linked to its platelet-binding function. We depleted platelets with an anti-GPIbα antibody to induce the short thrombocytopenia (TCP) regimen we previously described (8) prior TC injection in syngeneic mouse model of experimental metastasis (**Fig.3A-B**) and longitudinally tracking lung metastatic burden of TC. At the moment of TC seeding and extravasation (up to 3 dpi) (31), platelet depletion impaired extravasation of 4T1 shScramble cells but not 4T1 shCD24 cells (**Fig.3C**). This suggests that CD24-mediated TC-platelet interaction is required for early lung metastatic colonization. When assessing the platelet and CD24 effect on later metastatic outgrowth (14dpi), we further validated that platelets depletion at the time of TC injection massively reduce metastatic outgrowth in both conditions (**Fig.3D**), synergistically blunting metastatic outgrowth in CD24 knock-down condition. Yet, 4T1 shCD24 cells retained a residual metastatic potential in mice with normal platelet counts (**Fig.3D and Fig.S3A-C**), suggesting, as expected, that CD24 is not the sole molecular glue for TC-platelet interaction. To investigate the mechanisms that may underpin the late metastatic outgrowth, metastatic lungs were surgically resected on day 14. Macroscopic inspection of 4T1 shScramble and shCD24 metastatic lung revealed that early TCP significantly reduced the percentage of metastatic area, in agreement with the defect in lung colonization highlighted at 3 dpi and the subsequent lower bioluminescent signal observed at 14dpi (**Fig.3E**). However, these lesions displayed similar surface area and number of $Ki67^{pos}$ cells (**Fig. 3E-F**), suggesting that, while platelet control early lung metastatic colonization through CD24, they do not impact the later proliferation of 4T1 cells during the outgrowth of already-established metastatic foci. Moreover, the lack of difference in $Ki67^{pos}$ cells, consistent with the absence of variations in *in vitro* proliferation (**Fig.S3D**), indicated that our observations were not

due to a cell-intrinsic proliferation defect in the 4T1 sublines caused by the disruption of CD24 known role in modulating TC proliferation (32). Altogether, our results suggest that CD24 promotes metastasis by impacting early platelet-dependent seeding and colonization of circulating TC, independently of controlling their proliferation status.

Early CD24-mediated tumor-cell-platelet interaction controls later tumor immune microenvironment composition.

CD24 knock-down reduced the late metastatic outgrowth of 4T1 cancer cells in the lungs starting at 10 dpi (**Fig.3 and Fig.S3**), suggesting an enhanced adaptive immune response to metastasis. Indeed, we already previously demonstrate the ability of platelet to tune the metastatic TiME and, likely, alter TC fitness and outgrowth (8). Hence, we further explored the mechanisms underlying the reduced metastatic burden in 4T1 shCD24-injected mice using multiparametric flow cytometry. We examined the immune microenvironment of metastasis-bearing lungs of mice with normal platelet counts and found that 4T1 shScramble metastatic nodules induced a more immunosuppressive TiME compared to 4T1 shCD24 nodules (**Fig.4A**). Notably, 4T1 shScramble metastatic outgrowth was associated with a strong enrichment in total neutrophils and in their pro-tumoral Siglec-F^+ subtype (33) (**Fig.4A**). Conversely, CD24 knock-down rewired lung metastatic microenvironment towards a lymphoid response,as highlighted by the global augmentation in B-, NK- and T cells observed in 4T1 shCD24-tumor bearing mice (**Fig.4A**). Although the proportion of $CD4^+$ and $CD8^+$ T cells are similar between 4T1 shScramble- and shCD24 lung metastatic lesions, both infiltrated $CD4^+$ and $CD8^+$ T cells presented an increase in activated populations as per CD44 expression (**Fig.4A**). Remarkably, we also observed a rise in dendritic cells infiltration, further confirming the invigorated T cells activation (**Fig.4A**). Besides, we noticed a significant eosinophils recruitment (**Fig.4A**), which was previously described as promoting the mounting of a lymphocyte-mediated anti-tumor immunity (34). Further analysis of the soluble metastatic lung parenchyma milieu revealed an enrichment in pro-metastatic molecules such as matrix metalloproteases (MMP-3 and MMP-9) (35,36) in the 4T1 shScramble-injected mice whereas 4T1 shCD24 metastatic lesions were associated with an increase in lymphoid and dendritic cells chemoattractants such as CXCL12, CXCL13 and MIP1-α/CCL3 (37–39) (**Fig.S4A**). Importantly, we found that the TiME changes did not correlate with the number of metastases when either 4T1 shScramble and shCD24 lung metastatic lesions were analyzed, suggesting

that was unlikely to be the consequence of the impaired colonization and subsequent decreased metastatic burden in the lungs of 4T1 shCD24-injected mice (**Fig.S4B**). Overall, these results suggest that early CD24-mediated TC-platelet interaction controls later metastatic TiME, inducing an immunosuppressive environment. Interestingly, additional analysis of publicly available TNBC databases based on the FUSCC classification revealed that high *CD24* expression level was associated with poor prognosis particularly in the basal-like immune-suppressed (BLIS) TNBC subtypes, further validating its potential role in TiME immunosuppressive phenotype (**Fig.S4C**).

Discussion

This manuscript identifies for the first time CD24-mediated binding of TC to platelet as the determinant of platelets pro-metastatic role. We have previously shown that despite presenting different platelet binding efficacy, TC behave as platelets weak agonist, inducing their aggregation to a similar extend (8). Here, comparing TC presenting different platelet binding abilities, we revealed that they differ in CD24 expression levels. By screening publicly available databases, we revealed that high expression of CD24 in patients correlates with increased malignancy, poorer overall survival as highlighted also in a meta-analysis study (40). We further highlighted that CD24 high expression correlated with a bad prognosis in lymph node-positive TNBC patients, underlining its role in cancer progression. When analyzing our TC collection, we observed that CD24 expression on TC positively correlates with the number of platelets bound to TC and to the metastatic potential of the cell lines, in line with the increased platelet score in lung metastatic vs primary TME. Taking advantage of a shRNA approach, we knocked-down CD24 and we demonstrated that TCs unequal binding to platelets is, in part, mediated by CD24. Of note, CD24-expressing TC displayed bound platelet with a spread morphology whereas platelets binding on CD24-negative TC remained discoid. Upon their activation, platelets express P-selectin at their surface (41) which is essential for their stable binding (20). As CD24 is a ligand of P-selectin, we can hypothesize that while TC similarly activate platelets (8) only the ones expressing CD24 are able to stably bind activated, P-selectin^{pos} platelets. Further invigorating its involvement, we showed that CD24 is required to tune platelets pro-metastatic clustering and resistance to anoikis *in vitro*. As TC-platelet interaction is key to protect TC from shear stress and immune recognition in the

bloodstream (4,5), these data suggest that the expression of CD24 might attend this binding hence sustaining the metastatic spreading of $CD24^{pos}$ cells. Prompted by these results, we validated this notion *in vivo* assessing the lung metastatic colonization. In a shortTCP setting, we demonstrated that the early reduction of platelets combined with the depletion of CD24 on TCs completely blunted metastases outgrowth. This additive effect further identifies the early CD24-mediated TC-platelet interaction as a determinant of TC seeding and subsequent metastasis burden. Indeed, 4T1 shCD24 presented a reduced metastatic burden and a significantly diminished number of lung metastatic nodules. Of note, the absence of difference in lung colonization between 4T1 shScramble and 4T1 shCD24 in a shortTCP setting shed a new light on previously published results (14,15), suggesting that platelet but not endothelial P-selectin expression contributes to TC arrest in the lung.

Besides, we found that CD24 expression profoundly impact the metastatic immune microenvironment. Our results are in line with what recently observed in ΔCD24 4T1 primary tumors (42), where authors suggest that the loss of CD24 transform the TME from a “cold” to a “hot” state hence triggering the host response to tumor cells. Furthermore, our data also showed that this immune alteration is linked to a profound rewiring of the cytokine milieu as observed in the cytokine array. A previous study on lung and ovarian cancer already demonstrated that the targeting of CD24, via a blocking antibody, modifies the tumor secretome and reduces tumor growth *in vivo* (43). Whether these effects rely solely on platelets and, moreover, on their early or later recruitment within the tumor bed is still unknown. Indeed, platelets deeply contribute to the reshaping of the TME engaging in a feed-forward communication with TC both through secreted factors or direct exchange (44). In addition, platelets have already been described to infiltrate established primary tumors and activate in contact of TC expressing CD24 (16). Based on these pieces of evidence, we can speculate that CD24-mediated platelets binding influence metastatic outgrowth by *i*) promoting TC colonization and *ii*) rewiring the TiME towards an immunosuppressive one. Altogether, our results suggest that CD24 is, in part, responsible for the differential binding of platelets to TC and the subsequent pro-metastatic function of platelets. In addition, these findings identify CD24 as a potential druggable target to counteract TC-platelet interaction and metastatic progression, avoiding the collateral hemostatic perturbations of classical anti-platelet agents.

Acknowledgements

We thank all members of JGG and PM teams for their constant discussions on this topic. Image acquisition was performed on the Imaging Platform of the CRBS, PIC-STRA UMS 38, Inserm, Unistra. This work has been directly funded by the French National Institute for Cancer (INCa) grant (PLBIO 2023-173) and by the support of the Ligue Contre le Cancer (labelisation), the Association Ruban Rose, and the SATT Conectus (Strasbourg). VM was supported by a fellowship from the French Ministry of Science (MESRI) and a fourth-year thesis fellowship from the Fondation ARC pour la recherche sur le cancer as well as by the Association Ruban Rose. C.L. and S.M.G.T. are supported by INCa (PLBIO 2023-173). LB is supported by a doctoral fellowship from the Fondation pour la Recherche Médicale.

Authorship contributions

Conceptualization, V.M., C.L., M.J.G-L., O.L., and J.G.G.; Methodology, O.L.; Investigation, V.M., C.L., C.M., S.M.G.T., L.B., A.F., L.P., and O.L.; Formal Analysis, V.M., C.L., and O.L.; Writing – Original Draft, V.M., C.L., O.L., J.G.G.; Writing – Review & Editing, V.M., C.L., O.L., P.M.; J.G.G.; Supervision, P.M., and J.G.G.; Funding Acquisition, P.M. and J.G.G.

Material and Methods

Murine RNA-sequencing analysis

Bulk RNA-sequencing data of 4T1 and 67NR cells obtained by Affymetrix microarray were downloaded from the Gene Expression Omnibus (GEO) database (45) under accession number PRJNA106771. Bulk RNA-sequencing data of 4T1 and B16F10 cells obtained by Illumina HiSeq 2000 were downloaded from the European Nucleotide Archive (ENA) at EMBL-EBI (https://www.ebi.ac.uk/ena/browser/search) under the accession numbers PRJEB5797 (4T1 cells) and PRJEB5299 (B16F10 cells). Sequence reads were mapped to *Mus musculus* mm10 using STAR to obtain a BAM (Binary Alignment Map) file. An abundance matrix was generated based on read counts identified by FeatureCounts.

Human tumor bulk RNA-sequencing analysis

Gene expression levels and survival analysis. RNA-sequencing data regarding expression levels for *CD24* and *PODXL* from human tumors and matched healthy tissues were downloaded as $\log_2$ (normalized counts +1) values from UCSC Xena (46) (https://xenabrowser.net) with the query "TCGA Breast Cancer (BRCA)". To analyze CD24 expression during TNBC progression, patients were classified according to their lymph node positivity in the Miller cohort (47) and the TCGA BRCA dataset. For global survival analysis, patients were stratified into high *versus* low *CD24* or *PODXL* expression using their median expression values. For cancer progression survival and progression-free analyses, patients were divided in two groups (LN^{pos} and LN^{neg}) based on their lymph node positivity and stratified into high *versus* low *CD24* expression using their median expression values. For survival analyses of TNBC subtypes, data were retrieved using the Pronostic module of bc-GenExMiner (https://bcgenex.ico.unicancer.fr/) (48). Patient data extracted from GSE33926, GSE12276, GSE19615, GSE21653, GSE76124, GSE58812, GSE83937 were categorized into BLIS, BLIA, LAR and MLIA subtypes and stratified into high *versus* low *CD24* expression using their median expression values. Kaplan-Meier plots were generated and analyzed using Prism 9.0.

Tumor microenvironment landscape assessment. Bulk RNA-sequencing data of primary breast cancer and matched lung metastatic lesions obtained by Illumina HiSeq 2000 were downloaded from the Gene Expression Omnibus (GEO) database (45) under accession number PRJNA794830. Sequence reads were mapped to *Homo sapiens* hg19 using STAR to obtain a BAM (Binary Alignment Map) file. An abundance matrix was generated based on read counts identified by HTSeq-count. Normalized bulk RNA-sequencing data were used as an input in xCell (http://xCell.ucsf.edu/) (49) to quantify relative cell type abundance within primary and metastatic TME.

Genes correlation. The Spearman correlation coefficient ρ was calculated with the Gene_Corr module of TIMER2.0 (http://timer.comp-genomics.org/) (50) to evaluate the co-expression patterns between *GP6* and the following genes: *CD24*, *CD44*, *SELPLG*, *PODXL*, *PDPN*, *ITGAV*, *ITGB3*, *CD97*, and *LGALS3* in the TNBC subset of the TCGA BRCA cohort.

Single-cell RNA-sequencing analysis

Single-cell RNA-sequencing data from (24) were accessed on the Broad Institute Single Cell portal (https://singlecell.broadinstitute.org/single_cell) with the query "*CD24*" and "*PODXL*". Mean gene expressions at the single cell level for each annotated cell types and percentage of expressing cells were extracted from the dot plot representation.

Cell culture

The mouse breast cancer cell lines 4T1, 67NR, AT3, D2A1 and the mouse melanoma cell line B16F10, were cultured under standard conditions (37°C, 5% CO_2) using RPMI-1640, supplemented with 10% FBS and 1% penicillin-streptomycin solution. The human embryonic kidney HEK293T cell line was cultured under standard conditions (37°C, 5% CO_2) using DMEM, supplemented with 10% FBS and 1% penicillin-streptomycin solution. Cell viability *in vitro* was assayed before experiment by a Countess 3® automated cell counter (ThermoFisher).

Generation of 4T1 sub-lines

Plasmid construction. Control or CD24 double stranded oligos targeting sequences (**Table S1**) were inserted into the AgeI to EcoRI sites of pLKO.1 vector (Addgene #10878).

Lentivirus production. HEK293T cells were seeded in a 6 well plate and transfected using JetPrime reagent (Polyplus, #101000027) with either pLKO.1-shScramble or pLKO.1-shCD24, together with pLP1, pLP2 and pLP3/VSV-G lentiviral packaging plasmids (Invitrogen). Two days later, the viral lentivirus-containing supernatant was filtered through a 0.22µm filter and the viral particles were precipitated using the Lenti-X concentrator (Clontech, #PT4421-2). After centrifugation at 1500*g* during 45 min at 4°C, the high-titer virus-containing pellets were resuspended in 1 mL of PBS and aliquoted before storage at -80°C.

4T1 cells transduction. 4T1-Luc cells were seeded in a 6 well plate and transduced with one aliquot (100µL) of pLKO.1-shScramble or pLKO.1-shCD24 lentivirus, in the presence of 5µg/mL of polybrene (Sigma Aldrich, #H9268). Two days later, transduced 4T1-Luc cells were selected with blasticidin at 5 µg/mL (Sigma Aldrich, #15205-100MG), to generate the stable 4T1-Luc-shScramble or shCD24 sublines.

RT-qPCR analysis.

To measure CD24 predominant (201) and minor (202) isoforms expression, total RNA was extracted using TRI Reagent (Molecular Research Center). Next, complementary DNA (cDNA) was prepared with the High-Capacity cDNA Reverse Transcription Kit (Applied Biosystems #4368814), according to the manufacturer's instructions. Semi-quantitative PCR analysis on each biological sample was performed using technical replicates with the FastStart Universal SYBR Green Probe Master (ROX) mix for CD24 isoforms or the TaqMan system for the GAPDH housekeeping gene on a 7500 Real-Time PCR system. The cDNA concentration of target genes was normalized by amplification of GAPDH and fold changes in gene expression were obtained using the $2^{-\Delta\Delta Ct}$ method. Custom primers for CD24 isoforms were CD24_201 (Forward: TCTCTTTGGAATTGAACGTTTTG; Reverse: TGCCTGGCACATGTTAATTACT) and CD24_202 (Forward: TCGTCTTCCCCTTCTCAGG; Reverse: TCTGGTGGTAGCGTTACTTGG). TaqMan probe for GAPDH (Mm99999915_g1).

CD24 surface expression

Murine tumor cells (4T1 native, 4T1 shScramble, 4T1 shCD24, 67NR or B16F10) were washed with EDTA 0.48 mM (Versene, Gibco) and gently detached using a 0.25% trypsin-0.02% EDTA solution (Gibco). After a wash in media containing 10% FBS, cells were resuspended in PBS containing 2% FBS and 2mM EDTA. Murine tumor cells were stained with FITC anti-CD24 (1:200, BioLegend, clone M1/69) or its control isotype (Rat IgG2bk, eBioscience, clone eB149/10H5) for 15 minutes at 4°C. Samples were acquired with Attune NxT (Invitrogen) flow cytometer and data were analyzed using FlowJo™ v10 Software (ThreeStar).

Citrated platelet-rich plasma preparation

Murine blood was collected by aortic puncture in sodium citrate (0.315%). Citrated platelet-rich plasma (cPRP) was obtained by centrifuging whole blood in microtubes during 1 min at 1,900*g* at 37°C. The platelet count was adjusted to $300x10^3$/µl with citrated platelet-free plasma (cPFP). Mice were anesthetized (intra-peritoneal, *i.p.*, ketamine 100mg/kg, xylazine 10mg/kg) during the procedure and sacrificed by cervical dislocation at the end.

Platelet binding to tumor cell

For TC-platelet interaction, 6,000 tumor cells (4T1 native, 4T1 shScramble, 4T1 shCD24, 67NR or B16F10) were seeded per well on a 12 wells chamber and let to adhere overnight in complete medium. The following day, cPRP was added to each well at the ratio of 500 platelet/cell and let to interact for 30 minutes at 37°C 5% CO_2 in PBS. During the last two minutes of interaction, Wheat Germ Agglutinin-iFluor 488 (10µg/mL) was added. After three PBS washes, cells were fixed in PFA 0.5% in PBS for 20 minutes at room temperature. Cells were washed three times and stained with Alexa Fluor 647 coupled anti-RAM.1 antibodies (2µg/mL) for 1 hour at room temperature. Slides were then washed and mounted in Fluoromount-G™ with DAPI. Images were acquired with 60x/water objective at Olympus Spinning disk confocal microscope. A z-stack covering the full height of the tumor cell was acquired to ensure that only platelets in direct contact with the cells were imaged. Maximum intensity z-projections were generated using Fiji 2.15.1, and the number platelet engaging in interactions with tumor cell was manually quantified. Final data processing was performed in Excel 6.0 and GraphPad Prism 9.5 for statistical analysis.

Platelet circularity

To assess platelet circularity, images acquired for TC-platelet interaction were processed with Fiji 2.15.1. Fluorescence channels were split and platelet fluorescence, corresponding to anti-RAM.1 antibody signal, was segmented using the 'Default' thresholding method. Then, segmented platelet circularity was measure using the 'Analyzed particles' plugin. Data were post-processed in Excel 6.0 and GraphPad Prism 9.5 for statistical analysis.

Tumor cell clusters formation upon platelet binding

To form TC clusters in vitro, 2.10^6 4T1 shScramble or shCD24 cells in suspension were co-incubated with 2.10^7 murine cPRP for 2 hours at 37°C 5%CO_2 on a tilting tray. Cells were then washed with serum-free medium, and clusters were imaged on an inverted microscope. Macroscopic RGB images with identical zooming were loaded on ImageJ and clusters' area was measured after polygon selection definition.

Anoikis resistance assay upon platelet binding

To determine the response to anoikis clustered cells were plated at 500,000 cells/mL in 6-well ultra-low adherence plate in complete culture medium for 24h. At the end of the incubation, cells were harvested and stained with Zombie NIR (1:1,000; Biolegend, #423105) for 15 minutes at RT in the dark, prior to wash and signals' acquisition on an Attune NxT (Invitrogen) flow cytometer (20,000 events/conditions). Data were analyzed using FlowJo™ v10 Software (TreeStar).

Mice

All animals were housed and handled at INSERM (mouse facility agreement number: #C67-482-33) according to the guidelines of INSERM and the ethical committee of Alsace (CREMEAS), following French and European Union animal welfare guidelines (Directive 2010/63/EU on the protection of animals used for scientific purposes). All procedures were performed in accordance with French and European Union animal welfare guidelines and supervised by local ethics committee under the following APAFIS authorization #37433-2022052016445806.

Eight-week-old female wild-type immunocompetent BALB/c mice (028BALB/C; Charles River) were used in all experiments. Animals were housed in pathogen-free conditions with food and water *ad libitum* and appropriate enrichment (sterile pulp paper and coarsely litter). Mice were monitored daily, and terminally sick animals were euthanized under an approved protocol.

Experimental pulmonary metastasis assay and bioluminescent imaging

For the experimental pulmonary metastasis experiment, subconfluent 4T1-Luc (shScramble or shCD24) were washed with EDTA 0.48 mM (Versene, Gibco), gently detached using a 0.25% trypsin-0.02% EDTA solution (Gibco), washed in media containing 10% FBS, resuspended at 1.5 x 10^6 TC/mL in serum-free media, filtered through a 40 µm mesh (Falcon) and kept on ice until injection. Viability (>85% prior injection) was determined by Trypan Blue exclusion. Tumor cells (100µL, containing 150,000 cells) were injected through the lateral tail vein (intra-venously, *i.v.*) with a 25-gauge needle. *In vivo* imaging was performed shortly after to establish initial lung seeding (15 minutes post-injection) by *i.p.* injection of D-luciferin solution (150mg/kg) and subsequent signal acquisition in isofluorane (Isoflo, Zeotis)-anesthetized mice with an IVIS Lumina III (Perkin Elmer) imaging system. The rate of total light emission of

the lung metastatic area was analyzed using the Living Image software (Perkin Elmer) and expressed as numbers of photons emitted per second (p/s). Metastatic outgrowth was longitudinally followed by subsequent imaging at 1-, 3-, 7-, 10- and 14-days post-injection (dpi). For these later timepoints, the relative total light emission of the lung metastatic area compared to day 0 was calculated and represented.

Platelets depletion

Severe thrombocytopenia was induced by retro-orbital *i.v.* injection of 2 mg/kg of in-house-produced αGPIb antibody (RAM.6) (51) or IgG isotype control per mouse. RAM.6 or IgG were administrated the day before TC injection to induce a short thrombocytopenia (shortTCP). To validate platelet depletion, murine whole blood was collected into EDTA (6 mM) after severing the mouse tail. Platelet count and size were determined in an automatic cell counter (Element HT5, Heska).

Lung immune microenvironment analysis by flow cytometry

Single cell suspension was obtained from freshly harvested left lung lobes. Tissue was cut into approximately 2mm^3 pieces using a scalpel, then enzymatically digested with the mouse tumor dissociation kit (MiltenyiBiotec, #130-096-730) at 37°C for 42 minutes using the gentleMACS Octo Dissociator (MiltenyiBiotec) according to manufacturer's protocol. Cell suspension was filtered through a 50µm mesh and red blood cells were lysed in ACK Buffer [150mM NH_4Cl, 10mM $KHCO_3$, 0.1mM Na_2EDTA]. Non-viable cells were stained with Fixable Viability Dye-eFluor™780 (1:1,000; eBioscience, #65-0865-14) for 15 minutes at room temperature in the dark. Aspecific antibodies' binding was minimized with anti-CD32/CD16 blocking antibody (TruStain FcX 1:50, Biolegend #101320) for 20 minutes at 4°C. Primary conjugated (**Table S1**) were incubated for 15 minutes at 4°C. Samples were acquired with Attune NxT (Invitrogen) flow cytometer and data were analyzed using FlowJo™ v10 Software (ThreeStar). Gating strategies are displayed in Fig.S5.

Tissue array

Tissue homogenates were prepared according to manufacturer's instructions (Mouse angiogenesis kit (#ARY0015) and Cytokine panel kit (#ARY006)). Briefly, lungs were collected and snap frozen in liquid nitrogen at time of sacrifice. Frozen tissues were dissociated with Bead Ruptor 4 dissociator (OMNI International) using 1.5mm Triple-

Pure High Impact Zirconium beads (Benchmark) in PBS containing Protease/Phosphatase inhibitors (Pierce). Triton X-100 (Sigma) at the 1% final concentration was added at the end of the process. Supernatants were obtained after spinning the homogenates at 10,000*g* for 5 minutes at frozen at -80°C until analysis. Three-hundred µg of proteins (quantified by Bradford assay – BioRad) were applied per membrane following manufacturer's instructions and incubated overnight at 4°C in end-to-end shaking. Membranes were revealed using iBright1500 (Invitrogen) after sequential exposure. Images were analyzed in Fiji 6.0. and data were then post-processed in Excel 6.0 and GraphPad Prism 9.5 for statistical analysis.

Tissue histology and immunofluorescence

At the sacrifice, lungs were inflated in OCT (Tissue freezing media, Leica) before embedding and freezing at -80°C. Slices (7µm) were cut on SuperFrost UltraPlus slides (Thermo Fisher Scientific). After rehydration in PBS, slices were permeabilized in with 0.3% Triton X-100 in PBS for two consecutive 10 minutes incubations. Aspecific antibody binding was minimized by incubating for 1 hour in a Histoblock solution (3% bovine serum albumin-BSA, 5% non-heat inactivated FBS, 20mM $MgCl_2$ and 0.3% Triton X-100, in PBS). Immunostaining was performed by diluting the primary antibodies (**Table S1**) in the Histoblock solution and incubating them overnight at 4°C. After two washes in PBS, the appropriate secondary antibodies (**Table S1**) were incubated for 1 hour at room temperature in BSA 5% before mounting (Fluoromount/DAPI). Background and nonspecific staining controls were used. Slides were imaged with a 20X/NA0.8 air-objective on a Slide Scanner microscope VS200 (Olympus). Images were processed using QuPath 0.5.0 (52) and analyzed using consecutive thresholding methods and/or positive cell detection plug-in ($Ki67^+$ analysis). For the analyses of metastatic areas, metastases were manually annotated as area presenting high PanCK staining. Data were then post-processed in Excel 6.0 and GraphPad Prism 9.5 for statistical analysis.

Statistics

Statistical analysis was performed with GraphPad Prism 9.5. The normal distribution of the data sets was assessed by the Shapiro–Wilk normality test. According to the number of data sets compared, Student's t-test test or One-way ANOVA test with original FDR method of Benjamini-Hochberg were applied (*$p<0.05$; **$p<0.01$,

***p<0.001, ****p<0.0001). In all cases, the α-level was set at 0.05. All the data in graphs were presented as median ± standard deviation.

Data Availability

All data supporting the findings of this study are available from the corresponding authors on reasonable request.

References

1. Follain G, Herrmann D, Harlepp S, Hyenne V, Osmani N, Warren SC, et al. Fluids and their mechanics in tumour transit: shaping metastasis. Nature Reviews Cancer. Nature Research; 2020;20:107–24.
2. Yu M, Bardia A, Wittner BS, Stott SL, Smas ME, Ting DT, et al. Circulating Breast Tumor Cells Exhibit Dynamic Changes in Epithelial and Mesenchymal Composition. Science. 2013;339:580–4.
3. Labelle M, Begum S, Hynes RO. Platelets guide the formation of early metastatic niches. Proceedings of the National Academy of Sciences. National Academy of Sciences; 2014;111:E3053–61.
4. Egan K, Cooke N, Kenny D. Living in shear: platelets protect cancer cells from shear induced damage. Clin Exp Metastasis. 2014;31:697–704.
5. Nieswandt B, Hafner M, Echtenacher B, Männel DN. Lysis of tumor cells by natural killer cells in mice is impeded by platelets. Cancer research. 1999;59:1295–300.
6. Schumacher D, Strilic B, Sivaraj KK, Wettschureck N, Offermanns S. Platelet-Derived Nucleotides Promote Tumor-Cell Transendothelial Migration and Metastasis via P2Y2 Receptor. Cancer Cell. 2013;24:130–7.
7. Rayes J, Watson SP, Nieswandt B. Functional significance of the platelet immune receptors GPVI and CLEC-2. Journal of Clinical Investigation. 2019;129:12–23.
8. Garcia-Leon MJ, Liboni C, Mittelheisser V, Bochler L, Follain G, Mouriaux C, et al. Platelets favor the outgrowth of established metastases. Nat Commun. 2024;15:3297.
9. Barkal AA, Brewer RE, Markovic M, Kowarsky M, Barkal SA, Zaro BW, et al. CD24 signalling through macrophage Siglec-10 is a target for cancer immunotherapy. Nature. 2019;572:392–6.
10. Kristiansen G, Winzer K-J, Mayordomo E, Bellach J, Schlüns K, Denkert C, et al. CD24 expression is a new prognostic marker in breast cancer. Clin Cancer Res. 2003;9:4906–13.
11. Meyer MJ, Fleming JM, Ali MA, Pesesky MW, Ginsburg E, Vonderhaar BK. Dynamic regulation of CD24 and the invasive, CD44posCD24negphenotype in breast cancer cell lines. Breast Cancer Res. 2009;11:R82.
12. Aigner S, Sthoeger ZM, Fogel M, Weber E, Zarn J, Ruppert M, et al. CD24, a mucin-type glycoprotein, is a ligand for P-selectin on human tumor cells. Blood. 1997;89:3385–95.
13. Aigner S, Ramos CL, Hafezi-Moghadam A, Lawrence MB, Friederichs J, Altevogt P, et al. CD24 mediates rolling of breast carcinoma cells on P-selectin. FASEB j. 1998;12:1241–51.
14. Kim YJ, Borsig L, Varki NM, Varki A. P-selectin deficiency attenuates tumor growth and metastasis. Proc Natl Acad Sci USA. 1998;95:9325–30.
15. Friederichs J, Zeller Y, Hafezi-Moghadam A, Gröne HJ, Ley K, Altevogt P. The CD24/P-selectin binding pathway initiates lung arrest of human A125 adenocarcinoma cells. Cancer Res. 2000;60:6714–22.
16. Kuznetsov HS, Marsh T, Markens BA, Castaño Z, Greene-Colozzi A, Hay SA, et al. Identification of Luminal Breast Cancers That Establish a Tumor-Supportive Macroenvironment Defined by Proangiogenic Platelets and Bone Marrow–Derived Cells. Cancer Discovery. 2012;2:1150–65.
17. Zimmerman GA. Two by two: The pairings of P-selectin and P-selectin

glycoprotein ligand 1. Proc Natl Acad Sci USA. 2001;98:10023–4.
18. Suzuki-Inoue K, Kato Y, Inoue O, Kaneko MK, Mishima K, Yatomi Y, et al. Involvement of the Snake Toxin Receptor CLEC-2, in Podoplanin-mediated Platelet Activation, by Cancer Cells. Journal of Biological Chemistry. 2007;282:25993–6001.
19. Alves CS, Burdick MM, Thomas SN, Pawar P, Konstantopoulos K. The dual role of CD44 as a functional P-selectin ligand and fibrin receptor in colon carcinoma cell adhesion. American Journal of Physiology-Cell Physiology. 2008;294:C907–16.
20. Lonsdorf AS, Krämer BF, Fahrleitner M, Schönberger T, Gnerlich S, Ring S, et al. Engagement of αIIbβ3 (GPIIb/IIIa) with αvβ3 Integrin Mediates Interaction of Melanoma Cells with Platelets. Journal of Biological Chemistry. 2012;287:2168–78.
21. Ward Y, Lake R, Faraji F, Sperger J, Martin P, Gilliard C, et al. Platelets Promote Metastasis via Binding Tumor CD97 Leading to Bidirectional Signaling that Coordinates Transendothelial Migration. Cell Reports. 2018;23:808–22.
22. Mammadova-Bach E, Gil-Pulido J, Sarukhanyan E, Burkard P, Shityakov S, Schonhart C, et al. Platelet glycoprotein VI promotes metastasis through interaction with cancer cell-derived Galectin-3. Blood. Blood; 2020;135:1146–60.
23. Aslakson CJ, Miller FR. Selective events in the metastatic process defined by analysis of the sequential dissemination of subpopulations of a mouse mammary tumor. Cancer Res. 1992;52:1399–405.
24. Wu SZ, Roden DL, Wang C, Holliday H, Harvey K, Cazet AS, et al. Stromal cell diversity associated with immune evasion in human triple-negative breast cancer. The EMBO Journal. 2020;39:e104063.
25. Harbeck N, Penault-Llorca F, Cortes J, Gnant M, Houssami N, Poortmans P, et al. Breast cancer. Nat Rev Dis Primers. 2019;5:66.
26. Kaur J, Chandrashekar DS, Varga Z, Sobottka B, Janssen E, Kowalski J, et al. Distinct Gene Expression Profiles of Matched Primary and Metastatic Triple-Negative Breast Cancers. Cancers. 2022;14:2447.
27. Garcia-Recio S, Hinoue T, Wheeler GL, Kelly BJ, Garrido-Castro AC, Pascual T, et al. Multiomics in primary and metastatic breast tumors from the AURORA US network finds microenvironment and epigenetic drivers of metastasis. Nature Cancer. 2023;4:128–47.
28. Kanaji S. Thrombopoietin initiates demethylation-based transcription of GP6 during megakaryocyte differentiation. Blood. 2005;105:3888–92.
29. Holmsen H. Significance of testing platelet functions *in vitro*. Eur J Clin Investigation. 1994;24:3–8.
30. Aceto N, Bardia A, Miyamoto DT, Donaldson MC, Wittner BS, Spencer JA, et al. Circulating Tumor Cell Clusters Are Oligoclonal Precursors of Breast Cancer Metastasis. Cell. 2014;158:1110–22.
31. Labelle M, Hynes RO. The Initial Hours of Metastasis: The Importance of Cooperative Host–Tumor Cell Interactions during Hematogenous Dissemination. Cancer Discovery. 2012;2:1091–9.
32. Baumann P, Cremers N, Kroese F, Orend G, Chiquet-Ehrismann R, Uede T, et al. CD24 Expression Causes the Acquisition of Multiple Cellular Properties Associated with Tumor Growth and Metastasis. Cancer Research. 2005;65:10783–93.
33. Pfirschke C, Engblom C, Gungabeesoon J, Lin Y, Rickelt S, Zilionis R, et al. Tumor-Promoting Ly-6G+ SiglecFhigh Cells Are Mature and Long-Lived Neutrophils. Cell Reports. 2020;32:108164.
34. Grisaru-Tal S, Dulberg S, Beck L, Zhang C, Itan M, Hediyeh-zadeh S, et al. Metastasis-Entrained Eosinophils Enhance Lymphocyte-Mediated Antitumor Immunity. Cancer Research. 2021;81:5555–71.

35. Sternlicht MD, Lochter A, Sympson CJ, Huey B, Rougier J-P, Gray JW, et al. The Stromal Proteinase MMP3/Stromelysin-1 Promotes Mammary Carcinogenesis. Cell. 1999;98:137–46.
36. Itoh T, Tanioka M, Matsuda H, Nishimoto H, Yoshioka T, Suzuki R, et al. Experimental metastasis is suppressed in MMP-9-deficient mice. Clinical & Experimental Metastasis. 1999;17:177–81.
37. Bleul CC, Fuhlbrigge RC, Casasnovas JM, Aiuti A, Springer TA. A highly efficacious lymphocyte chemoattractant, stromal cell-derived factor 1 (SDF-1). The Journal of experimental medicine. 1996;184:1101–9.
38. Gu-Trantien C, Loi S, Garaud S, Equeter C, Libin M, De Wind A, et al. CD4+ follicular helper T cell infiltration predicts breast cancer survival. J Clin Invest. 2013;123:2873–92.
39. Castellino F, Huang AY, Altan-Bonnet G, Stoll S, Scheinecker C, Germain RN. Chemokines enhance immunity by guiding naive CD8+ T cells to sites of CD4+ T cell–dendritic cell interaction. Nature. 2006;440:890–5.
40. Lee JH, Kim SH, Lee ES, Kim YS. CD24 overexpression in cancer development and progression: A meta-analysis. Oncol Rep [Internet]. 2009 [cited 2024 Sep 25];22. Available from: http://www.spandidos-publications.com/or/22/5/1149
41. Diacovo TG, Puri KD, Warnock RA, Springer TA, Von Andrian UH. Platelet-Mediated Lymphocyte Delivery to High Endothelial Venules. Science. 1996;273:252–5.
42. Chan S-H, Tseng H-J, Wang L-H. CD24a knockout transforms the tumor microenvironment from cold to hot by promoting tumor-killing immune cell infiltration in a murine triple-negative breast cancer model [Internet]. 2024 [cited 2024 Sep 25]. Available from: http://biorxiv.org/lookup/doi/10.1101/2024.07.15.603489
43. Salnikov AV, Bretz NP, Perne C, Hazin J, Keller S, Fogel M, et al. Antibody targeting of CD24 efficiently retards growth and influences cytokine milieu in experimental carcinomas. Br J Cancer. 2013;108:1449–59.
44. Li S, Lu Z, Wu S, Chu T, Li B, Qi F, et al. The dynamic role of platelets in cancer progression and their therapeutic implications. Nat Rev Cancer. 2024;24:72–87.
45. Edgar R, Domrachev M, Lash AE. Gene Expression Omnibus: NCBI gene expression and hybridization array data repository. Nucleic Acids Res. 2002;30:207–10.
46. Goldman MJ, Craft B, Hastie M, Repečka K, McDade F, Kamath A, et al. Visualizing and interpreting cancer genomics data via the Xena platform. Nat Biotechnol. 2020;38:675–8.
47. Miller LD, Smeds J, George J, Vega VB, Vergara L, Ploner A, et al. An expression signature for p53 status in human breast cancer predicts mutation status, transcriptional effects, and patient survival. Proc Natl Acad Sci USA. 2005;102:13550–5.
48. Jézéquel P, Campone M, Gouraud W, Guérin-Charbonnel C, Leux C, Ricolleau G, et al. bc-GenExMiner: an easy-to-use online platform for gene prognostic analyses in breast cancer. Breast Cancer Res Treat. 2012;131:765–75.
49. Aran D, Hu Z, Butte AJ. xCell: digitally portraying the tissue cellular heterogeneity landscape. Genome Biol. 2017;18:220.
50. Li T, Fu J, Zeng Z, Cohen D, Li J, Chen Q, et al. TIMER2.0 for analysis of tumor-infiltrating immune cells. Nucleic Acids Research. 2020;48:W509–14.
51. Strassel C, David T, Eckly A, Baas M, Moog S, Ravanat C, et al. Synthesis of GPIbβ with novel transmembrane and cytoplasmic sequences in a Bernard–Soulier patient resulting in GPIb-defective signaling in CHO cells. Journal of Thrombosis and

Haemostasis. 2006;4:217–28.
52. Bankhead P, Loughrey MB, Fernández JA, Dombrowski Y, McArt DG, Dunne PD, et al. QuPath: Open source software for digital pathology image analysis. Sci Rep. 2017;7:16878.

Figure legends

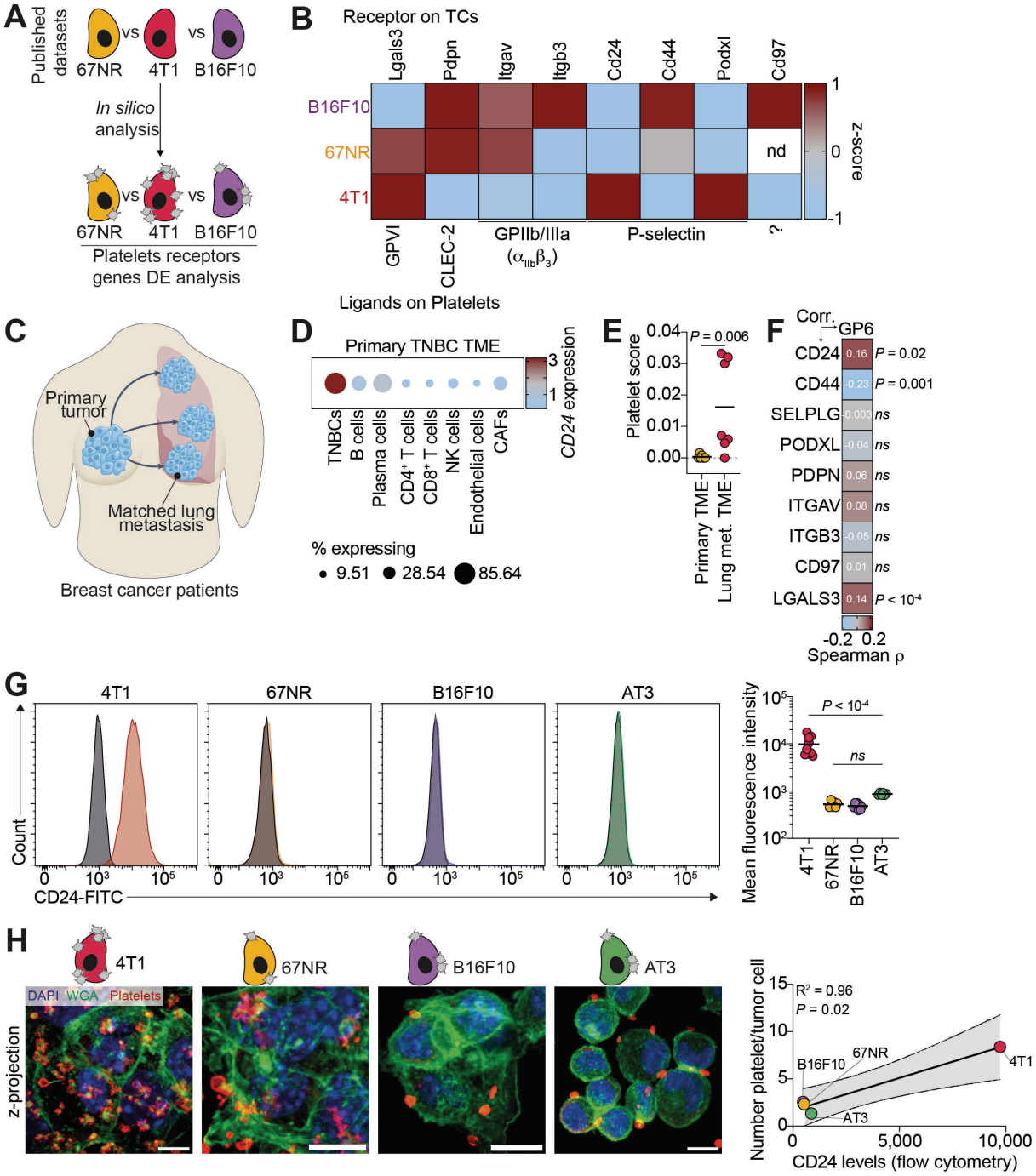

Figure 1 - Mittelheisser *et al.*

Figure 1. Platelet binding to TC scales with poor prognosis CD24 expression levels.

A. Infographics illustrating the pipeline of the *in silico* analysis. **B**. Heat-map showing Z-score values for RNA expression of platelet-cognate receptor on tumor cell (TC). Receptors on TC are represented on the top, while cognate receptors on platelet are

represented on the bottom. TC analyzed are listed on the left. **C**. Infographics illustrating breast cancer patients' samples. **D**. Bubble plot displaying *CD24* gene expression at the single-cell level across different cell types in the triple-negative breast cancer (TNBC) primary tumor microenvironment (TME). Bubble size represents percentage of *CD24*-expressing cells and color represent mean *CD24* expression. CAFs: Cancer Associated Fibroblasts. **E**. Platelet score value evaluating platelet infiltration in primary TNBC and their matched lung metastatic TME. Data are representative of 7 different patients from 2 independent clinical studies. Mann-Whitney test was applied after assessment of gaussian data distribution by Shapiro-Wilk test. **F**. Correlation between *GP6* and *CD24*, *CD44*, *SELPLG*, *PODXL*, *PDPN*, *ITGAV*, *ITGB3*, *CD97*, or *LGALS3* expression levels (Log_2 TPM) in the TNBC subset of the TCGA BRCA cohort (*n* = 191 patients). Color represents the value of Spearman ρ per correlation (legend on the bottom). **G**. Flow cytometry assessment of CD24 expression in selected TC. Left: Representative histograms of the relative expression levels of CD24-FITC. Isotype signal is represented in black in each graph. Right: Quantification of the mean fluorescent intensity signal for CD24-FITC. Data are presentative of between 6 to 9 independent experiments. One-way ANOVA with original FDR method of Benjamini-Hochberg was applied after assessment of gaussian distribution by Shapiro-Wilk test. **H**. *In vitro* platelet-TC interaction. Left: Representative confocal micrographs of platelet-TC binding. In green Wheat Germ Agglutinin (WGA)-iFluor488, in red platelet RAM.1 (Alexa Fluor 647), and in blue nuclei (DAPI). Scale bar = 10µm. Right: Pearson correlation between the number of platelets bound to tumor cell and mean CD24 expression levels on tumor cells – 4 xy pairs; $R^2 = 0.96$ – 95% confidence interval [0.31-0.99]. Number of platelets interacting with tumor cell were quantified from 10 fields of view from 2 independent experiments. MeanCD24 expression levels quantified by flow cytometry from G panel were used.

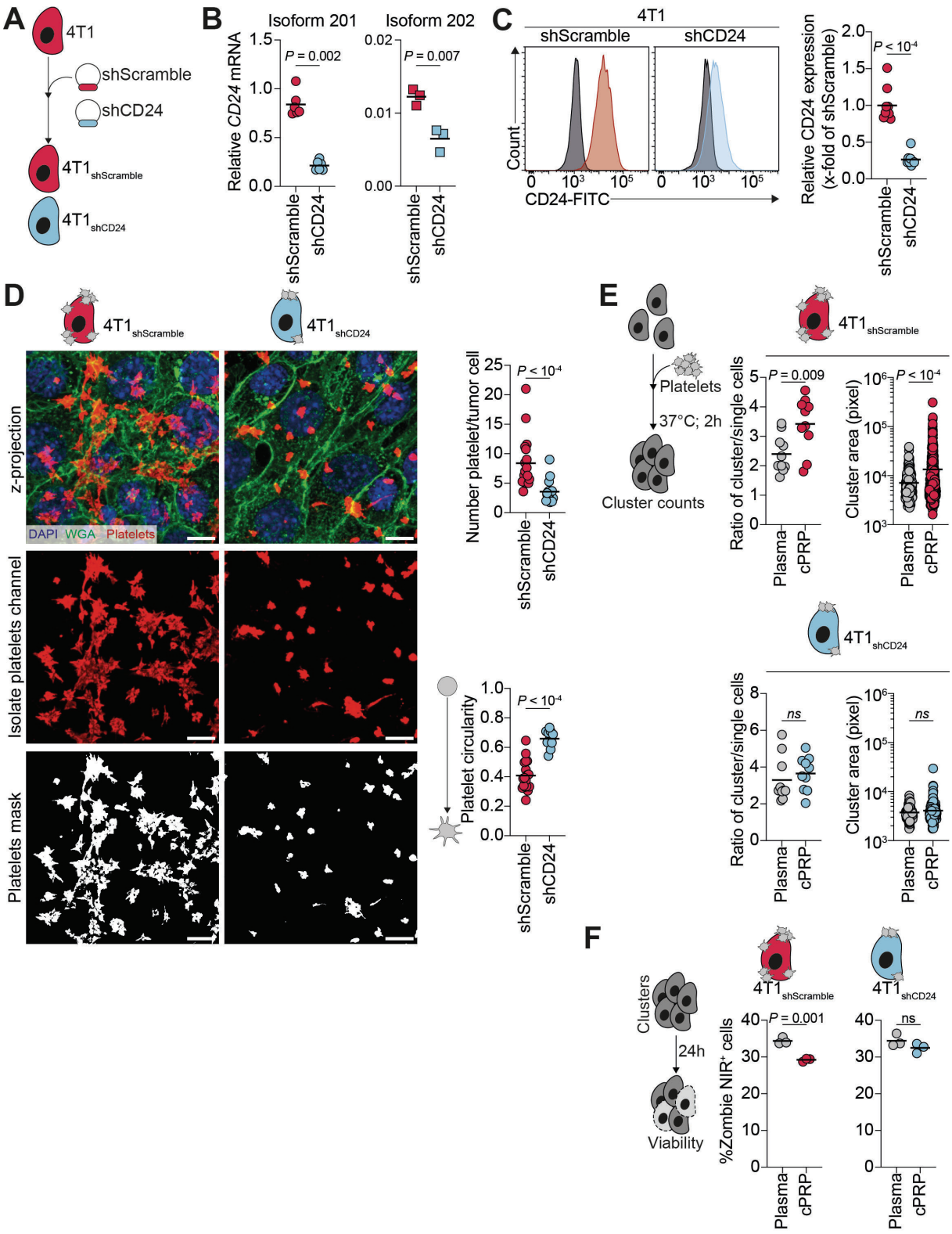

Figure 2 - Mittelheisser *et al.*

Figure 2. CD24-mediated binding tunes pro-metastatic function of platelets. A. Infographics illustrating the generation of shRNA-mediated CD24 knock-down 4T1 cells. **B**. 4T1 shScramble and 4T1 shCD24 cells expression of CD24 predominant isoform (201) mRNA expression calculated using the $2^{-\Delta\Delta Ct}$ method (housekeeping: *GAPDH*). Data are representative of 6 independent experiments. Mann-Whitney test was applied after assessment of gaussian data distribution by Shapiro-Wilk test. **C**. 4T1 shScramble and 4T1 shCD24 cells expression of CD24 minor isoform (202) mRNA expression calculated using the $2^{-\Delta\Delta Ct}$ method (housekeeping: *GAPDH*). Data are representative of 3 independent experiments. Student t-test was applied after assessment of gaussian data distribution by Shapiro-Wilk test. **C**. Flow cytometry assessment of CD24 expression 4T1 shScramble and 4T1 shCD24 cells. Left: Representative histograms of the relative expression levels of CD24-FITC. Isotype signal is represented in black in each graph. Right: Quantification of the mean fluorescent intensity signal for CD24-FITC as fold decrease compared to 4T1 shScramble signal. Data are representative of 10 independent experiments. Mann-Whitney test was applied after assessment of gaussian data distribution by Shapiro-Wilk test. **D**. *In vitro* platelet-TC interaction. Left top: Representative confocal micrographs of platelet-TC binding. In green Wheat Germ Agglutinin (WGA)-iFluor488, in red platelet RAM.1 (Alexa Fluor 647), and in blue nuclei (DAPI). Scale bar = 10µm. Left center: isolated platelet fluorescence channel. Left bottom: binary mask applied on isolated platelet fluorescence channel for circularity analysis. Right top: Quantification of the number of platelets bound per tumor cell. Right bottom: Quantification of platelet circularity. Data are representative of 10 fields of view from 2 independent experiments. Mann-Whitney test (number of platelet/tumor cell) and Student t-test (platelet circularity) were applied after assessment of gaussian data distribution by Shapiro-Wilk test. **E**. Tumor cell clustering upon platelet binding. Left: Infographics illustrating the experimental setting for the TC-platelet cluster formation *in vitro*. Right: Quantifications of the ratio of clusters per single cells and of the cluster area in absence (plasma) or presence (cPRP) of platelet. Ratio of clusters per single cells: Data are representative of 10 fields of view from 2 independent experiments. Student t-test (4T1 shScramble) and Mann-Whitney test (4T1 shCD24) were applied after assessment of gaussian data distribution by Shapiro-Wilk test. Cluster area: Data are representative of between 453 and 498 cells from 2 independent experiments. Mann-Whitney test was applied after assessment of gaussian data distribution by

Shapiro-Wilk test. **F**. Tumor cell cluster resistance to anoikis. Left: Infographics illustrating the experimental setting of the anoikis resistance assay. Right: Percentage of Zombie NIR^{pos} (dead) cells as quantified by flow cytometry at 24 hours post clusters formation in absence (plasma) or presence (cPRP) of platelet. Data are representative of 20,000 cells analyzed per conditions from 3 independent experiments. Student t-test was applied after assessment of gaussian data distribution by Shapiro-Wilk test.

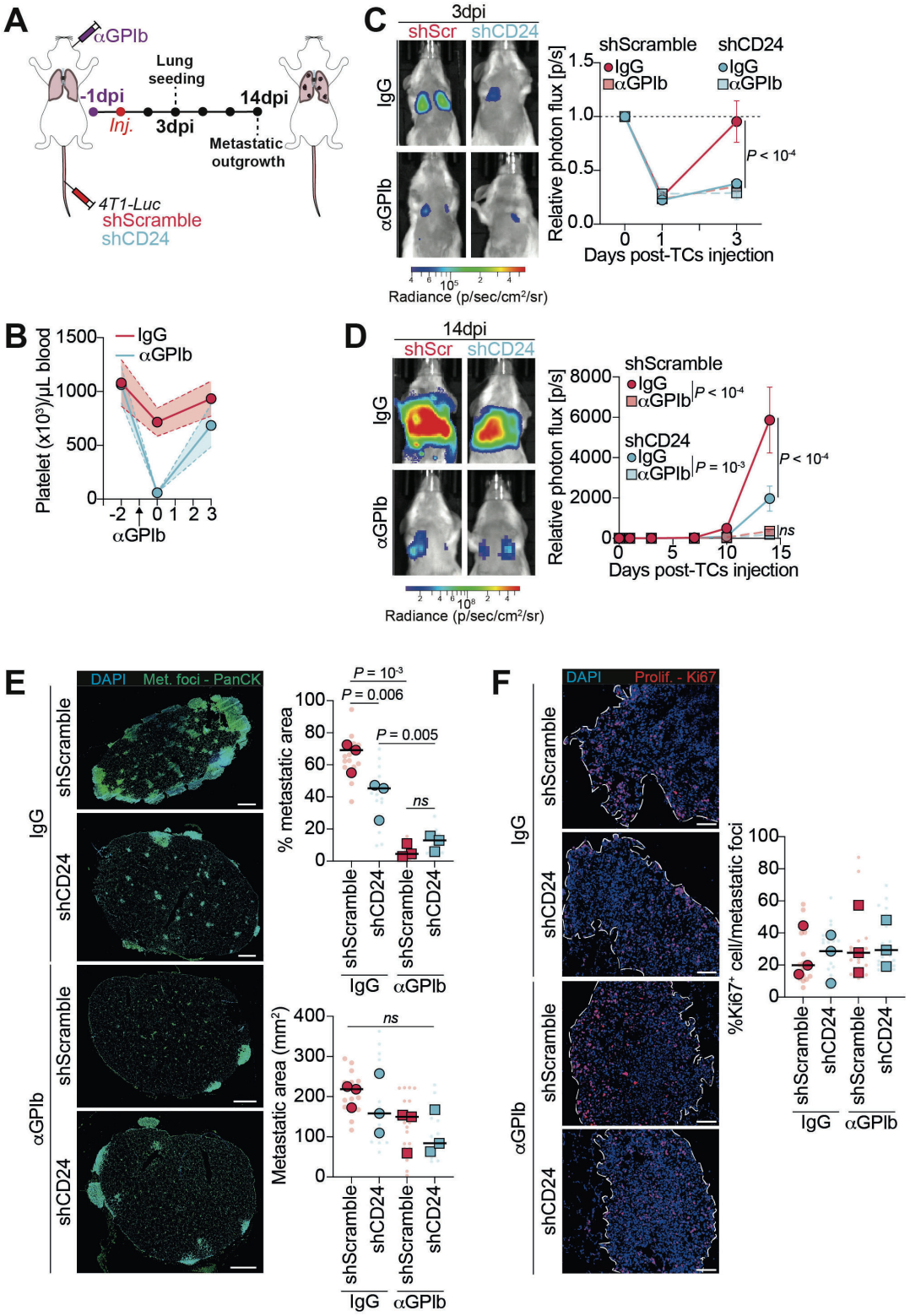

860 **Fig.3** - Mittelheisser *et al.*

861 **Figure 3. CD24-mediated platelets binding controls early steps of lung**
862 **colonization and subsequent metastatic outgrowth. A.** Infographics of short
863 thrombocytopenia regimen (short TCP) within the experimental metastasis model. **B.**

Platelet counts in IgG- and αGPIb-treated BALB/c mice. **C-D**. *In vivo* longitudinal Body Luminescence Index (BLI) measurement of 4T1 shScramble or 4T1 shCD24 lung seeding and metastatic outgrowth in normal and TCP mice. **C**. Left: Representative BLI images at 3 dpi (lung seeding). Right: Quantification of the BLI signal represented as the relative photon flux (p/s) on D_0 signal. Data are representative of 5 mice per group from 1 experiment. Two-way ANOVA corrected with original FDR method of Benjamini-Hochberg was applied. **D**. Left: Representative BLI images at 14 dpi (metastatic outgrowth). Right: Quantification of the BLI signal represented as the relative photon flux (p/s) on D_0 signal. Data are representative of 5 mice per group from 1 experiment. Two-way ANOVA corrected with original FDR method of Benjamini-Hochberg was applied. **E**. Metastatic burden immunofluorescence staining from OCT-embedded lungs at 14 dpi. Top: Representative images showing (from left to right): DAPI channel (nuclei), PanCK channel (metastatic foci) and merged channels. Scale bar = 1mm. Bottom: Quantification of percentage of metastatic area per slide and metastasis average size (metastatic area). Data are representative of 4 to 6 images per mouse from 3 mice per group and 1 experiment and displayed as mean per mouse (large points) superimposed on the value per single image (small points). One-way ANOVA with original FDR method of Benjamini-Hochberg was applied after assessment of gaussian distribution of the data by Shapiro-Wilk test. **F**. Metastatic tumor cell proliferation immunofluorescence staining from OCT-embedded lungs at 14dpi. Top: Representative images showing, from the left, DAPI channel (nuclei), Ki67 channel (proliferation) and channels merging. Scale bar = 100µm. Bottom: quantification of the percentage of $Ki67^{pos}$ cells per metastatic foci. Data are representative of 4 to 6 images per mouse from 3 mice per group and 1 experiment and displayed as mean per mouse (large points) superimposed on the value per single image (small points). One-way ANOVA with original FDR method of Benjamini-Hochberg was applied after assessment of gaussian distribution of the data by Shapiro-Wilk test.

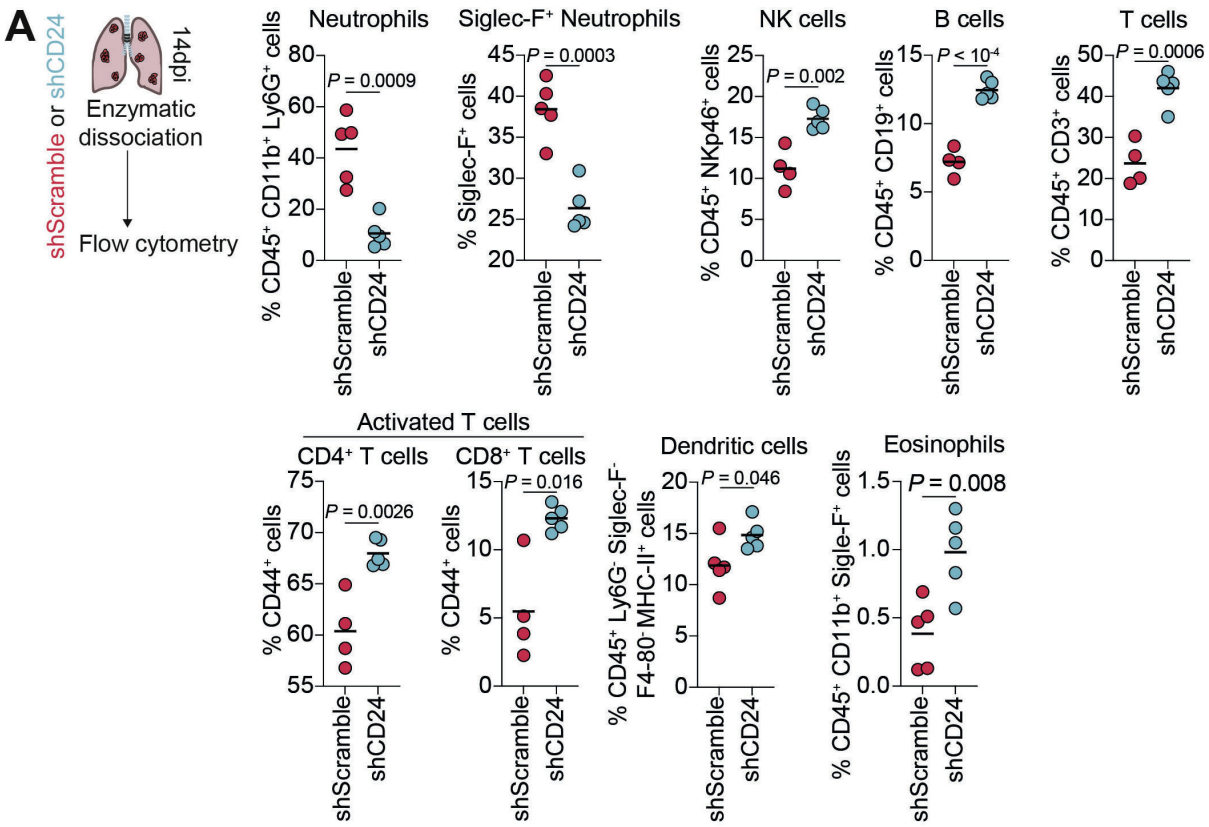

Figure 4 - Mittelheisser *et al.*

Figure 4. Early CD24-mediated tumor-cell-platelet interaction controls later tumor immune microenvironment composition. A. *Ex vivo* multiparametric flow cytometry of immune cells infiltrating mice bearing lung metastases. Left: Infographics describing the experimental scheme. Right: Immune cells population as percentage of their parental cells assessed by flow cytometry analysis at 14dpi. Data are representative of 4 mice per group from 1 experiment. Mann-Whitney (Activated $CD8^+$ T cells) or Student t-test (Neutrophils, Siglec-F^+ neutrophils, NK cells, B cells, T cells, Activated $CD4^+$ T cells, Dendritic cells, Eosinophils) were applied after assessment of gaussian data distribution by Shapiro-Wilk test.

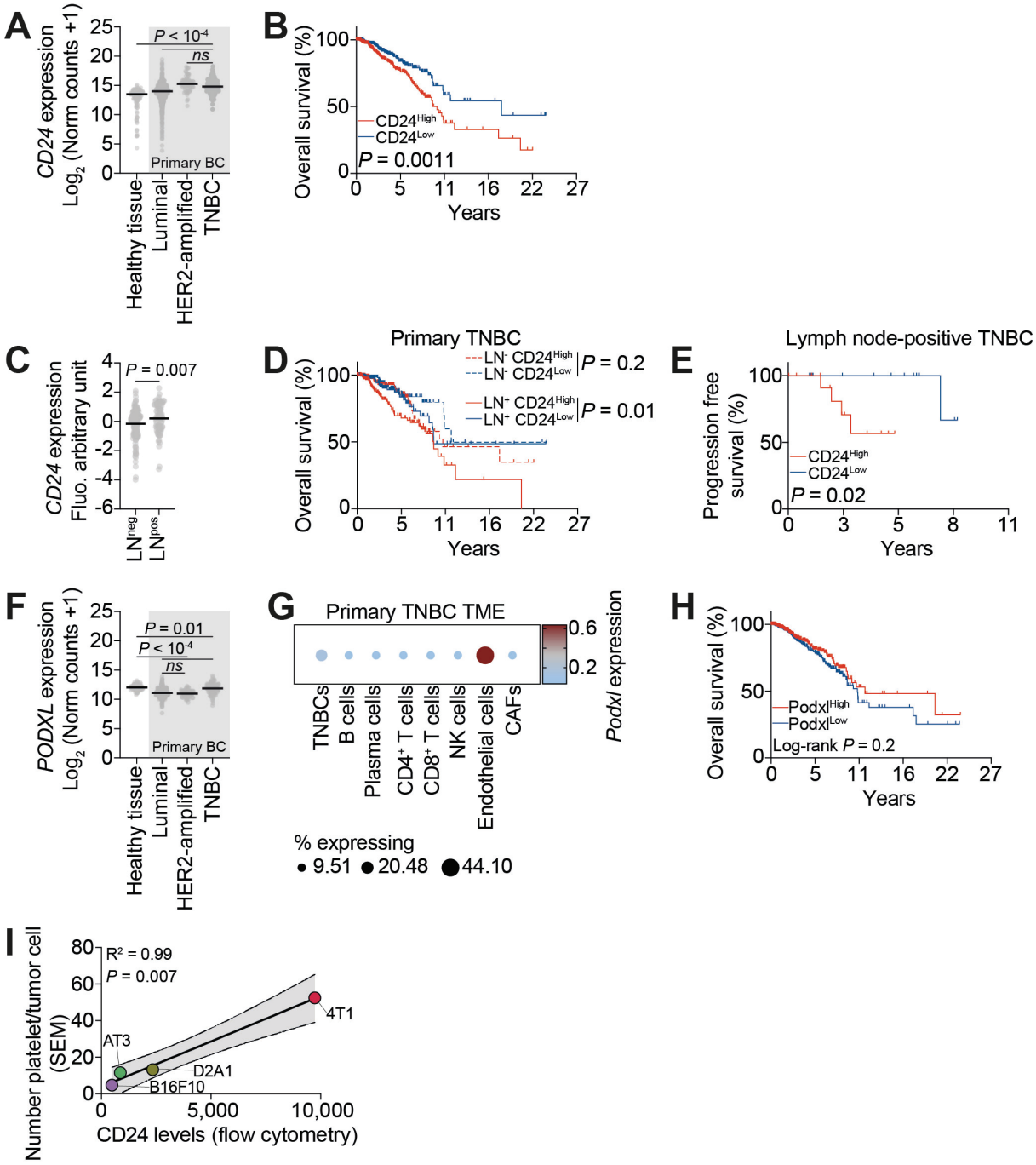

Figure S1 related to Fig.1 - Mittelheisser *et al.*

Supplementary Figure 1 related to Figure 1. A. *CD24* gene expression in healthy and neoplastic breast tissues, with primary breast cancer classified according to the main molecular subtypes. Kruskal-Wallis test with original FDR method of Benjamini-Hochberg was applied after assessment of gaussian distribution of the data by Shapiro-Wilk test. **B**. Overall survival percentage for breast cancer patients (n = 1080) with *CD24*^{high} versus *CD24*^{low} expression as defined by median. Two-sided P value

computed by a log-rank (Mantel-Cox) test. **C**. *CD24* gene expression (Affymetrix array) comparing patients without (LN^{neg}, $n = 158$) or with (LN^{pos}, $n = 84$) lymph node invasion. Mann-Whitney test was applied after assessment of gaussian data distribution by Shapiro-Wilk test. **D**. Overall survival percentage for LN^{pos} ($n = 405$) and LN^{neg} ($n = 384$) breast cancer patients with $CD24^{high}$ versus $CD24^{low}$ expression as defined by median. Two-sided *P* value computed by a log-rank (Mantel-Cox) test. **E**. Progression-free survival percentage for LN^{pos} ($n = 30$) breast cancer patients with $CD24^{high}$ versus $CD24^{low}$ expression as defined by median. Two-sided *P* value computed by a log-rank (Mantel-Cox) test. **F**. Podocalyxin (*PODXL*) gene expression in healthy and neoplastic breast tissues, with primary breast cancer classified according to the main molecular subtypes. Kruskal-Wallis test with original FDR method of Benjamini-Hochberg was applied after assessment of gaussian distribution of the data by Shapiro-Wilk test. **G**. Bubble plot displaying *PODXL* gene expression at the single-cell level across different cell types in the triple-negative breast cancer (TNBC) primary tumor microenvironment (TME). Bubble size represents percentage of *PODX*L-expressing cells and color represent mean *PODXL* expression. CAFs: Cancer Associated Fibroblasts. **H**. Overall survival percentage for breast cancer patients ($n = 1080$) with $PODXL^{high}$ versus $PODXL^{low}$ expression as defined by median. Two-sided *P* value computed by a log-rank (Mantel-Cox) test. **I**. Pearson correlation between the number of platelets bound to tumor cell and mean CD24 expression levels on tumor cells – 4 xy pairs; $R^2 = 0.99$ – 95% confidence interval [0.71-0.99]. Number of platelets interacting with tumor cell were quantified by scanning electron microscopy in (8). Mean CD24 expression levels were quantified by flow cytometry from Fig.1G.

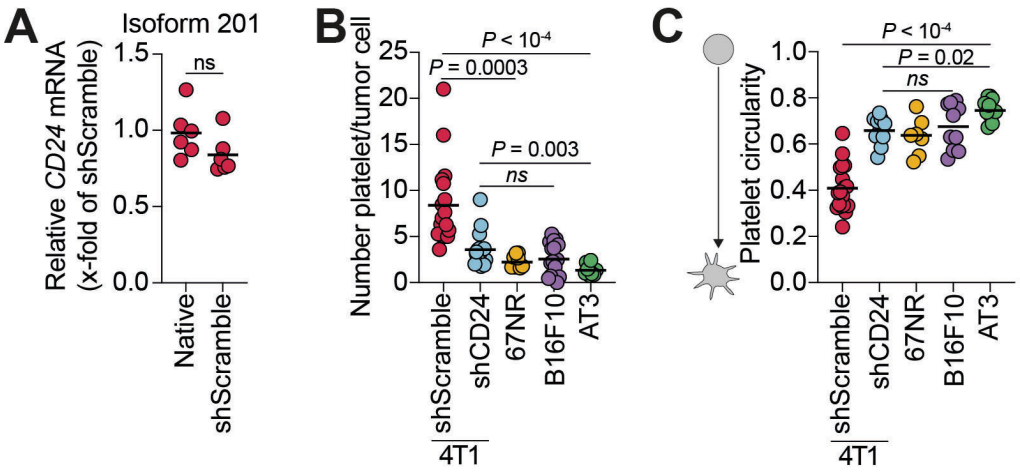

Figure S2 related to Fig.2 - Mittelheisser *et al.*

Supplementary Figure 2 related to Figure 2. A. 4T1 native and 4T1 shScramble cells expression of CD24 predominant isoform (201) mRNA expression calculated using the $2^{-\Delta\Delta Ct}$ method (housekeeping: *GAPDH*). Data are representative of 6 independent experiments. Mann-Whitney test was applied after assessment of gaussian data distribution by Shapiro-Wilk test. **B**. Number of platelets bound per tumor cell as quantified by immunofluorescence staining. Data are representative of 10 fields of view from 2 independent experiments. Kruskal-Wallis test with original FDR method of Benjamini-Hochberg was applied after assessment of gaussian distribution by Shapiro-Wilk test. **C**. Platelet circularity as measured by immunofluorescence staining. Data are representative of 10 fields of view from 2 independent experiments. One-way ANOVA with original FDR method of Benjamini-Hochberg was applied after assessment of gaussian distribution by Shapiro-Wilk test.

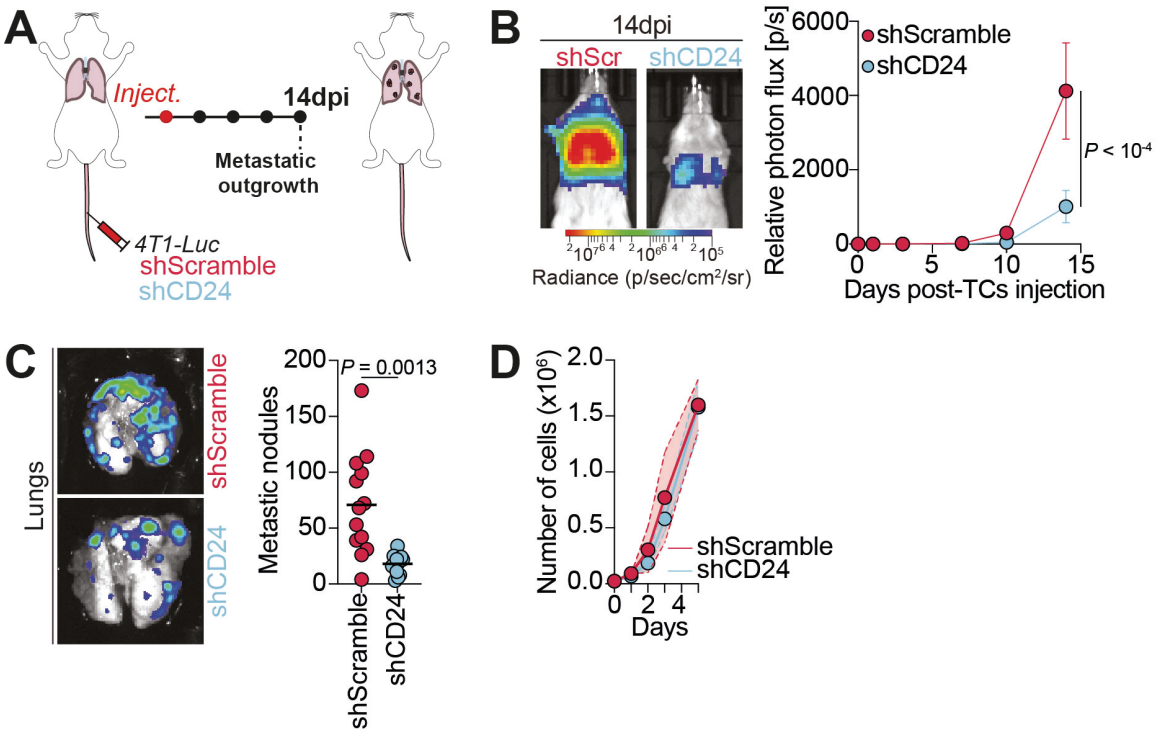

Figure S3 related to Fig.3 - Mittelheisser *et al.*

Supplementary Figure 3 related to Figure 3. A. Infographics of the experimental metastasis model. **B**. *In vivo* longitudinal Body Luminescence Index (BLI) measurement. Left: Representative BLI images at 14 dpi (metastatic outgrowth). Right: Quantification of the BLI signal represented as the relative photon flux (p/s) on D_0 signal. Data are representative of 10 mice from 2 independent experiments. Two-way ANOVA corrected with original FDR method of Benjamini-Hochberg was applied. **C**. Lungs macroscopic nodules count. Left: Representative BLI images of *ex vivo* lungs at 14 dpi. Right: Quantification of the number of metastatic nodules per lung. Data are representative of 13 mice from 3 independent experiments. Welch's t-test was applied after assessment of gaussian data distribution by Shapiro-Wilk test. **D**. Number of 4T1 shScramble and 4T1 shCD24 cells per culture days as measured by automatic counter. Data are presentative from 3 independent experiments. Two-way ANOVA corrected with original FDR method of Benjamini-Hochberg was applied.

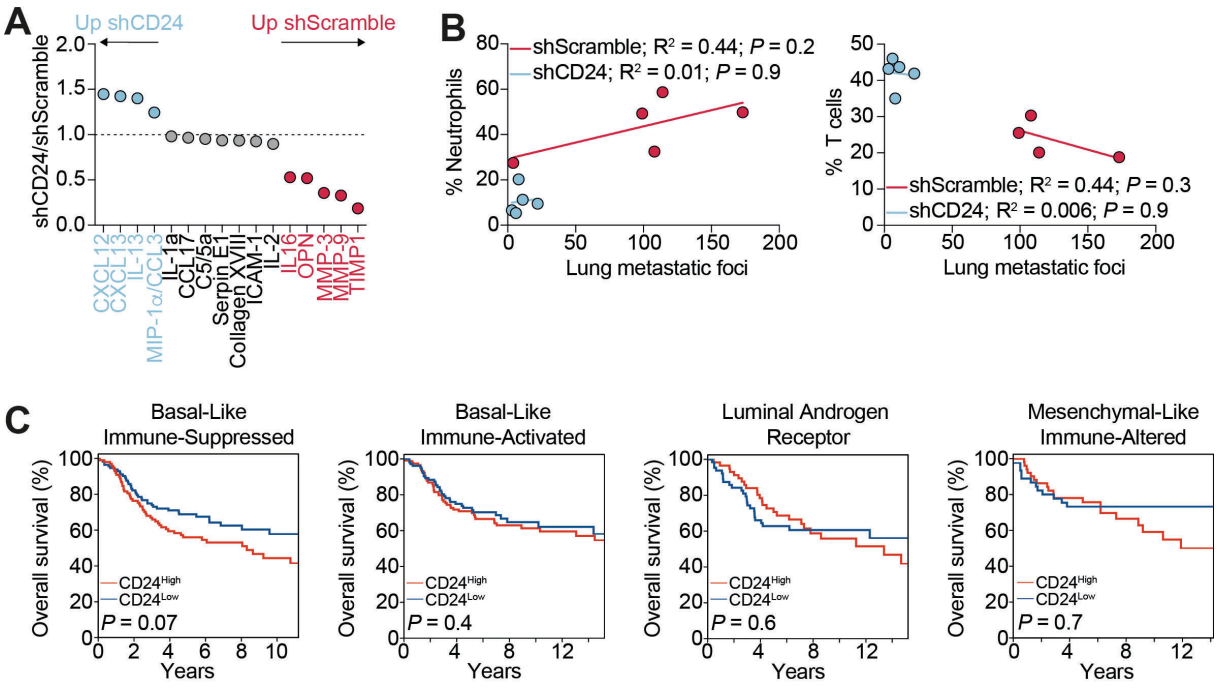

963 **Figure S4 related to Fig.4** - Mittelheisser *et al.*

964 **Supplementary Figure 4 related to Figure 4. A**. Tissue array analysis. Relative mean
965 signal per cytokine/chemokine is represented. Data are representative of 2 mice per
966 group from 1 experiment. **B**. Relationship between metastatic burden and infiltration of
967 neutrophils and T cells in the lungs of 4T1 shScramble- (n = 5) or 4T1 shCD24- (n =
968 5) bearing mice at 14 dpi. Pearson correlation was calculated on 5 xy pairs. **C**. Overall
969 survival percentage for TNBC breast cancer patients (n = 1,015) with different subtypes
970 based on *CD24*^{high} versus *CD24*^{low} expression as defined by median. Two-sided P
971 value computed by a log-rank (Mantel-Cox) test.

Chapter II

Biomechanical regulation of cancer immunosurveillance

Platelets not only interact with TCs and immune cells but also with stromal cells. Through these interactions, they participate to the global stiffening of tissues caused by extracellular matrix excessive deposition and remodeling (*Chapter I*). Mechanical changes constitute a signature trait of solid tumor that facilitates TCs invasion (Goetz et al., 2011; Levental et al., 2009; Provenzano et al., 2006). Accumulating evidences suggest that TCs are mechanically "dynamic and adaptable", a feature that confers them a selective advantage in almost all the steps of cancer progression (Gensbittel et al., 2021). Immune responses might be influenced by the mechanical aspects of tumor progression. Indeed, a growing body of evidence indicates that immune cells also sense and respond to mechanical signals from their environment. It remains unclear, however, how these mechanical aspects of immune surveillance are regulated during cancer progression.

This Chapter II is based on our review published in *Nature Nanotechnology* which highlights how mechanosensitive properties of immune cells influence their responses in various diseases and how targeting the biomechanical features of the disease milieu or immune cells is a promising strategy for manipulating therapeutic outcomes.

Publication associated to this chapter:

Mittelheisser V*, Gensbittel V*, Bonati L*, Li W*, Tang L[#], Goetz JG[#]. "***Evidence and therapeutic implications of biomechanically regulated immunosurveillance in cancer and other diseases.***"

Nature Nanotechnology 19:281–297 (2024) – doi:10.1038/s41565-023-01535-8

nature nanotechnology

Review article

https://doi.org/10.1038/s41565-023-01535-8

Evidence and therapeutic implications of biomechanically regulated immunosurveillance in cancer and other diseases

Received: 31 January 2023

Accepted: 26 September 2023

Published online: 29 January 2024

Check for updates

Vincent Mittelheisser[1,2,3,4,7], Valentin Gensbittel[1,2,3,4,7], Lucia Bonati[5,7], Weilin Li[5,7], Li Tang[5,6] ✉ & Jacky G. Goetz[1,2,3,4] ✉

Disease progression is usually accompanied by changes in the biochemical composition of cells and tissues and their biophysical properties. For instance, hallmarks of cancer include the stiffening of tissues caused by extracellular matrix remodelling and the softening of individual cancer cells. In this context, accumulating evidence has shown that immune cells sense and respond to mechanical signals from the environment. However, the mechanisms regulating these mechanical aspects of immune surveillance remain partially understood. The growing appreciation for the 'mechano-immunology' field has urged researchers to investigate how immune cells sense and respond to mechanical cues in various disease settings, paving the way for the development of novel engineering strategies that aim at mechanically modulating and potentiating immune cells for enhanced immunotherapies. Recent pioneer developments in this direction have laid the foundations for leveraging 'mechanical immunoengineering' strategies to treat various diseases. This Review first outlines the mechanical changes occurring during pathological progression in several diseases, including cancer, fibrosis and infection. We next highlight the mechanosensitive nature of immune cells and how mechanical forces govern the immune responses in different diseases. Finally, we discuss how targeting the biomechanical features of the disease milieu and immune cells is a promising strategy for manipulating therapeutic outcomes.

Disease progression is often associated with dynamic changes in mechanical properties at cellular and tissue levels. Such mechanical aspects of disease progression have been extensively studied in various pathological conditions, including cystic fibrosis[1], viral[2] and bacterial[3] infections, inflammation[4] and cancer[5]. Evidence shows that immune cells experience and respond to passive and active mechanical forces throughout their lifecycles. These mechanical forces have important roles in regulating the development, activation, migration, differentiation and effector functions of immune cells[6]. In particular, growing evidence has shown that T cells are mechanosensitive[7]. Upon cognate

[1]Tumor Biomechanics, INSERM UMR_S1109, Strasbourg, France. [2]Université de Strasbourg, Strasbourg, France. [3]Fédération de Médecine Translationnelle de Strasbourg (FMTS), Strasbourg, France. [4]Equipe Labellisée Ligue Contre le Cancer, Strasbourg, France. [5]Institute of Bioengineering, École Polytechnique Fédérale de Lausanne (EPFL), Lausanne, Switzerland. [6]Institute of Materials Science and Engineering, EPFL, Lausanne, Switzerland. [7]These authors contributed equally: Vincent Mittelheisser, Valentin Gensbittel, Lucia Bonati, Weilin Li. ✉e-mail: li.tang@epfl.ch; jacky.goetz@inserm.fr

https://doi.org/10.1038/s41565-023-01535-8

BOX 1

Relevant technologies for mechanical immunoengineering

Full dissection of the mechano-surveillance mechanisms inevitably relies on accurate methods for measuring forces. A plethora of in vitro techniques, such as micropipette aspiration, atomic force microscopy (AFM) and biomembrane force probe, have been available for measuring the mechanical properties of single cells, tissues and interaction forces between cells[7,211]. Although extensively used to highlight differences in mechanical properties between healthy and diseased cells and tissues, these techniques suffer from low throughput. More recently, microfluidic approaches have been developed to address this issue and allow high-throughput mechanical single-cell measurements. The development of real-time deformability cytometry (RT-DC) now allows to probe instant deformation and elasticity of cells at high throughput[212] and should soon expand its potential to allow fast measurements of viscoelastic properties[213]. The techniques mentioned above are all perfectly compatible with ex vivo measurements of patient-derived samples.

While certainly more challenging, probing forces and mechanical properties in vivo has a bright future ahead owing to recent technological breakthroughs. Brillouin microscopy has emerged to allow extraction of elastic and viscous properties of living tissues[214] and has been applied for mapping mechanical properties of cancer nodules in three dimensions[215]. Particle-tracking microrheology has been used to compare how mechanical properties of normal versus carcinoma cells evolve in living mice[216]. Hydrostatic pressure of fluid-filled cavities can be directly measured via the insertion of pressure-measuring micropipettes. Such methods were initially designed to measure pressure inside blood vessels[217] and can now be applied to measure cytoplasmic pressure in single cells[218]. Optical tweezers have been used to quantify haemodynamic and adhesion forces in the zebrafish embryo model[219]. Slightly invasive methods based on inclusion of deformable probes such as microdroplets/microbeads can quantify the mechanical stress acting on cells within living tissues[220,221]. Likewise, a recently developed microparticle-based platform was injected into tissues, allowing the characterization of the force profile of individual T cells in vivo[222]. Förster resonance energy transfer (FRET) tension sensors provide mechanical stress quantification when coupled with intravital imaging. These molecular springs can be genetically encoded in living cells/tissues, which then emit fluorescence that reports the local mechanical tension[223,224]. Such sensors have notably been used to quantify intercellular tension within endothelial cell monolayers exposed to fluid shear stress[225]. Similarly, viscosity can be followed in vivo by using molecular rotors that will adjust their conformational states upon viscosity changes[226,227]. Finally, breakthroughs in in vivo mechanical measurements have benefited researchers and found applications in the clinic. Novel diagnostic tools such as acoustic radiation force impulse[53] or magnetic resonance elastography[228] have allowed the probing of mechanical properties of patient-derived tissues in the clinic. In addition, recent progress in tissue mechanical dissociation coupled with RT-DC approaches will allow rapid probing of mechanical properties of surgically removed cells. This will help clinical decision-making during extemporaneous histological analysis[229]. Fine-tuning, spreading and combining these novel techniques will allow researchers to measure and investigate mechanical forces in the context of immune surveillance at all relevant scales, from whole tissues to single force-bearing receptors at immune synapses.

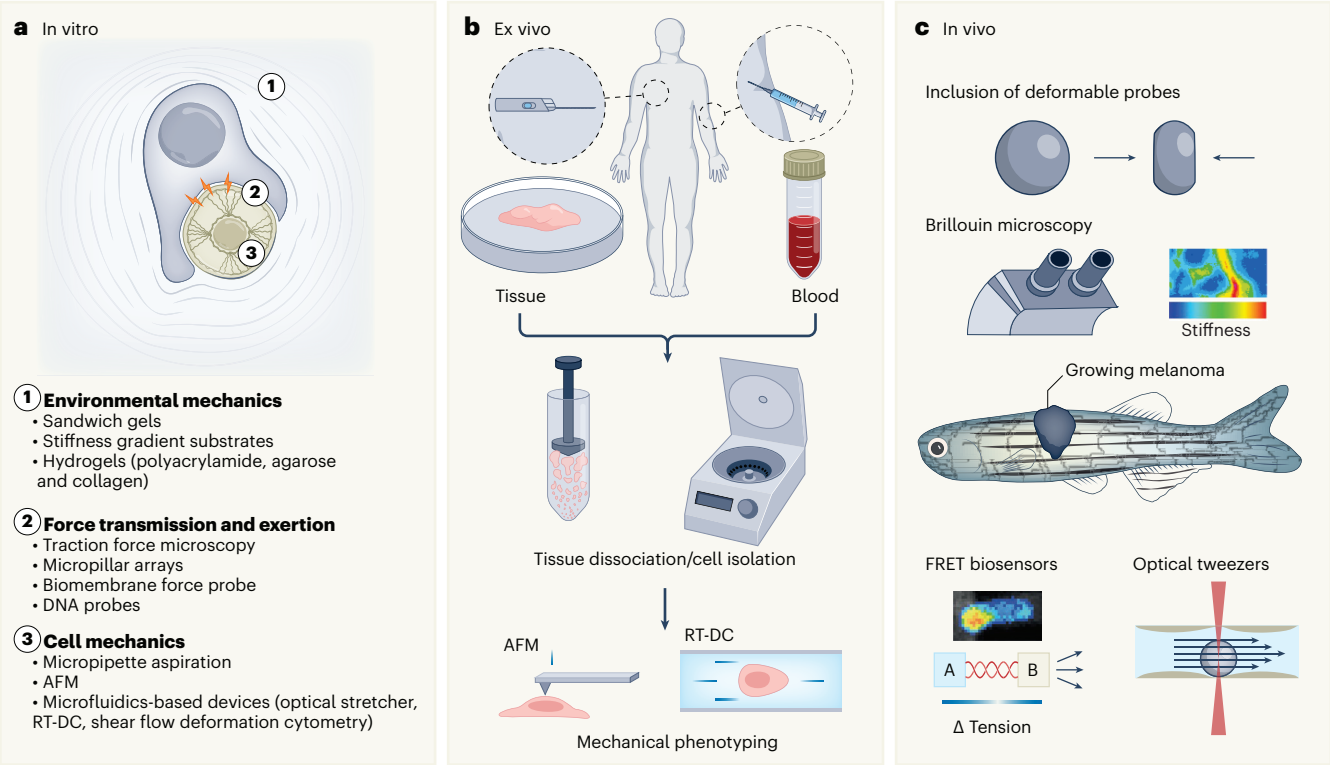

Relevant technologies for mechanical immunoengineering. **a**–**c**, A wide range of techniques are available to researchers for investigating environmental mechanics, interaction forces and cell properties in vitro (**a**), ex vivo (**b**) and in vivo (**c**).

antigen recognition, T cells form a well-defined nanostructure at their interface with antigen-presenting cells, called the immunological synapse (IS). T cells and their target cells are known to engage in extensive mechanical exchanges at the IS, which have been possible to investigate through the development of multiple nanotechnologies (see Box 1 on techniques). Both mouse and human $CD4^+$ T cells are activated to higher extents and secrete more effector cytokines when seeded on stiff substrates[8–11]. T cells exert mechanical forces to potentiate the killing of cancer cells[12]. In addition, T-cell-mediated lysis of tumour cells is enhanced when cancer cells are stiffened and decreased when they are softened[13–15]. These results provide solid evidence that mechanical aspects of pathologies do indeed impact immune responses.

Currently, most immunotherapies target biochemical cues of diseased tissues and immune cells. However, the growing appreciation of the mechanobiology of immune cells offers a good foundation for developing new engineering strategies aiming at mechanically modulating immune cells or target cells for enhanced therapies against various diseases. For example, emerging studies have been aiming at stiffening cancer cells to sensitize them to immune surveillance[14,15]. Expanding this concept to engineering strategies focusing on the mechanical modification of immunity–disease interactions shows enormous promise for developing next-generation immunotherapies. Here we first review the mechanical changes during pathological progression in several diseases, including cancer, fibrosis and infection. We then highlight the mechanosensing abilities of immune cells and the mechanosensitive nature of the immune response in various pathologies. Finally, we discuss how targeting the mechanical features of the disease milieu and immune cells is a viable strategy to enhance current immunotherapies. We also highlight several challenges yet to be addressed in this emerging field of 'mechanical immunoengineering'.

Altered mechanics in disease initiation and progression

Cancer

Mechanical changes in tissues constitute a signature trait of solid tumour pathologies that has long been exploited for diagnosing diseases, notably in breast cancer cases where mechanical probing of the tissues is routinely performed (palpation, mammography or elastography) (Fig. 1a). The mechanisms underlying the stiffening of tumour tissues and their metastatic secondary foci are well understood and have been expertly reviewed in the past[5]. Increases in the synthesis of matrix proteins, collagen crosslinking, integrin clustering and focal adhesion are the main contributors to extracellular matrix (ECM) remodelling. This is caused mainly by the concerted action of stromal cells and tumour growth-mediated solid stress, which leads to the stiffening of cancer tissues[16–18]. The pro-inflammatory environment of the initial malignant progression also sustains ECM stiffening. More specifically, cytokines and chemokines released by innate immune cells act in a paracrine way on stromal cells, driving their differentiation into 'activated fibroblasts' bearing a myofibroblast-like phenotype[19]. These 'activated fibroblasts', collectively named cancer-associated fibroblasts (CAFs), express higher levels of α-smooth muscle actin and collagen, and acquire greater contractile and proliferating capacities. Deposition of a stiff and non-elastic ECM in cancer results in impeded diffusion of chemotherapeutic molecules[20,21] and hinders infiltration of immune cells[22], which are key features of malignant progression. Other noteworthy changes during this desmoplastic reaction include disorganized and leaky vascularization. This results in a subsequent imbalance of interstitial fluid pressure, further preventing efficient delivery of chemotherapeutic molecules to the tumour[23].

Surprisingly, the stiffening at the scale of cancer (or metastatic) tissues can hardly be a representation or a consequence of the stiffness level of individual tumour cells. Although tumour tissues are stiffer than healthy tissues, it is so far widely accepted that tumour cells are softer than their healthy counterparts[24]. Consistently, nanomechanical profiling of tumour tissues has shown intratumoural stiffness to be highly heterogeneous compared with healthy tissues, with tumour cells constituting the softest spots of the probed cancer tissues[25]. As such, two very distinct scales must be considered when discussing mechanical changes in cancer diseases: (1) the whole-tissue scale, where solid cancer tissues, in general, are known to be stiffer than healthy tissues, and (2) the single-cell scale, where individual tumour cells are often thought to be softer than healthy cells. However, whether the consensus on the softer mechanical phenotype of single cancer cells is truly relevant remains debatable, as proper in vivo demonstrations have been lacking. As such, the potential link between the mechanical properties of tumour cells and disease progression remains unclear, despite some evidence hinting that both parameters probably affect each other. In addition, stromal components of tumours (fibroblast and immune cells mostly) are active elements from a mechanical standpoint and contribute to physical aspects of tumour progression, whose targeting offers a promising future for cancer therapy[26].

We recently speculated that cancer cells are not simply 'softer' but rather mechanically 'dynamic and adaptable', a feature that would undoubtedly grant them an important advantage for completing the metastatic cascade[27]. Accumulating evidence suggests that the mechanical properties of tumour cells confer a selective advantage in almost all the steps of cancer progression. A study investigating the link between mechanical phenotype and tumourigenicity of cancer stem cells found that only soft cancer stem cells could lead to primary tumour initiation[28]. This suggests that the mechanical properties of tumour cells are critical at the earliest stage of cancer progression. Tumour cells that later find themselves inside a growing primary tumour are subjected to increasing compressive stress levels and proliferate more efficiently by becoming spherical and stiffening their cell cortex[29]. Cancer cells that subsequently become invasive and escape the primary tumour site are softer and are subjected to gene expression changes associated with the epithelial–mesenchymal transition[30]. Such a softer mechanical phenotype facilitates migration through the ECM, as this process often requires extensive cell and nucleus deformation[31]. During intravasation, circulating tumour cells (CTCs) face drastic environmental changes. As their diameter is generally substantially larger than that of normal circulating cells, such as leukocytes, CTCs are more prone to shear-stress-induced destruction in mechanically hostile blood flow[32]. To cope with haemodynamic forces, CTCs have been shown to undergo stiffening and improve their chances of survival[33]. Tumour cells might again get softer once they have stably arrested and require performing extravasation through diapedesis[34]. Such an example of a dynamic adaptation mechanism to perform extravasation has recently been observed for primordial germ cells in avian embryos[35]. How mechanical properties of tumour cells evolve after extravasation remains largely unknown at this stage. However, one study suggested that freshly extravasated pericyte-like tumour cells might stiffen in a yes-associated protein (YAP)- and myocardin-related transcription factor (MRTF)-dependent manner to facilitate colonization of perivascular niches[36]. Such post-extravasation mechanical adaptation may impact or be impacted by the state that tumour cells might enter next: dormant or proliferative. In conclusion, the mechanical plasticity of tumour cells is an additional hallmark of metastatic progression.

Viral and bacterial infections

Similarly to cancer, two scales must be considered when discussing mechanical changes associated with viral and bacterial infections (Fig. 1b). Indeed, at the intracellular scale, bacteria and viruses can hijack the cytoskeleton of host cells to enhance transportation to the cytoplasm where they will replicate and assemble. In addition, bacteria and viruses can promote local actin polymerization to generate a mechanical force facilitating their progression. This phenomenon applies to several viruses, such as coronavirus[37] and respiratory syncytial virus[38]. Cytoskeleton changes do not occur exclusively in the

https://doi.org/10.1038/s41565-023-01535-8

host cells infected by viruses (that is, angiotensin-converting enzyme 2-positive cells in the case of severe acute respiratory syndrome coronavirus 2), but also in the immune cells at the infection site. Indeed, a recent study showed lymphocyte stiffening due to the clinical syndrome of coronavirus disease 2019[39]. Like cancer cells, pathogens, and more specifically bacteria, can also be affected by fluid shear stress[40,41] and develop strategies to resist it[42].

At the whole-tissue scale, bacteria and viruses can alter the biophysical properties of the infected tissue by changing the ECM structure and/or composition. Upon viral infection by rhinovirus, stromal cells markedly increase their production and deposition of fibronectin, perlecan and collagen IV in response to activation of Toll-like receptor (TLR)-3 and -7/8[43]. In parallel, TLR activation in stromal and epithelial cells triggers the secretion of high-molecular-weight hyaluronic acid[44], which traps fluid arriving through permeable endothelium and swells tissue, causing oedema and increased stiffness[44]. Oedema formation can be further fostered by secreted matrix metalloproteinases that degrade the endothelial barrier, resulting in abnormal Starling forces and fluid diffusion[45]. Upon acute inflammation, the lymph node architecture may undergo a late remodelling process, resulting in increased collagen deposition and ECM remodelling, which can profoundly impact tissue stiffness, such as scarring and eventually fibrosis[46]. Mechanical changes are actively experienced by immune cells as they travel through different tissue environments and contribute to the early recognition of danger and the induction of immune responses.

Fibrosis

Fibrotic diseases, such as idiopathic pulmonary fibrosis or scleroderma, are accompanied by numerous mechanical alterations (Fig. 1c). Fibrosis is the wound-healing response following iterative injuries of chemical (asbestos, alcohol and so on), mechanical or microbiological (hepatitis viruses, *Mycobacterium tuberculosis* and so on) origins[47,48]. Regardless of the underlying cause, chronic injury causes parenchymal cell death associated with a positive feedback loop between inflammatory damages, fibroblast proliferation and matrix deposition[49]. In some cases of acute stress, such as myocardial infarction, the emergence of fibrotic scars is crucial to replace the necrotic tissue and avoid cardiac rupture[50].

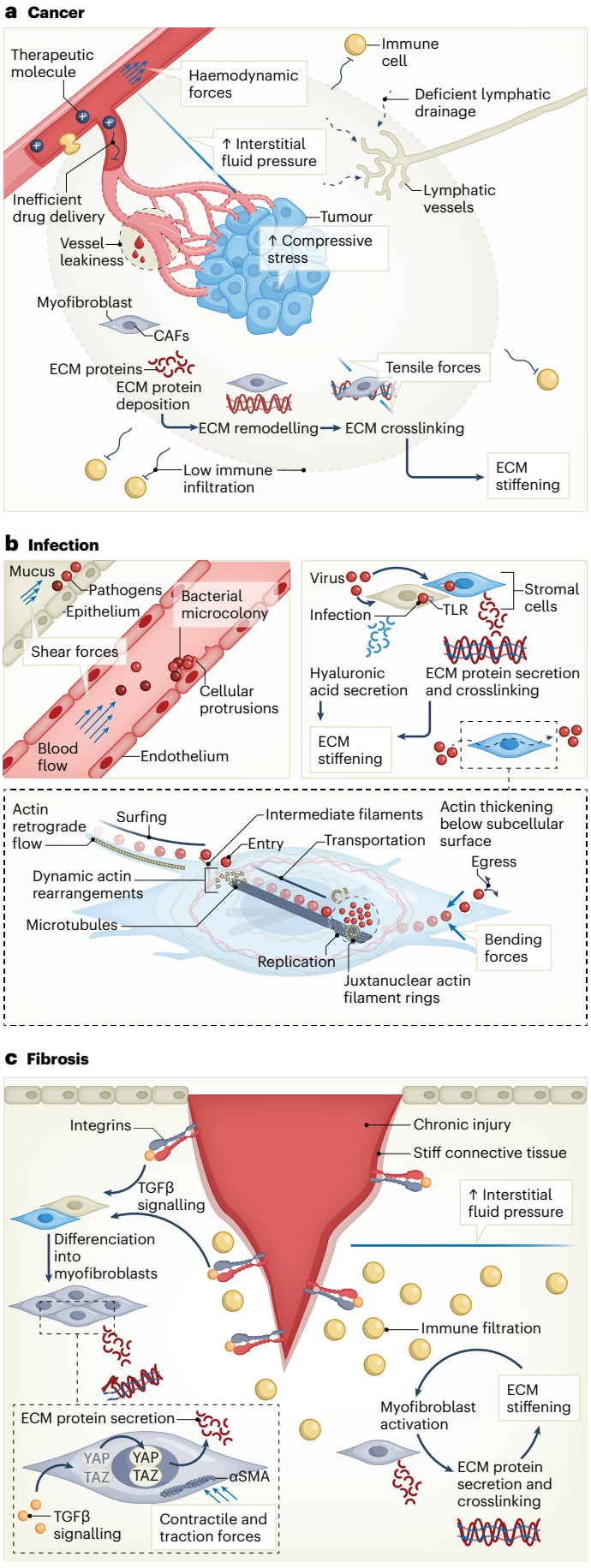

Fig. 1 | Different disease settings share common mechanical cues. a, Solid cancer diseases come with a variety of mechanical features that lead to the characteristic stiffness of tumour tissues. Compressive stress arises as the tumour volume expands and interstitial fluid pressure increases because of vessel leakiness and inefficient lymphatic drainage. Activated CAFs exert tensile forces on ECM fibres that they also secrete, remodel and crosslink. As a result of these changes, immune infiltration and delivery of therapeutic molecules to the tumour site are compromised. **b**, Mechanical forces are also at play in infectious diseases. Pathogens are sensitive to shear forces they encounter in mucus as they attempt to cross an epithelium or in the blood flow. Bacteria form microcolonies to deal with such forces. Stromal cells infected by viruses drive ECM stiffening by secreting hyaluronic acid and ECM proteins upon TLR activation. At the intracellular level, viruses hijack the cytoskeleton of their host cell to complete their replication and thrive. Viruses take advantage of actin retrograde flow in protrusions to 'surf' to their entry point. Entry is allowed by actin rearrangements and intermediate filaments acting as co-receptors at the cell surface. Microtubules are exploited for transportation to the replication site where acid filament rings come into play. Finally, actin thickening below the cell surface generate the bending forces necessary for freshly replicated virus particles to exit. **c**, Fibrotic diseases share very similar traits to cancer. Integrin-mediated TGFβ signalling originating from stiff connective tissue causes stromal cells to differentiate into activated myofibroblasts that secrete and crosslink ECM fibres and also exert high α-smooth actin-driven contractile and traction forces. The resulting ECM stiffening further activates myofibroblasts, thus creating a feedback loop that endlessly drives cellular activation and fibrosis. In addition, the chronic inflammation state of fibrotic tissues also leads to immune and fluid infiltrations that increase local hydrostatic pressure and further contribute to the stiffening of fibrotic tissues. α-SMA, α-Smooth muscle actin (α-SMA).

Increases in collagen and glycosaminoglycan depositions in the ECM promote the development of non-contractile fibrotic areas, leading to progressive tissue stiffening, which is a hallmark of fibrotic diseases. Indeed, various studies have shown that the elastic modulus of lung[51], liver[52] and kidney[53] tissues increased upon fibrosis when compared with healthy tissues. Several diseases, such as myocardial infarction, inflammatory cardiomyopathy or non-alcoholic fatty liver disease, can evolve into fibrosis[48,54]. A chronic inflammatory state can also occur with ageing. Indeed, unresolved systemic inflammation is a hallmark of immune ageing[55]. This persistent low-grade inflammation can lead to arteriosclerosis characterized by a stiff and thickened artery wall, resulting in the decline of cardiac function[56].

Although more work is needed to understand how matrix stiffness regulates tissue fibrosis comprehensively, accumulating evidence indicates that stiffening of connective tissue directly contributes to the progression of the fibrosis by promoting three fundamental profibrotic mechanisms: (1) mechano-activation of myofibroblasts through mechanotransduction pathways, (2) integrin-mediated activation of latent transforming growth factor β1 (TGFβ1), and (3) activation of non-canonical TGFβ1 signalling pathways. Mechanically induced activation triggers myofibroblast secretion of multiple types of ECM protein as well as matrix-crosslinking enzymes, resulting in a more stable and stiffer ECM[57]. This effect results in a positive feedback loop, leading to persistent cellular activation and fibrosis[58]. Moreover, reinforced activation of myofibroblasts also leads to upregulation of α-smooth muscle actin, further increasing their contractility[59]. As a result of this hypercontractile state, myofibroblasts exert higher traction forces on the stiff fibrotic ECM, which leads to more matrix remodelling and stiffening and integrin-mediated latent TGFβ1 activation (integrin αvβ6, αvβ5 and αvβ1), thus completing the fibrosis amplification loop[60]. Consequently, matrix stiffening in fibrosis should not simply be viewed as a by-product but as a key initiator and regulator of profibrotic fibrogenesis[61].

Mechanosensing and mechanotransduction of the immune system

Immune cells respond to various biochemical signals arising from pathogen-associated molecular patterns or specific activating ligands expressed at the surface of infected or transformed cells[62]. These signals are first detected by sentinel cells of the innate immune system, such as macrophages, dendritic cells (DCs) and natural killer (NK) cells. The innate immune system recognizes biochemical signals quickly through germ-line-encoded pattern-recognition receptors (PRRs) and other cell surface molecules, orchestrating inflammatory responses[63]. The effector functions of innate immune cells further drive adaptive immune responses by recruiting and activating T and B cells[63]. Professional antigen-presenting cells (APCs) expressing co-stimulatory molecules (CD80, CD86 and so on) prime T cells by presenting them cognate antigens as peptides bound to major histocompatibility complex (MHC) molecules[64].

In addition to their biochemical activation, immune cells encounter numerous forces as they circulate throughout the body to perform immunosurveillance and effector functions. Accumulating evidence shows that immune cells are sensitive to mechanical stimuli, such as shear stress, hydrostatic pressure and tension of their surrounding environment. Such forces are sensed and converted from mechanical cues to biochemical signals, thus activating cellular pathways and influencing their function. Current understanding of the mechanosensing of immune cells has been enabled largely by in vitro models of ligand-coated artificial substrates (for example, polydimethylsiloxane (PDMS), polyacrylamide gels, beads) that allow the decoupling of biophysical cues and biochemical signals involved in the interactions of immune cells with their environment and target cells[65,66]. As the physical properties of their surrounding microenvironment are essential to immune cell function, PDMS hydrogels offer an ideal model to manipulate and test the impact of stiffness[67]. Yet, the stiffness of PDMS gels typically spans from 100 kPa to 10 MPa (ref. 68), whereas the physiological stiffness normally ranges from 100 Pa (brain) to 100 kPa (carcinoma), except bones[69]. Therefore, polyacrylamide gels (typical stiffness ranging from 10 kPa to 10 kPa) might be more suitable to recapitulate the physiological stiffness of tissues[70]. Nevertheless, efforts are needed to generate models that better mimic the dynamic mechanical environment and cellular stiffness to model cell–cell interactions.

Monocytes and macrophages

Monocytes and macrophages are important innate immune cells that have a pivotal role in the initial recognition and elimination of pathogens through phagocytosis and/or cytokine secretion. Monocytes circulate in the peripheral blood for approximately one to three days and then migrate into tissues throughout the body where they differentiate into macrophages and DCs[71]. As these cells scout the body using body fluids, they are subjected to hostile fluid forces. For example, patrolling monocytes can sense haemodynamic forces, such as fluid shear stress, through mechano-gated ion channels[72,73]. The responses of circulating monocytes to high shear stress include enhanced adhesion, activation of CD11b integrin, phagocytosis and pro-inflammatory cytokine secretion[74].

Macrophages are terminally differentiated monocytes that reside in tissues, actively sensing their surroundings and launch effector responses accordingly. Macrophages are markedly affected by the wide range of phagocytic targets (pathogens, cancer cells, apoptotic bodies and so on) and their mechanical parameters[75–77]. Macrophages sense opsonized target stiffness through the Fcγ receptor, triggering integrin localization into the phagocytic cup. This further allows macrophages to close the phagocytic cup and complete phagocytosis[78]. Furthermore, target stiffness can overpower the signal-regulatory proteinα (SIRPα)-CD47 'don't eat me' signal[76]. In addition to phagocytosis, substrate stiffness is instrumental in tuning macrophage migration[77] and differentiation into anti-inflammatory ('M2 like') and pro-inflammatory ('M1 like') phenotypes[77]. Multiple research groups have shown that macrophages cultured on soft substrates have reduced inflammatory activation compared with those cultured on stiff surfaces[77]. Macrophages can sense their substrate's mechanical properties through integrins[79] and ion channels, such as PIEZO1 and transient receptor potential vanilloid 4 (TRPV4). The stiffness of the substrate favours the influx of Ca^{2+} ions through PIEZO1, a mechano-gated ion channel, and subsequent nuclear factor kappa B (NF-κB) activation and secretion of inflammatory cytokines leading to a more prominent 'M1 like' inflammatory phenotype[79].

Furthermore, the concerted action of PIEZO1 and TLR-4 is necessary to achieve innate responses against pathogens, including phagocytosis, reactive-oxygen-species production and bacterial clearance[80]. In addition to ion-channel-mediated mechanosensing, yes-associated protein and its functional partner, the transcriptional co-activator with PDZ-binding motif (YAP/TAZ) signalling orchestrates the response of macrophages to biophysical cues. Indeed, the translocation of YAP/TAZ to the nucleus, which allows the regulatory activity of downstream gene expression, is impacted by ECM stiffness[81]. When modelled in vitro, the stiffness of the culture substrate regulates the nuclear translocation of YAP and its downstream functions in various cell types[82–84]. In particular, macrophages cultured on hydrogels with a stiffness of 20 kPa or more have increased nuclear YAP, enhancing their response to the inflammatory agonist lipopolysaccharide[84].

Dendritic cells

DCs are the dominant population of professional APCs that present antigens to naive T cells and B cells[85]. Activation of DCs by their endogenous PRR or other inflammatory mediators leads to the overexpression of specific activation markers, such as CD80, CD83, CD86, and MHC class I and class II. In addition to biochemical stimuli[86–88],

DCs sense mechanical cues through ion channels, integrins and the YAP/TAZ pathway, influencing DC biology (migration, antigen uptake, IS formation)[88–90]. Shear stress activates mechano-gated ion channels of circulating DCs, inducing high expression of activation markers MHC class I and CD86[91] and forming podosomes, which improve their adhesion and migration abilities[91,92]. Once infiltrated in the inflamed stiff tissue, DCs adjust their activation levels and cytokine secretion. DCs cultured on stiff substrates show high YAP/TAZ nuclear translocation, leading to enhanced expression of downstream genes regulating DC activation, co-stimulatory molecule (that is, CD80/CD86) expression, proliferation and metabolism[93]. In addition, DCs modulate their antigen internalization and presentation capacities according to substrate stiffness[93,94]. A partial explanation can be found in the recent description of substrate stiffness responsiveness of the C-type lectin receptors, which are essential for antigen internalization by DCs[94,95]. Other studies show that DC activation through antigen uptake increases their cortical stiffness without necessarily increasing the expression of their maturation markers[96]. Thus, increased DC cortical stiffness is an additional feature of maturation that further lowers the antigen concentration threshold needed for efficient T-cell activation[11]. Indeed, actin cytoskeleton changes in mature DCs restrain the intercellular adhesion molecule (ICAM) lateral mobility, which promotes T-cell priming via affinity regulation of the lymphocyte function-associated antigen 1 (LFA-1) expressed by interacting T cells[97]. Finally, stiffness of the environment impacts mechano-gated ion channels that regulate the secretion of polarizing cytokine interleukin-12 (IL-12) by DCs, resulting in T helper cell 1 (T_H1) differentiation, inhibition of regulatory-T-cell lineage commitment and tumour growth inhibition[98].

Lymphocytes (T cells, NK cells and B cells)

Upon scouting throughout the body, lymphocytes recognize characteristic biochemical features that lead to their activation. Lymphoid cells also encounter different environments in which they can sense mechanical cues through mechanosensitive receptors, including integrins[99,100], ion channels (for example, TRPV4, PIEZO)[101], the T-cell receptor (TCR)[102,103] and cytoskeletal components[104,105], and convert these biomechanical stimuli to biochemical signals (migration, scanning, activation and so on). Emerging evidence shows mechanical cues govern $CD4^+$ and $CD8^+$ T-cell activation and effector functions. When seeded on stiff artificial substrates presenting CD3 and CD28 antibodies, mouse and human naive $CD4^+$ T cells show higher proliferation, metabolism and cytokine production[8,10,106]. TCR-related ZAP70 and Src kinases are phosphorylated in response to mechanosensing[8,107]. The stiffening of professional APCs also seems to enhance $CD4^+$ and $CD8^+$ T-cell activation[11]. Upon activation, the TCR not only senses mechanical cues of its environment but also exerts active pulling forces against their antigen[102,108,109]. DNA-based tension sensors (see Box 1 on techniques) revealed that T cells harness cytoskeletal coupling to transmit 12–19 pN forces per TCR, initiating strong T-cell activation[103,110]. Co-stimulation by CD28 further increases cellular force generation on TCR adhesions[108]. Moreover, TCR activation induces the inside-out upregulation of integrins, providing synergistic adhesive strength and mediating force transmission at the IS[111–113]. Other mechanoreceptors, such as PIEZO1, also synergize with TCR mechano-activation[114]. Mechano-activation of lymphocytes by TCR signalling also triggers cytoskeleton changes, inducing cytotoxic granule polarization and IS formation[111,112,115,116]. Besides, cytoskeleton disruption by pharmacological small molecule inhibitors (for example, latrunculin A, blebbistatin, nocodazole) completely abolishes immune cell stiffness-dependent activation and cytokine secretion[14,15,117]. In that way, cytoskeleton changes act as a second layer of mechanosensing by T cells. While naive T cells have a stiff cortical cytoskeleton, effector T cells are typically softer, resulting in the formation of larger IS with APCs[104]. This observation suggests that in addition to TCR mechanosensing and force exertion, the baseline cytoskeletal state controls T-cell responsiveness.

Similarly, NK cells sense the mechanical features of their environment that synergize with biochemical signals to modulate their activation and inhibition[11,66,118,119]. Stiff substrates coated with antibodies directed against LFA-1 or the natural cytotoxicity receptor NKp30 stimulate NK-cell degranulation by recruiting phosphorylated ZAP70 to the NK IS[120,121]. Stiff substrates also induce strong clustering of DNAX-protein 10, whose hexametric complex with NKG2D activates signalling in NK cells[66,122]. On the contrary, softer substrates impair microtubule organizing centre polarization, lytic granule polarization and F-actin accumulation at NK IS, leading to the formation of unstable asymmetrical synapses and decreased degranulation[123]. How NK cells sense the mechanical features of their environment is still unclear, but a recent study leans towards mechano-gated ion channels[124].

Like T and NK cells, B-cell activation is also modulated by the mechanical properties of their environment and partners, notably by the stiffness of the APCs[125]. Antigens presented on stiff substrates induce higher B-cell receptor microcluster formation compared with antigens tethered to soft substrates, leading to increased B-cell activation[125]. In addition, B cells are also able to differentiate high-affinity antigens from low-affinity antigens tethered on the APC by using diacylglycerol kinase ζ and myosin IIa to pull-out and invaginate the APC membranes presenting high-affinity antigens[126,127]. Therefore, substrate stiffness has a crucial role in B-cell activation, affinity maturation, class switch and antibody responses[128,129]. Although stiff substrates have been reported to induce better B-cell receptor clustering, high-affinity antigen extraction and affinity maturation, soft substrates, on the other hand, appear to be preferable for class switch and T-cell-independent antibody responses[128]. Altogether, the physical extraction of environmental signals by B cells accelerates their adaptation but may also cause the extinction of unfitted cell populations[130].

Evidence and mechanisms of mechano-immune surveillance

Anti-infection mechano-immunology

Viruses and bacteria can modify the host mechanobiology at the single cell or the tissue levels to evade immunosurveillance. At the host-cell level, the mechanical evasion from immunosurveillance is often mediated by a remodelling of the actin cytoskeleton. For example, upon infection, the human cytomegalovirus expresses the pUL135 protein, inducing remodelling of the actin cytoskeleton. Such a process is characterized by actin stress fibre loss, which markedly reduces the efficiency of IS formation upon recognition by immune cells[131]. This trait is exploited by human cytomegalovirus to protect the host cell against cytotoxic immune effector cells and to promote viral proliferation. Likewise, bacteria can also impair IS assembly by either reducing antigen presentation by APCs in *M. tuberculosis* infections[132] or by increasing T-cell actin polymerization, thereby impairing the ability of T cells to scan APCs in *Shigella*-mediated diarrhoeal diseases[133].

Nevertheless, actin cytoskeleton modifications can eventually serve as damage-associated molecular patterns to activate the immune system. For instance, F-actin is recognized by the dendritic cell natural killer group receptor-1 (DNGR-1) specifically expressed in DCs, leading to cross-priming of cytotoxic T lymphocytes (CTLs) in virus-infected mice[134]. Actin polymerization is also required to induce the NLR family CARD domain-containing 4 (NLRC4) inflammasome and to secrete antimicrobial molecules by bone-marrow-derived macrophages[135].

While altered biophysical properties of infected cells lead to immune evasion at the single-cell scale, pathogen-infected tissues with altered mechanical properties at the tissue level induce potent immune activation. Early activation of PRRs in Langerhans cells and stromal cells activated by virus- and bacteria-derived danger signals triggers the secretion of copious amounts of hyaluronic acid to promote oedema and attract immune cells to the infection site[44]. Mechanical forces applied on immune cells when they squeeze through the endothelium and dense ECM drive chromatin changes that promote

inflammation and chemotaxis-related transcripts[136]. At the same time, oedema-induced tensile stress and hydrostatic pressure encountered by innate immune cells activate their mechanosensitive ion channels (PIEZO1, TRP and so on), priming them for bioenergetic demands of activation and reducing the threshold required for optimal PRR stimulation[80,93,137]. These ion channels play an important role in the early immune response against infections as their depletion abrogates the inflammatory response that clears pathogens[137,138].

Upon immune-response progression, T cells migrate and proliferate in the lymph node, which causes local stiffening and swelling[139]. Lymph node tissue mechanics can be sensed by T cells, which further promotes their proliferation, activation and metabolism while lowering the antigen dose needed to elicit effector responses[139]. Stiffness of the environment can be sufficient to prime T cells, as reported in a recent study. Indeed, T cells that crawl through stiff 40 kPa matrices show enhanced activation, regardless of the stiffness level of the APC that interacts with them[106]. Activated T cells will eventually migrate to an infection site where they will experience multiple mechanical stimuli. Notably, migrating T cells interact with secreted hyaluronic acid through CD44, a key mechanosensitive receptor involved in T-cell extravasation[140]. Additional studies will be necessary to decipher whether this interaction promotes or suppresses T-cell activation. Finally, mechanical changes in tissues are reverted during infection resolution, with dissolution of hyaluronic acid, reduced oedema and impaired immunity to danger signals. However, chronic inflammation can sometimes arise from a positive association of mechanical stimulation, T-cell-dependent T_H2 cytokine (IL-4 and IL-13) and chemokine (monocyte chemoattractant protein-1(MCP-1)) signalling, leaving a lasting mechanical imprint at the inflammatory response site[141].

Anticancer mechano-immune surveillance

Anticancer immune surveillance kicks in early after malignancy and the immune system patrols throughout the body to identify and destroy nascent tumours[142]. NK cells and CTLs recognize transformation-associated molecules and tumour-associated antigens expressed on the surface of tumour cells[143]. Upon formation of the IS between cancer cells and lymphocytes, lymphocytes secrete the pore-forming protein perforin, which allows entry of death-inducing toxic granzymes and lysis of target cancer cells[144]. Although tumour cell killing had been mostly linked to canonical signalling pathways involving receptor–ligand recognition, recent evidence demonstrates that lymphocytes also sense tumour-dependent mechanical cues (see the 'Mechanosensing and mechanotransduction of the immune system' section) and respond accordingly towards target cells. Upon tumour infiltration and IS formation, NK cells and CTLs exert up to nanonewton-scale cellular forces towards target cells[102,108,109]. The force exerted at the IS regulates the cytotoxic responses in several ways. Mechanical cues are transduced inside lymphocytes from the plasma membrane into the nucleus through the linker of the nucleoskeleton and cytoskeleton complex. This leads to the expression of target genes (for example, *CD69*, *IL2*, *IFNG*), lymphocyte activation and the formation of a mature IS[145]. Forces exerted at the IS also directly influence lymphocyte-mediated cytotoxicity by increasing membrane tension and potentiating lysis of target cells[12,15]. During this process, surface receptors (for example, TCR, $\alpha_L\beta_2$ integrin LFA-1, NKG2D) at the IS change their conformation to form catch bonds with their respective ligands. Such catch bonds were found to rely on forces to achieve high affinity for their ligands[103,146,147]. The forces exerted at the IS heavily depend on the target cell's mechanical profile and compliance. Hence, it is important to note that the biophysical properties of the targeted tumour cells profoundly regulate the killing processes[12]. We and others recently found that the softness of cancer cells, independently of other biochemical features, acts as an 'immune checkpoint' of mechanical nature (or termed 'mechanical immune checkpoint'), which induces immune evasion of lymphocyte-mediated cytotoxicity[13–15]. The immune system is consequently more sensitive to stiff(er) tumour cells, yet the mechanisms must be fully unravelled (Fig. 2). First, stiff cancer cells may allow higher synaptic force exertion by lymphocytes, which potentiates cytotoxicity by enhancing target cell membrane tension to facilitate pore formation mediated by perforin[12,15]. Second, the mechanics of target cells probably impact the strength and morphology of the IS. Lymphocytes spatiotemporally coordinate the force exertion and perforin secretion within the synapse by forming Wiskott–Aldrich-syndrome-dependent interfacial actin-based protrusions[112,148,149], which could be enhanced when encountering stiffer target cells. Third, stronger activating signalling through lymphocyte's mechanosensitive receptors exerted by stiffer target cells could also increase the degranulation and cytokine production, leading to enhanced cytotoxicity[14,15]. Once cancer cell killing is achieved, immune cells sense the cytoskeletal contraction of apoptotic targets and respond to this mechanosensory feedback by dissolving the IS. Such IS turnout is critical for serial killing by CTLs and apoptotic body clearance by patrolling phagocytes[150]. Altogether, immune cells, particularly CTL and NK cells, modulate their activation and cytotoxic functions according to the biophysical status of the cancer cells that they probe. This biophysical angle of immunosurveillance has led to the emergence of a new unique field of 'mechano-immune surveillance'.

Several strategies have been reported to stiffen cancer cells for therapeutic purposes. Cholesterol enrichment in the plasma membrane reduces the cortical (plasma membrane and the underlying dense actin network) stiffness of cancer cells[151,152] in many types of cancer. One can thus envision that stiffening tumour cells by depleting membrane cholesterol with methyl-β-cyclodextrin (MeβCD), a cholesterol scavenger, could be a promising therapeutic intervention[15]. Treatment with MeβCD efficiently decreased the cholesterol levels at the plasma membrane of mouse and human cancer cells. It further increased the target cell stiffness, and sensitized the cancer cells towards T-cell-mediated killing in vitro and in vivo. Impressively, the combination therapy of MeβCD and adoptive transfer of tumour-specific T cells adjuvanted with an IL-15 super-agonist (IL-15SA) increased the rate of complete tumour eradication to 41.7% compared with 0% in the case of immunotherapy alone. In another elegant study, a subset of metastatic cancer cells was found to overexpress MRTFs, a cytoskeletal-associated transcriptional factor known to promote cancer migration and metastasis[36].

Interestingly, MRTF overexpression also enhances F-actin polymerization and, thereby, the stiffness of cancer cells. By inducing MRTF overexpression, the cancer cells increase their membrane tension, becoming more susceptible to T-cell and NK-cell-mediated cytotoxicity due to increased degranulation and cytokine production[14]. Of note, the selective depletion of F-actin in cancer cells completely abolishes the immune sensitization induced by MRTF overexpression, confirming the biophysical basis of these observations. Similarly, treating cancer cells with jasplakinolide, an actin polymerization promotor, also increased the stiffness of tumour-repopulating cells, a specific population among tumour cells that show features of self-renewal, low differentiation, high tumourigenicity and, in particular, softness and resistance towards T-cell-mediated killing[13]. Therefore, the combination of jasplakinolide, adoptive T-cell transfer therapy and programmed cell death protein 1 (PD-1) antibody improved the therapeutic efficacy in a mouse melanoma model.

Towards mechanical immunoengineering strategies to improve immunotherapies

Targeting mechanical adaptability of tumour cells

As discussed above, antitumour mechanical immune checkpoints can be targeted therapeutically. Indeed, soft cancer cells can be stiffened and sensitized towards current immunotherapies, including immune checkpoint blockade antibodies and adoptive T-cell transfer[13–15] (Fig. 3). Such discovery is also clinically relevant as soft human cancer cells also show resistance to perforin-mediated killing[13].

https://doi.org/10.1038/s41565-023-01535-8

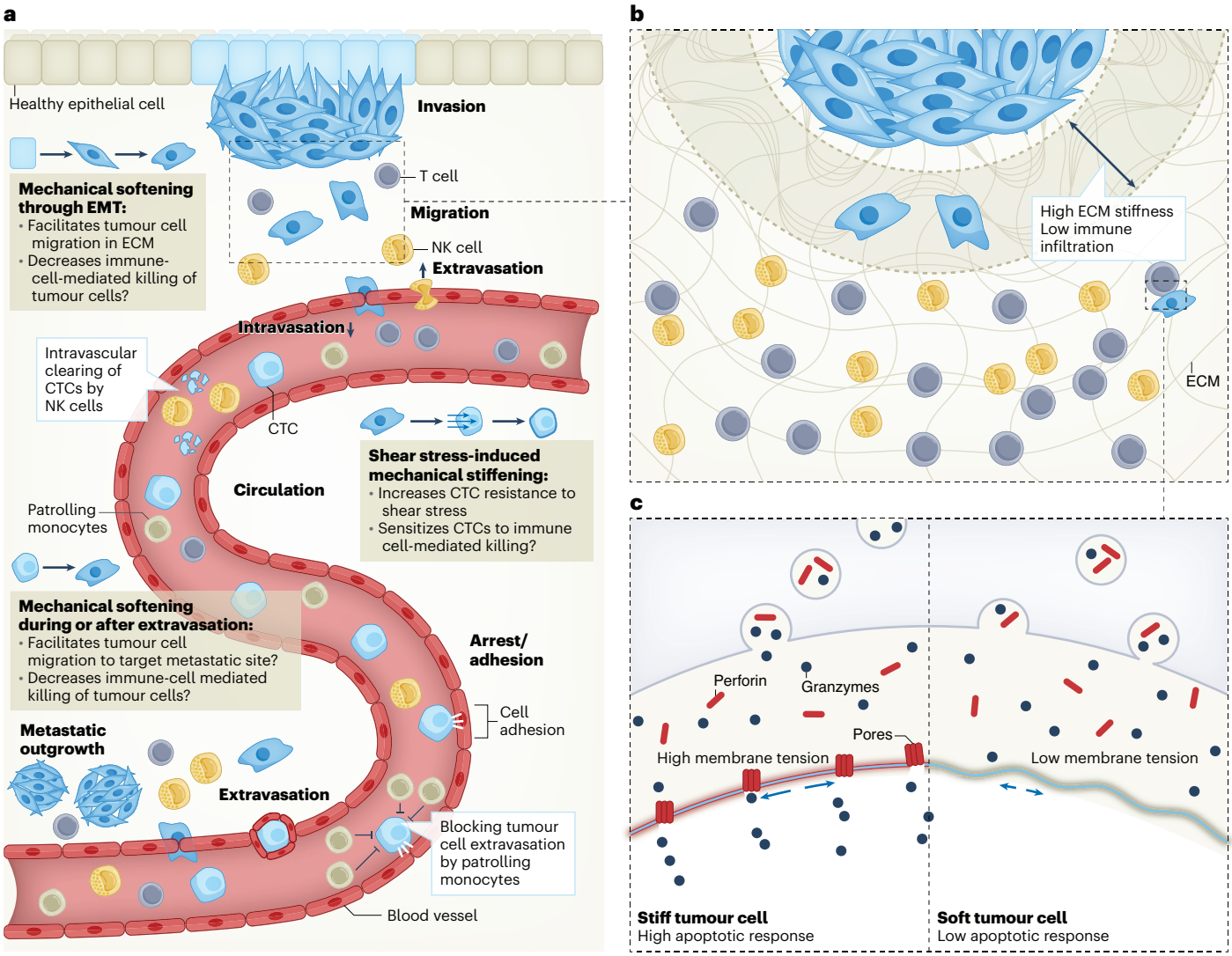

Fig. 2 | Spatiotemporal windows for optimal mechanical antitumour activity of immune cells. a, Tumour cells are probably adjusting their mechanical properties as they progress through the metastatic cascade. Following transformation of healthy epithelial cells and rise of a primary tumour, a select number of cancer cells will get softer as they go through the epithelial–mesenchymal transition (EMT) and perform invasion and migration. They later undergo stiffening as they enter the blood flow and become CTCs. As such, taking advantage of the optimal time windows when interactions between immune cells and stiffened tumour cells are most likely to occur might be key when establishing therapeutic strategies. Examples include NK cells performing intravascular clearing of CTCs and patrolling monocytes blocking tumour cell extravasation. **b**, Alternatively, windows in which immune cells show shortcomings could be identified to leverage mechanical immunoengineering and help them overcome them. The primary tumour site with its stiffened ECM and softened tumour cells represents a good example of such windows, with suboptimal mechanical features for NK- and T-cell antitumour activity. **c**, The aim should be to get immune cells in contact with tumour cells as stiff as possible as increased target cell stiffness favours IS formation and potentiates perforin and granzyme-dependent cytotoxic activity of immune cells.

Moreover, patients with melanoma exhibiting constitutive actin cytoskeleton-mediated stiffening are found to present enhanced responsiveness to immune checkpoint blockade therapy[14]. Yet, tumour cell mechanics cannot be a binary process where softness would fully explain and correlate with malignancy and metastatic progression. On the contrary, we believe that cancer cells are 'dynamic and adaptable' to perform and survive through the multiple mechanical and biochemical constraints they face along their path to metastasis[27] (as discussed in the 'Altered mechanics in disease initiation and progression' section). Their mechanical plasticity is an additional hallmark of metastatic progression that is likely to impact mechano-immune surveillance with, in theory, spatiotemporal windows in which immune cells can most efficiently recognize and kill tumour cells. As CTCs may get stiffened in response to the hostile haemodynamic forces in the circulation, we expect them to be, at this moment, the most vulnerable to T- and NK-cell-mediated killing, whose efficiency is likely also impacted by shear forces[101].

Recent studies have reported that CTCs could indeed be sensitive to immune cell-mediated killing, which contributes in part to the inefficiency of the metastatic process[153–155]. One of them showed that NK cells could clear tumour cells in the intravascular environment around the liver site and limit tumour cell seeding at a distant site in the lung. That same study highlighted an efficient synergy between NK cells and T cells, with the NK cells killing tumour cells in circulation and promoting T-cell recruitment, which would then restrict metastatic foci growth in situ[154]. In addition, patrolling monocytes might also contribute to antitumour activity in the circulation by directly scavenging tumour materials, secreting cytokines[156] and recruiting NK cells[153,157]. While evidence of intravascular antitumour activity of immune cells exist, this metastasis stage appears challenging to exploit because of the highly

https://doi.org/10.1038/s41565-023-01535-8

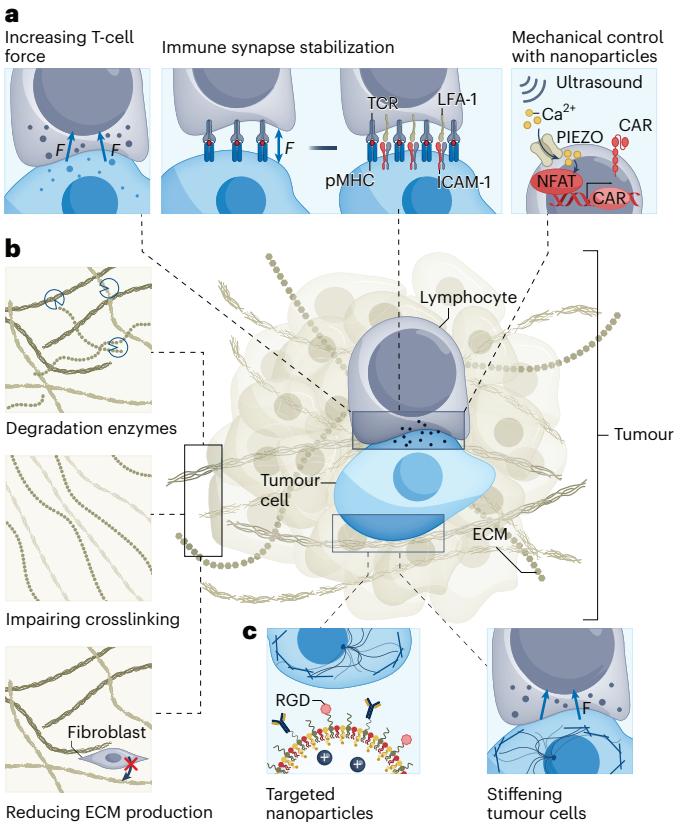

Fig. 3 | Improving therapies through mechanical immunoengineering of tumours and immune cells. Immune cells, tumour cells or the ECM of the tumour environment can be targeted using different strategies aiming at modulating the mechanical features of the immune response. **a**, Potentiating the mechanical activity of T cells (grey) can be achieved by enhancing their force exertion abilities (F), increasing the stability of immune synapses composed of the TCR (blue) recognizing tumour-associated antigens presented by MHC class I (pMHC, dark grey) and integrins, or controlling spatiotemporal activation of key genes through novel tools (for example, microbubbles and ultrasounds activating genes expression under the nuclear factor of activated T-cells (NFAT) promoter). **b**, Inducing ECM remodelling through release of degradation enzymes, impairing ECM crosslinking with inhibitors, or decreasing ECM protein production in fibroblasts can improve immune cell infiltration to target disease sites. **c**, Altering the mechanical properties of tumour cells (blue) to increase force transmission at the IS and potentiate antitumour activity of immune cells can be achieved by using stiffening agents such as MeβCD, or antibodies/arginylglycylaspartic acid (RGD) targeted nanoparticles loaded with anticancer drug or gene therapy.

dynamic movement and low frequency of tumour antigen-specific T cells in the circulation[158].

Instead, stiffening tumour cells during the invasion and migration processes, at which stage they typically display soft mechanical phenotypes, may be a promising strategy to sensitize them to T- and NK-cell-mediated killing. Enhancing cancer cell stiffness could also favour macrophage engulfment as the target stiffness could partially override the SIRPα-CD47 'don't eat me' immune checkpoint[76]. Previous studies have shown that depleting membrane cholesterol using MeβCD[15], activating myosin with 4-hydroxyacetophenone (4-HAP)[159] or inducing actin crosslinking with jasplakinolide[13,28] can stiffen cancer cells. However, none of these pharmacological approaches are specific. A challenging aspect of such strategies is to find ways to specifically stiffen the tumour cells without stiffening the ECM, which would hinder immune cell infiltration, possibly trigger pro-metastatic mechanotransduction in tumour cells and all-in-all be counterproductive. Tumour-targeted-nanoparticles might be a promising tool for achieving specific stiffening of tumour cells[160]. Moreover, their own mechanical properties can be tuned to foster their internalization in tumour cells. Soft nanomaterials and microparticles tend to better accumulate in tumour tissues and be preferentially taken up by cancer cells[161,162]. In a recent example, anticancer drug-loaded nanoparticles were developed to target soft cancer stem cells, allowing their specific elimination in vitro and in vivo with minimal side effects[163]. Besides, recent studies have also demonstrated that cancer cells can be transiently stiffened through increased F-actin polymerization upon internalization of iron oxide nanoparticles[164]. Cytoskeleton alterations and cell stiffening upon nanoparticle internalization have been described in macrophages[165] and such an approach might also be applied to tumour cells. As an alternative mechanical intervention approach, gene therapies for overexpression of MRTF and acyl-CoA:cholesterol acyltransferase 1 might be promising to facilitate specific stiffening of cancer cells[14,15].

Targeting tumour ECM mechanics for enhanced immunotherapy

The tumour microenvironment (TME) is known to impair anticancer immune responses. In addition to the highly immunosuppressive biochemical signals in the TME[166], its biophysical properties play a crucial role in immune cell migration and activation. During malignant progression, increased ECM stiffness together with other biochemical changes (for example, integrin clustering, altered chemokine profile) alter infiltration of T cells and other anticancer immune cells, and restricts them away from tumour cell nests, which reduces their antitumoural capacities[22,167,168]. Factors including TGFβ, matrix components and integrins are known to control the mechanical properties of the tumour ECM and its sensing by cancer cells. In addition, recent studies have shed light on how ECM mechanical properties might impact tumour cell dormancy[169,170]. Therefore, targeting actors of ECM stiffness and improving the diffusion of chemotherapeutic drugs and/or immune cells is a therapeutic approach with clinical potential[171] (Fig. 3). Inhibiting the production of matrix components by fibroblasts can be achieved by blocking the TGFβ profibrotic pathway. The use of neutralizing antibodies or the repurposing of angiotensin inhibitors, such as Losartan, has been shown to efficiently reduce collagen and hyaluronic acid production[172,173]. Collagen fibre alignment can also be reduced by targeting the discoidin domain receptor 1 (DDR1) ectodomain with monoclonal antibodies[169]. This strategy restores T-cell invasion into the tumour bed, resulting in remission in 56% of treated mice bearing triple-negative breast cancer. Conversely, DDR1 has been described to sustain tumour cell dormancy by maintaining type III collagen fibre at a low degree of alignment[170]. Hence, DDR1 depletion and subsequent realignment of collagen fibres was found to be a key trait of the dormancy-to-reactivation transition[170]. Of note, this study also indicates that enriching the TME with collagen III could promote or even induce a dormant state, thus preventing the formation of metastases[170].

Hyaluronic acid can also be reduced in the tumour ECM by using degradative enzymes, such as the pegvorhyaluronidase alfa investigated in a phase III clinical trial in association with gemcitabine for patients presenting hyaluronan-high metastatic pancreatic adenocarcinoma (NCT02715804)[174]. However, the use of hyaluronidase might also degrade avascular cartilage. A hyaluronidase nanoformulation showed no accumulation at these sites[175]. When combined with gemcitabine to treat a pancreatic ductal adenocarcinoma mouse model, the hyaluronidase nanoformulation resulted in a near doubling of overall survival[175]. The safety of use can be further improved by developing TME-responsive nanoparticles. Reactive-oxygen-species-activatable collagenase is selectively activated in the TME, relieving ECM stress and increasing paclitaxel penetration[176]. Degradative enzymes of ECM components can be used to enhance adoptive cell transfer immunotherapies. One strategy relies on engineered chimeric antigen receptor (CAR)-T cells secreting heparanase, which degrades heparan sulfate

proteoglycans, one of the main components of the ECM[177]. These heparanase-secreting CAR-T cells showed improved ECM degradation capacity, which promoted immune cell infiltration in tumour xenografts, resulting in increased survival of treated mice[177]. Recently, new strategies based on the bioorthogonal modification of the surface of immune cells to avoid viral transfection have been developed[178,179]. CAR-T cells cultured with azide-containing saccharides allowed for metabolic incorporation and membrane expression of azide groups for further conjugation with dibenzocyclooctyne-modified hyaluronidase through click chemistry[180]. These hyaluronidase-modified CAR-T cells presented better infiltration in the tumour, which correlated with improved tumour regression and survival.

As an alternative strategy, ECM stiffness can be reduced by preventing matrix crosslinking. Lysyl oxidase (LOX) is an enzyme responsible for the reticulation of collagen fibres[17]. Its inhibition by β-aminopropionitrile allowed to overcome chemoresistance and increase intratumoural T-cell migration, thus improving response to anti-PD-1 therapy[181,182]. The co-encapsulation of LOX inhibitors and epirubicin resulted in better biocompatibility and prolonged survival, providing an all-in-one nanoparticle-based ECM-targeting chemotherapy for cancer treatment[183]. Nanoparticle-based approaches can also be used to assess LOX activity in the tumour ECM and allow selection of patients that may benefit from LOX inhibitor treatments in addition to their chemotherapy[184]. Other studies have shown that LOX antibodies functionalized on polymeric poly(lactic-*co*-glycolic acid) (PLGA) nanoparticles efficiently decrease the expansion of breast cancer[185].

Finally, inhibiting fibroblast contractility may help to reduce global ECM integrity. Among the different targets, the use of fasudil to inhibit the Rho-associated protein kinase leads to loss of stress fibres and focal adhesion complexes[186]. Fasudil treatment, hence, alters cytoskeleton-based contractility of fibroblasts, disrupting ECM integrity and improving chemotherapy effectiveness[186]. Other studies have shown that focal adhesion kinases can be directly inhibited, reducing ECM force transmission to the actomyosin complex, and thus reducing cellular response to matrix mechanical cues. A focal-adhesion-kinase inhibitor (AMP945) improved response to gemcitabine in a pancreatic adenocarcinoma model and is now being investigated in a phase II clinical trial for this indication (NCT05355298)[187]. However, these molecules can lead to life-threatening adverse events, such as hypotension, hepatotoxicity and excessive bleeding. Efforts to develop targeted formulations of these molecules are still required to improve their safety in clinics. CAFs expressing the fibroblast activation protein (FAP) are found in nearly all solid tumours and can be depleted by using anti-FAP CAR-T cells. Several studies have evaluated the use of anti-FAP CAR-T cells, and it has been shown that depletion of FAP^+ stromal cells results in decreased tumour growth in an immune-dependent fashion[188,189]. Of interest, this strategy is also investigated to treat post-cardiac infraction fibrosis and to restore cardiac function[190]. While killing fibroblasts at the primary tumour site could reduce global ECM stiffness, their destruction in target organs of dissemination could help to maintain tumour cell dormancy[191]. Indeed, hepatic stellate cell activation upon chronic liver injury induces a myofibroblast-like phenotype that further disrupts NK-cell-sustained breast cancer dormancy[191]. As FAP is also expressed by skeletal muscle, adipose tissue and pancreas, depleting FAP^+ stromal cells can lead to muscle atrophy, bone marrow hypoplasia and rapid weight loss[192].

Strategies to soften the ECM have been extensively studied to enhance the diffusion of chemotherapeutic drugs into the tumour bed and could favour tumour targeting of other therapeutics, such as antibodies or CAR-T cells, whose access is also hindered by the stiff ECM[22,193]. Yet, only a few studies have investigated the perspective of ECM stiffness disruption to increase intratumoural T-cell migration and response to PD-1 blockade[169,177,180,182]. As ECM proteins cover a large part of the physical barrier hindering immune cell migration, strategies involving engineered CAR-T cells capable of degrading ECM proteins are elegant due to their abilities to degrade ECM while migrating and performing tumour cell killing. The therapeutic advantage of ECM softening in immune checkpoint blockage and cellular immunotherapies remains to be evaluated. Yet, due to the potential opposite functions of some targeted molecules, any therapeutic strategy aimed at influencing the ECM architecture will require careful planning and timing. Finally, combining these approaches with methods to control cell mechanics in an all-mechanics strategy, could synergistically enhance antitumour immune surveillance.

Mechanically enhanced T- and NK-cell-based immunotherapies

Most immunotherapies currently aim at targeting biochemical cues of tumours and immune cells to enhance the immune response. The emergence of the 'mechano-immune surveillance' concept paves the way for developing next-generation therapeutic strategies targeting biophysical features of immune cells to boost their functions against various diseases. Selective delivery to immune cells could be achieved by targeting selective immune markers with antibody–nanoparticle conjugates[160]. One such approach of mechanical immunoengineering could aim at enhancing the tumour infiltration of T cells. As described previously, tumour ECM presents a mechanical hurdle for antitumour immune cells to access the tumour bed[22,167,168]. One could circumvent that by further favouring the through-matrix migration potential of immune cells. For example, pharmacological or genetic manipulation of microtubules of T cells increases Rho-pathway-dependent cortical contractility, which favoured infiltration in a three-dimensional environment in vitro by shifting $CD4^+$ T cells towards an amoeboid phenotype[194]. In stark contrast, microtubule stabilization with a commonly used drug, taxol, induced a marked reduction in T-cell infiltration abilities.

Another strategy is to enhance the mechanosensitivity of immune cells. Mechanical force exertion and underlying actin remodelling are essential for IS formation and stabilization[109,112,115,116]. Indeed, treatment of T cells with the actin polymerization inhibitor latrunculin A resulted in complete abrogation of force exertion by T cells and consequent loss of activation and effector functions[12]. In contrast, modulation of actin polymerization-stimulating proteins at the lymphocyte/APC interface could provide a strategy for enhancing T-cell force exertion and thereby, possibly enhancing effector function and cytotoxicity. A series of studies showed that CTLs with phosphatase and tensin homologue (PTEN) knockdown show increased force exertion and enhanced tumour cell killing in vitro[12]. While CTL granule polarization and release were unaffected by PTEN knockdown, this strategy led to limited improvement of tumour growth control in vivo[195]. Nevertheless, the involvement of PTEN in numerous cellular processes makes it challenging for systemic inhibition of PTEN using pharmacological or genetic therapies, representing a key limitation in this strategy.

As an alternative approach, one may engineer T cells capable of developing a stable IS (Fig. 3). The canonical IS is characterized by a concentric architecture in which a central cluster of antigen-presenting receptors is surrounded by concentric, annular accumulations of integrins and F-actin[140]. In contrast to the IS of the TCR:peptide–MHC complex, the non-classical CAR IS shows less-organized structures with diffusive CAR:antigen clustering and reduced actin distribution[196]. As the IS structure and morphology influence the effector functions, CAR-NK cells have recently been engineered with a novel receptor that modulates and tunes the IS to a more ordered state[197]. Fusing a second-generation CAR with the post-synaptic density protein 95, *Drosophila* disc large tumour suppressor and zonula occludens-1 protein (PDZ) domain of a molecule implicated in IS formation, the cytotoxic and regulatory-T-cell-associated molecule, resulted in increased synaptic area and accumulation of pZAP70, a key kinase in T-cell signalling[197]. Moreover, the PDZ domain enabled additional scaffolding crosslinks between the CAR and the cytoskeleton via mediators such as ezrin.

Anchoring the receptor to cytoskeletal components enhanced the avidity and binding strength of IS thus succeeding in higher antitumour activity. CAR-T and CAR-NK cells were elegantly developed with synthetic Notch receptor (SynNotch) or apelin-based synthetic Notch receptor to increase their safety and expand the set of targetable antigens[198]. Activation of these receptors by their cognate ligand caused the proteolytic cleavage of their intramembrane domain, releasing a transcriptional factor that could activate a specific transcriptional programme (expression of a CAR, cytokines and so on)[199]. Structure-guided mutagenesis was also used to develop new cutting-edge designs of SynNotch receptors capable of increasing mechanical sensitivity to the piconewton range[200]. In response to varying tensile forces, these receptors are expected to enact tailored transcriptional programmes. These studies provide evidence that tuning the IS via anchoring domains or by repurposing SynNotch receptors to increase mechanosensitivity might offer an orthogonal and complementary dimension to biochemical engineering for CAR-based immunotherapies.

In addition, nanoparticles can be leveraged to improve immune cell activation. Several types of artificial APC composed of nanoparticles coated with anti-CD3, anti-CD28 or peptide–MHC complex have been developed[201] and can be used to trigger T-cell activation and expansion in vitro by TCR clustering under a magnetic field[202,203]. After adoptive cell transfer, these ex vivo-activated T cells showed better tumour control. Some ultrasmall silica nanoparticles can directly ligate the TCR:CD3 complex and activate the T cells[204]. As ultrasmall nanoparticles avoid liver accumulation and are quickly eliminated by renal clearance, they present very promising clinical translation prospects. A similar strategy has been evaluated for NK-cell activation. Magneto-activated NK cells show increased secretion of lytic granules correlating with therapeutic efficacies against hepatocellular carcinoma[205,206]. Other optomechanical actuators can be used to trigger immune cell activation such as optical systems[207] or ultrasounds[208]. However, these optical systems are poorly transferable in vivo due to the low light penetration through tissues (mirometres to millimetres)[209]. On the other hand, ultrasounds can penetrate tissues up to several centimetres. A sonic stimulus of integrin-bound microbubbles was used to induce calcium influx[210] through PIEZO1 channels in T cells in vitro. This was followed by the nuclear factor of activated T cells transcription factor translocation to the nucleus, which drove expression of T-cell activation genes. Despite the originality of this approach, in vivo translation is limited as shear forces will probably damage or burst the microbubbles coupled to T cells during their migration and extravasation.

Outlook

This Review has outlined the changes in cellular and tissular biomechanical properties arising in several pathological processes such as infectious diseases, fibrosis and, most importantly, cancer. We highlighted how immune cells sense these biomechanical changes and tune their response accordingly. The recent advances in the understanding of disease mechanobiology impact on immune surveillance mechanisms gave birth to a promising mechanical immunoengineering field where additional in vivo studies in preclinical models will be instrumental to develop efficient therapies. Preliminary studies have shown that different approaches can leverage immune cell mechano-activation. Nevertheless, each target should be thoroughly analysed and evaluated for its potential for desired therapeutic applications. In the context of cancer in particular, a further and closer inspection of tumour cell mechanics and how it evolves and adapts throughout disease progression is warranted to optimize the inhibitory tools. Although many challenges arise, mechanical modulation of effectors and/or targets, through genetic, pharmacogenetic or nanomedicine approaches is expected to evolve and gain precision in the future. We envision that mechanical immunoengineering will lead to a paradigm shift in the design of next-generation immunotherapy by combining approaches targeting biochemical and biophysical disease–immune interactions.

References

1. Klotter, V. et al. Assessment of pathologic increase in liver stiffness enables earlier diagnosis of CFLD: results from a prospective longitudinal cohort study. *PLoS ONE* **12**, e0178784 (2017).
2. Medrano, L. M. et al. Elevated liver stiffness is linked to increased biomarkers of inflammation and immune activation in HIV/hepatitis C virus-coinfected patients. *AIDS* **32**, 1095–1105 (2018).
3. Tomlin, H. & Piccinini, A. M. A complex interplay between the extracellular matrix and the innate immune response to microbial pathogens. *Immunology* **155**, 186–201 (2018).
4. Martinez-Vidal, L. et al. Causal contributors to tissue stiffness and clinical relevance in urology. *Commun. Biol.* **4**, 1011 (2021).
5. Mohammadi, H. & Sahai, E. Mechanisms and impact of altered tumour mechanics. *Nat. Cell Biol.* **20**, 766–774 (2018).
6. Du, H. et al. Tuning immunity through tissue mechanotransduction. *Nat. Rev. Immunol.* https://doi.org/10.1038/s41577-022-00761-w (2022).
7. Zhu, C., Chen, W., Lou, J., Rittase, W. & Li, K. Mechanosensing through immunoreceptors. *Nat. Immunol.* **20**, 1269–1278 (2019).
8. Judokusumo, E., Tabdanov, E., Kumari, S., Dustin, M. L. & Kam, L. C. Mechanosensing in T lymphocyte activation. *Biophys. J.* **102**, L5–L7 (2012).
9. O'Connor, R. S. et al. Substrate rigidity regulates human T cell activation and proliferation. *J. Immunol.* **189**, 1330–1339 (2012).
10. Saitakis, M. et al. Different TCR-induced T lymphocyte responses are potentiated by stiffness with variable sensitivity. *eLife* **6**, e23190 (2017).
11. Blumenthal, D., Chandra, V., Avery, L. & Burkhardt, J. K. Mouse T cell priming is enhanced by maturation-dependent stiffening of the dendritic cell cortex. *eLife* **9**, e55995 (2020).
Important work that sheds light on the mechanical aspect of dendritic cell-mediated activation of T cells.
12. Basu, R. et al. Cytotoxic T cells use mechanical force to potentiate target cell killing. *Cell* **165**, 100–110 (2016).
Seminal study that highlights the critical role of mechanical forces in cytotoxic activity of T cells.
13. Liu, Y. et al. Cell softness prevents cytolytic T-cell killing of tumor-repopulating cells. *Cancer Res.* **81**, 476–488 (2021).
14. Tello-Lafoz, M. et al. Cytotoxic lymphocytes target characteristic biophysical vulnerabilities in cancer. *Immunity* **54**, 1037–1054.e7 (2021).
15. Lei, K. et al. Cancer-cell stiffening via cholesterol depletion enhances adoptive T-cell immunotherapy. *Nat. Biomed. Eng.* **5**, 1411–1425 (2021).
Influential studies (refs. 14,15) that show that stiffening tumour cells through genetic manipulation targeting MRTF or by depleting cholesterol of the cell membrane results in higher vulnerabiliy to T-cell-mediated killing.
16. Provenzano, P. P. et al. Collagen reorganization at the tumor-stromal interface facilitates local invasion. *BMC Med.* **4**, 38 (2006).
17. Levental, K. R. et al. Matrix crosslinking forces tumor progression by enhancing integrin signaling. *Cell* **139**, 891–906 (2009).
18. Goetz, J. G. et al. Biomechanical remodeling of the microenvironment by stromal caveolin-1 favors tumor invasion and metastasis. *Cell* **146**, 148–163 (2011).
19. Massagué, J. TGFβ in cancer. *Cell* **134**, 215–230 (2008).
20. Insua-Rodríguez, J. et al. Stress signaling in breast cancer cells induces matrix components that promote chemoresistant metastasis. *EMBO Mol. Med.* **10**, e9003 (2018).
21. He, X. et al. Extracellular matrix physical properties govern the diffusion of nanoparticles in tumor microenvironment. *Proc. Natl Acad. Sci. USA* **120**, e2209260120 (2023).

22. Salmon, H. et al. Matrix architecture defines the preferential localization and migration of T cells into the stroma of human lung tumors. *J. Clin. Invest.* **122**, 899–910 (2012).
23. Salnikov, A. V. et al. Lowering of tumor interstitial fluid pressure specifically augments efficacy of chemotherapy. *FASEB J.* **17**, 1756–1758 (2003).
24. Guck, J. et al. Optical deformability as an inherent cell marker for testing malignant transformation and metastatic competence. *Biophys. J.* **88**, 3689–3698 (2005).
25. Plodinec, M. et al. The nanomechanical signature of breast cancer. *Nat. Nanotechnol.* **7**, 757–765 (2012).
26. Chen, Y., McAndrews, K. M. & Kalluri, R. Clinical and therapeutic relevance of cancer-associated fibroblasts. *Nat. Rev. Clin. Oncol.* **18**, 792–804 (2021).
27. Gensbittel, V. et al. Mechanical adaptability of tumor cells in metastasis. *Dev. Cell* **56**, 164–179 (2021).
This review presents the hypothesis that tumour cells adjust their mechanical properties throughout their metastatic journey.
28. Lv, J. et al. Cell softness regulates tumorigenicity and stemness of cancer cells. *EMBO J.* **40**, e106123 (2021).
29. Matthews, H. K. et al. Oncogenic signaling alters cell shape and mechanics to facilitate cell division under confinement. *Dev. Cell* **52**, 563–573.e3 (2020).
30. Young, K. M. et al. Correlating mechanical and gene expression data on the single cell level to investigate metastatic phenotypes. *iScience* **26**, 106393 (2023).
31. Rianna, C., Radmacher, M. & Kumar, S. Direct evidence that tumor cells soften when navigating confined spaces. *Mol. Biol. Cell* **31**, 1726–1734 (2020).
32. Regmi, S., Fu, A. & Luo, K. Q. High shear stresses under exercise condition destroy circulating tumor cells in a microfluidic system. *Sci. Rep.* **7**, 39975 (2017).
33. Moose, D. L. et al. Cancer cells resist mechanical destruction in circulation via rhoa/actomyosin-dependent mechano-adaptation. *Cell Rep.* **30**, 3864–3874.e6 (2020).
34. Chen, J. et al. Efficient extravasation of tumor-repopulating cells depends on cell deformability. *Sci. Rep.* **6**, 19304 (2016).
35. Saito, D. et al. Stiffness of primordial germ cells is required for their extravasation in avian embryos. *iScience* **25**, 105629 (2022).
36. Er, E. E. et al. Pericyte-like spreading by disseminated cancer cells activates YAP and MRTF for metastatic colonization. *Nat. Cell Biol.* **20**, 966–978 (2018).
37. Wen, Z., Zhang, Y., Lin, Z., Shi, K. & Jiu, Y. Cytoskeleton—a crucial key in host cell for coronavirus infection. *J. Mol. Cell. Biol.* **12**, 968–979 (2021).
38. Paluck, A. et al. Role of ARP2/3 complex-driven actin polymerization in RSV infection. *Pathogens* **11**, 26 (2021).
39. Kubánková, M. et al. Physical phenotype of blood cells is altered in COVID-19. *Biophys. J.* **120**, 2838–2847 (2021).
40. Yang, J., Barrila, J., Roland, K. L., Ott, C. M. & Nickerson, C. A. Physiological fluid shear alters the virulence potential of invasive multidrug-resistant non-typhoidal *Salmonella typhimurium* D23580. *npj Microgravity* **2**, 16021 (2016).
41. Padron, G. C. et al. Shear rate sensitizes bacterial pathogens to H_2O_2 stress. *Proc. Natl Acad. Sci. USA* **120**, e2216774120 (2023).
42. Mikaty, G. et al. Extracellular bacterial pathogen induces host cell surface reorganization to resist shear stress. *PLoS Pathog.* **5**, e1000314 (2009).
43. Kuo, C. et al. Rhinovirus infection induces extracellular matrix protein deposition in asthmatic and nonasthmatic airway smooth muscle cells. *Am. J. Physiol. Lung Cell. Mol. Physiol.* **300**, L951–L957 (2011).
44. Nagy, N. et al. Hyaluronan in immune dysregulation and autoimmune diseases. *Matrix Biol.* **78–79**, 292–313 (2019).
45. Fingleton, B. Matrix metalloproteinases as regulators of inflammatory processes. *Biochim. Biophys. Acta Mol. Cell Res.* **1864**, 2036–2042 (2017).
46. Krishnamurty, A. T. & Turley, S. J. Lymph node stromal cells: cartographers of the immune system. *Nat. Immunol.* **21**, 369–380 (2020).
47. Wynn, T. A. Integrating mechanisms of pulmonary fibrosis. *J. Exp. Med.* **208**, 1339–1350 (2011).
48. Tschöpe, C. et al. Myocarditis and inflammatory cardiomyopathy: current evidence and future directions. *Nat. Rev. Cardiol.* **18**, 169–193 (2021).
49. Fabre, T. et al. Identification of a broadly fibrogenic macrophage subset induced by type 3 inflammation. *Sci. Immunol.* **8**, eadd8945 (2023).
50. de Boer, R. A. et al. Towards better definition, quantification and treatment of fibrosis in heart failure. A scientific roadmap by the Committee of Translational Research of the Heart Failure Association (HFA) of the European Society of Cardiology. *Eur. J. Heart Fail.* **21**, 272–285 (2019).
51. Liu, F. et al. Feedback amplification of fibrosis through matrix stiffening and COX-2 suppression. *J. Cell Biol.* **190**, 693–706 (2010).
52. Georges, P. C. et al. Increased stiffness of the rat liver precedes matrix deposition: implications for fibrosis. *Am. J. Physiol. Gastrointest. Liver Physiol.* **293**, G1147–G1154 (2007).
53. Stock, K. F. et al. ARFI-based tissue elasticity quantification in comparison to histology for the diagnosis of renal transplant fibrosis. *Clin. Hemorheol. Microcirc.* **46**, 139–148 (2010).
54. Gadd, V. L. et al. The portal inflammatory infiltrate and ductular reaction in human nonalcoholic fatty liver disease. *Hepatology* **59**, 1393–1405 (2014).
55. Mogilenko, D. A., Shchukina, I. & Artyomov, M. N. Immune ageing at single-cell resolution. *Nat. Rev. Immunol.* **22**, 484–498 (2022).
56. Roman, M. J. et al. Arterial stiffness in chronic inflammatory diseases. *Hypertension* **46**, 194–199 (2005).
57. Klingberg, F., Hinz, B. & White, E. S. The myofibroblast matrix: implications for tissue repair and fibrosis: the myofibroblast matrix. *J. Pathol.* **229**, 298–309 (2013).
58. Liu, F. et al. Mechanosignaling through YAP and TAZ drives fibroblast activation and fibrosis. *Am. J. Physiol. Lung Cell. Mol. Physiol.* **308**, L344–L357 (2015).
59. Tomasek, J. J., Gabbiani, G., Hinz, B., Chaponnier, C. & Brown, R. A. Myofibroblasts and mechano-regulation of connective tissue remodelling. *Nat. Rev. Mol. Cell Biol.* **3**, 349–363 (2002).
60. Munger, J. S. et al. A mechanism for regulating pulmonary inflammation and fibrosis: the integrin αvβ6 binds and activates latent TGF β1. *Cell* **96**, 319–328 (1999).
61. Santos, A. & Lagares, D. Matrix stiffness: the conductor of organ fibrosis. *Curr. Rheumatol. Rep.* **20**, 2 (2018).
62. Morvan, M. G. & Lanier, L. L. NK cells and cancer: you can teach innate cells new tricks. *Nat. Rev. Cancer* **16**, 7–19 (2016).
63. Janeway, C. A. How the immune system works to protect the host from infection: a personal view. *Proc. Natl Acad. Sci. USA* **98**, 7461–7468 (2001).
64. Dustin, M. L. T-cell activation through immunological synapses and kinapses. *Immunol. Rev.* **221**, 77–89 (2008).
65. Feng, Y., Zhao, X., White, A. K., Garcia, K. C. & Fordyce, P. M. A bead-based method for high-throughput mapping of the sequence- and force-dependence of T cell activation. *Nat. Methods* **19**, 1295–1305 (2022).
66. Mordechay, L. et al. Mechanical regulation of the cytotoxic activity of natural killer cells. *ACS Biomater. Sci. Eng.* **7**, 122–132 (2021).

67. Lei, K., Kurum, A. & Tang, L. Mechanical immunoengineering of T cells for therapeutic applications. *Acc. Chem. Res.* **53**, 2777–2790 (2020).
Comprehensive review on recent advances in mechanical immunoengineering and their potential therapeutic applications.
68. Seghir, R. & Arscott, S. Extended PDMS stiffness range for flexible systems. *Sens. Actuators Phys.* **230**, 33–39 (2015).
69. Guimarães, C. F., Gasperini, L., Marques, A. P. & Reis, R. L. The stiffness of living tissues and its implications for tissue engineering. *Nat. Rev. Mater.* **5**, 351–370 (2020).
70. Denisin, A. K. & Pruitt, B. L. Tuning the range of polyacrylamide gel stiffness for mechanobiology applications. *ACS Appl. Mater. Interfaces* **8**, 21893–21902 (2016).
71. Geissmann, F. et al. Development of monocytes, macrophages, and dendritic cells. *Science* **327**, 656–661 (2010).
72. Follain, G. et al. Fluids and their mechanics in tumour transit: shaping metastasis. *Nat. Rev. Cancer* **20**, 107–124 (2020).
73. Baratchi, S. et al. Transcatheter aortic valve implantation represents an anti-inflammatory therapy via reduction of shear stress–induced, piezo-1–mediated monocyte activation. *Circulation* **142**, 1092–1105 (2020).
74. Serafini, N. et al. The TRPM4 channel controls monocyte and macrophage, but not neutrophil, function for survival in sepsis. *J. Immunol.* **189**, 3689–3699 (2012).
75. Beningo, K. A. & Wang, Y. Fc-receptor-mediated phagocytosis is regulated by mechanical properties of the target. *J. Cell Sci.* **115**, 849–856 (2002).
76. Sosale, N. G. et al. Cell rigidity and shape override CD47's 'self'-signaling in phagocytosis by hyperactivating myosin-II. *Blood* **125**, 542–552 (2015).
77. Sridharan, R., Cavanagh, B., Cameron, A. R., Kelly, D. J. & O'Brien, F. J. Material stiffness influences the polarization state, function and migration mode of macrophages. *Acta Biomater.* **89**, 47–59 (2019).
78. Hu, Y. et al. Molecular force imaging reveals that integrin-dependent mechanical checkpoint regulates Fcγ-receptor-mediated phagocytosis in macrophages. *Nano Lett.* **23**, 5562–5572 (2023).
79. Atcha, H. et al. Mechanically activated ion channel Piezo1 modulates macrophage polarization and stiffness sensing. *Nat. Commun.* **12**, 3256 (2021).
80. Geng, J. et al. TLR4 signalling via Piezo1 engages and enhances the macrophage mediated host response during bacterial infection. *Nat. Commun.* **12**, 3519 (2021).
81. Dupont, S. et al. Role of YAP/TAZ in mechanotransduction. *Nature* **474**, 179–183 (2011).
82. Rice, A. J. et al. Matrix stiffness induces epithelial–mesenchymal transition and promotes chemoresistance in pancreatic cancer cells. *Oncogenesis* **6**, e352 (2017).
83. Oliver-De La Cruz, J. et al. Substrate mechanics controls adipogenesis through YAP phosphorylation by dictating cell spreading. *Biomaterials* **205**, 64–80 (2019).
84. Meli, V. S. et al. YAP-mediated mechanotransduction tunes the macrophage inflammatory response. *Sci. Adv.* **6**, eabb8471 (2020).
85. Steinman, R. M. Decisions about dendritic cells: past, present, and future. *Annu. Rev. Immunol.* **30**, 1–22 (2012).
86. Moreau, H. D. et al. Macropinocytosis overcomes directional bias in dendritic cells due to hydraulic resistance and facilitates space exploration. *Dev. Cell* **49**, 171–188.e5 (2019).
87. Laplaud, V. et al. Pinching the cortex of live cells reveals thickness instabilities caused by myosin II motors. *Sci. Adv.* **7**, eabe3640 (2021).
88. Barbier, L. et al. Myosin II activity is selectively needed for migration in highly confined microenvironments in mature dendritic cells. *Front. Immunol.* **10**, 747 (2019).
89. Chabaud, M. et al. Cell migration and antigen capture are antagonistic processes coupled by myosin II in dendritic cells. *Nat. Commun.* **6**, 7526 (2015).
90. Leithner, A. et al. Dendritic cell actin dynamics control contact duration and priming efficiency at the immunological synapse. *J. Cell Biol.* **220**, e202006081 (2021).
91. Kang, J.-H. et al. Biomechanical forces enhance directed migration and activation of bone marrow-derived dendritic cells. *Sci. Rep.* **11**, 12106 (2021).
92. van den Dries, K. et al. Geometry sensing by dendritic cells dictates spatial organization and PGE2-induced dissolution of podosomes. *Cell. Mol. Life Sci.* **69**, 1889–1901 (2012).
93. Chakraborty, M. et al. Mechanical stiffness controls dendritic cell metabolism and function. *Cell Rep.* **34**, 108609 (2021).
94. Mennens, S. F. B. et al. Substrate stiffness influences phenotype and function of human antigen-presenting dendritic cells. *Sci. Rep.* **7**, 17511 (2017).
95. Figdor, C. G., van Kooyk, Y. & Adema, G. J. C-type lectin receptors on dendritic cells and langerhans cells. *Nat. Rev. Immunol.* **2**, 77–84 (2002).
96. Bufi, N. et al. Human primary immune cells exhibit distinct mechanical properties that are modified by inflammation. *Biophys. J.* **108**, 2181–2190 (2015).
97. Comrie, W. A., Babich, A. & Burkhardt, J. K. F-actin flow drives affinity maturation and spatial organization of LFA-1 at the immunological synapse. *J. Cell Biol.* **208**, 475–491 (2015).
98. Wang, Y. et al. Dendritic cell Piezo1 directs the differentiation of T_H1 and T_{reg} cells in cancer. *eLife* **11**, e79957 (2022).
99. Valignat, M.-P. et al. Lymphocytes can self-steer passively with wind vane uropods. *Nat. Commun.* **5**, 5213 (2014).
100. Roy, N. H., MacKay, J. L., Robertson, T. F., Hammer, D. A. & Burkhardt, J. K. Crk adaptor proteins mediate actin-dependent T cell migration and mechanosensing induced by the integrin LFA-1. *Sci. Signal.* **11**, eaat3178 (2018).
101. Hope, J. M. et al. Fluid shear stress enhances T cell activation through Piezo1. *BMC Biol.* **20**, 61 (2022).
102. Husson, J., Chemin, K., Bohineust, A., Hivroz, C. & Henry, N. Force generation upon T cell receptor engagement. *PLoS ONE* **6**, e19680 (2011).
An elegant use of a biomembrane force probe technique for measuring forces exerted by T cells upon engagement with antigen-presenting cells.
103. Liu, B., Chen, W., Evavold, B. D. & Zhu, C. Accumulation of dynamic catch bonds between TCR and agonist peptide–MHC triggers T cell signaling. *Cell* **157**, 357–368 (2014).
104. Thauland, T. J., Hu, K. H., Bruce, M. A. & Butte, M. J. Cytoskeletal adaptivity regulates T cell receptor signaling. *Sci. Signal.* **10**, eaah3737 (2017).
105. Gaertner, F. et al. WASp triggers mechanosensitive actin patches to facilitate immune cell migration in dense tissues. *Dev. Cell* **57**, 47–62.e9 (2022).
106. Majedi, F. S. et al. T-cell activation is modulated by the 3D mechanical microenvironment. *Biomaterials* **252**, 120058 (2020).
107. Wang, H. et al. ZAP-70: an essential kinase in T-cell signaling. *Cold Spring Harb. Perspect. Biol.* **2**, a002279 (2010).
108. Bashour, K. T. et al. CD28 and CD3 have complementary roles in T-cell traction forces. *Proc. Natl Acad. Sci. USA* **111**, 2241–2246 (2014).
109. Hu, K. H. & Butte, M. J. T cell activation requires force generation. *J. Cell Biol.* **213**, 535–542 (2016).
110. Liu, Y. et al. DNA-based nanoparticle tension sensors reveal that T-cell receptors transmit defined pN forces to their antigens for enhanced fidelity. *Proc. Natl Acad. Sci. USA* **113**, 5610–5615 (2016).
111. Tabdanov, E. et al. Micropatterning of TCR and LFA-1 ligands reveals complementary effects on cytoskeleton mechanics in T cells. *Integr. Biol.* **7**, 1272–1284 (2015).

112. Govendir, M. A. et al. T cell cytoskeletal forces shape synapse topography for targeted lysis via membrane curvature bias of perforin. *Dev. Cell* **57**, 2237–2247.e8 (2022).
113. Wang, M. S. et al. Mechanically active integrins target lytic secretion at the immune synapse to facilitate cellular cytotoxicity. *Nat. Commun.* **13**, 3222 (2022).
114. Liu, C. S. C. et al. Cutting edge: Piezo1 mechanosensors optimize human T cell activation. *J. Immunol.* **200**, 1255–1260 (2018).
115. Jin, W. et al. T cell activation and immune synapse organization respond to the microscale mechanics of structured surfaces. *Proc. Natl Acad. Sci. USA* **116**, 19835–19840 (2019).
116. Kumari, S. et al. Cytoskeletal tension actively sustains the migratory T-cell synaptic contact. *EMBO J.* **39**, e102783 (2020).
117. Huby, R. D. J., Weiss, A. & Ley, S. C. Nocodazole inhibits signal transduction by the T cell antigen receptor. *J. Biol. Chem.* **273**, 12024–12031 (1998).
118. Le Saux, G. et al. Nanoscale mechanosensing of natural killer cells is revealed by antigen-functionalized nanowires. *Adv. Mater.* **31**, 1805954 (2019).
119. Bhingardive, V. et al. Nanowire based mechanostimulating platform for tunable activation of natural killer cells. *Adv. Funct. Mater.* **31**, 2103063 (2021).
120. Brumbaugh, K. M. et al. Functional role for Syk tyrosine kinase in natural killer cell-mediated natural cytotoxicity. *J. Exp. Med.* **186**, 1965–1974 (1997).
121. Matalon, O. et al. Actin retrograde flow controls natural killer cell response by regulating the conformation state of SHP-1. *EMBO J.* **37**, e96264 (2018).
122. Garrity, D., Call, M. E., Feng, J. & Wucherpfennig, K. W. The activating NKG2D receptor assembles in the membrane with two signaling dimers into a hexameric structure. *Proc. Natl Acad. Sci. USA* **102**, 7641–7646 (2005).
123. Friedman, D. et al. Natural killer cell immune synapse formation and cytotoxicity are controlled by tension of the target interface. *J. Cell Sci.* **134**, jcs258570 (2021).
124. Yanamandra, A. K. et al. PIEZO1-mediated mechanosensing governs NK cell killing efficiency in 3D. Preprint at https://doi.org/10.1101/2023.03.27.534435 (2023).
125. Wan, Z. et al. B cell activation is regulated by the stiffness properties of the substrate presenting the antigens. *J. Immunol.* **190**, 4661–4675 (2013).
126. Natkanski, E. et al. B cells use mechanical energy to discriminate antigen affinities. *Science* **340**, 1587–1590 (2013).
127. Merino-Cortés, S. V. et al. Diacylglycerol kinase ζ promotes actin cytoskeleton remodeling and mechanical forces at the B cell immune synapse. *Sci. Signal.* **13**, eaaw8214 (2020).
128. Zeng, Y. et al. Substrate stiffness regulates B-cell activation, proliferation, class switch, and T-cell-independent antibody responses in vivo: Cellular immune response. *Eur. J. Immunol.* **45**, 1621–1634 (2015).
129. Nowosad, C. R., Spillane, K. M. & Tolar, P. Germinal center B cells recognize antigen through a specialized immune synapse architecture. *Nat. Immunol.* **17**, 870–877 (2016).
130. Jiang, H. & Wang, S. Immune cells use active tugging forces to distinguish affinity and accelerate evolution. *Proc. Natl Acad. Sci. USA* **120**, e2213067120 (2023).
131. Stanton, R. J. et al. HCMV pUL135 remodels the actin cytoskeleton to impair immune recognition of infected cells. *Cell Host Microbe* **16**, 201–214 (2014).
132. Pai, R. K., Convery, M., Hamilton, T. A., Boom, W. H. & Harding, C. V. Inhibition of IFN-γ-induced class II transactivator expression by a 19-kDa lipoprotein from *Mycobacterium tuberculosis*: a potential mechanism for immune evasion. *J. Immunol.* **171**, 175–184 (2003).
133. Samassa, F. et al. *Shigella* impairs human T lymphocyte responsiveness by hijacking actin cytoskeleton dynamics and T cell receptor vesicular trafficking. *Cell. Microbiol.* **22**, e13166 (2020).
134. Hanč, P. et al. Structure of the complex of F-actin and DNGR-1, a C-type lectin receptor involved in dendritic cell cross-presentation of dead cell-associated antigens. *Immunity* **42**, 839–849 (2015).
135. Man, S. M. et al. Actin polymerization as a key innate immune effector mechanism to control *Salmonella* infection. *Proc. Natl Acad. Sci. USA* **111**, 17588–17593 (2014).
136. Jacobson, E. C. et al. Migration through a small pore disrupts inactive chromatin organization in neutrophil-like cells. *BMC Biol.* **16**, 142 (2018).
137. Solis, A. G. et al. Mechanosensation of cyclical force by PIEZO1 is essential for innate immunity. *Nature* **573**, 69–74 (2019).
138. Robledo-Avila, F. H., Ruiz-Rosado, J., de, D., Brockman, K. L. & Partida-Sánchez, S. The TRPM2 ion channel regulates inflammatory functions of neutrophils during *Listeria monocytogenes* infection. *Front. Immunol.* **11**, 97 (2020).
139. Meng, K. P., Majedi, F. S., Thauland, T. J. & Butte, M. J. Mechanosensing through YAP controls T cell activation and metabolism. *J. Exp. Med.* **217**, e20200053 (2020).
This study sheds light on T cells sensing the mechanical signals of their environment and tuning their response accordingly.
140. Al-Aghbar, M. A., Jainarayanan, A. K., Dustin, M. L. & Roffler, S. R. The interplay between membrane topology and mechanical forces in regulating T cell receptor activity. *Commun. Biol.* **5**, 40 (2022).
141. Wong, V. W. et al. Mechanical force prolongs acute inflammation via T-cell-dependent pathways during scar formation. *FASEB J.* **25**, 4498–4510 (2011).
142. Chen, D. S. & Mellman, I. Oncology meets immunology: the cancer-immunity cycle. *Immunity* **39**, 1–10 (2013).
143. O'Donnell, J. S., Teng, M. W. L. & Smyth, M. J. Cancer immunoediting and resistance to T cell-based immunotherapy. *Nat. Rev. Clin. Oncol.* **16**, 151–167 (2019).
144. Dustin, M. L. & Long, E. O. Cytotoxic immunological synapses: NK and CTL synapses. *Immunol. Rev.* **235**, 24–34 (2010).
145. González-Granado, J. M. et al. Nuclear envelope lamin-A couples actin dynamics with immunological synapse architecture and T cell activation. *Sci. Signal.* **7**, ra37 (2014).
146. González, C. et al. Nanobody-CD16 catch bond reveals NK cell mechanosensitivity. *Biophys. J.* **116**, 1516–1526 (2019).
147. Fan, J. et al. NKG2D discriminates diverse ligands through selectively mechano-regulated ligand conformational changes. *EMBO J.* **41**, e107739 (2022).
148. Tsopoulidis, N. et al. T cell receptor–triggered nuclear actin network formation drives $CD4^+$ T cell effector functions. *Sci. Immunol.* **4**, eaav1987 (2019).
149. Tamzalit, F. et al. Interfacial actin protrusions mechanically enhance killing by cytotoxic T cells. *Sci. Immunol.* **4**, eaav5445 (2019).
150. Sanchez, E. E. et al. Apoptotic contraction drives target cell release by cytotoxic T cells. *Nat. Immunol.* https://doi.org/10.1038/s41590-023-01572-4 (2023).
151. Händel, C. et al. Cell membrane softening in human breast and cervical cancer cells. *N. J. Phys.* **17**, 083008 (2015).
152. Huang, B., Song, B. & Xu, C. Cholesterol metabolism in cancer: mechanisms and therapeutic opportunities. *Nat. Metab.* **2**, 132–141 (2020).
153. Hanna, R. N. et al. Patrolling monocytes control tumor metastasis to the lung. *Science* **350**, 985–990 (2015).

154. Vyas, M. et al. Natural killer cells suppress cancer metastasis by eliminating circulating cancer cells. *Front. Immunol.* **13**, 1098445 (2023).
155. Hu, B., Xin, Y., Hu, G., Li, K. & Tan, Y. Fluid shear stress enhances natural killer cell's cytotoxicity toward circulating tumor cells through NKG2D-mediated mechanosensing. *APL Bioeng.* **7**, 036108 (2023).
156. Boussommier-Calleja, A. et al. The effects of monocytes on tumor cell extravasation in a 3D vascularized microfluidic model. *Biomaterials* **198**, 180–193 (2019).
157. Soderquest, K. et al. Monocytes control natural killer cell differentiation to effector phenotypes. *Blood* **117**, 4511–4518 (2011).
158. Kumar, B. V., Connors, T. J. & Farber, D. L. Human T cell development, localization, and function throughout life. *Immunity* **48**, 202–213 (2018).
159. Surcel, A. et al. Pharmacological activation of myosin II paralogs to correct cell mechanics defects. *Proc. Natl Acad. Sci. USA* **112**, 1428–1433 (2015).
160. Mittelheisser, V. et al. Optimal physicochemical properties of antibody–nanoparticle conjugates for improved tumor targeting. *Adv. Mater.* **34**, 2110305 (2022).
161. Guo, P. et al. Nanoparticle elasticity directs tumor uptake. *Nat. Commun.* **9**, 130 (2018).
162. Liang, Q. et al. The softness of tumour-cell-derived microparticles regulates their drug-delivery efficiency. *Nat. Biomed. Eng.* **3**, 729–740 (2019).
163. Chen, X. et al. Nanoparticle-mediated specific elimination of soft cancer stem cells by targeting low cell stiffness. *Acta Biomater.* **135**, 493–505 (2021).
164. Perez, J. E. et al. Transient cell stiffening triggered by magnetic nanoparticle exposure. *J. Nanobiotechnol.* **19**, 117 (2021).
165. Liu, Y. X. et al. Single-cell mechanics provides an effective means to probe in vivo interactions between alveolar macrophages and silver nanoparticles. *J. Phys. Chem. B* **119**, 15118–15129 (2015).
166. Binnewies, M. et al. Understanding the tumor immune microenvironment (TIME) for effective therapy. *Nat. Med.* **24**, 541–550 (2018).
167. Hartmann, N. et al. Prevailing role of contact guidance in intrastromal T-cell trapping in human pancreatic cancer. *Clin. Cancer Res.* **20**, 3422–3433 (2014).
168. Kuczek, D. E. et al. Collagen density regulates the activity of tumor-infiltrating T cells. *J. Immunother. Cancer* **7**, 68 (2019).
169. Sun, X. et al. Tumour DDR1 promotes collagen fibre alignment to instigate immune exclusion. *Nature* **599**, 673–678 (2021).
170. Di Martino, J. S. et al. A tumor-derived type III collagen-rich ECM niche regulates tumor cell dormancy. *Nat. Cancer* **3**, 90–107 (2021).
171. Lampi, M. C. & Reinhart-King, C. A. Targeting extracellular matrix stiffness to attenuate disease: from molecular mechanisms to clinical trials. *Sci. Transl. Med.* **10**, eaao0475 (2018).
172. Diop-Frimpong, B., Chauhan, V. P., Krane, S., Boucher, Y. & Jain, R. K. Losartan inhibits collagen I synthesis and improves the distribution and efficacy of nanotherapeutics in tumors. *Proc. Natl Acad. Sci. USA* **108**, 2909–2914 (2011).
173. Liu, J. et al. TGF-β blockade improves the distribution and efficacy of therapeutics in breast carcinoma by normalizing the tumor stroma. *Proc. Natl Acad. Sci. USA* **109**, 16618–16623 (2012).
174. Van Cutsem, E. et al. Randomized phase III trial of pegvorhyaluronidase alfa with nab-paclitaxel plus gemcitabine for patients with hyaluronan-high metastatic pancreatic adenocarcinoma. *J. Clin. Oncol.* **38**, 3185–3194 (2020).
175. Provenzano, P. P. et al. Enzymatic targeting of the stroma ablates physical barriers to treatment of pancreatic ductal adenocarcinoma. *Cancer Cell* **21**, 418–429 (2012).
176. Zhong, Y. et al. Tumor microenvironment-activatable nanoenzymes for mechanical remodeling of extracellular matrix and enhanced tumor chemotherapy. *Adv. Funct. Mater.* **31**, 2007544 (2021).
177. Caruana, I. et al. Heparanase promotes tumor infiltration and antitumor activity of CAR-redirected T lymphocytes. *Nat. Med.* **21**, 524–529 (2015).
178. Prescher, J. A., Dube, D. H. & Bertozzi, C. R. Chemical remodelling of cell surfaces in living animals. *Nature* **430**, 873–877 (2004).
179. Meng, D. et al. In situ activated NK cell as bio-orthogonal targeted live-cell nanocarrier augmented solid tumor immunotherapy. *Adv. Funct. Mater.* **32**, 2202603 (2022).
180. Zhao, Y. et al. Bioorthogonal equipping CAR-T cells with hyaluronidase and checkpoint blocking antibody for enhanced solid tumor immunotherapy. *ACS Cent. Sci.* **8**, 603–614 (2022).
181. Saatci, O. et al. Targeting lysyl oxidase (LOX) overcomes chemotherapy resistance in triple negative breast cancer. *Nat. Commun.* **11**, 2416 (2020).
182. Nicolas-Boluda, A. et al. Tumor stiffening reversion through collagen crosslinking inhibition improves T cell migration and anti-PD-1 treatment. *eLife* **10**, e58688 (2021).
183. De Vita, A. et al. Lysyl oxidase engineered lipid nanovesicles for the treatment of triple negative breast cancer. *Sci. Rep.* **11**, 5107 (2021).
184. Kim, H. Y. et al. Detection of lysyl oxidase activity in tumor extracellular matrix using peptide-functionalized gold nanoprobes. *Cancers* **13**, 4523 (2021).
185. Kanapathipillai, M. et al. Inhibition of mammary tumor growth using lysyl oxidase-targeting nanoparticles to modify extracellular matrix. *Nano Lett.* **12**, 3213–3217 (2012).
186. Vennin, C. et al. Transient tissue priming via ROCK inhibition uncouples pancreatic cancer progression, sensitivity to chemotherapy, and metastasis. *Sci. Transl. Med.* **9**, eaai8504 (2017).
A compelling demonstration that altering the mechanical features of the tumour environment holds great potential for improving therapies.
187. Murphy, K. J. et al. Intravital imaging technology guides FAK-mediated priming in pancreatic cancer precision medicine according to Merlin status. *Sci. Adv.* **7**, eabh0363 (2021).
188. Tran, E. et al. Immune targeting of fibroblast activation protein triggers recognition of multipotent bone marrow stromal cells and cachexia. *J. Exp. Med.* **210**, 1125–1135 (2013).
189. Wang, L.-C. S. et al. Targeting fibroblast activation protein in tumor stroma with chimeric antigen receptor T cells can inhibit tumor growth and augment host immunity without severe toxicity. *Cancer Immunol. Res.* **2**, 154–166 (2014).
190. Rurik, J. G. et al. CAR T cells produced in vivo to treat cardiac injury. *Science* **375**, 91–96 (2022).
191. Correia, A. L. et al. Hepatic stellate cells suppress NK cell-sustained breast cancer dormancy. *Nature* **594**, 566–571 (2021).
192. Roberts, E. W. et al. Depletion of stromal cells expressing fibroblast activation protein-α from skeletal muscle and bone marrow results in cachexia and anemia. *J. Exp. Med.* **210**, 1137–1151 (2013).
193. Fujimori, K., Covell, D. G., Fletcher, J. E. & Weinstein, J. N. Modeling analysis of the global and microscopic distribution of immunoglobulin G, F(ab')2, and Fab in tumors. *Cancer Res.* **49**, 5656–5663 (1989).

194. Tabdanov, E. D. et al. Engineering T cells to enhance 3D migration through structurally and mechanically complex tumor microenvironments. *Nat. Commun.* **12**, 2815 (2021).
195. Whitlock, B. *Enhancing Cytotoxic T Cell Killing by PTEN Depletion* (Weill Cornell Medicine, 2018).
196. Li, R., Ma, C., Cai, H. & Chen, W. The CAR T-cell mechano-immunology at a glance. *Adv. Sci.* **7**, 2002628 (2020).
197. Chockley, P. J., Ibanez-Vega, J., Krenciute, G., Talbot, L. J. & Gottschalk, S. Synapse-tuned CARs enhance immune cell anti-tumor activity. *Nat. Biotechnol.* https://doi.org/10.1038/s41587-022-01650-2 (2023).
This study shows that improving the immunological synapse architecture of CAR-NK cells leads to superior therapeutic efficacy.
198. Roybal, K. T. et al. Precision tumor recognition by T cells with combinatorial antigen-sensing circuits. *Cell* **164**, 770–779 (2016).
199. Gordon, W. R. et al. Mechanical allostery: evidence for a force requirement in the proteolytic activation of notch. *Dev. Cell* **33**, 729–736 (2015).
200. Sloas, D. C., Tran, J. C., Marzilli, A. M. & Ngo, J. T. Tension-tuned receptors for synthetic mechanotransduction and intercellular force detection. *Nat. Biotechnol.* https://doi.org/10.1038/s41587-022-01638-y (2023).
201. Mittelheisser, V. et al. Leveraging immunotherapy with nanomedicine. *Adv. Ther.* **3**, 2000134 (2020).
202. Perica, K. et al. Magnetic field-induced T cell receptor clustering by nanoparticles enhances T cell activation and stimulates antitumor activity. *ACS Nano* **8**, 2252–2260 (2014).
203. Majedi, F. S. et al. Augmentation of T-cell activation by oscillatory forces and engineered antigen-presenting cells. *Nano Lett.* **19**, 6945–6954 (2019).
204. Vis, B. et al. Ultrasmall silica nanoparticles directly ligate the T cell receptor complex. *Proc. Natl Acad. Sci. USA* **117**, 285–291 (2020).
205. Kim, K.-S. et al. Cationic nanoparticle-mediated activation of natural killer cells for effective cancer immunotherapy. *ACS Appl. Mater. Interfaces* **12**, 56731–56740 (2020).
206. Sim, T. et al. Magneto-activation and magnetic resonance imaging of natural killer cells labeled with magnetic nanocomplexes for the treatment of solid tumors. *ACS Nano* **15**, 12780–12793 (2021).
207. Liu, Z. et al. Nanoscale optomechanical actuators for controlling mechanotransduction in living cells. *Nat. Methods* **13**, 143–146 (2016).
208. Farhadi, A., Ho, G. H., Sawyer, D. P., Bourdeau, R. W. & Shapiro, M. G. Ultrasound imaging of gene expression in mammalian cells. *Science* **365**, 1469–1475 (2019).
209. Wang, X., Chen, X. & Yang, Y. Spatiotemporal control of gene expression by a light-switchable transgene system. *Nat. Methods* **9**, 266–269 (2012).
210. Pan, Y. et al. Mechanogenetics for the remote and noninvasive control of cancer immunotherapy. *Proc. Natl Acad. Sci. USA* **115**, 992–997 (2018).
211. González-Bermúdez, B., Guinea, G. V. & Plaza, G. R. Advances in micropipette aspiration: applications in cell biomechanics, models, and extended studies. *Biophys. J.* **116**, 587–594 (2019).
212. Otto, O. et al. Real-time deformability cytometry: on-the-fly cell mechanical phenotyping. *Nat. Methods* **12**, 199–202 (2015).
Introduction of the state-of-the-art and high-throughput RT-DC technology for measuring the mechanical properties of cells.
213. Gerum, R. et al. Viscoelastic properties of suspended cells measured with shear flow deformation cytometry. *eLife* **11**, e78823 (2022).
214. Sánchez-Iranzo, H., Bevilacqua, C., Diz-Muñoz, A. & Prevedel, R. A 3D Brillouin microscopy dataset of the in-vivo zebrafish eye. *Data Brief.* **30**, 105427 (2020).
215. Conrad, C., Gray, K. M., Stroka, K. M., Rizvi, I. & Scarcelli, G. Mechanical characterization of 3D ovarian cancer nodules using Brillouin confocal microscopy. *Cell. Mol. Bioeng.* **12**, 215–226 (2019).
216. Wu, P.-H. et al. Particle tracking microrheology of cancer cells in living subjects. *Mater. Today* **39**, 98–109 (2020).
217. Falchuk, K. & Berliner, R. Hydrostatic pressures in peritubular capillaries and tubules in the rat kidney. *Am. J. Physiol.* **220**, 1422–1426 (1971).
218. Petrie, R. J. & Koo, H. Direct measurement of intracellular pressure. *Curr. Protoc. Cell Biol.* **63**, (2014).
219. Harlepp, S., Thalmann, F., Follain, G. & Goetz, J. G. Hemodynamic forces can be accurately measured in vivo with optical tweezers. *Mol. Biol. Cell* **28**, 3252–3260 (2017).
220. Mongera, A. et al. A fluid-to-solid jamming transition underlies vertebrate body axis elongation. *Nature* **561**, 401–405 (2018).
221. Mongera, A. et al. Mechanics of the cellular microenvironment as probed by cells in vivo during zebrafish presomitic mesoderm differentiation. *Nat. Mater.* **22**, 135–143 (2023).
222. Vorselen, D. et al. Microparticle traction force microscopy reveals subcellular force exertion patterns in immune cell–target interactions. *Nat. Commun.* **11**, 20 (2020).
223. Meng, F., Suchyna, T. M. & Sachs, F. A fluorescence energy transfer-based mechanical stress sensor for specific proteins in situ: mechanical stress sensor. *FEBS J.* **275**, 3072–3087 (2008).
224. Grashoff, C. et al. Measuring mechanical tension across vinculin reveals regulation of focal adhesion dynamics. *Nature* **466**, 263–266 (2010).
225. Conway, D. E. et al. Fluid shear stress on endothelial cells modulates mechanical tension across VE-cadherin and PECAM-1. *Curr. Biol.* **23**, 1024–1030 (2013).
226. Pan, X. et al. Assessment of cancer cell migration using a viscosity-sensitive fluorescent probe. *Chem. Commun.* **58**, 4663–4666 (2022).
227. Shimolina, L. E. et al. Imaging tumor microscopic viscosity in vivo using molecular rotors. *Sci. Rep.* **7**, 41097 (2017).
228. Sack, I. Magnetic resonance elastography from fundamental soft-tissue mechanics to diagnostic imaging. *Nat. Rev. Phys.* **5**, 25–42 (2022).
229. Soteriou, D. et al. Rapid single-cell physical phenotyping of mechanically dissociated tissue biopsies. *Nat. Biomed. Eng.* https://doi.org/10.1038/s41551-023-01015-3 (2023).

Acknowledgements

L.T. acknowledges the grant support from Swiss National Science Foundation (315230_204202, IZLCZ0_206035, CRSII5_205930), European Research Council under the ERC grant agreement MechanoIMM (805337), Swiss Cancer Research Foundation (KFS-4600-08-2018), Kristian Gerhard Jebsen Foundation, Anna Fuller Fund, Xtalpi Inc., and EPFL. J.G.G. acknowledges support from INSERM, University of Strasbourg and charities (Ligue contre le Cancer, Fondation ARC pour la recherche sur le cancer, Association Ruban Rose), which also support fellowships to V.M. and V.G. This work was also supported by grants from Plan Cancer to J.G.G. We apologize to the authors whose work could not be cited due to size constraints.

Author contributions

V.M., V.G., L.B., W.L., L.T. and J.G.G. researched data for the paper. All authors made substantial contributions to the discussion of content, wrote the paper and reviewed and/or edited the paper before submission.

Competing interests

L.T. is a co-founder, shareholder and advisor for Leman Biotech. The interests of L.T. were reviewed and managed by EPFL. The other authors declare no competing interests.

Additional information

Correspondence and requests for materials should be addressed to Li Tang or Jacky G. Goetz.

Peer review information *Nature Nanotechnology* thanks Claire Hivroz and the other, anonymous, reviewer(s) for their contribution to the peer review of this work.

Reprints and permissions information is available at www.nature.com/reprints.

Publisher's note Springer Nature remains neutral with regard to jurisdictional claims in published maps and institutional affiliations.

Springer Nature or its licensor (e.g. a society or other partner) holds exclusive rights to this article under a publishing agreement with the author(s) or other rightsholder(s); author self-archiving of the accepted manuscript version of this article is solely governed by the terms of such publishing agreement and applicable law.

© Springer Nature Limited 2024

Chapter III

Tumor targeting with antibody-nanoparticles conjugates

Targeting TME actors to regulate cancer progression and improving the diffusion of chemotherapeutic drugs and/or immune cells infiltration in tumors is now widely appreciated (Bejarano et al., 2021). Despite their high therapeutic potential, these approaches are limited by the toxicity and the side effects of the drugs. Cytotoxic molecules selective delivery can be achieved by conjugating them on antibodies targeting TCs (Drago et al., 2021). However, antibody-drug conjugates (ADCs) have relatively low drug/antibody ratios (≈ 4 molecules/antibody) (Hamblett et al., 2004). To circumvent drug loading limitations without impacting the antigen recognition or the pharmacokinetic parameters of ADCs, nanoparticles (NPs) vectorization approaches have been developed. Antibody targeted-NPs offer broad payload selections, high drug to antibody ratios (≈ 100 molecules/NPs) and the ability to finely tailor drug release (Johnston and Scott, 2018).

In this Chapter III, we will discuss the main NPs classes, focusing on those that we used for our studies, and describe the antibodies conjugation methods with NPs. We will then present our meta-analysis published in *Advanced Materials* which seeks the identification of the optimal antibody-NPs combination for further targeted NPs rational development. Finally, we will introduce the development of highly biocompatible TCs targeted-nanoemulsion obtained in collaboration with the laboratory of Andrey Klymchenko.

Publications associated to this chapter:

Mittelheisser V, Coliat P, Moeglin E, Goepp L, Goetz JG, Charbonnière LJ, Pivot X, Detappe A. "***Optimal Physicochemical Properties of Antibody-Nanoparticle Conjugates for Improved Tumor Targeting.***"

Advanced Materials 34:2110305 (2022) – doi:10.1002/adma.202110305

Boide Trujillo V-J*, **Mittelheisser V***, Liu F*, Lefebvre O, Andreiuk B, Yudhistira T, Anton N, Goetz JG [#] and Klymchenko AS[#]. "***Functionalization of lipid nanoemulsions with humanized antibodies using plug-and-play cholesterol anchor for targeting cancer cells***"

In preparation.

1. Nanoparticles in oncology

1.1. Nanoparticles definitions

According to the IUPAC (*International Union of Pure and Applied Chemistry*) and the ISO technical specification ISO/TS 80004:2023, nanoparticles (NPs) are defined as particles of any shape with a diameter between 1 and 100 nanometers. One of their primary biomedical applications was to improve the stability and solubility of encapsulated cargos and to direct therapeutic drugs delivery to cancer cells.

NPs applications in cancer treatment allowed to reduce chemotherapeutic molecules off-target effects and improved their therapeutic window by increasing the efficacy-to-toxicity ratio. NPs tumor targeting is traditionally ascribed to the enhanced permeability and retention (EPR) effect (Matsumura and Maeda, 1986). During the EPR effect, NPs pass through inter-endothelial gaps (up to 2,000 nm), which are formed as a consequence of the continuous pro-angiogenic stimulatory signals of tumor ECs (Di Tomaso et al., 2005). Solid tumor tissues also lack efficient drainage of lymphatic system, which results in the retention of extravasated NPs in tumor bed (Leu et al., 2000) (**Figure 11**). However, the EPR effect is very heterogeneous not only between tumor types, but also within the same patient tumor upon progression (Tanaka et al., 2017). In addition, tumor associated high IFP, and convective interstitial fluid flow (*General introduction*) suggest that NPs passive accumulation is not the only mechanism driving their retention in the tumor mass. Recent studies indeed challenged the EPR effect by showing that up to 97% of NPs enter tumors using an active trans-endothelial transport (Sindhwani et al., 2020) (**Figure 11**). Another study from the same group later challenged the impaired lymphatic drainage demonstrating that NPs can efficiently exit the tumor through lymphatic vessels and return the blood circulation, thus allowing several rounds of NPs interaction with the tumor tissues (Nguyen et al., 2023). The central dogma of NPs accumulation into tumors is shifting from the EPR effect to a new active transport and retention (ATR) principle.

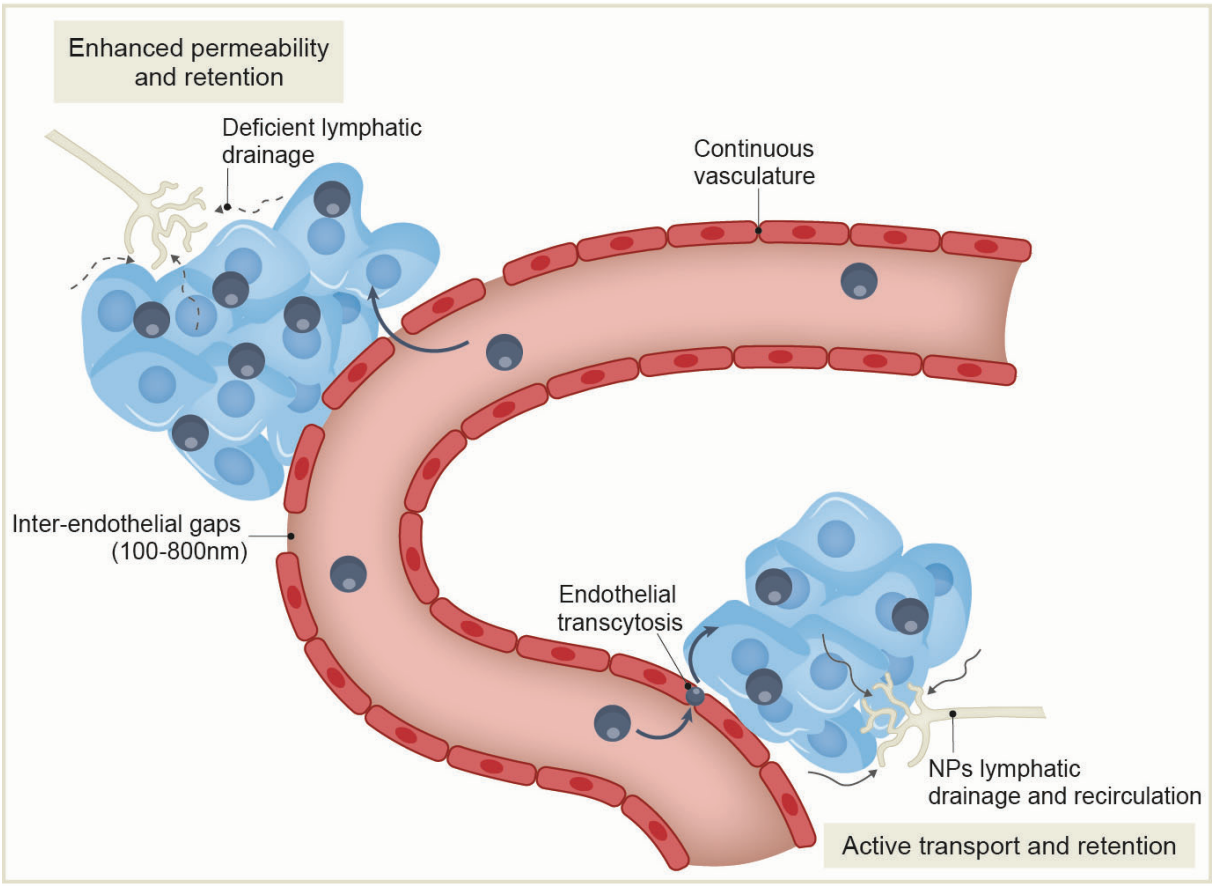

Figure 11 – Nanoparticles delivery to tumors.
The delivery of NPs to tumors may result from a mixture of both EPR and ATR mechanisms. The EPR effect posits that NPs enter tumors through inter-endothelial gaps and are unable to exit owing to impaired lymphatic drainage. The ATR principle posits that NPs enter tumors mainly through endothelial transcytosis, followed by nanoparticle trafficking and retention in tumors by partial NPs clearance through intra- and peritumoral lymphatics.

While the exact mechanism of NPs accumulation into tumors is still under investigation, lipid NPs have already made their way to clinic. In France, 4 liposomes are currently used to deliver doxorubicin (CAELYX®, ZOLSKETIL®), irinotecan (ONIVYDE®) or a cytarabine/daunorubicin combination (VYXEOX®). Although drugs encapsulation into liposomes improve their pharmacokinetic and biodistribution in comparison to free drugs, no marketed liposomal therapeutic agents have yet demonstrated a significant increase in overall survival versus the standard agent (O'Brien et al., 2004; Petersen et al., 2016). Nevertheless, improved safety profiles justify liposomal formulation use in patients with increased risk factors of chemotherapy adverse events (*e.g.*, cardiac disease, previous use of the free drug).

1.2. Liposomes and lipid-based nanoparticles

Liposomes were the first drug delivery system developed (Bangham et al., 1965). Liposomes are composed of an amphipathic phospholipid bilayer enclosing a hydrophilic core. Their amphiphilic structure allows encapsulation of both hydrophilic (in the core) and hydrophobic (within the lipid bilayer) active pharmaceutical ingredients (Allen and Cullis, 2013). However, due to the limited bilayer space, achieving high drug loading and retention of highly hydrophobic drugs in liposomes remains challenging (Allen and Cullis, 2013). Other lipid-based NPs, such as nanoemulsions droplets, have been developed to circumvent this limitation (Singh et al., 2017). Nanoemulsions are composed of a hydrophobic liquid core stabilized by phospholipid monolayer, allowing the encapsulation of highly hydrophobic molecules, such as drugs and contrast agents (Singh et al., 2017). Nanoemulsions are easy to prepare and can be prepared from edible oils with a low risk of toxicity (Constantinides et al., 2004).

Due to their high biocompatibility and biodegradability, lipid-based NPs were the first therapeutic vectors used in clinical to delivery chemotherapeutic molecules (*see above*) or nucleic acid-based drugs, such as siRNA (ONPATTRO®) (Akinc et al., 2019) or more recently mRNA for vaccine approaches during the COVID-19 pandemic (Polack et al., 2020). Despite their wide clinical use, lipid-based NPs are limited by their low encapsulation rates, uncontrolled drug release, stability and short blood circulation time. Improved stability and prolonged blood circulation time can be achieved by synthetizing lipid-based NPs with phospholipid grafted with long polyethylene glycol (PEG) chains (Lainé et al., 2014). However, lipid-based NPs PEGylation raised novel issues as their repeated injection is associated an “accelerated blood clearance” (Dams et al., 2000; Ishida et al., 2003). Furthermore, repeated administration of PEGylated lipid-based NPs may trigger a complement activation-related pseudo-allergy (CARPA) (Szebeni, 2005). CARPA is a non-IgE-mediated hypersensitivity reaction, that induces potentially lethal anaphylaxis symptoms (*e.g.*, facial swelling and cardiopulmonary distress) (Szebeni, 2014).

1.3. Polymeric nanoparticles

Polymeric NPs can be synthesized from natural (*e.g.*, poly(amino acids), polysaccharides) or synthetic materials (*e.g.*, polyesters, polyethyleneimine), allowing

for a wide variety of possible structures and characteristics (Beach et al., 2024). Polymeric NPs can encapsulate molecules in their core, entrapped in the polymer matrix or chemically conjugated to the polymer. Therapeutic cargoes can also be conjugated at the polymer NPs surface. Polymeric NPs synthesis is tightly controllable, allowing precise drug loading of hydrophobic and hydrophilic compounds, as well as cargos with different molecular weights (*e.g.*, proteins, nucleic acids) (Danhier et al., 2012).

Among the different polyesters-based polymeric NPs, the poly(lactic-*co*-glycolic) acid (PLGA) is one of the most attractive and successfully used therapeutic vector for drug delivery or biomaterial applications. PLGA is a copolymer composed of two monomers: the poly(lactic acid) (PLA) and the poly(glycolic acid) (PGA) (Beach et al., 2024). The PLGA NPs are usually identified by the PLA:PGA monomers ratio used for their synthesis. Interestingly, changing this PLA:PGA controlled PLGA NPs degradation rates and thereby drug release kinetic. Due to the presence of methyl groups, PLA is more hydrophobic than PGA (Beach et al., 2024). High PLA:PGA ratios resulted in slower diffusion of water in the PLGA NPs, and thus in a slower degradation rate. Conversely, low PLA:PGA ratios led to more degradable PLGA NPs (Vey et al., 2011). These differences in degradation allow to finely tune drug release properties of PLGA NPs by modulating the PLA:PGA ratios. PLGA NPs are greatly biodegradable, and their hydrolysis generates the original monomers: lactic acid and glycolic acid, which acidify the PLGA matrix, resulting in the bulk erosion of the NPs (Fu et al., 2000; Göpferich, 1997). Since lactic acid and glycolic acid are endogenous and easily metabolized by the body via the Krebs cycle and are degraded as carbon dioxide (CO_2) and water (H_2O), a minimal systemic toxicity is associated with the use of PLGA NPs.

Polymeric NPs present several advantages in terms of simplicity of formulation, encapsulation rate, stability and biocompatibility. In addition, PLGA copolymers expressed terminal carboxyl group, allowing easy surface functionalization with targeting moieties (McCarron et al., 2008; Valcourt et al., 2020). The Food and Drug Administration (FDA) and the European Medicines Agency (EMA) already approved several PLGA-based systems. However, no PLGA NPs formulations are currently available on the global market. Several PLGA NPs encapsulating docetaxel (Autio et al., 2018; Von Hoff et al., 2016) or the tumor antigen NY-ESO-1 (Creemers et al., 2021) are currently under clinical trials.

1.4. Carbon-based nanoparticles

Carbon-based NPs are carbon allotropes of various dimensionality: fullerenes (0D) (Kroto et al., 1985), carbon nanotubes (1D) (Iijima, 1991) and graphene (2D) (Novoselov et al., 2004). Among these carbon allotropes, carbon nanotubes (CNTs) are seamless cylindrical tubes formed by the winding of graphene sheets. Depending on the number of graphene sheets coaxially arranged, CNTs can be classified in single-walled CNTs (Iijima and Ichihashi, 1993) or multi-walled CNTs with a space of about 0.34-0.39 nm between adjacent graphene layers (Iijima, 1991). CNTs have attracted escalating attention for drug delivery due to their unique physicochemical properties (high specific surface area and hollow hydrophobic internal cavity) (Peigney et al., 2001) and their morphology that facilitates their translocation across the biological membranes (Höfinger et al., 2011; Lacerda et al., 2012).

Specific surface area | CNTs high specific surface area enables multiple surface functionalization that are crucial to improve their solubility, reduce bundling effects and avoid the toxicity of the pristine CNTs (Heister et al., 2010; Schipper et al., 2008). CNTs tips reactivity is considerably higher than that of the sidewalls, allowing selective acid oxidation of the tips, while the sidewalls remain inert (Tasis et al., 2006). Carboxylic acid groups generated after oxidation can later be functionalized through amidation (Chen et al., 1998). New functional groups can be further modified with chemotherapeutic molecules (Georgakilas et al., 2002; Pastorin et al., 2006) or targeting moieties (Venturelli et al., 2011) to create CNTs endowed with targeted pharmacological activity. In addition, CNTs sidewalls can also be functionalized by bio-reactive groups *via* 1,3-dipolar cycloaddition (Georgakilas et al., 2002). As after oxidation/amidation, the introduced bio-reactive groups can be further derivatized to conjugate small molecules (Pastorin et al., 2006) or targeting moieties (McDevitt et al., 2007; Villa et al., 2008). Besides, due to their structure CNTs can adsorb aromatic anti-cancer agents such as doxorubicin, 5-fluorouracil or paclitaxel via non-covalent π-π stacking onto their sidewalls (Ali-Boucetta et al., 2008; González-Lavado et al., 2019; Karnati and Wang, 2018). Interestingly, the difference in reactivity between CNTs tips and sidewalls allows sequential oxidation/amidation and cycloaddition leading to the generation of doubly functionalized CNTs (Wu et al., 2005).

Hollow internal cavity | CNTs acid oxidation also leads to their opening, allowing the entrapment of chemotherapeutic drugs inside their hollow hydrophobic internal cavity. Drug encapsulation within CNTs core is particularly attractive for pro-drug such as platinum(IV) to protect them from premature activation (Chin et al., 2014; Li et al., 2012).

Optical properties | Due to their optical properties CNTs can also be considered as a "first-generation theranostic NPs". Indeed, their photoacoustic and echogenic properties (Delogu et al., 2012) make them suitable for medical imaging and can be coupled with their strong near-infrared light absorption to identify and photo-thermally ablate tumor cells (Hashida et al., 2014).

Despite these numerous advantages, drug delivery by CNTs is inadequately controllable. Encapsulating highly hydrophobic drugs in the hollow internal cavity would lead to poor their release from CNTs in aqueous conditions due to strong hydrophobic-hydrophobic interactions. Furthermore, drug release rate is dependent on CNTs length and diameter (Muzi et al., 2015; Panczyk et al., 2013), yet long CNTs are associated with high toxicity (Kostarelos, 2008). Finally, CNTs similarity with asbestos fibers and prolonged *in vivo* persistence in the liver exclude them of the design of drug nanocarriers and require thorough toxicity evaluation before further pre-clinical development (Schipper et al., 2008).

1.5. Theranostic nanoparticles

While most of NPs are designed to primarily improve the drug delivery, theranostic NPs (*i.e.*, NPs carrying both imaging and therapeutic agents) emerged over the last two decades. Amid all the theranostic NPs, inorganic NPs made of high atomic number (Z) metals such as gadolinium (Z = 64) (Le Duc et al., 2011; Sancey et al., 2014), hafnium (Z = 72) (Bonvalot et al., 2017), gold (Z = 79) (Hainfeld et al., 2004) or bismuth (Z = 82) (Detappe et al., 2017) display advantageous theranostic properties. Over exposure to external radiation therapy, high atomic number species absorb X-rays energy and undergo inner-shell ionization inducing an increased electrons production. This subsequently increases the amount of reactive oxygen species in the tumor bed improving the radiation therapeutic efficacy (Kuncic and Lacombe, 2018). Despite a significant number of pre-clinical studies reports demonstrating the potential

efficacy of theranostic NPs, only a hafnium-based NPs (NBTXR3, Hensify) (Bonvalot et al., 2019) and a gadolinium-based NPs (Thivat et al., 2023) have been translated to clinical radio-enhancers.

Among all the inorganic NPs that translated into clinic gadolinium-based NPs also possess excellent MRI positive contrast properties thanks to the paramagnetic properties of Gd^{3+} gadolinium ions (Bianchi et al., 2014). Owing to silica sol-gel chemistry (Jeelani et al., 2020; Singh et al., 2014), Gd^{3+} gadolinium ions were successfully chelated into DOTAGA engrafted at the top of the silica matrix (Mignot et al., 2013). This approach allowed the development of biodegradable USM with a highly controlled hydrodynamic diameter close to 5 nm ensuring their renal elimination (Lux et al., 2011). In addition, silica sol-gel chemistry facilitated the easy functionalization of silica-based gadolinium NPs with antibodies which potentiate their imaging and radio-enhancing abilities (Detappe et al., 2020, 2019).

2. Antibodies conjugation to nanoparticles

After their administration, NPs passive accumulation into the tumor bed via EPR effect remains limited (≈1-3 % of the injected dose) and does not guarantee internalization into tumor cells (Mittelheisser et al., 2022; Wilhelm et al., 2016). Consequently, it remains essential to improve NPs tumor targeting. One of the most attractive targeting approaches relies on conjugating anti-tumor antigens antibodies via three main routes: (*i*) amines carried by lysines, (*ii*) thiols after reduction of disulfide bridges and (*iii*) carboxylic acids carried by aspartic and glutamic acids (Wu et al., 2022).

2.1. Lysines

Lysines (Lys, K) are among the most abundant amino acids in proteins. Lysyl residues have a ε-amino group protonated at neutral pH (pKa ≈ 10), which contributes to the antibody aqueous solubility. Human IgG contains around 100 lysyl residues located on both the heavy and light chains, around half of which are exposed to solvents and therefore easily exploitable for the conjugation of exogenous reagents such as NPs (Gautier et al., 2015; Kim et al., 2014).

Once deprotonated by a moderate rise in the pH (pH 7-9), the ε-amino group acts as a nucleophile that can further react with a *N*-Hydroxysuccinimide (NHS) ester

electrophilic carbon (**Figure 12**). The formed isopeptide bond between the antibody and the NP is stable at physiological pH, limiting the risk of NP release. Of note, this approach can lead to non-specific coupling reactions with tyrosyl residues (Leavell et al., 2004; Mädler et al., 2009). They can be avoided by controlling the reaction conditions: tyrosines are more reactive under acidic conditions (pH 6) whereas lysines modifications are favored under basic conditions (pH 8.4) (Leavell et al., 2004).

Lysine amidation decreases antibody total charge, which may reduce its solubility. Furthermore, given the wide distribution of lysines in the antibody backbone, potential NPs conjugation in its variable chain may impact antigen recognition by steric hindrance.

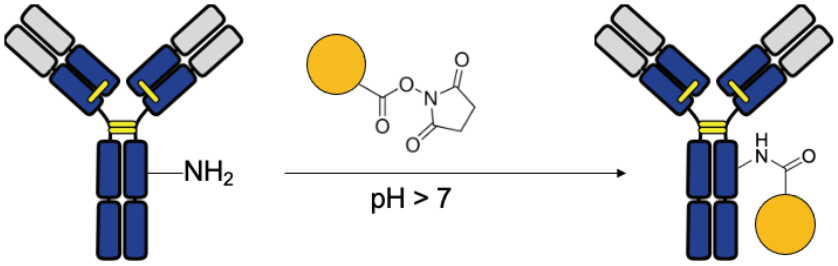

Figure 12 – Lysines amidation.
The nucleophilic center ε-amino group react with NPs bearing NHS-ester ester groups.

2.2. Cysteines

Cysteine (Cys, C) is one of the rarest amino acids in proteins (1-2%), found mainly in the form of disulfide bonds and very little in its free form (0.2%). Human IgG1 contains 32 cysteyl residues, all of which are involved in the formation of inter- and intra-chain disulfide bonds (4 and 12, respectively) (Liu and May, 2012). Their reduction by dithiothreitol (DTT), 2-mercaptoethanol (β-mercaptoethanol) or tris(2-carboxyethyl)phosphine (TCEP) can provide 0, 2, 4, 6, or 8 free reactive thiol groups for conjugation per antibody (**Figure 13**) (Hamblett et al., 2004). However, free thiols generation by reduction may lead to degradation of the inter-chain disulfide bridges and thus to antibody denaturation. To avoid disulfide bridges reduction, free thiol groups can be introduced in the antibody structure by derivatization of lysines ε-amino group with Traut's (2-iminothiolane) or *N*-Succinimidyl S-acetylthioacetate (SATA) reagents (Duncan et al., 1983; Traut et al., 1973).

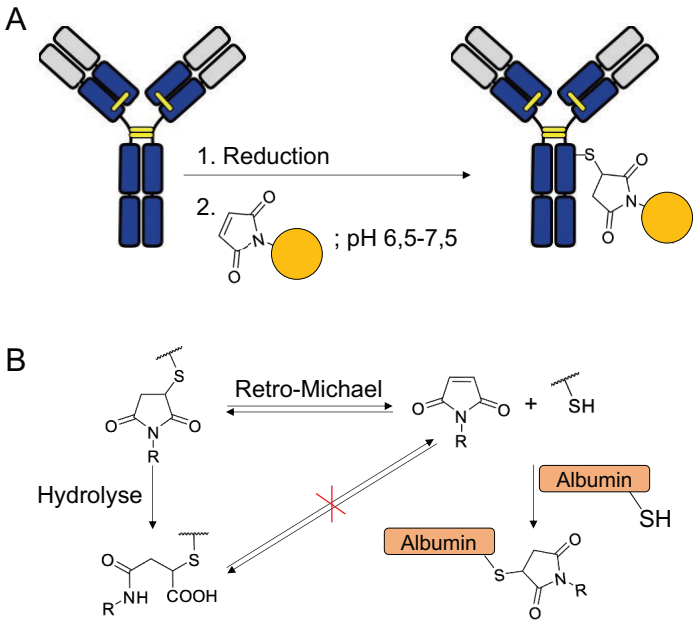

Figure 13 – Cysteine modification by Michael reaction.
Thiols generated by antibody reduction react with maleimide groups carried by NPs (A). However, the bond is unstable and may degrade, leading to NP release (B).

Due to thiol groups rarity and strong nucleophilic nature at physiological pH, cysteines represent prime targets for selective, site-specific bioconjugation. Thiols react with electrophilic Michael acceptors (*e.g.*, maleimides, vinyl sulfones) forming thiosuccinimide adducts. However, these thiosuccinimides bounds are unstable in physiological conditions and undergoes deconjugation through a retro-Michael pathway, leading to loss of NPs and reduction efficacy (**Figure 13**). The maleimide-NPs conjugate can then be bound to other plasma thiols (*e.g.*, human serum albumin) leading to off-site toxicities and reduced efficacy (Alley et al., 2008; Shen et al., 2012). Retro-Michael deconjugation pathway can be eliminated by hydrolyzing the thiosuccinimide ring to form a stable succinamic acid thioether (Fontaine et al., 2015; Tumey et al., 2014). Another method to circumvent the instability of the maleimide-cysteine conjugates relies on the use of novel maleimide scaffolds (*e.g.*, *N*-aryl maleimides, β-amino maleimides) that produce physiologically stable bioconjugates (Christie et al., 2015; Lyon et al., 2014). Of note, maleimide scaffolds can also react with lysines ε-amino group, leading to the formation of intra-antibody bridges (Chen et al., 2016). Thiol-michael addition chemoselectivity can be controlled by the reaction conditions: at pH 7 the kinetics of the thiol-maleimide reaction are around 1,000 times faster than the amine-maleimide reaction (Brewer and Riehm, 1967).

2.3. Aspartic and glutamic acids

Aspartic (Asp, D) and glutamic (Glu, E) acids are highly abundant in proteins (Gilis et al., 2001). As they are the only negatively charged amino acids at physiological pH, they play a key role in protein solubility and aggregation prevention (Kramer et al., 2012; Trainor et al., 2017).

The relatively low reactivity of carboxylic acids towards nucleophilic attack in aqueous solvents generally complicate the targeting of Asp and Glu residues. Yet, carboxylic acids can be activated by carbodiimide crosslinker such as 1-ethyl-3-(3-dimethylaminopropyl)carbodiimide (EDC) or N-ethyl-5-phenylisoxazolium-3'-sulfonate (Woodward's reagent) and form *O*-acylisourea intermediates. In most cases, NHS is further added to the reaction to form stable activated esters, thereby enhancing *O*-acylisourea displacement by nucleophilic attack from primary amine groups present on NPs (Totaro et al., 2016; Woodward et al., 1961) (**Figure 14**). The amide bond formed between the antibody carboxyl group and the NPs primary amine was one of the first methods for antibody bioconjugation (Hurwitz et al., 1975; Rowland et al., 1975). However, this method carries the risk of non-specific reactions with nearby lysines, which can lead to antibody aggregation and altered pharmacokinetics (Novák and Kruppa, 2008; Winkelhake, 1977).

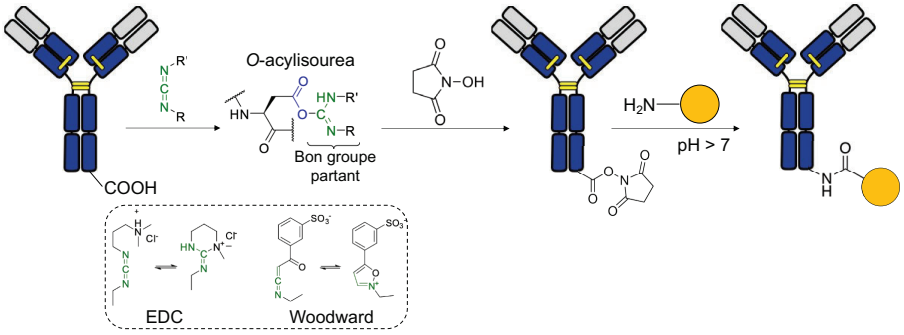

Figure 14 – Conjugation to carboxylic acids.
Once transformed into activated esters by EDC or Woodward reagents, carboxylic acids can react efficiently with amine functions carried by NPs.

2.4. Bioorthogonal reactions

To avoid non-specific reactions that can lead to inter- or intra-protein bridging, or to altered antibody functions, bio-orthogonal approaches have been developed. Bio-orthogonal click chemistry is a class of high-yielding chemical reactions that proceed rapidly and selectively under physiological conditions without side reactions towards endogenous functional groups (Sletten and Bertozzi, 2009).

Antibody can be derivatized with bio-orthogonal groups such as azide (-N_3) by non-natural carbohydrates introduction via glycosyltransferases on the *N*-glycosylated Asn^{297} residue (Agarwal and Bertozzi, 2015; Van Geel et al., 2015) or by photo-crosslinking (Light Activated Site-Specific Conjugation) of a low-molecular-weight (≈ 8kDa) reactive group to the CH2 domain of the antibody (Hui et al., 2015, 2014) (**Figure 15**).

The first click chemistry reaction developed was the Cu(I)-catalyzed 1,3-dipolar Huisgen cycloaddition between an azide and an alkyne (CuAAC) (Rostovtsev et al., 2002) (**Figure 15**). However, Cu(I)-catalyzed reactions led to reactive oxygen species (ROS) generation that affect structural integrity. Later, development of copper-free 1,3-dipolar cycloaddition reactions known as strain-promoted azide-alkyne cycloaddition (SPAAC) avoided proteins denaturation caused by Cu(I)-catalyzed reactions (Agard et al., 2006). SPAAC reactions are nonetheless slow and non-stereospecific. To enhance reaction kinetics, new strained cyclooctenes (dibenzocyclooctyne, DBCO; difluorocyclooctyne, DIFO or bicyclo[6.1.0]non-4yne, BCN) were synthesized to react with tetrazines in an inverse demand Diels-Alder (iEDDA) manner (Dommerholt et al., 2014; Van Geel et al., 2015).

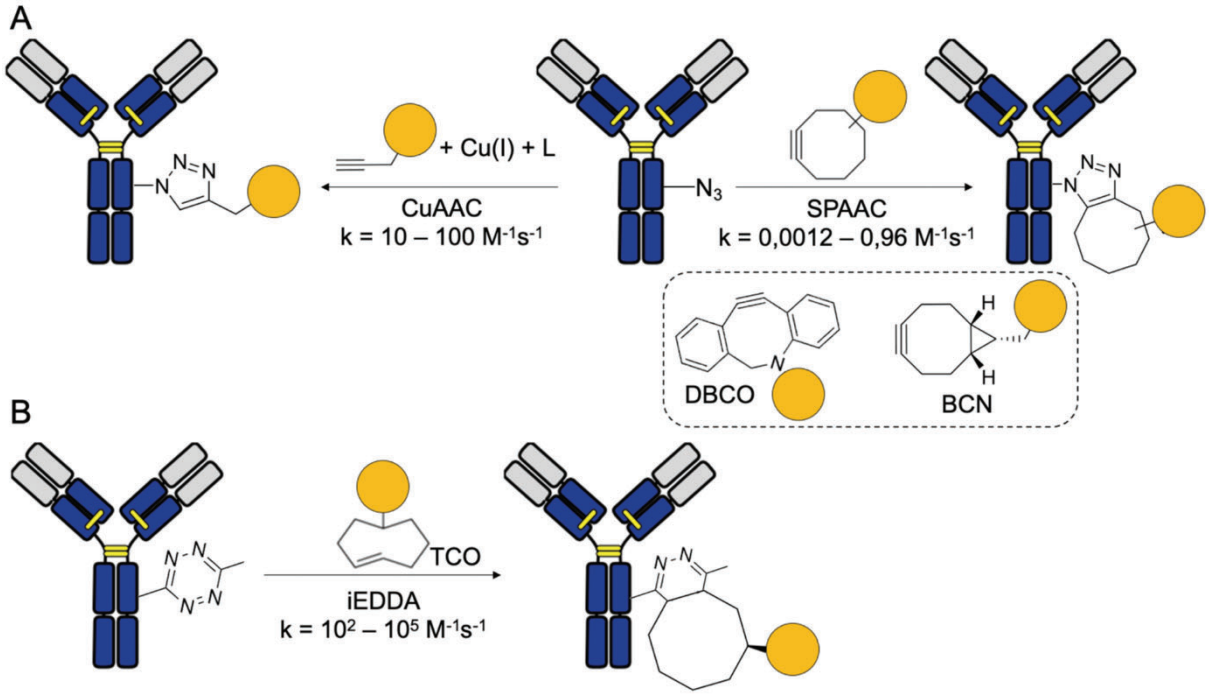

Figure 15 – Bio-orthogonal chemical click reaction.
Once introduced on the antibody backbone, N_3 react with alkynes in a reaction either catalyzed by copper (CuAAC) or without catalyst (SPAAC) (A). Using a 1,2,4,5-tetrazine enables an inverse demand Diels-Alder (B).

3. Optimal physicochemical properties of antibody-targeted NPs

Antibody-targeted NPs represent an innovative strategy to improve the delivery of drug-loaded NPs to the tumor. However, the physicochemical properties of antibody-targeted NPs remain to be optimized to achieve efficient tumor targeting. By performing a meta-analysis of literature data, we seek at the identification of the optimal antibody moiety (full antibodies or fragments)-NPs combination leading to the highest NPs tumor uptake.

In the following manuscript, we highlight that antibody-targeted NPs significantly improves their tumoral uptake. Yet, the biodistribution and pharmacokinetics profiles remain dictated by the NPs physicochemical properties independently of the use of monoclonal antibodies or antibody fragments. In addition, we also determine that to achieve high tumor uptake lipidic NPs should be conjugated with antibody fragments whereas polymeric and organic/inorganic NPs must be decorated with full antibodies.

This perspective confirms that, to improve tumor delivery, NPs design should be optimized based on their physicochemical properties and that targeting moieties must be selected based on NPs materials.

ADVANCED MATERIALS

www.advmat.de

Optimal Physicochemical Properties of Antibody-Nanoparticle Conjugates for Improved Tumor Targeting

*Vincent Mittelheisser, Pierre Coliat, Eric Moeglin, Lilian Goepp, Jacky G. Goetz, Loic J. Charbonnière, Xavier Pivot, and Alexandre Detappe**

Tumor-targeted antibody (mAb)/fragment-conjugated nanoparticles (NPs) represent an innovative strategy for improving the local delivery of small molecules. However, the physicochemical properties of full mAb–NPs and fragment–NPs—that is, NP material, size, charge, as well as the targeting antibody moiety, and the linker conjugation strategies—remain to be optimized to achieve an efficient tumor targeting. A meta-analysis of 161 peer-reviewed studies is presented, which describes the use of tumor-targeted mAb–NPs and fragment–NPs from 2009 to 2021. The use of these targeted NPs is confirmed to result in significantly greater tumor uptake of NPs than that of naked NPs (7.9 ± 1.9% ID g^{-1} versus 3.2 ± 0.6% ID g^{-1}, respectively). The study further demonstrates that for lipidic NPs, fragment–NPs provide a significantly higher tumor uptake than full mAb–NPs. In parallel, for both polymeric and organic/inorganic NPs, full mAb–NPs yield a significant higher tumor uptake than fragment–NPs. In addition, for both lipidic and polymeric NPs, the tumor uptake is improved with the smallest sizes of the conjugates. Finally, the pharmacokinetics of the conjugates are demonstrated to be driven by the NPs and not by the antibody moieties, independently of using full mAb–NPs or fragment–NPs, confirming the importance of optimizing the NP design to improve the tumor uptake.

1. Introduction

Improving the targeting specificity of small molecules is a primary focus in cancer treatment for reducing associated toxicities and to improve their therapeutic index.[1] Antibody–drug conjugates (ADC) and nanoparticles (NPs) have been developed to fulfill these roles. The former are widely accepted in the clinic with routine applications for the treatment of hematological malignancies and breast cancers with an effective antitumoral activity.[2–4] NPs mostly rely on the use of the passive targeting route to increase the delivery of small molecules to the tumor through the enhanced permeability and retention (EPR) effect.[5–7] Depending on their physicochemical structures, they are able to conjugate up to 10 times as many small molecules as the ADCs. However, the passive tumor targeting route was demonstrated to be limited, with an average delivery of only 0.7% of the injected dose (ID) delivered to the tumor[8] and large heterogeneity not only between tumor types, but also within the same patients' tumors.[9–13] In contrast, ADCs usually demonstrate high tumor targeting, but with relatively low average drug-to-antibody ratios (DAR) (from 2 to 4), preventing recognition by scavenger B receptors in the liver.

As such, combining the targeting selectivity of antibodies to the drug loading ability of NPs seems a logical step to advance this field. Several strategies have been reported based on either full monoclonal antibody (full mAb–NPs) or antibody fragment conjugates (fragment–NPs).[14]

This study presents a meta-analysis of literature data, seeking the identification of the optimal antibody moiety (full mAb or fragment)–NPs combination leading to the highest NP tumor uptake. The criteria for a rational selection were based on the material of the NPs (lipidic, polymeric, and organic/inorganic) with a particular emphasis on their size, their charge, the antibody-targeting moieties (full mAb or fragment), the linker conjugation strategy, and the overall impact of these parameters on the pharmacokinetic and non-specific biodistribution of these conjugates. The search item "antibody-targeted nanoparticles AND tumor targeting" was used to identified peer-reviewed publications with in vivo studies presenting biodistribution and/or pharmacokinetic data. A total of 80 new peer reviewed

V. Mittelheisser, P. Coliat, E. Moeglin, L. Goepp, X. Pivot, A. Detappe
Institut de Cancérologie Strasbourg-Europe
Strasbourg 67000, France
E-mail: a.detappe@icans.eu

V. Mittelheisser, J. G. Goetz
INSERM UMR_S1109
Strasbourg 67000, France

V. Mittelheisser, J. G. Goetz
Fédération de Médecine Translationnelle de Strasbourg (FMTS)
Strasbourg 67000, France

L. J. Charbonnière, A. Detappe
Institut Pluridisciplinaire Hubert Curien
CNRS UMR-7178
Strasbourg 67200, France

A. Detappe
Strasbourg Drug Discovery and Development Institute (IMS)
Strasbourg 67000, France

The ORCID identification number(s) for the author(s) of this article can be found under https://doi.org/10.1002/adma.202110305.

© 2022 The Authors. Advanced Materials published by Wiley-VCH GmbH. This is an open access article under the terms of the Creative Commons Attribution License, which permits use, distribution and reproduction in any medium, provided the original work is properly cited.

DOI: 10.1002/adma.202110305

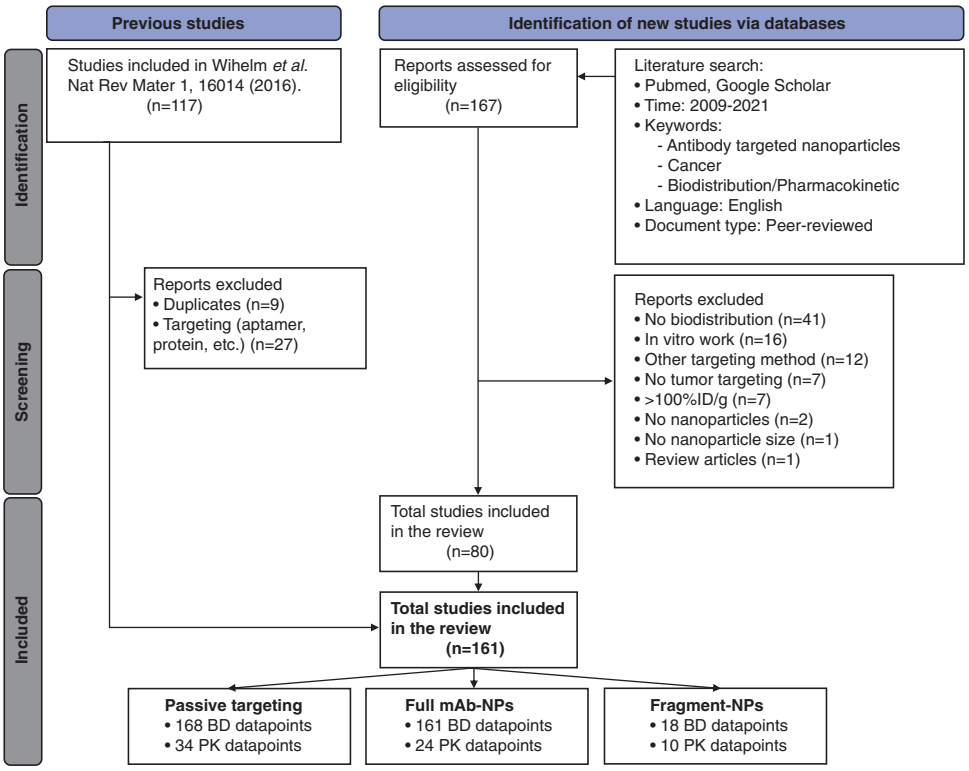

Figure 1. Procedure, strategies, and inclusion criteria for the literature search. Following a literature search of the PubMed and Google Scholar databases, 188 peer-reviewed publications between 2009 and 2021 were identified for the subsequent meta-analysis.

publications assessing full mAb/fragment–NPs (**Figure 1** and Table S1, Supporting Information) were identified in the PubMed and Google Scholar databases. Additionally, we added 108 datapoints[15–96] from the perspective article from Wilhelm et al.[8] describing passively targeted NPs. Among the selected peer-reviewed articles displaying antibody/fragment-targeted NPs data, 76% (61/80) reported the use of full mAb–NPs and 22% (18/80) of the fragment–NPs in order to improve the NP tumor uptake.

2. Nanoparticles Dictate the Pharmacokinetic and Biodistribution Profiles of Full mAb/Fragment–NPs

Among the 80 publications describing either full mAb–NPs or fragment–NPs, only 42% (34/80) presented a pharmacokinetic (PK) study (Table S2, Supporting Information), 22% (18/80) provided enough information to calculate the area under the curve ($AUC_{0-\infty}$) of the conjugate, 11% (9/80) had enough information to calculate the C_{max}, and 42% (34/80) presented the half-life of the NPs in the blood. No statistical differences (p-value = 0.69, 0.95, and 0.29, respectively, Mann–Whitney test) were observed for any of these parameters between the non-targeted NPs and the full mAb–NPs and fragment–NPs (**Figure 2**A,B and Figure S1, Supporting Information). The $AUC_{0-\infty}$ is defined as $\sum_{0}^{t_{last}} \frac{(C_i + C_{ii})}{2} \times (t_{ii} - t_i) + \frac{C_{last}}{k_e}$, and C_{max} is defined as the maximum serum concentration.

Interestingly, we observed a higher variability in the half-life for the full mAb–NP conjugates (p-value = 0.0013, Fisher–Snedecor test) (Figure 2B) than for the fragment–NP conjugates. Such variabilities were observed for the -ximab isotype full mAb–NPs (p-value = 0.0029, Fisher–Snedecor test) (Figure 2C), but not for the -omab full mAbs isotype, nor for the fragment–NP conjugates (p-value = 0.81, and 0.74, respectively, Fisher–Snedecor test) (Figure 2B,C).

The half-life variabilities observed for the full -ximab–NPs could be attributed to: i) the antibody-driven PK interindividual variability;[97–99] ii) an improper binding to the FcRn justified by the injection of chimeric antibodies in a murine model;[100,101] iii) and/or the amount of NPs per mAb that can fluctuate based on the conjugation route employed; and/or iv) the unspecific NP site-conjugation onto the Fc or the Fab part of the mAb that may generate a loss of specificity of the mAb.

The lack of significant half-life PK variabilities for the -zumab–NPs is mostly attributed to the size of the cohort analysis. As a result, we also evaluated the role of the linker conjugation for the full mAb–NPs (Figure S2, Supporting Information). The thiol conjugation strategy led to significant half-life variabilities in comparison to the amine conjugation strategies (p-value = 0.0042, and 0.16, respectively, Fisher–Snedecor test, Figure S2, Supporting Information). The thiol conjugation being non-specific, we sought to additionally quantify the impact of the number of NPs per mAb as this one may vary from one study to another, but also batch to batch. However, such information was rarely explicitly mentioned; this variable was removed from the analysis.

© 2022 The Authors. Advanced Materials published by Wiley-VCH GmbH

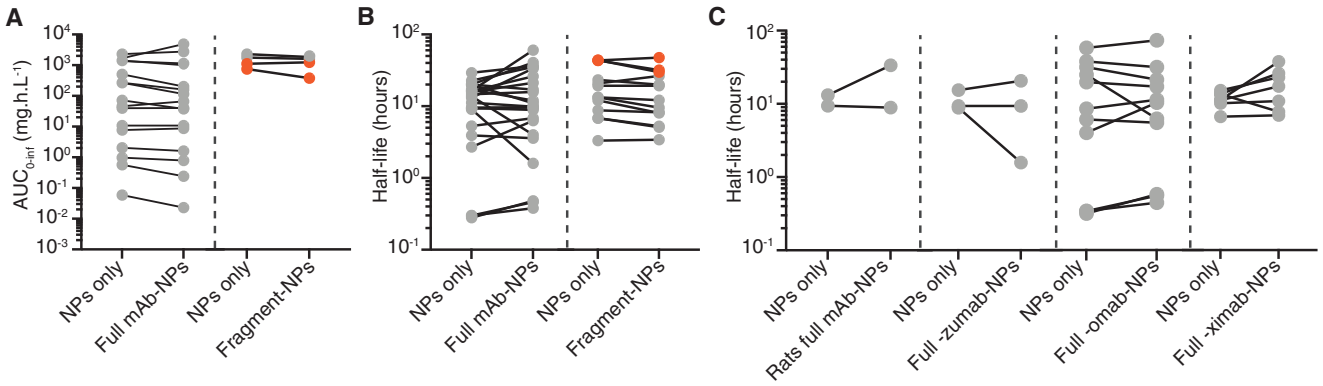

Figure 2. Analysis of the pharmacokinetic parameters of antibody.moiety-targeted nanoparticles. A) $AUC_{0-\infty}$ before and after conjugation of the NP to a full-monoclonal antibody (mAb) or to a fragment. B) Half-life before and after conjugation of the NP to a full monoclonal antibody (mAb) or to a fragment. The orange dots represent the data extracted from nanoparticles currently in clinical trials. C) Half-life before and after conjugation of the NP to a full mAb based on the isotype. No significant differences were observed between the groups (Mann–Whitney test).

This PK analysis confirms that the use of the targeting antibody moieties did not significantly improve the circulation time of the NPs relative to the non-conjugated NPs. All the half-lives of these NP conjugates are orders of magnitude below the usual half-life of mAbs in the blood (approximately a few weeks),[2] confirming that, independent of the NPs, the PK of these conjugates are mostly driven by the NPs.

We then analyzed the biodistribution of the passive and antibody/fragment–NPs in the 3 major organs known to eliminate the NPs of the body, i.e., liver, spleen, and kidneys (**Figure 3**). In comparison to the naked NPs, no clear differences were observed with the full mAb–NPs or the fragment–NPs. Similar to previously published studies deciphering the physicochemical properties of untargeted NPs and their relationships to organ accumulation,[102] we observed a pattern of biodistribution with the functionalized NPs where the largest complexes tended to accumulate in the liver (Figure 3A), the smallest accumulated mostly in the kidneys (Figure 3B), and no clear differences were observed in the spleen (Figure 3C).[103] No differences were observed in terms of biodistribution in those 3 organs between the full mAb–NPs and fragment–NPs based on the NP material (Figure S3, Supporting Information). The charge of the antibody–NPs/fragment–NPs being mostly dictated by the NPs, a similar biodistribution profile than for the naked NPs was observed (Figure S4, Supporting Information). Interestingly, the majority of these studies used negatively charged NPs to the conjugates with mAbs/fragments in order to reduce the passive internalization of the conjugates in major organs as much as possible but also to optimize the specificity of recognition of the antigens by the mAb/fragments. As a result, independent of the use of full mAb–NPs or fragment–NPs, the total accumulation of NPs in each of the three organs (liver, spleen, and kidneys) was similar to that of the naked NPs (Figure 3), confirming that the NP properties drive the biodistribution properties of the targeted complex.

3. Full-Antibody- and Fragment-Conjugated NPs Improve the Tumor NP Uptake

It was previously demonstrated that the use of targeted NPs improves the tumor uptake over passive targeting.[8] In this meta-analysis, we confirmed that the use of full mAb–NPs and fragment–NPs significantly improves the accumulation of the NPs into the tumor compared to the naked NPs ($7.9 \pm 1.9\%$ ID g^{-1} versus $3.2 \pm 0.6\%$ ID g^{-1}; p-value $= 4.07 \times 10^{-10}$, Mann–Whitney). The targeting moieties, that is, full mAb versus fragments, provided a comparable NPs tumor uptake ($8.2 \pm 2.4\%$ ID g^{-1} versus $6.2 \pm 1.8\%$ ID g^{-1}, respectively) (**Figure 4**A). However, the specificity of the targeting moiety that was selected significantly impacted the efficiency of the antibody–NPs and fragment–NPs to reach the tumor. As a result, targeting the HER2 antigen with Trastuzumab (anti-HER2 mAb) provided significantly better tumor uptake than targeting the EGFR with Cetuximab (anti-EGFR mAb) ($11.2 \pm 6.1\%$ ID g^{-1} versus $4.4 \pm 1.9\%$ ID g^{-1}; p-value = 0.023, Mann–Whitney) (Figure 4B). Interestingly, no clear patterns of tumor uptake were observed based on the size of the complex of the antibody–NPs and fragment–NPs (p-value = 0.1 and 0.6, respectively, Spearman correlation) (Figure 4C). No clear differences compared to the naked NPs were observed based on the charge of the conjugates (p-value = 0.4 and 0.7, respectively, Spearman correlation) (Figure 4D) nor between the different full mAb isotypes employed (p-value = 0.08 Kruskal–Wallis) (Figure 4E). However, due to their predominant use in therapeutic studies, only IgG were analyzed in this meta-analysis. These conclusions cannot be extrapolated to other type of antibodies (IgA, IgE, IgM, or IgD) and their respective fragments. Finally, for the full mAb–NPs, despite the non-specificity of the lysine, thiol, or carboxylic acid conjugation strategies employed to conjugate the mAb to the NPs, no statistical differences in tumor uptake were observed between these different conjugation strategies (p-value = 0.6, Kruskal–Wallis) (Figure 4F). These unspecific conjugation strategies lead to an uncontrolled amount of antibody-targeting moieties per NPs but also to the non-controlled orientation of the full mAb conjugated at the surface of the NPs. This latter parameter is known to lead to a decrease of antigen recognition abilities.[104–107] Such limitations are less observed with fragment–NPs because this strategy allows a better control of the fragment orientation at the NP surface.[108] Additionally, and importantly, the preclinical heterotopic tumor model employed to evaluate these conjugates did not contribute to any statistical tumor uptake differences (Figure S5, Supporting Information)

© 2022 The Authors. Advanced Materials published by Wiley-VCH GmbH

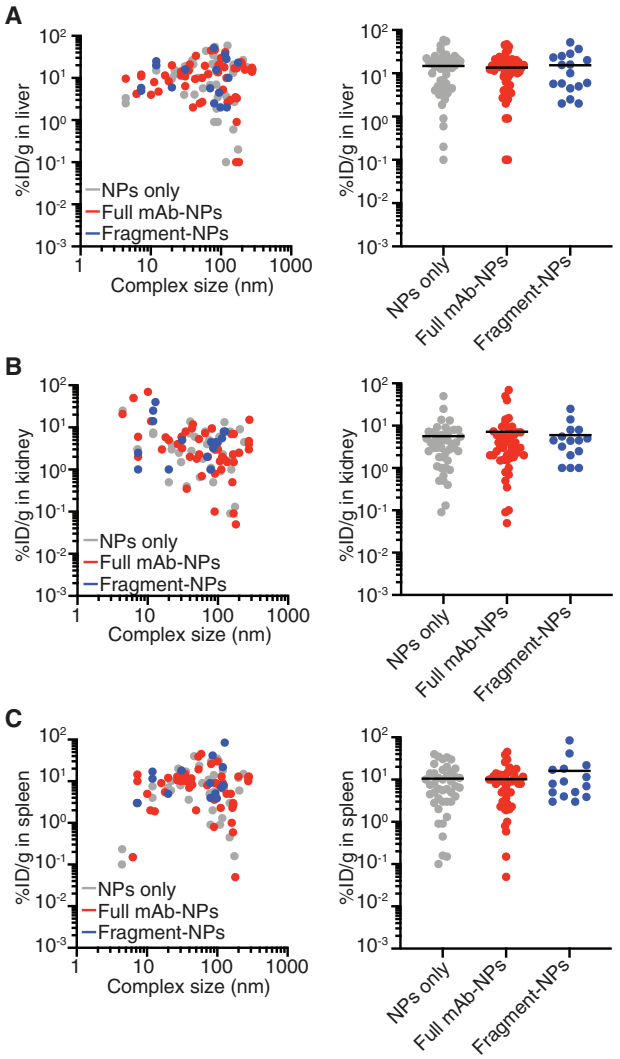

Figure 3. Analysis of the biodistribution of antibody–NP/fragment–NP complex. A) Liver uptake, B) kidneys uptake, and C) spleen uptake of the NPs based on the size of the complex (left) and independently on the size (right). The black solid lines indicate the mean values. No statistical differences were observed between the different groups. A Mann–Whitney statistical test was performed but no significant *p*-values were found.

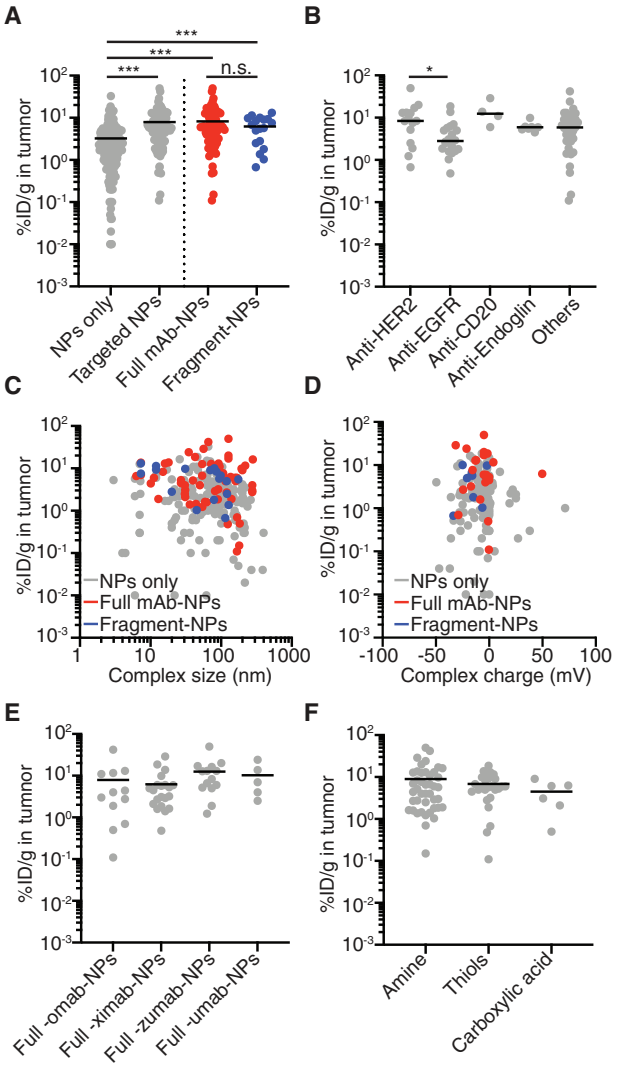

Figure 4. Analysis of antibody-targeted nanoparticles tumor uptake efficacy between 2009 and 2021. A) Tumor-uptake-based passive-targeted NP, full monoclonal antibody (mAb)–NPs, and fragment–NPs. B) Tumor uptake for both full mAb–NPs and fragment–NPs based on the target site. C) Tumor uptake based on the size of the complex. D) Tumor uptake based on the charge of the complex. E) Tumor uptake based on the isotype of the full mAb and fragments. F) Tumor uptake for the full mAb–NPs based on the conjugation strategy to conjugate the NPs to the mAb. The black solid lines indicate the mean values. *p*-values are calculated with a Mann–Whitney statistical test. **p*-value < 0.05; ***p*-value < 0.01, ****p*-value < 0.001, *****p*-value < 0.0001.

between the tumor-targeted NPs conjugate groups. Still, interspecies variation is an important aspect to consider. Pharmacologically, small-animal xenograft models exhibit a more pronounced vascularization compared to human malignancies[109,110] leading to higher nanoparticle tumor uptake. Similarly, higher PK variabilities are observed between animal species.[111,112] Thus, to perform interspecies scaling and predict human parameters, the PK parameters should be extrapolated through allometric scaling laws and physiologically based pharmacokinetic (PBPK) models.[113,114] Of note, the method used to quantify the BD (in vivo nuclear or fluorescence imaging, ex vivo NPs or drugs quantification) does not seem to influence the observed values (Table S1 and Figure S6, Supporting Information). Finally, we performed a univariate analysis to confirm these results (**Figure 5** and Figure S7, Supporting Information). The analysis confirmed that the use of a targeting approach led to a better NP tumor uptake independent of the NP type selected. However, for both polymeric and organic/inorganic NPs, the conjugation to full mAbs provide an improved NP tumor uptake in comparison to fragment–NPs, independent of the overall size of the conjugates. In contrast, for the lipidic NPs, fragment–NPs provide increased tumor uptake directly related with the size of the complex.

4. Conclusion

Anticancer treatments remain associated with major adverse effects. Several approaches have been developed to improve

© 2022 The Authors. Advanced Materials published by Wiley-VCH GmbH

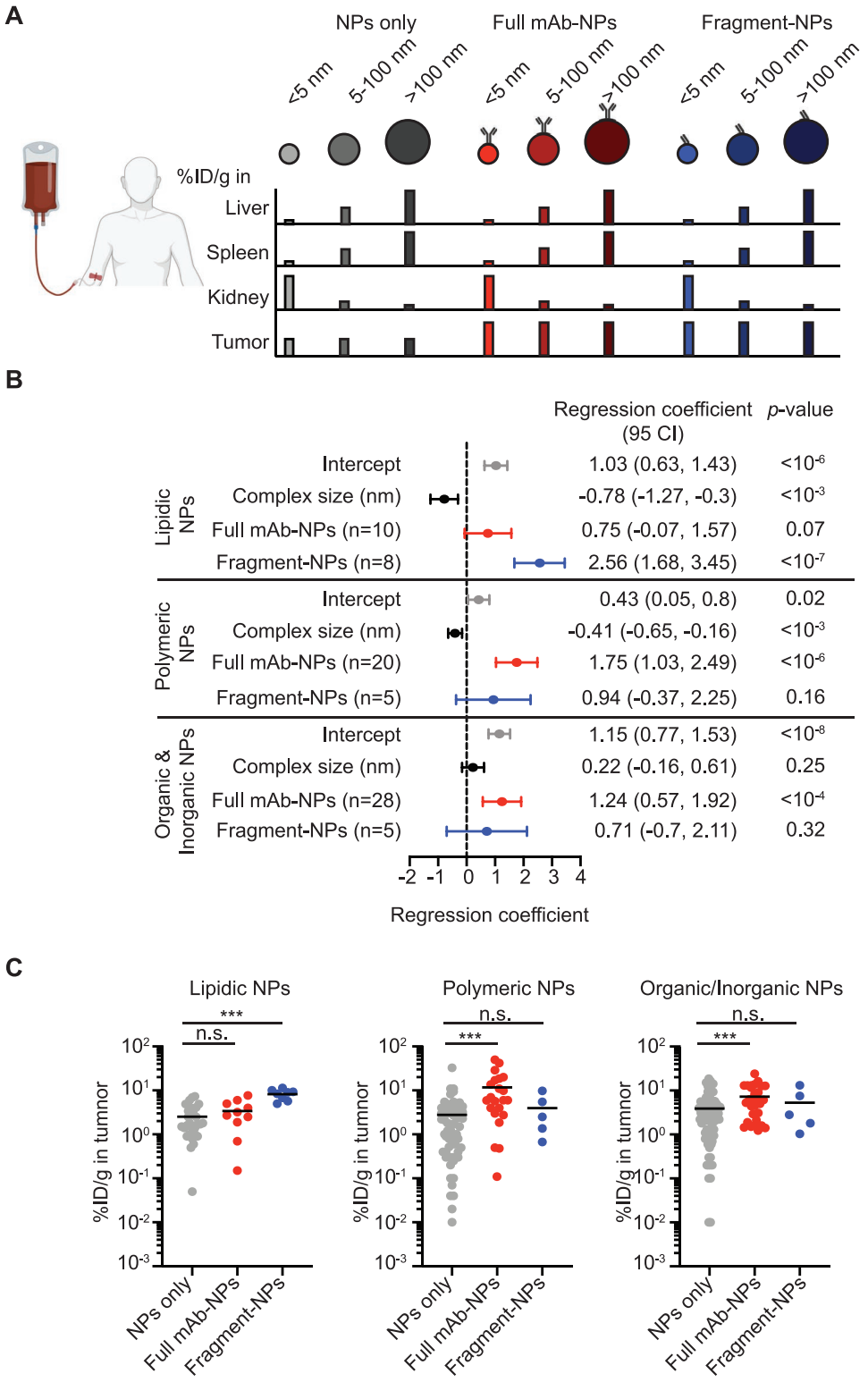

Figure 5. Tumor targeting efficiency based on the material type of the NPs. A) Schematic representation of the biodistribution of passively targeted NPs, full mAb–NPs, and fragment–NPs based on abovementioned results. B) Univariate analysis recapitulating the role of material used, the size of the complex, and the optimal conjugation moiety to employ for improved tumor uptake. C) These results were confirmed based on Mann–Whitney tests performed on the extracted data.

© 2022 The Authors. Advanced Materials published by Wiley-VCH GmbH

Table 1. Antibody-conjugated nanoparticles in clinical trials. C225-ILs: anti-EGFR immunoliposomes; TNBC: triple negative breast cancer; TfR: transferrin receptor; CNS: central nervous system; ✠ discontinued for clinical ineffectiveness; ▲ loss of funding.

Name	Size [nm]	Payload	Target	Clinical indications	Phases
MM-302	75–110	Doxorubicin	scFv anti-HER2	$HER2^+$ breast cancer	Phase II✠
C225-ILs	85	Doxorubicin	Fab′ anti-EGFR	TNBC $EGFR^+$	Phase II
MCC-465	140	Doxorubicin	$F(ab')_2$ anti-GAH	Metastatic gastric cancer	Phase I▲
SGT-53	90	Plasmid *TP53*	scFv anti-TfR	Pediatric solid tumors	Phase I
				Pediatric CNS tumors	Phase I
				Recurrent glioblastoma	Phase II
				Metastatic pancreatic cancer	Phase II
SGT-94	90	Plasmid *RB94*	scFv anti-TfR	RB negative tumors	Phase I

the therapeutic index and PK profiles of chemotherapies. Full antibody–NPs and fragment–NPs represent an innovative strategy for improving the delivery of these molecules to the tumor. While targeting NPs with antibodies or fragments significantly improves their uptake into the tumor over nontargeted NPs, the pharmacokinetics and the biodistribution profiles of both full antibody–NPs and fragment–NPs remained dictated by the physicochemical properties of the NPs (Figure 5A). We have demonstrated in this study that the size of the antibody-targeting moieties did not directly impact its ability to target the tumor cells or the PK properties of the NPs.

Interestingly, these results demonstrate that, for most of the NP conjugates, using a fragment or a full mAb conjugation strategy did not provide many differences in terms of tumor uptake, half-life in the blood, and off-target uptake. However, because of the chemistry employed to generate full mAb–NPs, some variabilities have been observed in terms of PK, which could be attributed to random site conjugation or uncontrolled amount of mAb per NPs. Additionally, it remains necessary to determine the optimal density for every individual mAb conjugated at the surface of the NPs to maintain the binding capacity of the complex.[115–117] Such PK variabilities induced by orientation challenges of the full mAbs are not present with fragment–NPs. As a result, it is almost logical to notate that the use of fragment–lipidic NPs is the first generation of tumor-targeted NPs being validating in the clinic (**Table 1**). However, while preclinical results seem to validate the interest of using antibody-targeted NPs rather than passively targeted NPs, the cost versus effectiveness still remains to be addressed through further clinical evaluations. Phase-I clinical trials confirm preclinical studies and validate the feasibility and the potential of targeted delivery.[118] However, the therapeutic efficacy results in breast cancer remain dismal.[119,120] Depending on the results of the on-going phase-II clinical trials,[121] the cost of production (antibodies production, NPs synthesis, conjugation, and batch reproducibility)[122,123] versus therapeutic improvement will need further analysis to justify such conjugation strategy.

More specifically, this study suggests that to optimize the tumor targeting efficiencies of NPs, selecting full mAb or fragments should be driven by the material type of the NPs. Of note, these results need to be taken with precautions due to the relatively limited size sample evaluated.

Supporting Information

Supporting Information is available from the Wiley Online Library or from the author.

Acknowledgements

This project was, in part, funded by the ICANS grant #2020-02-06 (A.D) and by the Inserm Plan Cancer (A.D., J.G.G, and L.J.C.). A.D is also supported by the European Research Council (ERC) Starting Grant TheranoImmuno, grant agreement No. 95010. V.M. is supported by a fellowship from the French Ministry of Science (MESRI).

Conflict of Interest

The authors declare no conflict of interest.

Keywords

active targeting, antibodies, biodistribution, nanomedicine, pharmacokinetics

Received: December 17, 2021
Revised: February 1, 2022
Published online:

[1] D. Rosenblum, N. Joshi, W. Tao, J. M. Karp, D. Peer, *Nat. Commun.* **2018**, *9*, 1410.
[2] J. Z. Drago, S. Modi, S. Chandarlapaty, *Nat. Rev. Clin. Oncol.* **2021**, *18*, 327.
[3] K. J. Hamblett, P. D. Senter, D. F. Chace, M. M. C. Sun, J. Lenox, C. G. Cerveny, K. M. Kissler, S. X. Bernhardt, A. K. Kopcha, R. F. Zabinski, D. L. Meyer, J. A. Francisco, *Clin. Cancer Res.* **2004**, *10*, 7063.
[4] Y. T. Adem, K. A. Schwarz, E. Duenas, T. W. Patapoff, W. J. Galush, O. Esue, *Bioconjugate Chem.* **2014**, *25*, 656.
[5] Y. Matsumura, H. Maeda, *Cancer Res.* **1986**, *46*, 6387.
[6] H. Maeda, *J. Pers. Med.* **2021**, *11*, 229.
[7] H. Maeda, *Bioconjugate Chem.* **2010**, *21*, 797.
[8] S. Wilhelm, A. J. Tavares, Q. Dai, S. Ohta, J. Audet, H. F. Dvorak, W. C. W. Chan, *Nat. Rev. Mater.* **2016**, *1*, 16014.
[9] N. Tanaka, S. Kanatani, R. Tomer, C. Sahlgren, P. Kronqvist, D. Kaczynska, L. Louhivuori, L. Kis, C. Lindh, P. Mitura,

© 2022 The Authors. Advanced Materials published by Wiley-VCH GmbH

A. Stepulak, S. Corvigno, J. Hartman, P. Micke, A. Mezheyeuski, C. Strell, J. W. Carlson, C. Fernández Moro, H. Dahlstrand, A. Östman, K. Matsumoto, P. Wiklund, M. Oya, A. Miyakawa, K. Deisseroth, P. Uhlén, *Nat. Biomed. Eng.* **2017**, *1*, 796.

[10] K. J. Harrington, S. Mohammadtaghi, P. S. Uster, D. Glass, A. M. Peters, R. G. Vile, J. S. W. Stewart, *Clin. Cancer Res.* **2001**, *7*, 243.

[11] M. I. Koukourakis, S. Koukouraki, A. Giatromanolaki, S. Kakolyris, V. Georgoulias, A. Velidaki, S. Archimandritis, N. N. Karkavitsas, *Acta Oncol.* **2000**, *39*, 207.

[12] A. E. Hansen, A. L. Petersen, J. R. Henriksen, B. Boerresen, P. Rasmussen, D. R. Elema, P. M. A. Rosenschöld, A. T. Kristensen, A. Kjær, T. L. Andresen, *ACS Nano* **2015**, *9*, 6985.

[13] S. Kunjachan, A. Detappe, R. Kumar, T. Ireland, L. Cameron, D. E. Biancur, V. Motto-Ros, L. Sancey, S. Sridhar, G. M. Makrigiorgos, R. I. Berbeco, *Nano Lett.* **2015**, *15*, 7488.

[14] S.-Y. Wu, F.-G. Wu, X. Chen, *Adv. Mater.* **2022**, *34*, 2109210.

[15] J. Zhong, L. Wen, S. Yang, L. Xiang, Q. Chen, D. Xing, *Nanomed.: Nanotechnol., Biol., Med.* **2015**, *11*, 1499.

[16] X. D. Zhang, Z. Luo, J. Chen, S. Song, X. Yuan, X. Shen, H. Wang, Y. Sun, K. Gao, L. Zhang, S. Fan, D. T. Leong, M. Guo, J. Xie, *Sci. Rep.* **2015**, *5*, 8669.

[17] L. Karmani, D. Labar, V. Valembois, V. Bouchat, P. G. Nagaswaran, A. Bol, J. Gillart, P. Levêque, C. Bouzin, D. Bonifazi, C. Michiels, O. Feron, V. Grégoire, S. Lucas, T. Vander Borght, B. Gallez, *Contrast Media Mol. Imaging* **2013**, *8*, 402.

[18] Y. Wang, Y. Liu, H. Luehmann, X. Xia, P. Brown, C. Jarreau, M. Welch, Y. Xia, *ACS Nano* **2012**, *6*, 5880.

[19] N. B. Shah, G. M. Vercellotti, J. G. White, A. Fegan, C. R. Wagner, J. C. Bischof, *Mol. Pharmaceutics* **2012**, *9*, 2146.

[20] L. C. Kennedy, A. S. Bear, J. K. Young, N. A. Lewinski, J. Kim, A. E. Foster, R. A. Drezek, *Nanoscale Res. Lett.* **2011**, *6*, 283.

[21] A. J. Gormley, A. Malugin, A. Ray, R. Robinson, H. Ghandehari, *J. Drug Targeting* **2011**, *19*, 915.

[22] Arnida, M. M. Janát-Amsbury, A. Ray, C. M. Peterson, H. Ghandehari, *Eur. J. Pharm. Biopharm.* **2011**, *77*, 417.

[23] S. D. Perrault, C. Walkey, T. Jennings, H. C. Fischer, W. C. W. Chan, *Nano Lett.* **2009**, *9*, 1909.

[24] R. P. Chauhan, R. Mathur, G. Singh, N. Bag, S. Singh, K. Chuttani, B. S. H. Kumar, S. K. Agrawal, A. K. Mishra, *J. Mater. Sci.* **2013**, *48*, 3913.

[25] R. P. Chauhan, R. Mathur, G. Singh, A. Kaul, N. Bag, S. Singh, H. Kumar, M. Patra, A. K. Mishra, *J. Biomed. Nanotechnol.* **2013**, *9*, 323.

[26] X. Yang, H. Hong, J. J. Grailer, I. J. Rowland, A. Javadi, S. A. Hurley, Y. Xiao, Y. Yang, Y. Zhang, R. J. Nickles, W. Cai, D. A. Steeber, S. Gong, *Biomaterials* **2011**, *32*, 4151.

[27] C. Zhang, C. Li, Y. Liu, J. Zhang, C. Bao, S. Liang, Q. Wang, Y. Yang, H. Fu, K. Wang, D. Cui, *Adv. Funct. Mater.* **2015**, *25*, 1314.

[28] R. Chakravarty, S. Goel, H. Hong, F. Chen, H. F. Valdovinos, R. Hernandez, T. E. Barnhart, W. Cai, *Nanomedicine* **2015**, *10*, 1233.

[29] M. Chen, X. Fang, S. Tang, N. Zheng, *Chem. Commun.* **2012**, *48*, 8934.

[30] F. Chen, H. Hong, S. Shi, S. Goel, H. F. Valdovinos, R. Hernandez, C. P. Theuer, T. E. Barnhart, W. Cai, *Sci. Rep.* **2014**, *4*, 5080.

[31] F. Chen, T. R. Nayak, S. Goel, H. F. Valdovinos, H. Hong, C. P. Theuer, T. E. Barnhart, W. Cai, *Mol. Pharmaceutics* **2014**, *11*, 4007.

[32] M. Benezra, O. Penate-Medina, P. B. Zanzonico, D. Schaer, H. Ow, A. Burns, E. DeStanchina, V. Longo, E. Herz, S. Iyer, J. Wolchok, S. M. Larson, U. Wiesner, M. S. Bradbury, *J. Clin. Invest.* **2011**, *121*, 2768.

[33] F. Chen, H. Hong, Y. Zhang, H. F. Valdovinos, S. Shi, G. S. Kwon, C. P. Theuer, T. E. Barnhart, W. Cai, *ACS Nano* **2013**, *7*, 9027.

[34] J. Wang, R. Bai, R. Yang, J. Liu, J. Tang, Y. Liu, J. Li, Z. Chai, C. Chen, *Metallomics* **2015**, *7*, 516.

[35] F. Chen, H. Hong, S. Goel, S. A. Graves, H. Orbay, E. B. Ehlerding, S. Shi, C. P. Theuer, R. J. Nickles, W. Cai, *ACS Nano* **2015**, *9*, 3926.

[36] J. Yu, W. Yin, X. Zheng, G. Tian, X. Zhang, T. Bao, X. Dong, Z. Wang, Z. Gu, X. Ma, Y. Zhao, *Theranostics* **2015**, *5*, 931.

[37] X. D. Zhang, J. Chen, Y. Min, G. B. Park, X. Shen, S. S. Song, Y. M. Sun, H. Wang, W. Long, J. Xie, K. Gao, L. Zhang, S. Fan, F. Fan, U. Jeong, *Adv. Funct. Mater.* **2014**, *24*, 1718.

[38] J. D. Meyers, Y. Cheng, A. M. Broome, R. S. Agnes, M. D. Schluchter, S. Margevicius, X. Wang, M. E. Kenney, C. Burda, J. P. Basilion, *Part. Part. Syst. Charact.* **2015**, *32*, 448.

[39] P. Mi, D. Kokuryo, H. Cabral, M. Kumagai, T. Nomoto, I. Aoki, Y. Terada, A. Kishimura, N. Nishiyama, K. Kataoka, *J. Controlled Release* **2014**, *174*, 63.

[40] H. Hong, F. Wang, Y. Zhang, S. A. Graves, S. B. Z. Eddine, Y. Yang, C. P. Theuer, R. J. Nickles, X. Wang, W. Cai, *ACS Appl. Mater. Interfaces* **2015**, *7*, 3373.

[41] K. Chen, Z. B. Li, H. Wang, W. Cai, X. Chen, *Eur. J. Nucl. Med. Mol. Imaging* **2008**, *35*, 2235.

[42] W. Cai, K. Chen, Z. B. Li, S. S. Gambhir, X. Chen, *J. Nucl. Med.* **2007**, *48*, 1862.

[43] W. A. T. Al-Jamal, K. T. Al-Jamal, B. Tian, A. Cakebread, J. M. Halket, K. Kostarelos, *Mol. Pharmaceutics* **2009**, *6*, 520.

[44] S. Goel, F. Chen, H. Hong, H. F. Valdovinos, R. Hernandez, S. Shi, T. E. Barnhart, W. Cai, *ACS Appl. Mater. Interfaces* **2014**, *6*, 21677.

[45] S. J. Denardo, G. L. Denardo, A. Natarajan, L. A. Miers, A. R. Foreman, C. Gruettner, G. N. Adamson, R. Ivkov, *J. Nucl. Med.* **2007**, *48*, 1338.

[46] H. Yu, Z. Tang, D. Zhang, W. Song, Y. Zhang, Y. Yang, Z. Ahmad, X. Chen, *J. Controlled Release* **2015**, *205*, 89.

[47] J. Guo, H. Hong, G. Chen, S. Shi, Q. Zheng, Y. Zhang, C. P. Theuer, T. E. Barnhart, W. Cai, S. Gong, *Biomaterials* **2013**, *34*, 8323.

[48] Y. Shi, R. Van Der Meel, B. Theek, E. Oude Blenke, E. H. E. Pieters, M. H. A. M. Fens, J. Ehling, R. M. Schiffelers, G. Storm, C. F. Van Nostrum, T. Lammers, W. E. Hennink, *ACS Nano* **2015**, *9*, 3740.

[49] E. A. Sykes, J. Chen, G. Zheng, W. C. W. Chan, *ACS Nano* **2014**, *8*, 5696.

[50] M. P. Kai, A. W. Keeler, J. L. Perry, K. G. Reuter, J. C. Luft, S. K. O'Neal, W. C. Zamboni, J. M. Desimone, *J. Controlled Release* **2015**, *204*, 70.

[51] Y. Chen, W. Zhang, Y. Huang, F. Gao, X. Sha, X. Fang, *Int. J. Pharm.* **2015**, *488*, 44.

[52] H. Oliveira, J. Thevenot, E. Garanger, E. Ibarboure, P. Calvo, P. Aviles, M. J. Guillen, S. Lecommandoux, *Pharm. Res.* **2014**, *31*, 983.

[53] M. Ding, N. Song, X. He, J. Li, L. Zhou, H. Tan, Q. Fu, Q. Gu, *ACS Nano* **2013**, *7*, 1918.

[54] K. S. Chu, W. Hasan, S. Rawal, M. D. Walsh, E. M. Enlow, J. C. Luft, A. S. Bridges, J. L. Kuijer, M. E. Napier, W. C. Zamboni, J. M. DeSimone, *Nanomed.: Nanotechnol., Biol., Med.* **2013**, *9*, 686.

[55] K. S. Chu, A. N. Schorzman, M. C. Finniss, C. J. Bowerman, L. Peng, J. C. Luft, A. J. Madden, A. Z. Wang, W. C. Zamboni, J. M. DeSimone, *Biomaterials* **2013**, *34*, 8424.

[56] Y. Ma, M. Sadoqi, J. Shao, *Int. J. Pharm.* **2012**, *436*, 25.

[57] X. Guo, C. Shi, J. Wang, S. Di, S. Zhou, *Biomaterials* **2013**, *34*, 4544.

[58] S. Sumitani, M. Oishi, Y. Nagasaki, *React. Funct. Polym.* **2011**, *71*, 684.

[59] Y. Bae, N. Nishiyama, K. Kataoka, *Bioconjugate Chem.* **2007**, *18*, 1131.

[60] H. Hu, P. Huang, O. J. Weiss, X. Yan, X. Yue, M. G. Zhang, Y. Tang, L. Nie, Y. Ma, G. Niu, K. Wu, X. Chen, *Biomaterials* **2014**, *35*, 9868.

© 2022 The Authors. Advanced Materials published by Wiley-VCH GmbH

[61] H. Cabral, N. Nishiyama, S. Okazaki, H. Koyama, K. Kataoka, *J. Controlled Release* **2005**, *101*, 223.
[62] Y. Bae, N. Nishiyama, S. Fukushima, H. Koyama, M. Yasuhiro, K. Kataoka, *Bioconjugate Chem.* **2005**, *16*, 122.
[63] L. E. van Vlerken, Z. Duan, S. R. Little, M. V. Seiden, M. M. Amiji, *Mol. Pharmaceutics* **2008**, *5*, 516.
[64] R. Rossin, D. Pan, K. Qi, J. L. Turner, X. Sun, K. L. Wooley, M. J. Welch, *J. Nucl. Med.* **2005**, *46*, 1210.
[65] N. Mondal, K. K. Halder, M. M. Kamila, M. C. Debnath, T. K. Pal, S. K. Ghosal, B. R. Sarkar, S. Ganguly, *Int. J. Pharm.* **2010**, *397*, 194.
[66] A. Pathak, P. Kumar, K. Chuttani, S. Jain, A. K. Mishra, S. P. Vyas, K. C. Gupta, *ACS Nano* **2009**, *3*, 1493.
[67] S. Shi, K. Yang, H. Hong, H. F. Valdovinos, T. R. Nayak, Y. Zhang, C. P. Theuer, T. E. Barnhart, Z. Liu, W. Cai, *Biomaterials* **2013**, *34*, 3002.
[68] H. Hong, K. Yang, Y. Zhang, J. W. Engle, L. Feng, Y. Yang, T. R. Nayak, S. Goel, J. Bean, C. P. Theuer, T. E. Barnhart, Z. Liu, W. Cai, *ACS Nano* **2012**, *6*, 2361.
[69] H. Xu, M. Fan, A. M. A. Elhissi, Z. Zhang, K. W. Wan, W. Ahmed, D. A. Phoenix, X. Sun, *Nanomedicine* **2015**, *10*, 1247.
[70] S. Shi, K. Yang, H. Hong, F. Chen, H. F. Valdovinos, S. Goel, T. E. Barnhart, Z. Liu, W. Cai, *Biomaterials* **2015**, *39*, 39.
[71] X. Liu, H. Li, Y. Chen, Q. Jin, K. Ren, J. Ji, *Adv. Healthcare Mater.* **2014**, *3*, 1439.
[72] H. Hong, Y. Zhang, J. W. Engle, T. R. Nayak, C. P. Theuer, R. J. Nickles, T. E. Barnhart, W. Cai, *Biomaterials* **2012**, *33*, 4147.
[73] Z. Liu, W. Cai, L. He, N. Nakayama, K. Chen, X. Sun, X. Chen, H. Dai, *Nat. Nanotechnol.* **2007**, *2*, 47.
[74] G. Song, D. B. Darr, C. M. Santos, M. Ross, A. Valdivia, J. L. Jordan, B. R. Midkiff, S. Cohen, N. Nikolaishvili-Feinberg, C. R. Miller, T. K. Tarrant, A. B. Rogers, A. C. Dudley, C. M. Perou, W. C. Zamboni, *Clin. Cancer Res.* **2014**, *20*, 6083.
[75] C. Pérez-Medina, D. Abdel-Atti, Y. Zhang, V. A. Longo, C. P. Irwin, T. Binderup, J. Ruiz-Cabello, Z. A. Fayad, J. S. Lewis, W. J. M. Mulder, T. Reiner, *J. Nucl. Med.* **2014**, *55*, 1706.
[76] S. Hirsjärvi, L. Sancey, S. Dufort, C. Belloche, C. Vanpouille-Box, E. Garcion, J. L. Coll, F. Hindré, J. P. Benoît, *Int. J. Pharm.* **2013**, *453*, 594.
[77] C. C. Tsai, C. H. Chang, L. C. Chen, Y. J. Chang, K. L. Lan, Y. H. Wu, C. W. Hsu, I. H. Liu, C. L. Ho, W. C. Lee, H. C. Ni, T. J. Chang, G. Ting, T. W. Lee, *Int. J. Nanomed.* **2011**, *6*, 2607.
[78] Y. Miyajima, H. Nakamura, Y. Kuwata, J. D. Lee, S. Masunaga, K. Ono, K. Maruyama, *Bioconjugate Chem.* **2006**, *17*, 1314.
[79] D. B. Kirpotin, D. C. Drummond, Y. Shao, M. R. Shalaby, K. Hong, U. B. Nielsen, J. D. Marks, C. C. Benz, J. W. Park, *Cancer Res.* **2006**, *66*, 6732.
[80] D. Paolino, D. Cosco, L. Racanicchi, E. Trapasso, C. Celia, M. Iannone, E. Puxeddu, G. Costante, S. Filetti, D. Russo, M. Fresta, *J. Controlled Release* **2010**, *144*, 144.
[81] W. C. Zamboni, S. Strychor, E. Joseph, D. R. Walsh, B. A. Zamboni, R. A. Parise, M. E. Tonda, N. Y. Yu, C. Engbers, J. L. Eiseman, *Clin. Cancer Res.* **2007**, *13*, 7217.
[82] G. P. Goodrich, L. Bao, K. Gill-Sharp, K. L. Sang, J. Wang, J. D. Payne, *J. Biomed. Opt.* **2010**, *15*, 018001.
[83] L. C. Chen, C. H. Chang, C. Y. Yu, Y. J. Chang, Y. H. Wu, W. C. Lee, C. H. Yeh, T. W. Lee, G. Ting, *Nucl. Med. Biol.* **2008**, *35*, 883.
[84] Z. P. Yuan, L. J. Chen, L. Y. Fan, M. H. Tang, G. L. Yang, H. S. Yang, X. B. Du, G. Q. Wang, W. X. Yao, Q. M. Zhao, B. Ye, R. Wang, P. Diao, W. Zhang, H. Bin Wu, X. Zhao, Y. Q. Wei, *Clin. Cancer Res.* **2006**, *12*, 3193.
[85] M. H. Chen, C. H. Chang, Y. J. Chang, L. C. Chen, C. Y. Yu, Y. H. Wu, W. C. Lee, C. H. Yeh, F. H. Lin, T. W. Lee, C. S. Yang, G. Ting, *Anticancer Res.* **2010**, *30*, 65.
[86] Y. J. Chang, C. H. Chang, C. Y. Yu, T. J. Chang, L. C. Chen, M. H. Chen, T. W. Lee, G. Ting, *Nucl. Med. Biol.* **2010**, *37*, 95.
[87] Y. J. Chang, C. H. Chang, T. J. Chang, C. Y. Yu, L. C. Chen, M. L. Jan, T. Y. Luo, T. W. Lee, G. Ting, *Anticancer Res.* **2007**, *27*, 2217.
[88] S. Sadekar, A. Ray, M. Janàt-Amsbury, C. M. Peterson, H. Ghandehari, *Biomacromolecules* **2011**, *12*, 88.
[89] T. Okuda, S. Kawakami, N. Akimoto, T. Niidome, F. Yamashita, M. Hashida, *J. Controlled Release* **2006**, *116*, 330.
[90] F. Zhang, P. Mastorakos, M. K. Mishra, A. Mangraviti, L. Hwang, J. Zhou, J. Hanes, H. Brem, A. Olivi, B. Tyler, R. M. Kannan, *Biomaterials* **2015**, *52*, 507.
[91] M. Wu, J. Shi, D. Fan, Q. Zhou, F. Wang, Z. Niu, Y. Huang, *Biomacromolecules* **2013**, *14*, 4032.
[92] S. Sadekar, O. Linares, G. J. Noh, D. Hubbard, A. Ray, M. Janát-Amsbury, C. M. Peterson, J. Facelli, H. Ghandehari, *Drug Delivery Transl. Res.* **2013**, *3*, 260.
[93] K. C. L. Black, Y. Wang, H. P. Luehmann, X. Cai, W. Xing, B. Pang, Y. Zhao, C. S. Cutler, L. V Wang, Y. Liu, Y. Xia, *ACS Nano* **2014**, *8*, 4385.
[94] J. H. Kim, Y. Kim, K. H. Bae, T. G. Park, J. H. Lee, K. Park, *Mol. Pharmaceutics* **2015**, *12*, 1230.
[95] L. Harivardhan Reddy, R. K. Sharma, K. Chuttani, A. K. Mishra, R. S. R. Murthy, *J. Controlled Release* **2005**, *105*, 185.
[96] J. Liu, M. Yu, X. Ning, C. Zhou, S. Yang, J. Zheng, *Angew. Chem., Int. Ed.* **2013**, *52*, 12572.
[97] T. M. Allen, *Nat. Rev. Cancer* **2002**, *2*, 750.
[98] K. L. Gill, K. K. Machavaram, R. H. Rose, M. Chetty, *Clin. Pharmacokinet.* **2016**, *55*, 789.
[99] F. Li, M. L. Ulrich, V. F. S. Shih, J. H. Cochran, J. H. Hunter, L. Westendorf, J. Neale, D. R. Benjamin, *Mol. Cancer Ther.* **2019**, *18*, 780.
[100] T. Suzuki, A. Ishii-Watabe, M. Tada, T. Kobayashi, T. Kanayasu-Toyoda, T. Kawanishi, T. Yamaguchi, *J. Immunol.* **2010**, *184*, 1968.
[101] A. V. Kamath, *Drug Discovery Today Technol.* **2016**, *21-22*, 75.
[102] E. Blanco, H. Shen, M. Ferrari, *Nat. Biotechnol.* **2015**, *33*, 941.
[103] D. Peer, J. M. Karp, S. Hong, O. C. Farokhzad, R. Margalit, R. Langer, *Nat. Nanotechnol.* **2007**, *2*, 751.
[104] B. Saha, T. H. Evers, M. W. J. Prins, *Anal. Chem.* **2014**, *86*, 8158.
[105] N. Tajima, M. Takai, K. Ishihara, *Anal. Chem.* **2011**, *83*, 1969.
[106] K. Tripathi, J. D. Driskell, *ACS Omega* **2018**, *3*, 8253.
[107] M. E. Wiseman, C. W. Frank, *Langmuir* **2012**, *28*, 1765.
[108] D. A. Richards, A. Maruani, V. Chudasama, *Chem. Sci.* **2016**, *8*, 63.
[109] F. Yuan, M. Dellian, D. Fukumura, M. Leunig, D. A. Berk, V. P. Torchilin, R. K. Jain, *Cancer Res.* **1995**, *55*, 3752.
[110] N. Bertrand, J. Wu, X. Xu, N. Kamaly, O. C. Farokhzad, *Adv. Drug Delivery Rev.* **2014**, *66*, 2.
[111] W. P. Caron, G. Song, P. Kumar, S. Rawal, W. C. Zamboni, *Clin. Pharmacol. Ther.* **2012**, *91*, 802.
[112] S. W. Jones, R. A. Roberts, G. R. Robbins, J. L. Perry, M. P. Kai, K. Chen, T. Bo, M. E. Napier, J. P. Y. Ting, J. M. DeSimone, J. E. Bear, *J. Clin. Invest.* **2013**, *123*, 3061.
[113] Z. Lin, N. A. Monteiro-Riviere, R. Kannan, J. E. Riviere, *Nanomedicine* **2016**, *11*, 107.
[114] M. S. Valic, G. Z. Prof, *Theranostics* **2019**, *9*, 3365.
[115] A. Rodallec, C. Franco, S. Robert, G. Sicard, S. Giacometti, B. Lacarelle, F. Bouquet, A. Savina, R. Lacroix, F. Dignat-George, J. Ciccolini, P. Poncelet, R. Fanciullino, *Sci. Rep.* **2020**, *10*, 4147.
[116] M. Li, J. Dong, F. Cheng, C. Li, H. Wang, T. Sun, W. He, Q. Wang, *Mol. Pharmaceutics* **2021**, *18*, 1196.
[117] M. Colombo, L. Fiandra, G. Alessio, S. Mazzucchelli, M. Nebuloni, C. De Palma, K. Kantner, B. Pelaz, R. Rotem, F. Corsi, W. J. Parak, D. Prosperi, *Nat. Commun.* **2016**, *7*, 13818.
[118] C. Mamot, R. Ritschard, A. Wicki, G. Stehle, T. Dieterle, L. Bubendorf, C. Hilker, S. Deuster, R. Herrmann, C. Rochlitz, *Lancet Oncol.* **2012**, *13*, 1234.

© 2022 The Authors. Advanced Materials published by Wiley-VCH GmbH

[119] K. Miller, J. Cortes, S. A. Hurvitz, I. E. Krop, D. Tripathy, S. Verma, K. Riahi, J. G. Reynolds, T. J. Wickham, I. Molnar, D. A. Yardley, *BMC Cancer* **2016**, *16*, 352.
[120] A. Wicki, C. Mamot, U. Hasler-Strub, S. Riniker, Q. Li, L. Holer, D. Baertschi, K. Zaman, R. von Moos, K. J. Dedes, U. Novak, A. Bodmer, R. Ritschard, E. Obermann, C. J. Ackermann, V. Membrez-Antonioli, U. Zuerrer, C. B. Caspar, C. Rochlitz, R. C. Winterhalder, *Ann. Oncol.* **2021**, *32*, S479.
[121] B. Kasenda, D. König, M. Manni, R. Ritschard, U. Duthaler, E. Bartoszek, A. Bärenwaldt, S. Deuster, G. Hutter, D. Cordier, L. Mariani, J. Hench, S. Frank, S. Krähenbühl, A. Zippelius, C. Rochlitz, C. Mamot, A. Wicki, H. Läubli, *ESMO Open* **2022**, *7*, 100365.
[122] Z. Cheng, A. Al Zaki, J. Z. Hui, V. R. Muzykantov, A. Tsourkas, *Science* **2012**, *338*, 903.
[123] W. C. Zamboni, V. Torchilin, A. K. Patri, J. Hrkach, S. Stern, R. Lee, A. Nel, N. J. Panaro, P. Grodzinski, *Clin. Cancer Res.* **2012**, *18*, 3229.

© 2022 The Authors. Advanced Materials published by Wiley-VCH GmbH

4. Green chemistry-driven antibody-targeted nanoemulsion development for cancer therapy

Real-life data demonstrate that no marketed liposomal agents trigger a significantly increased therapeutic response compared to the standard agent (Petersen et al., 2016). Owing to targeted NPs development, antibody fragments were conjugated at the surface of liposome to improve their delivery in the tumor bed. Despite improving tumor targeting in preclinical models, these immunoliposomes did not make their way to clinical use due to a lack of efficacy. One could infer that clinical translation failure was due to the limited liposomal drug loading and retention.

To circumvent these limitations, nanoemulsions (NEs) appear to be an attractive solution thanks to their high loading potential (Bouchaala et al., 2016; Liu et al., 2021) and their highly biocompatible composition (*e.g.*, lipids, edible oils and PEGs) (Anton and Vandamme, 2011; Singh et al., 2017). In a longstanding collaboration with the laboratory of Andrey Klymchenko (CNRS UMR_7021, Laboratoire de Bioimagerie et Pathologies), the Tumor Biomechanics lab demonstrated with a Förster resonance energy transfer (FRET) approach that NEs are stable in the blood and release their content upon tumor entry (Bouchaala et al., 2016). Continuing our collaboration, we developed NEs allowing pH-sensitive delivery of doxorubicin, which further decrease cargo leakage at physiological pH (Liu et al., 2021). The next logical step of our established collaboration was to engineer antibody-targeted NEs to enhance their tumor selectivity. Using a green chemistry approach based on *generally recognized as safe* compounds, we successfully conjugate trastuzumab or cetuximab at the NEs surface. We demonstrate that antibody-targeted NEs selectively recognized their cognate receptors expressed on TCs. Additionally, antibody-targeted NEs display significantly higher internalization in TCs compared to untargeted NEs passive uptake.

Nota bene: The reader should note that other members of the Nanotranslational lab develop a versatile NPs functionalization approach based on the use of peptide building blocks. This strategy allows to overcome complex chemistry and batch-dependent variation by synthetizing large quantity of “pre-targeted” NPs that can be further conjugated on-demand with antibody fragments. This grants broad targeting

possibilities from tumor-associated antigens to immune cell-associated antigens for drug delivery or imaging approaches (Mathieu et al., 2024)

Functionalization of lipid nanoemulsions with humanized antibodies using plug-and-play cholesterol anchor for targeting cancer cells

Valeria Jose Boide-Trujillo[1,*], Vincent Mittelheisser[2,*], Fei Liu[1,3,*], Olivier Lefebvre[2], Bohdan Andreiuk[1], Nicolas Anton[3], Jacky G. Goetz[2,#], and Andrey S. Klymchenko[1,#]

[1]Laboratoire de Bioimagerie et Pathologies, CNRS UMR_7021, ITI SysChem-Chimie des Systèmes Complexes, Université de Strasbourg; Illkirch (France)

[2]Tumor Biomechanics Lab, INSERM UMR_S1109, Fédération de Médecine Translationnelle de Strasbourg, Université de Strasbourg, Equipe labélisée Ligue Nationale Contre le Cancer ; Strasbourg (France).

[3]Regenerative Nanomedicine (RNM), INSERM UMR_1260, Fédération de Médecine Translationnelle de Strasbourg, Université de Strasbourg; Strasbourg (France)

[*]**Equal contribution:**
VJBT, VM and FL have contributed equally to this work.

[#]**Correspondence and co-last authors:**
Andrey S. Klymchenko, andrey.klymchenko@unistra.fr
CNRS UMR_7021, Faculté de Pharmacie, Université de Strasbourg, Institut Thématique Interdisciplinaire SysChem, Illkirch F-67400, France.

Jacky G. Goetz, jacky.goetz@inserm.fr
INSERM UMR_S1109, Tumor Biomechanics Lab, Centre de Recherche en Biomédecine de Strasbourg (CRBS), Fédération de Médecine Translationnelle de Strasbourg (FMTS), 67000 Strasbourg, France. Web: www.goetzlab.fr

Abstract

Lipid NEs are promising green nanocarriers for diagnostic and therapeutic applications, but their functionalization with biomolecules, such as antibodies, remains a challenge due to liquid nature of their core. Here, we developed an original plug-and-play strategy to graft an antibody (trastuzumab) at the surface of NEs, using components generally recognized as safe (GRAS). We synthesized a reactive derivative of cholesterol and a Biotin-PEG_{3000}-Lysine linker, which can react within one-pot formulation to form an amphiphilic carbamate Biotin-PEG_{3000}-Cholesterol. The cholesterol ensures anchorage of the linker, which effectively exposes biotin moiety at the surface of NEs for further antibody grafting using a biotin-neutravidin coupling. The reaction between the Biotin-PEG_{3000}-Lysine linker and NPC-Chol was confirmed by ^{1}H-NMR and absorption spectroscopy. The obtained biotinylated 50-nm NEs loaded with a near-infrared dye were successfully targeted to neutravidin-coated glass surfaces and imaged at the single-droplet level. The biotinylated NEs bearing the trastuzumab antibody targeted specifically HER2-amplified breast cancer models HCC-1954 and SKBR3, in contrast to control MDA-MB-231 (HER2-low) cells. Altogether, our study proposes an efficient methodology for grafting antibodies to the surface of NEs, which offers new opportunities of application of these green nanocarriers in biomedicine.

Introduction

Cancer nanomedicine has initially emerged to improve the delivery selectivity of chemotherapeutics to reduce associated toxicities.[1, 2] Among existing nanoparticles (NPs), nanoemulsions (NEs) constitute sustainable, biomimetic nanomaterials mainly composed of lipids and PEGs, which are materials *generally recognized as safe* (GRAS). [3-5] Their oil core serves as an ideal reservoir for encapsulating lipophilic compounds, including cytotoxic drugs and imaging agents.[6-8] In particular, encapsulation of fluorescent dyes transforms them into bright fluorescence imaging agents.[6] Dye-loaded NEs enable imaging vasculature and tumors,[8] crossing brain blood barrier[9] and intranasal brain delivery[10] as well as tracking individual particles[11] *in vivo*. Their long circulation time and potential of therapeutic molecules loading into their core render them particularly attractive for *in vivo* imaging and drug delivery.[6-8] These nanocarriers are known to passively accumulate in the tumor through the enhanced permeability and retention (EPR) effect.[8, 12] However, as defined in meta-analyses, this passive targeting remains suboptimal and thus requires implementing strategies for specific targeting.[13, 14]

Enhancing the targeting selectivity of drugs and contrast agents is a primary focus in cancer diagnostics and treatment to minimize systemic exposure and increase their efficacy.[15] One major strategy has been the development of antibody-drug conjugates (ADCs), which merge the targeting specificity of monoclonal antibodies with the potency of cytotoxic drugs. These features have led to the widespread clinical adoption of ADCs, with routine applications for the treatment of hematological malignancies and HER2-amplified breast cancers due to their strong antitumoral activity.[16] However, to maintain favorable pharmacokinetic and pharmacodynamic profiles, ADCs have relatively low drug/antibody ratios (≈ 4 molecules/antibody).[17] To overcome this limitation, nanoparticles (NPs) delivery systems have been explored, which can carry >10 times as many small molecules as ADCs.[2, 18] The same concerns contrast agents, where single NP can carry molecules, such as fluorescent dyes, this enhancing sensitivity of detection.[19, 20] As such, combining the targeting selectivity of antibodies with the drug/contrast agent loading ability of NPs seems a logical step to advance this field. We recently confirmed the interest of developing such targeted formulations by highlighting that antibody-targeted nanoparticles demonstrate greater tumor uptake than non-decorated ones.[14] However, functionalization of NEs with antibodies has been poorly explored to date.[6]

The major challenge in surface modifications of NEs is the dynamic nature of their liquid/liquid interface of NEs, which renders surface grafting poorly stable. In previous studies, NEs were functionalized with a peptide arginylglycylaspartic acid (RGD) using lipids[21] or fatty acids,[22] allowing the increased targeting of $\alpha_v\beta_3$ integrin rich cells. However, this approach does not guarantee stable grafting for antibodies, because lipid/fatty acid residues may exchange with other lipid components of serum, as for instance was shown for other lipid nanoparticles.[23] To overcome this limitation, we recently proposed to use NEs with amphiphilic polymers bearing biotin[24] or an antibody.[25] However, the limitation here is the use of non-biodegradable polymer, which raises concerns about long-term toxicity of this approach. Overall, antibodies are an excellent targeting ligand for delivery and imaging applications because of high affinity and specificity to the target.[26, 27] They were found highly efficient for targeting different NPs in drug delivery applications.[14, 28, 29] To achieve effective functionalization of NEs with antibodies and preserve GRAS characteristics and biomimetic nature, a "green" approach should be developed, which would involve exclusively natural/biocompatible components.

In the present work, we engineered antibody-targeted NEs to enhance tumor cell selectivity and improve their potential for clinical translation. To this end, we used biotinylation strategy which is commonly used in molecular biology and bio-nanotechnology for its rapid, efficient and robust bio-conjugation.[30, 31] We synthesized a reactive derivative of cholesterol and a Biotin-PEG_{3000}-Lysine linker, which can react within one-pot formulation to form an amphiphilic carbamate Biotin-PEG_{3000}-Cholesterol. Cholesterol moiety was expected to ensure its firm anchorage in NEs, whereas the long hydrophilic PEG_{3000} chain was expected to expose biotin moiety at the surface of NEs for further antibody grafting using a biotin-neutravidin coupling. Successful NE biotinylation was confirmed by fluorescence staining on a glass surface. These biotinylated-NEs were further functionalized with biotinylated antibodies using neutravidin as a bridge. We selected trastuzumab as the targeting antibody due to its routine use as part of the therapeutic arsenal as a single agent or in ADCs formulations to treat HER2-amplified patients.[32] Trastuzumab-functionalized NEs effectively recognized their cognate receptors and selectively accumulated into HER2-expressing cancer cell lines (in comparison to HER2-low ones). Overall, this study presents a highly biocompatible, modular and stable way to functionalize NEs surfaces with antibodies. These antibody-targeted NEs demonstrated enhanced and antigen-

selective tumor cell targeting *in vitro*, suggesting that NEs are promising vehicles for targeted delivery and imaging.

Results and discussion

Design and synthesis of GRAS-compatible building blocks for NEs surface functionalization

We aimed at developing NEs decorated with an antibody to enable targeting tumor cell membrane expressing the cognate antigen. Given the liquid nature of the oil core, we considered that efficient anchoring of large biomolecules at the surface, can only be achieved by a linking with a highly hydrophobic anchor counterpart. To this end, we considered developing a plug-and-play appracoh, where a functional unit is “implanted” into the nano-droplet core by two cholesterol units though a long spacer. Cholesterol is a highly hydrophobic neutral lipid, which makes it attractive as a non-toxic anchor for NEs. We synthesized a reactive cholesterol derivative, (4-nitrophenyl) carbonate of cholesterol (NPC-Chol), which would allow attachment of the anchor group directly during preparation of NEs. We also designed and synthesized a PEG linker bearing lysine moiety on one end and biotin on the other. The two amino groups of lysine are expected to react with NPC-Chol thus anchoring the PEG linker in the oil core of the nano-droplets after their formulation. Due to sufficiently long PEG3000 linker, we expect that the biotin moiety would be exposed well outside of NEs surface. Then, biotinylated antibody is coupled to biotinylated-NEs though a neutravidin (avidin analogue) bridge. The selected antibody was trastuzumab, which is a commonly used therapeutic antibodies for targeting HER2 receptor

To address the current limitations of anti-HER2 ADCs and NPs, we aimed to develop trastuzumab-functionalized NEs capable of targeting their cognate antigen expressed on the surface of tumor cells. However, given the liquid nature of the NE oil core, efficient surface anchoring of large biomolecules such as the humanized IgG1 antibody trastuzumab requires conjugation to a highly hydrophobic anchor. To this end, we adopted a plug-and-play approach using GRAS compounds by designing reactive cholesterol derivative that can firmly anchor a functional linker within one-pot protocol. Cholesterol’s strong hydrophobic character and biocompatibility make it an attractive anchor for functionalization with an antibody at the NE surface. To this end, cholesterol was converted into reactive (4-nitrophenyl) carbonate of cholesterol (NPC-Chol) in one step by reaction with p-nitrophenyl chloroformate under basic conditions.[33] Biotin-

PEG_{3000}-Lysine linker, which was synthesized in several steps (*see Supporting Information*) (**Figure 1**). Biotin was reacted with Mono-Boc-protected PEG_{3000} diamine to give compound **1**, which, after Boc removal in TFA, yielded compound **2**. Compound **2** was further reacted with Di-Boc-protected lysine to produce conjugate **3**. Then, the Boc groups of conjugate **3** were deprotected in TFA, yielding the final Biotin-PEG_{3000}-Lysine linker (compound **4**). The identity of each synthesis intermediate as well as the final compound was confirmed by ^{1}H-NMR and mass spectrometry (**Figure S1-5**). This linker is composed of three GRAS blocks. The lysine moiety, among the most common amino acids, are expected to react with NPC-Chol through their amino groups, thus anchoring the linker in the NE oil core after formulation. The spacer made of PEG, a widely used component in drug delivery, would allow exposure of derivatizable moieties away from the NE surface. The biotin, a water-soluble vitamin, is a convenient handle for further functionalization. Altogether, we designed and synthesized a GRAS, derivatizable anchor-linker system for subsequent conjugation with targeting ligands such as trastuzumab.

Formulation of *in situ* biotinylated lipid nanoemulsion

In our approach, the reactive anchor NPC-Chol was first coupled with the linker Biotin-PEG_{3000}-Lysine in THF in the presence of a base trimethylamine and Vitamin E acetate, which later on will serve as the oil core. After evaporation of the solvent and the base, the NMR spectra of the reaction mixture showed new peaks, corresponding to the liberated p-nitrophenol (**Figure 2B**). The integral of the new peaks suggested 18.5% conversion of the used NPC-Chol. Considering that complete reaction of one amino group of the linker with NPC-Chol would result in 23 % conversion of the latter, the observed 18.5% conversion suggests that at these conditions we grafted one cholesterol anchor per linker. Then, surfactant and water were added to the oil mixture containing the *in situ* generated Biotin-PEG_{3000}-Chol, under intense stirring in order to obtain NEs by spontaneous nanoemulsification. In order to make independent verification that the NPC-Chol reacted with Biotin-PEG_{3000}-Lysine, absorption spectrum of the obtained NEs mixture was recorded in order to identify the presence of released p-nitrophenol. Importantly, the reaction mixture showed the characteristic peak around 400 nm,[34] whereas the control conditions without the linker showed negligible contribution of p-nitrophenol absorption. Thus, we confirmed that the reaction took place, which led to release of p-nitrophenol.

Then, to quench the non-reacted NPC-Chol, we incubated the NEs mixture with an excess of n-butylamine, which lead to further increase in the absorbance of p-nitrophenol. The reaction was incubated until no significant increase in absorbance was observed (**Figure 2C**). Assuming that after incubation with n-butylamine, 100% of NPC-Chol reacted with the amines liberating all p-nitrophenol, we could estimate that 17.1 % of NPC-Chol reacted Liotin-PEG_{3000}-Lysine. This estimation is in line with the NMR data above, confirming formation of the linker-cholesterol conjugate. Then, the mixture was dialyzed to remove non-reacted linker, non-reacted butylamine and liberated p-nitrophenol. Dynamic light scattering (DLS) of the dialyzed product suggested the presence of nano-droplets of 64 ± 4 nm diameter with a polydispersity index of 0.2 ± 0.03 (Table S1). Altogether, we developed a one-pot green chemistry approach for NEs biotinylation using GRAS components, thereby reducing the risk of ligand detachment from the NEs surface.

Validation of surface biotin activity via neutravidin binding assay

To assess the presence of active biotin units on the surface of NEs, we formulated biotinylated-NEs loaded with a hydrophobic cyanine 5.5 derivative and its bulky counterion tetraphenylborate (Cy5.5-LP/TPB) at 2 wt% in the oil phase (**Figure 3A**). This counterion has been shown to be essential to ensure efficient encapsulation of the dye within NEs with minimal dye leakage and aggregation-caused quenching.[8, 11] According to DLS, the obtained Cy5.5-loaded biotinylated NEs were 53 ± 2 nm in diameter, with a polydispersity index of 0.16 ± 0.01 (**Table S1**). The absorption and emission spectra of these NEs showed single bands with maxima at 700 and 727 nm, were close to those for Cy5.5-LP in labrafac oil (**Figure 3B**). Using this Cy5.5-labeling, we characterized the biotinylated-NEs immobilized on glass surface at the single-particle level by fluorescence microscopy (**Figure 3B**). As a conjugation biomolecule for biotin, we used neutravidin, which is an avidin analogue presenting higher selectivity and lower non-specific binding.[35] Hence, neutravidin is frequently used for immobilization of biotinylated molecules and nanoparticles on the surface.[24, 31, 36, 37] To test interaction of neutravidin with biotin on NEs surface, we coated a glass surface with BSA-biotin, followed by a layer of neutravidin based on established protocols (**Figure 3A**).[36, 37] With this surface at hand, we compared targeting specificity of biotinylated-NEs with control NEs without grafted biotin. Biotinylated-NEs were clearly visible on the glass surface by fluorescence microscopy in form of dots (**Figure 3D-E**).

The density of dots and the overall intensity on the images increased with higher NEs concentration (**Figure 3D-E**). In case of control non-modified NEs, fluorescent dots were absent already for the highest used NEs concentration (**Figure 3C**). These results clearly show that the grafted biotin remains accessible and functionally active, as evidenced by its specific interaction with neutravidin, while non-specific interactions with the NEs with the surface are negligible.

Functionalization NEs with trastuzumab

Prompted by these results, we next generated NEs decorated with therapeutic antibodies to enable selective targeting of tumor cells expressing cognate antigens. For this purpose, trastuzumab – a clinically approved anti-HER2 antibody[34] – was conjugated to biotin via its amino groups at physiological pH using a biotin-NHS ester,[34] and unreacted reagent was removed by ultrafiltration. Efficient biotinylation was confirmed by strong membrane staining in a cell binding assay on HER2-amplified HCC1954, using Streptavidin-AF647 (SA-AF647) to detect accessible biotin sites (**Figure 4A**). The specificity of the biotin–streptavidin interaction was validated by pre-blocking with neutravidin, which abolished membrane-localized fluorescence (**Figure 4B**). Next, biotinylated trastuzumab was coupled to biotinylated NEs via a neutravidin bridge. This interaction is rapid, highly specific, and extremely stable ($K_d \approx 10^{-15}$ mol.L^{-1}).[30, 31] Unbound antibodies were then removed by size exclusion chromatography using Sephacryl S300 HR, which is specially adapted for separating relatively large macromolecules or globular proteins in the range 10 to 150 KDa. UV-visible absorbance spectra of the eluted fractions showed that trastuzumab-decorated NEs were recovered in early fractions (f3–f5), with coincident absorbance at 280 nm (protein) and 700 nm (Cy5.5-LP) (**Figure S6**). In contrast, free trastuzumab eluted in later fractions (f6–f8), showing absorbance only at 280 nm. This result suggests that the first fraction presenting both 280 and 700 nm absorbance (f3-f5) correspond to both NEs and conjugated trastuzumab, while the following fractions correspond to proteins (free antibodies and possibly neutravidin). The first fractions were combined and studied again by the same chromatography method. This time only a one band corresponding to the first fractions was observed, presenting absorbance in both 280 and 700 nm (**Figure S7**). Thus, size exclusion method allows separation of the of NEs from non-conjugated protein molecules. Importantly, antibody functionalization had negligible impact on NE hydrodynamic diameter (56 ± 2 nm) with preserved good

polydispersity of 0.12 ± 0.03 (**Table S1**). To confirm that trastuzumab conjugation did not impair antigen recognition, we determined the apparent affinity constant (K_d) of trastuzumab-decorated NEs by flow cytometry, using biotinylated NEs without antibody as a negative control. Fitting the binding data to a one-site Langmuir isotherm yielded an apparent K_d of 3.5 ± 1.8 nmol·L^{-1} (**Figure 4C**), consistent with previously reported values for trastuzumab in cell-based assays.[38, 39]

Trastuzumab-functionalized NEs target HER2-amplified tumor cells *in vitro* with high selectively

Building on these results, we next evaluated whether trastuzumab-functionalized NEs can target specifically tumor cells with high expression of HER2 receptor (HCC-1954) (**Figure 5A-B**) using confocal fluorescence imaging, of NEs loaded with Cy5.5-LP (2 wt% vs oil). Trastuzumab-functionalized NEs showed markedly increased internalization in HER2-amplified HCC-1954 cells compared to passive uptake by biotinylated NEs alone (**Figure 5C**). To confirm HER2 dependency, we assessed internalization in $HER2^{low}$ MDA-MB-231 cells, where no detectable differences were observed between targeted and untargeted NEs (**Figure 5C**). To further validate the targeting selectivity, we extended the analysis to an additional HER2-positive cell line, SKBR3, which also showed preferential uptake of trastuzumab-targeted NEs over control formulations (**Figure S8**). To evaluate the biocompatibility of the formulation approach, we assessed whether NEs uptake induced cytotoxic effects. Treating both HER2-amplified and $HER2^{low}$ cell lines with either trastuzumab-targeted or untargeted NEs had no effect on cell viability (**Figure S9**). Altogether, these results demonstrate the enhanced targeting selectivity of trastuzumab-functionalized NEs toward HER2-expressing tumor cells. This strategy provides a versatile and biocompatible platform for antibody-based surface functionalization of NEs to improve tumor-targeting efficiency.

Conclusions

Functionalization of lipid NEs with biomolecules for selective targeting remains a challenge. Here, we developed an original plug-and-play strategy to graft an antibody (trastuzumab) at the surface of NEs, using GRAS components. For this purpose, we synthesized a reactive derivative of cholesterol, cholesteryl (4-nitrophenol) carbonate (NPC-Chol), which can be readily encapsulated in the oil core of NEs and react with

amines. We also designed a Biotin-PEG_{3000}-Lysine linker with two amino groups of lysine at one end for reaction with NPC-Chol to form the amphiphilic carbamate Biotin-PEG_{3000}-Chol. Cholesterol moiety was expected to ensure its firm anchorage in NEs. On the other end of the linker, the long hydrophilic PEG_{3000} chain is expected to expose biotin moiety at the surface of NEs for further antibody grafting using a biotin-neutravidin coupling. The reaction between the Biotin-PEG_{3000}-Lysine linker and NPC-Chol was confirmed by ^{1}H-NMR and absorption spectroscopy. Using one-pot approach, the obtained conjugate with oil and surfactant were formulated into 50-nm NEs, which were expected to bear biotin ligand. The successful biotinylation was confirmed by fluorescence microscopy: biotinylated-NEs loaded with a near-infrared dye were successfully targeted to neutravidin-coated glass surfaces in contrast to non-modified NEs. The obtained fluorescent biotinylated-NEs were grafted with biotinylated anti-HER2 (trastuzumab) monoclonal antibodies via a neutravidin bridge. The described approach presents several unique features compared to previously proposed methods. Compared to the previously proposed method based on amphiphilic polymers[24, 25] the present approach uses GRAS and biodegradable components, which addresses the issues of safely. On the other hand, compared to methods based on fatty acids [22] or PEGylated lipids,[21] the use of cholesterol increases the strength of anchoring with lower chance of exchange in biological medium due to higher hydrophobicity of the latter.

The targeting selectivity of the trastuzumab-decorated NEs was evaluated *in vitro* by confocal microscopy on relevant breast cancer models HCC-1954 and SKBR3 (HER2-amplified) and MDA-MB-231 ($HER2^{low}$). Targeted NEs presented higher cellular internalization compared to control NEs in corresponding positive cell lines. In contrast, in control cell lines with low HER2 expression, no internalization was observed for both targeted and non-targeted formulations. These results show receptor dependent targeting of our NEs functionalized with antibodies.

Altogether, our study showed that combining the high encapsulation properties of the NEs with the trastuzumab surface decoration allowed receptor selective targeting of HER2-amplified breast cancer cells. These easily tunable functionalized NEs systems provide a platform for conjugation of different monoclonal antibodies and encapsulation of a large variety of contrast agents and drugs and thus can be used for imaging, therapeutic and targeted drug delivery applications. However, further improvements are still required. Indeed, the streptavidin analogue neutravidin used to bridge

antibodies to NEs can be immunogenic[40] and could eventually be replaced by direct biorthogonal conjugation methods such as click chemistry.[25, 41, 42] In this case, the same green chemistry could be applied, where the biotin unit is replaced with corresponding reactive group. In addition, the NEs used in this study are lipidic nanoparticles and thus should, according to our meta-analysis results, be targeted with fragments rather than full antibodies for significantly higher accumulation.[14] These improvements will be further complemented with *in vivo* experiments of mice bearing tumor models in order to evaluate the full potential of functionalized NEs in biomedical applications.

Acknowledgements

We thank all members of the JGG and ASK labs for helpful discussions. ASK team and VJBT were supported by ANR SenEmul and by the Interdisciplinary Thematic Institute SysChem, via the IdEx Unistra (ANR-10-IDEX-0002), the CSC Graduate School (CSC-IGS ANR-17-EURE-
0016) within the French Investments for the Future Program. FL was supported by China Scholarship council (CSC). Work and people in JGG lab are mostly supported by the INCa (Institut National Du Cancer, French National Cancer Institute), La Ligue contre le Cancer, the Association pour la Recherche contre le Cancer (ARC), the Fondation pour la Recherche Médicale (FRM), the National Plan Cancer initiative, the Region Grand Est, INSERM and the University of Strasbourg as well as from local donators (Rohan Athlétisme Saverne, Trailers De La Rose, Club Féminin Lampertheim). VM was funded by a Ph.D. fellowship from the French Ministry of Science (MESRI) and by the Foundation ARC. We thank Pascal Kessler and Ignacio Busnelli from PICSTRA (CRBS). We thank Alexandre Detappe for providing Trastuzumab.

References

1. Rosenblum, D.; Joshi, N.; Tao, W.; Karp, J. M.; Peer, D., Progress and challenges towards targeted delivery of cancer therapeutics. *Nat Commun* **2018,** *9* (1), 1410.
2. Mitchell, M. J.; Billingsley, M. M.; Haley, R. M.; Wechsler, M. E.; Peppas, N. A.; Langer, R., Engineering precision nanoparticles for drug delivery. *Nat Rev Drug Discov* **2021,** *20* (2), 101-124.
3. Tayeb, H. H.; Felimban, R.; Almaghrabi, S.; Hasaballah, N., Nanoemulsions: Formulation, characterization, biological fate, and potential role against COVID-19 and other viral outbreaks. *Colloid Interface Sci Commun* **2021,** *45*, 100533.
4. Anton, N.; Vandamme, T. F., Nano-emulsions and micro-emulsions: clarifications of the critical differences. *Pharm Res* **2011,** *28* (5), 978-85.
5. Singh, Y.; Meher, J. G.; Raval, K.; Khan, F. A.; Chaurasia, M.; Jain, N. K.; Chourasia, M. K., Nanoemulsion: Concepts, development and applications in drug delivery. *J Control Release* **2017,** *252*, 28-49.
6. Klymchenko, A. S.; Liu, F.; Collot, M.; Anton, N., Dye-Loaded Nanoemulsions: Biomimetic Fluorescent Nanocarriers for Bioimaging and Nanomedicine. *Advanced Healthcare Materials* **2021,** *10* (1), 2001289-2001289.
7. Liu, F.; Niko, Y.; Bouchaala, R.; Mercier, L.; Lefebvre, O.; Andreiuk, B.; Vandamme, T.; Goetz, J. G.; Anton, N.; Klymchenko, A., Drug-Sponge Lipid Nanocarrier for in Situ Cargo Loading and Release Using Dynamic Covalent Chemistry. *Angewandte Chemie International Edition* **2021**, anie.202014259-anie.202014259.
8. Bouchaala, R.; Mercier, L.; Andreiuk, B.; Mély, Y.; Vandamme, T.; Anton, N.; Goetz, J. G.; Klymchenko, A. S., Integrity of lipid nanocarriers in bloodstream and tumor quantified by near-infrared ratiometric FRET imaging in living mice. *Journal of Controlled Release* **2016,** *236*, 57-67.
9. Khalin, I.; Adarsh, N.; Schifferer, M.; Wehn, A.; Groschup, B.; Misgeld, T.; Klymchenko, A.; Plesnila, N., Size-Selective Transfer of Lipid Nanoparticle-Based Drug Carriers Across the Blood Brain Barrier Via Vascular Occlusions Following Traumatic Brain Injury. *Small* **2022,** *18* (18), 2200302.
10. Alleva, M.; Baranyai, Z.; Esteban-Pérez, N.; Martínez-Vicente, P.; Martín-Rapún, R.; Moros, M.; Martínez de la Fuente, J., Förster Resonance Energy Transfer (FRET) Demonstrates In Vitro Chitosan-Coated Nanocapsules Suitability for Intranasal Brain Delivery. *ACS Applied Materials & Interfaces* **2025,** *17* (18), 26348-26360.
11. Kilin, V. N.; Anton, H.; Anton, N.; Steed, E.; Vermot, J.; Vandamme, T. F.; Mely, Y.; Klymchenko, A. S., Counterion-enhanced cyanine dye loading into lipid nano-droplets for single-particle tracking in zebrafish. *Biomaterials* **2014,** *35* (18), 4950-7.
12. Matsumura, Y.; Maeda, H., A new concept for macromolecular therapeutics in cancer chemotherapy: mechanism of tumoritropic accumulation of proteins and the antitumor agent smancs. *Cancer Res* **1986,** *46* (12 Pt 1), 6387-92.

13. Wilhelm, S.; Tavares, A. J.; Dai, Q.; Ohta, S.; Audet, J.; Dvorak, H. F.; Chan, W. C. W., Analysis of nanoparticle delivery to tumours. *Nature Reviews Materials* **2016,** *1* (5), 16014.
14. Mittelheisser, V.; Coliat, P.; Moeglin, E.; Goepp, L.; Goetz, J. G.; Charbonnière, L. J.; Pivot, X.; Detappe, A., Optimal Physicochemical Properties of Antibody–Nanoparticle Conjugates for Improved Tumor Targeting. *Advanced Materials* **2022,** *34* (24), 2110305.
15. Rosenblum, D.; Joshi, N.; Tao, W.; Karp, J. M.; Peer, D., Progress and challenges towards targeted delivery of cancer therapeutics. *Nature Communications* **2018,** *9* (1), 1410.
16. Drago, J. Z.; Modi, S.; Chandarlapaty, S., Unlocking the potential of antibody–drug conjugates for cancer therapy. *Nature Reviews Clinical Oncology* **2021,** *18* (6), 327-344.
17. Hamblett, K. J.; Senter, P. D.; Chace, D. F.; Sun, M. M.; Lenox, J.; Cerveny, C. G.; Kissler, K. M.; Bernhardt, S. X.; Kopcha, A. K.; Zabinski, R. F.; Meyer, D. L.; Francisco, J. A., Effects of drug loading on the antitumor activity of a monoclonal antibody drug conjugate. *Clin Cancer Res* **2004,** *10* (20), 7063-70.
18. Johnston, M. C.; Scott, C. J., Antibody conjugated nanoparticles as a novel form of antibody drug conjugate chemotherapy. *Drug Discovery Today: Technologies* **2018,** *30*, 63-69.
19. Howes, P. D.; Chandrawati, R.; Stevens, M. M., Bionanotechnology. Colloidal nanoparticles as advanced biological sensors. *Science* **2014,** *346* (6205), 1247390.
20. Ashoka, A. H.; Aparin, I. O.; Reisch, A.; Klymchenko, A. S., Brightness of fluorescent organic nanomaterials. *Chemical Society Reviews* **2023,** *52* (14), 4525-4548.
21. Goutayer, M.; Dufort, S.; Josserand, V.; Royère, A.; Heinrich, E.; Vinet, F.; Bibette, J.; Coll, J. L.; Texier, I., Tumor targeting of functionalized lipid nanoparticles: assessment by in vivo fluorescence imaging. *Eur J Pharm Biopharm* **2010,** *75* (2), 137-47.
22. Attia, M. F.; Swasy, M. I.; Akasov, R.; Alexis, F.; Whitehead, D. C., Strategies for High Grafting Efficiency of Functional Ligands to Lipid Nanoemulsions for RGD-Mediated Targeting of Tumor Cells In Vitro. *ACS Applied Bio Materials* **2020,** *3* (8), 5067-5079.
23. Sobot, D.; Mura, S.; Yesylevskyy, S. O.; Dalbin, L.; Cayre, F.; Bort, G.; Mougin, J.; Desmaële, D.; Lepetre-Mouelhi, S.; Pieters, G.; Andreiuk, B.; Klymchenko, A. S.; Paul, J.-L.; Ramseyer, C.; Couvreur, P., Conjugation of squalene to gemcitabine as unique approach exploiting endogenous lipoproteins for drug delivery. *Nature Communications* **2017,** *8* (1), 15678.
24. Bou, S.; Wang, X.; Anton, N.; Bouchaala, R.; Klymchenko, A. S.; Collot, M., Lipid-core/polymer-shell hybrid nanoparticles: synthesis and characterization by fluorescence labeling and electrophoresis. *Soft Matter* **2020,** *16* (17), 4173-4181.
25. Belcastro, E.; Rehman, A. U.; Remila, L.; Park, S.-H.; Gong, D. S.; Anton, N.; Auger, C.; Lefebvre, O.; Goetz, J. G.; Collot, M.; Klymchenko, A. S.;

Vandamme, T. F.; Schini-Kerth, V. B., Fluorescent nanocarriers targeting VCAM-1 for early detection of senescent endothelial cells. *Nanomedicine: Nanotechnology, Biology and Medicine* **2021**, 102379-102379.
26. Atreya, R.; Neumann, H.; Neufert, C.; Waldner, M. J.; Billmeier, U.; Zopf, Y.; Willma, M.; App, C.; Münster, T.; Kessler, H.; Maas, S.; Gebhardt, B.; Heimke-Brinck, R.; Reuter, E.; Dörje, F.; Rau, T. T.; Uter, W.; Wang, T. D.; Kiesslich, R.; Vieth, M.; Hannappel, E.; Neurath, M. F., In vivo imaging using fluorescent antibodies to tumor necrosis factor predicts therapeutic response in Crohn's disease. *Nat Med* **2014,** *20* (3), 313-8.
27. Schnell, U.; Dijk, F.; Sjollema, K. A.; Giepmans, B. N., Immunolabeling artifacts and the need for live-cell imaging. *Nat Methods* **2012,** *9* (2), 152-8.
28. Peer, D.; Karp, J. M.; Hong, S.; FaroKhzad, O. C.; Margalit, R.; Langer, R., Nanocarriers as an emerging platform for cancer therapy. *Nature Nanotechnology* **2007,** *2* (12), 751-760.
29. Colombo, M.; Fiandra, L.; Alessio, G.; Mazzucchelli, S.; Nebuloni, M.; De Palma, C.; Kantner, K.; Pelaz, B.; Rotem, R.; Corsi, F.; Parak, W. J.; Prosperi, D., Tumour homing and therapeutic effect of colloidal nanoparticles depend on the number of attached antibodies. *Nature Communications* **2016,** *7* (1), 13818.
30. Nau, F.; Guérin-Dubiard, C.; Croguennec, T., Avidin. *Bioactive Egg Compounds* **2007**, 75-80.
31. Wayment, J. R.; Harris, J. M., Biotin-avidin binding kinetics measured by single-molecule imaging. *Analytical Chemistry* **2009,** *81* (1), 336-342.
32. Swain, S. M.; Shastry, M.; Hamilton, E., Targeting HER2-positive breast cancer: advances and future directions. *Nat Rev Drug Discov* **2023,** *22* (2), 101-126.
33. Vangala, M.; Shinde, G. P., p-Nitrophenyl carbonate promoted ring-opening reactions of DBU and DBN affording lactam carbamates. *BEILSTEIN JOURNAL OF ORGANIC CHEMISTRY* **2016,** *12*, 2086-2092.
34. Bowers, G. N., Jr; McComb, R. B.; Christensen, R. G.; Schaffer, R., High-purity 4-nitrophenol: purification, characterization, and specifications for use as a spectrophotometric reference material. *Clinical Chemistry* **1980,** *26* (6), 724-729.
35. Jain, A.; Barve, A.; Zhao, Z.; Jin, W.; Cheng, K., Comparison of Avidin, Neutravidin, and Streptavidin as Nanocarriers for Efficient siRNA Delivery. *Molecular Pharmaceutics* **2017,** *14* (5), 1517-1527.
36. Melnychuk, N.; Klymchenko, A. S., DNA-Functionalized Dye-Loaded Polymeric Nanoparticles: Ultrabright FRET Platform for Amplified Detection of Nucleic Acids. *Journal of the American Chemical Society* **2018,** *140* (34), 10856-10865.
37. Yudhistira, T.; Da Silva, E. C.; Combes, A.; Lehmann, M.; Reisch, A.; Klymchenko, A. S., Biotinylated Fluorescent Polymeric Nanoparticles for Enhanced Immunostaining. *Small Methods* **2023**, e2201452.
38. Coussens, L.; Yang-Feng, T. L.; Liao, Y.-C.; Chen, E.; Gray, A.; McGrath, J.; Seeburg, P. H.; Libermann, T. A.; Schlessinger, J.; Francke, U.; Levinson, A.; Ullrich, A., Tyrosine Kinase Receptor with Extensive Homology to EGF Receptor

Shares Chromosomal Location with neu Oncogene. *Science* **1985,** *230* (4730), 1132-1139.
39. Slamon, D. J.; Godolphin, W.; Jones, L. A.; Holt, J. A.; Wong, S. G.; Keith, D. E.; Levin, W. J.; Stuart, S. G.; Udove, J.; Ullrich, A.; et al., Studies of the HER-2/neu proto-oncogene in human breast and ovarian cancer. *Science* **1989,** *244* (4905), 707-12.
40. Yumura, K.; Ui, M.; Doi, H.; Hamakubo, T.; Kodama, T.; Tsumoto, K.; Sugiyama, A., Mutations for decreasing the immunogenicity and maintaining the function of core streptavidin. *Protein Sci* **2013,** *22* (2), 213-21.
41. Rehman, A. U.; Anton, N.; Bou, S.; Schild, J.; Messaddeq, N.; Vandamme, T.; Akram, S.; Klymchenko, A.; Collot, M., Tunable functionalization of nano-emulsions using amphiphilic polymers. *Soft Matter* **2021,** (December).
42. Prévot, G.; Duonor-Cérutti, M.; Larivière, M.; Laroche-Traineau, J.; Jacobin-Valat, M. J.; Barthélémy, P.; Clofent-Sanchez, G.; Crauste-Manciet, S., Data on atherosclerosis specific antibody conjugation to nanoemulsions. *Data in Brief* **2017,** *15*, 824-827.

Figure legends

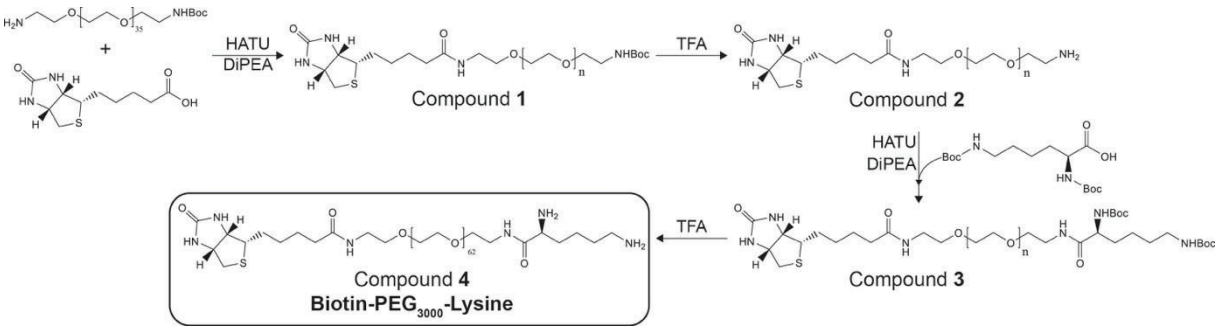

Figure 1. Synthesis of the Biotin-PEG$_{3000}$-Lysine linker.

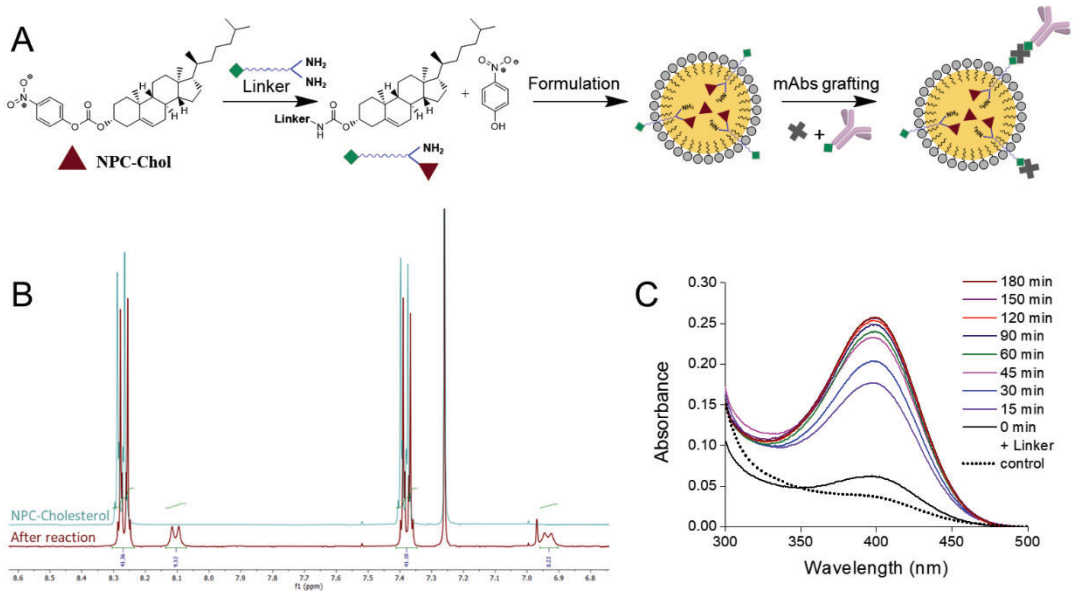

Figure 2. *In situ* biotinylation of lipid nanoemulsions. (**A**) *In situ* reaction between the Biotin-PEG$_{3000}$-Lysine linker and the NPC-Chol generating the Biotin-PEG$_{3000}$-Chol conjugate and releasing p-nitrophenol. (**B**) Superimposed ^{1}H-NMR spectra of the NPC-Chol aromatic region, before and after the reaction with the Biotin-PEG$_{3000}$-Lysine linker. (**C**) Absorption spectra of the released p-nitrophenol. The control experiment was done without Biotin-PEG$_{3000}$-Lysine.

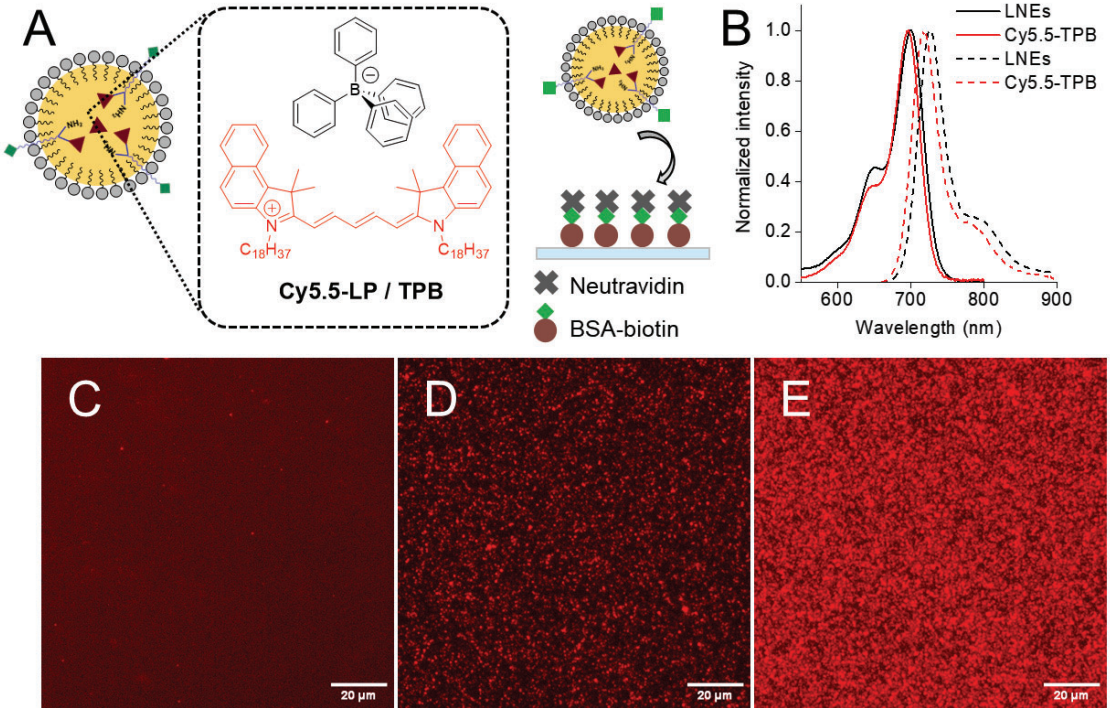

Figure 3. Validation of biotinylated nanoemulsions. (**A**) Schematic representation of Cy5.5-LP/TPB loaded NEs and their immobilization on a glass surface coated with BSA-biotin and neutravidin. (**B**) Absorption (solid line) and emission (dashed line) spectra of NEs loaded with Cy5.5-LP/TPB in water, and Cy5.5-LP/TPB in labrafac. (**C-E**) Fluorescence microscopy of neutravidin-coated glass surface incubated with bare NEs (30,000-fold dilution) (**C**) or biotin-decorated NEs (100,000- (**D**) or 30,000-fold (**E**) dilution). Scale bar = 20µm.

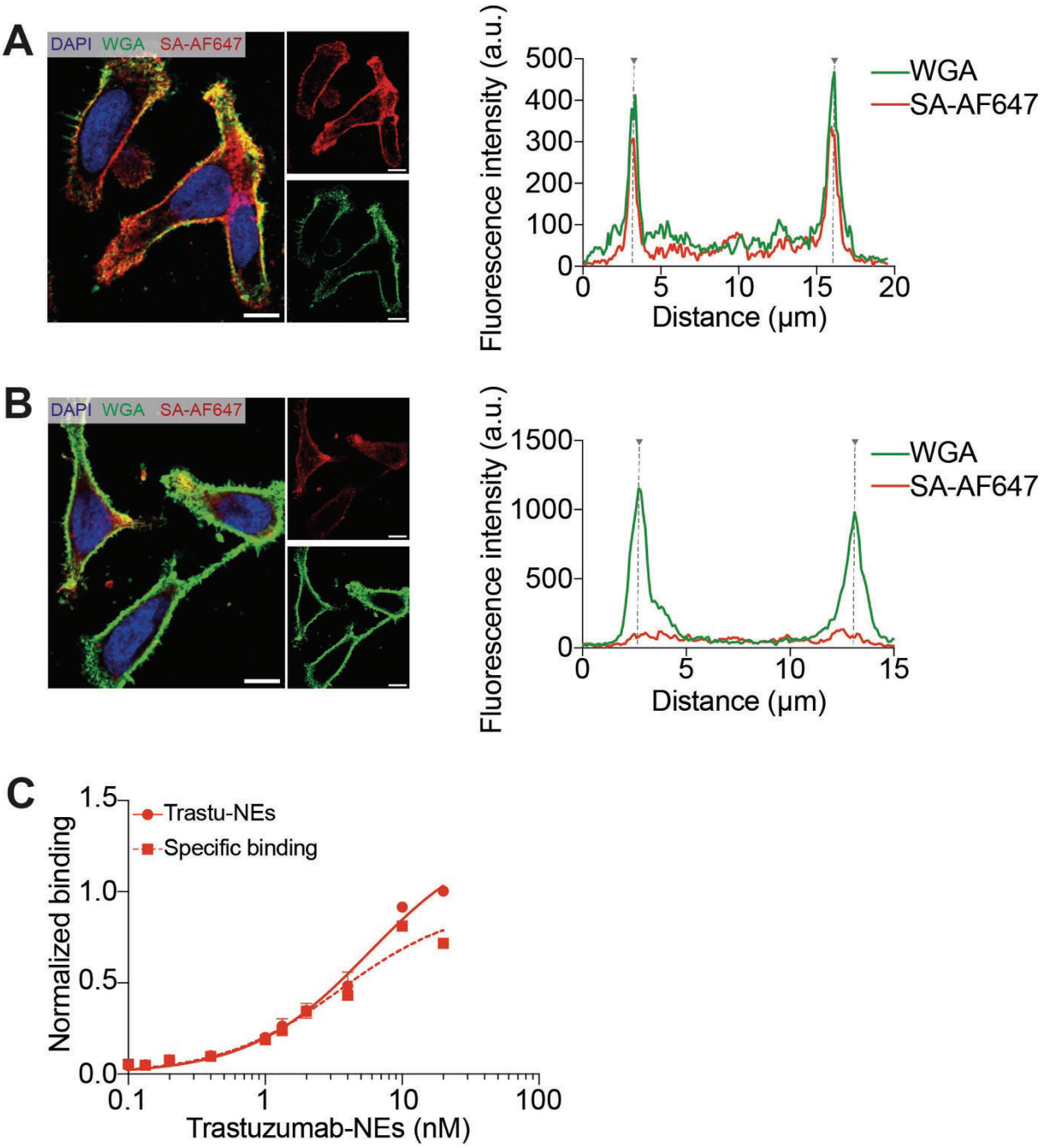

Figure 4. **Validation of biotinylated trastuzumab on HER2-amplified HCC1954 cells.** (**A-B**) Quantification of the trastuzumab-biotin membrane staining by following Streptavidin-AF647 (SA-AF647) fluorescence without (**A**) or with (**B**) pre-blocking with neutravidin. Cell membranes were labeled with Wheat Germ Agglutinin-AF488 (green). Scale bar is 10μm. Cell edges are marked by dot lines on the fluorescence profil plots. (**C**) Flow cytometry study determining the apparent binding affinity of the trastuzumab-functionalized nanoemulsions on HER2-amplified HCC-1954 cells.

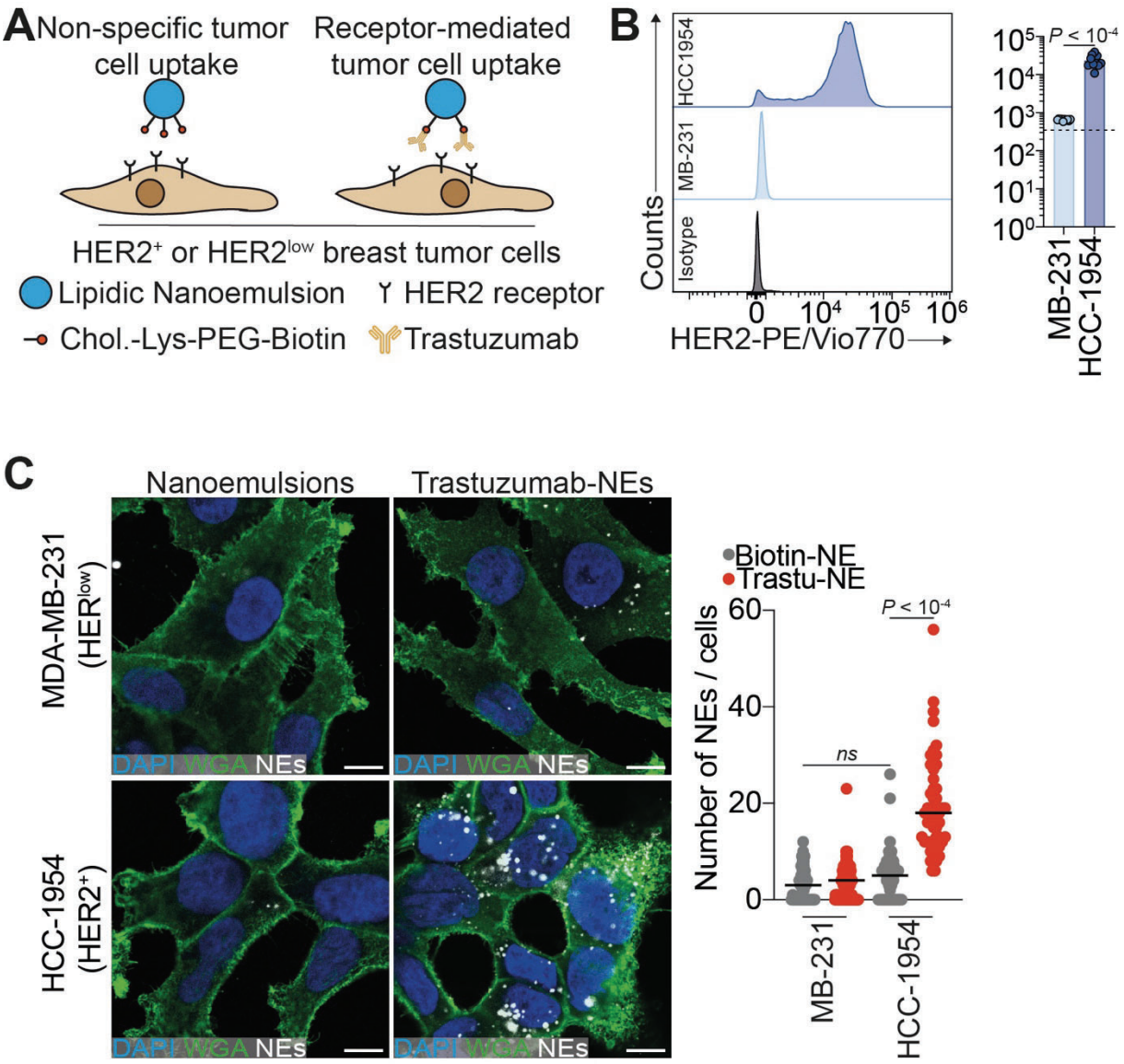

Figure 5. **Trastuzumab-functionalized nanoemulsions target breast cancer cells in an antigen-antibody manner.** (A) Biotinylated-NEs or Trastuzumab-targeted NEs interactions were assessed using HER2-amplified HCC-1954 cells or HER2^{low} MDA-MB-231 cells. (B) Flow cytometry analysis of HCC-1954 and MDA-MB-231 HER2 status. (C-D) Quantification of the nanoemulsion uptake in HER2^{low} (upper panel) and HER2-amplified (lower panel) cells. Cells incubated for 3h with 1.1 nM of Cy5.5-loaded (red) biotinylated NEs (right) or Trastuzumab-targeted NEs (left). Cell membranes were labeled with Wheat Germ Agglutinin-AF488 (green). Scale bar is 10 µm.

Supporting information

Functionalization of lipid nanoemulsions with humanized antibodies using plug-and-play cholesterol anchor for targeting cancer cells

Valeria Jose Boide-Trujillo[1,*], Vincent Mittelheisser[2,*], Fei Liu[1,3,*], Olivier Lefebvre[2], Bohdan Andreiuk[1], Nicolas Anton[3], Jacky G. Goetz[2,#], and Andrey S. Klymchenko[1,#]

[1]Laboratoire de Bioimagerie et Pathologies, CNRS UMR_7021, ITI SysChem-Chimie des Systèmes Complexes, Université de Strasbourg; Illkirch (France)

[2]Tumor Biomechanics Lab, INSERM UMR_S1109, Fédération de Médecine Translationnelle de Strasbourg, Université de Strasbourg, Equipe labélisée Ligue Nationale Contre le Cancer ; Strasbourg (France).

[3]Regenerative Nanomedicine (RNM), INSERM UMR_1260, Fédération de Médecine Translationnelle de Strasbourg, Université de Strasbourg; Strasbourg (France)

[*]**Equal contribution:**
VJBT, VM and FL have contributed equally to this work.

[#]**Correspondence and co-last authors:**
Andrey S. Klymchenko, andrey.klymchenko@unistra.fr
CNRS UMR_7021, Faculté de Pharmacie, Université de Strasbourg, Institut Thématique Interdisciplinaire SysChem, Illkirch F-67400, France.

Jacky G. Goetz, jacky.goetz@inserm.fr
INSERM UMR_S1109, Tumor Biomechanics Lab, Centre de Recherche en Biomédecine de Strasbourg (CRBS), Fédération de Médecine Translationnelle de Strasbourg (FMTS), 67000 Strasbourg, France. Web: www.goetzlab.fr

Materials and methods

Materials

Boc-NH-PEG-NH_2 (3 kDa) was purchased from Iris Biotech GmbH. Biotin (97%) and diBoc-lysine (98%) were acquired from abcr GmbH. 2-(7-Aza-1H-benzotriazole-1-yl)-1,1,3,3-tetramethyluronium hexafluorophosphate (HATU) was provided by Fluorochem. N,N-Diisoprozlethylamine (DiPEA) (>99%), Kolliphor® ELP, triethylamine, butylamine (99.5%), and BSA-biotin were supplied by Sigma-Aldrich. Trifluoro acetic acid (TFA) (99%), NHS-Biotin, and NeutrAvidin were obtained from ThermoFisher. Herceptin® (Trastuzumab) was purchased from the ICANS Pharmacy. Vitamin E acetate (>97.0%) was acquired from TCI. Dulbecco's Phosphate-buffer saline (DPBS) (without Ca^{2+} and Mg^{2+}) was provided by Dominique Dutscher. Buffer preparations and formulation of lipid nanoemulsions (NEs) were done with filter-sterilized Milli-Q water. Borate buffer (pH 8.4) was prepared with sodium tetraborate (25 mM), NaCl (25 mM), and EDTA (1 mM). Phosphate buffer (pH 8.5) was prepared with dipotassium hydrogen phosphate (40 mM) and NaCl (150 mM). Final pH values were adjusted with 1 M hydrochloric acid or 1 M sodium hydroxide.

Equipment

Size distributions of NEs were determined by dynamic light scattering using a Zetasizer Nano series DTS 1060 (Malvern Instruments). Absorption Spectra were recorded on a Cary 500-UV-vis-NIR spectrophotometer (Agilent). NMR spectra were recorded at 20 °C on a Bruker Avance III 400 MHz NMR spectrometer (Bruker). Conjugation experiments were carried out in DNA low-binding tubes 1.5 mL (Eppendorf) at atmospheric pressure at room temperature unless otherwise stated. Ultrafiltration was carried out in centrifugal filters Amicon® Ultra 0.5 mL (Merck Millipore) with a molecular weight cut-off (MWCO) of 50 kDa. Centrifugation was carried out on a MiniSpin plus (Eppendorf) operating at 10.000 rpm at room temperature. Size exclusion chromatography was performed on an ÄKTA start (Cytivia) operating at a flow speed of 0.5 mL/min. Sephacryl S-300 High-Resolution (GE Healthcare) resin was used to pack the column. Epifluorescence microscopy images were recorded on an ECLIPSE Ti (Nikon). Confocal microscopy was performed on an inverted Olympus Spinning-disk.

Synthesis

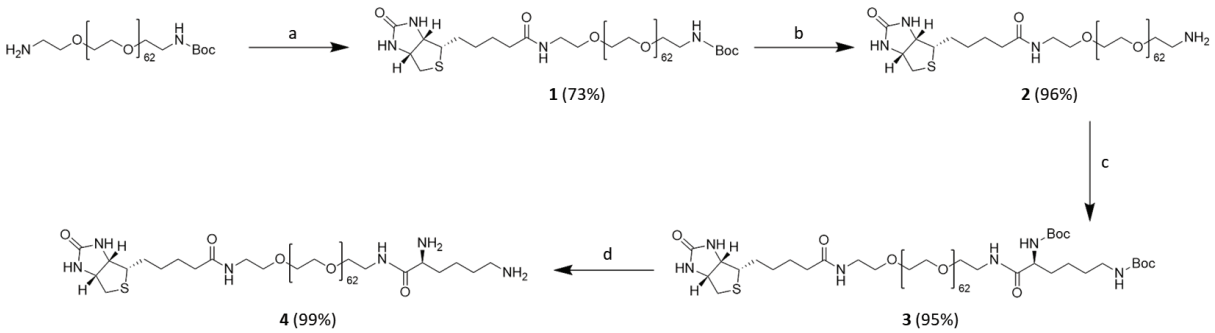

Scheme 1. Biotin-PEG-lysine synthesis (**4**): a) Biotin, HATU, DiPEA, DMF, 40 °C, overnight; b) TFA, DCM, rt, 3 hours; c) Boc-lysine(Boc)-OH, HATU, DiPEA, DMF, 40 °C, overnight; b) TFA, DCM, rt, 3 hours.

Compound 1 - Biotin (5 eq., 62.3 mg., 0.25 mmol) and HATU (5 eq., 100.0 mg, 0.25 mmol) were dissolved in 5 mL of dry DMF. DiPEA (18 eq., 145 µL, 0.85 mmol) was added and stirred for 15 min. A 5 mL solution of Boc-H-PEG-NH_2 (1 eq., 140.0 mg, 0.03 mmol) in dry DMF was added to the previous mixture, and the final mixture was stirred overnight at 40 °C. The crude was purified by size exclusion chromatography LH-20 (DCM:MeOH, 1:1) to afford compound **1** (107.0 mg, 0.03 mmol, 73 %) as a colorless wax. ^{1}H-NMR (400 MHz, CD_3OD) δ 4.50 (m, 1H), 4.31 (dd, J = 4.4, 7.8 Hz, 1H), 3.81 (t, J = 4.8 Hz, 2H), 3.70-3.58 (m, ~285H), 3.55 (m, 2H), 3.51 (t, J = 5.7 Hz, 1H), 3.46 (t, J = 4.7 Hz, 1H), 3.36 (m, 2H), 3.22 (p, J = 5.7 Hz, 3H), 2.93 (dd, J = 5.0, 12.7 Hz, 1H), 2.71 (d, J = 12.7 Hz, 1H), 2.23 (t, J = 7.4 Hz, 2H), 1.81-1.54 (bs, 4H), 1.48-1.41 (10H).

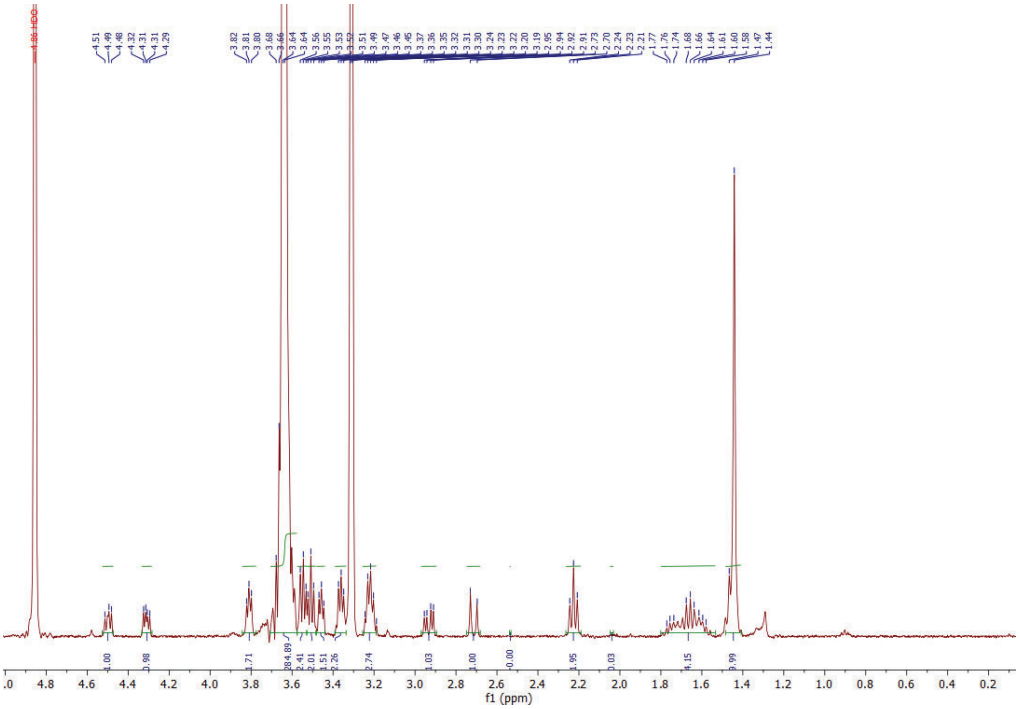

Figure S1. ^{1}H-NMR of compound **1** in CD_3OD.

Compound 2 - Compound **1** (1 eq., 107.0 mg, 0.03 mmol) was dissolved in dry DCM (2 mL). Trifluoroacetic acid (150 eq., 0.34 mL, 4.48 mmol) was added, followed by 3 hours of stirring at room temperature. DCM was removed under reduced pressure. Co-evaporation with methanol (1 mL) was done several times to remove the remaining trifluoroacetic acid, affording compound **2** (102.0 mg, 0.03 mmol, 96 %) as light-yellow wax. ^{1}H-NMR (400 MHz, CD_3OD) δ 4.50 (dd, J = 4.9, 7.9 Hz, 1H), 4.31 (dd, J = 4.5, 7.9 Hz, 1H), 3.74-3.35 (m, ~278H),3.83-3.75 (m, 4H), 3.54 (t, J = 5.5 Hz, 2H), 3.46 (m, 1H), 3.36 (m, 3H), 3.20 (m, 3H), 2.93 (dd, J = 5.0, 12.8 Hz, 1H), 2.71 (d, J = 12.7 Hz, 1H), 2.23 (t, J = 7.3 Hz, 2H), 1.77- 1.53 (bs, 4H), 1.46 (q, J = 7.5 Hz, 2H).

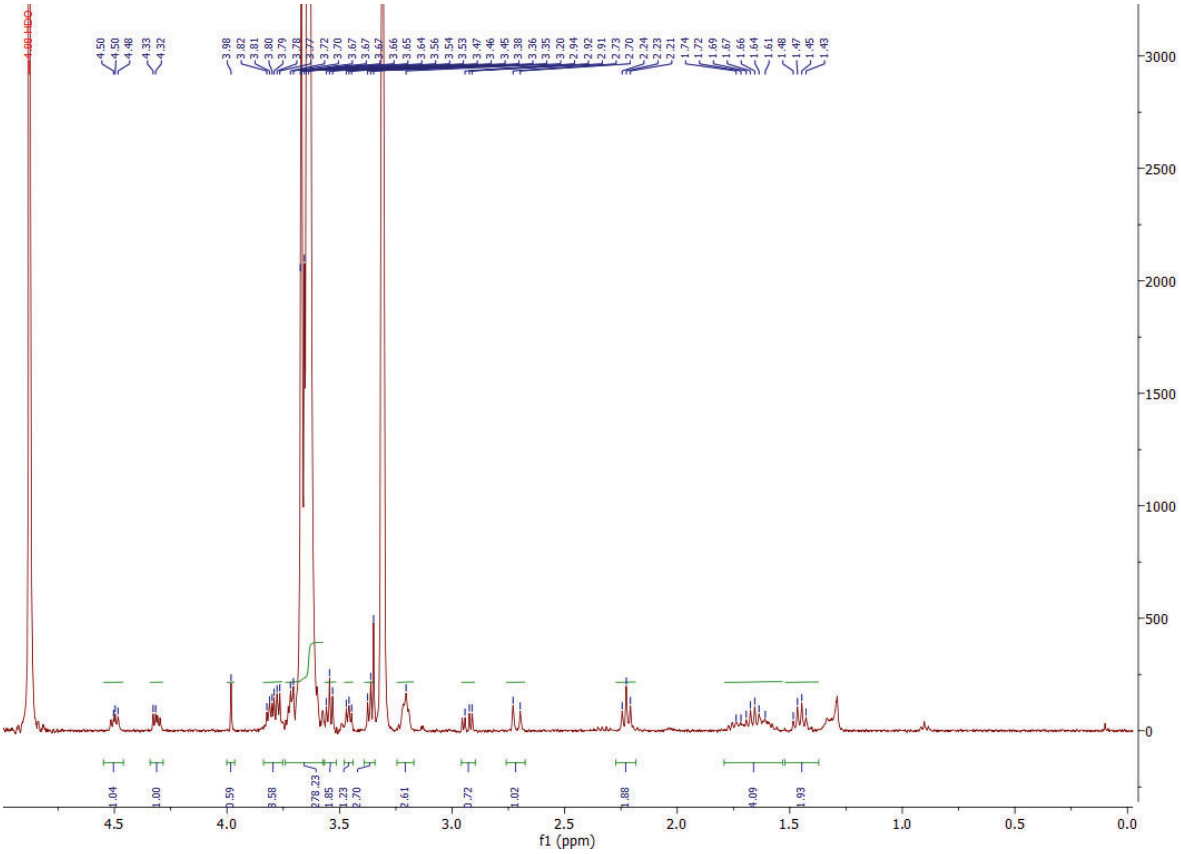

Figure S2. ^{1}H-NMR of compound **2** in CD_3OD.

Compound 3 - diBoc-lysine (3 eq., 51.4 mg., 0.09 mmol) and HATU (2.5 eq., 31.0 mg, 0.07 mmol) were dissolved in 5 mL of dry DMF. DiPEA (10 eq., 55 µL, 0.32 mmol) was added and stirred for 15 min. A 5 mL solution of compound **2** (1 eq., 102.0 mg, 0.03 mmol) in dry DMF was added to the previous mixture, and the final mixture was stirred overnight at 40 °C. The crude was purified by size exclusion chromatography LH-20 (DCM:MeOH, 1:1) to afford compound **3** (105.0 mg, 0.03 mmol, 95 %) as a colorless wax. ^{1}H-NMR (400 MHz, CD_3OD) δ 4.50 (dd, J =4.8, 7.7 Hz, 1H), 4.31 (dd, J = 4.4, 7.9 Hz, 1H), 3.99 (m, 1H), 3.81 (m, 2H) 3.70-3.58 (m, ~315 H), 3.54 (t, J = 5.4 Hz, 5H), 3.45 (m, 2H), 3.37 (q, J = 5.5 Hz, 4H), 3.21 (m, 1H), 3.03 (t, J = 5.9 Hz, 2H), 2.93 (dd, J = 5.0, 12.7 Hz, 1H), 2.72 (d, J = 12.7 Hz 1H), 2.23 (t, J = 7.4 Hz, 2H), 1.81-1.54 (m, 7H), 1.52-1.40 (m, 25H).

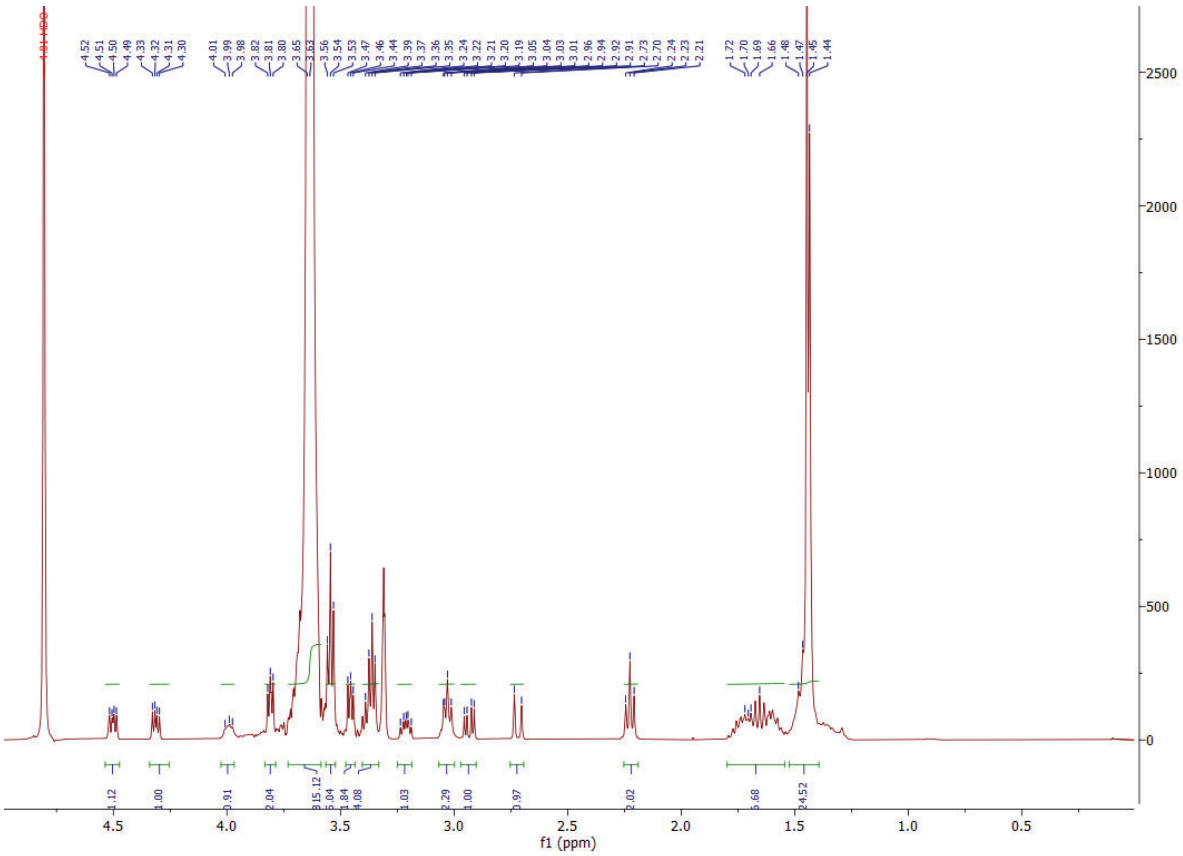

Figure S3. ^{1}H-NMR of compound **3** in CD_3OD.

Compound 4 - Compound **3** (1 eq., 105.0 mg, 0.03 mmol) was dissolved in 2 mL of dry DCM. Trifluoroacetic acid (150 eq., 0.34 mL, 4.48 mmol) was added, followed by 3 hours of stirring at room temperature. DCM was removed under reduced pressure. Co-evaporation with methanol (1mL) was done several times to remove the remaining trifluoroacetic acid, affording compound **4** (104.0 mg, 0.03 mmol, 99 %) as light-yellow wax. ^{1}H-NMR (400 MHz, CD_3OD) δ 4.49 (dd, J = 4.8, 8.0, 1H), 4.30 (dd, J = 4.3, 7.8, 1H), 3.95 (t, J = 6.6 Hz, 1H), 3.8 (t, J = 4.8 Hz, 2H) 3.71– 3.56 (m, ~306 H), 3.54 (t, J = 5.4 Hz, 3H), 3.45 (m, 2H), 3.35 (m, 2H), 3.20 (dt, J = 5.2, 9.9 Hz, 1H), 3.02 (t, J = 7.9 Hz, 2H), 2.92 (dd, J = 5.0, 12.8 Hz, 1H), 2.70 (d, J = 12.4 Hz, 1H), 2.22 (t, J = 7.3 Hz, 2H), 1.91 (q, J = 7.9 Hz, 2H), 1.80-1.55 (m, 6H), 1.55 -1.40 (m, 4H). Mass data: $C_{144}H_{286}N_6O_{66}S$ (Exact mass expected 3187.92). Mass detected: 1617.70 and 1086.09 (calc.: $(M+2Na^+)/2$=1616.96 and $(M+3Na^+)/3$=1085.64).

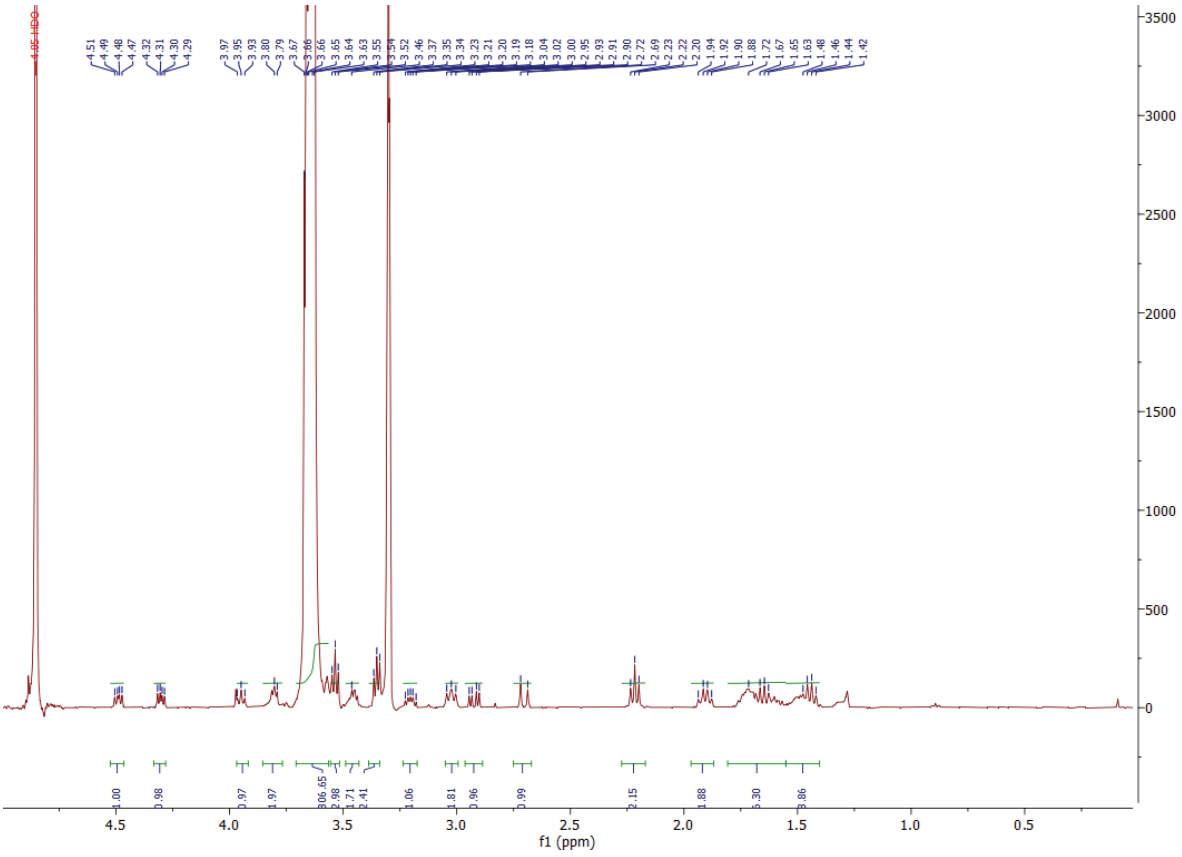

Figure S4. ^{1}H-NMR of compound **4** in CD_3OD.

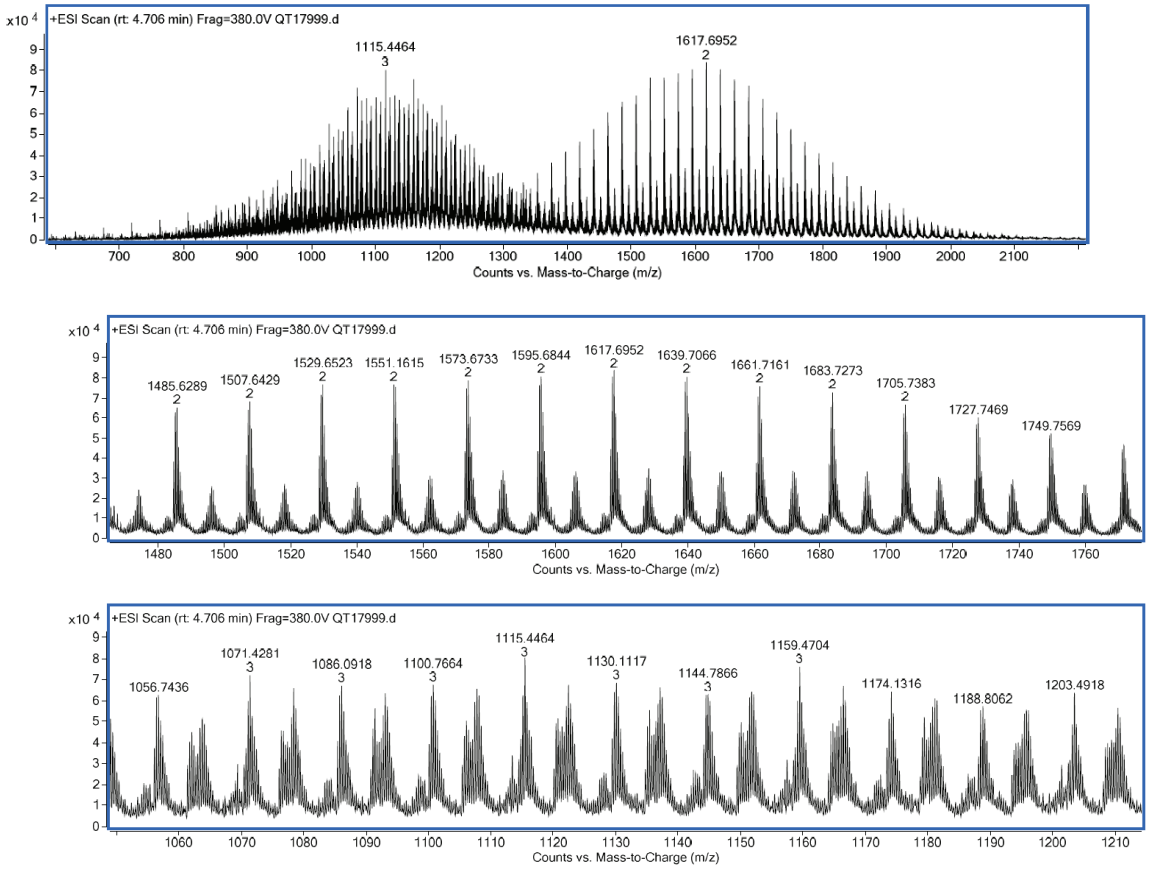

Figure S5. Mass spectra of compound **4** in CD_3OD.

Formation non-functionalized nanoemulsions (NEs)

NEs were produced by spontaneous nanoemulsification: 55 mg Vitamin E acetate containing 6% of NPC-Cholesterol with Cy5.5-TPB at 2% and 45 mg Kolliphor® ELP are mixed at 60 °C for 5 min. To the Oil:Surfactant mixture, 230 µL of filtered Milli-Q water is added, followed by 30 s of shaking with vortex, and 10 min with ThermoShaker (60°C, 1400 rpm).

Nanoemulsion biotinylation

55 mg Vitamin E acetate containing 6% of NPC-Cholesterol (with or without Cy5.5-TPB at 2%), Biotin-PEG-lysine (5 mg), and triethylamine (1.3 µL) were mixed in THF (500 µL), overnight at 60°C. THF and triethylamine were removed under reduced pressure. Kolliphor® ELP (45 mg) and filtered Milli-Q water (460 µL) were added according to the general protocol for nanoemulsion formulation. Then, 66 µL of biotinylated-NEs were diluted into 100 µL phosphate buffer (pH 8.5). Butylamine (1.6 µL) was added, followed by 2 hours of incubation on a ThermoShaker (room temperature, 400 rpm). Absorbance spectra were recorded before and after the addition of butylamine to determine the extent of the reaction with the biotin-linker. Finally, Biotin-NEs were purified by dialysis in Milli-Q water using a 14 kDa MWCO membrane.

NPC-Cholesterol conversion

NCP-Cholesterol (3.3 mg), Biotin-PEG-lysine (5 mg), and triethylamine (1.3 µL) were mixed in THF (500 µL), overnight at 60 °C. THF and triethylamine were removed under reduced pressure. The residue was dissolved in CDCl3 (100 µL) and transferred to a 3 mm diameter tube for ^{1}H-NMR acquisition.

Trastuzumab conjugation with biotin-NHS ester

500 µL of Trastuzumab (32 µM in borate buffer) was mixed with 5 µL of NHS-biotin (100 mM in DMSO). The reaction was incubated overnight on a ThermoShaker (room temperature, 300 rpm). Afterward, purification was done by ultrafiltration (50 kDa MWCO) using PBS. The Biotin-Trastuzumab was stored at 4°C in DPBS, in the presence of 0.05% (w/v) of sodium azide, for conservation.

Nanoemulsion functionalization with trastuzumab

200 µL of NeutrAvidin (22 µM in DPBS) and 200 µL of biotinylated antibody (11 µM in DPBS) were incubated for 24 hours at room temperature in a DNA low-bidding Eppendorf. Then, 100 µL of biotinylated-NEs were added, followed by 24 hours of further incubation. Finally, antibody-NEs were purified by size exclusion chromatography using using Sephacryl S300 HR gel column, which is specially adapted for separating relatively large macromolecules or globular proteins in the range 10 to 150 KDa, and DPBS as an eluent.

Biotin-NEs immobilization protocol

8-well LabTek® chambers were treated with 500 µL KOH (1 M) each and incubated for 30 min. Similar treatments were done with 100 µL BSA-biotin (0.5 mg/mL) and 100 µL NeutrAvidin (0.5 mg/mL), each followed by 30 min incubation. Finally, the chambers were treated with biotinylated and non-biotinylated NEs as control, followed by 30 min incubation in darkness. Both biotinylated and non-biotinylated NEs were loaded with Cy5.5-TPB (2% with respect to the oil). All treatments were done at room temperature with DPBS washings in between.

Cell experiments

Cell culture. MDA-MB-231 and HCC-1954 were grown in RPMI1640 with L-Glutamine, supplemented with 10% fetal calf serum and penicillin (100UI/mL) and streptomycin (100µg/mL) at 37°C in a humidified atmosphere containing 5% CO_2.

Cytotoxicity. 2,500 MDA-MB-231 and 7,500 HCC-1954 were plated in a 96-well plate and let adhere overnight. The day after, medium was changed for medium containing increasing concentration of bare NEs or antibody-targeted NEs. After 72h, cells were washed, fixed with PFA 4% and stained for 1h with 2% Cristal violet. Excess of cristal violet was washed with tap water and plates were let dry before destaining by acetic acid. Cristal violet absorbance was measured at 595nm using a MultiSkan FC plate-reader.

Nanoemulsion internalization. 30,000 MDA-MB-231 or HCC-1954 were plated in an 8-well LabTek slide with coverlid and let adhere overnight. The day after, medium was changed for medium containing 1.1nM of bare NEs or antibody-targeted NEs in Opti-MEM. After 4h of incubation at 37°C, cells were wash and their membranes were stained with wheat germ agglutinin (WGA) Alexa-Fluor 488 (5 µg/mL in PBS) over 5

min at 37°C. After an additional wash, cells were fixed in PFA 4% and mounted in Fluoromount/DAPI. Slides were imaged using a 60X water-immersion objective on an inverted OIympus Spinning-disk. The comparions of SKBR3 vs MDA-MB 231 was done in another set of experiments. SKBR3 and MDA-MB 231 cells were grown in Dulbecco's modified Eagle medium (DMEM, Gibco) supplemented with FBS (10%), sodium pyruvate (1 mM), L-glutamine (4 mM), and phenol red. For imaging experiments, cells were seeded in 35 mm glass bottom dishes (Ibidi) and incubated over 2 days, at 37 °C under a humidified 5% CO2 atmosphere. Then, cells were washed with DPBS, followed by 30 min incubation in darkness with Hoechst 33342. After washing with DPBS, cells were incubated with Antibody-NEs (0.2 nM in OptiMem) on ice for 1 hour. Finally, they were washed with OptiMem.

Statistical analysis

Statistical analysis was performed with GraphPad Prism 9 software. The normal distribution of the data was tested using the Shapiro–Wilk normality test. When comparing two groups, a Mann-Whitney analysis were used, for more than 2 groups a Kruskal-Wallis test followed by the original FDR method of Benjamini and Hochberg post-test was used. $p<0.05$, *; $p<0.01$, ** . $p<0.001$, ***; $p<0.0001$, ****. Data in graphs are presented as mean ± Standard Deviation.

Supplementary Figure legends

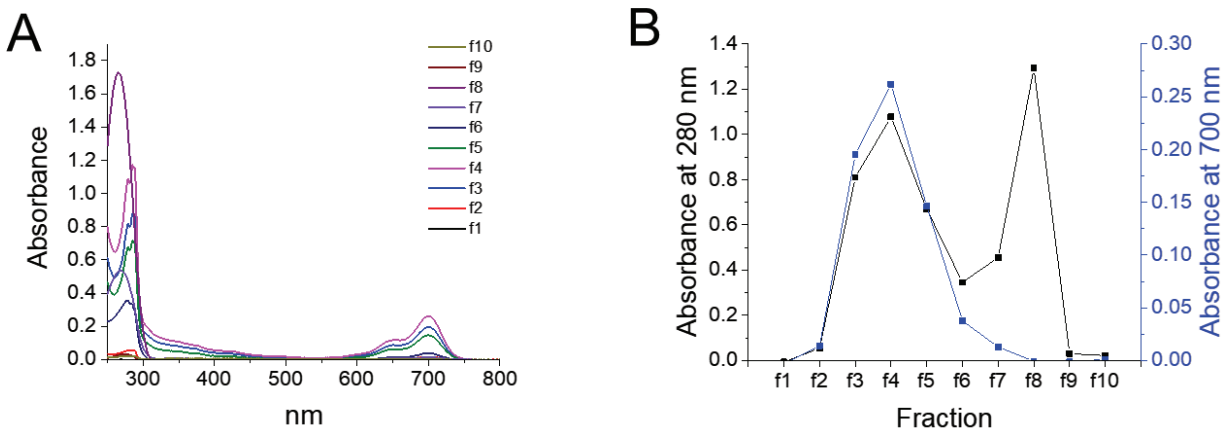

Figure S6. (A) Absorption spectra of different fractions of non-purified mixture containing NEs, neutravidin and biotinylated mAbs. (B) Absorbance value for different fractions recorded at 280 and 700 nm.

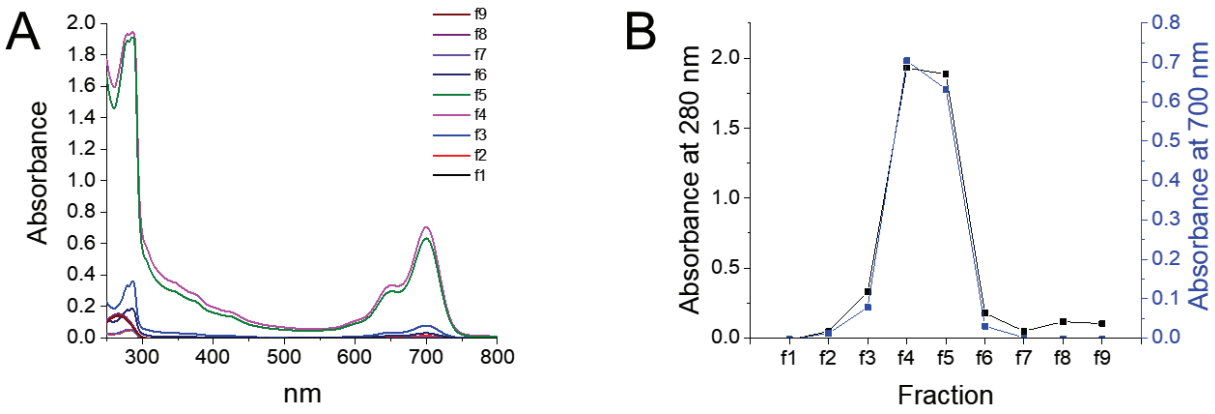

Figure S7. (A) Absorption spectra of different fractions of NEs conjugated with mAbs after purification. (B) Absorbance value for different fractions recorded at 280 and 700 nm.

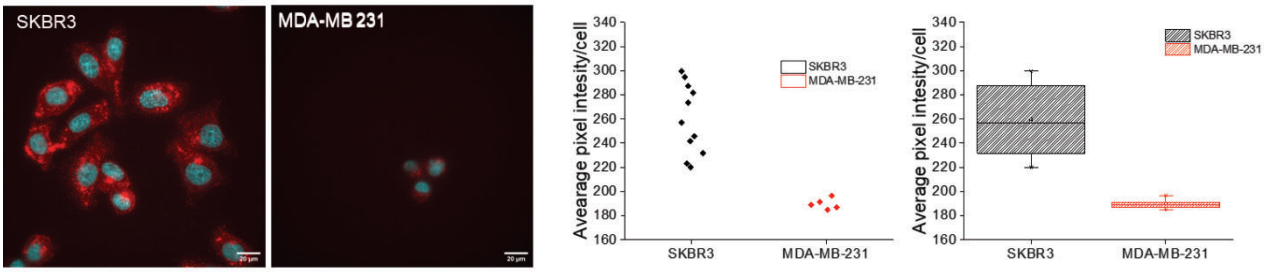

Figure S8. Epifluorescence microscopy images from SKBR3 and MDA-MB 231 cells after 1h incubation on ice with Antibody-NEs (0.2 nM) containing 2% of Cy5.5-TPB. Data on the left are the quantitative image analysis.

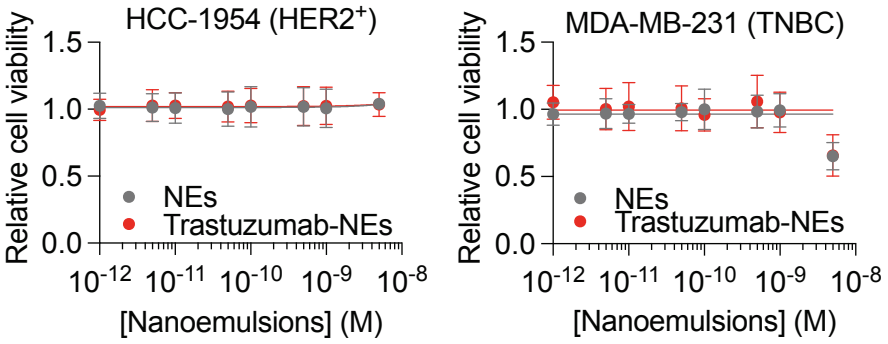

Figure S9. Nanoemulsions cytotoxicity was measured after a 72h treatment with NEs increasing concentrations of HER2-amplified HCC-1954 (left) and HER2^{low} MDA-MB-231 (right) cells. Cytotoxicity was assessed using a crystal violet staining.

Table S1. Size of NEs measured by DLS.

NEs type	Diameter (nm)	Polydispersity index (PdI)
Non-functionalized (6 wt. % NPC-Chol and 2 wt. % Cy5.5-TPB)	53.3 ± 0.2	0.13 ± 0.02
Biotinylated (no dye)	64 ± 4	0.20 ± 0.03
Biotinylated (2 wt. % Cy5.5-TPB)	53 ± 2	0.16 ± 0.01
Antibody (2 wt. % Cy5.5-TPB)	56 ± 2	0.12 ± 0.03

Chapter IV

Leveraging immunotherapies with nanomedicine

Pathologists have long recognized that some tumors are densely infiltrated by cells of both the innate and adaptive immune systems (Dvorak, 1986). In this Chapter IV, we will describe the major cellular actors of the anti-tumoral immune response and how immunoselected TCs variants induce an immunosuppressive TME, thereby sabotaging the tumoricidal functions of immune cells. The emergence of cancer immunotherapies approaches allows to tackle the TME immunosuppression, but these therapies are associated with low response rate and life-threatening immune-related adverse events. Consequently, improving cancer immunotherapy efficacy and safety remains a priority.

Based on our review published in *Advanced Therapeutics*, we will discuss the utilization of nanoimmunotherapy approaches to modulate the immune response in a controlled spatiotemporal manner. While nanoimmunotherapies successfully reactivate immune cells in several preclinical studies, the impact of drug-free nanomaterials on immune cells remains unknown. To address this gap, we characterize the response of human NK cells and pan T cells to a selection of five NPs commonly used in biomedical applications. We identify PLGA NPs as suitable and promising candidates for further targeting approaches aiming to reactivate the immune system of cancer patients.

Publications associated to this chapter:

Mittelheisser V, Banerjee M, Pivot X, Charbonnière LJ, Goetz JG, Detappe A. "***Leveraging immunotherapy with nanomedicine.***"
Advanced Therapeutics 3:2000134 (2020) – doi:10.1002/adtp.202000134

Mittelheisser V, Lefebvre O, Banerjee M, Soltani R, Ghosh S, Dupas A, Diringer MC, Blumberger J, Bochler L, Harlepp S, Larnicol A, Pichot A, Stemmelen T, Molitor A, Rompai M, Carapito C, Carapito R, Ménard-Moyon C, Bianco A, Charbonnière LJ, Lux F, Tillement O, JG* and Detappe A*

"***Nanomaterials trigger functional responses in primary human immune cells***"

In revision

Immune system role in repressing the growth of carcinomas was first predicted in 1908 Paul Ehrlich (Ehrlich, 1908). Immunosurveillance theory gained understanding fifty years later, when Frank Macfarlane Burnet and Lewis Thomas revisited the theory of anti-tumoral immune protection. Frank Macfarlane Burnet enunciated that TC-specific neo-antigens could provoke an effective immunologic reaction that would eliminate developing cancers (Burnet, 1971, 1964, 1957). In parallel, Lewis Thomas conjectured a more evolutionary hypothesis in which complex long-lived organisms must possess protection mechanisms against neoplastic disease (Thomas, 1959). Further implications of the immune system in TCs clearance were underpinned when immunodeficient patients were described as more prone to cancer progression compared to immunocompetent individuals (Penn, 1982). Yet, the first experimental evidence of immunosurveillance only arose in the 1990-2000's. Pivotal studies on IFNγ (Dighe et al., 1994; Shankaran et al., 2001; Street et al., 2001) and perforin (Smyth et al., 2000; Street et al., 2001; Van Den Broek et al., 1996) highlighted the role of cytotoxic immune cells as a key element of anti-tumor immune responses in both chemically induced and spontaneous tumors.

While we acknowledge the participation of all immune cells in an extensively coordinated anti-tumoral immune response, we will stress the role of the two immune cells that we selected for our study, namely the Natural Killer (NK) cells and the T cells. We decided to specifically work on NK- and T cells for their potent antitumoral effector functions. Circulating NK cells killing capacity correlates with reduced cancer progression, underpinning their importance in the innate anti-tumoral response (Imai et al., 2000). Similarly, scoring T cells infiltration in the TME is a good prognostic value for predicting patient overall and disease-free survival (*i.e.*, time to relapse) (Pagès et al., 2009).

1. Anti-tumoral immune response

1.1. NK cell-mediated anti-tumoral response

NK cells are cytotoxic innate lymphoid cells that were first described in 1973 (Greenberg et al., 1973). Their ability to kill various TCs types without the need for prior sensitization and through the secretion of their preformed lytic granules coined them the name "natural" killer" cells (Kiessling et al., 1975). NK cells are commonly found penetrating the TME (Cózar et al., 2021). Their infiltration levels correlate with an

increased overall survival in patients with gastric cancer (Ishigami et al., 2000), pulmonary adenocarcinoma (Takanami et al., 2001), melanoma (Cursons et al., 2019), and breast cancer (Muntasell et al., 2019). NK cells recruitment in the TME occurs owing to their expression of a unique and broad repertoire of chemokine receptors to control their migration (Grégoire et al., 2007).

1.1.1. NK cells recognition of tumor cells and activation

As opposed to T and B lymphocytes, NK cells utilize germ-line encoded activating and inhibitory receptors to detect foreign, stressed, infected, or cancerous cells and destroy them once activated. Therefore, complex signals arising from multiple ligand-receptor interactions are integrated and the balance between activating, co-stimulatory and inhibitory signals determine the outcome of NK-cell activation (**Figure 16**).

Missing self | NK cells constitutively express a variety of killer immunoglobulin-like receptors (KIRs) (Campbell and Purdy, 2011) and the CD94-NKG2A heterodimer (Lazetic et al., 1996). Inhibitory KIRs are critical for NK cells education, as these receptors recognize classical polymorphic self-major histocompatibility complex (MHC) class I molecules (Kim et al., 2005). This step termed “licensing” or “arming” allows NK cells to distinguish between healthy self-tissue (expressing the MHC-I molecules) and stressed, infected, foreign or transformed cells. Indeed, to escape $CD8^+$ T-cell immunosurveillance, neoplastic cells frequently downregulate classical MHC-I molecules expression (Algarra et al., 2000), alleviating NK cells inhibition and rendering them more prone to activation via a plethora of activating receptors described hereafter.

Stress-induced ligands | NK cells are equipped with an armory of other activating receptors able to recognize stress-induced ligands strongly expressed in TCs but not in healthy tissues (Moretta et al., 2001). Natural cytotoxicity receptors (NCRs), namely NKp46 (*NCR1*/CD335) (Sivori et al., 1997), NKp44 (*NCR2*/CD336) (Vitale et al., 1998) and NKp30 (*NCR3*/CD337) (Pende et al., 1999) belong to the immunoglobulin superfamily and are essential to fully activate NK cells. The identification of ligands for the NCRs family is still a matter of ongoing research, hindering a complete understanding of their role in NK cells immunosurveillance. An exception resides in the

identification of NKp30 ligands: the B7 immunoreceptor family member B7-H6 (Brandt et al., 2009) and the Bcl-2-associated athanogene 6, Bag-6 protein (Pogge Von Strandmann et al., 2007). Beside NCRs, the lectin-like type 2 transmembrane receptor NKG2D plays a crucial role in NK cell-mediated tumor cell killing by recognizing a variety of MHC-related ligands such as MHC class I polypeptide-related sequence A or B (MICA/MICB) (Bauer et al., 1999) and several UL16-binding proteins (ULBPs) (Cosman et al., 2001). Like NKG2D, NKp80 is a C-type lectin-like receptor that co-stimulates NK cells activation (Vitale et al., 2001) by binding the activation-induced C-type lectin (Welte et al., 2006). Another potent NK cells activator is the CD16 receptor, predominantly expressed on the $CD56^{Dim}CD16^{Hi}$ subset (Bruhns, 2012). CD16 (or FcγRIIIA) recognizes IgG_1 antibody-coated TCs through their highly conserved Fc region and mediates antibody-dependent cell-mediated cytotoxicity (ADCC) (Cartron et al., 2002).

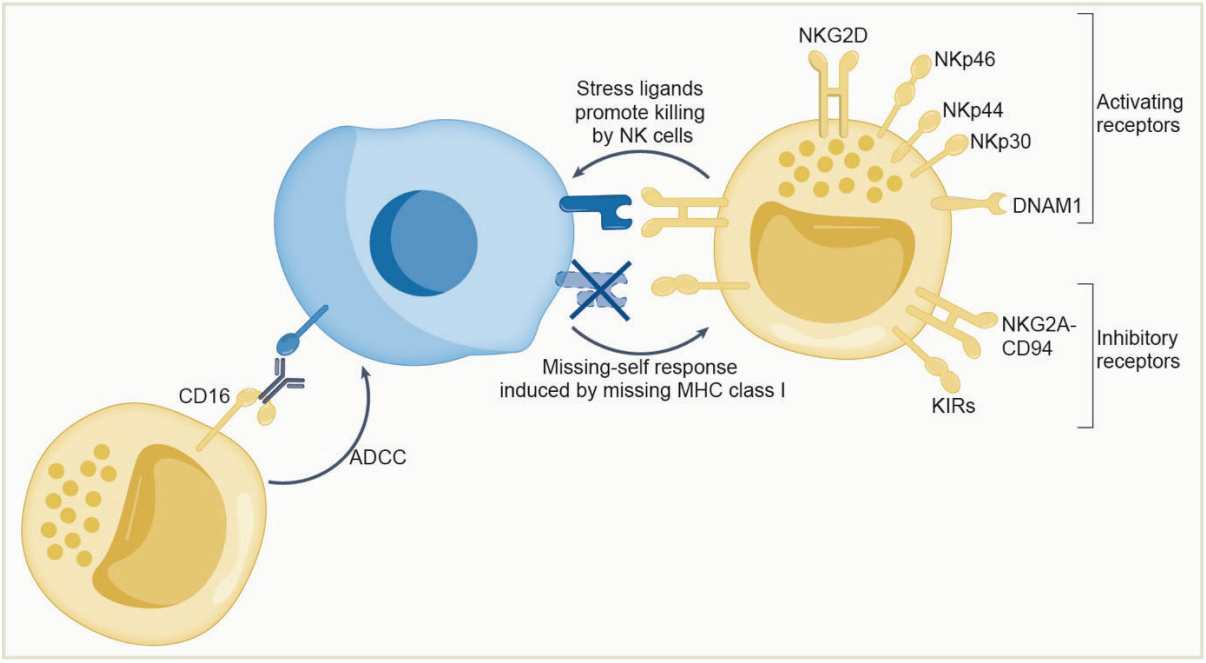

Figure 16 – Mechanisms of NK cells activation.
NK cells activation relies on the complex integration of inhibiting and activating cues. On one hand, MHC class I-deficient TCs do not present inhibitory signals to NK cells. On the other hand, in addition to alleviate NK cells inhibition, TCs express stress ligands that activate NK cells by engaging their cognate receptors such as NKG2D, NKp46, NKp44, NKp30 and DNAM1. Besides, NK cells also engage opsonized TCs via the Fc fragment of the antibody initiating antibody-dependent cellular cytotoxicity (ADCC).

Adhesion molecules | In addition to activating receptors, adhesion molecules also promote NK cell activation by acting as coreceptors. Lymphocyte function-associated antigen-1 (LFA-1) expressed on NK cells interacts with intercellular adhesion molecules (ICAMs) on target cells, thereby enhancing NK cell-mediated cytotoxicity through improved polarization of the cytoskeleton machinery (Urlaub et al., 2017). Upon binding its ligands (CD155 or CD112) expressed by TCs (Bottino et al., 2003), DNAX accessory molecule-1 (CD226/DNAM-1) also contributes to promote NK cell adhesion, migration and cytotoxic functions (Martinet et al., 2015).

1.1.2. NK cell-mediated tumor cells lysis

Once activated, NK cells induce apoptosis of local and disseminated TCs either by releasing cytotoxic proteins (*e.g.*, perforin, granzymes, granulysin) within the immunological synapse or by death receptor signaling.

Cytotoxic granules | NK cell lytic function is exerted through the formation of an immunological synapse (IS), which enables focused lytic granules secretion and mitigate bystander killing. Upon recognizing TCs, NK cells initiate the formation of an immune synapse (IS) (Chen et al., 2005; Warren et al., 1996). Next, NK cells engage firm adhesion through integrins interactions (LFA-1-ICAMs), resulting in IS maturation (Barber et al., 2004; Riteau et al., 2003). During IS maturation, NK cells undergo cytoskeletal reorganization leading to the formation of central and peripheral supramolecular activation clusters (SMAC). Adhesion molecules (*e.g.*, LFA-1) and filamentous actin networks segregate into the peripheral SMAC (Carpén et al., 1983; Orange et al., 2003; Vyas et al., 2001), where they provide co-stimulation signals to the NK cells (Perez et al., 2004; Riteau et al., 2003) (**Figure 17**). Peripheral SMAC form a ring through which lytic granules traffic to reach the central SMAC where they fuse with the NK cells plasma membrane (McCann et al., 2003; Stinchcombe et al., 2011) (**Figure 17**). Upon their secretion at the IS cleft, lytic granules release the membrane-disrupting protein, perforin (Nakata et al., 1992; Salcedo et al., 1993), and proteolytic serine proteases, the granzymes (Salcedo et al., 1993). Following its release from the lytic granules, perforin inserts itself into the TC membrane, oligomerizes, and generates 10-25 nm range pores in a calcium-dependent mechanism (Law et al., 2010). Granzymes are then able to diffuse through the perforin pore into the cytosol of TCs (Keefe et al., 2005), where they induce apoptosis through

caspase-dependent (Medema et al., 1997) and -independent mechanisms (*e.g.*, Bcl-2 family member BID cleavage to activate the mitochondrial death pathway) (Barry et al., 2000) (**Figure 17**).

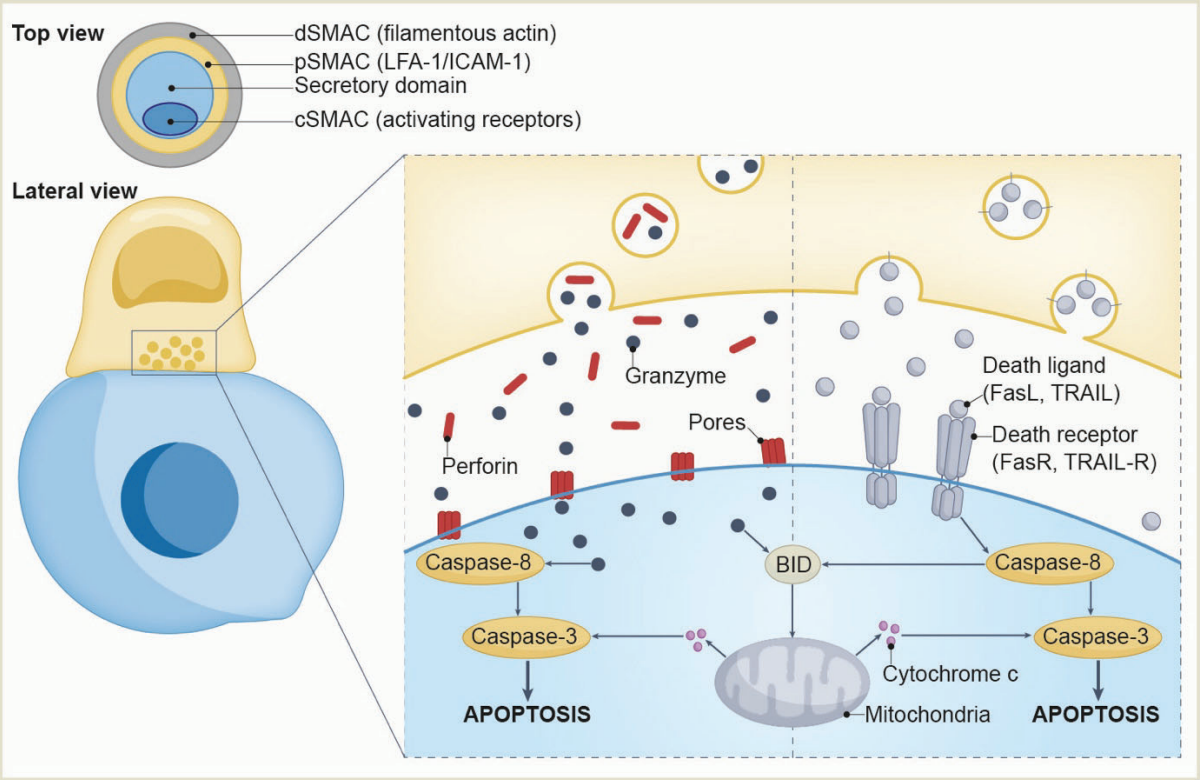

Figure 17 – NK cell-mediated tumor cell lysis.
After target recognition, NK cells induce its apoptosis by releasing cytotoxic proteins or by death receptor signaling. Granzymes diffuse through the perforin pore into the cytosol of the TC (left) and trigger caspase-dependent and independent apoptosis. Death receptor signaling (right) occurs when death ligands released by NK cells bind their cognate receptors expressed by the TC.

Death ligands | Additionally, activation of NK cells induces the expression of death-inducing ligands of the TNF family, such as Fas ligand (FasL/CD95L) or TNF-related apoptosis-inducing ligand (TRAIL) at their surface (Kischkel et al., 1995; Sprick et al., 2000) (**Figure 17**). These ligands can bind to death receptors express on TCs (FasR and TRAIL-R) leading to caspase enzymatic cascade activation and eventually inducing their apoptosis (Scaffidi, 1998). Death receptor signaling plays notably important roles in NK cell-mediated control of liver metastasis (Smyth et al., 2001).

1.1.3. Orchestration of the adaptive immune response by NK cells

When activated by TCs interactions or by cytokines in the microenvironment, NK cells secrete numerous cytokines (*e.g.*, IFNγ, tumour necrosis factor, TNFα),

chemokines (e.g., CCL5, lymphotactin, XCL1) and growth factors (*e.g.*, GM-CSF, G-CSF and M-CSF) that shape the innate and adaptive immune responses (Vivier et al., 2011).

Regulation of adaptive immune responses by NK cells occurs mainly by cross-talks with dendritic cells (DCs) (Walzer et al., 2005). DCs are professional antigen presenting cells crucial for T cell-mediated immune responses, hence bridging the gap between the innate and adaptive immune systems. Initial studies showed that NK cells play an important role in shaping DC responses either by promoting monocytes differentiation in DCs via GM-CSF (Zhang et al., 2007) or by inducing their maturation through IFNγ (Adam et al., 2005; Mocikat et al., 2003). IFNγ-activated DCs present an increased expression in MHC-I and II molecules, an upregulation of costimulatory molecules and an upregulation in antigen processing (Pan et al., 2004). In addition to promote DCs activation by IFNγ, NK cells also secrete IL-12 and IL-15, which directly foster the induction of antitumoral responses by $CD4^+$ T_H1 and cytotoxic $CD8^+$ T cells (Manetti et al., 1993; Morandi et al., 2009). Moreover, NK cells are also key regulators of DCs recruitment, retention, and/or survival in the TME. NK cell-secreted CCL5 and XCL1 recruit into the tumor myeloid-derived conventional type 1 DCs (cDC1s), which are specialized in cross-presenting antigens to $CD8^+$ T cells (Böttcher et al., 2018). NK cells also secrete the cytokine FLT3LG, thereby increasing the survival of cDC1s within the TME (Barry et al., 2018). Besides inducing an IFNγ-dependent priming of cDC1, NK cells can directly act on T cells functions by stimulating an anti-tumoral T_H1 cell polarization (Bradley et al., 1996) and by increasing antigen presentation in TCs, leading to increased tumor immunogenicity (Shankaran et al., 2001).

1.2. T cell-mediated anti-tumoral response

During their continuous proliferation, TCs accumulate somatic mutations that can be translated into immunogenic neoantigens. High tumor mutational burden (TMB) leads to the accumulation of missense and frameshift mutations that results in the production of virtually random tumor-associated antigens (TAAs) with a highly dissimilar to germline epitopes (Schischlik et al., 2019; Turajlic et al., 2017). Generated TAAs trigger the adaptive immune system, inducing T cells priming, expansion and specific TCs recognition. The adaptive anti-tumoral response can be described as a

cyclic process initiated by DCs engulfment of TAAs and ending by TCs eradication by T cells (Chen and Mellman, 2013) (**Figure 18**).

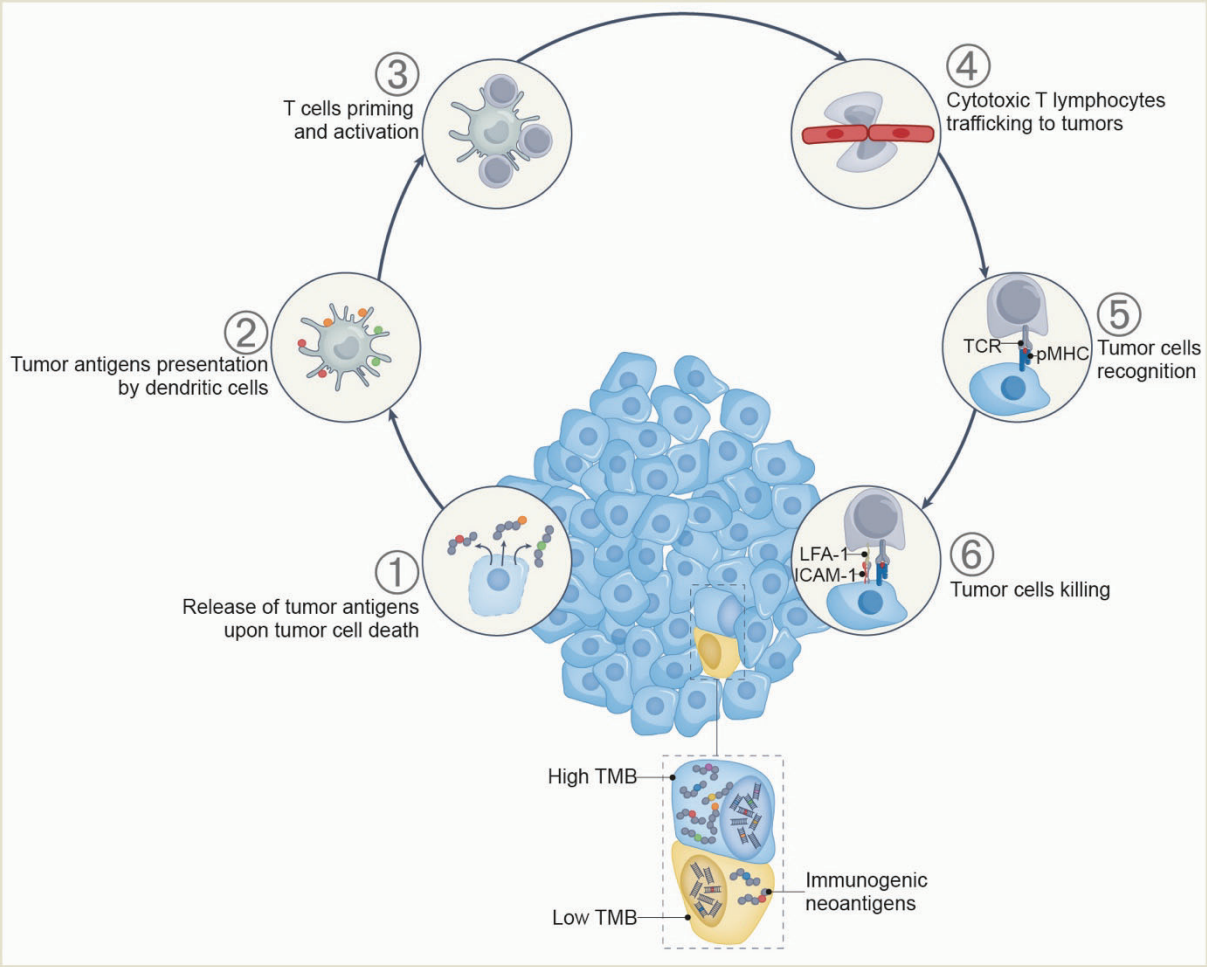

Figure 18 – T cell-mediated anti-tumoral response.
The anti-tumoral T cell-mediated immune response is a self-perpetuating cycle that is divided in 6 stages. The destruction of TCs leads to the release of immunogenic neoantigens (1), which are captured and processed by dendritic cells (2) to be presented to T cells in lymph nodes (3). Tumor associated antigens presentation induces differentiation of naïve $CD8^+$ T cells in cytotoxic T lymphocytes, which then migrate and infiltrate the tumor (4), with the aim of specifically recognizing tumor cells (5) and destroying them (6).

1.2.1. Naïve T cells activation

Tumor-infiltrating immature DCs engulf TAAs released in the TME from TCs undergoing immunogenic or necrotic cell death (Ferguson et al., 2011). Immature DCs require further activation signals provided by damage-associated molecular patterns (DAMPs) (Messmer et al., 2004; Obeid et al., 2007) or tumor-infiltrating NK cells (Gerosa et al., 2002) to fully mature and present TAAs. Maturating DCs upregulate CCR7 which trigger their rapid migration to lymphoid organs, allowing TAAs drainage

to the draining lymph nodes (Förster et al., 1999; Roberts et al., 2016). In addition, DCs maturation process is associated with TAAs processing as well as upregulation of the co-stimulatory molecules CD40, CD80 (B7-1) and CD86 (B7-2) (Inaba et al., 2000; Turley et al., 2000). Once in the lymphoid organs, mature DCs present MHC-I/MHC-II-loaded TAAs to $CD4^+$ or $CD8^+$ T cells in paracortical regions (Dieu et al., 1998; Ngo et al., 1998).

Helper T cells | Naïve $CD4^+$ T cells recognize MHC-II-loaded TAAs epitopes presented by mature DCs. To fully activate, naïve T cells require co-stimulatory signals involving interactions between T cells CD28 and its cognate ligands CD80 (B7-1) and CD86 (B7-2) expressed by mature DCs (Mc Adam et al., 1998). After having completed their activation, T cells undergo clonal expansion through autocrine IL-2 signaling via the high affinity IL-2Rα (Sojka et al., 2004) (**Figure 19**). Activated and proliferating $CD4^+$ T cells become T_H0 cells that can be further polarized in T_H1 or T_H2 cells depending on their cytokinic microenvironment. In the context of anti-tumoral response, mature DCs induce a T_H1 polarization via IL-12 and IL-18 secretion (Macatonia et al., 1995; Stoll et al., 1998) (**Figure 19**). Interestingly, IL-18 secreted by mature DCs can activate NK cells and trigger secretion of IFNγ which in turn further fuels T_H1 differentiation (Wong et al., 2013).

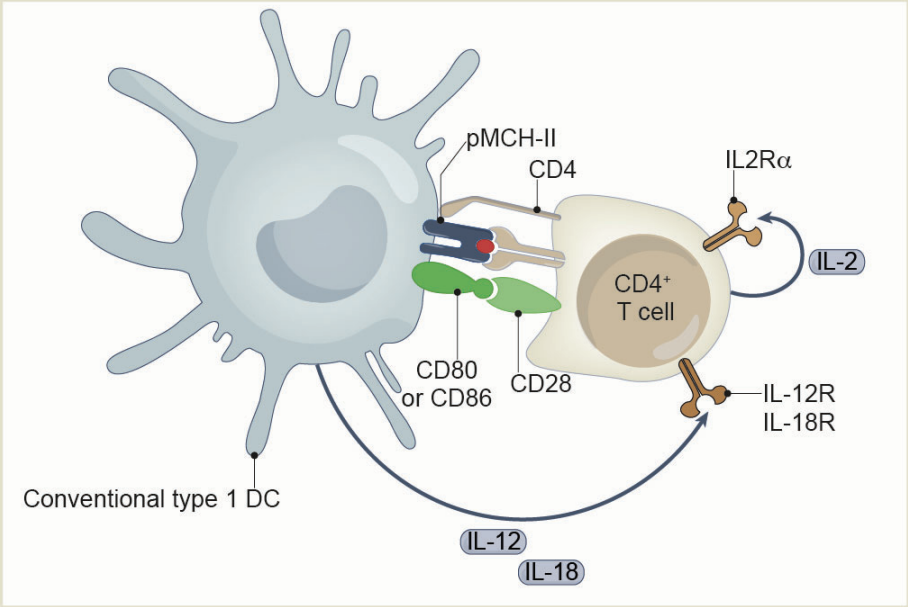

Figure 19 – $CD4^+$ helper T cells activation by dendritic cells.
Naïve $CD4^+$ T cells encounter mature DCs in lymphoid organs. DC-mediated naïve $CD4^+$ T cells polarization towards T_H1 cells requires three signals: (1) recognition of the peptide:MHC-II complex by the TCR; (2) the interaction of the co-stimulatory

molecules (CD28, CD80 and CD86) and (2) the release of T_H1 polarizing cytokines (IL-12 and IL-18). The activated $CD4^+$ T cells also produce IL-2 which allows their survival and clonal expansion.

Cytotoxic T cells | While TAAs epitopes presentation by DCs happens simultaneously, $CD4^+$ and $CD8^+$ T cells activation is sequentially around the DCs. Naïve $CD8^+$ T cells recognize MHC-I-loaded TAAs epitopes presented by mature DCs. Besides, $CD8^+$ T cells also rely on co-stimulatory signals for their activation (Mc Adam et al., 1998). In addition, to become cytotoxic T lymphocytes (CTLs), naïve $CD8^+$ T cells require a "*ménage à trois*" with T_H1 cells and mature DCs (Bennett et al., 1997; Ridge et al., 1998) (**Figure 20**). During this process, T_H1 cells "license" mature DCs to increase their MHC-I and costimulatory molecules expression, thereby providing potent activating signals to naïve $CD8^+$ T cells (Lanzavecchia, 1998). Mature DCs licensing proceeds by the secretion of IFNγ by T_H1 cells (Tau et al., 2001) as well as through the signaling between CD40L on the T_H1 cells and their cognate CD40 receptor expressed by DCs (Bennett et al., 1998; Schoenberger et al., 1998).

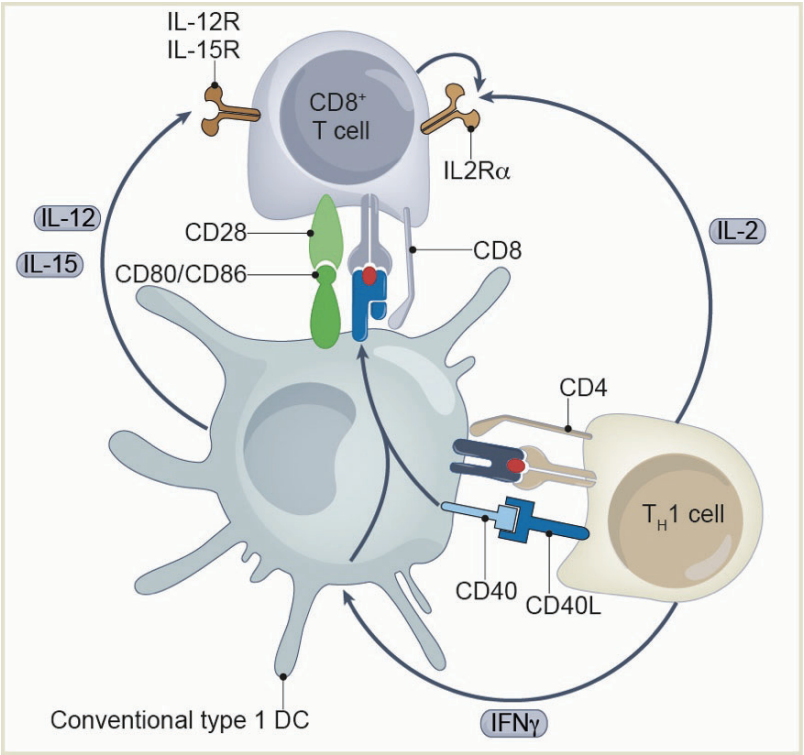

Figure 20 – $CD8^+$ T cells activation.
In the second step of T_H1 cells priming, antigen presentation DCs stimulate CD40L expression by effector $CD4^+$ T cells. CD40L-CD40 interaction coupled with IFNγ expression by T_H1 cells "license" DCs to increase their antigen presentation ability and expression of co-stimulatory ligands and cytokines. IL-12 and IL-15 produced by

cDC1s act directly on $CD8^+$ T cells to support their differentiation into effector cytotoxic T lymphocytes (CTLs).

1.2.2. Anti-tumoral response

Once activated, CTLs undergo clonal expansion through T_H1-secreted IL-2 and migrate towards the tumor bed where they will exert their cytotoxic functions. TAAs-educated CTLs recognize their epitope presented by MHC-I molecules expressed at the surface of the TCs. Initial binding of the TCR to its cognate antigenic peptide induces a massive reorganization of CTLs cytoskeleton leading to the formation of an IS (Grakoui et al., 1999; Wülfing and Davis, 1998). Actin remodeling at the IS promotes CTL spreading on the interacting TC surface (Gomez et al., 2006; Le Floc'h et al., 2013; Nolz et al., 2006), thus increasing cell-cell contact and IS maturation. Mature CTL IS present a similar architecture than NK cells IS (**Figure 17**). Adhesion molecules (*e.g.*, LFA-1) and filamentous actin networks are segregated in the peripheral SMAC (Kaizuka et al., 2007; Monks et al., 1998) whereas the activating TCR-MHC complexes are found in the central SMAC (Dustin and Cooper, 2000; Monks et al., 1998). This architecture forms a so-called "bull's eye" IS with actin hypodense central SMAC through which CTLs lytic granules traffic before to fuse with the plasma membrane (Le Floc'h et al., 2013; Murugesan et al., 2016). After their secretion, perforins and granzymes contained in the lytic granules enables the efficient killing of TCs with similar mechanisms to the ones previously described for NK cells (**Figure 17**). Besides, CTLs are also able to induce TCs apoptosis through death ligands signaling.

1.3. Cancer immune escape

During their progression, cancers are under constant surveillance of the immune system. In the introductory materials of this Chapter IV, we described the "elimination" phase during which cytotoxic NK and T cells successfully identify and eradicate the TCs (**Figure 21**). Yet, immune cells-mediated elimination leads to a selection pressure leading to the emergence of resistant TC clones. During this "equilibrium" period, the tumor mass enters an immuno-mediated dormancy where the balance between TCs proliferation and their elimination by the immune system is null (Schreiber et al., 2011). Surviving TCs accumulate mutations conferring them the ability to modulate the TME by using immune rheostats (**Figure 21**).

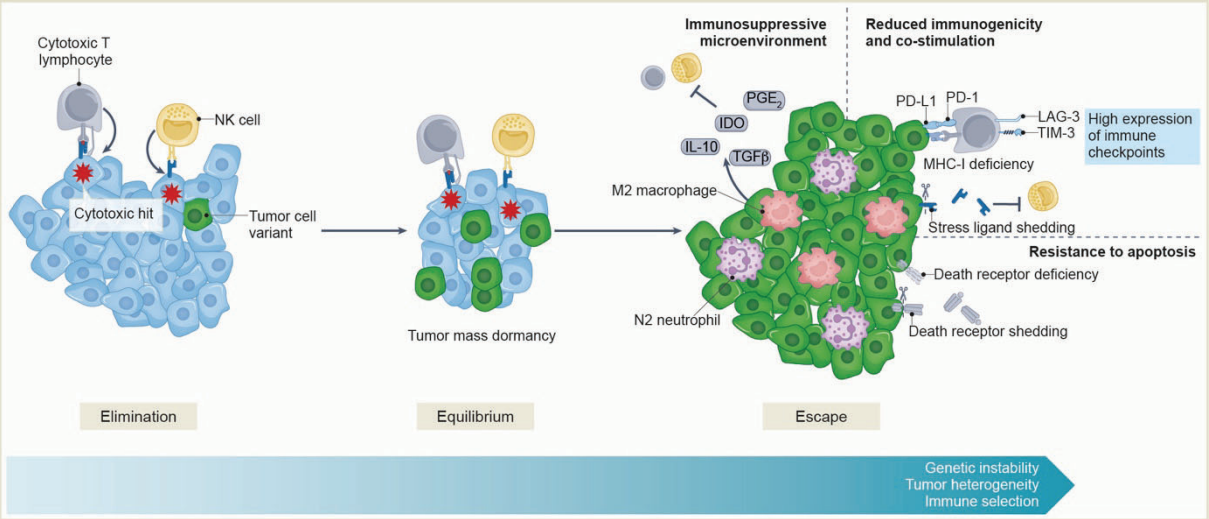

Figure 21 – Immuno-editing and immune escape.
Cancer immuno-editing describes the intricate relationship between a tumor and its infiltrating immune system. In the first phase (left), the immune system efficiently eliminates TCs. In the second phase (center), the tumor mass enters an immuno-mediated dormancy and the immuno-resistant TCs variants arise. TCs variants have increasing capacity to survive immune attack, such that in the third phase (right), the tumor escapes immune control and proliferate, leading to a clinically detectable tumor mass. The escape phase is characterized by a multitude of tumor-intrinsic and extrinsic mechanisms that can be classified into three categories: (1) lack of TCs recognition due to a lowered immunogenicity (decreased MHC-I expression, increased immune checkpoints receptors); (2) resistance to apoptosis induced by cytotoxic cells and (3) establishment of an active immune suppression in the microenvironment through cytokine production (TGFβ, IL-10) and recruitment of immunosuppressive cells.

1.3.1. Reduced immunogenicity

During immune escape, TCs become “invisible” to the immune system. To evade CTL-induced recognition and specific lysis, many tumors develop MHC-I molecules deficient variants (Algarra et al., 1997; Cabrera et al., 1996) or variants with defect in TAAs production (de Vries et al., 1997) or processing (Restifo et al., 1993; Sanda et al., 1995). Yet, these MHC-I deficient TCs can still be eliminated by NK cells. Hence, TCs able to escape NK cells lysis are also immunoselected. This phenomenon occurs through the proteolytic shedding of stress-induced NK cells ligands. Soluble NKG2D ligands act as a decoy for NK cells, inducing their strong functional impairment (Groh et al., 2002; Kaiser et al., 2007). Another mechanism relies on TCs overexpression of HLA-E non-classical MHC-I molecules. HLA-E binding to its cognate CD94-NKG2A inhibitory receptor inhibits NK cell effector functions (Le Dréan et al., 1998).

1.3.2. Reduced immune cells co-activation

Tumor "invisibility" can also be mediated by the expression of immune checkpoints that act as brakes for the immune response. CTLA-4 primarily attenuates T cells activation during the priming phase. CTLA-4 has higher affinity for co-stimulatory ligands CD80 (B7-1) and CD86 (B7-2) than their CD28 receptor (Hathcock et al., 1993), thereby outcompeting CD28 in binding CD80 and CD86 and reducing T cells activation (Linsley et al., 1994). CTLA-4 also hinder T cells activation by promoting CD80 and CD86 active removal from the DCs surface (Qureshi et al., 2011). Nevertheless, another study hints that CTLA-4 expressed by melanoma cells can impair T cells functional response, further suggesting a potential role for CTLA4 in peripheral tissues (Mo et al., 2018). PD-L1 major role is to limit T cells activity in peripheral tissues. PD-L1 binding to its cognate receptor PD-1 expressed on T cells induces the recruitment of a tyrosine phosphatase 2 (SHP2), which dephosphorylates the proximal TCR signaling molecules (Yokosuka et al., 2012) and CD28-associated molecules (Hui et al., 2017) thereby leading to T cells anergy or exhaustion in peripheral tissues. In addition to CTLA-4 and PD-L1, other immune checkpoints have been described. For instance, tumor-specific CTLs co-express PD-1 and T-cell immunoglobulin and mucin-domain containing-3 (TIM-3) (Fourcade et al., 2010). TIM-3 binding to galectin-9 expressed by TCs triggers intracellular calcium flux and CTLs death (Zhu et al., 2005). Besides TIM-3, PD-1^{+} CTLs also upregulate Lymphocyte-activation gene 3 (LAG-3). LAG-3 binding to fibrinogen-like protein 1 expressed by TCs disrupts co-receptor CD4/CD8 interactions with Lck tyrosine kinase by local pH acidification and Zn^{2+} cations sequestration thereby limiting downstream TCR signaling and T cells functions (Guy et al., 2022).

1.3.3. Immunosuppressive microenvironment

Other studies underline that TCs overproduce immunosuppressive factors, such as TGFβ (Gorelik and Flavell, 2001), galectin-1 (Rubinstein et al., 2004), galectin-3 (Wang et al., 2014), indoleamine-pyrrole 2,3-dioxygenase (IDO) (Uyttenhove et al., 2003), IL-10 (Sharma et al., 1999) and prostaglandin E_2 (PGE_2) (Zelenay et al., 2015). These immunosuppressive factors further promote tumor immune escape by the recruitment and activation of immunosuppressive immune cells such as myeloid-derived suppressor cells (Gallina et al., 2006), regulatory T (T_{reg}) cells (Sutmuller et al.,

2001) as well as pro-tumoral M2 macrophages (Mantovani et al., 2017) and pro-tumoral N2 neutrophils (Fridlender et al., 2009). In turn, these cells maintain an immunosuppressive TME via additionally secreting TGFβ, IL-10, arginase-1 (Norian et al., 2009), and IDO. Altogether, the establishment of a strongly immunosuppressive TME triggers the rapid functional impairment of immune cells after their infiltration. Tumor-infiltrating NK cells display an enrichment of a $CD56^{Bright}$ $Perforin^{Low}$ non-cytotoxic subpopulation (Carrega et al., 2014) that also expresses higher inhibitory receptors levels (De Andrade et al., 2019). Immunosuppressive TME also hinders adaptive immune response either by inducing a dysfunctional DCs phenotype that prevents CTLs proper polarization (Bayerl et al., 2023; Wang et al., 2004) or by inhibiting CTL-induced TCs lysis directly (Liu et al., 2003; Munn et al., 2005).

1.3.4. Resistance to apoptosis

Besides becoming “invisible” to immune cells, TCs also develop resistance mechanisms to immune-mediated apoptosis. During immune selection, TCs variants downregulating (Strand et al., 1996) or presenting truncated form (Cascino et al., 1996; Shin et al., 2001) of the death receptors FasR and TRAIL-R may arise. Resistant TCs variants are also able to produce soluble form of the FasR that competitively inhibit FasL/FasR signaling (Cheng et al., 1994; Ugurel et al., 2001). In addition to modulating death receptors expression, TCs can also express caspase 8-inhibitory proteins that hinder the death-inducing signaling complex triggered by death receptors signaling (Irmler et al., 1997; Tepper and Seldin, 1999) or serine protease inhibitor PI-9/SPI-6, which inhibits granzyme B pro-apoptotic activity (Medema et al., 2001).

2. Leveraging immunotherapy with nanomedicine

Tumor-induced immunosuppression is a decade long black box for efficient and durable anti-tumoral responses. Efforts to tackle intra-tumoral immunosuppression led to the emergence of cancer immunotherapies approaches aiming at restoring an efficient immune response. Several antibodies targeting TAAs to trigger an ADCC response (*e.g.*, trastuzumab, anti-HER2) reached the clinics (Slamon et al., 2001). More recently, antibodies targeting immune checkpoints (*e.g.*, ipilimumab, anti-CTLA-4 or atezolizumab, anti-PD-L1) have been developed and used to treat melanoma (Hodi et al., 2010) or non-small-cell lung cancer (Herbst et al., 2020). Yet only 15-30% patients respond to immunotherapies (Vogel et al., 2002; Yarchoan et al., 2017) and their administration can induce grade-3 or grade-4 immune related adverse events (*e.g.*, myocarditis, maculopapular rash or colitis) (Berner et al., 2019; Johnson et al., 2016). Therefore, improving cancer immunotherapy efficacy and safety remains a priority.

One of the most promising solution lies in the utilization of nanoimmunotherapy approaches that combine the drug loading capacities of NPs and the selective targeting abilities of antibodies. In the following review we discussed how nanoimmunotherapy would allow to selectively deliver immunomodulatory molecules to immune cells, thereby activating *in vivo* the immune system to foster anti-tumoral responses through a tightly controlled spatiotemporal immunomodulation.

Nota bene: The reader should note that no nanoimmunotherapy targeting NK cells had been developed at the time we wrote this review. Recently, a NKp46-targeted lipid NPs encapsulating siRNA was described to efficiently target NK cells and silence inhibitory checkpoint signaling molecules *in vivo* (Biber et al., 2022; Sabag et al., 2024), reinvigorating their immune response. Another study managed to reactivate NK cells anti-tumoral response by using NPs coated with anti-NKG2A/anti-TIGIT antibodies (Ye et al., 2024).

ADVANCED THERAPEUTICS
www.advtherap.com

Leveraging Immunotherapy with Nanomedicine

*Vincent Mittelheisser, Mainak Banerjee, Xavier Pivot, Loïc J. Charbonnière, Jacky Goetz, and Alexandre Detappe**

Considerable progress has been made in the development and understanding of immunotherapy, notably with the emergence of novel chimeric antigen receptor T cells (CAR-T) which changed the perception of personalized therapy. However, cell-based immunotherapy not only lacks therapeutic efficiency in various solid cancers but also raises concerns related to important side effects. The convergence of immunotherapy and nanomedicine is timely as nanoparticles can now be easily conjugated to various antibodies and peptides enabling outstanding abilities to target specific cell populations in vivo. Here, the state of the art of immunonanotherapy that activates the immune system in vivo, by acting either as vaccines or as tumor microenvironment (TME) activators is described. Then, the development of ex vivo immune-cell surface labeling strategies is discussed to exploit immune cells as trojan horses and thereby improving the delivery of the therapeutics in the TME. Such a strategy is likely to considerably amplify the efficacy of immunotherapy.

1. Introduction

Cancer immunotherapies lead to specific and durable anticancer responses, overcoming traditional cancer treatment limitations. Successful immunotherapy approach aims to restore an immune response by either stimulating or suppressing the immune system.[1,2] Thanks to the recent advancement of novel monoclonal antibodies (mAbs) and immune cell-based therapies, the field of immunotherapy has oriented our perception of medicine toward a personalized approach.

Hence, different therapeutic modalities have been evaluated clinically to improve cancer immunotherapy by harnessing the immune system. These include, among others, the use of mAbs blocking pro-angiogenic factors or immune checkpoints inhibitors (e.g., NCT01274338, NCT02252042, NCT02125461). Targeting immune-checkpoints proteins with anti-cytotoxic T lymphocyte-associated antigen-4 (CTLA-4) and anti-programmed cell death receptor-1 (PD-1) antibodies demonstrated outstanding results when compared to cytotoxic chemotherapies or to targeted therapies.[3,4] Although results remain modest in the majority of solid cancers, immune checkpoints inhibitors have become a standard of care in some advanced setting (e.g., melanoma, nonsmall-cell lung carcinoma, basal breast cancer, head and neck cancer, etc.).[5,6] These moderate effects could be partly explained because solid tumors exhibit low immunogenicity together with primary or acquired mechanisms of resistance.[7–10] In addition, the safety profile of immunotherapy remains a challenge to overcome (e.g., cytokine release syndrome).[11,12] Currently, administration of immunotherapeutic agents is limited by the induction of systemic autoimmunity (e.g., myocarditis, colitis, etc.), and grade-3 or grade-4 adverse events such as gastrointestinal, renal, or pulmonary toxicities.[13,14] As such, a paramount need in improving efficacy as well as safety in cancer immunotherapy remains.

The use of cell-based therapies has recently emerged (e.g., dendritic cell (DC)-based vaccines, chimeric antigen receptor (CAR) T and CAR NK cells, etc.) and led to promising results in several clinical trials (e.g., NCT03274219, NCT02498912, NCT02408016, NCT02311621, etc.).[15–18] DC-based vaccines use nanoparticles (NPs) to pulse cancer cell lysates, DNA, or mRNA into DCs to prime tumor-specific T cells[19,20] while CAR T and CAR NK cells act in a HLA-independent mechanism without requiring antigen presentation.[21] These recent approaches

V. Mittelheisser, Dr. M. Banerjee, Dr. A. Detappe
Centre Paul Strauss
Strasbourg 67000, France
E-mail: a.detappe@ICANS.eu
V. Mittelheisser, Dr. J. Goetz
INSERM UMR_S1109
Strasbourg 67000, France
V. Mittelheisser, Dr. L. J. Charbonnière, Dr. J. Goetz, Dr. A. Detappe
Université de Strasbourg
Strasbourg 67000, France
V. Mittelheisser, Dr. J. Goetz
Fédération de Médecine Translationnelle de Strasbourg (FMTS)
Strasbourg 67000, France
Dr. M. Banerjee, Prof. X. Pivot, Dr. A. Detappe
Institut de Cancérologie Strasbourg Europe
Strasbourg 67000, France
Dr. M. Banerjee, Dr. L. J. Charbonnière, Dr. A. Detappe
Institut Pluridisciplinaire Hubert Curien
CNRS UMR-7178
Strasbourg 67087, France

The ORCID identification number(s) for the author(s) of this article can be found under https://doi.org/10.1002/adtp.202000134

© 2020 The Authors. Published by Wiley-VCH GmbH. This is an open access article under the terms of the Creative Commons Attribution License, which permits use, distribution and reproduction in any medium, provided the original work is properly cited.

DOI: 10.1002/adtp.202000134

allow to overcome the low immunogenicity of tumors that might hinder the tumor-associated antigen presentation, and thus the cytotoxic response. However, the response remains heterogenous throughout the population.[19,22] Transition of DCs and engineered immune cells into an in vivo immunosuppressive environment may alter their viability and functionality and thus jeopardize their ability to induce an antitumor immune response. Cancer cells can also undergo antigenic modulation (i.e., antigen loss or downregulation) that enables immune escape.[22] Moreover, the efficiency of these patient-derived cell-based therapies is strongly dependent on the patient's immune system exhaustion level when the cells are harvested.[23] Finally, such therapies have limited efficacy in patients with solid tumors.[22]

Nanomedicine was originally developed to improve the therapeutic index of small molecules by decreasing their side effects or improve the specificity of the drug delivery into the tumor.[24,25] Once injected in the bloodstream, the NPs were designed to passively accumulate in the tumor by using the leaky vasculature produced by the rapid tumor neoangiogenesis and impaired lymphatic vessels (also called enhanced permeability and retention (EPR) effect).[26] However, this passive targeting method recently raised some concerns because of the limited amount of NPs reaching the tumor cells.[27] For this reason, improving the targeted delivery of NPs to the tumor remains a challenge.

Liposomal NPs were the first generation of drug carriers. Although drugs encapsulation into liposomes improve their pharmacokinetic and biodistribution in comparison to free drugs, no marketed liposomal therapeutic agents have yet demonstrated a significant increase in overall survival versus the standard agent.[28] Further liposome PEGylation allows a decreased plasma clearance and results in a longer retention time in the bloodstream.[29,30] Nevertheless, improved safety profiles justified PEG-liposomal NPs routine use in tumors where the original active ingredient has failed to provide results (e.g., liposomal doxorubicin in ovarian cancer: DOXIL, CAELYX). Liposomal deliveries are however seriously limited by their loading capacities, their stability, and their uncontrolled drug delivery abilities (i.e., dose dumping).

Second NP generation based on micelles and NPs obtained from synthetic polymers (e.g., poly(d,l-lactic-*co*-glycolic acid)-*b*-poly(ethylene glycol); PLGA-PEG, organic-based NPs, dendrimers, etc.) has been developed for several biomedical applications such as drug delivery or medical imaging.[31–34] These long-circulating polymeric NPs demonstrated an improved therapeutic index in comparison to small molecules, but their use in the clinic remains limited, notably because of their high liver internalization and remaining toxicity concerns.[35]

More recently, theranostic NPs (i.e., carrying both imaging and therapeutic agents) have emerged. Their conjugation with near-infrared fluorescent dyes, magnetic resonance imaging tracers, or positron emission tomography contrast agents allows to track the NPs through noninvasive and whole-body imaging and thus facilitates triggered drug delivery to tumor site.[36,37] This application is only at its beginning and multiple clinical trials are currently ongoing.[38,39] Altogether, the different generations of NPs aim to improve the therapeutic window of free drugs by either reducing the toxicity, increasing the total amount of small molecules delivered to the tumor, or enabling the delivery of highly toxic molecules.[40–42] In vivo tracking of NPs further provides an additional level of understanding and can even better improve their therapeutic benefit with personalized therapy.[43–45] However, despite the advancements of nanotechnology over the last decade, a retrospective analysis demonstrated that no more than 0.9% of the injected dose reach the tumor cells on average.[27] The EPR effect was questioned as to be the best route of delivery in patients. Indeed, its effect varies significantly between both patients and tumor types (and vascularization), with some differences within the same patient or tumor type over tumor progression.[46,47] These findings also questioned the use of the appropriate animal model to better assess the NP efficacy.[48] Additionally, alternatively to the known EPR effect used for the passive targeting delivery of NPs, a recent study demonstrated that NPs tend to actually predominantly enter the tumors through active transcytosis process through endothelial cells rather than using the neovasculature gaps.[49] A deeper mechanistic understanding of its delivery mechanism could help in designing NPs with improved accumulation in the tumors. Despite all the questioning regarding the passive uptake mechanisms, some NPs still confirm their effective tumor internalization in patients through passive targeting delivery.[50,51]

To overcome the low yield of NPs reaching the tumor, some routes have been investigated (**Figure 1**A); i) the tumor blood vessel normalization approach consists in using antiangiogenic agents to transiently normalize the tumor neovascularization to decrease the tumor hypoxia and to increase the efficacy of conventional therapies by increasing the total amount of NPs (smaller than 12 nm) or small molecules to be delivered.[52–54] ii) More recently, the use of an external trigger combined with NPs has been investigated. This trigger could be ultrasounds,[55–57] photothermal therapy,[57–59] photodynamic therapy,[57,60,61] or even radiation therapy.[62,63] Most often, the approach consists in targeting the tumor blood vessel using an $\alpha v\beta 3$ peptide to disrupt the neovessels with the external trigger in order to improve the delivery of the drug in a second time (Figure 1B). iii) An alternative approach consisting in priming the liver with "blanked" liposomal NPs prone to be highly accumulated this organ. A second injection consisting in the therapeutic compound is then administrated and avoid liver retention, resulting in an increased accumulation of NPs or small molecules to be delivered at the tumor[64,65] (Figure 1C). Altogether, these novel passive targeting methods seem to alleviate the NPs tumor uptake and/or improve the drug delivery.

In parallel, novels strategies have been studies to deliver the therapeutic agent to the cancer cells (**Table 1**). This is achieved through the design of therapeutic vaccines, or the conjugation of peptides and monoclonal, bispecific, or trispecific antibodies[66,67] to activate immune cells (both circulating and within the tumor microenvironment). While active targeting based on the use of peptides, or antibodies, conjugated at the surface of the NPs was first employed to improve the NP tumor uptake, such strategy only improved the delivery specificity of NPs to the tumor cells without improving the total amount of tumor internalization.[68–70] As such, utilizing nanomedicine to specifically target immune cells could hence improve the efficiency of immunotherapies or at least, to decrease their toxicities.

In this review, we will discuss how nanomedicine could foster the benefit of immune cell-based therapy and overcome the usual therapeutic-limiting secondary effects by either i) activating

© 2020 The Authors. Published by Wiley-VCH GmbH

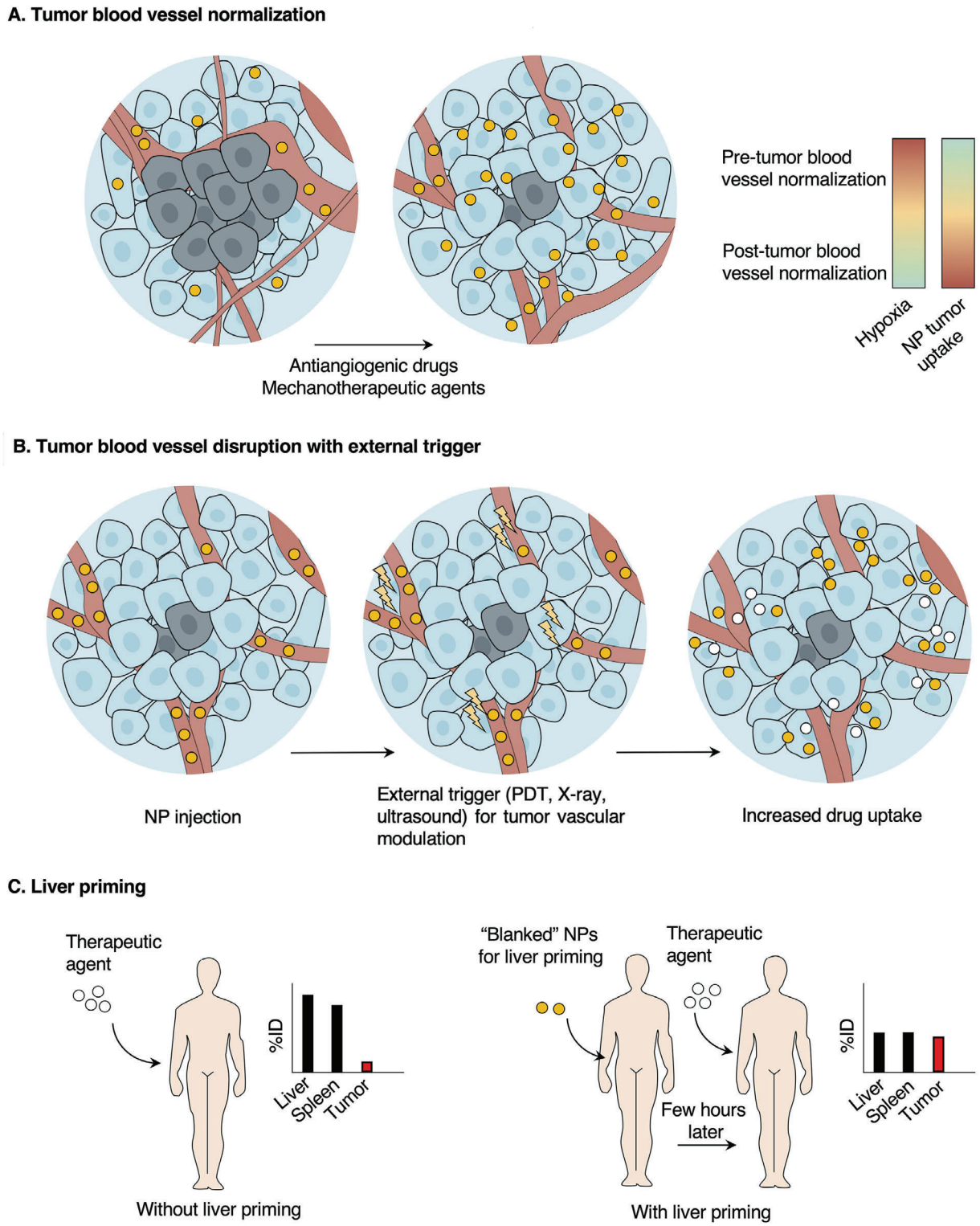

Figure 1. Improving the passive targeting strategy. A) Tumor blood vessel normalization consists of using antiangiogenic drugs or mechanotherapeutic agents in order to decrease tumor hypoxia levels but also in normalizing the sizes of the endothelial gaps. Below 12 nm diameter size, the NPs can benefit from this approach to increase their tumor uptake.[52–54] B) Tumor blood vessel disruption by an external element (e.g., radiation, UV, ultrasound) can dramatically improve NP uptake and drug delivery.[50–58] C) The liver priming consists in injecting blanked liposomes known into the liver followed by the therapeutics an hour later to override the hepatic metabolism and hence increase their circulation time in the body, resulting in an improved uptake in the tumor.[64,65]

© 2020 The Authors. Published by Wiley-VCH GmbH

Table 1. Systematic review of cancer type, animal models, and NP types used for immunonanotherapeutic preclinical studies.

Nanotherapeutic approach	Cancer type (injection site)	Animal models	NP types[a)]	Targeting	Complex size	Injection route[a)]	Ref.
Myeloid cells activation	Xenograft MC38 colon cancer	C57BL/6	Cyclodextrin	Optimized size for phagocytosis	30 nm	i.v.	[76]
	Orthotopic KP1.9 lung cancer						
	Xenograft B16.F10 melanoma						
	Orthotopic 4T1 mammary cancer	C57BL/6	Glucan (BG34-10 kDa)	Glucan-decorated	17 nm	i.t.	[79]
		BALB/c					
	Orthotopic ID8 ovarian cancer	C57BL/6	PLGA	Mannose-decorated	100 nm	i.v.	[80]
	Orthotopic B16.F10 melanoma						
	PDGFβ-driven glioma	PDG mice					
	Xenograft 4T1 mammary cancer	BALB/c	Albumin	G-CSF-decorated	67 nm	i.v.	[84]
	Xenograft B16.F10 melanoma	C57BL/6	PEG-Lipidic	Anti-CD47/anti-SIRPα-functionalized	70 nm	i.v./i.t.	[90]
T cells activation	Xenograft MC38 colon cancer	C57BL/6	PLGA-PEG	Anti-CD8-functionalized	273 nm	i.v.	[94]
	Xenograft B16.F10 melanoma	C57BL/6	PEGylated liposome	Anti-CD40-functionalized	148 nm	i.t.	[102]
	Xenograft B16.F10 melanoma	BALB/c		Anti-CD137/IL-2Fc-functionalized	160 nm	i.t.	[103]
	Xenograft A20 lymphoma	C57BL/6					
	Xenograft TC-1 lung cancer						
	Xenograft B16.F10 melanoma	C57BL/6	Iron-dextran	Anti-4-1BB/anti-PD-L1-functionalized	80 nm	i.v.	[104]
	Orthotopic 4T1 mammary cancer	BALB/c	PLGA-PEG	Anti-OX40/anti-PD-1-functionalized	167 nm	i.v.	[105]
Artificial APCs	Xenograft E.G7-OVA lymphoma	C57BL/6	Polymer	Optimized size for lymph node targeting	30 nm	i.d.	[117]
	Xenograft B16.F10 melanoma						
TAA and adjuvants codelivery	OVA immunization (*s.c.*)	C57BL/6	PEGylated multilamellar liposome	None	263 nm	s.c.	[119]
	OVA immunization (*s.c.*)	C57BL/6	Polymer	Optimized size for lymph node targeting	25 nm	s.c.	[121]
Recruitment of neoantigens post-radiotherapy	Xenograft B16.F10 melanoma	C57BL/6	Polymer	Optimized size for lymph node targeting	30 nm	i.t.	[128]
	Xenograft B16.F10 melanoma	C57BL/6	PLGA	None	100 nm	i.t.	[141]
	Orthotopic 4T1 mammary cancer						
T cells backpacking	Xenograft B16.F10 melanoma	C57BL/6	PEGylated multilamellar liposome	T cells tumor homing properties	200 nm	i.v.	[170]
	Xenograft EL4 lymphoma						
	Orthotopic Eμ-myc $Arf^{-/-}$ cells				136 nm	i.v.	[93]
	Xenograft B16.F10 melanoma	C57BL/6	PEG-PLL		90 nm	i.v.	[172]

[a)] PLGA-PEG, poly(d,l-lactic-*co*-glycolic acid)-*b*-poly(ethylene glycol); PEG-PLL, poly(ethylene glycol)-*b*-poly(L-lysine); i.v., intravenous; i.t., intratumoral; i.d., intradermal; s.c., subcutaneous.

in vivo the immune system to turn poorly immunogenic tumors into inflamed tumors or ii) by modifying ex vivo the immune cells behavior before infusion to enable targeted drug delivery as well as immune activation in the tumor site.

2. Nanomedicine to Improve Immunotherapy

Rather than trying to target directly the tumor, and because of the low tumor uptake of NPs, novel strategies to specifically target circulating immune cells have emerged. The advantage of this approach is based on the fact that, once activated, the immune cells will propagate the message to turn the tumor into a "hot tumor" and will recruit more native resting immune cells, resulting in a potent immunotherapeutic response. Immune cells targeting can be performed by conjugating peptides, antibodies, or ligands at the surface of the NPs (**Figure 2**). It was demonstrated that the biodistribution and pharmacokinetics of ultrasmall NPs (< 5 nm diameter) are dictated by their ligand decoration, increasing their circulation time in the body and

© 2020 The Authors. Published by Wiley-VCH GmbH

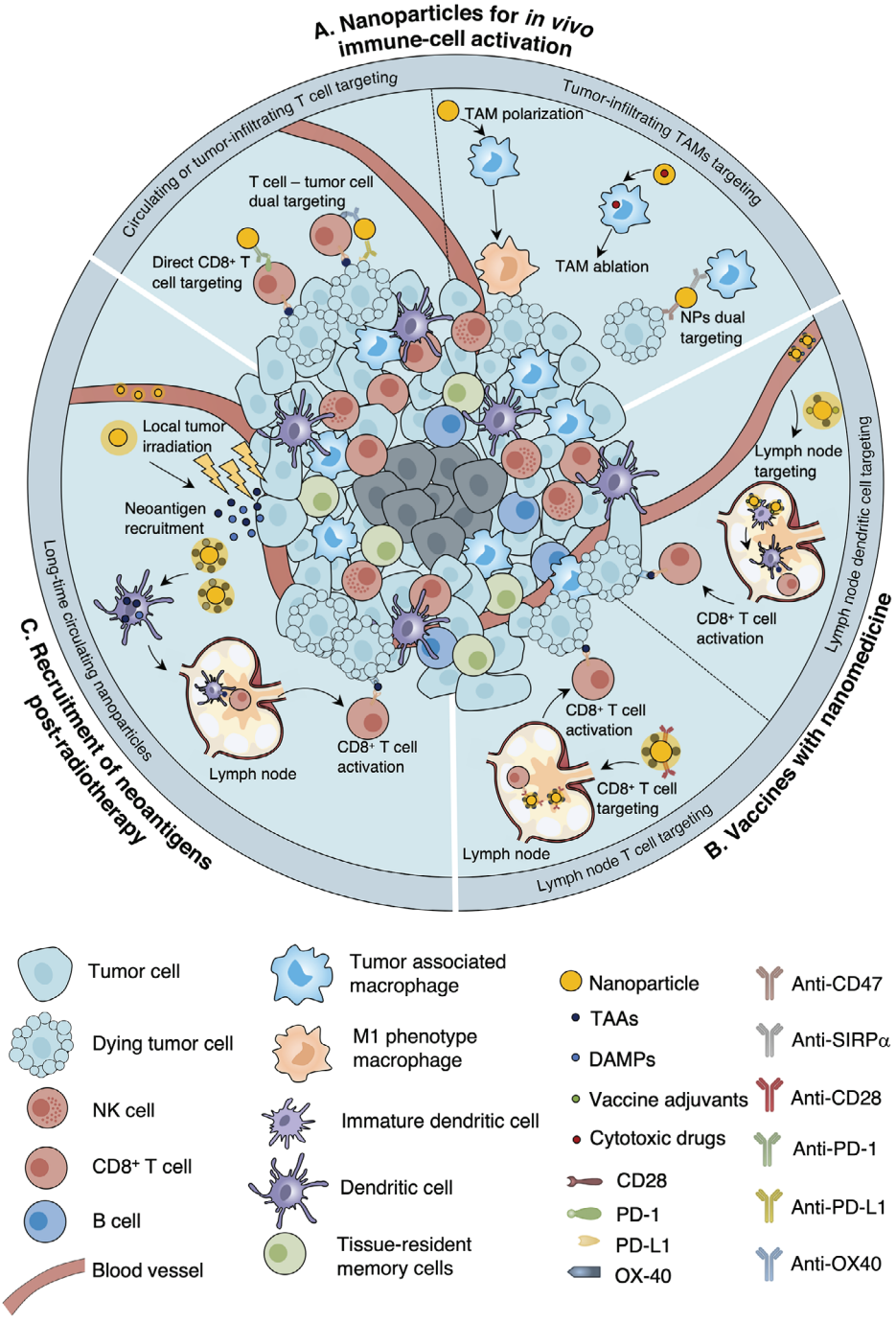

Figure 2. Nanomedicine to improve immunotherapy. A) NPs can be used for lymphocytes activation by targeting either the T- or NK cells or both immune and tumor cells. NPs can be used to target other immune cells present in the tumor microenvironment such as TAMs. They can either i) polarize TAMs toward a more antitumor M1 phenotype with mRNA, siRNA, or TLR agonists. ii) Ablate them with cytotoxic drug delivery or iii) co-target TAMs and tumor cells to promote their phagocytosis. This activation can potentiate the delivery of small molecules that tackle the immunosuppressive tumor microenvironment.[76–83,90],[93–96] B) NPs can also be used as artificial antigen presenting cells to directly activate $CD8^+$ T cells in the lymph node (lower panel)[115–118] or to co-deliver tumor-associated antigens (TAAs) and adjuvants (e.g., CpG, Poly(I:C)) (upper panel).[119–121] C) Radiotherapy leads to high TAAs and DAMPs release in tumor microenvironment captured by antigen-capturing NPs.[141] These NPs are uptake by dendritic cells that migrate to the lymph nodes to activate $CD8^+$ T cells activation.

© 2020 The Authors. Published by Wiley-VCH GmbH

hence improving tumor cells accumulation.[71] However, because of their size, a high drug loading is difficult to achieve, orienting their use mostly for medical imaging applications.[33,34,71] At the opposite, the biodistribution and pharmacokinetics properties of large NPs (> 50 nm diameter) are dictated by the NP, resulting in a large accumulation in the liver and lymph nodes.[72,73] This preferential accumulation into lymphatic vessels and lymph nodes is of interest to target immune cells for vaccination approach or for neoantigen recruitment after radiotherapy.[73,74]

3. NPs for In Vivo Immune Cells Activation

In vivo activation of immune cells remains the main goal of immunotherapy. While activating T cells or tumor-associated macrophages (TAMs) has resulted in great therapeutic responses, the co-stimulation of several immune cells simultaneously is a goal not yet fully achieved.

3.1. Circulating and Tumor-Infiltrating Myeloid Cells

Myeloid cells such as TAMs or immature myeloid-derived suppressor cells (MDSCs) play an important role in initiating the immunosuppressive environment that strongly suppresses the function of cytotoxic immune cells, negatively impacting the immunotherapy efficacy.[75] NPs-based therapies can either polarize TAMs toward a more antitumor M1 phenotype (i.e., producing pro-inflammatory cytokines such as TNF-α, IL-12, or nitric oxide) or completely neutralize or kill them (Figure 2A). A prominent approach to reprogram TAM toward an M1 antitumor phenotype is to deliver Toll-like receptor (TLR) agonists. R848, a TLR7/8 agonist, loaded in β-cyclodextrin (β-CD) NPs potently drive TAM polarization toward the M1 phenotype, leading to efficient tumor growth control in multiple mouse models and synergized anti-PD-1 antibodies effects.[76] Another strategy to reeducate TAM is to interfere with intracellular mRNAs by delivering siRNA, miRNA, or mRNA via mannosylated NPs due to high expression of mannose receptor 1 on TAMs surface.[77–80] Glycan-decorated NPs allow in vivo delivery of specific anti-macrophage migration inhibitory siRNA which results in macrophage polarization toward an antitumor phenotype expressing pro-inflammatory cytokines such as TNF-α and IL-2 which subsequently enhanced T cell infiltration and function at the tumor site.[79] More recently, mannose-modified PLGA-based NPs allow delivery of mRNA encoding the M1-polarizing interferon regulatory factor 5 transcription factor to TAMs, which reverse the immunosuppressive, protumorigenic phenotype of TAMs and reprogram them to an antitumor one inducing immunity and inhibiting tumor growth in models of ovarian cancer, melanoma, and glioblastoma.[80]

Another approach to modulate the tumor immune microenvironment myeloid compartment is to completely neutralize or kill TAMs by delivering them cytotoxic molecules through ligand-decorated NPs that target the TAMs overexpressed receptors (e.g., mannose receptor, folate receptor beta, etc.).[81–83] Similarly, granulocyte-colony stimulating factor (G-CSF) decoration of albumin NPs promotes preferential in vivo accumulation in MDSCs in a 4T1 metastatic triple-negative breast mouse model.[84] This system could provide a cell lineage-specific delivery of indocyanine green, an effective photothermal and photosensitizing agent that can be used for MDSCs ablation in highly immunosuppressed patients.[85,86]

In parallel, cancer cells upregulate CD47 that ligates with SIRPα present on TAMs surface and eventually inhibit their phagocytic functions. Blocking CD47 and/or SIRPα with mAbs showed interesting but limited results notably due to low bioavailability at the tumor site.[87–89] The co-delivery of CD47 and SIRPα sequestrated on a multivalent lipid-based phagocytosis nanoenhancer enables simultaneous engagement of TAMs and cancer cells at significantly lower concentrations of antibodies than the ones used in recent studies (2 mg kg^{-1} vs 5 mg kg^{-1})[90] (Figure 2A). TAMs activation allows intratumoral infiltration of effector T cells and NK cells, leading to significantly enhanced tumor growth inhibition as well as increased survival in B16F10 melanoma tumor-bearing mice.

However, widespread expression of some receptors led to readily uptake of these targeted drug delivery systems by normal macrophages, mononuclear phagocyte system, or even liver sinusoidal endothelial cells.[91,92]

3.2. Circulating and Tumor-Infiltrating T Cells

In order to override the abovementioned limitations, NPs-based approaches have been designed to leverage T cells as drug carriers and demonstrated greater drug levels in the tumor than ones delivered by NPs alone[93–96] (Figure 2A). This could notably be explained by the ability of the T cells to freely circulate in the body, and hence being used as trojan horse for the NPs to avoid macrophages and direct liver accumulation after their first pass in blood system.[97] In one approach, immunoliposomes decorated with engineered interleukin-2 (IL-2) molecule on an Fc framework or an antibody $F(ab')_2$ fragment against a congenic cell surface receptor were used to effectively target in vivo adoptively transferred T cells (> 95%). Using $F(ab')_2$ fragments to decorate NPs demonstrated high target specificity and avidity along with little interactions with Fc receptors expressed by the mononuclear phagocyte system, which is a major way of NPs clearance.[98] Conjugation of immunoliposomes to the surface of exogenous T cells induced repeated waves of cells expansion, improving their potency.[95,96] Nevertheless, cell-bound NPs become diluted over cell proliferation, and adoptive cell transfer (ACT) remains a cumbersome and costly procedure. In another approach, PLGA NPs were used to encapsulate either SD-208, a TGFβR1 inhibitor, to restore T cells function, or a TLR7/TLR8 agonist to recruit lymphocytes to non-inflammed tumors.[94] PLGA NPs were decorated by anti-PD-1 antibody $F(ab')_2$ fragments via thiol-maleimide minute-process, such that the NPs bound ≈5% of the circulating and tumor-infiltrating $CD8^+$ $PD1^+$ T cells.[94,99] Targeted delivery of a TGFβR1 inhibitor led to extended survival in a mouse model of colorectal cancer compared with free drugs at similar dosages, while TLR7/TLR8 agonist increased the proportion of tumor-infiltrating $CD8^+$ T cells and sensitized tumors to anti-PD-1 therapy when compared to NPs lacking the targeting moiety or equivalent doses of the free drugs.[94]

With the recent development and clinical demonstration of the efficiency of bispecific antibodies, or at the preclinical level with tri-specific antibodies, these approaches demonstrated tremendous results. While these antibodies have already been

© 2020 The Authors. Published by Wiley-VCH GmbH

conjugated to drugs to form antibody-drug conjugates, they could now be used to ease NPs decoration for multiple targeting. Interestingly, based on a click-chemistry approach, generating dual-targeted NPs or tri-specific NPs is a minute-process,[100,101] allowing to quickly evaluate novel targeting conjugations. NPs platform combining immune checkpoint blockade agents along with co-stimulatory signals have been developed to overcome the autoimmune-mediated dose-limiting toxicities of free mAbs.[14] These dual targeting systems redirect effector T cells to recognize cancer cells while simultaneously blocking checkpoint inhibitors.[102–105] Various NPs types (e.g., liposome, PEG-PLGA, etc.) have been decorated with different T cells agonists (e.g., anti-4-1BB mAb, anti-OX40 mAb, etc.) and immune checkpoint blockade agents (e.g., anti-PD-L1 mAb, anti-PD-1 mAb, etc.). These approaches resulted in a marketed therapeutic activity as demonstrated by tumor regression, tumor-specific T cells expansion, and immune responses in B16 melanoma and 4T1 breast cancer models.[102–105]

Targeting NPs-based immunotherapies to blood circulating and tumor-infiltrating immune cells rather than tumor cells directly allows efficient in vivo activation of immune cells with limited doses administration, and thus lowers immune-mediated adverse events occurrence. These NPs-based immunotherapeutic approaches can also be used to target immune cells in the lymph node as cancer vaccination tool that elicits a potent antitumor immune response.

4. Vaccines with Nanomedicine

The antitumor vaccines directed against tumor-associated antigens (TAAs) or tumor-specific antigens were among the first immunotherapeutic agents developed since the late 1980s.[106,107] Cancer cell lysates, DNA, or mRNA are pulsed into dendritic cells (e.g., FDA-approved Sipuleucel-T, PROVENGE for prostate cancer) to activate T cells by presenting them the tumor antigen, leading to a cytotoxic T cells (CTL) response.[108,109] Because DCs can be inhibited by the cancer cells or the tumor microenvironment, and because the antitumor vaccines are difficult to standardize due to their requirement of highly immunogenic antigen as well as potent adjuvant, this strategy shows decreased potency to eradicate tumors.[107,110] Newly developed nanoengineered vaccines demonstrated better efficacy in cancer treatment over former antitumor vaccines which come with major limitations such as poor immunogenicity and off-target side effects.[111–113]

The size of the nanomaterial has a detrimental effect in therapeutic outcome in cancer vaccination. NPs sizes ranging from 10 to 100 nm in diameter and negatively charged (−3 to −15 mV) tend to preferentially accumulate into lymphatic vessels and lymph nodes.[73,74] The lymph nodes-targeted NPs behave as artificial antigen presenting cells (APCs) to directly stimulate $CD8^+$ T cells. To achieve their activation, T cells recognized the Ag through their T cell receptor (TCR). This recognition is followed by a co-stimulatory signal procured by the interaction between the CD28 from the T cells and its receptors present at the DC surface (i.e., CD80 or CD86). A third signal mediated through IL-2 can enhance T cells stimulation but is not required for their activation.[114] Artificial APCs are coated with TAA and anti-CD28 antibodies recapitulate both mandatory signals for T cells activations[115–118] (Figure 2B). The other benefit for nanomaterials-based vaccines relies on their ability to co-deliver the TAAs and adjuvants simultaneously, at a controlled ratio, and at the same location (e.g., CpG, Poly(I:C)), improving the ability of APCs to present up taken antigens with MHC-I molecules to $CD8^+$ T cells and enhancing CTL responses[119–121] (Figure 2B). Although nanoengineered vaccines lead to a potent activation of the immune system, delivery through lymphatic draining depends on NPs composition, morphology, and surface chemistry. Alternatively, other NP designs have been sought to target specifically the spleen to activate B lymphocytes[122] or to recruit, through the use of hydrogels, e.g., dendritic cells.[123] These approaches enabled a specific targeting of immune cells without decorating the NPs with conventional peptides or antibodies.

However, it is important to note that whereas small animal models are essential tools for proof-of-concept studies, these preclinical studies often fail to be successfully translated in nonhuman primates and humans.

5. Recruitment of Neoantigens Post-Radiotherapy

Radiation oncology combined with immunotherapy has gained a substantial interest due to its inherent ability to generate an abscopal effect defined as transforming "cold tumor" into "hot tumor" as defined by the total amount of tumor antigen, APC deficit, absence of T cells, and impaired trafficking to the tumor mass post-radiation.[13,124] By irradiating the tumor bed, which includes the tumor microenvironment, the radiation beams generate additional immune response inside the tumor microenvironment. It was demonstrated that the irradiation of the tumor leads to the liberation of TAAs that are endocytosed by APCs and then presented to $CD8^+$ T cells.[125] This process increases the diversity of the TCR repertoire of intra-tumoral T cells and leads to a tumor-specific immune response directed against primary tumor and metastatic tumor sites.[126,127] Unfortunately, the presence of immunosuppressive cells (e.g., MDSCs and T_{reg} cells) producing immunosuppressive cytokines (e.g., IL-10 and TGFβ) in the tumor microenvironment hampers the development of robust and sustained abscopal responses even with combination approaches.[7–9] This combination therapy led only to a limited abscopal effect due to T cells exhaustion mediated by the upregulation of PD-L1 on tumor cells. As such, multiple strategies have been attempted to increase this tumor immunogenicity to boost the abscopal effect. Among them, targeted NPs have been used to deliver potent immunotherapeutic compounds to the tumor microenvironment and tumor draining lymph nodes in order to reverse immunosuppression, as illustrated by the use of CpG oligodeoxynucleotides conjugated to polymer NPs.[128] This compound was developed to activate DCs in the lymph node, resulting in an increased activation of $CD8^+$ T cells/T_{reg} ratio.[128] Activating DCs or tumor-infiltrating immune cells by immune checkpoint inhibitors or TLR agonists potentiates the abscopal effect, leading to delayed tumor growth. However, little is known about potential adverse effects emerging from combining radiotherapy with immune-checkpoint inhibition.[129]

Alternatively, rather than activating the DCs by using targeted NPs, boosting the abscopal effect through the use of radiation therapy enhancer NPs made of high-atomic number atoms (gold, gadolinium, or hafnium NPs, among others) was also evaluated. The radiosensitization properties of these inorganic NPs are

© 2020 The Authors. Published by Wiley-VCH GmbH

attributed to an increase of Auger electrons production via the photoelectric effect leading to an increased amount of reactive oxygen species in the tumor bed.[130–137] Altogether, physical and biological boost effects induced by the presence of metallic inorganic NPs during the radiation treatment increased local DNA damage.[138] The local boost of radiation dose deposition is hypothesized to enable a higher release of TAAs upon tumor cells death that potentiate the abscopal response through an increased tumor immunogenicity.[139,140] Toward these findings, the development of antigen-capturing NPs (AC-NPs) to exploit the release of TAAs upon radiotherapy in order to boost the abscopal effect was also performed[141] (Figure 2C). By formulating polymeric PLGA NPs with diverse surface modifications (decoration with 1,2-dioleoyloxy-3-(trimethylammonium)propane, DOTAP; maleimide, NH_2; mPEG; or unmodified PLGA) to determine the effects of NP surface chemistry on antigen capture efficiency, it was demonstrated that NPs allow to capture efficiently tumor neoantigens post-radiation.[142] Interestingly, these AC-NPs also captured a number of damage-associated molecular pattern proteins (DAMPs) that potentiated the immune response by being efficiently internalized by APCs and trafficked to lymphoid tissues. In a B16F10 melanoma bilateral tumor model, they showed that intratumoral injection of NPs in one tumor significantly improved the efficacy of anti-PD-1 antibodies and enhanced abscopal responses, generating a 20% cure rate compared to 0% without any NPs. The mechanistic studies revealed that AC-NPs induced an expansion of $CD8^+$ cytotoxic T cells and increased both $CD4^+$ T cells/T_{reg} and $CD8^+$ T cells/T_{reg} ratios.

Although harnessing the immune system to enhance the abscopal effect demonstrated promising results, these approaches are still at their stammering. However, to elicit a potent abscopal effect, most of these studies require an intratumoral injection of the NPs into the tumor bed to achieve a concentration leading to these therapeutic effects. While this approach is easy to be translated for melanoma and some specific cancers (head and neck, e.g.), this administration route could limit their clinical translation in the vast majority of irradiated cancers. There is a great impetus for more cross-disciplinary research combining radiotherapy and immunotherapy with NPs in boosting the abscopal effect, thereby improving the treatment of both local and metastatic disease.

6. Immune Cells-Based Therapy with Ex Vivo Nanomedicine Labeling

Alongside with immune checkpoints blockade, adoptively transferred autologous T cells have shown tremendous therapeutics effects. Patients-isolated T or NK cells can be genetically engineered to express a CAR that recognizes tumor cells in an HLA-independent mechanism without requiring antigen presentation.[21] These CAR T cells, CAR NK cells, or more recently CAR macrophages showed impressive results in treating acute lymphoblastic leukemia, refractory large B cell lymphomas, or multiple myelomas.[15–17,143] However, CAR cells remain costly, time consuming, and only allow the addition of a single targeting moiety at the time.[144] Moreover, the overall response to these therapies remains heterogenous and CAR immune cells have shown only moderate successes in treating solid cancers.[22] Once infused into patients, adoptively transferred cells migrate to the tumor sites and require a sustained supply of oxygen, nutrients, and cytokines to support their viability, functions, and proliferation. Moreover, cells have to overcome the immunosuppressive tumor microenvironment.[8,9] To promote their antitumoral actions, adjuvant cytokines and immune-checkpoint blockade agents can be administered.[145–147] However, systemic administration of such drugs requires repeated injection to maintain therapeutic levels resulting in dose-limiting toxicities.[148,149] In order to overcome the aforementioned limitations and enhance ACT potency, cell surface bioengineering strategies have been developed.[150] Immune cells are an attractive option for cell surface bioengineering because of their natural abilities to circulate in the bloodstream and pass challenging biological barriers before to accumulate into the tumor microenvironment.

7. Cell Surface Conjugation Routes

Cell surface conjugation strategies have to satisfy the following biocompatibility fundamental principles: i) any cell surface modifications should not have detrimental effects either on cell viability or cellular functions. ii) Bioengineering should further minimize alterations in membrane fluidity or bending elasticity that are critical for cell adhesion, migration, and signaling. iii) Moreover, surface-engineered immune cells are exposed to in vivo shear stress and hemodynamic forces that can dissociate the NPs from the cell surface. Thus, the introduced modifications have to be compatible with the in vivo complex mechanical and biochemical interactions. iv) Finally, they should also not lead to the apparition of severe adverse effects such as thrombus formation after infusion.[151]

As such, to design novel and smarter immune cells, diverse bioengineering methodologies have been investigated. They can be subdivided in noncovalent physical biointeraction and covalent chemical conjugation (**Figure 3**).

7.1. Non-covalent Non-specific Biointeractions

Non-covalent conjugation of NPs can be achieved using non-specific (e.g., hydrophobic, electrostatic, etc.) interactions or specific ligand–receptors ones[150] (Figure 3A). Since the plasma membrane is composed of a hydrophobic lipid bilayer, NPs conjugated with hydrophobic moieties such as glycoinositol phospholipids (GPIs) can spontaneously be anchored into the membrane.[152,153] Besides being hydrophobic, the plasma membrane is also negatively charged, as a result of phosphate groups of phospholipids, carboxylate groups on proteins, and sialic acid termination of glycoproteins.[154] Thus, NPs harboring many cationic sites can bind to cell surfaces via electrostatic interactions. Nevertheless, non-covalent non-specific conjugations have intrinsic tremendous drawbacks. Indeed, GPI-anchored NPs recapitulate natural membrane-associated molecules turnover rates and are thus rapidly internalized ($t_{1/2}$ between 3.8 and 20 h).[155,156] Moreover, the electrostatic interactions between the negatively charged plasma membrane and the NPs positive surface can trigger local membrane depolarization and lead to cellular uptake.[157] As such, non-specific non-covalent interactions are a rapid and easy route of conjugation but yet suffer from in

© 2020 The Authors. Published by Wiley-VCH GmbH

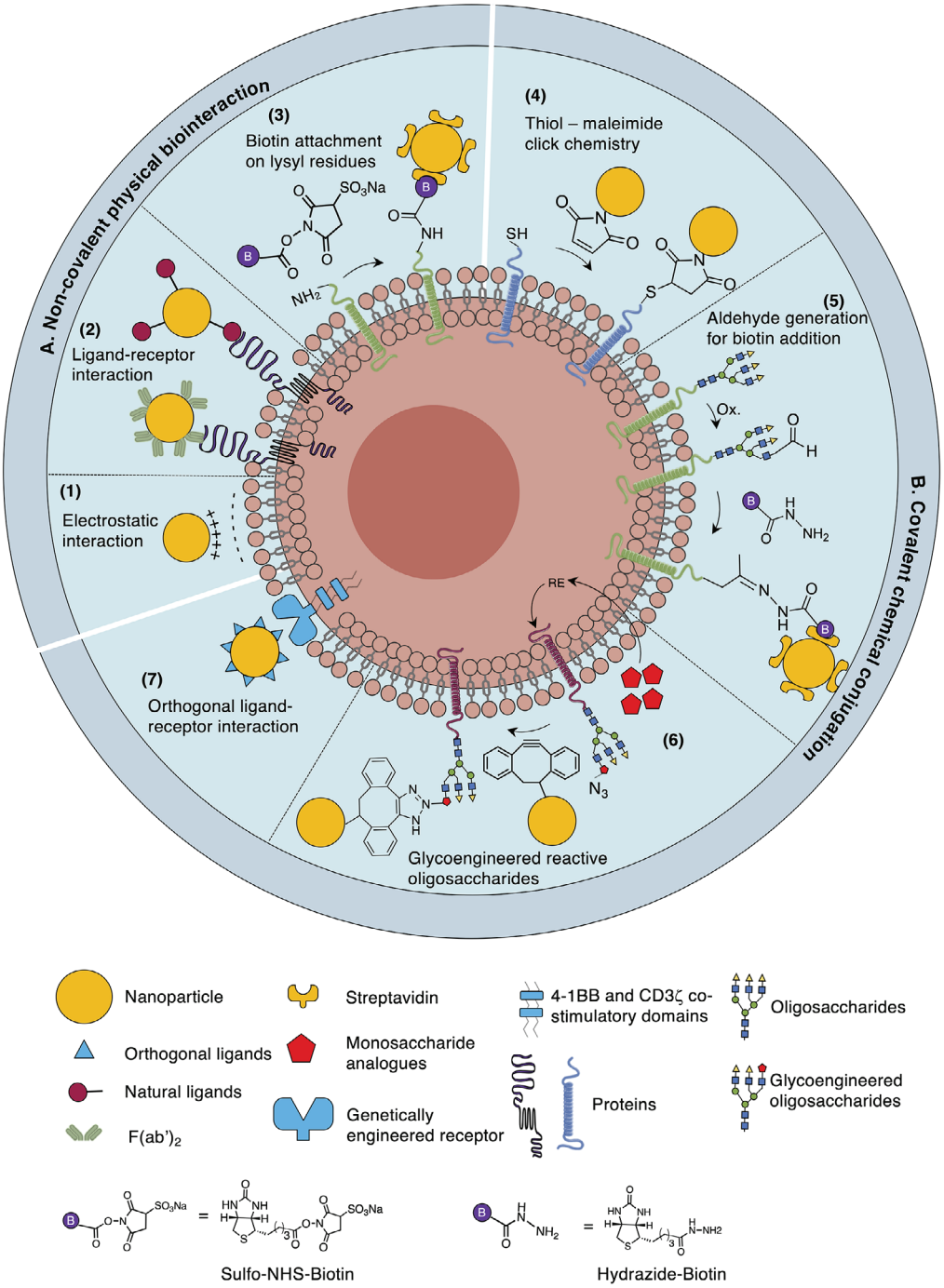

Figure 3. Immune cells-based therapy with ex vivo nanomedicine labeling. Various biochemical strategies have been employed to conjugate antibodies or NPs to yield active immune cells and can be broadly subdivided in A) noncovalent physical bio-interactions and B) covalent chemical conjugation. 1) Non-covalent conjugation of NPs to cell surface can be achieved between the negatively charged plasma membrane and NPs harboring cationic sites via electrostatic interactions.[150] 2) Cell surface also expresses receptors can be targeted by NPs functionalized with their respective ligands or antibodies fragments directed against them.[158] 3) Chemical groups existing on membrane proteins (e.g., -NH_2, -SH) can be leverage to successfully bonded biotin moieties[162–164] or 4) maleimide-decorated therapeutic nanomaterial cargos.[170–172] 5) Biotin hydrazide-mediated amidation of natural oligosaccharides can also be used to bind streptavidin functionalized NP[162,163,165] and 6) glycoengineered oligosaccharides metabolically incorporated into living cell can be targeted with NPs presenting azides or alkynes groups at their surface.[175–177] 7) Finally, immune cells receptors can be genetically engineered to provide an exclusive orthogonal ligand–receptor interaction.[181,182]

© 2020 The Authors. Published by Wiley-VCH GmbH

vivo shear stress exposure in the systemic circulation or endothelial diapedesis. More specific and robust interactions have thus been designed.

7.2. Non-covalent Specific Biointeractions

Specific ligand–receptor interactions can be highly specific but yet pose the risk of undesired cellular responses. Cell surface expressed transmembrane receptors that can be targeted to conjugate NPs functionalized with their respective ligands. Hyaluronic acid-functionalized cell patch can target leukocytes and M1 macrophages through the CD44 hyaluronic acid receptor.[158,159] Loading these backpacks with interferon gamma allows to maintain the M1 phenotype upon adoptive transfer in the immunosuppressive tumor microenvironment.[159] However, these ligand–receptors interactions are transient and dictated by their intrinsic binding and dissociation kinetics (K_D) which hinder stable coupling of NPs on cell surface[160,161] (Figure 3A).

Biotin–avidin interactions have also been extensively studied as specific, non-covalent cell surface interactions.[162,163] This approach requires the introduction of a biotin group on cell surfaces. Biotin moieties can be covalently attached whether by amide bond formation with lysine residues[164] or aldehyde groups formation through mild oxidation of cell surface monosaccharides followed by functionalization with a hydrazide-biotin crosslinker.[165] However, streptavidin as an immunogenic xenoprotein can elicit neutralizing antibodies that lead to opsonization and phagocytic clearance of the engineered cell.[166]

Sialylated carbohydrate ligands such as sialyl-lewis^X are naturally present at the surface of leukocytes and can provide other opportunities for non-covalent, specific biointeractions. As an example, E-selectin/TRAIL-coated or anti-NK1.1/TRAIL-coated liposomes were designed to interact with the sialylated carbohydrates present at the surface of the leukocytes and with the TRAIL receptors expressed by circulating tumor cells (CTCs).[167,168] This approach allowed CTCs elimination and prevention of lymph nodes metastasis formation in patient-derived xenograft model.

7.3. Covalent Chemical Conjugation

Covalent approaches were performed by i) targeting native functional groups (e.g., thiols, amines) present on the cell surface, by ii) chemical generation of reactive groups (e.g., aldehydes) or by iii) using metabolic strategies to introduce nonnatural functional groups (Figure 3B).

7.4. Native Functional Groups

The naturally expressed thiol groups help to protect cells against oxygen radicals.[169] Maleimide-functionalized NPs (e.g., liposomes, multilamellar liposomes, PLGA, etc.) have efficiently been conjugated to immune cells surface[170–172] and their release can be triggered by the reduction potential of the tumor microenvironment (e.g., glutathione increase, etc.).[173] In addition to thiol groups, aldehydes have also been successfully targeted to covalently tether NPs on cell surfaces. However, aldehydes have to be generated by mild oxidation of primary alcohols contained in carbohydrates natively present on the cell surface.[174]

7.5. Metabolic Strategies

Metabolic glycoengineering strategies use bio-orthogonal chemistry to modify natural oligosaccharides present on live cells. Alkyne- or azide-modified monosaccharides such as sialic acid or *N*-acetylmannosamine are metabolically incorporated into living cells and processed through natural biosynthetic pathways to be eventually incorporated into the membrane as glycoengineered oligosaccharides that will react with azides or alkynes groups[175–177] (Figure 3B). Up to now, glycoengineered glycan are used for broad range of diagnostic, therapeutic, or theranostic approaches.[176,178] However, an emerging strategy using a dibenzocyclooctyne alkyne-decorated polyamidoamine dendrimer to target *N*-azidoacetylmannosamine-expressing macrophages demonstrated the feasibility of creating hybrid cell-NPs by bio-orthogonal chemistry to develop personalized immunotherapy.[179] Although this approach exhibited no cell viability, intracellular signaling pathways, and motility altering, its toxicity and efficacy have to be evaluated in vivo. In parallel, the recent development of bio-orthogonal cleavage chemistry opens new perspectives for NPs release and specific drug delivery.[180]

7.6. Receptor Genetical Engineering

The aforementioned approaches result in stable interactions between the NPs and the cell surface but provide only moderate control over the resulting cell surface engineering. Thus, stable and controlled cell–NPs interactions have been sought. Immune cells naturally express receptors at their surface which can be genetically engineered to provide an exclusive orthogonal ligand–receptor interaction[181] (Figure 3B). NK cells, T cells, and some macrophages present the NKG2D receptors on their surfaces that recognize the MHC class I polypeptide-related sequences (MIC) ligands family overexpressed on cells stressed by viral infection or cancer transformation. Leveraging the natural $\alpha1-\alpha2$ binding domain of these ligands through protein engineering allows to develop an exclusive orthogonal ligand–receptor interaction to generate the components of a universal CAR T cell platform.[181] The engineered extracellular domain of the inert NKG2D receptors (iNKG2D) is fused to the intracellular 4-1BB and CD3ζ co-signaling domains to generate the CAR while the mutant ligand domains that specifically bind to the iNKG2D are fused to intact human antibodies. Up to now, efficacy of rituximab-based convertible CAR T cells has been investigated in NSG (NOD scid gamma) mice bearing Burkitt lymphoma and demonstrated dose-dependent control of tumor mass. Similarly, SpyCatcher technology can be used to develop a universal immune receptor.[182] SpyCatcher fused to the intracellular 4-1BB and CD3ζ co-signaling domains is used as an immune receptor that is armed with an antibody fused with SpyTag moieties. These new approaches can be exploited for cell surface modification. NPs can be decorated by the orthogonal ligands mutated $\alpha1-\alpha2$ domain or SpyTag moieties to be conjugated on iNKG2D- or SpyCatcher-expressing immune cells, respectively.

© 2020 The Authors. Published by Wiley-VCH GmbH

7.7. Cell Surface Retention

As previously mentioned, cell membrane components (e.g., lipids and proteins) are continuously internalized, degraded, and replaced.[183] Therefore, means to prolong cell surface retention of NPs have been studied.[171,172,184–189] In a thiol-maleimide approach, NPs-binding proteins have been identified by mass spectrometry.[171] The leukocyte common antigen CD45 is predominantly bound by maleimide-functionalized NPs. Other surface proteins such as LFA-1, CD2, or CD97 have also been identified. However, depending on the cell type, the direct targeting of a surface receptor can trigger undesired cellular responses. Consequently, other ways to increase cell surface retention have been investigated.[184–189] Depending on their compositions and the type of interaction with the cell, NPs can be internalized by different mechanisms (e.g., clathrin- and/or caveolae-mediated endocytosis).[190] Converging in vitro and in vivo evidences demonstrated that the antimalarial agent chloroquine effectively inhibits NPs clathrin-mediated endocytosis by depleting the phosphatidylinositol binding clathrin assembly protein.[184,185] Similar results were found by studying the antipsychotic drug chlorpromazine.[186–188] Nonetheless, these results have not been validated in in vivo models. More recent trial demonstrated that the antiemetic and antipsychotic drug prochlorperazine (PCZ) can be repurposed to reversibly inhibit dynamin-mediated endocytosis of membrane proteins targeted by therapeutic mAbs.[189] In mouse models (squamous cell carcinoma, colon carcinoma, and renal carcinoma) and in a pilot clinical study on head and neck squamous cell carcinoma, treatment with PCZ led to increased clustering of receptors on the cell surface, enhancing tumor cell-NK cells contacts, and finally driving to improve antibody-dependent cell-mediated cytotoxicity in response to approved IgG1 mAbs, such as cetuximab (anti-EGFR mAb) and avelumab (anti-PD-L1 mAb).[189] However, PCZ did not affect targets that are not internalized by dynamin. Thus, this perspective might only be of interest in NPs anchoring targets with dynamin-mediated endocytosis. Although the abovementioned molecules showed promising results in vitro and in pilot clinical study, those molecules might have severe adverse effects in vivo (e.g., chloroquine: cardiac toxicities; chlorpromazine: agranulocytosis; and prochlorperazine: extrapyramidal symptoms) and must thus be carefully handled.

8. Application of T Cells Backpacking

Many cell therapy protocols require adjuvant drugs to maintain transferred cells functions, phenotype, and lifespan.[145–147] However, systemic administration of such drugs is challenging due to their pleiotropic activities, leading to dose-limiting toxicities.[148,149] NPs-targeting strategies with specific cell-targeting ligands, such as antibodies or small molecules have been investigated to deliver these molecules to the tumor site.[191,192] Nonetheless, it has been shown that targeting ligands do not modify the overall NPs biodistribution but rather enable more efficient reaching of the tumor site by targeted NPs.[68–70] Immune cells backpacking strategy with NPs-containing adjuvant cytokines and immune-checkpoint blockade agents has been explored to focus administration of such drugs on tumor site.[93,170–172]

Backpacking T cells with up to 100 (± 20) liposomes (200 nm in diameter) did not affect key cellular functions (e.g., activation, transendothelial migration, tumor homing properties, and antitumor functions) and allowed a 176-fold increase in NP accumulation into the EL4 tumor site when compared to free NP.[170] Loading interleukins 15 and 21 (IL-15 and IL-21, respectively) into the surface of multilamellar liposomes supported T cells antitumor function in an autocrine-like manner through a continuous release of bioactive interleukins over 7 days, and hence enhanced the therapeutic efficacy by efficiently preventing tumor growth up to 30 days after treatment. Moreover, the on-site drug action allowed the use of interleukins doses that are inefficient when systemically administered. Multilamellar liposomes loaded with SN-38, the active metabolite of irinotecan, a potent topoisomerase I poison have also been used to tether T cells.[93] In a Burkitt lymphoma mice model, tumor cells disseminated in lymph node were not sensitive to treatment with free SN-38 or liposomal formulation because of the drug-poor pharmacokinetics due to a short half-life ($t_{1/2}$ = 7 mins) and a rapid hepatic clearance[193] along with the lack of leaky neovasculature into the lymph node and thus, a lack of EPR effect. This lymph node homing property was exploited to deliver SN-38-loaded NPs on T cells in lymphoid organs enriched in lymphoma cells. SN-38-loaded NPs carried by T cells accumulated in lymph nodes 20 h after infusion and SN-38 concentrations were 63-fold greater than free NPs and were maintained for 4 days. SN-38 released in a paracrine-like manner leading to a 60-fold reduction in tumor burden and an extended survival of mice up to 12 days at relatively low doses (7 mg kg^{-1}) when compared to the free drug. Although these approaches allowed to increase the treatment potency, the payloads (e.g., IL-15, IL-21, SN-38, etc.) can passively leak out of the multilamellar liposomes and continually stimulate the T cells until their activation-induced depletion leading to a reduction in the effective dose of T cells trafficking to the tumor site.

To override this issue, a second generation of backpacking NPs has been designed.[172] Nanogel (NG) backpacks have been engineered to transport IL-15 to tumors together with adoptively transferred T cells. ALT-803, an IL-15 superagonist molecule was aggregated into an NG with a linker including reduction-sensitive disulfide bonds that senses the reducing potential of the environment.[194] To facilitate and prolong their cell surface retention, small quantities of anti-CD45 mAbs and poly(ethylene glycol)-*b*-poly(L-lysine) (PEG-PLL) were incorporated onto the NG surface. By engaging their cognate antigen in the tumor, activated T cells induce thiol groups emission at the cell surface, increasing their cell surface reduction potential that detaches the NGs. The release of IL-15 superagonist through this approach resulted in a 16-fold expansion of T cells in tumors, as compared with free IL-15. This approach allowed an eightfold higher dose of cytokine to be administered without toxicity, widening its therapeutic window and enabling a significant increased tumor clearance by ACT T cells and CAR T cells. However, stimulation of cell division will eventually lead to dilution of the backpacked NPs.

Cell-attached cargo actively transmigrate the endothelial barrier and accumulate in tumor sites, thereby enhancing their actions on transferred cells antitumor abilities and limiting systemic adverse effects. Given the plethora of available NPs tailored to deliver small molecules drugs, proteins, siRNA, or magnetic imaging agents, T cells backpacking

© 2020 The Authors. Published by Wiley-VCH GmbH

approaches profoundly open new perspectives for adoptive cell therapies and drug delivery that can be extended far beyond the small molecule drugs and recombinant proteins delivery aforementioned.

9. Conclusion

Immunonanotherapy aims to apply nanotechnology to overcome the issues encountered with immunotherapy. Historically, NPs have been used to improve in vivo activation of immune cells (e.g., vaccines, radiotherapy enhancers, or as tumor microenvironment activators), leading to an improved antitumor response. More recently, a deep focus on the immune cell surface bioengineering to tackle the intrinsic drawbacks of ACT of autologous immune cells or CAR cells is being investigated. These ex vivo immune cells labeling by NPs approaches will also allow NPs to either target the tumor microenvironment, or to use it as a trojan horse to enhance the tumor drug delivery. Using immune cells as NPs vectors allows more efficient targeting of the tumor site compared to the injection of "free" NPs using passive accumulation in the tumor or active tumor targeting methods. This new cell therapy approach is one of the most promising strategy in cancer treatment but requires deepen biodistribution and immune cell behavior characterization upon reinjection. Several other outstanding issues including the immunonanotherapy efficacy, immune cells reaction to surface labeling, and immunonanotherapy translation toward clinic remain challenges that have to be prospectively addressed. In addition, the inherent limitations to NPs synthesis remain to be overcome,[195] such as the scale up of the NPs production to enable following the good manufacturing processes is required, or in depth toxicology, pharmacology, and biodistribution studies in the case the NPs are being separated from the immune cell during its circulation in the body.

Acknowledgements

A.D. acknowledges the generous support of the International Myeloma Foundation.

Conflict of Interest

The authors declare no conflict of interest.

Keywords

cancers, immune cells, immunonanotherapy, nanomedicines, surface labeling

Received: June 8, 2020
Revised: July 28, 2020
Published online:

[1] I. Mellman, G. Coukos, G. Dranoff, *Nature* **2011**, *480*, 480.
[2] D. N. Khalil, E. L. Smith, R. J. Brentjens, J. D. Wolchok, *Nat. Rev. Clin. Oncol.* **2016**, *13*, 273.
[3] D. M. Pardoll, *Nat. Rev. Cancer* **2012**, *12*, 252.
[4] S. L. Topalian, C. G. Drake, D. M. Pardoll, *Cancer Cell* **2015**, *27*, 450.
[5] M. Yarchoan, A. Hopkins, E. M. Jaffee, *N. Engl. J. Med.* **2017**, *377*, 2500.
[6] N. L. Syn, M. W. L. Teng, T. S. K. Mok, R. A. Soo, *Lancet Oncol.* **2017**, *18*, e731.
[7] H. Garner, K. E. de Visser, *Nat. Rev. Immunol.* **2020**, *20*, 483.
[8] M. Binnewies, E. W. Roberts, K. Kersten, V. Chan, D. F. Fearon, M. Merad, L. M. Coussens, D. I. Gabrilovich, S. Ostrand-Rosenberg, C. C. Hedrick, R. H. Vonderheide, M. J. Pittet, R. K. Jain, W. Zou, T. K. Howcroft, E. C. Woodhouse, R. A. Weinberg, M. F. Krummel, *Nat. Med.* **2018**, *24*, 541.
[9] N. Nagarsheth, M. S. Wicha, W. Zou, *Nat. Rev. Immunol.* **2017**, *17*, 559.
[10] P. Sharma, S. Hu-Lieskovan, J. A. Wargo, A. Ribas, *Cell* **2017**, *168*, 707.
[11] B. Santomasso, C. Bachier, J. Westin, K. Rezvani, E. J. Shpall, *Am. Soc. Clin. Oncol. Educ. Book* **2019**, *39*, 433.
[12] J. N. Brudno, J. N. Kochenderfer, *Nat. Rev. Clin. Oncol.* **2018**, *15*, 31.
[13] M. A. Postow, M. K. Callahan, C. A. Barker, Y. Yamada, J. Yuan, S. Kitano, Z. Mu, T. Rasalan, M. Adamow, E. Ritter, C. Sedrak, A. A. Jungbluth, R. Chua, A. S. Yang, R.-A. Roman, S. Rosner, B. Benson, J. P. Allison, A. M. Lesokhin, S. Gnjatic, J. D. Wolchok, *N. Engl. J. Med.* **2012**, *366*, 925.
[14] F. Martins, L. Sofiya, G. P. Sykiotis, F. Lamine, M. Maillard, M. Fraga, K. Shabafrouz, C. Ribi, A. Cairoli, Y. Guex-Crosier, T. Kuntzer, O. Michielin, S. Peters, G. Coukos, F. Spertini, J. A. Thompson, M. Obeid, *Nat. Rev. Clin. Oncol.* **2019**, *16*, 563.
[15] S. L. Maude, N. Frey, P. A. Shaw, R. Aplenc, D. M. Barrett, N. J. Bunin, A. Chew, V. E. Gonzalez, Z. Zheng, S. F. Lacey, Y. D. Mahnke, J. J. Melenhorst, S. R. Rheingold, A. Shen, D. T. Teachey, B. L. Levine, C. H. June, D. L. Porter, S. A. Grupp, *N. Engl. J. Med.* **2014**, *371*, 1507.
[16] N. Raje, J. Berdeja, Y. Lin, D. Siegel, S. Jagannath, D. Madduri, M. Liedtke, J. Rosenblatt, M. V. Maus, A. Turka, L.-P. Lam, R. A. Morgan, K. Friedman, M. Massaro, J. Wang, G. Russotti, Z. Yang, T. Campbell, K. Hege, F. Petrocca, M. T. Quigley, N. Munshi, J. N. Kochenderfer, *N. Engl. J. Med.* **2019**, *380*, 1726.
[17] E. Liu, D. Marin, P. Banerjee, H. A. MacApinlac, P. Thompson, R. Basar, L. N. Kerbauy, B. Overman, P. Thall, M. Kaplan, V. Nandivada, I. Kaur, A. N. Cortes, K. Cao, M. Daher, C. Hosing, E. N. Cohen, P. Kebriaei, R. Mehta, S. Neelapu, Y. Nieto, M. Wang, W. Wierda, M. Keating, R. Champlin, E. J. Shpall, K. Rezvani, *N. Engl. J. Med.* **2020**, *382*, 545.
[18] C. E. Brown, D. Alizadeh, R. Starr, L. Weng, J. R. Wagner, A. Naranjo, J. R. Ostberg, M. S. Blanchard, J. Kilpatrick, J. Simpson, A. Kurien, S. J. Priceman, X. Wang, T. L. Harshbarger, M. D'Apuzzo, J. A. Ressler, M. C. Jensen, M. E. Barish, M. Chen, J. Portnow, S. J. Forman, B. Badie, *N. Engl. J. Med.* **2016**, *375*, 2561.
[19] C. M. Le Gall, J. Weiden, L. J. Eggermont, C. G. Figdor, *Nat. Mater.* **2018**, *17*, 474.
[20] S. Anguille, E. L. Smits, E. Lion, V. F. Van Tendeloo, Z. N. Berneman, *Lancet Oncol.* **2014**, *15*, e257.
[21] M. Sadelain, I. Rivière, S. Riddell, *Nature* **2017**, *545*, 423.
[22] N. N. Shah, T. J. Fry, *Nat. Rev. Clin. Oncol.* **2019**, *16*, 372.
[23] F. Pagès, B. Mlecnik, F. Marliot, G. Bindea, F. S. Ou, C. Bifulco, A. Lugli, I. Zlobec, T. T. Rau, M. D. Berger, I. D. Nagtegaal, E. Vink-Börger, A. Hartmann, C. Geppert, J. Kolwelter, S. Merkel, R. Grützmann, M. Van den Eynde, A. Jouret-Mourin, A. Kartheuser, D. Léonard, C. Remue, J. Y. Wang, P. Bavi, M. H. A. Roehrl, P. S. Ohashi, L. T. Nguyen, S. Han, H. L. MacGregor, S. Hafezi-Bakhtiari, *Lancet* **2018**, *391*, 2128.
[24] B. Y. S. Kim, J. T. Rutka, W. C. W. Chan, *N. Engl. J. Med.* **2010**, *363*, 2434.
[25] R. K. Jain, T. Stylianopoulos, *Nat. Rev. Clin. Oncol.* **2010**, *7*, 653.
[26] Y. Matsumura, H. Maeda, *Cancer Res.* **1986**, *46*, 6387.

 © 2020 The Authors. Published by Wiley-VCH GmbH

[27] S. Wilhelm, A. J. Tavares, Q. Dai, S. Ohta, J. Audet, H. F. Dvorak, W. C. W. Chan, *Nat. Rev. Mater.* **2016**, *1*, 16014.
[28] G. H. Petersen, S. K. Alzghari, W. Chee, S. S. Sankari, N. M. La-Beck, *J. Controlled Release* **2016**, *232*, 255.
[29] J.-W. Yoo, E. Chambers, S. Mitragotri, *Curr. Pharm. Des.* **2010**, *16*, 2298.
[30] T. M. Allen, P. R. Cullis, *Adv. Drug Delivery Rev.* **2013**, *65*, 36.
[31] R. Gref, Y. Minamitake, M. T. Peracchia, V. Trubetskoy, V. Torchilin, R. Langer, *Science* **1994**, *263*, 1600.
[32] K. Zhang, X. Tang, J. Zhang, W. Lu, X. Lin, Y. Zhang, B. Tian, H. Yang, H. He, *J. Controlled Release* **2014**, *183*, 77.
[33] G. T. Tietjen, S. A. Hosgood, J. DiRito, J. Cui, D. Deep, E. Song, J. R. Kraehling, A. S. Piotrowski-Daspit, N. C. Kirkiles-Smith, R. Al-Lamki, S. Thiru, J. A. Bradley, K. Saeb-Parsy, J. R. Bradley, M. L. Nicholson, W. M. Saltzman, J. S. Pober, *Sci. Transl. Med.* **2017**, *9*, eaam6764.
[34] F. Chen, K. Ma, B. Madajewski, L. Zhuang, L. Zhang, K. Rickert, M. Marelli, B. Yoo, M. Z. Turker, M. Overholtzer, T. P. Quinn, M. Gonen, P. Zanzonico, A. Tuesca, M. A. Bowen, L. Norton, J. A. Subramony, U. Wiesner, M. S. Bradbury, *Nat. Commun.* **2018**, *9*, 4141.
[35] P. L. Turecek, M. J. Bossard, F. Schoetens, I. A. Ivens, *J. Pharm. Sci.* **2016**, *105*, 460.
[36] T. Sun, Y. S. Zhang, B. Pang, D. C. Hyun, M. Yang, Y. Xia, *Angew. Chem., Int. Ed.* **2014**, *53*, 123.
[37] A. Detappe, M. Bustoros, T. H. Mouhieddine, P. P. Ghoroghchian, *Trends Mol. Med.* **2018**, *24*, 560.
[38] D. Singh, F. Dilnawaz, S. K. Sahoo, *Nanomedicine* **2020**, *24*, 560.
[39] H. Lee, A. F. Shields, B. A. Siegel, K. D. Miller, I. Krop, C. X. Ma, P. M. Lorusso, P. N. Munster, K. Campbell, D. F. Gaddy, S. C. Leonard, E. Geretti, S. J. Blocker, D. B. Kirpotin, V. Moyo, T. J. Wickham, B. S. Hendriks, *Clin. Cancer Res.* **2017**, *23*, 4190.
[40] R. Qi, Y. Wang, P. M. Bruno, H. Xiao, Y. Yingjie, T. Li, S. Lauffer, W. Wei, Q. Chen, X. Kang, H. Song, X. Yang, X. Huang, A. Detappe, U. Matulonis, D. Pepin, M. T. Hemann, M. J. Birrer, P. P. Ghoroghchian, *Nat. Commun.* **2017**, *8*, 2166.
[41] J. E. Lancet, G. L. Uy, J. E. Cortes, L. F. Newell, T. L. Lin, E. K. Ritchie, R. K. Stuart, S. A. Strickland, D. Hogge, S. R. Solomon, R. M. Stone, D. L. Bixby, J. E. Kolitz, G. J. Schiller, M. J. Wieduwilt, D. H. Ryan, A. Hoering, M. Chiarella, A. C. Louie, B. C. Medeiros, *J. Clin. Oncol.* **2016**, *34*, 7000.
[42] W. J. Gradishar, S. Tjulandin, N. Davidson, H. Shaw, N. Desai, P. Bhar, M. Hawkins, J. O'Shaughnessy, *J. Clin. Oncol.* **2005**, *23*, 7794.
[43] T. Lammers, L. Y. Rizzo, G. Storm, F. Kiessling, *Clin. Cancer Res.* **2012**, *18*, 4889.
[44] B. Theek, L. Y. Rizzo, J. Ehling, F. Kiessling, T. Lammers, *Clin. Transl. Imaging* **2014**, *2*, 67.
[45] T. Lammers, S. Aime, W. E. Hennink, G. Storm, F. Kiessling, *Acc. Chem. Res.* **2011**, *44*, 1029.
[46] N. Tanaka, S. Kanatani, R. Tomer, C. Sahlgren, P. Kronqvist, D. Kaczynska, L. Louhivuori, L. Kis, C. Lindh, P. Mitura, A. Stepulak, S. Corvigno, J. Hartman, P. Micke, A. Mezheyeuski, C. Strell, J. W. Carlson, C. F. Moro, H. Dahlstrand, A. Östman, K. Matsumoto, P. Wiklund, M. Oya, A. Miyakawa, K. Deisseroth, P. Uhlén, *Nat. Biomed. Eng.* **2017**, *1*, 796.
[47] K. J. Harrington, S. Mohammadtaghi, P. S. Uster, D. Glass, A. M. Peters, R. G. Vile, J. S. W. Stewart, *Clin. Cancer Res.* **2001**, *7*, 243.
[48] Z. Tao, M. D. Muzumdar, A. Detappe, X. Huang, E. S. Xu, Y. Yu, T. H. Mouhieddine, H. Song, T. Jacks, P. P. Ghoroghchian, *Nano Lett.* **2018**, *18*, 2195.
[49] S. Sindhwani, A. M. Syed, J. Ngai, B. R. Kingston, L. Maiorino, J. Rothschild, P. MacMillan, Y. Zhang, N. U. Rajesh, T. Hoang, J. L. Y. Wu, S. Wilhelm, A. Zilman, S. Gadde, A. Sulaiman, B. Ouyang, Z. Lin, L. Wang, M. Egeblad, W. C. W. Chan, *Nat. Mater.* **2020**, *19*, 566.
[50] H. Ragelle, F. Danhier, V. Préat, R. Langer, D. G. Anderson, *Expert Opin. Drug Delivery* **2017**, *19*, 566.
[51] G. Bort, F. Lux, S. Dufort, Y. Crémillieux, C. Verry, O. Tillement, *Theranostics* **2020**, *10*, 1319.
[52] R. K. Jain, *Science* **2005**, *307*, 58.
[53] J. D. Martin, H. Cabral, T. Stylianopoulos, R. K. Jain, *Nat. Rev. Clin. Oncol.* **2020**, *17*, 251.
[54] V. P. Chauhan, T. Stylianopoulos, J. D. Martin, Z. PopoviÄ, O. Chen, W. S. Kamoun, M. G. Bawendi, D. Fukumura, R. K. Jain, *Nat. Nanotechnol.* **2012**, *7*, 383.
[55] O. Couture, J. Foley, N. F. Kassell, B. Larrat, J. F. Aubry, *Transl. Cancer Res.* **2014**, *3*, 494.
[56] T. Boissenot, A. Bordat, E. Fattal, N. Tsapis, *J. Controlled Release* **2016**, *241*, 144.
[57] S. Mura, J. Nicolas, P. Couvreur, *Nat. Mater.* **2013**, *12*, 991.
[58] M. M. Shenoi, N. B. Shah, R. J. Griffin, G. M. Vercellotti, J. C. Bischof, *Nanomedicine* **2011**, *6*, 545.
[59] D. S. Chauhan, A. B. Bukhari, G. Ravichandran, R. Gupta, L. George, R. Poojari, A. Ingle, A. K. Rengan, A. Shanavas, R. Srivastava, A. De, *Sci. Rep.* **2018**, *8*, 16673.
[60] Z. Zhen, W. Tang, Y. J. Chuang, T. Todd, W. Zhang, X. Lin, G. Niu, G. Liu, L. Wang, Z. Pan, X. Chen, J. Xie, *ACS Nano* **2014**, *8*, 6004.
[61] J. L. Paris, G. Villaverde, S. Gómez-Graña, M. Vallet-Regí, *Acta Biomater.* **2020**, *101*, 459.
[62] S. Kunjachan, A. Detappe, R. Kumar, T. Ireland, L. Cameron, D. E. Biancur, V. Motto-Ros, L. Sancey, S. Sridhar, G. M. Makrigiorgos, R. I. Berbeco, *Nano Lett.* **2015**, *15*, 7488.
[63] S. Kunjachan, S. Kotb, R. Pola, M. Pechar, R. Kumar, B. Singh, F. Gremse, R. Taleeli, F. Trichard, V. Motto-Ros, L. Sancey, A. Detappe, S. Yasmin-Karim, A. Protti, I. Shanmugam, T. Ireland, T. Etrych, S. Sridhar, O. Tillement, M. Makrigiorgos, R. I. Berbeco, *Sci. Rep.* **2019**, *9*, 15844.
[64] M. Germain, M. E. Meyre, L. Poul, M. Paolini, C. Berjaud, F. Mpambani, M. Bergere, L. Levy, A. Pottier, *Sci. Rep.* **2018**, *8*, 4797.
[65] K. E. Ibrahim, A. O. Bakhiet, M. E. Awadalla, H. A. Khan, *Nanomedecine* **2018**, *13*, 313.
[66] K. Runcie, D. R. Budman, V. John, N. Seetharamu, *Mol. Med.* **2018**, *24*, 50.
[67] L. Wu, E. Seung, L. Xu, E. Rao, D. M. Lord, R. R. Wei, V. Cortez-Retamozo, B. Ospina, V. Posternak, G. Ulinski, P. Piepenhagen, E. Francesconi, N. El Murr, C. Beil, T. Dabdoubi, B. Cameron, T. Bertrand, P. Ferrari, S. Pouzieux, C. Lemoine, C. Prades, A. Park, H. Qiu, Z. Song, B. Zhang, F. Sun, M. Chiron, S. Rao, K. Radosevic, Y. Zhi-yong, G. J. Nabel, *Nat. Cancer* **2020**, *1*, 86.
[68] D. B. Kirpotin, D. C. Drummond, Y. Shao, M. R. Shalaby, K. Hong, U. B. Nielsen, J. D. Marks, C. C. Benz, J. W. Park, *Cancer Res.* **2006**, *66*, 6732.
[69] D. W. Bartlett, H. Su, I. J. Hildebrandt, W. A. Weber, M. E. Davis, *Proc. Natl. Acad. Sci. USA* **2007**, *104*, 15549.
[70] S. Kunjachan, R. Pola, F. Gremse, B. Theek, J. Ehling, D. Moeckel, B. Hermanns-Sachweh, M. Pechar, K. Ulbrich, W. E. Hennink, G. Storm, W. Lederle, F. Kiessling, T. Lammers, *Nano Lett.* **2014**, *14*, 972.
[71] A. Detappe, M. Reidy, Y. Yu, C. Mathieu, H. V. T. Nguyen, T. P. Coroller, F. Lam, P. Jarolim, P. Harvey, A. Protti, Q. D. Nguyen, J. A. Johnson, Y. Cremillieux, O. Tillement, I. M. Ghobrial, P. P. Ghoroghchian, *Nanoscale* **2019**, *11*, 20485.
[72] E. Blanco, H. Shen, M. Ferrari, *Nat. Biotechnol.* **2015**, *33*, 941.
[73] A. Schudel, D. M. Francis, S. N. Thomas, *Nat. Rev. Mater.* **2019**, *4*, 415.
[74] S. T. Reddy, A. J. Van Der Vlies, E. Simeoni, V. Angeli, G. J. Randolph, C. P. O'Neil, L. K. Lee, M. A. Swartz, J. A. Hubbell, *Nat. Biotechnol.* **2007**, *25*, 1159.
[75] C. Engblom, C. Pfirschke, M. J. Pittet, *Nat. Rev. Cancer* **2016**, *16*, 447.
[76] C. B. Rodell, S. P. Arlauckas, M. F. Cuccarese, C. S. Garris, R. Li, M. S. Ahmed, R. H. Kohler, M. J. Pittet, R. Weissleder, *Nat. Biomed. Eng.* **2018**, *2*, 578.

 © 2020 The Authors. Published by Wiley-VCH GmbH

[77] R. A. Ortega, W. Barham, K. Sharman, O. Tikhomirov, T. D. Giorgio, F. E. Yull, *Int. J. Nanomed.* **2016**, *11*, 2163.
[78] R. A. Ortega, W. J. Barham, B. Kumar, O. Tikhomirov, I. D. McFadden, F. E. Yull, T. D. Giorgio, *Nanoscale* **2015**, *7*, 500.
[79] M. Zhang, L. Yan, J. A. Kim, *Cancer Gene Ther.* **2015**, *22*, 463.
[80] F. Zhang, N. N. Parayath, C. I. Ene, S. B. Stephan, A. L. Koehne, M. E. Coon, E. C. Holland, M. T. Stephan, *Nat. Commun.* **2019**, *10*, 3974.
[81] S. Zhu, M. Niu, H. O'Mary, Z. Cui, *Mol. Pharmaceutics* **2013**, *10*, 3525.
[82] W. Xia, A. R. Hilgenbrink, E. L. Matteson, M. B. Lockwood, J. X. Cheng, P. S. Low, *Blood* **2009**, *113*, 438.
[83] A. Puig-Kröger, E. Sierra-Filardi, A. Domínguez-Soto, R. Samaniego, M. T. Corcuera, F. Gómez-Aguado, M. Ratnam, P. Sánchez-Mateos, A. L. Corbí, *Cancer Res.* **2009**, *69*, 9395.
[84] K. Margulis, A. Honkala, I. Kalashnikova, S. E. Noll, M. Hill, R. N. Zare, B. R. Smith, *Nanoscale* **2020**, *12*, 2752.
[85] B. M. Barth, E. I. Altinoğlu, S. S. Shanmugavelandy, J. M. Kaiser, D. Crespo-Gonzalez, N. A. Divittore, C. McGovern, T. M. Goff, N. R. Keasey, J. H. Adair, T. P. Loughran, D. Claxton, M. Kester, *ACS Nano* **2011**, *5*, 5325.
[86] C. Shirata, J. Kaneko, Y. Inagaki, T. Kokudo, M. Sato, S. Kiritani, N. Akamatsu, J. Arita, Y. Sakamoto, K. Hasegawa, N. Kokudo, *Sci. Rep.* **2017**, *7*, 13958.
[87] B. Edris, K. Weiskopf, A. K. Volkmer, J. P. Volkmer, S. B. Willingham, H. Contreras-Trujillo, J. Liu, R. Majeti, R. B. West, J. A. Fletcher, A. H. Beck, I. L. Weissman, M. van de Rijn, *Proc. Natl. Acad. Sci. USA* **2012**, *109*, 6656.
[88] N. G. Ring, D. Herndler-Brandstetter, K. Weiskopf, L. Shan, J. P. Volkmer, B. M. George, M. Lietzenmayer, K. M. McKenna, T. J. Naik, A. McCarty, Y. Zheng, A. M. Ring, R. A. Flavell, I. L. Weissman, *Proc. Natl. Acad. Sci. USA* **2017**, *114*, E10578.
[89] Y. Murata, D. Tanaka, D. Hazama, T. Yanagita, Y. Saito, T. Kotani, P. A. Oldenborg, T. Matozaki, *Cancer Sci.* **2018**, *109*, 1300.
[90] A. Ramesh, S. Kumar, A. Nguyen, A. Brouillard, A. Kulkarni, *Nanoscale* **2020**, *12*, 1875.
[91] A. Mantovani, S. Sozzani, M. Locati, P. Allavena, A. Sica, *Trends Immunol.* **2002**, *23*, 549.
[92] J. M. Irache, H. H. Salman, C. Gamazo, S. Espuelas, *Expert Opin. Drug Delivery* **2008**, *5*, 703.
[93] B. Huang, W. D. Abraham, Y. Zheng, S. C. Bustamante López, S. S. Luo, D. J. Irvine, *Sci. Transl. Med.* **2015**, *7*, 291ra94.
[94] D. Schmid, C. G. Park, C. A. Hartl, N. Subedi, A. N. Cartwright, R. B. Puerto, Y. Zheng, J. Maiarana, G. J. Freeman, K. W. Wucherpfennig, D. J. Irvine, M. S. Goldberg, *Nat. Commun.* **2017**, *8*, 1747.
[95] Y. Zheng, M. T. Stephan, S. A. Gai, W. Abraham, A. Shearer, D. J. Irvine, *J. Controlled Release* **2013**, *172*, 426.
[96] Y. Zheng, L. Tang, L. Mabardi, S. Kumari, D. J. Irvine, *ACS Nano* **2017**, *11*, 3089.
[97] B. V. Kumar, T. J. Connors, D. L. Farber, *Immunity* **2018**, *48*, 202.
[98] V. Mirshafiee, R. Kim, S. Park, M. Mahmoudi, M. L. Kraft, *Biomaterials* **2016**, *75*, 295.
[99] A. Gros, P. F. Robbins, X. Yao, Y. F. Li, S. Turcotte, E. Tran, J. R. Wunderlich, A. Mixon, S. Farid, M. E. Dudley, K.-I. Hanada, J. R. Almeida, S. Darko, D. C. Douek, J. C. Yang, S. A. Rosenberg, *J. Clin. Invest.* **2014**, *124*, 2246.
[100] G. Yi, J. Son, J. Yoo, C. Park, H. Koo, *Biomater. Res.* **2018**, *22*, 13.
[101] B. L. Kenry, *Trends Chem.* **2019**, *1*, 763.
[102] B. Kwong, H. Liu, D. J. Irvine, *Biomaterials* **2011**, *32*, 5134.
[103] B. Kwong, S. A. Gai, J. Elkhader, K. D. Wittrup, D. J. Irvine, *Cancer Res.* **2013**, *73*, 1547.
[104] A. K. Kosmides, J. W. Sidhom, A. Fraser, C. A. Bessell, J. P. Schneck, *ACS Nano* **2017**, *11*, 5417.
[105] Y. Mi, C. C. Smith, F. Yang, Y. Qi, K. C. Roche, J. S. Serody, B. G. Vincent, A. Z. Wang, *Adv. Mater.* **2018**, *30*, 1706098.
[106] U. Sahin, Ö. Türeci, *Science* **2018**, *359*, 1355.
[107] Z. Hu, P. A. Ott, C. J. Wu, *Nat. Rev. Immunol.* **2018**, *18*, 168.
[108] M. Schmitz, H. Jähnisch, S. Füssel, A. Kiessling, R. Wehner, S. Zastrow, M. Bachmann, E. P. Rieber, M. P. Wirth, *Clin. Dev. Immunol.* **2010**, *2010*, 517493.
[109] G. Di Lorenzo, C. Buonerba, P. W. Kantoff, *Nat. Rev. Clin. Oncol.* **2011**, *8*, 551.
[110] C. R. Perez, M. De Palma, *Nat. Commun.* **2019**, *10*, 5408.
[111] M. S. Goldberg, *Nat. Rev. Cancer* **2019**, *19*, 587.
[112] D. J. Irvine, M. C. Hanson, K. Rakhra, T. Tokatlian, *Chem. Rev.* **2015**, *115*, 11109.
[113] L. Galluzzi, A. Buqué, O. Kepp, L. Zitvogel, G. Kroemer, *Nat. Rev. Immunol.* **2017**, *17*, 97.
[114] L. Chen, D. B. Flies, *Nat. Rev. Immunol.* **2013**, *17*, 402.
[115] K. Shao, S. Singha, X. Clemente-Casares, S. Tsai, Y. Yang, P. Santamaria, *ACS Nano* **2015**, *9*, 16.
[116] D. J. Irvine, M. A. Swartz, G. L. Szeto, *Nat. Mater.* **2013**, *12*, 978.
[117] L. Jeanbart, M. Ballester, A. De Titta, P. Corthésy, P. Romero, J. A. Hubbell, M. A. Swartz, *Cancer Immunol. Res.* **2014**, *2*, 436.
[118] K. R. Rhodes, J. J. Green, *Mol. Immunol.* **2018**, *98*, 13.
[119] J. J. Moon, H. Suh, A. Bershteyn, M. T. Stephan, H. Liu, B. Huang, M. Sohail, S. Luo, S. Ho Um, H. Khant, J. T. Goodwin, J. Ramos, W. Chiu, D. J. Irvine, *Nat. Mater.* **2011**, *10*, 243.
[120] H. Dewitte, R. Verbeke, K. Breckpot, S. C. De Smedt, I. Lentacker, *Nano Today* **2014**, *9*, 743.
[121] J. T. Wilson, S. Keller, M. J. Manganiello, C. Cheng, C. C. Lee, C. Opara, A. Convertine, P. S. Stayton, *ACS Nano* **2013**, *7*, 3912.
[122] O. S. Fenton, K. J. Kauffman, J. C. Kaczmarek, R. L. McClellan, S. Jhunjhunwala, M. W. Tibbitt, M. D. Zeng, E. A. Appel, J. R. Dorkin, F. F. Mir, J. H. Yang, M. A. Oberli, M. W. Heartlein, F. DeRosa, R. Langer, D. G. Anderson, *Adv. Mater.* **2017**, *29*, 1606944.
[123] O. S. Fenton, M. W. Tibbitt, E. A. Appel, S. Jhunjhunwala, M. J. Webber, R. Langer, *Biomacromolecules* **2019**, *20*, 4430.
[124] R. R. Weichselbaum, H. Liang, L. Deng, Y. X. Fu, *Nat. Rev. Clin. Oncol.* **2017**, *14*, 365.
[125] A. Gardner, B. Ruffell, *Trends Immunol.* **2016**, *37*, 855.
[126] G. D. Grass, N. Krishna, S. Kim, *Curr. Probl. Cancer* **2016**, *40*, 10.
[127] M. E. Rodríguez-Ruiz, C. Vanpouille-Box, I. Melero, S. C. Formenti, S. Demaria, *Trends Immunol.* **2018**, *39*, 644.
[128] S. N. Thomas, E. Vokali, A. W. Lund, J. A. Hubbell, M. A. Swartz, *Biomaterials* **2014**, *35*, 814.
[129] W. L. Hwang, L. R. G. Pike, T. J. Royce, B. A. Mahal, J. S. Loeffler, *Nat. Rev. Clin. Oncol.* **2018**, *15*, 477.
[130] R. I. Berbeco, A. Detappe, P. Tsiamas, D. Parsons, M. Yewondwossen, J. Robar, *Med. Phys.* **2016**, *43*, 436.
[131] S. J. McMahon, W. B. Hyland, M. F. Muir, J. A. Coulter, S. Jain, K. T. Butterworth, G. Schettino, G. R. Dickson, A. R. Hounsell, J. M. O'Sullivan, G. Schettino, F. J. Currell, D. G. Hirst, K. M. Prise, *Sci. Rep.* **2011**, *7*, 26736.
[132] J. F. Hainfeld, D. N. Slatkin, H. M. Smilowitz, *Phys. Med. Biol.* **2004**, *49*, N309.
[133] L. Sancey, F. Lux, S. Kotb, S. Roux, S. Dufort, A. Bianchi, Y. Crémillieux, P. Fries, J. L. Coll, C. Rodriguez-Lafrasse, M. Janier, M. Dutreix, M. Barberi-Heyob, F. Boschetti, F. Denat, C. Louis, E. Porcel, S. Lacombe, G. Le Duc, E. Deutsch, J. -L. Perfettini, A. Detappe, C. Verry, R. Berbeco, K. T. Butterworth, S. J. McMahon, K. M. Prise, P. Perriat, O. Tillement, *Br. J. Radiol.* **2014**, *87*, 20140134.
[134] A. Detappe, S. Kunjachan, J. Rottmann, J. Robar, P. Tsiamas, H. Korideck, O. Tillement, R. Berbeco, *Cancer Nanotechnol.* **2015**, *6*, 4.
[135] A. Detappe, E. Thomas, M. W. Tibbitt, S. Kunjachan, O. Zavidij, N. Parnandi, E. Reznichenko, F. Lux, O. Tillement, R. Berbeco, *Nano Lett.* **2017**, *17*, 1733.
[136] A. Detappe, S. Kunjachan, L. Sancey, V. Motto-Ros, D. Biancur, P. Drane, R. Guieze, G. M. Makrigiorgos, O. Tillement, R. Langer, R. Berbeco, *J. Controlled Release* **2016**, *238*, 103.

 © 2020 The Authors. Published by Wiley-VCH GmbH

[137] A. Detappe, S. Kunjachan, P. Drané, S. Kotb, M. Myronakis, D. E. Biancur, T. Ireland, M. Wagar, F. Lux, O. Tillement, R. Berbeco, *Sci. Rep.* **2016**, *6*, 34040.
[138] A. Detappe, P. Tsiamas, W. Ngwa, P. Zygmanski, M. Makrigiorgos, R. Berbeco, *Med. Phys.* **2013**, *40*, 031706.
[139] W. Ngwa, O. C. Irabor, J. D. Schoenfeld, J. Hesser, S. Demaria, S. C. Formenti, *Nat. Rev. Cancer* **2018**, *18*, 313.
[140] M. Moreau, S. Yasmin-Karim, S. Kunjachan, N. Sinha, F. Gremse, R. Kumar, K. F. Chow, W. Ngwa, *Front. Oncol.* **2018**, *8*, 56.
[141] Y. Min, K. C. Roche, S. Tian, M. J. Eblan, K. P. McKinnon, J. M. Caster, S. Chai, L. E. Herring, L. Zhang, T. Zhang, J. M. DeSimone, J. E. Tepper, B. G. Vincent, J. S. Serody, A. Z. Wang, *Nat. Nanotechnol.* **2017**, *12*, 877.
[142] D. V. Krysko, A. D. Garg, A. Kaczmarek, O. Krysko, P. Agostinis, P. Vandenabeele, *Nat. Rev. Cancer* **2012**, *12*, 860.
[143] M. Klichinsky, M. Ruella, O. Shestova, X. M. Lu, A. Best, M. Zeeman, M. Schmierer, K. Gabrusiewicz, N. R. Anderson, N. E. Petty, K. D. Cummins, F. Shen, X. Shan, K. Veliz, K. Blouch, Y. Yashiro-Ohtani, S. S. Kenderian, M. Y. Kim, R. S. O'Connor, S. R. Wallace, M. S. Kozlowski, D. M. Marchione, M. Shestov, B. A. Garcia, C. H. June, S. Gill, *Nat. Biotechnol.* **2020**, *38*, 947.
[144] S. R. Bailey, M. V. Maus, *Nat. Biotechnol.* **2019**, *37*, 1425.
[145] R. A. Morgan, M. E. Dudley, J. R. Wunderlich, M. S. Hughes, J. C. Yang, R. M. Sherry, R. E. Royal, S. L. Topalían, U. S. Kammula, N. P. Restifo, Z. Zheng, A. Nahvi, C. R. De Vries, L. J. Rogers-Freezer, S. A. Mavroukakis, S. A. Rosenberg, *Science* **2006**, *314*, 126.
[146] R. Zeng, R. Spolski, S. E. Finkelstein, S. K. Oh, P. E. Kovanen, C. S. Hinrichs, C. A. Pise-Masison, M. F. Radonovich, J. N. Brady, N. P. Restifo, J. A. Berzofsky, W. J. Leonard, *J. Exp. Med.* **2005**, *201*, 139.
[147] A. Wallace, V. Kapoor, J. Sun, P. Mrass, W. Weninger, D. F. Heitjan, C. June, L. R. Kaiser, L. E. Ling, S. M. Albelda, *Clin. Cancer Res.* **2008**, *14*, 3966.
[148] J. A. Thompson, D. J. Lee, W. W. Cox, C. G. Lindgren, C. Collins, K. A. Neraas, R. A. Dennin, A. Fefer, *Cancer Res.* **1987**, *47*, 4202.
[149] S. C. Berger, M. Berger, R. C. Hackman, M. Gough, C. Elliott, M. C. Jensen, S. R. Riddell, *Blood* **2009**, *114*, 2417.
[150] M. T. Stephan, D. J. Irvine, *Nano Today* **2011**, *6*, 309.
[151] C. Sperling, M. Fischer, M. F. Maitz, C. Werner, *Biomaterials* **2009**, *30*, 4447.
[152] M. G. Paulick, C. R. Bertozzi, *Biochemistry* **2008**, *47*, 6991.
[153] H. Liu, B. Kwong, D. J. Irvine, *Angew. Chem., Int. Ed.* **2011**, *50*, 7052.
[154] B. Alberts, J. Lewis, *Molecular Biology of the Cell*, 6th edition, Garland Science, New York, NY, **2014**, 1464 pp., ISBN 9780815344322.
[155] K. Bojkowska, F. Santoni De Sio, I. Barde, S. Offner, S. Verp, C. Heinis, K. Johnsson, D. Trono, *Chem. Biol.* **2011**, *18*, 805.
[156] B. R. Peterson, *Org. Biomol. Chem.* **2005**, *3*, 3607.
[157] R. R. Arvizo, O. R. Miranda, M. A. Thompson, C. M. Pabelick, R. Bhattacharya, J. David Robertson, V. M. Rotello, Y. S. Prakash, P. Mukherjee, *Nano Lett.* **2010**, *10*, 2543.
[158] A. J. Swiston, C. Cheng, S. H. Um, D. J. Irvine, R. E. Cohen, M. F. Rubner, *Nano Lett.* **2008**, *8*, 4446.
[159] C. Wyatt Shields, M. A. Evans, L. L. Wang, N. Baugh, S. Iyer, D. Wu, Z. Zhao, A. Pusuluri, A. Ukidve, D. C. Pan, S. Mitragotri, *Sci. Adv.* **2020**, *6*, eaaz6579.
[160] W. Chen, V. I. Zarnitsyna, K. K. Sarangapani, J. Huang, C. Zhu, *Cell. Mol. Bioeng.* **2008**, *1*, 276.
[161] V. A. Kickhoefer, M. Han, S. Raval-Fernandes, M. J. Poderycki, R. J. Moniz, D. Vaccari, M. Silvestry, P. L. Stewart, K. A. Kelly, L. H. Rome, *ACS Nano* **2009**, *3*, 27.
[162] R. Mooney, Y. Weng, E. Garcia, S. Bhojane, L. Smith-Powell, S. U. Kim, A. J. Annala, K. S. Aboody, J. M. Berlin, *J. Controlled Release* **2014**, *191*, 82.
[163] A. Jain, K. Cheng, *J. Controlled Release* **2017**, *245*, 27.
[164] H. Cheng, C. J. Kastrup, R. Ramanathan, D. J. Siegwart, M. Ma, S. R. Bogatyrev, Q. Xu, K. A. Whitehead, R. Langer, D. G. Anderson, *ACS Nano* **2010**, *4*, 425.
[165] Y. Krishnamachari, M. E. Pearce, A. K. Salem, *Adv. Mater.* **2008**, *20*, 989.
[166] G. Paganelli, M. Malcovati, A. G. Siccardi, E. Villa, F. Sudati, C. Rossetti, F. Fazio, *Cancer Res.* **1991**, *51*, 5960.
[167] M. J. Mitchell, E. Wayne, K. Rana, C. B. Schaffer, M. R. King, *Proc. Natl. Acad. Sci. USA* **2014**, *111*, 930.
[168] S. Chandrasekaran, M. F. Chan, J. Li, M. R. King, *Biomaterials* **2016**, *77*, 66.
[169] K. Ulrich, U. Jakob, *Free Radicals Biol. Med.* **2019**, *576*, 301.
[170] M. T. Stephan, J. J. Moon, S. H. Um, A. Bersthteyn, D. J. Irvine, *Nat. Med.* **2010**, *16*, 1035.
[171] M. T. Stephan, S. B. Stephan, P. Bak, J. Chen, D. J. Irvine, *Biomaterials* **2012**, *33*, 5776.
[172] L. Tang, Y. Zheng, M. B. Melo, L. Mabardi, A. P. Castaño, Y. Q. Xie, N. Li, S. B. Kudchodkar, H. C. Wong, E. K. Jeng, M. V. Maus, D. J. Irvine, *Nat. Biotechnol.* **2018**, *36*, 707.
[173] L. Wayteck, H. Dewitte, L. De Backer, K. Breckpot, J. Demeester, S. C. De Smedt, K. Raemdonck, *Biomaterials* **2016**, *77*, 243.
[174] C. A. Holden, Q. Yuan, W. A. Yeudall, D. A. Lebman, H. Yang, *Int. J. Nanomed.* **2010**, *5*, 25.
[175] C. Büll, T. Heise, N. van Hilten, J. F. A. Pijnenborg, V. R. L. J. Bloemendal, L. Gerrits, E. D. Kers-Rebel, T. Ritschel, M. H. den Brok, G. J. Adema, T. J. Boltje, *Angew. Chem., Int. Ed.* **2017**, *56*, 3309.
[176] C. Agatemor, M. J. Buettner, R. Ariss, K. Muthiah, C. T. Saeui, K. J. Yarema, *Nat. Rev. Chem.* **2019**, *3*, 605.
[177] J. A. Prescher, D. H. Dube, C. R. Bertozzi, *Nature* **2004**, *430*, 873.
[178] H. A. Badr, D. M. M. AlSadek, M. E. El-Houseini, C. T. Saeui, M. P. Mathew, K. J. Yarema, H. Ahmed, *Biomaterials* **2017**, *116*, 158.
[179] L. Xu, O. Y. Zolotarskaya, W. A. Yeudall, H. Yang, *Adv. Healthcare Mater.* **2014**, *3*, 1430.
[180] J. Li, P. R. Chen, *Nat. Chem. Biol.* **2016**, *12*, 129.
[181] K. Landgraf, S. R. Williams, D. Steiger, D. Gebhart, S. Lok, D. W. Martin, K. T. Roybal, K. C. Kim, *Communications Biology* **2020**, *3*, 296.
[182] N. G. Minutolo, P. Sharma, M. Poussin, L. C. Shaw, D. P. Brown, E. E. Hollander, A. Smole, A. Rodriguez-Garcia, J. Z. Hui, F. Zappala, A. Tsourkas, D. J. Powell, *J. Am. Chem. Soc.* **2020**, *142*, 6554.
[183] R. E. Cone, J. J. Marchalonis, R. T. Rolley, *J. Exp. Med.* **1971**, *134*, 1373.
[184] J. Wolfram, S. Nizzero, H. Liu, F. Li, G. Zhang, Z. Li, H. Shen, E. Blanco, M. Ferrari, *Sci. Rep.* **2017**, *7*, 13738.
[185] T. Y. Hu, M. Frieman, J. Wolfram, *Nat. Nanotechnol.* **2020**, *15*, 247.
[186] A. Alshehri, A. Grabowska, S. Stolnik, *Sci. Rep.* **2018**, *8*, 3748.
[187] H. Gao, Z. Yang, S. Zhang, S. Cao, S. Shen, Z. Pang, X. Jiang, *Sci. Rep.* **2013**, *3*, 2534.
[188] N. Bloise, A. Massironi, C. Della Pina, J. Alongi, S. Siciliani, A. Manfredi, M. Biggiogera, M. Rossi, P. Ferruti, E. Ranucci, L. Visai, *Front. Bioeng. Biotechnol.* **2020**, *8*, 132.
[189] H. Y. Chew, P. O. De Lima, J. L. Gonzalez Cruz, B. Banushi, G. Echejoh, L. Hu, S. R. Joseph, B. Lum, J. Rae, J. S. O'Donnell, L. Merida de Long, S. Okano, B. King, R. Barry, D. Moi, R. Mazzieri, R. Thomas, F. Souza-Fonseca-Guimaraes, M. Foote, A. McCluskey, P. J. Robinson, I. H. Frazer, N. A. Saunders, R. G. Parton, R. Dolcetti, K. Cuff, J. H. Martin, B. Panizza, E. Walpole, J. W. Wells, F. Simpson, *Cell* **2020**, *180*, 895.
[190] S. Behzadi, V. Serpooshan, W. Tao, M. A. Hamaly, M. Y. Alkawareek, E. C. Dreaden, D. Brown, A. M. Alkilany, O. C. Farokhzad, M. Mahmoudi, *Chem. Soc. Rev.* **2017**, *46*, 4218.
[191] J. Park, S. H. Wrzesinski, E. Stern, M. Look, J. Criscione, R. Ragheb, S. M. Jay, S. L. Demento, A. Agawu, P. Licona Limon, A. F. Ferrandino, D. Gonzalez, A. Habermann, R. A. Flavell, T. M. Fahmy, *Nat. Mater.* **2012**, *11*, 895.

© 2020 The Authors. Published by Wiley-VCH GmbH

[192] S. U. Frick, M. P. Domogalla, G. Baier, F. R. Wurm, V. Mailänder, K. Landfester, K. Steinbrink, *ACS Nano* **2016**, *10*, 9216.
[193] R. Atsumi, O. Okazaki, H. Hakusui, *Biol. Pharm. Bull.* **1995**, *18*, 1024.
[194] P. R. Rhode, J. O. Egan, W. Xu, H. Hong, G. M. Webb, X. Chen, B. Liu, X. Zhu, J. Wen, L. You, L. Kong, A. C. Edwards, K. Han, S. Shi, S. Alter, J. B. Sacha, E. K. Jeng, W. Cai, H. C. Wong, *Cancer Immunol. Res.* **2016**, *4*, 49.
[195] J. M. Metselaar, T. Lammers, *Drug Delivery Transl. Res.* **2020**, *10*, 721.

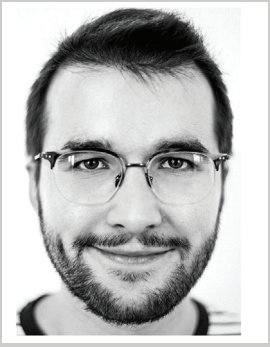

Vincent Mittelheisser: Vincent Mittelheisser is a graduate Pharmacy student (Strasbourg, France). After a Master's degree in Immunology, he was awarded a Ministère français de l'Enseignement supérieur, de la Recherche et de l'Innovation Doctoral Research Fellowship in 2020 to pursue his Ph.D. under the supervision of Dr. Alexandre Detappe and Dr. Jacky Goetz. His research interests include the immune cells surface modifications with nanoparticles and therapeutic-related applications as well as the interaction between immune cells and nanoparticles.

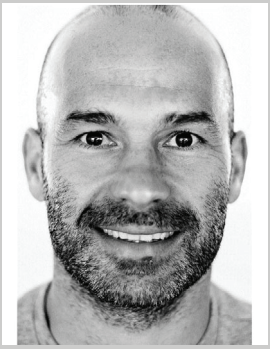

Jacky Goetz: Trained as cell biologist, he developed intravital correlative microscopy for tracking metastasis in animal models. His group focuses on dissecting the biomechanics of metastasis and showed that fluid mechanics are key regulators of tumormetastasis. They also aim at elucidating the establishment of pre-metastatic niches.



Alexandre Detappe: Dr. Alexandre Detappe is an assistant professor and head of the Nanotranslational Laboratory at Centre Paul Strauss/Institut de Cancérologie Strasbourg Europe. He completed his Ph.D. degree under the supervision of Prof. Olivier Tillement and Prof. Ross Berbeco at the University of Lyon and was a postdoctoral fellow with Prof. Irene Ghobrial at Dana-Farber Cancer Institute/Harvard Medical School. His research focuses on the development of novel organic and inorganic macromolecules for biomedical applications.

© 2020 The Authors. Published by Wiley-VCH GmbH

3. Nanomaterials trigger functional responses in primary human immune cells

Recently, a paradigm shift occurred in nanomedicine. Instead of targeting TCs with chemotherapeutics, NPs were loaded with immunomodulatory agents and targeted to immune cells (Sofias et al., 2021). Nevertheless, the impact of drug-free nanomaterials on immune cells remains surprisingly unexplored.

To address this black box, we screen untargeted and unloaded NPs impact on innate NK cells and adaptive pan T cells sourced from healthy donors. Through a proteogenomic mapping of immune cells response we highlight that PLGA NPs trigger pro-inflammatory transcriptional programs in NK and pan T cells. We further observe that pro-inflammatory transcriptional priming of NK cells resulted in an improved tumoricidal NK cells functions.

Overall, our study provides a useful resource of the impact of drug-free nanomaterials on human NK and pan T cells that will be beneficial to the tailoring of nanoimmunotherapeutic strategies in oncology.

Nanomaterials trigger functional anti-tumoral responses in primary human immune cells

Vincent Mittelheisser[1-6], Olivier Lefebvre[1-5], Mainak Banerjee[5-7], Shayamita Ghosh[5-7], Amandine Dupas[1-5], Marie-Charlotte Diringer[5-7], Juliette Blumberger[5-7], Louis Bochler[1-5], Sébastien Harlepp[5-7], Annabel Larnicol[1-5], Angélique Pichot[2-4,8], Tristan Stemmelen[2-4,8], Anne Molitor[2-4,9], Chloé Moritz[9], Christine Carapito[9], Raphaël Carapito[2-4,8,10], Loïc J. Charbonnière[11], François Lux[12,13], Olivier Tillement[12], Jacky G. Goetz[1-5,*] and Alexandre Detappe[5-7,11,*]

[1]Tumour Biomechanics lab, Strasbourg, France.
[2]INSERM UMR_S1109, Strasbourg, France.
[3]Université de Strasbourg, Strasbourg, France.
[4]Fédération de Médecine Translationnelle de Strasbourg (FMTS), Strasbourg, France.
[5]Équipe Labellisée Ligue Contre le Cancer.
[6]Nanotranslational lab, Institut de cancérologie Strasbourg Europe.
[7]Strasbourg Drug Discovery and Development Institute (IMS), Strasbourg, France.
[8]Plateforme GENOMAX, Institut thématique interdisciplinaire (ITI) de Médecine de Précision de Strasbourg Transplantex NG, Faculté de Médecine.
[9]Laboratoire de Spectrométrie de Masse BioOrganique (LSMBO), IPHC UMR 7178, CNRS, Université de Strasbourg, Infrastructure nationale ProFI FR 2048, Strasbourg, France.
[10]Service d'Immunologie Biologique, Plateau Technique de Biologie, Pôle de Biologie, Nouvel Hôpital Civil, Hôpitaux Universitaires de Strasbourg, 1 Place de l'Hôpital, 67091, Strasbourg, France.
[11]Institut Pluridisciplinaire Hubert Curien CNRS UMR 7178, Strasbourg, France.
[12]Institut Lumière Matière, CNRS UMR 5306, Université Claude Bernard – Lyon 1, Villeurbanne, France.
[13]Institut Universitaire de France (IUF), Paris, France.

***Correspondence and co-last authors**

Jacky G. Goetz, jacky.goetz@inserm.fr

Tumour Biomechanics lab, INSERM UMR_S1109, Centre de Recherche en Biomédecine de Strasbourg

1 rue Eugène Boeckel, 67000 Strasbourg.

Web: www.goetzlab.fr, @GoetzJacky

Alexandre Detappe, a.detappe@icans.eu

Institut de Cancérologie Strasbourg

3, rue de la porte de l'Hôpital, 67000 Strasbourg France

Web: www.detappelab.com, @AlxDetappe

Abstract

Targeting the immune system with nanoparticles (NPs) to deliver immunomodulatory molecules emerged as a solution to address intra-tumoral immunosuppression and enhance therapeutic response. While the potential of nanoimmunotherapies in reactivating immune cells has been evaluated in several preclinical studies, the impact of drug-free nanomaterials on the immune system remains unknown. Here, we characterize the molecular and functional response of human NK cells and pan T cells to a selection of five NPs that are commonly used in biomedical applications. After a pre-screen to evaluate the toxicity of these nanomaterials on immune cells, we selected ultrasmall silica-based gadolinium (Si-Gd) NPs and poly(lactic-*co*-glycolic acid) (PLGA) NPs for further investigation. Bulk RNA-sequencing and flow cytometry analysis showcase that PLGA NPs trigger a transcriptional priming towards activation in NK and pan T cells. While PLGA NPs improved NK cells anti-tumoral functions in cytokines-deprived environment, Si-Gd NPs significantly impaired T cells activation as well as functional responses to a polyclonal antigenic stimulation. Altogether, we identified PLGA NPs as an attractive strategy for reactivating the immune system of cancer patients.

Keywords: Immunotherapy, nanomaterial, proteogenomics

Introduction

Over the past decade, immunotherapies became increasingly attractive for cancer treatment[1–4]. Among them, adoptive cell therapy (ACT) emerge as one of the most promising approaches[5]. These therapies aim to modify *ex vivo* the immune cells to induce the expression of an exogenous antigen receptor, enabling the detection of tumor antigens and hence resulting in potent anti-tumoral responses. T cells isolated from blood or tumor tissue were the first genetically reprogrammed immune cells for ACT[6–8]. The infusion of autologous modified T cells demonstrate positive clinical outcomes in relapsed hematological malignancies[9,10], yet, adoptively transferred T cells are often associated with severe life-threatening side effects such as graft-versus-host disease, cytokine release syndrome (CRS), and neurological toxicities[11]. To overcome these limitations, emerging strategies utilizing the cytotoxic activity of non-MHC restricted NK cells are being evaluated clinically[12]. Allogeneic engineered NK cells administered to patients have shown tremendous potential to treat cancer patients, as they do not induce the abovementioned limitations while offering the possibility to be used off-the shelf[13,14]. In contrast to hematological malignancies, intratumoral infiltration of immune cells is restricted in solid tumors that quickly build an immunosuppressive tumor microenvironment (TME) which induces a rapid functional impairment of immune cells[15–19]. The emergence of cancer immunotherapies approaches allows to tackle the TME immunosuppression, but these therapies are associated with low response rate and life-threatening immune-related adverse events [20–23]. Consequently, improving cancer immunotherapy efficacy and safety remains a priority.

One of the most promising solution lies in the utilization of nanoimmunotherapy approaches to specifically target immune cells and to promote immune cells mediated anti-tumoral responses through controlled spatiotemporal immunomodulation[24]. Specifically, nanoimmunotherapies have been evaluated using carbon nanotubes (CNTs) or a combination of CNTs and poly(lactic-*co*-glycolic acid) (PLGA) polymeric nanoparticles (NPs) conjugated with peptide-loaded MHC-I, and the co-stimulatory ligand anti-CD28 to act as artificial antigen presenting cells, which are pivotal for *ex vivo* T cells expansion in ACT manufacturing processes[25,26]. In addition, polymeric NPs have also been used to to deliver immune reactivating agents (such as the TGFβR1 inhibitor SD-208) directly to tumor-infiltrating T cells *in vivo*[27]. This class of NPs has also enable the generation of genetically engineered immune cells through

ex vivo and *in vivo* delivery of CAR-encoding plasmids, providing a virus-free alternative for transduction[28,29]. More recently, ultrasmall metallic NPs decorated with anti-PD-L1 V_HH were developed to monitor *in vivo* the expression of this immune checkpoint molecule in cancer[30]. While these nanoimmunotherapies show promising results in preclinical trials, most reported nanotoxicology evaluations have focused on cargo-loaded NPs effects on primary murine cells or human immortalized cell lines[31,32]. In contrast, the investigation of NPs chemistry impact on primary human immune cells at subcellular levels remains limited. Capturing these material-specific effects on human immune cells is crucial for developing and implementing NPs in relevant clinical settings[33].

Here, we use untargeted and drug-free NPs to precisely investigate the impact of their material on innate NK cells and adaptive pan T cells sourced from healthy donors to explore the fate of NPs post-internalization in immune cells, to ensure their safety profile and guide the selection of specific NPs based on the therapeutic need. To conduct pre-screening studies integrating cytotoxicity assessments and comprehensive proteomic analysis, we selected five nanosystems from the broad array being explored in both pre-clinical and clinical research. Hence, we prioritized a rational selection of nanomaterials that are representative of lipidic, organic, and inorganic nanomaterial classes, ensuring that key variables such as material composition, size, and functionalization could be effectively evaluated. The nanomaterials included in this study were chosen not only based on their clinical relevance and frequent use in biomedical applications but also to address specific questions regarding their structure-activity relationships. We evaluated ultrasmall polysiloxane-based nanoparticles chelated with gadolinium (Si-Gd NPs) or terbium (Si-Tb NPs) to explore the role of metal chelation and core composition in modulating immune responses. Additionally, we investigated the impact of NP size by comparing ultrasmall terbium-doped silica nanoparticles (Si-Tb NPs) to larger terbium fluoride nanoparticles (Tb NPs). Furthermore, we incorporated lipid-polymer hybrid PLGA NPs and carbon nanotubes (oxCNTs) to examine how diverse physicochemical properties influence cytotoxicity and immune activation. This strategic approach enabled us to balance a broad characterization of nanomaterials with a focused comparative assessment of critical material attributes. By carefully selecting complementary systems, we provide novel insights into how key properties dictate immune cell

interactions and highlight generalizable trends that are crucial for the design of future nanoimmunotherapeutics.

Based on these results, we selected two NPs with minimal cytotoxicity and effects on the proteome. We further evaluated their internalization in primary immune cells and highlight efficient internalization of the two NPs in both primary NK and pan T cells, with $CD4^+$ T cells displaying higher internalization potential when compared to $CD8^+$ T cells. Proteogenomic mapping of immune cells response to the selected nanomaterial revealed that PLGA NPs trigger pro-inflammatory transcriptional programs in NK and pan T cells, while ultrasmall polysiloxane-based gadolinium NPs (Si-Gd NPs) do not alter their transcriptomes. We further probed the effect of NPs on the functional behavior of immune cells and observed that PLGA NPs transcriptional priming of NK cells improved anti-tumoral function of NK cells. Conversely, Si-Gd NPs treatment impaired pan T cells responses to polyclonal antigenic stimulation. This study provides a unique resource of the impact of NP materials on human NK and pan T cells that will be beneficial to the tailoring of nanoimmunotherapeutic strategies in oncology.

Results and Discussion

Unequal internalization and subsequent toxicities of nanomaterials on human innate and adaptative lymphocytes

We use a library of five NPs, composed of (*i*) oxidized carbon nanotubes (oxCNTs), (*ii*) ultrasmall polysiloxane-based gadolinium (Si-Gd) NPs and terbium (Si-Tb) synthesized with a bottom-up one pot synthesis[34], as well as (*iv*) unfunctionalized terbium fluoride (Tb) NPs and (*v*) PLGA NPs (**Fig.1A**). These five NPs were specifically chosen to enable direct comparisons between representative examples of pre-clinically and clinically relevant[35] inorganic (Si-Gd, Si-Tb, Tb NPs), polymeric (PLGA NPs), and carbon-based (oxCNTs) materials, allowing us to systematically assess the impact of diverse physicochemical parameters covering large range of hydrodynamic diameter distributions (from 5 to 120 nm) and ζ-potentials (from -50 to 40 mV), representing a wide spectrum of the nanomedicine field (**Fig.S1**) on human immune cells. PLGA NPs were selected as the representative polymeric platform due to their FDA-approved status and distinct advantages for immunological studies, including superior stability in biological fluids, tunable degradation kinetics enabling controlled release, and inherent immunomodulatory properties through complement activation,

features that distinguish them from lipid-based systems. While liposomes and lipid nanoparticles (LNPs) have clinical relevance, their lipid membrane fusion mechanisms represent fundamentally different cellular interaction profiles compared to the sustained-release polymeric degradation of PLGA, making PLGA more representative of the broader polymeric nanomaterial class. The inorganic silica-based particles (Si-Gd, Si-Tb) were included to represent theranostic applications, while the systematic size and composition variations (ultrasmall Si-Tb vs. larger Tb NPs) enable assessment of structure-activity relationships. Carbon nanotubes were incorporated to capture the unique immunological effects of one-dimensional morphology not present in spherical particles. This selection strategy ensures comprehensive coverage of major nanomaterial categories while maintaining clinical relevance and avoiding mechanistically redundant systems. To assess the impact of these NPs on primary human immune cells, we negatively isolate NK and pan T cells from healthy donor buffy coats with high purity (>95%) and subject them to a cytotoxicity-driven screening test (**Fig.S3A−B**). We incubate the sorted NK and pan T cells with increasing NPs concentration for 48 h (**Fig.1B**). We observe that oxCNTs markedly decrease NK cells (IC_{50} = 68.37µg/mL) and pan T cells (IC_{50} = 47.65µg/mL) viability at low concentrations. Inversely, the other tested nanomaterials do not significantly decrease immune cells viability (**Fig.1B**). We perform a whole proteome (liquid chromatography-tandem mass spectrometry, LC-MS/MS) analysis to further assess nanomaterials impact on immune cells (**Fig.S4A**).

While terbium-based NPs (Si-Tb and Tb NPs) do not overtly affect immune cell viability (**Fig.1B**), the whole proteome analysis reveals an upregulation of proteins linked with necroptosis (**Fig.S4A**). Based on this initial pre-screening that combines proteomic and viability read-outs, we exclude cytotoxic oxCNT and terbium-based NPs as they appear unattractive for further preclinical development in this context. On the other hand, Si-Gd and PLGA NPs display no toxicity towards primary human immune cells (IC_{50} > 1 mg/mL) (**Fig.1B**) and the observed deregulated proteins are not associated with specific gene ontology terms (**Fig.S4A**). We thus decided to further evaluate their impact on immune cells using concentrations of 150 µg/mL of Si-Gd NPs[36] and 50 µg/mL of PLGA NPs[37] (median of the tested range for immune cells viability assay).

We next confirm that Cyanine5.5-labelled Si-Gd NPs and PLGA NPs efficiently penetrate NK and pan T cells despite their low phagocytic potential (**Fig.1C**). Through an incubation on ice, we highlight that Cyanine5.5-labelled Si-Gd NPs and PLGA NPs

internalization in NK and pan T cells rely on their metabolism (**Fig.S3B**). Furthermore, we assess NPs cellular uptake via flow cytometry 48h post-treatment. We observe that Si-Gd NPs and PLGA NPs are uniformly internalized in NK cells, forming a single continuous population with no significant differences between $CD56^{High}$ and $CD56^{Low}$ NK cells (**Fig.1D-E**). Conversely, we notice that pan T cells exhibited two distinct populations based on the uptake levels - *i.e.* one with low internalization rates comparable to NK cells and another with significantly higher levels of both NPs (**Fig.1D**). Further flow cytometric analysis revealed that high internalizing T cells population predominantly comprises $CD4^+$ T cells, while the low internalizing population is enriched in $CD8^+$ T cells (**Fig.1F**). Although the exact mechanism underlying the difference in internalization abilities between $CD4^+$ and $CD8^+$ T cells remains unclear, it originates from $CD4^+$ T cells intrinsic higher metabolic potential[38] and unconventional phagocytic potential, a feature not observed in $CD8^+$ T cells[39,40]. Importantly, increasing the concentration of NPs resulted in a dose-dependent uptake in NK cells and low-internalizing pan T cells (**Fig.S4C**). At the opposite, the high internalizing pan T cells population reached a plateau starting at the lowest tested Si-Gd NPs concentration and only a marginal increase in PLGA NPs uptake at higher doses (**Fig.S4D**).

Altogether, we demonstrate that Si-Gd NPs and PLGA NPs are successfully internalized by NK and pan T cells without associated toxicities. Yet, NK cells and $CD4^+$ or $CD8^+$ T cells are not equal with regards to nanomaterials uptake.

PLGA NPs trigger a pro-inflammatory signature in immune cells

To provide a refined analysis of the impact of the NPs on human NK and pan T cells, we perform a gene expression analysis using bulk RNA sequencing after 48 hours of treatment. Unsupervised analysis of the entire transcriptome using principal component analysis (PCA) reveal that PLGA NPs-treated populations clustered separately from control (untreated) and Si-Gd NPs-treated cells in the principal component space, indicating significant transcriptomic differences (**Fig.2A**). We identify 249 differentially expressed genes (DEGs) in NK cells and 395 DEGs in pan T cells following PLGA NPs exposure (adjusted p-value ≤ 0.05 and fold-change > 2) (**Fig.S5A and Table S1-2**). In contrast and in agreement with the PCA analysis, only 16 and 11 genes are differentially expressed in Si-Gd NPs-treated NK cells and pan T cells respectively (**Fig.S5A and Table S1-2**).

Upstream regulators analysis of the deregulated genes following PLGA NPs treatment reveals that TNF was the most significant activated regulator (NK cells Z-score 7.79; pan T cells Z-score 5.354 and *p*-values of overlap were 2.82×10^{-42} and 4.60×10^{-38}, respectively). Other regulators in the top five included IL1B, NFκB, and IFN, all of which were predicted to be activated upon PLGA NPs treatment (**Fig.S5B**). When we compared expected protein-protein interactions network among upregulated genes in PLGA NPs-treated pan T cells, we found a complex interaction between TNF, NFκB, and IFN in NK- (**Fig.S5C**) and pan T cells (**Fig.S5D**).

Using an aggregate expression analysis, we confirm the global upregulation of tumor necrosis factor-α (TNFα) signaling via the nuclear factor-κB (NFκB) and interferon gamma (IFNγ) pathways in PLGA NPs-treated NK cells compared with the untreated and Si-Gd NPs-treated populations (**Fig.2B-C**). Overexpression of key downstream regulators NFκB and IRF1 mRNA is further confirmed by reverse transcription quantitative polymerase chain reaction (RT–qPCR) (**Fig.2D-E**). In addition to significant enrichments of upregulated genes in GO terms/pathways associated with cytokines signaling and several immune-associated pathways, we observe that PLGA NPs treatment also induce an upregulation of immune cells specific transcriptional programs such as NK cells cytotoxicity against tumour cells, α/β T cells activation and T_H1 immune response (**Fig.S5E**).

When probing transcriptional programs specific to immune cells activation, we observe that PLGA NPs treatment lead to a significant overexpression of genes linked to NK cells activating receptors (*NCR2*/NKp44), immediate-early response genes (*DUSP4*, and *EGR2*), and co-stimulatory receptors (*TNFRSF4*/OX-40, *TNFRSF9*/4-1BB, *TNFRSF18*/GITR, *CRTAM* and *TNFSF10*/TRAIL)[41,42] (**Fig.2F and Table S3**). Correlatively, PLGA NPs-treatment induce a trend increase in the early activation marker CD69 expression at the basal level in NK cells, which we further confirm by flow cytometry (**Fig.2G**). PLGA NPs also induced an overexpression of the high-affinity interleukin-2 receptor (*IL2RA*/CD25) and NME1 (Fold Change: 2.46; *q*-value = 4.02×10^{-4}) which are critical for NK cells activation and proliferation[43] (**Table S3**). Additionally, PLGA NPs-treated NK cells displayed an upregulation of *IFNG* (Fold Change: 7.46; *q*-value = 4.67×10^{-5}), *ICAM1* (Fold Change: 2.29; *q*-value = 2.86×10^{-5}) transcripts required for NK cells killing of tumour cells[13,44] as well as *XCL1* (Fold Charge: 2.15; *q*-value = 2.10×10^{-6}) transcripts linked to cDC1 recruitment and

orchestration of adaptive immunity by NK cells[45] (**Table S3**). Transcriptional programs analysis also revealed that PLGA NPs treatment induced the upregulation of genes associated with a NK cells adaptative/memory phenotype (*LAG3*, *IRF4* and *BCL2L11*/BIM)[46–48] (**Fig.2F and Table S3**). These NK cells also overexpressed *CCR7* (Fold change: 2.97; *q*-value = $8.63x10^{-10}$) and *CD83* (Fold change: 3.38; *q*-value = $1.07x10^{-23}$), genes associated with migratory and helper phenotypes leading to high ability to produce IFN-γ[49].

Similarly, transcriptional programs analysis of PLGA NPs treated pan T cells present a positive z-score for genes related with activation (*TNFRSF4*/OX-40, *TNFRSF9*/4-1BB, *TNFRSF18*/GITR), proliferation (*IL15*/*IL15RA, LIF*), and cell division (*G0S2*, *NME1*)[50,51] as well as effector functions (*GNLY*, *GZMB*, *SLAMF7*, *NKG7*)[52,53] (**Fig.2H and Table S3**). Alongside, PLGA NPs-treated pan T cells displayed an upregulation of ATF-like transcription factors such as *BATF* (Fold Change: 2.38; *q*-value = 0.001) and *BATF3* (Fold Change: 2.34; *q*-value = 0.04), that are essential checkpoints for early effector T cells differentiation[54,55]. Furthermore, as highlighted in the differentially expressed term analysis (**Fig.S5C**), these effector-primed T cells displayed a T_H1 transcriptional landscape (*STAT1*, *ADAM12*)[56,57] as well as a reduction in T_H2 transcription factors transcripts (*GATA3*) and cytokines (*IL12B*, *TNF*, *IL17F*, *XCL1, CCL3L1*, *CCL4L1*) known to prime and to be expressed during T_H1/TH_{17}-like pro-inflammatory response[58–60] (**Table S3**). Similarly to NK cells and in accordance with the upregulation of activation/effector-associated genes, PLGA NPs treatment increased CD69 expression at the basal level in pan T cells as observed by flow cytometry (**Fig.2I**). We confirmed such priming with a nanomaterial-induced dose-dependent decrease in CD3 expression (**Fig.S6A-B**) and with an increase in pan T cells size (**Fig.S6C-D**), that are classically associated with their activation[61]. On the other hand, and as expected, Si-Gd NPs did not induce pan T cells basal activation (**Fig.S6A-E**). Besides, transcriptional activation of pan T cells by PLGA NPs was further underpinned by the induction of multiple gene families associated with canonical IFN response module (*IFIT1*, *IFIT2*, *IFIT3*, *IFITM1*, *IFITM2*, *IRF1*, *IFI44*, *IFI44L*, *STAT1*, *GBP1*, *GBP4*, *GBP5*)[52,62,63] (**Table S2**). Of note, we also found a significant increase in the expression of immune checkpoint transcripts (*LAG3*, *HAVCR2*/TIM3) (**Fig.2H and Table S3**) that can be counteract by the upregulation of *EGR2* (**Table S3**) whose role was recently described in maintaining anti-tumor responses of exhausted T cells[64,65].

Altogether, we identify a transcriptional priming in NK and pan T cells upon drug-free PLGA NPs treatment, but not with Si-Gd NPs through bulk RNA sequencing of immune cells. Flow cytometry analysis further exhibit that drug-free PLGA NPs exposure was sufficient to trigger NK and pan T cells activation.

PLGA NPs enhance anti-tumor functions of NK cells

As PLGA NPs could transcriptionally prime NK cells, we sought to investigate whether they could functionally activate their tumor-lytic properties (**Fig.3A and Fig.S7A-B**). We co-culture NPs-treated NK cells with their prototypical targets lacking MHC class I molecules, the K562 cells, over 4h with or without supplementing the pro-survival cytokine IL-15 to mimic tumor microenvironments that often lack pro-survival cytokines required by cytotoxic NK cells[66] (**Fig.3A**). With IL-15, both Si-Gd NPs and PLGA NPs-treated NK cells successfully clear the K562 targets (**Fig.3B**). Without supplementary IL-15, only PLGA NPs-treated NK cells efficiently induce killing of 25% of the target cells (**Fig.3B**). Of note, NK cells anti-tumoral functions alterations observed in control NK cells or upon Si-Gd NPs treatment are not resulting from an impaired NK cells activation, as all conditions exhibited similar CD69 expression levels (**Fig.3C**). In addition, both NPs-treatment do not impair K562 target cells recognition, as observed through the measurement of available NKG2D receptor at the NK cells surface by flow cytometry (**Fig.3D**). Nevertheless, without IL-15, PLGA NPs treatment induces a significant increase in the number of conjugates between NK cells and their K562 target cells, as measured by flow cytometry (**Fig.3E**). Prompted by this result, we next induce IS formation and assess the distance between mature perforin and the plasma membrane of NK-K562 synapses (**Fig.3F**), using stable expression of palmitoylated tdTomato (**Fig.S6C**), as efficient cytotoxic granule polarization at the immune synapse (IS) is also critical for the killing capacity of NK cells. Without IL-15, PLGA NPs treatment favor cytotoxic granules convergence at the IS, as measured by the reduction of granules distance to the IS (**Fig.3F**). Concomitantly, PLGA NPs treatment increase the percentage of NK cells presenting a polarized IS (**Fig.3F**). In contrast, neither Si-Gd NPs treated, nor untreated NK cells present polarized IS (or reduced distance between perforin and the IS) (**Fig.3F**), suggesting that, as expected, PLGA NPs treatment induce efficient K562 cells lysis through an increase in NK cells perforin polarization. Coming back to our proteogenomic analysis, we highlight that PLGA NPs

induce the upregulation of proteins associated with NK cells maturation (IKZF3)[67], cell adhesion (VLA-1: ITGA1/ITGB1)[68] and vesicle transport (STX11)[69] (**Fig.S7D**). Conversely, Si-Gd NPs repress the expression of these proteins and stimulate the expression of proteins associated with NK cells inhibitory signaling (HLA-E and GSK3B)[70–72] that are less or not expressed in PLGA NPs-treated NK cells (**Fig.S7D**). NK cell-induced cytotoxicity requires both polarization of the cytotoxic granules and their fusion with the plasma membrane, allowing the release of their cytotoxic content. We next monitor NK cells degranulation by dosing the cytotoxic cytokines TNFα[73] and IFNγ[74] in the supernatant after 4h of NK cells co-incubated with their target K562 cells. Increased cytotoxic granules polarization in PLGA NPs-treated NK cells is corroborated by a trend, yet non-significant, augmentation in TNF-α and IFN-γ concentrations when compared to control and Si-Gd NPs-treated NK cells (**Fig.3G**). According to these results, we demonstrate that NK cells transcriptional priming towards an activated phenotype induced by PLGA NPs results in an enhancement of their anti-tumoral cytotoxic capacity *in vitro* in a cytokines-deprived (*i.e.*, immunosuppressive) environment.

Silica-based gadolinium NPs treatment impairs pan T cells functions

When investigating the impact of NPs on T cell functions, we notice from the unbiased proteomic approach previously described (**Fig.S4A**) that proteins involved in TCR downstream signaling are significantly downregulated (CD48, PLCG1 and CARD11)[75–77] upon Si-Gd NPs treatment (**Fig.4A**). These modifications are accompanied by a significant reduction in proteins associated with pan T cells cytoskeletal remodeling, including small GTPase (CDC42, RAC1 or SEPT7)[78,79], actin binding proteins (Ezrin, EZRI or WAVE2)[80,81] as well as formins (formin-like-1, FMNL1)[82] (**Fig.4A**). Si-Gd NPs-treated pan T cells also display a significant decrease in the levels of integrin β1, which sustains cytotoxic T cells functions[83,84] and their efficient intra-tumoral infiltration[85]. Similarly, we also observe a significant diminution in proteins required for terminal transport (KLC1 and KIF5B)[86] and membrane fusion (SNAP23 and VAMP8)[87,88] of lytic granule at the immune synapse (**Fig.4A**). Incidentally, PLGA NPs have no or little effects on these proteins (**Fig.4A**). Building on these observations, we aim at testing the effect of NPs on pan T cells function. We mimic stimulation of the TCR and co-receptors by coating surfaces with activating

antibodies against CD3 (part of the TCR complex) and CD28 (a costimulatory receptor) and measure how T cells activate and spread, as they would over the surfaces of antigen presenting cells (APCs)[89] (**Fig.4B**). We first observe that both Si-Gd and PLGA NPs treatment do not prevent global pan T cell activation when comparing CD69 expression after 24h of culture on a surface coated with increasing concentrations of anti-CD3 and a fixed concentration of anti-CD28 antibodies (hereafter, anti-CD3/CD28) (**Fig.4C**). This result further suggests that transcriptional priming is antigen-independent and mediated by intracellular cues. However, in the line with TCR signaling proteins downregulation observed in our proteomic data, Si-Gd NPs-treated pan T cells require higher anti-CD3/CD28 concentrations to reach similar activation levels than control and PLGA NPs-treated pan T cells, suggesting a reduced sensitivity to TCR activation (**Fig.4C**). We further confirm this weakened TCR signaling by measuring OX-40 expression, a co-stimulatory molecule selectively induced after TCR stimulation[90,91]. When normalizing to untreated pan T cells, we notice that Si-Gd NPs reduced by 25% OX-40 expression (**Fig.4D**).

Next, we sought to analyze NPs treatment effect on actin remodeling at the IS. We compare pan T cell spreading on glass surfaces coated with anti-CD3 together with a recombinant ICAM1-Fc chimera protein (**Fig.4B**). We monitor T cells morphology and cytoskeletal remodeling and observe that Si-Gd NPs, but not PLGA NPs, significantly reduce cell spreading and F-actin content (**Fig.4E**). T cells-mediated functions require not only spreading on the APCs surface but also degranulation. We thus assess the effect of NPs treatments on the degranulation of pan T cells as well as of their $CD4^+$ and $CD8^+$ subpopulations. To do so, we follow the cell surface expression of CD107a (LAMP-1) and cytokines release in T cells activated by anti-CD3/CD28 and ICAM1-Fc chimera protein. When compared to control, CD107a expression is significantly decreased by Si-Gd NPs treatment in pan T cells from all tested donors, hinting at an inhibition of their degranulation (**Fig.4F**). This phenotype is associated with a significant two-fold reduction in TNFα and IFNγ secretion (**Fig.4G**). We previously observe that $CD4^+$ and $CD8^+$ T cells internalized differentially the NPs (**Fig.1F**) and thus wonder whether the uptake level of NPs affect the T cells functionality. Hence, we further evaluate the CD107a expression of $CD4^+$ and $CD8^+$ T cells within the pan T cells population. Interestingly, $CD4^+$ and $CD8^+$ T cells exhibited similar significant two-fold diminution in CD107a expression upon Si-Gd NPs treatment, suggesting that their detrimental effect already occurs at low NP doses (**Fig.4H**).

Altogether, we highlight that Si-Gd NPs treatment widely impairs T cells activation, and functional responses to a polyclonal antigenic stimulation.

Conclusion

Nanoimmunotherapies, combining nanotechnology and immunotherapy, represent a promising therapeutic strategy to improve anti-tumoral immune response. Understanding how NPs materials impact immune cells post-internalization is essential to ensure their safety profile and rationally guide the selection of specific NPs based on the therapeutic need.

Here, we present a pioneering analysis of the material impact from untargeted and drug-free NPs on two human primary immune cell types. Through a pre-screen combining cytotoxicity measurement and whole proteome analysis of a panel of five different nanomaterials under preclinical and clinical evaluation, we first highlight the toxicity of oxCNTs and terbium-based NPs (Tb and Si-Tb NPs) on NK and pan T cells. Overt toxicity at low concentration induced by oxCNTs might be partially explained by the downregulation of a wide range of proteins associated with cellular metabolic processes as well as ribosomal associated proteins, as observed by whole proteome analysis (**Fig.S4A**). Of note, ribosomal associated proteins modulation was previously observed following co-culture of Jurkat T cells with carbon-based NPs[92].

Based on this pre-screen, we identify Si-Gd NPs and PLGA NPs as promising candidates for further preclinical development. We further examine Si-Gd NPs and PLGA NPs interactions with immune cells using a proteogenomic approach. Bulk RNA-sequencing reveal that PLGA NPs triggered a strong transcriptional priming towards activation in NK and pan T cells. We additionally validate by flow cytometry that drug-free PLGA NPs exposure was sufficient to activate NK and pan T cells, further confirming the transcriptional priming. Upstream regulators and aggregate expression analysis reveal that this priming is, in part, mediated by TNF-α via NFκB and IFN-γ pathways. Investigation of the expected protein-protein interactions network among upregulated genes in PLGA NPs-treated NK- and pan T cells (**Fig.S5C-D**) further underpin the complex interaction between TNF, NFκB, and IFN pathways. Although our study sheds light on which signaling pathway activated by PLGA NPs triggers NK- and pan T cells activation, the initial events and targets engaged during the immune cells-NPs interaction remain to be identified. One could combine modeling of potential interactions between NPs, their protein corona and immune sensors such as Toll-Like

Receptors or other Pattern Recognition Receptors (PRRs). Additionally, localization and possible colocalization of NPs with PRRs using high-resolution live-cell imaging could solve the mechanisms underlying NK and pan T cell activation. More detailed investigations of NK functions upon NPs exposure reveal that PLGA NPs treatment efficiently enhance NK cells tumoricidal activity in cytokines-deprived environment. In depth analysis showcase that the NK cells functional enhancement is mediated by an increase in conjugates formation, a better mature perforin polarization at the IS associated with a surge in cytotoxic cytokines release. Increased perforin polarization might be partially explained by an enhanced NK cells maturation and vesicles transport as observed in our proteogenomic data. In line with our results, another study recently demonstrated that drug-free polymer micropatches were able to activate murine neutrophils and induce an N1 anti-tumoral response[93]. Yet, our *in vitro* analysis does not allow to evaluate how NK cells priming integrate into the global adaptative immune system. Since NK cells are key player in the regulation of adaptive immune responses[94], notably by the recruitment dendritic cells via XCL1[45] (that is overexpressed by PLGA NPs-treated NK cells), thorough *in vivo* evaluation remained to be performed to decipher *ex vivo* primed NK cells tumoricidal enhancement on tumor burden regression and systemic immune response induction.

In parallel, explorations of pan T functions expose that Si-Gd NPs treatment widely impaired their activation, and functional responses to a polyclonal antigenic stimulation. Detailed analysis reveals that impairment was similar in $CD4^+$ and $CD8^+$ T cells despite different internalization rates, suggesting that their detrimental effect already occurs at low doses. Si-Gd NPs are under clinical evaluation as a MRI contrast agent[95] and radio-enhancer[96] (NCT04789486). Si-Gd NPs increase the radiation effects on tumor cells, inducing higher immunogenic cell death levels and higher immune cells recruitment to the tumor bed[97]. Therefore, a careful assessment of the impact of Si-Gd NPs on recruited immune cells is necessary. In addition, Si-Gd NPs were recently targeted with a programmed death-ligand 1 (PD-L1) V_HH to monitor immune checkpoint molecules expression *in vivo* through medical imaging[30]. However, human effector T cells are also PD-L1[98,99]. These results suggest that Si-Gd NPs development as medical imaging tracers to assess immune infiltration in tumors and to predict response to immunotherapy treatments should be carefully evaluated. Interestingly, a previous study exhibit that ultrasmall silica NPs were able to induce a dose-dependent $CD4^+$ and $CD8^+$ T cells activation[36]. These ultrasmall

silica NPs possess a hydrodynamic diameter similar than our Si-Gd NPs, suggesting than metallic loading can impact T cells response. Further investigations in that sense should be performed to evaluate other metals (such as gold or silver NPs). While transcriptomic analysis reveals that PLGA NPs seemed to promote a T_H1 anti-tumoral polarization signature, working with healthy pan T cells we were not able to investigate this aspect of the NPs impact. Indeed, healthy pan T cells do not possess a tumor antigen-specific TCR. Further evaluation working with T cells sourced from cancer patients or TCR-engineered T cells are required to evaluate the function impact of the transcriptional T_H1 polarization.

Our findings highlight the significant potential of drug-free PLGA NPs to activate human immune cells via the TNF-α and NFκB pathways. This study lays a strong foundation for future preclinical and clinical research into PLGA NP-based immunotherapies. Further exploration, including *in vivo* evaluations and studies involving tumor-infiltrating lymphocytes and primary tumor cells, may support the validation of such strategies. A first step, assessing the safety and immuno-modulatory effects of PLGA NPs in cancer-specific settings using humanized mouse models would be valuable. However, replicating the human immune system in mice remains challenging, as these models often display defective NK cells homeostasis[100] and limited immune functions due to the absence of lymph nodes for effective immune response mounting[101], and they rely on supraphysiological cytokine expression to compensate[102]. Additionally, our results offer valuable insights for the rational selection of NP materials in nanoimmunotherapeutic strategies. We identify drug-free PLGA NPs as promising candidates for targeted approaches aimed at reactivating the immune response in cancer patients. The intrinsic properties of PLGA NPs may also synergize with immuno-activating agents, providing a complementary mechanism to effectively modulate and enhance immune responses.

Experimental section

Nanoparticles synthesis.

Nanoparticles were synthetized as previously described. Briefly, carbon nanotubes have been shortened under strong acid conditions (H_2SO_4/HNO_3 3:1) and sonication for 24h to generate a high amount of carboxylic groups at the tips and around the side walls[103]. The ultra-small metal-based NPs are composed by a polysiloxane core, and a shell comprising amine function and metal complexed by DOTAGA (in same amount) and were provided by the Institut Lumière-Matière of the University of Lyon. Si-Gd were synthetized by a top-down process[104] and Si-Tb were synthetized in a one-pot protocol[34]. Lanthanide-doped $La_{0.9}Tb_{0.1}F_3$ NPs (hereafter, Tb NPs) were synthetized by dropwise addition of 0.9 $LaCl_3$ and 0.1 $TbCl_3$ to 3 NH_4F followed by heating at 150°C for 12 mins and purification, as described in[105]. Finaly, hybrid PLGA-lipid NPs were synthetized via self-assembly of poly(D,L-lactide-*co*-glycolide) acid (30-60 kDa, lactide:glycolide 50:50; Sigma #P2191) and 1,2-distearoyl-sn-glycero-3-phosphoethanolamine-N-[carboxy(polyethylene glycol)-2000] (sodium salt) (DSPE-PEG-CO_2H; Avanti Polar Lipids #880135) through a one-step nanoprecipitation method as described previously in[106]. Briefly, PLGA polymer was dissolved with or without 0.2% Cyanine 5.5 carboxylic acid (Lumiprobe #17090; $\lambda_{ex}/\lambda_{em}$: 684nm/710 nm) in acetonitrile at a concentration of 5 mg/mL. DSPE-PEG-CO_2H, at a weight ratio of 20% relative to PLGA polymer, was dissolved in 10 mL of 4 wt% ethanol aqueous solution and stirred vigorously at 65 °C. The PLGA solution was then added dropwise into the lipid solution using a syringe pump (0.5 mL/h) under constant stirring. The entire mixture was kept under gentle stirring for 2 hours at room temperature under a chemical hood. The remaining organic solvent and unloaded molecules were removed by washing the NP solution with ultrapure water using an Amicon Ultra-15 centrifugal filter from Millipore, France (cut-off: 50 kDa; 3 cycles, 3,000*g*, 10 min) via tangential centrifugation. The final NP formulation was reconstituted in 1 mL of ultrapure water.

Dynamic Light Scattering (DLS).

DLS measurements were conducted using a nano-ZS instrument (Malvern). The suspensions of NPs were prepared in a solution of nanopure water (Milli-Q). DLS measurements were performed in sets of 10 acquisitions. The average hydrodynamic diameters of the NPs were determined by analyzing the DLS correlation function through a regularization fitting method.

Human NK and pan T cells isolation.

Peripheral blood mononuclear cells (PBMC) were obtained by density gradient centrifugation (1,200*g*, 20mins) of buffy coats from healthy volunteer blood donors under written informed consent recruited at Établissement Français du Sang Grand-Est, Strasbourg, France (agreement A122395/2022). Following erythrolysis (MiltenyiBiotec #130-094-183), NK cells and pan T cells were isolated from PBMC by negative magnetic cell-sorting (MiltenyiBiotec #130-092-657and #130-096-535) following manufacturer instructions. The cell purity was then controlled by flow cytometry on a Attune NxT (Invitrogen) flow cytometer using PE anti-CD56 (1:100, MiltenyiBiotec #130-113-312) and FITC anti-CD3 (1:100, MiltenyiBiotec #130-126-882) staining and ranged from 90% to 99.2% (median 96.3%). Gating strategy is shown in Figure S2.

NK- and pan T cells (10^6 cells/mL) were cultured for further experiment in R10 medium: RPMI 1640 (Gibco #72400054) containing 2mM Glutamine, 25mM HEPES and completed with 10 % v/v of (fetal bovine serum) FBS (Gibco), 100 U/mL penicillin, 100 µg/mL streptomycin (PanBiotech #P06-07100) and 50 µM β-mercaptoethanol (Gibco #11508916).

Cell lines and cell line engineering.

The human chronic myelogenous leukemia cell line K562 (ATCC CCL-243) was cultured under standard conditions (37°C, 5% CO_2) using complete R10 medium. Cell viability *in vitro* was assayed before functional experiment by a Countess 3® automated cell counter (ThermoFisher).

For immune synapse formation, K562 cells were engineered to express a palmitoylated tdTomato. Briefly, the tdTomatoDNA fragment from the Addgene plasmid tdTomato-Lifeact-7 (#54528) was amplified by PCR to add the palmitoylation sequence of the *GAP43* gene and then cloned in pJET 1.2 vector according to manufactory instructions (ThermoFisher #K1231). The generated Mb-tdTomato fragment was then cloned in a lentivirus pLSFFV-IRES-Blasticidin vector. Lentivirus generated from the pLSFFV-Mb-tdTomato-IRES-Blasticidin construct were produced by transfection together with 3 additional vectors (pLP1, pLP2 and pLP3-VSV plasmids) in HEK293T cells using JetPRIME transfection reagent (Polyplus).

For K562 cells transduction, 6 wells plate was coated with Retronectin (Takara, 10µg/cm^2) for 2h at room temperature. Wells were washed in PBS before blocking with 2% BSA in PBS for 30 min. After a wash with PBS, 400.000 K562 cells were seeded and let adhere overnight under standard conditions (37°C, 5% CO_2). The day after, lentiviruses encoding for the pLSFFV-Mb-tdTomato-IRES-Blasticidin construct were added in the presence of polybrene (10µg/mL). After one day of transduction, selection with blasticidin (5µg/mL) was performed until highly fluorescent cells were FACS sorted.

Nanoparticles impact on immune cells viability.

Negatively sorted NK and pan T cells (100,000/wells) were treated with increasing concentrations of each NPs types in complete R10 medium. Cells were treated for 48h under standard conditions (37°C, 5% CO_2). Immune cells viability was measured at the endpoint using the CellTiterGlo® luminescent cell viability assay (Promega #G7570).

Immune cells RNA extraction and bulk RNA-sequencing.

RNA extraction and quantification. After 48h of culture, NK and pan T cells untreated or treated with NPs at the indicated concentrations were harvested and washed in ice-cold PBS. Total RNA was isolated using the RNAeasy kit (Qiagen #74136) with on-column DNAse I digestion (Qiagen #79256) according to manufacturer's instruction. RNA was eluted in 50µL final volume, and its concentration was assessed with the NanoPhotometer® N60 (Implemen). RNA integrity was assessed using a total RNA Pico Kit by Bioanalyzer 2100 Instrument (Agilent Technologies). All samples had RNA integrity numbers above 7.

Library preparation and sequencing. Sequencing libraries were prepared using "NEBNext Ultra II Directional RNA Library Prep Kit for Illumina" and enriched in mRNA using "NEB Ultra II polyA m RNA magnetic isolation" kit (New England Biolabs). Libraries were pooled and sequenced (single-end, 100bp) on a NextSeq2000 according to the manufacturer's instructions (Illumina Inc.).

Multidimensional scaling (MDS) and differential expression analysis. For each sample, quality control was carried out and assessed with the NGS Core Tools FastQC[107]. Sequence reads (minimum 22.4 million) were mapped to *Homo sapiens* hg19 using STAR[108] to obtain a BAM (Binary Alignment Map) file. An abundance matrix was

generated based on read counts identified by HTSeq-count[109]. Multidimensional scaling (MDS) was performed on gene expression counts normalized using the DESeq2 R package[110] to investigate relative similarities across the different conditions. The first two principal components were plotted against each other, along with their respective variances explained. Differential expression analysis was then performed between the NPs treated conditions and the control using DESeq2[110] package of the Bioconductor framework for RNASeq data[111]. Volcano plots were constructed based on $\log_2$ fold change (≥ or ≤ 2) and $-\log_{10}$ FDR adjusted *p*-value (<1.3).

Erichment analysis. Enrichment analysis of Gene Ontology (GO) terms a was conducted using Metascape (http://metascape.org)[112]. Functional analysis of gene expression changes was undertaken using Ingenuity Pathway Analysis (IPA, Ingenuity Systems).

Estimation of aggregate expression. Genes related to TNFα signaling via NFκB and IFNγ pathways were curated from the MSigDb Hallmark 2024 database (**Table S4**). For each experimental condition, aggregate expression levels of the indicated gene signatures were estimated by first performing a normalization on the cell counts. The normalized counts were then z-scored by gene (across all the conditions), after which the genes of interest were subsetted and their distribution of z-scored gene counts visualized as violin plots.

RT-qPCR analysis.

Downstreamed regulators expression was performed by generating complementary DNA (cDNA) with the High-Capacity cDNA Reverse Transcription Kit (Applied Biosystems #4368814), according to the manufacturer's instructions. qPCR analysis on each biological sample was performed using technical replicates with the TaqMan system on a QuantStudio™ 3. The cDNA concentration of target genes was normalized by amplification of GAPDH and fold changes in gene expression were obtained using the $2^{-\Delta\Delta Ct}$ method. TaqMan probes were NFKB1 (Hs00765730_m1), NFKB2 (Hs01028890_g1), RELA (Hs01042014_m1), RELB (Hs00232399_m1), IRF1 (Hs00971965_m1), GAPDH (Hs02786624_g1).

Whole proteome analysis.

Protein extraction and samples preparation. After 48h of culture, NK and pan T cells untreated or treated with NPs at the indicated concentrations were harvested and washed in ice-cold PBS. Immune cells dry pellets were flash frozen in liquid nitrogen. Cellular pellets were resuspended in 2% SDS, 62.5 mM Tris-HCl pH = 6.8 and lysed using a water bath sonicator cooled with ice. Protein concentration was estimated using the Biorad DC kit (Hercules). Proteins (2µg) were prepared using a modified SP3 workflow based on[113]. Briefly, proteins were reduced 30 minutes at 37°C with dithiothreitol (final conc. 12mM) and alkylated 30 minutes, RT, in the dark with iodoacetamide (final conc. 40mM). SP3 magnetic beads (Sera-Mag SpeedBeads) were rinsed 3 times with H_2O before being added to the sample (ratio 1:10 protein/beads). Acetonitrile (final conc. 50% v/v) was added to precipitate the proteins on the beads and the samples were incubated for 15min, RT, with agitation. The beads were washed twice with 200µL of 80% ethanol and once with 180µL of acetonitrile before being resuspended in 40µL of ammonium bicarbonate (100mM) followed by 5min sonication in a water bath. Trypsin/Lys-C was added to achieve a final ratio of 1:10 (enzyme:protein) and the proteins were digested overnight, 37°C, 600rpm. Samples were acidified with formic acid to a final conc. of 1% v/v and centrifuged for 10min at 3500rpm. The samples were incubated for 10 minutes on the magnetic rack and the supernatants containing the peptides were transferred to a new plate. Peptide clean-up was performed on a Bravo AssayMap (Agilent) using 5µL RP-C18 cartridges (Agilent) following the manufacturer's instructions.

nLC-MS/MS analysis. After evaporation, peptides were resuspended in H_2O/ACN/FA (98/2/0.1) and 1/6th of the peptides were injected in randomised order on a nanoAcquity (Waters) - Q-Exactive HF-X coupling (Thermo Fisher Scientific). Peptides were separated using a 79min gradient at a flow rate of 400nL/min. The amount of solvent B (ACN/FA, 99.9/0.1) started at 1%, increased to 8% in 2 mins and then to 35% B in 77 mins. The column was washed by increasing the percentage of B to 90% in 1min and for 5min before decreasing to 1% B in 2min and for 2min to re-equilibrate the column. MS analysis was performed using a TOP20 data-dependent acquisition. The scan range was 375 to 1500m/z with a dynamic exclusion of 40s. For precursor analysis, a resolution of 120,000 was used with an AGC target of 3.10^6 and a maximum injection time of 60ms. For fragment analysis, the resolution was 15,000 with an AGC target of 10^5, a maximum injection time of 60ms and an isolation window of 2m/z.

Data treatment and differential analysis. Data searches were performed on a local Mascot server (Matrix Science) using a database containing all human protein entries from the UniProtKB/SwissProt database and classical MS contaminant proteins. A tolerance of 5 ppm for precursors and 0.05 Da for fragments was applied. Carbamidomethylation of cysteine residues was defined as a fixed modification, while acetylation of the N-termini of the proteins and oxidation of methionines were defined as variable modifications. Proline studio[114] was used for validation of protein identifications and quantification using a 1% FDR at both the protein and PSM levels. The Prostar software (v 1.22.6)[115] was used for the differential analysis. The filtering keeps only proteins with at least two values for one condition. The abundance was normalised using a quantile centering normalisation over all the analysis. The imputation of the Partially Observed Value (POV) was realised using Structured Least Square Adaptative (SLSA) imputation whereas the imputation of the values Missing in an Entire Condition (MEC) was realised using det quantile imputation. The hypothesis testing used a Limma test for one condition in comparison to the control. Finally, the P-value calibration was realised using Benjamini-Hochberg calibration. Results were filtered to obtain an FDR of around 1%.

NK cells activation and K562 killing assay.

For NK cells activation, 40,000 K562 target cells were seeded per wells in a U-bottom 96-wells plate. Untreated or NPs-treated NK cells were washed and resuspended at 4.10^6 cells/mL in complete R10 medium and added at increasing effector-to-target ratios (0:1: 0.625:1; 1.25:1; 2.5:1 and 5:1) to K562 cells. NK were co-incubated with their target cells for 4h under standard conditions (37°C, 5% CO_2). After incubation, the cells were washed in PBS and non-viable cells were stained with Fixable Viability Dye-eFluor450 (eBioscience #65-0863-14) for 15 minutes at room temperature in the dark. Aspecific antibodies binding was minimized by treating the cells with TruStain FcX anti-CD32/CD16 blocking antibody (1:50, BioLegend # 422301) for 20 minutes at 4°C. Then, cells were stained with PE anti-CD56 (1:100, MiltenyiBiotec #130-113-312) and PE-Vio700 anti-CD69 (1:50, MiltenyiBiotec #130-112-615) and APC anti-NKG2D (1:50, MiltenyiBiotec #130-111-846) for 15 min at 4°C. Samples were acquired with Attune NxT (Invitrogen) flow cytometer and data were analyzed using FlowJo™ v10 Software (ThreeStar). Gating strategy is shown in Figure S6A-B.

NK cells conjugates formation.

For NK cells conjugates formation, NK cells were stained with 0.5µM CellTrace™ Violet (Invitrogen #C34557) for 15 mins under standard conditions (37°C, 5% CO_2) in PBS and then washed three times with complete R10 medium. In parallel, K562 target cells were stained with 0.5µM CellTrace™ CFSE (Invitrogen #C34554) under the same conditions. Cells were then resuspended at 10^6 cells/mL in complete R10 medium, mixed at a 1:1 ratio, and pelleted with a short spin before incubation for 20 mins under standard conditions (37°C, 5% CO_2) to assess conjugate formation rates. Then, unspecific conjugates were removed by pipetting and cells were fixed with 2% PFA in PBS for 20 min at room temperature. After washing the cells with PBS, conjugate formation was analyzed with Attune NxT (Invitrogen) flow cytometer and data were analyzed using FlowJo™ v10 Software (ThreeStar).

NK cells immune synapse formation.

Conjugates between untreated or NPs-treated NK cells and K562-palmitoylated tdTomato target cells at a 2:1 ratio were formed in suspension for 20 min at 37°C in serum-free R10 medium. Cells were then gently mixed and transferred to 0.01% poly-L-lysine coated 12-wells ibidi slides (ibidi #81201). Slides were incubated for 25 minutes under standard conditions (37°C, 5% CO_2) and then fixed with 2% PFA in PBS for 20 min at room temperature. Fixative was removed and wells were rinsed three times with 150 µl PBS. Cells were permeabilized with 0.1% Triton X-100 / 2% BSA in 1x PBS for 5 min and unspecific antibody binding was blocked for 1 h in blocking solution (3% bovine serum albumin-BSA, 5% FBS, 0.01% Triton X-100, in PBS). Immunostaining was performed with purified mouse anti-perforin (10µg/mL, BioLegend, clone dG9), incubated overnight at 4°C followed by secondary antibodies (Goat anti-mouse-AlexaFluor 647, 1:250, ThermoFisher #A-21236) and Phalloidin-iFluor488 (1:1,000, Abcam #ab176753) for 1h room temperature prior to slides mounting (Fluoromount/DAPI). Background and nonspecific staining controls were used.

Perforin-stained NK-K562 conjugates were imaged with a 60X water-immersion objective on an inverted Olympus Spinning-disk, and *z*-series images were acquired with a space of 0.45 µm. Images were processed using ImageJ software (National Institutes of Health). For scoring of cytotoxic granules distance to the immune synapse (based on perforin staining), 20 conjugates between NK cells and K562 target cells

were chosen randomly per condition. Distance quantification was performed using the ImageJ macro “Shortest_distance_between_objects” as described in[116].

Pan T cells activation analysis.

For T cells activation, F-bottom 96-wells plate were coated increasing anti-CD3 concentrations (ranging from 0.001 to 10µg/mL, BioLegend, clone OKT3) overnight at 4°C. Wells were washed once in PBS before adding the cells. Untreated or NPs-treated pan T cells were washed and resuspended at 10^6 cells/mL in complete R10 medium and anti-CD28 (5µg/mL, BioLegend, clone 28.2) was added to each condition. 100,000 cells per wells were incubated for 24h under standard conditions (37°C, 5% CO_2). After incubation, the cells were washed in PBS and non-viable cells were stained with Fixable Viability Dye-eFluor780 (eBioscience #65-0865-14) for 15 minutes at room temperature in the dark. Aspecific antibodies binding was minimized by treating the cells with TruStain FcX anti-CD32/CD16 blocking antibody (1:50, BioLegend #422301) for 20 minutes at 4°C. Then, cells were stained with FITC anti-CD3 (1:100, MiltenyiBiotec #130-126-882), PE-Vio700 anti-CD69 (1:50, MiltenyiBiotec #130-112-615) and Brilliant Violet 421 anti-OX40 (1:20, BioLegend, clone Ber-ACT35) for 15 min at 4°C. Samples were acquired with Attune NxT (Invitrogen) flow cytometer and data were analyzed using FlowJo™ v10 Software (ThreeStar).

Pan T cells spreading and F-actin analysis.

For T cells spreading, 8-wells ibidi slides (ibidi #80841) were coated with 0.01% poly-L-lysine for 45 min at room temperature. After washing in PBS, the coverslips were coated with anti-CD3 (10µg/mL, BioLegend, clone OKT3) and rhICAM1-Fc (2µg/mL, BioLegend #552906) overnight at 4°C. Coverslips were washed once in PBS before adding the cells. Untreated or NPs-treated pan T cells were washed and resuspended at 10^6 cells/mL in serum-free R10 medium for 1h under standard conditions (37°C, 5% CO_2). After, 100,000 cells per wells were incubated with anti-CD28 (5µg/mL, BioLegend, clone 28.2) for 25 min under standard conditions (37°C, 5% CO_2). Coverslips were then washed once with PBS and fixed with 2% PFA in PBS for 20 min at room temperature. Fixative was removed and wells were rinsed three times with 150 µl PBS. Cells were permeabilized with 0.1% Triton X-100 / 2% BSA in 1x PBS for 5 min and F-actin was stained by Phalloidin-iFluor488 (1:1,000, Abcam #ab176753) for 1h room temperature prior to slides mounting (Fluoromount/DAPI).

Phalloidin-stained pan T cells were imaged with a 60X water-immersion objective on an inverted Olympus Spinning-disk, and *z*-series images were acquired with a space of 0.45 µm. Images were processed using ImageJ software (National Institutes of Health). To analyze cell spreading on surfaces, only the z-stack plane corresponding to the contact between cells and the surface was considered, and a projection of the DAPI stain was used to individualize each cell. Briefly, cell areas were obtained by polygon selection definition and spreading area as well as F-actin intensity at the immunological synapse were measured. F-actin intensity was normalized by each cell area.

Pan T cells degranulation analysis.

For T cells degranulation, F-bottom 96-wells plate were coated anti-CD3 (10µg/mL, BioLegend, clone OKT3) and rhICAM1-Fc (2µg/mL, BioLegend #552906) overnight at 4°C. Wells were washed once in PBS before adding the cells. Untreated or NPs-treated pan T cells were washed and resuspended at 10^6 cells/mL in complete R10 medium and anti-CD28 (2µg/mL, BioLegend, clone 28.2) was added to each condition. 100,000 cells per wells were incubated for 1h under standard conditions (37°C, 5% CO_2) in presence of APC-conjugated anti-CD107a (1:50, MiltenyiBiotec #130-111-847). After 1h, protein transport inhibitor cocktail (1:500, eBioscience) was added in each well and cell were incubated for addition 4h under standard conditions (37°C, 5% CO_2). After incubation, the cells were washed in PBS and non-viable cells were stained with Fixable Viability Dye-eFluor780 (eBioscience #65-0865-14) for 15 minutes at room temperature in the dark. Aspecific antibodies binding was minimized by treating the cells with TruStain FcX anti-CD32/CD16 blocking antibody (1:50, BioLegend # 422301) for 20 minutes at 4°C. Then, cells were stained with VioBright B515 anti-CD3 (1:50, MiltenyiBiotec #130-126-882), Pacific Blue anti-CD4 (1:100, BioLegend, clone RPA-T4) and PE anti-CD8 (1:100, BioLegend, clone RPA-T8) for 15 min at 4°C. Samples were acquired with Attune NxT (Invitrogen) flow cytometer and data were analyzed using FlowJo™ v10 Software (ThreeStar).

Cytokine measurement.

Supernatants from 96-well plates were aliquoted after 4h of NK-K562 cells co-incubated or after 24h of pan T cells activation and stored at -20 °C. Cytokines were quantified by custom LEGENDplex (5-plex, BioLegend # 740510) with the Attune NxT

Flow Cytometer. Cytokine assays were analyzed using the LEGENDplex software Qognit (https://legendplex.qognit.com).

Statistics.

Statistical analysis was performed with GraphPad Prism 9.5. The normal distribution of the data sets was assessed by the Shapiro–Wilk normality test. According to the number of data sets compared, Student's t-test test or One-way ANOVA test with original FDR method of Benjamini-Hochberg were applied (*p<0.05; **p<0.01, ***p<0.001, ****p<0.0001). In all cases, the α-level was set at 0.05. All the data in graphs were presented as median ± standard deviation.

Data Availability.

Raw RNA-seq data have been deposited in the EMBL-EBI ArrayExpress archive (accession number E-MTAB-14550). Complete proteomics dataset has been deposited to the ProteomeXchange Consortium via the PRIDE partner repository[117] (accession number PXD056695). All the other data are available within the article and its Supplementary Information. Raw data are accessible through reasonable requests to the corresponding authors.

Acknowledgements

We thank all members of the JGG and AD labs for helpful discussions. The authors wish to thank R. Soltani and A. Bianco for kindly providing the oxidized carbon nanotubes. We thank Pascal Kessler (PICSTRA, CRBS) for assistance in imaging as well as Claudine Ebel and Muriel Philipps (IGBMC, Strasbourg, France) for assistance in FACS sorting. We are grateful to Alexandre F. Carisey (St. Jude Children's Research Hospital, Memphis, USA) for sharing K562 cells. This work was supported by a fellowship from the French Ministry of Science (MESRI) and a fourth-year thesis fellowship from the Fondation ARC pour la recherche sur le cancer to VM. Work and people in the lab of JGG are supported by the INSERM, the University of Strasbourg, as well as by La Ligue Nationale Contre le Cancer (LNCC) and the Association pour la Recherche contre le Cancer (ARC). LB is funded by FRM (Fondation pour la Recherche Médicale). We are also thankful for recent donators (Rohan Athlétisme Saverne and Traileurs de la Rose) to support our work. AD acknowledges funding from the Cancéropole Grand Est, the Fondation Française contre le Myélome et les

Gammapathies, the International Myeloma Foundation, as well as support from the Institut de Cancérologie Strasbourg Europe and the European Research Council (ERC) under the European Union's Horizon 2020 research and innovation program (ERC Starting Grant TheranoImmuno, grant agreement No. 950101) and the Ligue Nationale Contre le Cancer. Additionally, this work was also supported by the CNRS, the University of Strasbourg, the Agence National de la Recherche, the French Proteomics Infrastructure (ProFI FR2048; ANR-10-INBS-08-03), the Interdisciplinary Thematic Institute IMS, the drug discovery and development institute, as part of the ITI 2021-2028 program of the University of Strasbourg, CNRS and Inserm supported by IdEx Unistra (ANR-10-IDEX-0002) and SFRI-STRAT'US project (ANR-20-SFRI-0012) under the framework of the French Investments for the Future Program. We finally also acknowledge funding by IBiSA and Region Grand Est.

Disclosure and competing interest statement

A.D., O.T., and F.L. are shareholders of NH Theraguix who is translating to the clinic Gd-NPs. The other authors declare that they have no conflict of interest.

Authorship contributions

Conceptualization, V.M., O.L., J.G.G., and A.D.; Methodology, V.M., and O.L.; Investigation, V.M., M.C.D., J.B., A.L., A.P., and C.M.; Resources, M.B., S.G., L.J.C., F.L., and O.T.; Formal Analysis, V.M., O.L., A.D., M.C.D., L.B., S.H., , A.P., T.S., A.M., M.R., C.C., and R.C.; Writing – Original Draft, V.M., O.L., J.G.G., and A.D.; Writing – Review & Editing, V.M., O.L., C.C., R.C., L.J.C., F.L., O.T., J.G.G., and A.D.; Supervision, C.C., R.C., J.G.G., and A.D.; Funding Acquisition, J.G.G., and A.D.

References

[1] I. Mellman, G. Coukos, G. Dranoff, *Nature* **2011**, *480*, 480.
[2] J. Galon, D. Bruni, *Nat Rev Drug Discov* **2019**, *18*, 197.
[3] L. Galluzzi, J. Humeau, A. Buqué, L. Zitvogel, G. Kroemer, *Nat Rev Clin Oncol* **2020**, *17*, 725.
[4] L. Galluzzi, M. J. Aryankalayil, C. N. Coleman, S. C. Formenti, *Nat Rev Clin Oncol* **2023**, *20*, 543.
[5] M. A. Fischbach, J. A. Bluestone, W. A. Lim, *Sci. Transl. Med.* **2013**, *5*, DOI 10.1126/scitranslmed.3005568.
[6] Z. Eshhar, T. Waks, G. Gross, D. G. Schindler, *Proc. Natl. Acad. Sci. U.S.A.* **1993**, *90*, 720.
[7] J. Maher, R. J. Brentjens, G. Gunset, I. Rivière, M. Sadelain, *Nat Biotechnol* **2002**, *20*, 70.
[8] R. J. Brentjens, J.-B. Latouche, E. Santos, F. Marti, M. C. Gong, C. Lyddane, P. D. King, S. Larson, M. Weiss, I. Rivière, M. Sadelain, *Nat Med* **2003**, *9*, 279.
[9] S. L. Maude, T. W. Laetsch, J. Buechner, S. Rives, M. Boyer, H. Bittencourt, P. Bader, M. R. Verneris, H. E. Stefanski, G. D. Myers, M. Qayed, B. De Moerloose, H. Hiramatsu, K. Schlis, K. L. Davis, P. L. Martin, E. R. Nemecek, G. A. Yanik, C. Peters, A. Baruchel, N. Boissel, F. Mechinaud, A. Balduzzi, J. Krueger, C. H. June, B. L. Levine, P. Wood, T. Taran, M. Leung, K. T. Mueller, Y. Zhang, K. Sen, D. Lebwohl, M. A. Pulsipher, S. A. Grupp, *N Engl J Med* **2018**, *378*, 439.
[10] P. Rodriguez-Otero, S. Ailawadhi, B. Arnulf, K. Patel, M. Cavo, A. K. Nooka, S. Manier, N. Callander, L. J. Costa, R. Vij, N. J. Bahlis, P. Moreau, S. R. Solomon, M. Delforge, J. Berdeja, A. Truppel-Hartmann, Z. Yang, L. Favre-Kontula, F. Wu, J. Piasecki, M. Cook, S. Giralt, *N Engl J Med* **2023**, *388*, 1002.
[11] J. N. Brudno, J. N. Kochenderfer, *Blood* **2016**, *127*, 3321.
[12] E. Liu, D. Marin, P. Banerjee, H. A. Macapinlac, P. Thompson, R. Basar, L. Nassif Kerbauy, B. Overman, P. Thall, M. Kaplan, V. Nandivada, I. Kaur, A. Nunez Cortes, K. Cao, M. Daher, C. Hosing, E. N. Cohen, P. Kebriaei, R. Mehta, S. Neelapu, Y. Nieto, M. Wang, W. Wierda, M. Keating, R. Champlin, E. J. Shpall, K. Rezvani, *N Engl J Med* **2020**, *382*, 545.
[13] T. Bald, M. F. Krummel, M. J. Smyth, K. C. Barry, *Nat Immunol* **2020**, *21*, 835.
[14] O. Demaria, L. Gauthier, G. Debroas, E. Vivier, *Eur J Immunol* **2021**, *51*, 1934.
[15] H. Salmon, K. Franciszkiewicz, D. Damotte, M.-C. Dieu-Nosjean, P. Validire, A. Trautmann, F. Mami-Chouaib, E. Donnadieu, *J. Clin. Invest.* **2012**, *122*, 899.
[16] S. Platonova, J. Cherfils-Vicini, D. Damotte, L. Crozet, V. Vieillard, P. Validire, P. André, M.-C. Dieu-Nosjean, M. Alifano, J.-F. Régnard, W.-H. Fridman, C. Sautès-Fridman, I. Cremer, *Cancer Research* **2011**, *71*, 5412.
[17] N. E. Scharping, A. V. Menk, R. S. Moreci, R. D. Whetstone, R. E. Dadey, S. C. Watkins, R. L. Ferris, G. M. Delgoffe, *Immunity* **2016**, *45*, 374.
[18] A. R. Lim, W. K. Rathmell, J. C. Rathmell, *eLife* **2020**, *9*, e55185.
[19] I. Dean, C. Y. C. Lee, Z. K. Tuong, Z. Li, C. A. Tibbitt, C. Willis, F. Gaspal, B. C. Kennedy, V. Matei-Rascu, R. Fiancette, C. Nordenvall, U. Lindforss, S. M. Baker, C. Stockmann, V. Sexl, S. A. Hammond, S. J. Dovedi, J. Mjösberg, M. R. Hepworth, G. Carlesso, M. R. Clatworthy, D. R. Withers, *Nat Commun* **2024**, *15*, 683.
[20] D. J. Slamon, B. Leyland-Jones, S. Shak, H. Fuchs, V. Paton, A. Bajamonde, T. Fleming, W. Eiermann, J. Wolter, M. Pegram, J. Baselga, L. Norton, *N Engl J Med* **2001**, *344*, 783.
[21] F. S. Hodi, S. J. O'Day, D. F. McDermott, R. W. Weber, J. A. Sosman, J. B. Haanen, R. Gonzalez, C. Robert, D. Schadendorf, J. C. Hassel, W. Akerley, A. J. M.

Van Den Eertwegh, J. Lutzky, P. Lorigan, J. M. Vaubel, G. P. Linette, D. Hogg, C. H. Ottensmeier, C. Lebbé, C. Peschel, I. Quirt, J. I. Clark, J. D. Wolchok, J. S. Weber, J. Tian, M. J. Yellin, G. M. Nichol, A. Hoos, W. J. Urba, *N Engl J Med* **2010**, *363*, 711.
[22] F. Berner, D. Bomze, S. Diem, O. H. Ali, M. Fässler, S. Ring, R. Niederer, C. J. Ackermann, P. Baumgaertner, N. Pikor, C. G. Cruz, W. Van De Veen, M. Akdis, S. Nikolaev, H. Läubli, A. Zippelius, F. Hartmann, H.-W. Cheng, G. Hönger, M. Recher, J. Goldman, A. Cozzio, M. Früh, J. Neefjes, C. Driessen, B. Ludewig, A. N. Hegazy, W. Jochum, D. E. Speiser, L. Flatz, *JAMA Oncol* **2019**, *5*, 1043.
[23] D. B. Johnson, J. M. Balko, M. L. Compton, S. Chalkias, J. Gorham, Y. Xu, M. Hicks, I. Puzanov, M. R. Alexander, T. L. Bloomer, J. R. Becker, D. A. Slosky, E. J. Phillips, M. A. Pilkinton, L. Craig-Owens, N. Kola, G. Plautz, D. S. Reshef, J. S. Deutsch, R. P. Deering, B. A. Olenchock, A. H. Lichtman, D. M. Roden, C. E. Seidman, I. J. Koralnik, J. G. Seidman, R. D. Hoffman, J. M. Taube, L. A. Diaz, R. A. Anders, J. A. Sosman, J. J. Moslehi, *N Engl J Med* **2016**, *375*, 1749.
[24] V. Mittelheisser, M. Banerjee, X. Pivot, L. J. Charbonnière, J. Goetz, A. Detappe, *Adv. Therap.* **2020**, *3*, 2000134.
[25] T. R. Fadel, M. Look, P. A. Staffier, G. L. Haller, L. D. Pfefferle, T. M. Fahmy, *Langmuir* **2010**, *26*, 5645.
[26] T. R. Fadel, F. A. Sharp, N. Vudattu, R. Ragheb, J. Garyu, D. Kim, E. Hong, N. Li, G. L. Haller, L. D. Pfefferle, S. Justesen, K. C. Herold, T. M. Fahmy, *Nature Nanotech* **2014**, *9*, 639.
[27] D. Schmid, C. G. Park, C. A. Hartl, N. Subedi, A. N. Cartwright, R. B. Puerto, Y. Zheng, J. Maiarana, G. J. Freeman, K. W. Wucherpfennig, D. J. Irvine, M. S. Goldberg, *Nat Commun* **2017**, *8*, 1747.
[28] T. T. Smith, S. B. Stephan, H. F. Moffett, L. E. McKnight, W. Ji, D. Reiman, E. Bonagofski, M. E. Wohlfahrt, S. P. S. Pillai, M. T. Stephan, *Nature Nanotech* **2017**, *12*, 813.
[29] N. N. Parayath, S. B. Stephan, A. L. Koehne, P. S. Nelson, M. T. Stephan, *Nat Commun* **2020**, *11*, 6080.
[30] L. Carmès, G. Bort, F. Lux, L. Seban, P. Rocchi, Z. Muradova, A. Hagège, L. Heinrich-Balard, F. Delolme, V. Gueguen-Chaignon, C. Truillet, S. Crowley, E. Bello, T. Doussineau, M. Dougan, O. Tillement, J. D. Schoenfeld, N. Brown, R. Berbeco, *Nanoscale* **2024**, *16*, 2347.
[31] P. Sharma, A. Alakesh, S. Jhunjhunwala, *Trends in Pharmacological Sciences* **2022**, *43*, 305.
[32] X. Feng, W. Xu, Z. Li, W. Song, J. Ding, X. Chen, *Advanced Science* **2019**, *6*, 1900101.
[33] Y. Wang, Z. Xiao, Z. Wang, D. Lee, Y. Ma, S. Wilhelm, H. Wang, B. Y. S. Kim, W. Jiang, *Nat Rev Bioeng* **2024**, DOI 10.1038/s44222-024-00264-4.
[34] V.-L. Tran, V. Thakare, F. Rossetti, A. Baudouin, G. Ramniceanu, B.-T. Doan, N. Mignet, C. Comby-Zerbino, R. Antoine, P. Dugourd, F. Boschetti, F. Denat, C. Louis, S. Roux, T. Doussineau, O. Tillement, F. Lux, *J. Mater. Chem. B* **2018**, *6*, 4821.
[35] T. Lammers, *Advanced Materials* **2024**, *36*, 2312169.
[36] B. Vis, R. E. Hewitt, T. P. Monie, C. Fairbairn, S. D. Turner, S. D. Kinrade, J. J. Powell, *Proc. Natl. Acad. Sci. U.S.A.* **2020**, *117*, 285.
[37] S. Weller, X. Li, L. R. Petersen, P. Kempen, G. Clergeaud, T. L. Andresen, *International Immunopharmacology* **2024**, *129*, 111643.
[38] N. Jones, J. G. Cronin, G. Dolton, S. Panetti, A. J. Schauenburg, S. A. E. Galloway, A. K. Sewell, D. K. Cole, C. A. Thornton, N. J. Francis, *Front. Immunol.*

2017, *8*, 1516.
[39] N. Martínez-Martín, E. Fernández-Arenas, S. Cemerski, P. Delgado, M. Turner, J. Heuser, D. J. Irvine, B. Huang, X. R. Bustelo, A. Shaw, B. Alarcón, *Immunity* **2011**, *35*, 208.
[40] A. Cruz-Adalia, G. Ramirez-Santiago, J. Osuna-Pérez, M. Torres-Torresano, V. Zorita, A. Martínez-Riaño, V. Boccasavia, A. Borroto, G. Martínez Del Hoyo, J. M. González-Granado, B. Alarcón, F. Sánchez-Madrid, E. Veiga, *Nat Commun* **2017**, *8*, 1591.
[41] M. Vitale, C. Bottino, S. Sivori, L. Sanseverino, R. Castriconi, E. Marcenaro, R. Augugliaro, L. Moretta, A. Moretta, *The Journal of Experimental Medicine* **1998**, *187*, 2065.
[42] O. Dufva, S. Gandolfi, J. Huuhtanen, O. Dashevsky, H. Duàn, K. Saeed, J. Klievink, P. Nygren, J. Bouhlal, J. Lahtela, A. Näätänen, B. R. Ghimire, T. Hannunen, P. Ellonen, H. Lähteenmäki, P. Rumm, J. Theodoropoulos, E. Laajala, J. Härkönen, P. Pölönen, M. Heinäniemi, M. Hollmén, S. Yamano, R. Shirasaki, D. A. Barbie, J. A. Roth, R. Romee, M. Sheffer, H. Lähdesmäki, D. A. Lee, R. De Matos Simoes, M. Kankainen, C. S. Mitsiades, S. Mustjoki, *Immunity* **2023**, *56*, 2816.
[43] A. Pfefferle, B. Jacobs, H. Netskar, E. H. Ask, S. Lorenz, T. Clancy, J. P. Goodridge, E. Sohlberg, K.-J. Malmberg, *Cell Reports* **2019**, *29*, 2284.
[44] D. Urlaub, K. Höfer, M.-L. Müller, C. Watzl, *The Journal of Immunology* **2017**, *198*, 1944.
[45] J. P. Böttcher, E. Bonavita, P. Chakravarty, H. Blees, M. Cabeza-Cabrerizo, S. Sammicheli, N. C. Rogers, E. Sahai, S. Zelenay, C. Reis E Sousa, *Cell* **2018**, *172*, 1022.
[46] T. D. Holmes, R. V. Pandey, E. Y. Helm, H. Schlums, H. Han, T. M. Campbell, T. T. Drashansky, S. Chiang, C.-Y. Wu, C. Tao, M. Shoukier, E. Tolosa, S. Von Hardenberg, M. Sun, C. Klemann, R. A. Marsh, C. M. Lau, Y. Lin, J. C. Sun, R. Månsson, F. Cichocki, D. Avram, Y. T. Bryceson, *Sci. Immunol.* **2021**, *6*, eabc9801.
[47] E. K. Santosa, H. Kim, T. Rückert, J.-B. Le Luduec, A. J. Abbasi, C. K. Wingert, L. Peters, J. N. Frost, K. C. Hsu, C. Romagnani, J. C. Sun, *Nat Immunol* **2023**, *24*, 1685.
[48] G. Min-Oo, N. A. Bezman, S. Madera, J. C. Sun, L. L. Lanier, *Journal of Experimental Medicine* **2014**, *211*, 1289.
[49] R. B. Mailliard, S. M. Alber, H. Shen, S. C. Watkins, J. M. Kirkwood, R. B. Herberman, P. Kalinski, *The Journal of Experimental Medicine* **2005**, *202*, 941.
[50] P. Lee, T. Yamada, C. S. Park, Y. Shen, M. Puppi, H. D. Lacorazza, *Immunol Cell Biol* **2015**, *93*, 605.
[51] P. A. Szabo, H. M. Levitin, M. Miron, M. E. Snyder, T. Senda, J. Yuan, Y. L. Cheng, E. C. Bush, P. Dogra, P. Thapa, D. L. Farber, P. A. Sims, *Nat Commun* **2019**, *10*, 4706.
[52] L. Loyal, S. Warth, K. Jürchott, F. Mölder, C. Nikolaou, N. Babel, M. Nienen, S. Durlanik, R. Stark, B. Kruse, M. Frentsch, R. Sabat, K. Wolk, A. Thiel, *Nat Commun* **2020**, *11*, 6357.
[53] X.-Y. Li, D. Corvino, B. Nowlan, A. R. Aguilera, S. S. Ng, M. Braun, A. R. Cillo, T. Bald, M. J. Smyth, C. R. Engwerda, *Cancer Immunology Research* **2022**, *10*, 154.
[54] M. Kurachi, R. A. Barnitz, N. Yosef, P. M. Odorizzi, M. A. DiIorio, M. E. Lemieux, K. Yates, J. Godec, M. G. Klatt, A. Regev, E. J. Wherry, W. N. Haining, *Nat Immunol* **2014**, *15*, 373.
[55] Z. Qiu, C. Khairallah, G. Romanov, B. S. Sheridan, *The Journal of Immunology* **2020**, *205*, 901.

[56] K. J. Oestreich, A. S. Weinmann, *Current Opinion in Immunology* **2012**, *24*, 191.
[57] Y. Liu, R. Bockermann, M. Hadi, I. Safari, B. Carrion, M. Kveiborg, S. Issazadeh-Navikas, *Cell Mol Immunol* **2021**, *18*, 1904.
[58] U. Gubler, A. O. Chua, D. S. Schoenhaut, C. M. Dwyer, W. McComas, R. Motyka, N. Nabavi, A. G. Wolitzky, P. M. Quinn, P. C. Familletti, *Proc. Natl. Acad. Sci. U.S.A.* **1991**, *88*, 4143.
[59] G. S. Kelner, J. Kennedy, K. B. Bacon, S. Kleyensteuber, D. A. Largaespada, N. A. Jenkins, N. G. Copeland, J. F. Bazan, K. W. Moore, T. J. Schall, A. Zlotnik, *Science* **1994**, *266*, 1395.
[60] A. J. Ozga, M. T. Chow, A. D. Luster, *Immunity* **2021**, *54*, 859.
[61] R. Lachmann, M. Bajwa, S. Vita, H. Smith, E. Cheek, A. Akbar, F. Kern, *J Virol* **2012**, *86*, 1001.
[62] W. M. Schneider, M. D. Chevillotte, C. M. Rice, *Annu. Rev. Immunol.* **2014**, *32*, 513.
[63] E. Cano-Gamez, B. Soskic, T. I. Roumeliotis, E. So, D. J. Smyth, M. Baldrighi, D. Willé, N. Nakic, J. Esparza-Gordillo, C. G. C. Larminie, P. G. Bronson, D. F. Tough, W. C. Rowan, J. S. Choudhary, G. Trynka, *Nat Commun* **2020**, *11*, 1801.
[64] A. L. Symonds, W. Zheng, T. Miao, H. Wang, T. Wang, R. Kiome, X. Hou, S. Li, P. Wang, *Life Sci. Alliance* **2020**, *3*, e202000766.
[65] A. L. J. Symonds, T. Miao, Z. Busharat, S. Li, P. Wang, *Cancer Immunol Immunother* **2023**, *72*, 1139.
[66] M. Binnewies, E. W. Roberts, K. Kersten, V. Chan, D. F. Fearon, M. Merad, L. M. Coussens, D. I. Gabrilovich, S. Ostrand-Rosenberg, C. C. Hedrick, R. H. Vonderheide, M. J. Pittet, R. K. Jain, W. Zou, T. K. Howcroft, E. C. Woodhouse, R. A. Weinberg, M. F. Krummel, *Nat Med* **2018**, *24*, 541.
[67] M. L. Holmes, N. D. Huntington, R. P. Thong, J. Brady, Y. Hayakawa, C. E. Andoniou, P. Fleming, W. Shi, G. K. Smyth, M. A. Degli-Esposti, G. T. Belz, A. Kallies, S. Carotta, M. J. Smyth, S. L. Nutt, *The EMBO Journal* **2014**, *33*, 2721.
[68] E. Hegewisch-Solloa, S. Seo, B. L. Mundy-Bosse, A. Mishra, E. H. Waldman, S. Maurrasse, E. Grunstein, T. J. Connors, A. G. Freud, E. M. Mace, *The Journal of Immunology* **2021**, *207*, 950.
[69] O. D'Orlando, F. Zhao, B. Kasper, Z. Orinska, J. Müller, I. Hermans-Borgmeyer, G. M. Griffiths, U. Zur Stadt, S. Bulfone-Paus, *Eur J Immunol* **2013**, *43*, 194.
[70] E. Le Dréan, F. Vély, L. Olcese, A. Cambiaggi, S. Guia, G. Krystal, N. Gervois, A. Moretta, F. Jotereau, E. Vivier, *Eur. J. Immunol.* **1998**, *28*, 264.
[71] R. Parameswaran, P. Ramakrishnan, S. A. Moreton, Z. Xia, Y. Hou, D. A. Lee, K. Gupta, M. deLima, R. C. Beck, D. N. Wald, *Nat Commun* **2016**, *7*, 11154.
[72] F. Cichocki, B. Valamehr, R. Bjordahl, B. Zhang, B. Rezner, P. Rogers, S. Gaidarova, S. Moreno, K. Tuininga, P. Dougherty, V. McCullar, P. Howard, D. Sarhan, E. Taras, H. Schlums, S. Abbot, D. Shoemaker, Y. T. Bryceson, B. R. Blazar, S. Wolchko, S. Cooley, J. S. Miller, *Cancer Research* **2017**, *77*, 5664.
[73] Y. Kashii, R. Giorda, R. B. Herberman, T. L. Whiteside, N. L. Vujanovic, *J Immunol* **1999**, *163*, 5358.
[74] G. Z. Tau, S. N. Cowan, J. Weisburg, N. S. Braunstein, P. B. Rothman, *The Journal of Immunology* **2001**, *167*, 5574.
[75] M. Moran, M. C. Miceli, *Immunity* **1998**, *9*, 787.
[76] D. M. Desai, M. E. Newton, T. Kadlecek, A. Weiss, *Nature* **1990**, *348*, 66.
[77] J. L. Pomerantz, E. M. Denny, D. Baltimore, *EMBO J* **2002**, *21*, 5184.

[78] K. Chemin, A. Bohineust, S. Dogniaux, M. Tourret, S. Guégan, F. Miro, C. Hivroz, *The Journal of Immunology* **2012**, *189*, 2159.
[79] A. S. Zhovmer, A. Manning, C. Smith, A. Nguyen, O. Prince, P. J. Sáez, X. Ma, D. Tsygankov, A. X. Cartagena-Rivera, N. A. Singh, R. K. Singh, E. D. Tabdanov, *Sci. Adv.* **2024**, *10*, eadi1788.
[80] A. Roumier, J. C. Olivo-Marin, M. Arpin, F. Michel, M. Martin, P. Mangeat, O. Acuto, A. Dautry-Varsat, A. Alcover, *Immunity* **2001**, *15*, 715.
[81] J. C. Nolz, T. S. Gomez, P. Zhu, S. Li, R. B. Medeiros, Y. Shimizu, J. K. Burkhardt, B. D. Freedman, D. D. Billadeau, *Current Biology* **2006**, *16*, 24.
[82] T. S. Gomez, K. Kumar, R. B. Medeiros, Y. Shimizu, P. J. Leibson, D. D. Billadeau, *Immunity* **2007**, *26*, 177.
[83] B. P. Nicolet, A. Guislain, F. P. J. Van Alphen, R. Gomez-Eerland, T. N. M. Schumacher, M. Van Den Biggelaar, M. C. Wolkers, *Proc. Natl. Acad. Sci. U.S.A.* **2020**, *117*, 6686.
[84] B. P. Nicolet, A. Guislain, M. C. Wolkers, *The Journal of Immunology* **2021**, *207*, 2966.
[85] Z. Wang, J. Shang, Y. Qiu, H. Cheng, M. Tao, E. Xie, X. Pei, W. Li, L. Zhang, A. Wu, G. Li, *Cell Reports* **2024**, *43*, 113796.
[86] M. Kurowska, N. Goudin, N. T. Nehme, M. Court, J. Garin, A. Fischer, G. De Saint Basile, G. Ménasché, *Blood* **2012**, *119*, 3879.
[87] V. Das, B. Nal, A. Dujeancourt, M.-I. Thoulouze, T. Galli, P. Roux, A. Dautry-Varsat, A. Alcover, *Immunity* **2004**, *20*, 577.
[88] M. R. Marshall, V. Pattu, M. Halimani, M. Maier-Peuschel, M.-L. Müller, U. Becherer, W. Hong, M. Hoth, T. Tschernig, Y. T. Bryceson, J. Rettig, *Journal of Cell Biology* **2015**, *210*, 135.
[89] M. L. Dustin, *Cancer Immunology Research* **2014**, *2*, 1023.
[90] I. Gramaglia, A. D. Weinberg, M. Lemon, M. Croft, *J Immunol* **1998**, *161*, 6510.
[91] G. Verdeil, D. Puthier, C. Nguyen, A.-M. Schmitt-Verhulst, N. Auphan-Anezin, *The Journal of Immunology* **2006**, *176*, 4834.
[92] M. Pescatori, D. Bedognetti, E. Venturelli, C. Ménard-Moyon, C. Bernardini, E. Muresu, A. Piana, G. Maida, R. Manetti, F. Sgarrella, A. Bianco, L. G. Delogu, *Biomaterials* **2013**, *34*, 4395.
[93] N. Kumbhojkar, S. Prakash, T. Fukuta, K. Adu-Berchie, N. Kapate, R. An, S. Darko, V. Chandran Suja, K. S. Park, A. P. Gottlieb, M. G. Bibbey, M. Mukherji, L. L.-W. Wang, D. J. Mooney, S. Mitragotri, *Nat. Biomed. Eng* **2024**, *8*, 579.
[94] T. Walzer, M. Dalod, S. H. Robbins, L. Zitvogel, E. Vivier, *Blood* **2005**, *106*, 2252.
[95] C. Verry, S. Dufort, B. Lemasson, S. Grand, J. Pietras, I. Troprès, Y. Crémillieux, F. Lux, S. Mériaux, B. Larrat, J. Balosso, G. Le Duc, E. L. Barbier, O. Tillement, *Sci. Adv.* **2020**, *6*, eaay5279.
[96] C. Verry, S. Dufort, J. Villa, M. Gavard, C. Iriart, S. Grand, J. Charles, B. Chovelon, J.-L. Cracowski, J.-L. Quesada, C. Mendoza, L. Sancey, A. Lehmann, F. Jover, J.-Y. Giraud, F. Lux, Y. Crémillieux, S. McMahon, P. J. Pauwels, D. Cagney, R. Berbeco, A. Aizer, E. Deutsch, M. Loeffler, G. Le Duc, O. Tillement, J. Balosso, *Radiotherapy and Oncology* **2021**, *160*, 159.
[97] M. E. Rodriguez-Ruiz, I. Vitale, K. J. Harrington, I. Melero, L. Galluzzi, *Nat Immunol* **2020**, *21*, 120.
[98] B. Diskin, S. Adam, M. F. Cassini, G. Sanchez, M. Liria, B. Aykut, C. Buttar, E. Li, B. Sundberg, R. D. Salas, R. Chen, J. Wang, M. Kim, M. S. Farooq, S. Nguy, C.

Fedele, K. H. Tang, T. Chen, W. Wang, M. Hundeyin, J. A. K. Rossi, E. Kurz, M. I. U. Haq, J. Karlen, E. Kruger, Z. Sekendiz, D. Wu, S. A. A. Shadaloey, G. Baptiste, G. Werba, S. Selvaraj, C. Loomis, K.-K. Wong, J. Leinwand, G. Miller, *Nat Immunol* **2020**, *21*, 442.
[99] W. Piao, L. Li, V. Saxena, J. Iyyathurai, R. Lakhan, Y. Zhang, I. T. Lape, C. Paluskievicz, K. L. Hippen, Y. Lee, E. Silverman, M. W. Shirkey, L. V. Riella, B. R. Blazar, J. S. Bromberg, *Nat Commun* **2022**, *13*, 2176.
[100] T. Strowig, O. Chijioke, P. Carrega, F. Arrey, S. Meixlsperger, P. C. Rämer, G. Ferlazzo, C. Münz, *Blood* **2010**, *116*, 4158.
[101] S. Chappaz, D. Finke, *The Journal of Immunology* **2010**, *184*, 3562.
[102] M. A. Brehm, W. J. Racki, J. Leif, L. Burzenski, V. Hosur, A. Wetmore, B. Gott, M. Herlihy, R. Ignotz, R. Dunn, L. D. Shultz, D. L. Greiner, *Blood* **2012**, *119*, 2778.
[103] L. García-Hevia, R. Soltani, J. González, O. Chaloin, C. Ménard-Moyon, A. Bianco, M. L. Fanarraga, *Bioactive Materials* **2024**, *34*, 237.
[104] A. Mignot, C. Truillet, F. Lux, L. Sancey, C. Louis, F. Denat, F. Boschetti, L. Bocher, A. Gloter, O. Stéphan, R. Antoine, P. Dugourd, D. Luneau, G. Novitchi, L. C. Figueiredo, P. C. de Morais, L. Bonneviot, B. Albela, F. Ribot, L. Van Lokeren, I. Déchamps-Olivier, F. Chuburu, G. Lemercier, C. Villiers, P. N. Marche, G. Le Duc, S. Roux, O. Tillement, P. Perriat, *Chemistry A European J* **2013**, *19*, 6122.
[105] C. Charpentier, V. Cifliku, J. Goetz, A. Nonat, C. Cheignon, M. Cardoso Dos Santos, L. Francés-Soriano, K. Wong, L. J. Charbonnière, N. Hildebrandt, *Chemistry A European J* **2020**, *26*, 14602.
[106] L. Zhang, J. M. Chan, F. X. Gu, J.-W. Rhee, A. Z. Wang, A. F. Radovic-Moreno, F. Alexis, R. Langer, O. C. Farokhzad, *ACS Nano* **2008**, *2*, 1696.
[107] S. Andrews, “FastQC: a quality control tool for high throughput sequence data.,” can be found under https://www.bioinformatics.babraham.ac.uk/projects/fastqc/, **2010**.
[108] A. Dobin, C. A. Davis, F. Schlesinger, J. Drenkow, C. Zaleski, S. Jha, P. Batut, M. Chaisson, T. R. Gingeras, *Bioinformatics* **2013**, *29*, 15.
[109] S. Anders, P. T. Pyl, W. Huber, *Bioinformatics* **2015**, *31*, 166.
[110] M. I. Love, W. Huber, S. Anders, *Genome Biol* **2014**, *15*, 550.
[111] R. C. Gentleman, V. J. Carey, D. M. Bates, B. Bolstad, M. Dettling, S. Dudoit, B. Ellis, L. Gautier, Y. Ge, J. Gentry, K. Hornik, T. Hothorn, W. Huber, S. Iacus, R. Irizarry, F. Leisch, C. Li, M. Maechler, A. J. Rossini, G. Sawitzki, C. Smith, G. Smyth, L. Tierney, J. Y. Yang, J. Zhang, *Genome Biol* **2004**, *5*, R80.
[112] Y. Zhou, B. Zhou, L. Pache, M. Chang, A. H. Khodabakhshi, O. Tanaseichuk, C. Benner, S. K. Chanda, *Nat Commun* **2019**, *10*, 1523.
[113] C. S. Hughes, S. Moggridge, T. Müller, P. H. Sorensen, G. B. Morin, J. Krijgsveld, *Nat Protoc* **2019**, *14*, 68.
[114] D. Bouyssié, A.-M. Hesse, E. Mouton-Barbosa, M. Rompais, C. Macron, C. Carapito, A. Gonzalez De Peredo, Y. Couté, V. Dupierris, A. Burel, J.-P. Menetrey, A. Kalaitzakis, J. Poisat, A. Romdhani, O. Burlet-Schiltz, S. Cianférani, J. Garin, C. Bruley, *Bioinformatics* **2020**, *36*, 3148.
[115] S. Wieczorek, F. Combes, C. Lazar, Q. Giai Gianetto, L. Gatto, A. Dorffer, A.-M. Hesse, Y. Couté, M. Ferro, C. Bruley, T. Burger, *Bioinformatics* **2017**, *33*, 135.
[116] V. P. Sharma, B. Tang, Y. Wang, C. L. Duran, G. S. Karagiannis, E. A. Xue, D. Entenberg, L. Borriello, A. Coste, R. J. Eddy, G. Kim, X. Ye, J. G. Jones, E. Grunblatt, N. Agi, S. Roy, G. Bandyopadhyaya, E. Adler, C. R. Surve, D. Esposito, S. Goswami, J. E. Segall, W. Guo, J. S. Condeelis, L. M. Wakefield, M. H. Oktay, *Nat Commun* **2021**, *12*, 7300.

[117] Y. Perez-Riverol, J. Bai, C. Bandla, D. García-Seisdedos, S. Hewapathirana, S. Kamatchinathan, D. J. Kundu, A. Prakash, A. Frericks-Zipper, M. Eisenacher, M. Walzer, S. Wang, A. Brazma, J. A. Vizcaíno, *Nucleic Acids Research* **2022**, *50*, D543.

Figure legends

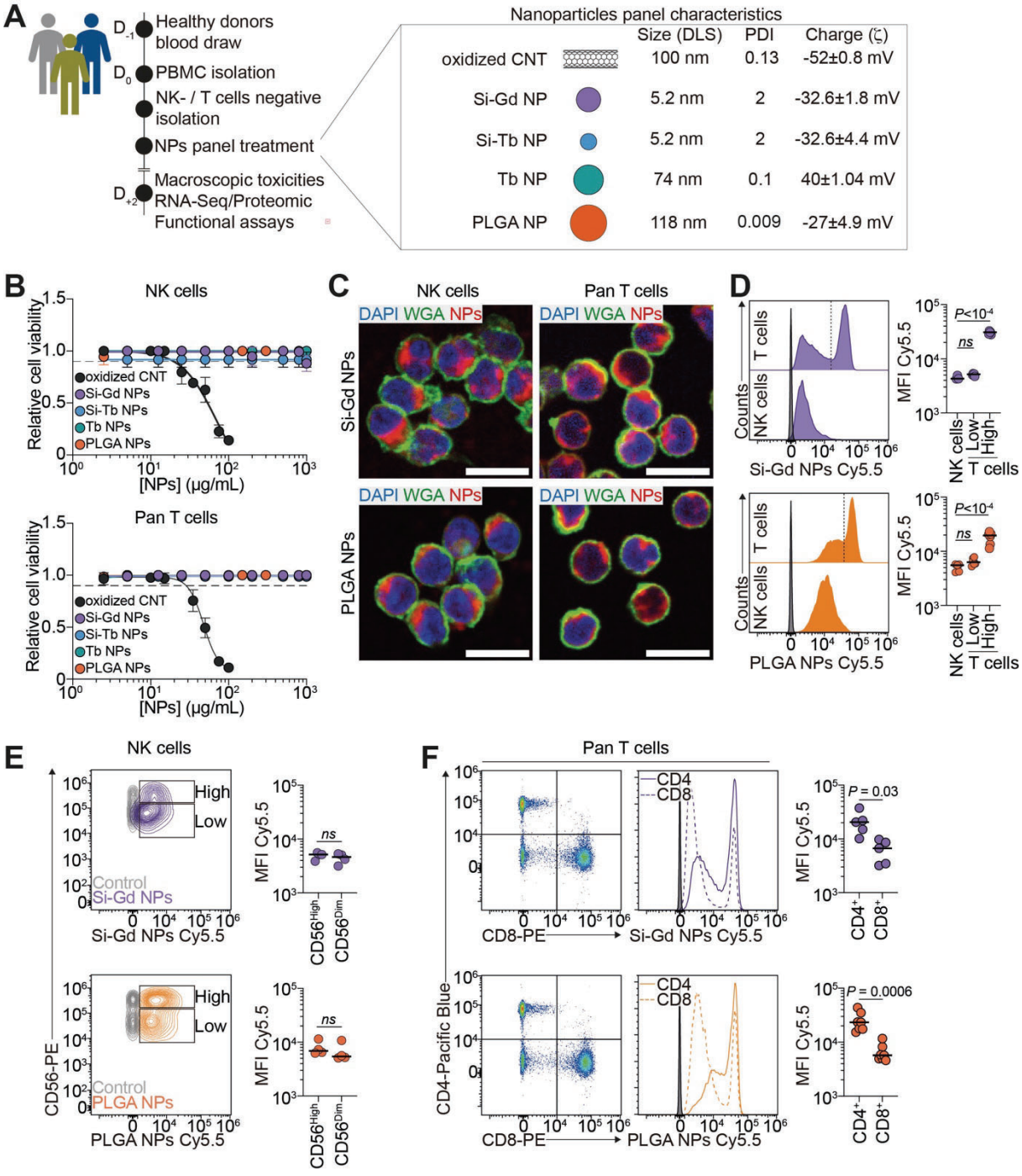

Figure 1 - Mittelheisser *et al.*

Figure 1. Nanomaterials internalization vary across human NK cells and pan T cells.

A. Infographics illustrating the pipeline of the assessment of nanomaterial impact on primary human NK- and pan T cells. Nanomaterial physicochemical characteristics are displayed on the right. **B**. Nanomaterials impact on NK cells (upper panel) and pan T cells (lower panel) viability measured using CellTiterGlo assay. Data are representative

of 3 independent donors. Data are presented as mean ± s.d. **C**. Representative confocal micrographs of NK cells and pan T cells showing internalized Si-Gd NPs and PLGA NPs after 4h co-incubation at 37°C. In green Wheat Germ Agglutinin (WGA), in red nanomaterial (Cyanine5.5-labelled), in blue nuclei (DAPI). Scale bar = 10µm. **D**. Flow-cytometry assessment of nanomaterials internalization in NK- and pan T cells after 48h co-incubation at 37°C. Left: Representative histograms of the relative internalization of Si-Gd NPs (upper panel) and PLGA NPs (lower panel). Grey histogram: untreated control. Right: Quantification of the mean fluorescent intensity signal of the Cyanine5.5-labelled nanomaterials. Data are representative of 3 to 6 independent donors and analyzed by a One-way ANOVA test with original FDR method of Benjamini-Hochberg after assessment of their gaussian distribution by Shapiro-Wilk test. **E**. Flow-cytometry assessment of nanomaterials internalization in $CD56^{High}$ and $CD56^{Low}$ NK cells after 48h co-incubation at 37°C. Left: Representative flow cytometry contour plots of the relative internalization of Si-Gd NPs (upper panel) and PLGA NPs (lower panel). Right: Quantification of the mean fluorescent intensity signal of the Cyanine5.5-labelled nanomaterials. Data are representative of 4 independent donors and analyzed by a Student's t-test (Si-Gd NPs) or Mann-Whitney test (PLGA NPs) after assessment of their gaussian distribution by Shapiro-Wilk test. **F**. Flow-cytometry assessment of nanomaterials internalization in $CD4^+$ and $CD8^+$ pan T cells after 48h co-incubation at 37°C. Left: Representative flow cytometry contour plots of the relative internalization of Si-Gd NPs (upper panel) and PLGA NPs (lower panel). Grey histogram: untreated control. Right: Quantification of the mean fluorescent intensity signal of the Cyanine5.5-labelled nanomaterials. Data are representative of 5 to 7 independent donors and analyzed by a Student's t-test with Welch's correction (Si-Gd NPs) or Mann-Whitney test (PLGA NPs) after assessment of their gaussian distribution by Shapiro-Wilk test.

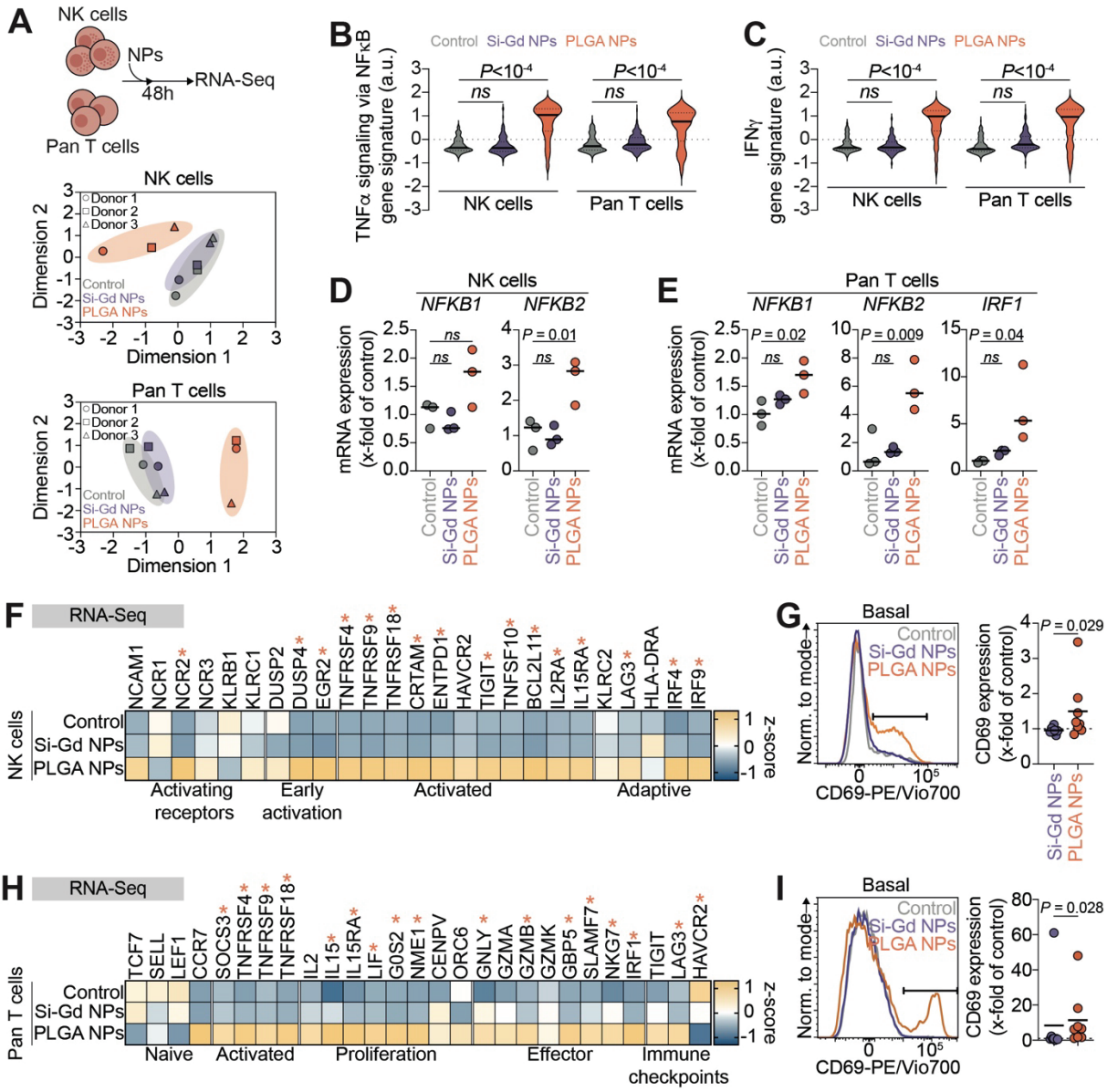

Figure 2 - Mittelheisser *et al.*

Figure 2. PLGA NPs transcriptionally prime immune cells activation.

A. Transcriptomic impact of Si-Gd NPs and PLGA NPs treatment on immune cells. Upper panel: Schematic representation of the pipeline of the assessment of nanomaterial impact on primary human NK- and pan T cells transcriptome. Lower panel: Principal component analysis of the entire transcriptomic profile of NK cells and pan T cells untreated and treated with Si-Gd NPs or PLGA NPs. Each point represents one independent replicate. Axis labels represent the percent of variance as in the respective principal components (dimension 1 and dimension 2). **B-C**. Violin plots comparing aggregate expression distribution of genes related to TNFα signaling via the NFκB pathway (**B**) or related to IFNγ signaling (**C**) according to the MSigDB Hallmark 2024 database. The solid line within each violin represents the median and

dotted lines represent quartiles. Data are analyzed by a Kruskal-Wallis test with original FDR method of Benjamini-Hochberg after assessment of their gaussian distribution by Shapiro-Wilk test. **D**. NK cells expression of *NKFB1* and *NFKB2* mRNA expression as fold change relative to untreated control calculated using the $2^{-\Delta\Delta Ct}$ method (housekeeping: *GAPDH*). Data are representative of 3 independent donors and analyzed by One-way ANOVA test with original FDR method of Benjamini-Hochberg after assessment of their gaussian distribution by Shapiro-Wilk test. **E**. Pan T cells expression of *NKFB1*, *NFKB2* and *IRF1* mRNA expression as fold change relative to untreated control calculated using the $2^{-\Delta\Delta Ct}$ method (housekeeping: *GAPDH*). Data are representative of 3 independent donors and analyzed by One-way ANOVA test with original FDR method of Benjamini-Hochberg after assessment of their gaussian distribution by Shapiro-Wilk test. **F**. Heat-map showing Z-score values for RNA expression of NK cells activation and function associated genes. Gene names are represented on the top while associations are represented on the bottom. Stars represent significant statistical difference between untreated control NK cells and PLGA NPs-treated NK cells. **G**. Flow-cytometry analysis of NK cells activation. Left: Representative histograms of CD69 expression at the NK cells surface in the different treatment conditions. Right: Quantification of CD69 expression as fold change relative to untreated control. Data are representative of 7 to 8 independent donors and analyzed by a Mann-Whitney test after assessment of their gaussian distribution by Shapiro-Wilk test. **H**. Heat-map showing Z-score values for RNA expression of pan T cells activation and function associated genes. Gene names are represented on the top while associations are represented on the bottom. Stars represent significant statistical difference between untreated control pan T cells and PLGA NPs-treated pan T cells. **G**. Flow-cytometry analysis of pan T cells activation. Left: Representative histograms of CD69 expression at the pan T cells surface in the different treatment conditions. Right: Quantification of CD69 expression as fold change relative to untreated control. Data are representative of 8 independent donors and analyzed by a Mann-Whitney test after assessment of their gaussian distribution by Shapiro-Wilk test.

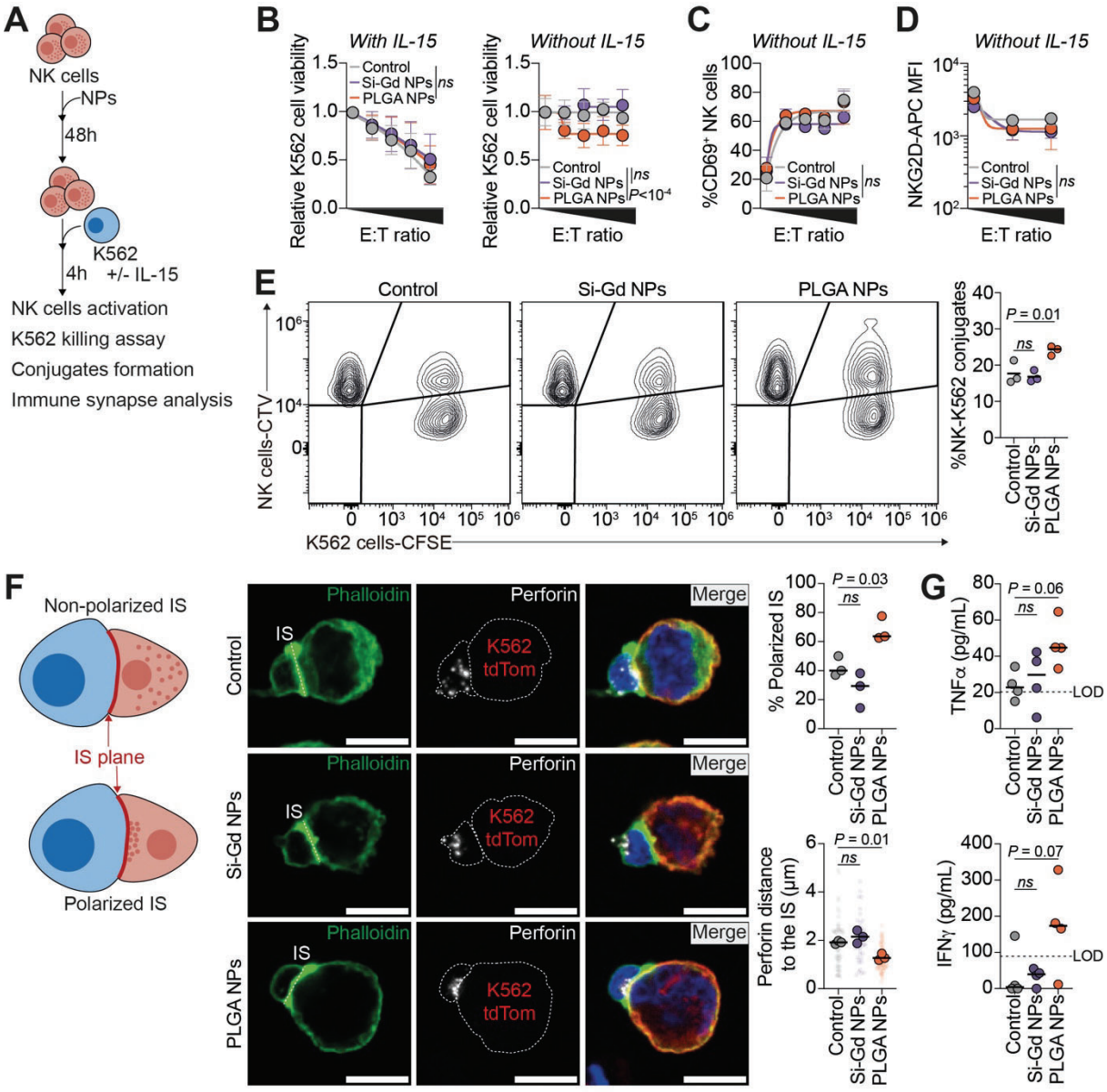

Figure 3 - Mittelheisser *et al.*

Figure 3. PLGA NPs enhance anti-tumor functions of NK cells by promoting perforin polarization at the immune synapse.

A. Schematic representation of the pipeline of the assessment of Si-Gd NPs and PLGA NPs functional impact on primary human NK cells. **B**. Flow-cytometry assessment of K562 lysis induced by increasing nanomaterials-treated NK cells ratio (0.625:1; 1.25:1; 2.5:1 and 5:1) after 4h of co-incubation with 10ng/mL of IL-15 (left) or without (right). Data are representative of 6 to 8 independent donors and analyzed by a Two-way ANOVA corrected with original FDR method of Benjamini-Hochberg. **C**. Percentage of CD69-positive NK cells assessed after co-incubation with K562 cells for 4h. Data are representative of 3 independent donors and analyzed by a Two-way ANOVA corrected

with original FDR method of Benjamini-Hochberg. **D**. Mean fluorescence intensity of NKG2D expressed at the NK cells surface after co-incubation with K562 cells for 4h. Data are representative of 3 independent donors and analyzed by a two-way ANOVA corrected with original FDR method of Benjamini-Hochberg. **E**. Representative conjugate formation assay. Left: Representative contour plots conjugates formed between CTV-stained NK cells and CFSE-stained K562 cells after co-incubation at a 1:1 ratio for 20 mins. Right: Quantification of the percentage of conjugates in each condition. Data are representative of 3 independent donors and analyzed by a two-way ANOVA corrected with original FDR method of Benjamini-Hochberg. **F**. Nanomaterials-treated NK cells immune synapse (IS) formation with K562. Left: Schematic representation of IS polarization and perforin distance evaluation. Center: Representative confocal micrographs of NK-K562 IS. In green Phalloidin-iFluor488, in white perforin dG9 (Alexa Fluor 647), in red K562 palmitoylated-tdTomato and in blue nuclei (DAPI). Scale bar = 10µm. Right: Percentage of polarized IS (upper panel) and mean perforin distance to the IS (lower panel). Data are representative of between 43 and 73 synapses coming from 3 independent donors displayed as mean per experiment. Data are analyzed by a One-way ANOVA test with original FDR method of Benjamini-Hochberg after assessment of their gaussian distribution by Shapiro-Wilk test. **G**. Concentration of TNFa (upper panel) and IFNg (lower panel) released in the supernatant after 4h of NK cells co-incubation with K562 cells at a 2:1 ratio. Data are representative of 4 independent donors and analyzed by a One-way ANOVA test with original FDR method of Benjamini-Hochberg (TNFα) or by a Kruskal-Wallis test (IFNγ) after assessment of their gaussian distribution by Shapiro-Wilk test. LOD: limit of detection.

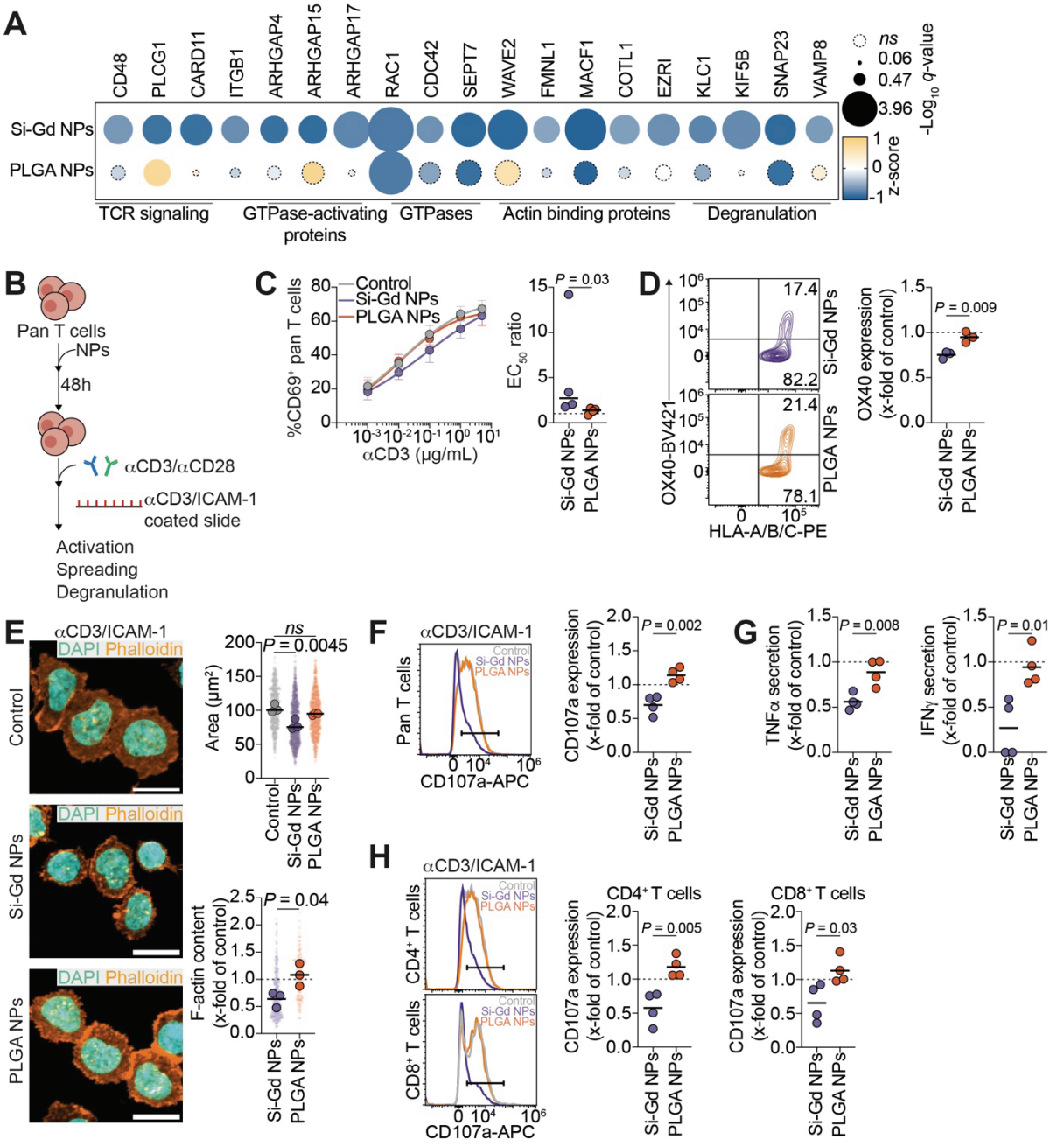

Figure 4 - Mittelheisser *et al.*

Figure 4. Silica-based gadolinium NPs treatment impairs pan T cells spreading and degranulation.

A. Bubble plot showing Z-score values for proteins expression associated with pan T cells functions. Protein names are represented on the top while associations are represented on the bottom. Bubble size represents -Log$_{10}$(*q*-value). Dashed lines bubbles correspond to non-significantly deregulated proteins. **B**. Schematic representation of the pipeline of the assessment of Si-Gd NPs and PLGA NPs functional impact on primary human pan T cells. **C**. Pan T cells sensibility to polyclonal activation. Left: Percentage of CD69-positive pan T cells assessed after culture on a

culture plate coated with increasing concentration of anti-CD3 antibodies for 24h. Right: Half maximal effective concentration (EC_{50}) calculated from the dose-response curve in the left graph. Data are representative of 4 independent donors and analyzed by a Mann-Whitney test after assessment of their gaussian distribution by Shapiro-Wilk test. **D**. Flow-cytometry assessment of OX-40 expression at the pan T cells surface after activation with 5µg/mL of anti-CD3 and 5µg/mL of anti-CD28 antibodies for 24h. Left: Representative flow cytometry contour plots of the relative OX-40 expression in activated pan T cells previously treated for 48h with Si-Gd NPs (upper panel) or PLGA NPs (lower panel). Right: Quantification of OX-40 expression as fold change relative to untreated control. Data are representative of 3 independent donors and analyzed by a Student's t-test after assessment of their gaussian distribution by Shapiro-Wilk test. **E**. Nanomaterials-treated pan T cells spreading on an antigen-presenting cells mimicking surface. Left: Representative confocal micrographs of pan T cells spreading. In orange Phalloidin-iFluor488, in cyan nuclei (DAPI). Scale bar = 10µm. Right: Pan T cells median spreading area. Left: Relative filamentous actin content in pan T cells as fold change relative to untreated control. Data are representative of 3 independent donors and analyzed by a One-way ANOVA test with original FDR method of Benjamini-Hochberg (Spreading area) or a Student's t-test (F-actin content) after assessment of their gaussian distribution by Shapiro-Wilk test. **F**. Flow-cytometry analysis of pan T cells degranulation. Left: Representative histograms of CD107a (LAMP-1) expression at the pan T cells surface after activation with 5µg/mL of anti-CD3 and 5µg/mL of anti-CD28 antibodies for 4h. Right: Quantification of CD107a expression as fold change relative to untreated control. Data are representative of 4 independent donors and analyzed by a Student's t-test after assessment of their gaussian distribution by Shapiro-Wilk test. **G**. TNFa (left panel) and IFNg (right panel) secretion in the supernatant after activation with 5µg/mL of anti-CD3 and 5µg/mL of anti-CD28 antibodies for 4h. Data are represented as fold change relative to untreated control. Data are representative of 4 independent donors and analyzed by a Student's t-test after assessment of their gaussian distribution by Shapiro-Wilk test. **H**. Flow-cytometry analysis of $CD4^+$ and $CD8^+$ T cells degranulation. Left: Representative histograms of CD107a (LAMP-1) expression at the $CD4^+$ T cells (upper panel) and $CD8^+$ T cells (lower panel) surface after activation with 5µg/mL of anti-CD3 and 5µg/mL of anti-CD28 antibodies for 4h. Right: Quantification of CD107a expression as fold change relative to untreated control. Data are representative of 4

independent donors and analyzed by a Student’s t-test after assessment of their gaussian distribution by Shapiro-Wilk test.

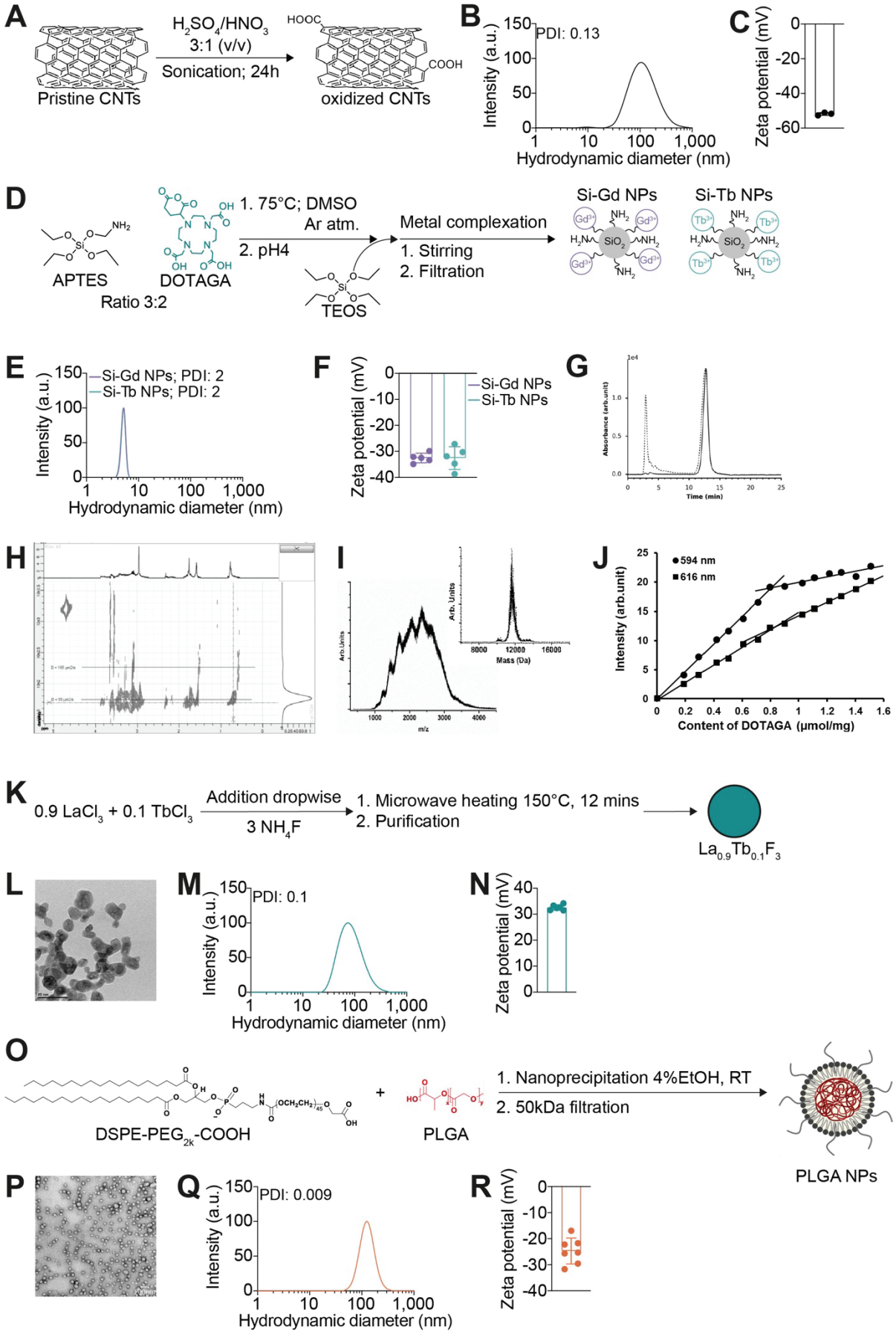

Figure S1 related to Fig.1 - Mittelheisser *et al.*

Supplementary Figure 1 related to Figure 1 – Nanomaterials synthesis and characterization. A. Prisitin CNTs were shortened under strong acid conditions (H_2SO_4/HNO_3 3:1) and sonication for 24h to generate a high amount of carboxylic groups. **B-C.** oxidated CNTs size and charge were measured by DLS. **D.** Ultrasmall polysiloxane-based gadolinium (Si-Gd) NPs were synthesized by a top-down method from core (gadolinium oxide) shell (polysiloxane) NPs whereas ultrasmall polysiloxane-based terbium (Si-Tb) NPs were synthesized with a bottom-up one pot synthesis. **E-F.** Si-Gd NPs and Si-Tb NPs size and charge were measured by DLS. **G**. Chromatograms of polysiloxane-based NPs before (dashed line) and after (solid line) tangential filtration. Absorbance was measured at 295 nm. **H**. NMR DOSY spectrum of polysiloxane nanoparticles. **I**. ESI-MS spectrum of polysiloxane nanoparticles. **J**. Europium titration of DOTAGA in polysiloxane nanoparticles. **K.** Terbium fluoride (Tb) NPs were synthetized by dropwise addition of 0.9 $LaCl_3$ and 0.1 $TbCl_3$ to 3 NH_4F followed by heating at 150°C for 12 mins and purification. **L.** Transmission electron microscopy of Tb NPs. **M-N.** Tb NPs size and charge were measured by DLS. **O.** PLGA NPs were synthetized by self-assembly of DSPE-PEG_{2k}-COOH and PLGA through a one-step nanoprecipitation. **P.** Transmission electron microscopy of PLGA NPs. **Q-R.** PLGA NPs size and charge were measured by DLS.

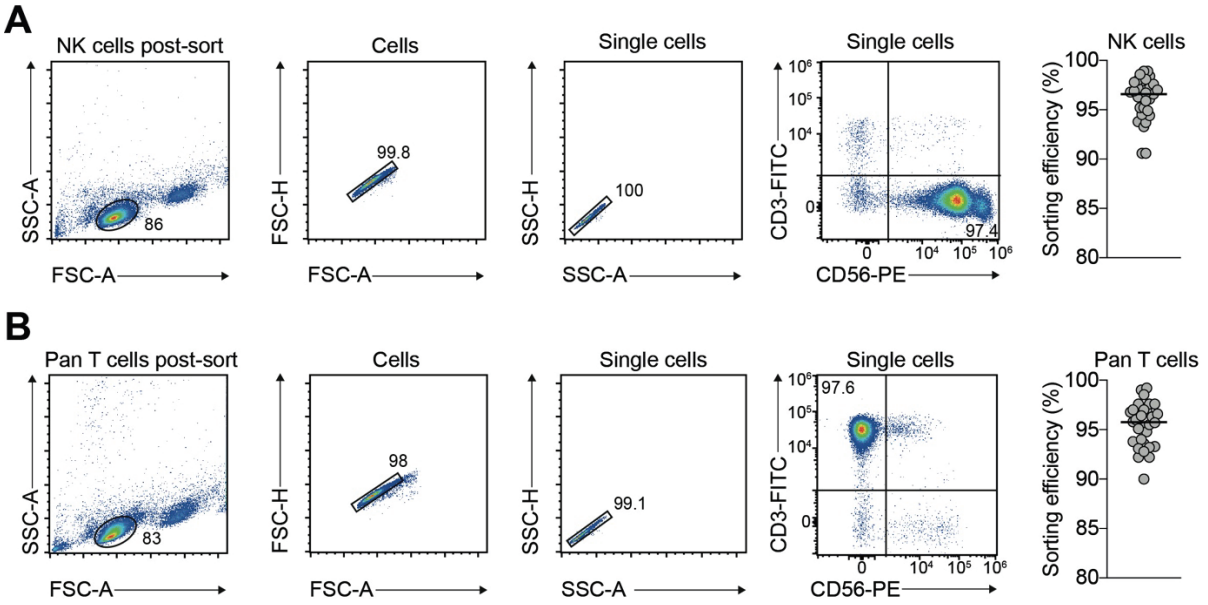

Figure S2 related to Fig.1 - Mittelheisser *et al.*

Supplementary Figure 3 related to Figure 1 – NK cells and pan T cells isolation. NK cells and pan T cells immunophenotyping. **A.** Left: Gating strategy for assessment of NK cells sorting efficiency. Right: Percentage of pure $CD3^-$ $CD56^+$ NK cells after sorting. Data are representative of 31 independent donors. Median of the data is presented. **B.** Left: Gating strategy for assessment of pan T cells sorting efficiency. Right: Percentage of pure $CD3^+$ pan T cells after sorting. Data are representative of 30 independent donors. Median of the data is presented.

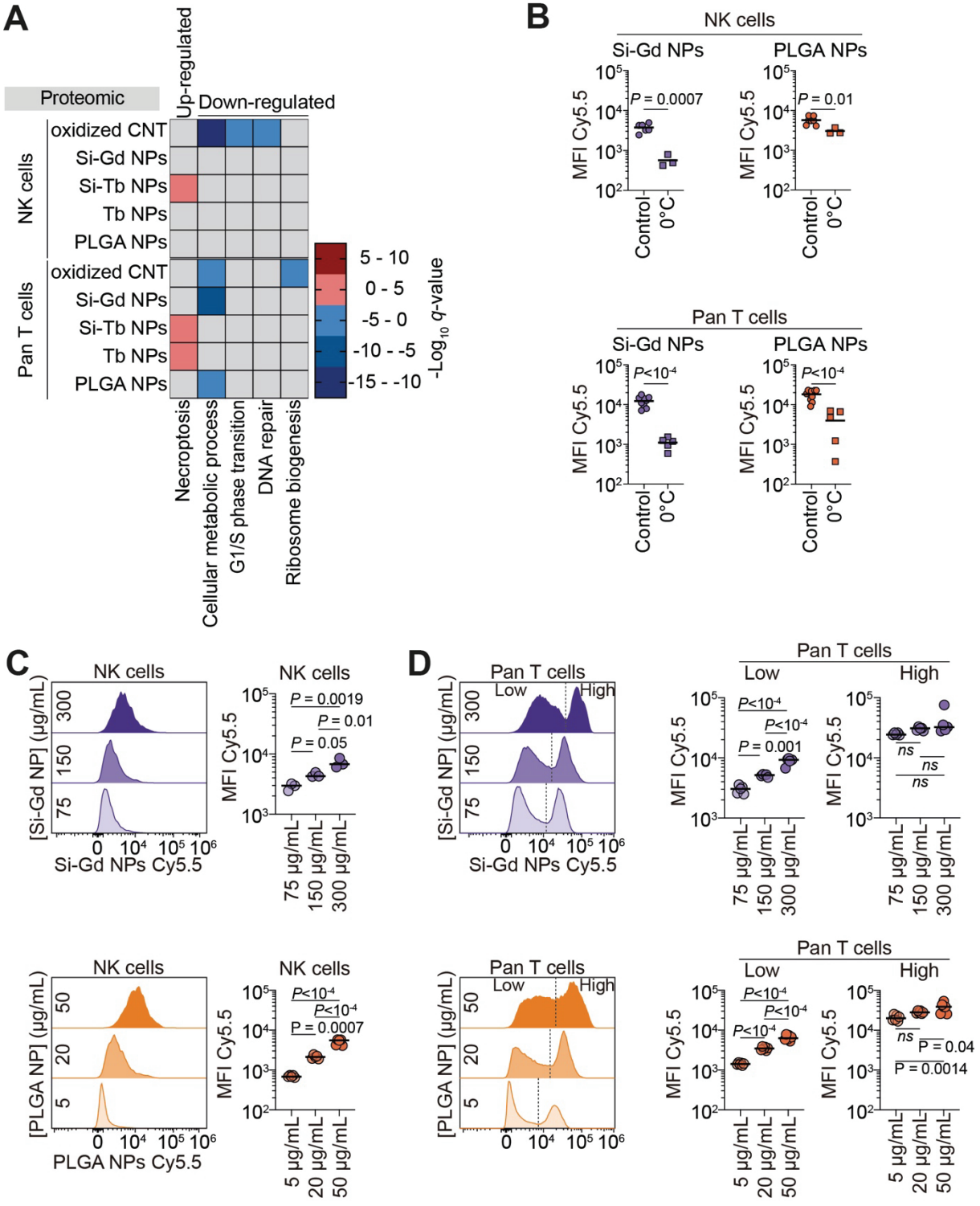

Figure S3 related to Fig.1 - Mittelheisser *et al.*

Supplementary Figure 4 related to Figure 1. A. Heat-map showing -Log$_{10}$(*q*-value) for up-regulated and down-regulated gene ontology terms in NK cells and pan T cells upon 48h treatment with different nanomaterials. **B**. Quantification of the mean fluorescent intensity signal of the Cyanine5.5-labelled nanomaterials to assess their internalization metabolism dependency in NK cells (upper panel) and pan T cells (lower

panel) after 8h co-incubation at 37°C (Control) or on ice (0°C). Data are representative of 3 to 11 independent donors and analyzed by a Student's t-test or a Mann-Whitney test (PLGA NPs in NK cells) after assessment of their gaussian distribution by Shapiro-Wilk test. **C.** Flow-cytometry assessment of nanomaterials internalization dose-dependency in NK cells after 48h co-incubation at 37°C. Left: Representative histograms of the relative internalization of Si-Gd NPs (upper panel) and PLGA NPs (lower panel). Right: Quantification of the mean fluorescent intensity signal of the Cyanine5.5-labelled nanomaterials. Data are representative of 3 to 6 independent donors and analyzed by a One-way ANOVA test with original FDR method of Benjamini-Hochberg after assessment of their gaussian distribution by Shapiro-Wilk test. **D.** Flow-cytometry assessment of nanomaterials internalization dose-dependency in pan T cells after 48h co-incubation at 37°C. Left: Representative histograms of the relative internalization of Si-Gd NPs (upper panel) and PLGA NPs (lower panel). Right: Quantification of the mean fluorescent intensity signal of the Cyanine5.5-labelled nanomaterials in low and high internalizing population as gated on the histograms. Data are representative of 5 to 6 independent donors and analyzed by a One-way ANOVA test with original FDR method of Benjamini-Hochberg after assessment of their gaussian distribution by Shapiro-Wilk test.

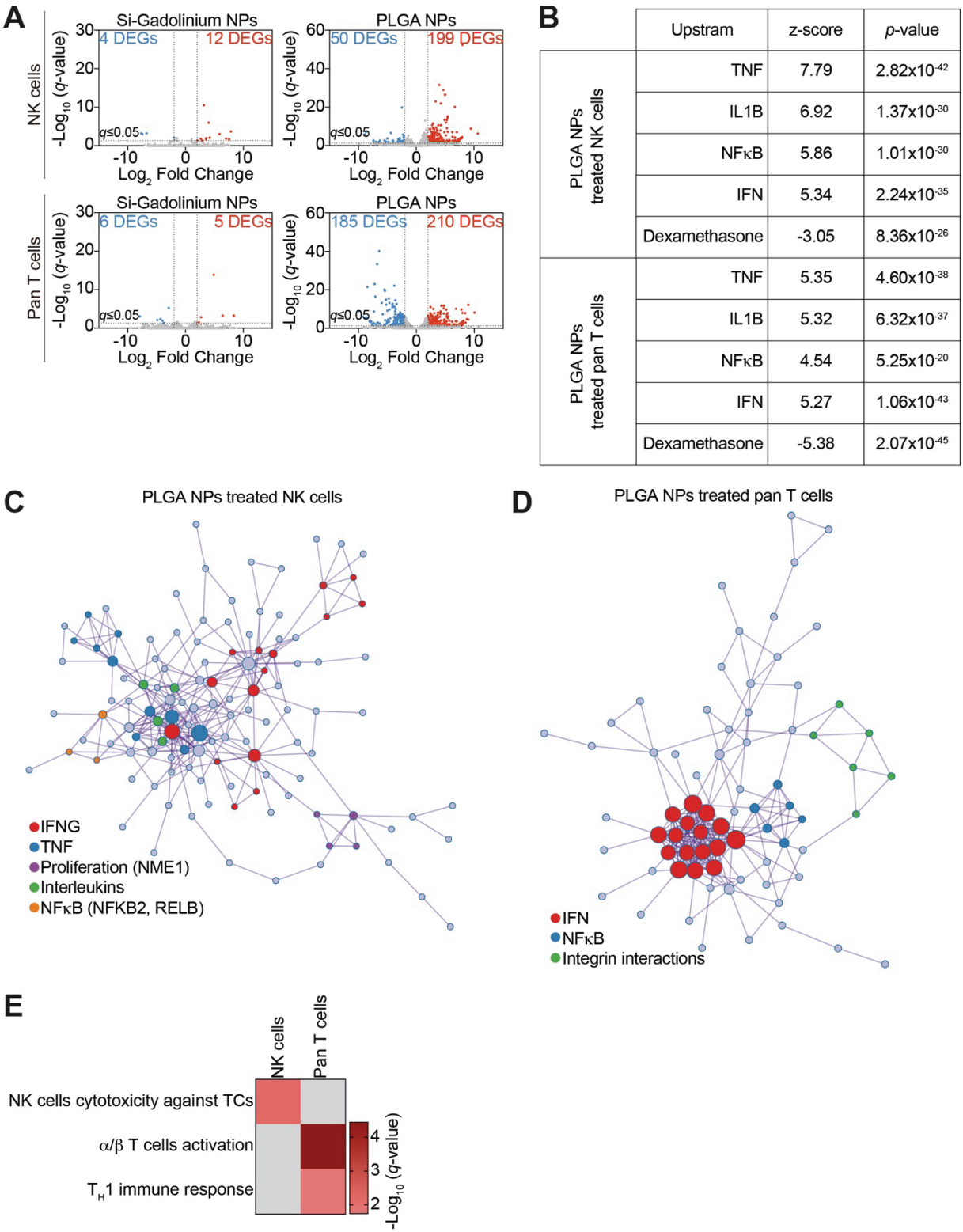

	Upstram	z-score	*p*-value
PLGA NPs treated NK cells	TNF	7.79	2.82×10^{-42}
	IL1B	6.92	1.37×10^{-30}
	NFκB	5.86	1.01×10^{-30}
	IFN	5.34	2.24×10^{-35}
	Dexamethasone	-3.05	8.36×10^{-26}
PLGA NPs treated pan T cells	TNF	5.35	4.60×10^{-38}
	IL1B	5.32	6.32×10^{-37}
	NFκB	4.54	5.25×10^{-20}
	IFN	5.27	1.06×10^{-43}
	Dexamethasone	-5.38	2.07×10^{-45}

Figure S4 related to Fig.2 - Mittelheisser *et al.*

Supplementary Figure 5 related to Figure 2. A. Volcano plot display differentially expressed genes between Si-Gd NPs- or PLGA NPs-treated NK cells (upper panel) or pan T cells (lower panel). Threshold -Log10 (*q*-value) ≤ 1.3 and fold-change > 2. *q*-value = adjusted *p*-value. **B.** Upstream analysis showing the top upstream molecules

predicted to cause the observed gene expression changes. **C-D.** STRING predicted protein-protein interactions based on the upregulated genes in PLGA NPs-treated NK cells (**B**) and pan T cells (**C**) and their functional annotations. **E.** Heat-map showing -Log10 (*q*-value) of immune cells specific gene ontology terms assignment from upregulated genes by PLGA NPs treatment of NK cells and pan T cells.

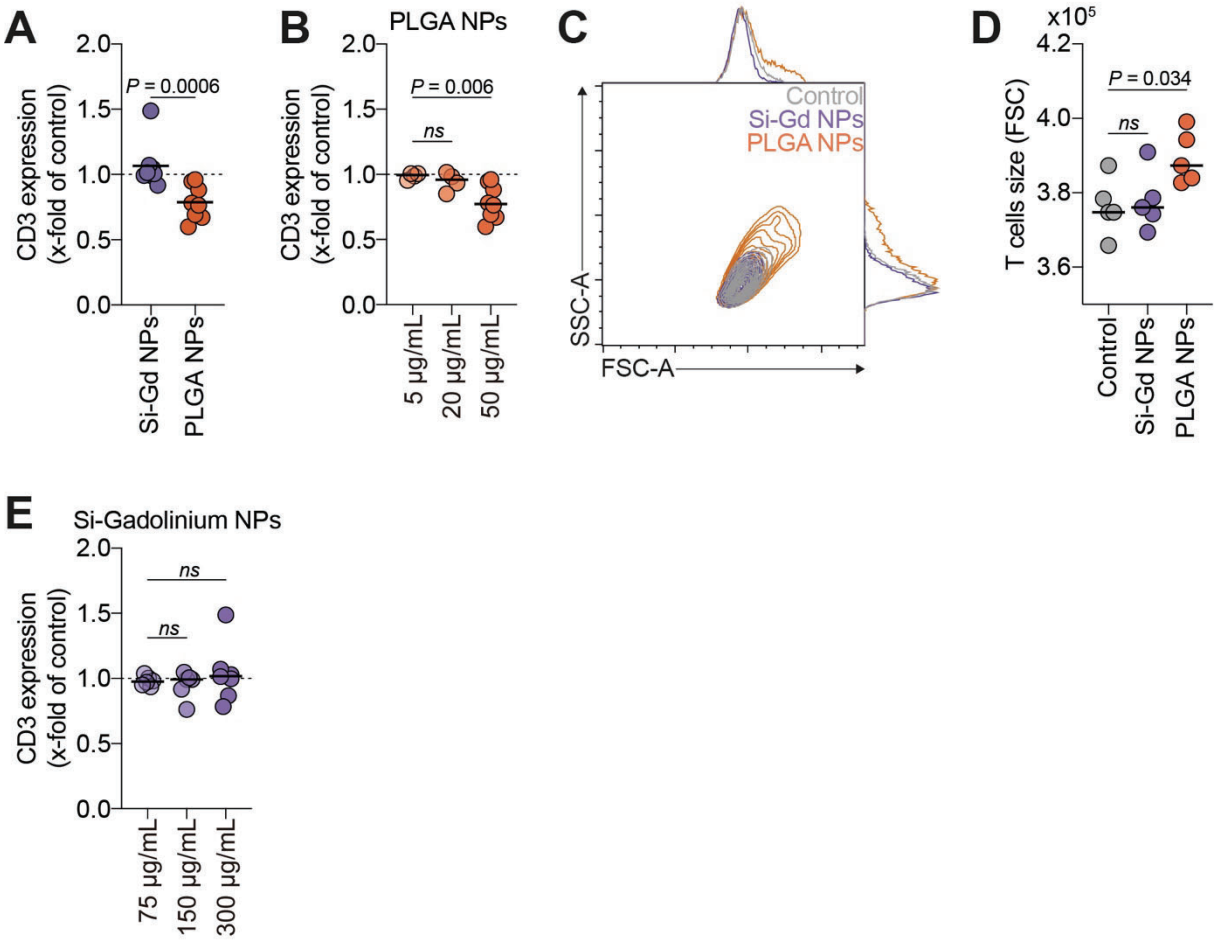

Figure S5 related to Fig.2 - Mittelheisser *et al.*

Supplementary Figure 6 related to Figure 2. A. Quantification of CD3 expression at the surface of pan T cells after 48h of treatment with Si-Gd NPs or PLGA NPs. Data are represented as fold change relative to untreated control. Data are representative of 8 independent donors and analyzed by a Mann-Whitney test after assessment of their gaussian distribution by Shapiro-Wilk test. **B.** Quantification of CD3 expression at the surface of pan T cells after 48h of treatment with increasing concentrations of PLGA NPs. Data are represented as fold change relative to untreated control. Data are representative of 4 to 8 independent donors and analyzed by a Brown-Forsythe and Welch's ANOVA test with original FDR method of Benjamini-Hochberg after assessment of their gaussian distribution by Shapiro-Wilk test. **C.** Representative flow cytometry contour plots of the pan T cells size (FSC) and structure (SSC) obtained by flow cytometry after Si-Gd NPs and PLGA NPs treatment of 48h. **D.** Quantification of pan T cells size based on (**C**) flow cytometry experiments after 48h of treatment with increasing concentrations of PLGA NPs. Data are representative of 5 independent donors and analyzed by a One-way ANOVA test with original FDR method of

Benjamini-Hochberg after assessment of their gaussian distribution by Shapiro-Wilk test. **D.** Quantification of CD3 expression at the surface of pan T cells after 48h of treatment with increasing concentrations of Si-Gd NPs. Data are represented as fold change relative to untreated control. Data are representative of 6 to 8 independent donors and analyzed by a Kruskal-Wallis test after assessment of their gaussian distribution by Shapiro-Wilk test.

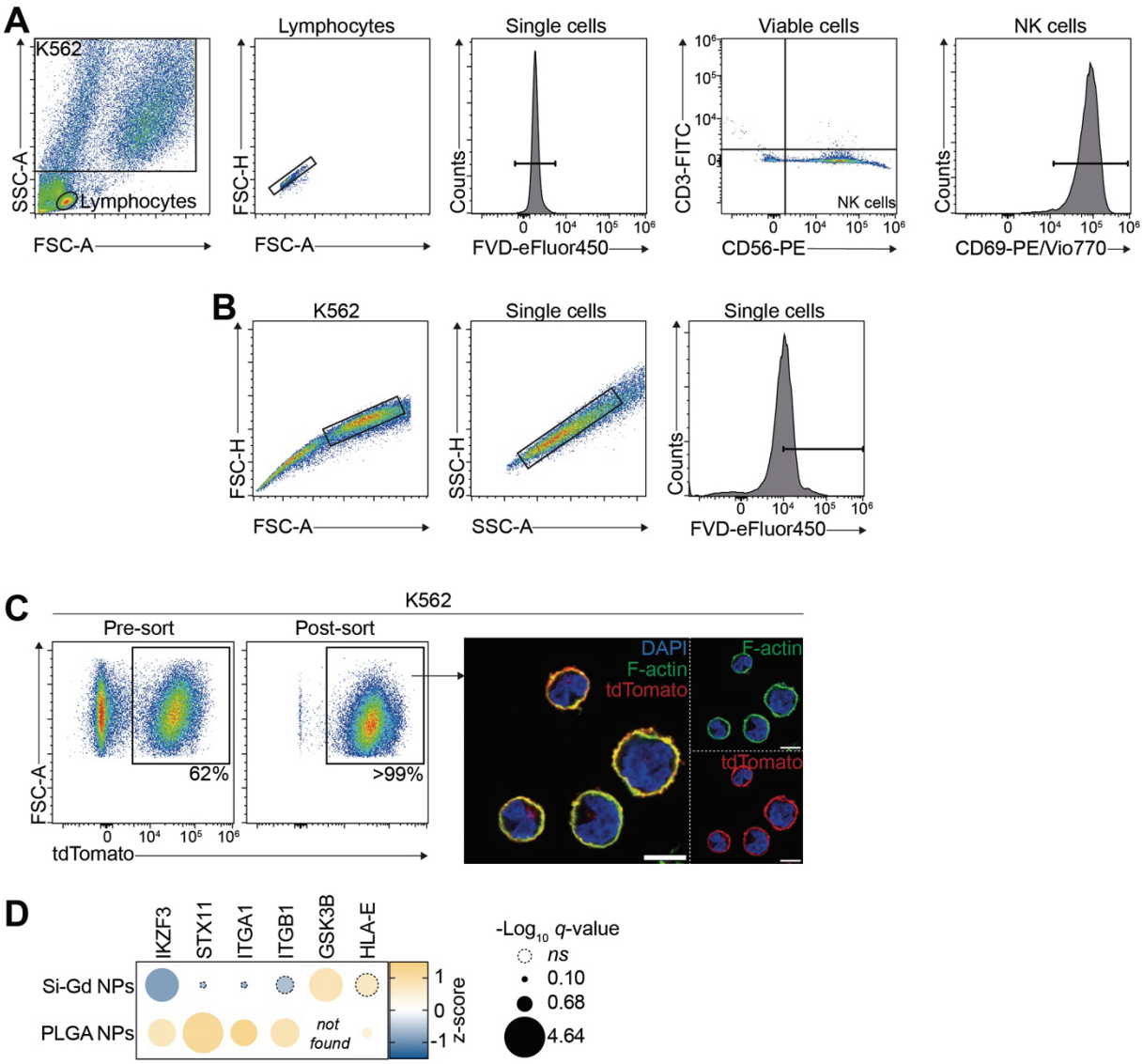

Figure S6 related to Fig.3 - Mittelheisser *et al.*

Supplementary Figure 7 related to Figure 3. A. Gating strategy for assessment of NK cells activation levels. **B.** Gating strategy for assessment of NK cells-induced K562 lysis. **C.** Generation of a K562 transgenic cells expressing palmitoylated-tdTomato at their surface. Right: Representative pseudo-color flow cytometry plot before and after fluorescence-activated cells sorting for high tdTomato fluorescence. Left: Representative confocal micrographs of K562-tdTomato cells. In green Phalloidin-iFluor488, in red palmitoylated-tdTomato, in blue nuclei (DAPI). Scale bar = 10µm. **D.** Bubble plot showing Z-score values for genes/proteins expression associated with NK cells functions. Bubble size represents -Log_{10}(*q*-value). Dashed lines bubbles correspond to non-significantly deregulated genes/proteins.

Discussion and perspectives

1. Platelets infiltration in metastatic foci

While previous reports found evidence of platelets inside primary tumors (Haemmerle et al., 2016; Li et al., 2014; Stone et al., 2012), no evidence proves that this could apply to metastasis. We now document for the first time that metastatic sites are populated by platelets (Garcia-Leon et al., 2024). Whether platelets seed metastases just by interacting and imprinting TCs in circulation or if they require extravasation remains an open question. Pathways involved in platelets' metastatic foci colonization can be further investigated by applying our experimental metastasis approach in $PF4^{Cre}FAK^{-/-}$ or $PF4^{Cre}$ $CX3CR1^{-/-}$ models as FAK and CX3CR1 were previously described to be involved in primary tumor infiltration by platelets (Haemmerle et al., 2016; Miao et al., 2020).

Besides, we particularly study platelets impact on lung metastasis. However, it was recently demonstrated that the lung substantially contributes to platelet biogenesis (≈ 50% of total platelet production) (Lefrançais et al., 2017). Intriguingly, lung megakaryocytes transcriptionally differ from BM ones, hinting probable different functions of lung-derived platelets. Therefore, additional efforts should be made to decipher the involvement of lung "resident" platelets in lung metastasis.

2. Molecular cues involved in late metastatic outgrowth

We highlight that, after having massively infiltrate lung metastatic lesions, platelets profoundly impact the immune TME thereby contributing to the outgrowth of the metastatic foci (Garcia-Leon et al., 2024). Whether these effects rely on platelets direct interactions with immune cells or if platelets secretome plays also a role remains to be demonstrated. Platelets may suppress the immune response by impairing DCs and T cells activation and downstreamed functions upon direct binding (Kissel et al., 2006; Zamora et al., 2017). However, the role of their secretome remains vague. Of note, platelets are not the only producers of pro-tumoral factors such as TGFβ, PGE_2, or maresin-1 (Half et al., 2002; Massagué, 2008; Serhan et al., 2009; Yoshimatsu et al., 2001) with other cell types possibly involved. Hence, further evaluation of the

metastatic TME upon late platelets depletion should be performed to better determine the origin of the pro-tumoral cytokines highlighted in our work. Moreover, we only analyzed the immune TME at 14 days post-TCs injection. However, one should note that the immune compartment of the TME is highly dynamic and varies upon cancer progression (Rozenblatt-Rosen et al., 2020).

In parallel to the immune TME, CAFs also undergo dynamic changes as tumors evolve. An increasing body of literature highlights that PDPN$^+$ fibroblasts diverge into pro-tumoral CAFs during cancer progression. PDPN$^+$ CAFs restrict anti-tumoral immune response and strongly correlate with poor clinical outcome (Assouline et al., 2024; Cords et al., 2024; Friedman et al., 2020). Interestingly, primary tumor infiltrating platelets are known to interact through CLEC-2 with PDPN$^+$ fibroblasts and activate them in PDPN$^+$ CAFs (Miyashita et al., 2019). Whether this interaction occurs in metastatic sites and promotes metastases outgrowth by impacting the immune TME remains an open question.

Altogether, immune and CAFs dynamics upon cancer progression warrant further spatiotemporal investigations to decipher platelets interactants and immune cells dynamics during metastatic outgrowth.

3. Place of antiplatelet agents in cancer therapy

Given the broad implications of platelets at each step of the cancer dissemination and during later metastatic outgrowth, the use of anti-platelet strategies to hamper cancer progression seems an appealing approach. Repurposing of clinically available anti-platelet agents such as cyclooxygenases inhibitors (*i.e.*, aspirin) (Lucotti et al., 2019) or purinergic $P2Y_{12}$ receptor antagonists (*e.g.*, clopidogrel or ticagrelor) (Gareau et al., 2018; Mezouar et al., 2015) in preclinical trials efficiently prevent cancer progression. Anti-platelet drugs not only reduce TCs metastatic potential but also dramatically enhance response to chemotherapy (Demers et al., 2011; Volz et al., 2019). Furthermore, anti-platelet agents potentiate immune checkpoint blockade (Motz et al., 2014; Riesenberg et al., 2019) and adoptive cell transfer efficacy (Rachidi et al., 2017). While anti-platelet agents gave promising results in preclinical models, their use in routine oncologic care remains unexplored due to their drug-drug interactions and their broad side effects (*e.g.*, increased bleeding risks, gastrointestinal hemorrhage risks and allergic asthma) (Falanga et al., 2022; Sostres and Lanas, 2011; Szczeklik

and Stevenson, 1999). The identification of the specific platelets targets that do not induce bleeding risks could open new therapeutic avenues.

We identify GPVI as a major player in platelet-driven metastases outgrowth (Garcia-Leon et al., 2024). To counteract GPVI function, we use the glenzocimab, a humanized anti-GPVI antibody Fab fragment, and successfully impair metastasis growth without inducing collateral hemostatic perturbations (Garcia-Leon et al., 2024; Lebozec et al., 2017). Of note, glenzocimab was recently successfully used to treat acute ischemic stroke in a phase Ib/IIa clinical trial (Mazighi et al., 2024). Yet, while glenzocimab exhibits great potential, it presents a very short half-life (≈ 10 hours) rendering impracticable its employment as an anti-metastatic strategy (Renaud et al., 2020). In a follow-up study, we highlight that CD24 expression on TCs influenced platelets binding and metastatic seeding (Mittelheisser et al. *In preparation*). These results identify CD24 as a potential druggable target to counteract platelets-TCs interaction and metastatic progression without collateral hemostatic perturbations. Indeed, different studies already exploit the CD24 targeting with the aim of improving immune response (Barkal et al., 2019; Salnikov et al., 2013). However, their action as a platelets-TCs binding disruptors was never investigated. Nevertheless prior to their application in oncologic care, an in-depth assessment of the time frame of CD24 implication in platelets pro-metastatic functions (*i.e.*, early vs late) is of the utmost urgency.

4. Improving antibody-targeted NPs design

While antibody-targeted NPs conjugates improve tumor biodistribution ensuing encouraging preclinical therapeutic results, they still suffer from poor clinical translation (He et al., 2019). As we highlighted in our meta-analysis, antibody-targeted NPs conjugates biodistribution and pharmacokinetics profiles remain dictated by the NPs physicochemical properties. Hence, capitalizing on NPs physicochemical properties (their size, charge, shape) could improve their biodistribution into specific organs (Blanco et al., 2015; Reddy et al., 2007). Besides simply tuning NPs size and charge, NP improvement relies in the addition of “selective organ targeting” component to traditional lipid NPs significantly alters their *in vivo* delivery profile and mediates tissue-specific delivery (Cheng et al., 2020; Kim et al., 2021; Wang et al., 2023).

Another parameter influencing antibody-targeted NPs penetration inside the tumor bed is the antibody size and affinity. Antibody's high molecular weight (150kDa) decreases their diffusion in tumors interstitial space. In addition, high cellular antigen expression act as antibody sinks, where few TCs trap extravasated antibodies (Fujimori et al., 1990; Juweid et al., 1992; Thurber et al., 2007; Thurber and Wittrup, 2008). In the case of antibody-drug conjugates and antibody-targeted NPs, the binding site barrier results in sub-optimal tumor exposure and thus decreased therapeutic efficacy (Cilliers et al., 2018; Rhoden and Wittrup, 2012; Singh et al., 2020). To circumvent the binding site barrier, co-injection of free antibodies prior the administration of antibody-targeted NPs could allow the saturation of perivascular TCs and lead to a deeper antibody-targeted NPs diffusion inside the tumor bed. Another approach to improve antibody-targeted NPs penetration include NPs conjugation with antibody fragments (Fabs, scFvs, VHHs) or low affinity antibodies. Antibody fragments uniformly diffuse throughout the tumour mass (Adams et al., 1998; Zhou et al., 2007). Low-affinity antibodies undergo multiple dissociation-association steps leading to their deeper diffusion prior to receptor-mediated internalization (Thurber et al., 2007).

Besides, understanding antibody-targeted NPs interactions with TCs is essential to design efficient conjugates. It remains particularly necessary to determine the optimal antibody density at the NPs surface that induce selective target recognition and maintain the binding capacity of the complex. One can hypothesize that an increasing density of ligands leads to better cellular uptake, but this relationship is not always linear (Alkilany et al., 2019). High antibody density leads to their orientation and/or steric hindrance, resulting in dismal target binding (Algar et al., 2011; Greene et al., 2020).

5. Reactivating NK cells with drug-free nanomaterials

While nanoimmunotherapies successfully reactivate immune cells in several preclinical studies (Mittelheisser et al., 2020), the impact of drug-free nanomaterials on immune cells remains unknown. Our last study provides new insights for the rational selection of NPs materials in nanoimmunotherapeutic strategies. We identify drug-free PLGAs NPs as suitable and promising candidates for further targeting approaches aiming to reactivate the immune system of cancer patients, and particularly NK and T cells. If we identify the signaling pathway involved in NK and T cells activation by PLGA

NPs, we still lack the precise identification of the first events and targets engaged during the immune cells-NPs interaction. This remaining black box requires further evaluation to decipher the exact mechanism of NK and pan T cells activation. PLGA NPs degrade into lactic acid and glycolic acid, which are metabolized in the Krebs cycle. Knowing that increased metabolism is linked with NK cells and pan T cells activation and enhanced anti-tumoral functions (Donnelly et al., 2014; Keating et al., 2016; Patsoukis et al., 2015), an interesting avenue would be to investigate whether PLGAs NPs treatment could induce NK cells and pan T cells metabolic response. We successfully demonstrated *in vitro* that PLGA NPs priming promoted efficient TCs lysis by increasing NK cell cytotoxicity. Given the important role of NK cells in the immune response against metastases (Chan and Ewald, 2022), thorough *in vivo* evaluation remained to be performed to decipher whether PLGA NP-primed NK cells exhibit tumoricidal enhancement on the tumor burden regression, how they synergize with other immuno-activating agents and how the NP-priming induces systemic immune response. Furthermore, NK cells are key player in the regulation of adaptive immune responses (Walzer et al., 2005).). If we revealed that PLGA NPs priming directly enhance TCs lysis by NK, our study did not allow to evaluate how NK cells priming integrate into the global adaptative immune system. The impact of PLGA NP-primed NK cells in shaping dendritic cells and subsequent T cells response remains to be evaluated. In addition, potential PLGAs NPs-mediated sustained activation of NK cells may lead to cytokine release and eventual cell exhaustion, thus impeding the tumoricial properties of NPs priming. These aspects might pose safety limitations and need to be investigated in future studies.

Besides, the recent development of “pre-targeted” NPs by the Nanotranslational lab (Mathieu et al., 2024) will enable us to easily conjugated PLGA NPs to NK and pan T cells targeting antibodies. Such conjugation permits to evaluate drug-free nanomaterials impact on immune cells when directly targeted *in vivo* and compare it to our *ex vivo* results. This will allow to expand our knowledge on drug-free nanomaterials impact on immune cells in complex environment and provide rational for further nanoimmunotherapies development.

BIBLIOGRAPHY

A

Aaronson SA. 1991. Growth Factors and Cancer. *Science* **254**:1146–1153. doi:10.1126/science.1659742

Aceto N, Bardia A, Miyamoto DT, Donaldson MC, Wittner BS, Spencer JA, Yu M, Pely A, Engstrom A, Zhu H, Brannigan BW, Kapur R, Stott SL, Shioda T, Ramaswamy S, Ting DT, Lin CP, Toner M, Haber DA, Maheswaran S. 2014. Circulating Tumor Cell Clusters Are Oligoclonal Precursors of Breast Cancer Metastasis. *Cell* **158**:1110–1122. doi:10.1016/j.cell.2014.07.013

Adam C, King S, Allgeier T, Braumüller H, Lüking C, Mysliwietz J, Kriegeskorte A, Busch DH, Röcken M, Mocikat R. 2005. DC-NK cell cross talk as a novel CD4+ T-cell–independent pathway for antitumor CTL induction. *Blood* **106**:338–344. doi:10.1182/blood-2004-09-3775

Adams DL, Martin SS, Alpaugh RK, Charpentier M, Tsai S, Bergan RC, Ogden IM, Catalona W, Chumsri S, Tang C-M, Cristofanilli M. 2014. Circulating giant macrophages as a potential biomarker of solid tumors. *Proc Natl Acad Sci USA* **111**:3514–3519. doi:10.1073/pnas.1320198111

Adams GP, Schier R, Marshall K, Wolf EJ, McCall AM, Marks JD, Weiner LM. 1998. Increased affinity leads to improved selective tumor delivery of single-chain Fv antibodies. *Cancer Res* **58**:485–490.

Agard NJ, Baskin JM, Prescher JA, Lo A, Bertozzi CR. 2006. A Comparative Study of Bioorthogonal Reactions with Azides. *ACS Chem Biol* **1**:644–648. doi:10.1021/cb6003228

Agarwal P, Bertozzi CR. 2015. Site-Specific Antibody–Drug Conjugates: The Nexus of Bioorthogonal Chemistry, Protein Engineering, and Drug Development. *Bioconjugate Chem* **26**:176–192. doi:10.1021/bc5004982

Aigner S, Sthoeger ZM, Fogel M, Weber E, Zarn J, Ruppert M, Zeller Y, Vestweber D, Stahel R, Sammar M, Altevogt P. 1997. CD24, a mucin-type glycoprotein, is a ligand for P-selectin on human tumor cells. *Blood* **89**:3385–3395.

Akinc A, Maier MA, Manoharan M, Fitzgerald K, Jayaraman M, Barros S, Ansell S, Du X, Hope MJ, Madden TD, Mui BL, Semple SC, Tam YK, Ciufolini M, Witzigmann D, Kulkarni JA, van der Meel R, Cullis PR. 2019. The Onpattro story and the clinical translation of nanomedicines containing nucleic acid-based drugs. *Nat Nanotechnol* **14**:1084–1087. doi:10.1038/s41565-019-0591-y

Albeiroti S, Ayasoufi K, Hill DR, Shen B, De La Motte CA. 2015. Platelet hyaluronidase-2: an enzyme that translocates to the surface upon activation to function in extracellular matrix degradation. *Blood* **125**:1460–1469. doi:10.1182/blood-2014-07-590513

Bibliography

Alberts B, Heald R, Johnson A, Morgan D, Raff M, Roberts K, Walter P, Wilson JH, Hunt T. 2022. Blood Vessels and Endothelial CellsMolecular Biology of the Cell. New York, NY London: W.W. Norton & Company.

Algar WR, Prasuhn DE, Stewart MH, Jennings TL, Blanco-Canosa JB, Dawson PE, Medintz IL. 2011. The Controlled Display of Biomolecules on Nanoparticles: A Challenge Suited to Bioorthogonal Chemistry. *Bioconjugate Chem* **22**:825–858. doi:10.1021/bc200065z

Algarra I, Cabrera T, Garrido F. 2000. The HLA crossroad in tumor immunology. *Human Immunology* **61**:65–73. doi:10.1016/S0198-8859(99)00156-1

Algarra I, Collado A, Garrido F. 1997. Altered MHC class I antigens in tumors. *Int J Clin Lab Res* **27**:95–102. doi:10.1007/BF02912442

Ali-Boucetta H, Al-Jamal KT, McCarthy D, Prato M, Bianco A, Kostarelos K. 2008. Multiwalled carbon nanotube–doxorubicin supramolecular complexes for cancer therapeutics. *Chem Commun* 459–461. doi:10.1039/B712350G

Alkilany AM, Zhu L, Weller H, Mews A, Parak WJ, Barz M, Feliu N. 2019. Ligand density on nanoparticles: A parameter with critical impact on nanomedicine. *Advanced Drug Delivery Reviews* **143**:22–36. doi:10.1016/j.addr.2019.05.010

Allen TA, Asad D, Amu E, Hensley MT, Cores J, Vandergriff A, Tang J, Dinh P-U, Shen D, Qiao L, Su T, Hu S, Liang H, Shive H, Harrell E, Campbell C, Peng X, Yoder JA, Cheng K. 2019. Circulating tumor cells exit circulation while maintaining multicellularity, augmenting metastatic potential. *Journal of Cell Science* **132**:jcs231563. doi:10.1242/jcs.231563

Allen TM, Cullis PR. 2013. Liposomal drug delivery systems: From concept to clinical applications. *Advanced Drug Delivery Reviews* **65**:36–48. doi:10.1016/j.addr.2012.09.037

Alley SC, Benjamin DR, Jeffrey SC, Okeley NM, Meyer DL, Sanderson RJ, Senter PD. 2008. Contribution of Linker Stability to the Activities of Anticancer Immunoconjugates. *Bioconjugate Chem* **19**:759–765. doi:10.1021/bc7004329

Alves CS, Burdick MM, Thomas SN, Pawar P, Konstantopoulos K. 2008. The dual role of CD44 as a functional P-selectin ligand and fibrin receptor in colon carcinoma cell adhesion. *American Journal of Physiology-Cell Physiology* **294**:C907–C916. doi:10.1152/ajpcell.00463.2007

Anderberg C, Li H, Fredriksson L, Andrae J, Betsholtz C, Li X, Eriksson U, Pietras K. 2009. Paracrine Signaling by Platelet-Derived Growth Factor-CC Promotes Tumor Growth by Recruitment of Cancer-Associated Fibroblasts. *Cancer Research* **69**:369–378. doi:10.1158/0008-5472.CAN-08-2724

Anton N, Vandamme TF. 2011. Nano-emulsions and Micro-emulsions: Clarifications of the Critical Differences. *Pharm Res* **28**:978–985. doi:10.1007/s11095-010-0309-1

Bibliography

Arwert EN, Harney AS, Entenberg D, Wang Y, Sahai E, Pollard JW, Condeelis JS. 2018. A Unidirectional Transition from Migratory to Perivascular Macrophage Is Required for Tumor Cell Intravasation. *Cell Reports* **23**:1239–1248. doi:10.1016/j.celrep.2018.04.007

Asgari A, Lesyk G, Poitras E, Govindasamy N, Terry K, To R, Back V, Rudzinski JK, Lewis JD, Jurasz P. 2021. Platelets stimulate programmed death-ligand 1 expression by cancer cells: Inhibition by anti-platelet drugs. *Journal of Thrombosis and Haemostasis* **19**:2862–2872. doi:10.1111/jth.15478

Assouline B, Kahn R, Hodali L, Condiotti R, Engel Y, Elyada E, Mordechai-Heyn T, Pitarresi JR, Atias D, Steinberg E, Bidany-Mizrahi T, Forkosh E, Katz LH, Benny O, Golan T, Hofree M, Stewart SA, Atlan KA, Zamir G, Stanger BZ, Berger M, Ben-Porath I. 2024. Senescent cancer-associated fibroblasts in pancreatic adenocarcinoma restrict CD8+ T cell activation and limit responsiveness to immunotherapy in mice. *Nat Commun* **15**:6162. doi:10.1038/s41467-024-50441-7

Augsten M, Sjöberg E, Frings O, Vorrink SU, Frijhoff J, Olsson E, Borg Å, Östman A. 2014. Cancer-Associated Fibroblasts Expressing CXCL14 Rely upon NOS1-Derived Nitric Oxide Signaling for Their Tumor-Supporting Properties. *Cancer Research* **74**:2999–3010. doi:10.1158/0008-5472.CAN-13-2740

Autio KA, Dreicer R, Anderson J, Garcia JA, Alva A, Hart LL, Milowsky MI, Posadas EM, Ryan CJ, Graf RP, Dittamore R, Schreiber NA, Summa JM, Youssoufian H, Morris MJ, Scher HI. 2018. Safety and Efficacy of BIND-014, a Docetaxel Nanoparticle Targeting Prostate-Specific Membrane Antigen for Patients With Metastatic Castration-Resistant Prostate Cancer: A Phase 2 Clinical Trial. *JAMA Oncol* **4**:1344. doi:10.1001/jamaoncol.2018.2168

Ay C, Simanek R, Vormittag R, Dunkler D, Alguel G, Koder S, Kornek G, Marosi C, Wagner O, Zielinski C, Pabinger I. 2008. High plasma levels of soluble P-selectin are predictive of venous thromboembolism in cancer patients: results from the Vienna Cancer and Thrombosis Study (CATS). *Blood* **112**:2703–2708. doi:10.1182/blood-2008-02-142422

B

Bach K, Pensa S, Zarocsinceva M, Kania K, Stockis J, Pinaud S, Lazarus KA, Shehata M, Simões BM, Greenhalgh AR, Howell SJ, Clarke RB, Caldas C, Halim TYF, Marioni JC, Khaled WT. 2021. Time-resolved single-cell analysis of Brca1 associated mammary tumourigenesis reveals aberrant differentiation of luminal progenitors. *Nat Commun* **12**:1502. doi:10.1038/s41467-021-21783-3

Bailey SE, Ukoumunne OC, Shephard EA, Hamilton W. 2017. Clinical relevance of thrombocytosis in primary care: a prospective cohort study of cancer incidence using English electronic medical records and cancer registry data. *Br J Gen Pract* **67**:e405–e413. doi:10.3399/bjgp17X691109

Bibliography

Bakewell SJ, Nestor P, Prasad S, Tomasson MH, Dowland N, Mehrotra M, Scarborough R, Kanter J, Abe K, Phillips D, Weilbaecher KN. 2003. Platelet and osteoclast β 3 integrins are critical for bone metastasis. *Proc Natl Acad Sci USA* **100**:14205–14210. doi:10.1073/pnas.2234372100

Baluk P, Hashizume H, McDonald DM. 2005. Cellular abnormalities of blood vessels as targets in cancer. *Current Opinion in Genetics & Development* **15**:102–111. doi:10.1016/j.gde.2004.12.005

Bangham AD, Standish MM, Watkins JC. 1965. Diffusion of univalent ions across the lamellae of swollen phospholipids. *Journal of Molecular Biology* **13**:238-IN27. doi:10.1016/S0022-2836(65)80093-6

Barber DF, Faure M, Long EO. 2004. LFA-1 Contributes an Early Signal for NK Cell Cytotoxicity. *The Journal of Immunology* **173**:3653–3659. doi:10.4049/jimmunol.173.6.3653

Barkal AA, Brewer RE, Markovic M, Kowarsky M, Barkal SA, Zaro BW, Krishnan V, Hatakeyama J, Dorigo O, Barkal LJ, Weissman IL. 2019. CD24 signalling through macrophage Siglec-10 is a target for cancer immunotherapy. *Nature* **572**:392–396. doi:10.1038/s41586-019-1456-0

Barrow AD, Edeling MA, Trifonov V, Luo J, Goyal P, Bohl B, Bando JK, Kim AH, Walker J, Andahazy M, Bugatti M, Melocchi L, Vermi W, Fremont DH, Cox S, Cella M, Schmedt C, Colonna M. 2018. Natural Killer Cells Control Tumor Growth by Sensing a Growth Factor. *Cell* **172**:534-548.e19. doi:10.1016/j.cell.2017.11.037

Barry KC, Hsu J, Broz ML, Cueto FJ, Binnewies M, Combes AJ, Nelson AE, Loo K, Kumar R, Rosenblum MD, Alvarado MD, Wolf DM, Bogunovic D, Bhardwaj N, Daud AI, Ha PK, Ryan WR, Pollack JL, Samad B, Asthana S, Chan V, Krummel MF. 2018. A natural killer–dendritic cell axis defines checkpoint therapy–responsive tumor microenvironments. *Nat Med* **24**:1178–1191. doi:10.1038/s41591-018-0085-8

Barry M, Heibein JA, Pinkoski MJ, Lee S-F, Moyer RW, Green DR, Bleackley RC. 2000. Granzyme B Short-Circuits the Need for Caspase 8 Activity during Granule-Mediated Cytotoxic T-Lymphocyte Killing by Directly Cleaving Bid. *Molecular and Cellular Biology* **20**:3781–3794. doi:10.1128/MCB.20.11.3781-3794.2000

Bastid J, Regairaz A, Bonnefoy N, Déjou C, Giustiniani J, Laheurte C, Cochaud S, Laprevotte E, Funck-Brentano E, Hemon P, Gros L, Bec N, Larroque C, Alberici G, Bensussan A, Eliaou J-F. 2015. Inhibition of CD39 Enzymatic Function at the Surface of Tumor Cells Alleviates Their Immunosuppressive Activity. *Cancer Immunology Research* **3**:254–265. doi:10.1158/2326-6066.CIR-14-0018

Bauer S, Groh V, Wu J, Steinle A, Phillips JH, Lanier LL, Spies T. 1999. Activation of NK Cells and T Cells by NKG2D, a Receptor for Stress-Inducible MICA. *Science* **285**:727–729. doi:10.1126/science.285.5428.727

Bibliography

Baxter LT, Jain RK. 1989. Transport of fluid and macromolecules in tumors. I. Role of interstitial pressure and convection. *Microvascular Research* **37**:77–104. doi:10.1016/0026-2862(89)90074-5

Bayerl F, Meiser P, Donakonda S, Hirschberger A, Lacher SB, Pedde A-M, Hermann CD, Elewaut A, Knolle M, Ramsauer L, Rudolph TJ, Grassmann S, Öllinger R, Kirchhammer N, Trefny M, Anton M, Wohlleber D, Höchst B, Zaremba A, Krüger A, Rad R, Obenauf AC, Schadendorf D, Zippelius A, Buchholz VR, Schraml BU, Böttcher JP. 2023. Tumor-derived prostaglandin E2 programs cDC1 dysfunction to impair intratumoral orchestration of anti-cancer T cell responses. *Immunity* **56**:1341-1358.e11. doi:10.1016/j.immuni.2023.05.011

Beach MA, Nayanathara U, Gao Y, Zhang C, Xiong Y, Wang Y, Such GK. 2024. Polymeric Nanoparticles for Drug Delivery. *Chem Rev* **124**:5505–5616. doi:10.1021/acs.chemrev.3c00705

Bejarano L, Jordão MJC, Joyce JA. 2021. Therapeutic Targeting of the Tumor Microenvironment. *Cancer Discovery* **11**:933–959. doi:10.1158/2159-8290.CD-20-1808

Bekes EM, Schweighofer B, Kupriyanova TA, Zajac E, Ardi VC, Quigley JP, Deryugina EI. 2011. Tumor-Recruited Neutrophils and Neutrophil TIMP-Free MMP-9 Regulate Coordinately the Levels of Tumor Angiogenesis and Efficiency of Malignant Cell Intravasation. *The American Journal of Pathology* **179**:1455–1470. doi:10.1016/j.ajpath.2011.05.031

Bennett SRM, Carbone FR, Karamalis F, Flavell RA, Miller JFAP, Heath WR. 1998. Help for cytotoxic-T-cell responses is mediated by CD40 signalling. *Nature* **393**:478–480. doi:10.1038/30996

Bennett SRM, Carbone FR, Karamalis F, Miller JFAP, Heath WR. 1997. Induction of a CD8+ Cytotoxic T Lymphocyte Response by Cross-priming Requires Cognate CD4+ T Cell Help. *The Journal of Experimental Medicine* **186**:65–70. doi:10.1084/jem.186.1.65

Bergers G, Brekken R, McMahon G, Vu TH, Itoh T, Tamaki K, Tanzawa K, Thorpe P, Itohara S, Werb Z, Hanahan D. 2000. Matrix metalloproteinase-9 triggers the angiogenic switch during carcinogenesis. *Nat Cell Biol* **2**:737–744. doi:10.1038/35036374

Berner F, Bomze D, Diem S, Ali OH, Fässler M, Ring S, Niederer R, Ackermann CJ, Baumgaertner P, Pikor N, Cruz CG, Van De Veen W, Akdis M, Nikolaev S, Läubli H, Zippelius A, Hartmann F, Cheng H-W, Hönger G, Recher M, Goldman J, Cozzio A, Früh M, Neefjes J, Driessen C, Ludewig B, Hegazy AN, Jochum W, Speiser DE, Flatz L. 2019. Association of Checkpoint Inhibitor–Induced Toxic Effects With Shared Cancer and Tissue Antigens in Non–Small Cell Lung Cancer. *JAMA Oncol* **5**:1043. doi:10.1001/jamaoncol.2019.0402

Bibliography

Bianchi A, Dufort S, Lux F, Fortin P-Y, Tassali N, Tillement O, Coll J-L, Crémillieux Y. 2014. Targeting and in vivo imaging of non-small–cell lung cancer using nebulized multimodal contrast agents. *Proc Natl Acad Sci USA* **111**:9247–9252. doi:10.1073/pnas.1402196111

Biber G, Sabag B, Raiff A, Ben-Shmuel A, Puthenveetil A, Benichou JIC, Jubany T, Levy M, Killner S, Barda-Saad M. 2022. Modulation of intrinsic inhibitory checkpoints using nano-carriers to unleash NK cell activity. *EMBO Mol Med* **14**:e14073. doi:10.15252/emmm.202114073

Billroth T. 1877. Lectures on surgical pathology and therapeutics : a handbook for students and practitioners, The New Sydenham Society ; v. 73, 76. London: New Sydenham Society.

Bizzozero J. 1882. Ueber einen neuen Formbestandtheil des Blutes und dessen Rolle bei der Thrombose und der Blutgerinnung: Untersuchungen. *Archiv f pathol Anat* **90**:261–332. doi:10.1007/BF01931360

Black WC, Welch HG. 1993. Advances in Diagnostic Imaging and Overestimations of Disease Prevalence and the Benefits of Therapy. *N Engl J Med* **328**:1237–1243. doi:10.1056/NEJM199304293281706

Blanco E, Shen H, Ferrari M. 2015. Principles of nanoparticle design for overcoming biological barriers to drug delivery. *Nat Biotechnol* **33**:941–951. doi:10.1038/nbt.3330

Bodnar AG, Ouellette M, Frolkis M, Holt SE, Chiu C-P, Morin GB, Harley CB, Shay JW, Lichtsteiner S, Wright WE. 1998. Extension of Life-Span by Introduction of Telomerase into Normal Human Cells. *Science* **279**:349–352. doi:10.1126/science.279.5349.349

Bonvalot S, Le Pechoux C, De Baere T, Kantor G, Buy X, Stoeckle E, Terrier P, Sargos P, Coindre JM, Lassau N, Ait Sarkouh R, Dimitriu M, Borghi E, Levy L, Deutsch E, Soria J-C. 2017. First-in-Human Study Testing a New Radioenhancer Using Nanoparticles (NBTXR3) Activated by Radiation Therapy in Patients with Locally Advanced Soft Tissue Sarcomas. *Clinical Cancer Research* **23**:908–917. doi:10.1158/1078-0432.CCR-16-1297

Bonvalot S, Rutkowski PL, Thariat J, Carrère S, Ducassou A, Sunyach M-P, Agoston P, Hong A, Mervoyer A, Rastrelli M, Moreno V, Li RK, Tiangco B, Herraez AC, Gronchi A, Mangel L, Sy-Ortin T, Hohenberger P, De Baère T, Le Cesne A, Helfre S, Saada-Bouzid E, Borkowska A, Anghel R, Co A, Gebhart M, Kantor G, Montero A, Loong HH, Vergés R, Lapeire L, Dema S, Kacso G, Austen L, Moureau-Zabotto L, Servois V, Wardelmann E, Terrier P, Lazar AJ, Bovée JVMG, Le Péchoux C, Papai Z. 2019. NBTXR3, a first-in-class radioenhancer hafnium oxide nanoparticle, plus radiotherapy versus radiotherapy alone in patients with locally advanced soft-tissue sarcoma (Act.In.Sarc): a multicentre, phase 2–3, randomised, controlled trial. *The Lancet Oncology* **20**:1148–1159. doi:10.1016/S1470-2045(19)30326-2

Bibliography

Bordeleau F, Mason BN, Lollis EM, Mazzola M, Zanotelli MR, Somasegar S, Califano JP, Montague C, LaValley DJ, Huynh J, Mencia-Trinchant N, Negrón Abril YL, Hassane DC, Bonassar LJ, Butcher JT, Weiss RS, Reinhart-King CA. 2017. Matrix stiffening promotes a tumor vasculature phenotype. *Proc Natl Acad Sci USA* **114**:492–497. doi:10.1073/pnas.1613855114

Borriello L, Coste A, Traub B, Sharma VP, Karagiannis GS, Lin Y, Wang Y, Ye X, Duran CL, Chen X, Friedman M, Sosa MS, Sun D, Dalla E, Singh DK, Oktay MH, Aguirre-Ghiso JA, Condeelis JS, Entenberg D. 2022. Primary tumor associated macrophages activate programs of invasion and dormancy in disseminating tumor cells. *Nat Commun* **13**:626. doi:10.1038/s41467-022-28076-3

Böttcher JP, Bonavita E, Chakravarty P, Blees H, Cabeza-Cabrerizo M, Sammicheli S, Rogers NC, Sahai E, Zelenay S, Reis E Sousa C. 2018. NK Cells Stimulate Recruitment of cDC1 into the Tumor Microenvironment Promoting Cancer Immune Control. *Cell* **172**:1022-1037.e14. doi:10.1016/j.cell.2018.01.004

Bottino C, Castriconi R, Pende D, Rivera P, Nanni M, Carnemolla B, Cantoni C, Grassi J, Marcenaro S, Reymond N, Vitale M, Moretta L, Lopez M, Moretta A. 2003. Identification of PVR (CD155) and Nectin-2 (CD112) as Cell Surface Ligands for the Human DNAM-1 (CD226) Activating Molecule. *The Journal of Experimental Medicine* **198**:557–567. doi:10.1084/jem.20030788

Bouchaala R, Mercier L, Andreiuk B, Mély Y, Vandamme T, Anton N, Goetz JG, Klymchenko AS. 2016. Integrity of lipid nanocarriers in bloodstream and tumor quantified by near-infrared ratiometric FRET imaging in living mice. *Journal of Controlled Release* **236**:57–67. doi:10.1016/j.jconrel.2016.06.027

Boucharaba A, Serre C-M, Grès S, Saulnier-Blache JS, Bordet J-C, Guglielmi J, Clézardin P, Peyruchaud O. 2004. Platelet-derived lysophosphatidic acid supports the progression of osteolytic bone metastases in breast cancer. *J Clin Invest* **114**:1714–1725. doi:10.1172/JCI200422123

Bradley LM, Dalton DK, Croft M. 1996. A direct role for IFN-gamma in regulation of Th1 cell development. *J Immunol* **157**:1350–1358.

Brandt CS, Baratin M, Yi EC, Kennedy J, Gao Z, Fox B, Haldeman B, Ostrander CD, Kaifu T, Chabannon C, Moretta A, West R, Xu W, Vivier E, Levin SD. 2009. The B7 family member B7-H6 is a tumor cell ligand for the activating natural killer cell receptor NKp30 in humans. *Journal of Experimental Medicine* **206**:1495–1503. doi:10.1084/jem.20090681

Bray F, Laversanne M, Sung H, Ferlay J, Siegel RL, Soerjomataram I, Jemal A. 2024. Global cancer statistics 2022: GLOBOCAN estimates of incidence and mortality worldwide for 36 cancers in 185 countries. *CA A Cancer J Clinicians* **74**:229–263. doi:10.3322/caac.21834

Brewer CF, Riehm JP. 1967. Evidence for possible nonspecific reactions between N-ethylmaleimide and proteins. *Analytical Biochemistry* **18**:248–255. doi:10.1016/0003-2697(67)90007-3

Brooks PC, Clark RAF, Cheresh DA. 1994. Requirement of Vascular Integrin $\alpha_v \beta_3$ for Angiogenesis. *Science* **264**:569–571. doi:10.1126/science.7512751

Brown WH. 1913. THE HISTOGENESIS OF BLOOD PLATELETS. *Journal of Experimental Medicine* **18**:278–286. doi:10.1084/jem.18.3.278

Bruhns P. 2012. Properties of mouse and human IgG receptors and their contribution to disease models. *Blood* **119**:5640–5649. doi:10.1182/blood-2012-01-380121

Bryan TM, Cech TR. 1999. Telomerase and the maintenance of chromosome ends. *Current Opinion in Cell Biology* **11**:318–324. doi:10.1016/S0955-0674(99)80043-X

Burnet FM. 1971. Immunological Surveillance in Neoplasia. *Immunological Reviews* **7**:3–25. doi:10.1111/j.1600-065X.1971.tb00461.x

Burnet M. 1964. Immunological factors in the process of carcinogenesis. *British Medical Bulletin* **20**:154–158. doi:10.1093/oxfordjournals.bmb.a070310

Burnet M. 1957. Cancer: a biological approach. III. Viruses associated with neoplastic conditions. IV. Practical applications. *Br Med J* **1**:841–847. doi:10.1136/bmj.1.5023.841

C

Cabrera T, Fernandez MA, Sierra A, Garrido A, Herruzo A, Escobedo A, Fabra A, Garrido F. 1996. High frequency of altered HLA class I phenotypes in invasive breast carcinomas. *Human Immunology* **50**:127–134. doi:10.1016/0198-8859(96)00145-0

Calvo F, Ege N, Grande-Garcia A, Hooper S, Jenkins RP, Chaudhry SI, Harrington K, Williamson P, Moeendarbary E, Charras G, Sahai E. 2013. Mechanotransduction and YAP-dependent matrix remodelling is required for the generation and maintenance of cancer-associated fibroblasts. *Nat Cell Biol* **15**:637–646. doi:10.1038/ncb2756

Camerer E, Qazi AA, Duong DN, Cornelissen I, Advincula R, Coughlin SR. 2004. Platelets, protease-activated receptors, and fibrinogen in hematogenous metastasis. *Blood* **104**:397–401. doi:10.1182/blood-2004-02-0434

Campbell KS, Purdy AK. 2011. Structure/function of human killer cell immunoglobulin-like receptors: lessons from polymorphisms, evolution, crystal structures and mutations: Structure/function of human KIR. *Immunology* **132**:315–325. doi:10.1111/j.1365-2567.2010.03398.x

Cao R, Björndahl MA, Religa P, Clasper S, Garvin S, Galter D, Meister B, Ikomi F, Tritsaris K, Dissing S, Ohhashi T, Jackson DG, Cao Y. 2004. PDGF-BB induces intratumoral lymphangiogenesis and promotes lymphatic metastasis. *Cancer Cell* **6**:333–345. doi:10.1016/j.ccr.2004.08.034

Carpén O, Virtanen I, Lehto VP, Saksela E. 1983. Polarization of NK cell cytoskeleton upon conjugation with sensitive target cells. *J Immunol* **131**:2695–2698.

Bibliography

Carrega P, Bonaccorsi I, Di Carlo E, Morandi B, Paul P, Rizzello V, Cipollone G, Navarra G, Mingari MC, Moretta L, Ferlazzo G. 2014. CD56brightPerforinlow Noncytotoxic Human NK Cells Are Abundant in Both Healthy and Neoplastic Solid Tissues and Recirculate to Secondary Lymphoid Organs via Afferent Lymph. *The Journal of Immunology* **192**:3805–3815. doi:10.4049/jimmunol.1301889

Cartron G, Dacheux L, Salles G, Solal-Celigny P, Bardos P, Colombat P, Watier H. 2002. Therapeutic activity of humanized anti-CD20 monoclonal antibody and polymorphism in IgG Fc receptor FcγRIIIa gene. *Blood* **99**:754–758. doi:10.1182/blood.V99.3.754

Cascino I, Papoff G, De Maria R, Testi R, Ruberti G. 1996. Fas/Apo-1 (CD95) receptor lacking the intracytoplasmic signaling domain protects tumor cells from Fas-mediated apoptosis. *J Immunol* **156**:13–17.

Cereceda L, Cardenas JC, Khoury M, Silva-Pavez E, Hidalgo Y. 2024. Impact of platelet-derived mitochondria transfer in the metabolic profiling and progression of metastatic MDA-MB-231 human triple-negative breast cancer cells. *Front Cell Dev Biol* **11**:1324158. doi:10.3389/fcell.2023.1324158

Chan IS, Ewald AJ. 2022. The changing role of natural killer cells in cancer metastasis. *Journal of Clinical Investigation* **132**:e143762. doi:10.1172/JCI143762

Chen DS, Mellman I. 2013. Oncology Meets Immunology: The Cancer-Immunity Cycle. *Immunity* **39**:1–10. doi:10.1016/j.immuni.2013.07.012

Chen J, Hamon MA, Hu H, Chen Y, Rao AM, Eklund PC, Haddon RC. 1998. Solution Properties of Single-Walled Carbon Nanotubes. *Science* **282**:95–98. doi:10.1126/science.282.5386.95

Chen R, Jin G, Li W, McIntyre TM. 2018. Epidermal Growth Factor (EGF) Autocrine Activation of Human Platelets Promotes EGF Receptor–Dependent Oral Squamous Cell Carcinoma Invasion, Migration, and Epithelial Mesenchymal Transition. *The Journal of Immunology* **201**:2154–2164. doi:10.4049/jimmunol.1800124

Chen S, Kawashima H, Lowe JB, Lanier LL, Fukuda M. 2005. Suppression of tumor formation in lymph nodes by L-selectin–mediated natural killer cell recruitment. *The Journal of Experimental Medicine* **202**:1679–1689. doi:10.1084/jem.20051473

Chen Y, Kim MT, Zheng L, Deperalta G, Jacobson F. 2016. Structural Characterization of Cross-Linked Species in Trastuzumab Emtansine (Kadcyla). *Bioconjugate Chem* **27**:2037–2047. doi:10.1021/acs.bioconjchem.6b00316

Cheng G, Tse J, Jain RK, Munn LL. 2009. Micro-Environmental Mechanical Stress Controls Tumor Spheroid Size and Morphology by Suppressing Proliferation and Inducing Apoptosis in Cancer Cells. *PLoS ONE* **4**:e4632. doi:10.1371/journal.pone.0004632

Bibliography

Cheng J, Zhou T, Liu C, Shapiro JP, Brauer MJ, Kiefer MC, Barr PJ, Mountz JD. 1994. Protection from Fas-Mediated Apoptosis by a Soluble Form of the Fas Molecule. *Science* **263**:1759–1762. doi:10.1126/science.7510905

Cheng Q, Wei T, Farbiak L, Johnson LT, Dilliard SA, Siegwart DJ. 2020. Selective organ targeting (SORT) nanoparticles for tissue-specific mRNA delivery and CRISPR–Cas gene editing. *Nat Nanotechnol* **15**:313–320. doi:10.1038/s41565-020-0669-6

Chin CF, Yap SQ, Li J, Pastorin G, Ang WH. 2014. Ratiometric delivery of cisplatin and doxorubicin using tumour-targeting carbon-nanotubes entrapping platinum(IV) prodrugs. *Chem Sci* **5**:2265–2270. doi:10.1039/C3SC53106F

Cho MS, Li J, Gonzalez-Delgado R, Lee H, Vasquez M, He T, He Y, Liu K, Sasano T, Nürnberg B, Sood AK, Wong STC, Afshar-Kharghan V. 2021. The effect of platelet G proteins on platelet extravasation and tumor growth in the murine model of ovarian cancer. *Blood Advances* **5**:1947–1951. doi:10.1182/bloodadvances.2020003410

Choquet D, Felsenfeld DP, Sheetz MP. 1997. Extracellular Matrix Rigidity Causes Strengthening of Integrin–Cytoskeleton Linkages. *Cell* **88**:39–48. doi:10.1016/S0092-8674(00)81856-5

Christie RJ, Fleming R, Bezabeh B, Woods R, Mao S, Harper J, Joseph A, Wang Q, Xu Z-Q, Wu H, Gao C, Dimasi N. 2015. Stabilization of cysteine-linked antibody drug conjugates with N-aryl maleimides. *Journal of Controlled Release* **220**:660–670. doi:10.1016/j.jconrel.2015.09.032

Christofori G, Naik P, Hanahan D. 1994. A second signal supplied by insulin-like growth factor II in oncogene-induced tumorigenesis. *Nature* **369**:414–418. doi:10.1038/369414a0

Cilliers C, Menezes B, Nessler I, Linderman J, Thurber GM. 2018. Improved Tumor Penetration and Single-Cell Targeting of Antibody–Drug Conjugates Increases Anticancer Efficacy and Host Survival. *Cancer Research* **78**:758–768. doi:10.1158/0008-5472.CAN-17-1638

Clark AG, Vignjevic DM. 2015. Modes of cancer cell invasion and the role of the microenvironment. *Current Opinion in Cell Biology* **36**:13–22. doi:10.1016/j.ceb.2015.06.004

Cluxton CD, Spillane C, O'Toole SA, Sheils O, Gardiner CM, O'Leary JJ. 2019. Suppression of Natural Killer cell NKG2D and CD226 anti-tumour cascades by platelet cloaked cancer cells: Implications for the metastatic cascade. *PLoS ONE* **14**:e0211538. doi:10.1371/journal.pone.0211538

Colarusso C, Falanga A, Terlizzi M, De Rosa I, Somma P, Sommella EM, Caponigro V, Panico L, Salviati E, Campiglia P, Salatiello G, Tramontano T, Maiolino P, Pinto A, Sorrentino R. 2023. High levels of PD-L1 on platelets of NSCLC patients contributes to the pharmacological activity of Atezolizumab. *Biomedicine & Pharmacotherapy* **168**:115709. doi:10.1016/j.biopha.2023.115709

Bibliography

Constantinides PP, Tustian A, Kessler DR. 2004. Tocol emulsions for drug solubilization and parenteral delivery. *Advanced Drug Delivery Reviews* **56**:1243–1255. doi:10.1016/j.addr.2003.12.005

Contrino J, Hair G, Kreutzer DL, Rickles FR. 1996. In situ detection of tissue factor in vascular endothelial cells: Correlation with the malignant phenotype of human breast disease. *Nat Med* **2**:209–215. doi:10.1038/nm0296-209

Cooke NM, Egan K, McFadden S, Grogan L, Breathnach OS, O'Leary J, Hennessy BT, Kenny D. 2013. Increased platelet reactivity in patients with late-stage metastatic cancer. *Cancer Medicine* **2**:564–570. doi:10.1002/cam4.86

Cools-Lartigue J, Spicer J, McDonald B, Gowing S, Chow S, Giannias B, Bourdeau F, Kubes P, Ferri L. 2013. Neutrophil extracellular traps sequester circulating tumor cells and promote metastasis. *J Clin Invest* **123**:3446–3458. doi:10.1172/JCI67484

Cords L, Engler S, Haberecker M, Rüschoff JH, Moch H, De Souza N, Bodenmiller B. 2024. Cancer-associated fibroblast phenotypes are associated with patient outcome in non-small cell lung cancer. *Cancer Cell* **42**:396-412.e5. doi:10.1016/j.ccell.2023.12.021

Cosman D, Müllberg J, Sutherland CL, Chin W, Armitage R, Fanslow W, Kubin M, Chalupny NJ. 2001. ULBPs, Novel MHC Class I–Related Molecules, Bind to CMV Glycoprotein UL16 and Stimulate NK Cytotoxicity through the NKG2D Receptor. *Immunity* **14**:123–133. doi:10.1016/S1074-7613(01)00095-4

Costa B, Eisemann T, Strelau J, Spaan I, Korshunov A, Liu H-K, Bugert P, Angel P, Peterziel H. 2019. Intratumoral platelet aggregate formation in a murine preclinical glioma model depends on podoplanin expression on tumor cells. *Blood Advances* **3**:1092–1102. doi:10.1182/bloodadvances.2018015966

Counter CM, Avilion AA, LeFeuvre CE, Stewart NG, Greider CW, Harley CB, Bacchetti S. 1992. Telomere shortening associated with chromosome instability is arrested in immortal cells which express telomerase activity. *The EMBO Journal* **11**:1921–1929. doi:10.1002/j.1460-2075.1992.tb05245.x

Coupland LA, Chong BH, Parish CR. 2012. Platelets and P-Selectin Control Tumor Cell Metastasis in an Organ-Specific Manner and Independently of NK Cells. *Cancer Research* **72**:4662–4671. doi:10.1158/0008-5472.CAN-11-4010

Cózar B, Greppi M, Carpentier S, Narni-Mancinelli E, Chiossone L, Vivier E. 2021. Tumor-Infiltrating Natural Killer Cells. *Cancer Discovery* **11**:34–44. doi:10.1158/2159-8290.CD-20-0655

Crawford Y, Kasman I, Yu L, Zhong C, Wu X, Modrusan Z, Kaminker J, Ferrara N. 2009. PDGF-C Mediates the Angiogenic and Tumorigenic Properties of Fibroblasts Associated with Tumors Refractory to Anti-VEGF Treatment. *Cancer Cell* **15**:21–34. doi:10.1016/j.ccr.2008.12.004

Creemers JHA, Pawlitzky I, Grosios K, Gileadi U, Middleton MR, Gerritsen WR, Mehra N, Rivoltini L, Walters I, Figdor CG, Ottevanger PB, De Vries IJM. 2021. Assessing the safety, tolerability and efficacy of PLGA-based immunomodulatory nanoparticles in patients with advanced NY-ESO-1-positive cancers: a first-in-human phase I open-label dose-escalation study protocol. *BMJ Open* **11**:e050725. doi:10.1136/bmjopen-2021-050725

Cursons J, Souza-Fonseca-Guimaraes F, Foroutan M, Anderson A, Hollande F, Hediyeh-Zadeh S, Behren A, Huntington ND, Davis MJ. 2019. A Gene Signature Predicting Natural Killer Cell Infiltration and Improved Survival in Melanoma Patients. *Cancer Immunology Research* **7**:1162–1174. doi:10.1158/2326-6066.CIR-18-0500

D

Dameron KM, Volpert OV, Tainsky MA, Bouck N. 1994. Control of Angiogenesis in Fibroblasts by p53 Regulation of Thrombospondin-1. *Science* **265**:1582–1584. doi:10.1126/science.7521539

Dams ET, Laverman P, Oyen WJ, Storm G, Scherphof GL, van Der Meer JW, Corstens FH, Boerman OC. 2000. Accelerated blood clearance and altered biodistribution of repeated injections of sterically stabilized liposomes. *J Pharmacol Exp Ther* **292**:1071–1079.

Danhier F, Ansorena E, Silva JM, Coco R, Le Breton A, Préat V. 2012. PLGA-based nanoparticles: An overview of biomedical applications. *Journal of Controlled Release* **161**:505–522. doi:10.1016/j.jconrel.2012.01.043

Dardik R, Kaufmann Y, Savion N, Rosenberg N, Shenkman B, Varon D. 1997. Platelets mediate tumor cell adhesion to the subendothelium under flow conditions: Involvement of platelet GPIIb-IIIa and tumor cell ?v integrins. *Int J Cancer* **70**:201–207. doi:10.1002/(SICI)1097-0215(19970117)70:2<201::AID-IJC11>3.0.CO;2-L

Davizon-Castillo P, McMahon B, Aguila S, Bark D, Ashworth K, Allawzi A, Campbell RA, Montenont E, Nemkov T, D'Alessandro A, Clendenen N, Shih L, Sanders NA, Higa K, Cox A, Padilla-Romo Z, Hernandez G, Wartchow E, Trahan GD, Nozik-Grayck E, Jones K, Pietras EM, DeGregori J, Rondina MT, Di Paola J. 2019. TNF-α–driven inflammation and mitochondrial dysfunction define the platelet hyperreactivity of aging. *Blood* **134**:727–740. doi:10.1182/blood.2019000200

De Andrade LF, Lu Y, Luoma A, Ito Y, Pan D, Pyrdol JW, Yoon CH, Yuan G-C, Wucherpfennig KW. 2019. Discovery of specialized NK cell populations infiltrating human melanoma metastases. *JCI Insight* **4**:e133103. doi:10.1172/jci.insight.133103

De Leval X, Benoit V, Delarge J, Julémont F, Masereel B, Pirotte B, Merville M-P, David J-L, Dogné J-M. 2003. Pharmacological evaluation of the novel thromboxane modulator BM-567 (II/II). Effects of BM-567 on osteogenic sarcoma-cell-induced platelet aggregation. *Prostaglandins, Leukotrienes and Essential Fatty Acids* **68**:55–59. doi:10.1016/S0952-3278(02)00235-1

Bibliography

De Palma M, Venneri MA, Galli R, Sergi LS, Politi LS, Sampaolesi M, Naldini L. 2005. Tie2 identifies a hematopoietic lineage of proangiogenic monocytes required for tumor vessel formation and a mesenchymal population of pericyte progenitors. *Cancer Cell* **8**:211–226. doi:10.1016/j.ccr.2005.08.002

de Vries TJ, Fourkour A, Wobbes T, Verkroost G, Ruiter DJ, van Muijen GN. 1997. Heterogeneous expression of immunotherapy candidate proteins gp100, MART-1, and tyrosinase in human melanoma cell lines and in human melanocytic lesions. *Cancer Res* **57**:3223–3229.

De Wever O, Nguyen Q, Van Hoorde L, Bracke M, Bruyneel E, Gespach C, Mareel M. 2004. Tenascin-C and SF/HGF produced by myofibroblasts in vitro provide convergent proinvasive signals to human colon cancer cells through RhoA and Rac. *FASEB j* **18**:1016–1018. doi:10.1096/fj.03-1110fje

Delarue M, Montel F, Vignjevic D, Prost J, Joanny J-F, Cappello G. 2014. Compressive Stress Inhibits Proliferation in Tumor Spheroids through a Volume Limitation. *Biophysical Journal* **107**:1821–1828. doi:10.1016/j.bpj.2014.08.031

Delogu LG, Vidili G, Venturelli E, Ménard-Moyon C, Zoroddu MA, Pilo G, Nicolussi P, Ligios C, Bedognetti D, Sgarrella F, Manetti R, Bianco A. 2012. Functionalized multiwalled carbon nanotubes as ultrasound contrast agents. *Proc Natl Acad Sci USA* **109**:16612–16617. doi:10.1073/pnas.1208312109

Demers M, Ho-Tin-Noé B, Schatzberg D, Yang JJ, Wagner DD. 2011. Increased efficacy of breast cancer chemotherapy in thrombocytopenic mice. *Cancer Res* **71**:1540–1549. doi:10.1158/0008-5472.CAN-10-2038

Detappe A, Mathieu C, Jin C, Agius MP, Diringer M-C, Tran V-L, Pivot X, Lux F, Tillement O, Kufe D, Ghoroghchian PP. 2020. Anti-MUC1-C Antibody–Conjugated Nanoparticles Potentiate the Efficacy of Fractionated Radiation Therapy. *International Journal of Radiation Oncology*Biology*Physics* **108**:1380–1389. doi:10.1016/j.ijrobp.2020.06.069

Detappe A, Reidy M, Yu Y, Mathieu C, Nguyen HV-T, Coroller TP, Lam F, Jarolim P, Harvey P, Protti A, Nguyen Q-D, Johnson JA, Cremillieux Y, Tillement O, Ghobrial IM, Ghoroghchian PP. 2019. Antibody-targeting of ultra-small nanoparticles enhances imaging sensitivity and enables longitudinal tracking of multiple myeloma. *Nanoscale* **11**:20485–20496. doi:10.1039/C9NR06512A

Detappe A, Thomas E, Tibbitt MW, Kunjachan S, Zavidij O, Parnandi N, Reznichenko E, Lux F, Tillement O, Berbeco R. 2017. Ultrasmall Silica-Based Bismuth Gadolinium Nanoparticles for Dual Magnetic Resonance–Computed Tomography Image Guided Radiation Therapy. *Nano Lett* **17**:1733–1740. doi:10.1021/acs.nanolett.6b05055

Di Martino JS, Nobre AR, Mondal C, Taha I, Farias EF, Fertig EJ, Naba A, Aguirre-Ghiso JA, Bravo-Cordero JJ. 2021. A tumor-derived type III collagen-rich ECM niche regulates tumor cell dormancy. *Nat Cancer* **3**:90–107. doi:10.1038/s43018-021-00291-9

Bibliography

Di Tomaso E, Capen D, Haskell A, Hart J, Logie JJ, Jain RK, McDonald DM, Jones R, Munn LL. 2005. Mosaic Tumor Vessels: Cellular Basis and Ultrastructure of Focal Regions Lacking Endothelial Cell Markers. *Cancer Research* **65**:5740–5749. doi:10.1158/0008-5472.CAN-04-4552

Dieu M-C, Vanbervliet B, Vicari A, Bridon J-M, Oldham E, Aït-Yahia S, Brière F, Zlotnik A, Lebecque S, Caux C. 1998. Selective Recruitment of Immature and Mature Dendritic Cells by Distinct Chemokines Expressed in Different Anatomic Sites. *The Journal of Experimental Medicine* **188**:373–386. doi:10.1084/jem.188.2.373

Dighe AS, Richards E, Old LJ, Schreiber RD. 1994. Enhanced in vivo growth and resistance to rejection of tumor cells expressing dominant negative IFNγ receptors. *Immunity* **1**:447–456. doi:10.1016/1074-7613(94)90087-6

Dillekås H, Rogers MS, Straume O. 2019. Are 90% of deaths from cancer caused by metastases? *Cancer Medicine* **8**:5574–5576. doi:10.1002/cam4.2474

Dilly A, Ekambaram P, Guo Y, Cai Y, Tucker SC, Fridman R, Kandouz M, Honn KV. 2013. Platelet-type 12-lipoxygenase induces MMP9 expression and cellular invasion *via* activation of PI3K/Akt/NF-κB: Overexpression of Platelet-Type 12-LOX in PC-3 Cells. *Int J Cancer* **133**:1784–1791. doi:10.1002/ijc.28165

Dimitroff CJ, Descheny L, Trujillo N, Kim R, Nguyen V, Huang W, Pienta KJ, Kutok JL, Rubin MA. 2005. Identification of Leukocyte E-Selectin Ligands, P-Selectin Glycoprotein Ligand-1 and E-Selectin Ligand-1, on Human Metastatic Prostate Tumor Cells. *Cancer Research* **65**:5750–5760. doi:10.1158/0008-5472.CAN-04-4653

Dommerholt J, Van Rooijen O, Borrmann A, Guerra CF, Bickelhaupt FM, Van Delft FL. 2014. Highly accelerated inverse electron-demand cycloaddition of electron-deficient azides with aliphatic cyclooctynes. *Nat Commun* **5**:5378. doi:10.1038/ncomms6378

Dongre A, Weinberg RA. 2019. New insights into the mechanisms of epithelial–mesenchymal transition and implications for cancer. *Nat Rev Mol Cell Biol* **20**:69–84. doi:10.1038/s41580-018-0080-4

Donnelly RP, Loftus RM, Keating SE, Liou KT, Biron CA, Gardiner CM, Finlay DK. 2014. mTORC1-Dependent Metabolic Reprogramming Is a Prerequisite for NK Cell Effector Function. *The Journal of Immunology* **193**:4477–4484. doi:10.4049/jimmunol.1401558

Drago JZ, Modi S, Chandarlapaty S. 2021. Unlocking the potential of antibody–drug conjugates for cancer therapy. *Nat Rev Clin Oncol* **18**:327–344. doi:10.1038/s41571-021-00470-8

Duncan RJS, Weston PD, Wrigglesworth R. 1983. A new reagent which may be used to introduce sulfhydryl groups into proteins, and its use in the preparation of conjugates for immunoassay. *Analytical Biochemistry* **132**:68–73. doi:10.1016/0003-2697(83)90426-8

Dustin ML, Cooper JA. 2000. The immunological synapse and the actin cytoskeleton: molecular hardware for T cell signaling. *Nat Immunol* **1**:23–29. doi:10.1038/76877

Dvorak HF. 1986. Tumors: Wounds That Do Not Heal. *N Engl J Med* **315**:1650–1659. doi:10.1056/NEJM198612253152606

E

Egan K, Cooke N, Kenny D. 2014. Living in shear: platelets protect cancer cells from shear induced damage. *Clin Exp Metastasis* **31**:697–704. doi:10.1007/s10585-014-9660-7

Egan K, Crowley D, Smyth P, O'Toole S, Spillane C, Martin C, Gallagher M, Canney A, Norris L, Conlon N, McEvoy L, Ffrench B, Stordal B, Keegan H, Finn S, McEneaney V, Laios A, Ducrée J, Dunne E, Smith L, Berndt M, Sheils O, Kenny D, O'Leary J. 2011. Platelet Adhesion and Degranulation Induce Pro-Survival and Pro-Angiogenic Signalling in Ovarian Cancer Cells. *PLoS ONE* **6**:e26125. doi:10.1371/journal.pone.0026125

Ehrlich P. 1908. Ueber den jetzigen Stand der Karzinomforschung.

El Ghissassi F, Baan R, Straif K, Grosse Y, Secretan B, Bouvard V, Benbrahim-Tallaa L, Guha N, Freeman C, Galichet L, Cogliano V, WHO International Agency for Research on Cancer Monograph Working Group. 2009. A review of human carcinogens--part D: radiation. *Lancet Oncol* **10**:751–752. doi:10.1016/s1470-2045(09)70213-x

Elyada E, Bolisetty M, Laise P, Flynn WF, Courtois ET, Burkhart RA, Teinor JA, Belleau P, Biffi G, Lucito MS, Sivajothi S, Armstrong TD, Engle DD, Yu KH, Hao Y, Wolfgang CL, Park Y, Preall J, Jaffee EM, Califano A, Robson P, Tuveson DA. 2019. Cross-Species Single-Cell Analysis of Pancreatic Ductal Adenocarcinoma Reveals Antigen-Presenting Cancer-Associated Fibroblasts. *Cancer Discovery* **9**:1102–1123. doi:10.1158/2159-8290.CD-19-0094

Elzey BD, Tian J, Jensen RJ, Swanson AK, Lees JR, Lentz SR, Stein CS, Nieswandt B, Wang Y, Davidson BL, Ratliff TL. 2003. Platelet-Mediated Modulation of Adaptive Immunity. *Immunity* **19**:9–19. doi:10.1016/S1074-7613(03)00177-8

Erler JT, Bennewith KL, Cox TR, Lang G, Bird D, Koong A, Le Q-T, Giaccia AJ. 2009. Hypoxia-Induced Lysyl Oxidase Is a Critical Mediator of Bone Marrow Cell Recruitment to Form the Premetastatic Niche. *Cancer Cell* **15**:35–44. doi:10.1016/j.ccr.2008.11.012

Etulain J, Martinod K, Wong SL, Cifuni SM, Schattner M, Wagner DD. 2015. P-selectin promotes neutrophil extracellular trap formation in mice. *Blood* **126**:242–246. doi:10.1182/blood-2015-01-624023

Ewing J. 1928. 10.1016/j.devcel.2018.02.015, Third edition. ed.

F

Falanga A, Leader A, Ambaglio C, Bagoly Z, Castaman G, Elalamy I, Lecumberri R, Niessner A, Pabinger I, Szmit S, Trinchero A, Ten Cate H, Rocca B. 2022. EHA Guidelines on Management of Antithrombotic Treatments in Thrombocytopenic Patients With Cancer. *HemaSphere* **6**:e750. doi:10.1097/HS9.0000000000000750

Feinauer MJ, Schneider SW, Berghoff AS, Robador JR, Tehranian C, Karreman MA, Venkataramani V, Solecki G, Grosch JK, Gunkel K, Kovalchuk B, Mayer FT, Fischer M, Breckwoldt MO, Brune M, Schwab Y, Wick W, Bauer AT, Winkler F. 2021. Local blood coagulation drives cancer cell arrest and brain metastasis in a mouse model. *Blood* **137**:1219–1232. doi:10.1182/blood.2020005710

Feitsma LJ, Brondijk HC, Jarvis GE, Hagemans D, Bihan D, Jerah N, Versteeg M, Farndale RW, Huizinga EG. 2022. Structural insights into collagen binding by platelet receptor glycoprotein VI. *Blood* **139**:3087–3098. doi:10.1182/blood.2021013614

Feng W, Madajka M, Kerr BA, Mahabeleshwar GH, Whiteheart SW, Byzova TV. 2011. A novel role for platelet secretion in angiogenesis: mediating bone marrow–derived cell mobilization and homing. *Blood* **117**:3893–3902. doi:10.1182/blood-2010-08-304808

Ferguson TA, Choi J, Green DR. 2011. Armed response: how dying cells influence T-cell functions. *Immunological Reviews* **241**:77–88. doi:10.1111/j.1600-065X.2011.01006.x

Ferjančič Š, Gil-Bernabé AM, Hill SA, Allen PD, Richardson P, Sparey T, Savory E, McGuffog J, Muschel RJ. 2013. VCAM-1 and VAP-1 recruit myeloid cells that promote pulmonary metastasis in mice. *Blood* **121**:3289–3297. doi:10.1182/blood-2012-08-449819

Fishel R, Lescoe MK, Rao MR, Copeland NG, Jenkins NA, Garber J, Kane M, Kolodner R. 1993. The human mutator gene homolog MSH2 and its association with hereditary nonpolyposis colon cancer. *Cell* **75**:1027–1038. doi:10.1016/0092-8674(93)90546-3

Fishman DA, Liu Y, Ellerbroek SM, Stack MS. 2001. Lysophosphatidic acid promotes matrix metalloproteinase (MMP) activation and MMP-dependent invasion in ovarian cancer cells. *Cancer Res* **61**:3194–3199.

Follain G, Osmani N, Azevedo AS, Allio G, Mercier L, Karreman MA, Solecki G, Garcia Leòn MJ, Lefebvre O, Fekonja N, Hille C, Chabannes V, Dollé G, Metivet T, Hovsepian FD, Prudhomme C, Pichot A, Paul N, Carapito R, Bahram S, Ruthensteiner B, Kemmling A, Siemonsen S, Schneider T, Fiehler J, Glatzel M, Winkler F, Schwab Y, Pantel K, Harlepp S, Goetz JG. 2018. Hemodynamic Forces Tune the Arrest, Adhesion, and Extravasation of Circulating Tumor Cells. *Developmental Cell* **45**:33-52.e12. doi:10.1016/j.devcel.2018.02.015

Fontaine SD, Reid R, Robinson L, Ashley GW, Santi DV. 2015. Long-Term Stabilization of Maleimide–Thiol Conjugates. *Bioconjugate Chem* **26**:145–152. doi:10.1021/bc5005262

Förster R, Schubel A, Breitfeld D, Kremmer E, Renner-Müller I, Wolf E, Lipp M. 1999. CCR7 Coordinates the Primary Immune Response by Establishing Functional Microenvironments in Secondary Lymphoid Organs. *Cell* **99**:23–33. doi:10.1016/S0092-8674(00)80059-8

Fourcade J, Sun Z, Benallaoua M, Guillaume P, Luescher IF, Sander C, Kirkwood JM, Kuchroo V, Zarour HM. 2010. Upregulation of Tim-3 and PD-1 expression is associated with tumor antigen–specific CD8+ T cell dysfunction in melanoma patients. *Journal of Experimental Medicine* **207**:2175–2186. doi:10.1084/jem.20100637

Fridlender ZG, Sun J, Kim S, Kapoor V, Cheng G, Ling L, Worthen GS, Albelda SM. 2009. Polarization of Tumor-Associated Neutrophil Phenotype by TGF-β: “N1” versus “N2” TAN. *Cancer Cell* **16**:183–194. doi:10.1016/j.ccr.2009.06.017

Friedman G, Levi-Galibov O, David E, Bornstein C, Giladi A, Dadiani M, Mayo A, Halperin C, Pevsner-Fischer M, Lavon H, Mayer S, Nevo R, Stein Y, Balint-Lahat N, Barshack I, Ali HR, Caldas C, Nili-Gal-Yam E, Alon U, Amit I, Scherz-Shouval R. 2020. Cancer-associated fibroblast compositions change with breast cancer progression linking the ratio of S100A4+ and PDPN+ CAFs to clinical outcome. *Nat Cancer* **1**:692–708. doi:10.1038/s43018-020-0082-y

Fu K, Pack DW, Klibanov AM, Langer R. 2000. Visual Evidence of Acidic Environment Within Degrading Poly(lactic-co-glycolic acid) (PLGA) Microspheres. *Pharmaceutical Research* **17**:100–106. doi:10.1023/A:1007582911958

Fujimori K, Covell DG, Fletcher JE, Weinstein JN. 1990. A modeling analysis of monoclonal antibody percolation through tumors: a binding-site barrier. *J Nucl Med* **31**:1191–1198.

Fukumura D, Xavier R, Sugiura T, Chen Y, Park E-C, Lu N, Selig M, Nielsen G, Taksir T, Jain RK, Seed B. 1998. Tumor Induction of VEGF Promoter Activity in Stromal Cells. *Cell* **94**:715–725. doi:10.1016/S0092-8674(00)81731-6

G

Gallina G, Dolcetti L, Serafini P, Santo CD, Marigo I, Colombo MP, Basso G, Brombacher F, Borrello I, Zanovello P, Bicciato S, Bronte V. 2006. Tumors induce a subset of inflammatory monocytes with immunosuppressive activity on CD8+ T cells. *Journal of Clinical Investigation* **116**:2777–2790. doi:10.1172/JCI28828

Gao Y, Bado I, Wang H, Zhang W, Rosen JM, Zhang XH-F. 2019. Metastasis Organotropism: Redefining the Congenial Soil. *Developmental Cell* **49**:375–391. doi:10.1016/j.devcel.2019.04.012

Garber JE, Offit K. 2005. Hereditary Cancer Predisposition Syndromes. *JCO* **23**:276–292. doi:10.1200/JCO.2005.10.042

Garcia-Leon MJ, Liboni C, Mittelheisser V, Bochler L, Follain G, Mouriaux C, Busnelli I, Larnicol A, Colin F, Peralta M, Osmani N, Gensbittel V, Bourdon C, Samaniego R, Pichot A, Paul N, Molitor A, Carapito R, Jandrot-Perrus M, Lefebvre O, Mangin PH, Goetz JG. 2024. Platelets favor the outgrowth of established metastases. *Nat Commun* **15**:3297. doi:10.1038/s41467-024-47516-w

Gareau AJ, Brien C, Gebremeskel S, Liwski RS, Johnston B, Bezuhly M. 2018. Ticagrelor inhibits platelet–tumor cell interactions and metastasis in human and murine breast cancer. *Clin Exp Metastasis* **35**:25–35. doi:10.1007/s10585-018-9874-1

Bibliography

Gasic GJ, Gasic TB, Stewart CC. 1968. Antimetastatic effects associated with platelet reduction. *Proc Natl Acad Sci USA* **61**:46–52. doi:10.1073/pnas.61.1.46

Gaudry M, Brégerie O, Andrieu V, El Benna J, Pocidalo M-A, Hakim J. 1997. Intracellular Pool of Vascular Endothelial Growth Factor in Human Neutrophils. *Blood* **90**:4153–4161. doi:10.1182/blood.V90.10.4153

Gautier V, Boumeester AJ, Lössl P, Heck AJR. 2015. Lysine conjugation properties in human IgGs studied by integrating high-resolution native mass spectrometry and bottom-up proteomics. *Proteomics* **15**:2756–2765. doi:10.1002/pmic.201400462

Geiger TR, Peeper DS. 2007. Critical Role for TrkB Kinase Function in Anoikis Suppression, Tumorigenesis, and Metastasis. *Cancer Research* **67**:6221–6229. doi:10.1158/0008-5472.CAN-07-0121

Gensbittel V, Kräter M, Harlepp S, Busnelli I, Guck J, Goetz JG. 2021. Mechanical Adaptability of Tumor Cells in Metastasis. *Developmental Cell* **56**:164–179. doi:10.1016/j.devcel.2020.10.011

Georgakilas V, Kordatos K, Prato M, Guldi DM, Holzinger M, Hirsch A. 2002. Organic Functionalization of Carbon Nanotubes. *J Am Chem Soc* **124**:760–761. doi:10.1021/ja016954m

Gerber HP, Kowalski J, Sherman D, Eberhard DA, Ferrara N. 2000. Complete inhibition of rhabdomyosarcoma xenograft growth and neovascularization requires blockade of both tumor and host vascular endothelial growth factor. *Cancer Res* **60**:6253–6258.

Gerosa F, Baldani-Guerra B, Nisii C, Marchesini V, Carra G, Trinchieri G. 2002. Reciprocal Activating Interaction between Natural Killer Cells and Dendritic Cells. *The Journal of Experimental Medicine* **195**:327–333. doi:10.1084/jem.20010938

Gil Del Alcazar CR, Huh SJ, Ekram MB, Trinh A, Liu LL, Beca F, Zi X, Kwak M, Bergholtz H, Su Y, Ding L, Russnes HG, Richardson AL, Babski K, Min Hui Kim E, McDonnell CH, Wagner J, Rowberry R, Freeman GJ, Dillon D, Sorlie T, Coussens LM, Garber JE, Fan R, Bobolis K, Allred DC, Jeong J, Park SY, Michor F, Polyak K. 2017. Immune Escape in Breast Cancer During *In Situ* to Invasive Carcinoma Transition. *Cancer Discovery* **7**:1098–1115. doi:10.1158/2159-8290.CD-17-0222

Gilis D, Massar S, Cerf NJ, Rooman M. 2001. Optimality of the genetic code with respect to protein stability and amino-acid frequencies. *Genome Biol* **2**:research0049.1. doi:10.1186/gb-2001-2-11-research0049

Goetz JG, Minguet S, Navarro-Lérida I, Lazcano JJ, Samaniego R, Calvo E, Tello M, Osteso-Ibáñez T, Pellinen T, Echarri A, Cerezo A, Klein-Szanto AJP, Garcia R, Keely PJ, Sánchez-Mateos P, Cukierman E, Del Pozo MA. 2011. Biomechanical Remodeling of the Microenvironment by Stromal Caveolin-1 Favors Tumor Invasion and Metastasis. *Cell* **146**:148–163. doi:10.1016/j.cell.2011.05.040

Bibliography

Gomez TS, McCarney SD, Carrizosa E, Labno CM, Comiskey EO, Nolz JC, Zhu P, Freedman BD, Clark MR, Rawlings DJ, Billadeau DD, Burkhardt JK. 2006. HS1 Functions as an Essential Actin-Regulatory Adaptor Protein at the Immune Synapse. *Immunity* **24**:741–752. doi:10.1016/j.immuni.2006.03.022

González-Lavado E, Valdivia L, García-Castaño A, González F, Pesquera C, Valiente R, Fanarraga ML. 2019. Multi-walled carbon nanotubes complement the anti-tumoral effect of 5-Fluorouracil. *Oncotarget* **10**:2022–2029. doi:10.18632/oncotarget.26770

Göpferich A. 1997. Polymer Bulk Erosion. *Macromolecules* **30**:2598–2604. doi:10.1021/ma961627y

Gorelik L, Flavell RA. 2001. Immune-mediated eradication of tumors through the blockade of transforming growth factor-β signaling in T cells. *Nat Med* **7**:1118–1122. doi:10.1038/nm1001-1118

Grakoui A, Bromley SK, Sumen C, Davis MM, Shaw AS, Allen PM, Dustin ML. 1999. The Immunological Synapse: A Molecular Machine Controlling T Cell Activation. *Science* **285**:221–227. doi:10.1126/science.285.5425.221

Greaves M, Maley CC. 2012. Clonal evolution in cancer. *Nature* **481**:306–313. doi:10.1038/nature10762

Greenberg AH, Hudson L, Shen L, Roitt IM. 1973. Antibody-dependent Cell-mediated Cytotoxicity due to a “Null” Lymphoid Cell. *Nature New Biology* **242**:111–113. doi:10.1038/newbio242111a0

Greene MK, Nogueira JCF, Tracey SR, Richards DA, McDaid WJ, Burrows JF, Campbell K, Longley DB, Chudasama V, Scott CJ. 2020. Refined construction of antibody-targeted nanoparticles leads to superior antigen binding and enhanced delivery of an entrapped payload to pancreatic cancer cells. *Nanoscale* **12**:11647–11658. doi:10.1039/D0NR02387F

Grégoire C, Chasson L, Luci C, Tomasello E, Geissmann F, Vivier E, Walzer T. 2007. The trafficking of natural killer cells. *Immunological Reviews* **220**:169–182. doi:10.1111/j.1600-065X.2007.00563.x

Grivennikov S, Karin E, Terzic J, Mucida D, Yu G-Y, Vallabhapurapu S, Scheller J, Rose-John S, Cheroutre H, Eckmann L, Karin M. 2009. IL-6 and Stat3 Are Required for Survival of Intestinal Epithelial Cells and Development of Colitis-Associated Cancer. *Cancer Cell* **15**:103–113. doi:10.1016/j.ccr.2009.01.001

Groh V, Wu J, Yee C, Spies T. 2002. Tumour-derived soluble MIC ligands impair expression of NKG2D and T-cell activation. *Nature* **419**:734–738. doi:10.1038/nature01112

Guck J, Schinkinger S, Lincoln B, Wottawah F, Ebert S, Romeyke M, Lenz D, Erickson HM, Ananthakrishnan R, Mitchell D, Käs J, Ulvick S, Bilby C. 2005. Optical Deformability as an Inherent Cell Marker for Testing Malignant Transformation and Metastatic Competence. *Biophysical Journal* **88**:3689–3698. doi:10.1529/biophysj.104.045476

Guo Q, Malloy MW, Roweth HG, McAllister SS, Italiano JE, Battinelli EM. 2022. Platelets upregulate tumor cell programmed death ligand 1 in an epidermal growth factor receptor-dependent manner in vitro. *Blood Advances* **6**:5668–5675. doi:10.1182/bloodadvances.2021006120

Guy C, Mitrea DM, Chou P-C, Temirov J, Vignali KM, Liu X, Zhang H, Kriwacki R, Bruchez MP, Watkins SC, Workman CJ, Vignali DAA. 2022. LAG3 associates with TCR–CD3 complexes and suppresses signaling by driving co-receptor–Lck dissociation. *Nat Immunol* **23**:757–767. doi:10.1038/s41590-022-01176-4

H

Haemmerle M, Bottsford-Miller J, Pradeep S, Taylor ML, Choi H-J, Hansen JM, Dalton HJ, Stone RL, Cho MS, Nick AM, Nagaraja AS, Gutschner T, Gharpure KM, Mangala LS, Rupaimoole R, Han HD, Zand B, Armaiz-Pena GN, Wu SY, Pecot CV, Burns AR, Lopez-Berestein G, Afshar-Kharghan V, Sood AK. 2016. FAK regulates platelet extravasation and tumor growth after antiangiogenic therapy withdrawal. *Journal of Clinical Investigation* **126**:1885–1896. doi:10.1172/JCI85086

Haemmerle M, Taylor ML, Gutschner T, Pradeep S, Cho MS, Sheng J, Lyons YM, Nagaraja AS, Dood RL, Wen Y, Mangala LS, Hansen JM, Rupaimoole R, Gharpure KM, Rodriguez-Aguayo C, Yim SY, Lee J-S, Ivan C, Hu W, Lopez-Berestein G, Wong ST, Karlan BY, Levine DA, Liu J, Afshar-Kharghan V, Sood AK. 2017. Platelets reduce anoikis and promote metastasis by activating YAP1 signaling. *Nat Commun* **8**:310. doi:10.1038/s41467-017-00411-z

Hainfeld JF, Slatkin DN, Smilowitz HM. 2004. The use of gold nanoparticles to enhance radiotherapy in mice. *Phys Med Biol* **49**:N309–N315. doi:10.1088/0031-9155/49/18/N03

Haining EJ, Lowe KL, Wichaiyo S, Kataru RP, Nagy Z, Kavanagh DP, Lax S, Di Y, Nieswandt B, Ho-Tin-Noé B, Mehrara BJ, Senis YA, Rayes J, Watson SP. 2021. Lymphatic blood filling in CLEC-2-deficient mouse models. *Platelets* **32**:352–367. doi:10.1080/09537104.2020.1734784

Half E, Tang XM, Gwyn K, Sahin A, Wathen K, Sinicrope FA. 2002. Cyclooxygenase-2 expression in human breast cancers and adjacent ductal carcinoma in situ. *Cancer Res* **62**:1676–1681.

Hall JM, Lee MK, Newman B, Morrow JE, Anderson LA, Huey B, King MC. 1990. Linkage of early-onset familial breast cancer to chromosome 17q21. *Science* **250**:1684–1689. doi:10.1126/science.2270482

Bibliography

Hamblett KJ, Senter PD, Chace DF, Sun MMC, Lenox J, Cerveny CG, Kissler KM, Bernhardt SX, Kopcha AK, Zabinski RF, Meyer DL, Francisco JA. 2004. Effects of Drug Loading on the Antitumor Activity of a Monoclonal Antibody Drug Conjugate. *Clinical Cancer Research* **10**:7063–7070. doi:10.1158/1078-0432.CCR-04-0789

Han YL, Ronceray P, Xu G, Malandrino A, Kamm RD, Lenz M, Broedersz CP, Guo M. 2018. Cell contraction induces long-ranged stress stiffening in the extracellular matrix. *Proc Natl Acad Sci USA* **115**:4075–4080. doi:10.1073/pnas.1722619115

Hanahan D, Folkman J. 1996. Patterns and Emerging Mechanisms of the Angiogenic Switch during Tumorigenesis. *Cell* **86**:353–364. doi:10.1016/S0092-8674(00)80108-7

Hanahan D, Weinberg RA. 2011. Hallmarks of Cancer: The Next Generation. *Cell* **144**:646–674. doi:10.1016/j.cell.2011.02.013

Hansemann D. 1890. Ueber asymmetrische Zelltheilung in Epithelkrebsen und deren biologische Bedeutung. *Archiv für pathologische Anatomie und Physiologie und für klinische Medicin* **119**:299–326.

Harano K, Kogawa T, Wu J, Yuan Y, Cohen EN, Lim B, Reuben JM, Ueno NT. 2017. Thrombocytosis as a prognostic factor in inflammatory breast cancer. *Breast Cancer Res Treat* **166**:819–832. doi:10.1007/s10549-017-4463-6

Harney AS, Arwert EN, Entenberg D, Wang Y, Guo P, Qian B-Z, Oktay MH, Pollard JW, Jones JG, Condeelis JS. 2015. Real-Time Imaging Reveals Local, Transient Vascular Permeability, and Tumor Cell Intravasation Stimulated by TIE2hi Macrophage–Derived VEGFA. *Cancer Discovery* **5**:932–943. doi:10.1158/2159-8290.CD-15-0012

Harper KL, Sosa MS, Entenberg D, Hosseini H, Cheung JF, Nobre R, Avivar-Valderas A, Nagi C, Girnius N, Davis RJ, Farias EF, Condeelis J, Klein CA, Aguirre-Ghiso JA. 2016. Mechanism of early dissemination and metastasis in Her2+ mammary cancer. *Nature* **540**:588–592. doi:10.1038/nature20609

Hashida Y, Tanaka H, Zhou S, Kawakami S, Yamashita F, Murakami T, Umeyama T, Imahori H, Hashida M. 2014. Photothermal ablation of tumor cells using a single-walled carbon nanotube–peptide composite. *Journal of Controlled Release* **173**:59–66. doi:10.1016/j.jconrel.2013.10.039

Hashizume H, Baluk P, Morikawa S, McLean JW, Thurston G, Roberge S, Jain RK, McDonald DM. 2000. Openings between Defective Endothelial Cells Explain Tumor Vessel Leakiness. *The American Journal of Pathology* **156**:1363–1380. doi:10.1016/S0002-9440(10)65006-7

Hathcock KS, Laszlo G, Dickler HB, Bradshaw J, Linsley P, Hodes RJ. 1993. Identification of an Alternative CTLA-4 Ligand Costimulatory for T Cell Activation. *Science* **262**:905–907. doi:10.1126/science.7694361

Häuselmann I, Roblek M, Protsyuk D, Huck V, Knopfova L, Grässle S, Bauer AT, Schneider SW, Borsig L. 2016. Monocyte Induction of E-Selectin–Mediated Endothelial Activation Releases VE-Cadherin Junctions to Promote Tumor Cell Extravasation in the Metastasis Cascade. *Cancer Research* **76**:5302–5312. doi:10.1158/0008-5472.CAN-16-0784

He H, Liu L, Morin EE, Liu M, Schwendeman A. 2019. Survey of Clinical Translation of Cancer Nanomedicines—Lessons Learned from Successes and Failures. *Acc Chem Res* **52**:2445–2461. doi:10.1021/acs.accounts.9b00228

Headley MB, Bins A, Nip A, Roberts EW, Looney MR, Gerard A, Krummel MF. 2016. Visualization of immediate immune responses to pioneer metastatic cells in the lung. *Nature* **531**:513–517. doi:10.1038/nature16985

Heister E, Lamprecht C, Neves V, Tîlmaciu C, Datas L, Flahaut E, Soula B, Hinterdorfer P, Coley HM, Silva SRP, McFadden J. 2010. Higher Dispersion Efficacy of Functionalized Carbon Nanotubes in Chemical and Biological Environments. *ACS Nano* **4**:2615–2626. doi:10.1021/nn100069k

Heldin C-H, Rubin K, Pietras K, Östman A. 2004. High interstitial fluid pressure — an obstacle in cancer therapy. *Nat Rev Cancer* **4**:806–813. doi:10.1038/nrc1456

Heldin CH, Westermark B, Wasteson A. 1981. Platelet-derived growth factor. Isolation by a large-scale procedure and analysis of subunit composition. *Biochemical Journal* **193**:907–913. doi:10.1042/bj1930907

Hellström M, Phng L-K, Hofmann JJ, Wallgard E, Coultas L, Lindblom P, Alva J, Nilsson A-K, Karlsson L, Gaiano N, Yoon K, Rossant J, Iruela-Arispe ML, Kalén M, Gerhardt H, Betsholtz C. 2007. Dll4 signalling through Notch1 regulates formation of tip cells during angiogenesis. *Nature* **445**:776–780. doi:10.1038/nature05571

Herbst RS, Giaccone G, De Marinis F, Reinmuth N, Vergnenegre A, Barrios CH, Morise M, Felip E, Andric Z, Geater S, Özgüroğlu M, Zou W, Sandler A, Enquist I, Komatsubara K, Deng Y, Kuriki H, Wen X, McCleland M, Mocci S, Jassem J, Spigel DR. 2020. Atezolizumab for First-Line Treatment of PD-L1–Selected Patients with NSCLC. *N Engl J Med* **383**:1328–1339. doi:10.1056/NEJMoa1917346

Hidari KI-PJ, Weyrich AS, Zimmerman GA, McEver RP. 1997. Engagement of P-selectin Glycoprotein Ligand-1 Enhances Tyrosine Phosphorylation and Activates Mitogen-activated Protein Kinases in Human Neutrophils. *Journal of Biological Chemistry* **272**:28750–28756. doi:10.1074/jbc.272.45.28750

Hilf N, Singh-Jasuja H, Schwarzmaier P, Gouttefangeas C, Rammensee H-G, Schild H. 2002. Human platelets express heat shock protein receptors and regulate dendritic cell maturation. *Blood* **99**:3676–3682. doi:10.1182/blood.V99.10.3676

Hinterleitner C, Strähle J, Malenke E, Hinterleitner M, Henning M, Seehawer M, Bilich T, Heitmann J, Lutz M, Mattern S, Scheuermann S, Horger M, Maurer S, Walz J, Fend F, Handgretinger R, Seitz C, Weigelin B, Singer S, Salih H, Borst O, Kopp H-G, Zender L. 2021. Platelet PD-L1 reflects collective intratumoral PD-L1 expression and predicts immunotherapy response in non-small cell lung cancer. *Nat Commun* **12**:7005. doi:10.1038/s41467-021-27303-7

Hodi FS, O'Day SJ, McDermott DF, Weber RW, Sosman JA, Haanen JB, Gonzalez R, Robert C, Schadendorf D, Hassel JC, Akerley W, Van Den Eertwegh AJM, Lutzky J, Lorigan P, Vaubel JM, Linette GP, Hogg D, Ottensmeier CH, Lebbé C, Peschel C, Quirt I, Clark JI, Wolchok JD, Weber JS, Tian J, Yellin MJ, Nichol GM, Hoos A, Urba WJ. 2010. Improved Survival with Ipilimumab in Patients with Metastatic Melanoma. *N Engl J Med* **363**:711–723. doi:10.1056/NEJMoa1003466

Höfinger S, Melle-Franco M, Gallo T, Cantelli A, Calvaresi M, Gomes JANF, Zerbetto F. 2011. A computational analysis of the insertion of carbon nanotubes into cellular membranes. *Biomaterials* **32**:7079–7085. doi:10.1016/j.biomaterials.2011.06.011

Ho-Tin-Noé B, Carbo C, Demers M, Cifuni SM, Goerge T, Wagner DD. 2009. Innate Immune Cells Induce Hemorrhage in Tumors during Thrombocytopenia. *The American Journal of Pathology* **175**:1699–1708. doi:10.2353/ajpath.2009.090460

Ho-Tin-Noé B, Goerge T, Cifuni SM, Duerschmied D, Wagner DD. 2008. Platelet Granule Secretion Continuously Prevents Intratumor Hemorrhage. *Cancer Research* **68**:6851–6858. doi:10.1158/0008-5472.CAN-08-0718

Hu Q, Hisamatsu T, Haemmerle M, Cho MS, Pradeep S, Rupaimoole R, Rodriguez-Aguayo C, Lopez-Berestein G, Wong STC, Sood AK, Afshar-Kharghan V. 2017. Role of Platelet-Derived Tgfβ1 in the Progression of Ovarian Cancer. *Clinical Cancer Research* **23**:5611–5621. doi:10.1158/1078-0432.CCR-16-3272

Huang J, Jochems C, Talaie T, Anderson A, Jales A, Tsang KY, Madan RA, Gulley JL, Schlom J. 2012. Elevated serum soluble CD40 ligand in cancer patients may play an immunosuppressive role. *Blood* **120**:3030–3038. doi:10.1182/blood-2012-05-427799

Hui E, Cheung J, Zhu J, Su X, Taylor MJ, Wallweber HA, Sasmal DK, Huang J, Kim JM, Mellman I, Vale RD. 2017. T cell costimulatory receptor CD28 is a primary target for PD-1–mediated inhibition. *Science* **355**:1428–1433. doi:10.1126/science.aaf1292

Hui JZ, Tamsen S, Song Y, Tsourkas A. 2015. LASIC: Light Activated Site-Specific Conjugation of Native IgGs. *Bioconjugate Chem* **26**:1456–1460. doi:10.1021/acs.bioconjchem.5b00275

Hui JZ, Zaki AA, Cheng Z, Popik V, Zhang H, Luning Prak ET, Tsourkas A. 2014. Facile Method for the Site-Specific, Covalent Attachment of Full-Length IgG onto Nanoparticles. *Small* **10**:3354–3363. doi:10.1002/smll.201303629

Hurwitz E, Levy R, Maron R, Wilchek M, Arnon R, Sela M. 1975. The covalent binding of daunomycin and adriamycin to antibodies, with retention of both drug and antibody activities. *Cancer Res* **35**:1175–1181.

I

Iijima S. 1991. Helical microtubules of graphitic carbon. *Nature* **354**:56–58. doi:10.1038/354056a0

Iijima S, Ichihashi T. 1993. Single-shell carbon nanotubes of 1-nm diameter. *Nature* **363**:603–605. doi:10.1038/363603a0

Ikeda M, Furukawa H, Imamura H, Shimizu J, Ishida H, Masutani S, Tatsuta M, Satomi T. 2002. Poor prognosis associated with thrombocytosis in patients with gastric cancer. *Annals of Surgical Oncology* **9**:287–291. doi:10.1007/BF02573067

Im JH, Fu W, Wang H, Bhatia SK, Hammer DA, Kowalska MA, Muschel RJ. 2004. Coagulation Facilitates Tumor Cell Spreading in the Pulmonary Vasculature during Early Metastatic Colony Formation. *Cancer Research* **64**:8613–8619. doi:10.1158/0008-5472.CAN-04-2078

Imai K, Matsuyama S, Miyake S, Suga K, Nakachi K. 2000. Natural cytotoxic activity of peripheral-blood lymphocytes and cancer incidence: an 11-year follow-up study of a general population. *The Lancet* **356**:1795–1799. doi:10.1016/S0140-6736(00)03231-1

Inaba K, Turley S, Iyoda T, Yamaide F, Shimoyama S, E Sousa CR, Germain RN, Mellman I, Steinman RM. 2000. The Formation of Immunogenic Major Histocompatibility Complex Class II–Peptide Ligands in Lysosomal Compartments of Dendritic Cells Is Regulated by Inflammatory Stimuli. *The Journal of Experimental Medicine* **191**:927–936. doi:10.1084/jem.191.6.927

Irmler M, Thome M, Hahne M, Schneider P, Hofmann K, Steiner V, Bodmer J-L, Schröter M, Burns K, Mattmann C, Rimoldi D, French LE, Tschopp J. 1997. Inhibition of death receptor signals by cellular FLIP. *Nature* **388**:190–195. doi:10.1038/40657

Ishida T, Masuda K, Ichikawa T, Ichihara M, Irimura K, Kiwada H. 2003. Accelerated clearance of a second injection of PEGylated liposomes in mice. *International Journal of Pharmaceutics* **255**:167–174. doi:10.1016/S0378-5173(03)00085-1

Ishigami S, Natsugoe S, Tokuda K, Nakajo A, Che X, Iwashige H, Aridome K, Hokita S, Aikou T. 2000. Prognostic value of intratumoral natural killer cells in gastric carcinoma. *Cancer* **88**:577–583.

Italiano JE, Lecine P, Shivdasani RA, Hartwig JH. 1999. Blood Platelets Are Assembled Principally at the Ends of Proplatelet Processes Produced by Differentiated Megakaryocytes. *The Journal of Cell Biology* **147**:1299–1312. doi:10.1083/jcb.147.6.1299

Italiano JE, Richardson JL, Patel-Hett S, Battinelli E, Zaslavsky A, Short S, Ryeom S, Folkman J, Klement GL. 2008. Angiogenesis is regulated by a novel mechanism: pro- and antiangiogenic proteins are organized into separate platelet α granules and differentially released. *Blood* **111**:1227–1233. doi:10.1182/blood-2007-09-113837

J

Jain S, Russell S, Ware J. 2009. Platelet glycoprotein VI facilitates experimental lung metastasis in syngenic mouse models. *Journal of Thrombosis and Haemostasis* **7**:1713–1717. doi:10.1111/j.1538-7836.2009.03559.x

Jain S, Zuka M, Liu J, Russell S, Dent J, Guerrero JA, Forsyth J, Maruszak B, Gartner TK, Felding-Habermann B, Ware J. 2007. Platelet glycoprotein Ibα supports experimental lung metastasis. *Proc Natl Acad Sci USA* **104**:9024–9028. doi:10.1073/pnas.0700625104

Jeelani PG, Mulay P, Venkat R, Ramalingam C. 2020. Multifaceted Application of Silica Nanoparticles. A Review. *Silicon* **12**:1337–1354. doi:10.1007/s12633-019-00229-y

Jiang L, Luan Y, Miao X, Sun C, Li K, Huang Z, Xu D, Zhang M, Kong F, Li N. 2017. Platelet releasate promotes breast cancer growth and angiogenesis via VEGF–integrin cooperative signalling. *Br J Cancer* **117**:695–703. doi:10.1038/bjc.2017.214

Jin DK, Shido K, Kopp H-G, Petit I, Shmelkov SV, Young LM, Hooper AT, Amano H, Avecilla ST, Heissig B, Hattori K, Zhang F, Hicklin DJ, Wu Y, Zhu Z, Dunn A, Salari H, Werb Z, Hackett NR, Crystal RG, Lyden D, Rafii S. 2006. Cytokine-mediated deployment of SDF-1 induces revascularization through recruitment of CXCR4+ hemangiocytes. *Nat Med* **12**:557–567. doi:10.1038/nm1400

Johnson DB, Balko JM, Compton ML, Chalkias S, Gorham J, Xu Y, Hicks M, Puzanov I, Alexander MR, Bloomer TL, Becker JR, Slosky DA, Phillips EJ, Pilkinton MA, Craig-Owens L, Kola N, Plautz G, Reshef DS, Deutsch JS, Deering RP, Olenchock BA, Lichtman AH, Roden DM, Seidman CE, Koralnik IJ, Seidman JG, Hoffman RD, Taube JM, Diaz LA, Anders RA, Sosman JA, Moslehi JJ. 2016. Fulminant Myocarditis with Combination Immune Checkpoint Blockade. *N Engl J Med* **375**:1749–1755. doi:10.1056/NEJMoa1609214

Johnston MC, Scott CJ. 2018. Antibody conjugated nanoparticles as a novel form of antibody drug conjugate chemotherapy. *Drug Discovery Today: Technologies* **30**:63–69. doi:10.1016/j.ddtec.2018.10.003

Jurasz P, Sawicki G, Duszyk M, Sawicka J, Miranda C, Mayers I, Radomski MW. 2001. Matrix metalloproteinase 2 in tumor cell-induced platelet aggregation: regulation by nitric oxide. *Cancer Res* **61**:376–382.

Juweid M, Neumann R, Paik C, Perez-Bacete MJ, Sato J, van Osdol W, Weinstein JN. 1992. Micropharmacology of monoclonal antibodies in solid tumors: direct experimental evidence for a binding site barrier. *Cancer Res* **52**:5144–5153.

K

Kahner BN, Shankar H, Murugappan S, Prasad GL, Kunapuli SP. 2006. Nucleotide receptor signaling in platelets. *Journal of Thrombosis and Haemostasis* **4**:2317–2326. doi:10.1111/j.1538-7836.2006.02192.x

Kaiser BK, Yim D, Chow I-T, Gonzalez S, Dai Z, Mann HH, Strong RK, Groh V, Spies T. 2007. Disulphide-isomerase-enabled shedding of tumour-associated NKG2D ligands. *Nature* **447**:482–486. doi:10.1038/nature05768

Kaizuka Y, Douglass AD, Varma R, Dustin ML, Vale RD. 2007. Mechanisms for segregating T cell receptor and adhesion molecules during immunological synapse formation in Jurkat T cells. *Proc Natl Acad Sci USA* **104**:20296–20301. doi:10.1073/pnas.0710258105

Kalagara T, Moutsis T, Yang Y, Pappelbaum KI, Farken A, Cladder-Micus L, Vidal-y-Sy S, John A, Bauer AT, Moerschbacher BM, Schneider SW, Gorzelanny C. 2018. The endothelial glycocalyx anchors von Willebrand factor fibers to the vascular endothelium. *Blood Advances* **2**:2347–2357. doi:10.1182/bloodadvances.2017013995

Kalluri R, Weinberg RA. 2009. The basics of epithelial-mesenchymal transition. *J Clin Invest* **119**:1420–1428. doi:10.1172/JCI39104

Kaplan RN, Riba RD, Zacharoulis S, Bramley AH, Vincent L, Costa C, MacDonald DD, Jin DK, Shido K, Kerns SA, Zhu Z, Hicklin D, Wu Y, Port JL, Altorki N, Port ER, Ruggero D, Shmelkov SV, Jensen KK, Rafii S, Lyden D. 2005. VEGFR1-positive haematopoietic bone marrow progenitors initiate the pre-metastatic niche. *Nature* **438**:820–827. doi:10.1038/nature04186

Karnati KR, Wang Y. 2018. Understanding the co-loading and releasing of doxorubicin and paclitaxel using chitosan functionalized single-walled carbon nanotubes by molecular dynamics simulations. *Phys Chem Chem Phys* **20**:9389–9400. doi:10.1039/C8CP00124C

Karreman MA, Bauer AT, Solecki G, Berghoff AS, Mayer CD, Frey K, Hebach N, Feinauer MJ, Schieber NL, Tehranian C, Mercier L, Singhal M, Venkataramani V, Schubert MC, Hinze D, Hölzel M, Helfrich I, Schadendorf D, Schneider SW, Westphal D, Augustin HG, Goetz JG, Schwab Y, Wick W, Winkler F. 2023. Active Remodeling of Capillary Endothelium via Cancer Cell–Derived MMP9 Promotes Metastatic Brain Colonization. *Cancer Research* **83**:1299–1314. doi:10.1158/0008-5472.CAN-22-3964

Kaser A, Brandacher G, Steurer W, Kaser S, Offner FA, Zoller H, Theurl I, Widder W, Molnar C, Ludwiczek O, Atkins MB, Mier JW, Tilg H. 2001. Interleukin-6 stimulates thrombopoiesis through thrombopoietin: role in inflammatory thrombocytosis. *Blood* **98**:2720–2725. doi:10.1182/blood.V98.9.2720

Kaushansky K. 1995. Thrombopoietin: the primary regulator of platelet production [see comments]. *Blood* **86**:419–431. doi:10.1182/blood.V86.2.419.bloodjournal862419
Keating SE, Zaiatz-Bittencourt V, Loftus RM, Keane C, Brennan K, Finlay DK, Gardiner CM. 2016. Metabolic Reprogramming Supports IFN-γ Production by CD56bright NK Cells. *The Journal of Immunology* **196**:2552–2560. doi:10.4049/jimmunol.1501783

Keefe D, Shi L, Feske S, Massol R, Navarro F, Kirchhausen T, Lieberman J. 2005. Perforin Triggers a Plasma Membrane-Repair Response that Facilitates CTL Induction of Apoptosis. *Immunity* **23**:249–262. doi:10.1016/j.immuni.2005.08.001

Kerr BA, McCabe NP, Feng W, Byzova TV. 2013. Platelets govern pre-metastatic tumor communication to bone. *Oncogene* **32**:4319–4324. doi:10.1038/onc.2012.447

Kiessling R, Klein E, Wigzell H. 1975. „Natural" killer cells in the mouse. I. Cytotoxic cells with specificity for mouse Moloney leukemia cells. Specificity and distribution according to genotype. *Eur J Immunol* **5**:112–117. doi:10.1002/eji.1830050208

Kim M, Jeong M, Hur S, Cho Y, Park J, Jung H, Seo Y, Woo HA, Nam KT, Lee K, Lee H. 2021. Engineered ionizable lipid nanoparticles for targeted delivery of RNA therapeutics into different types of cells in the liver. *Sci Adv* **7**:eabf4398. doi:10.1126/sciadv.abf4398

Kim MT, Chen Y, Marhoul J, Jacobson F. 2014. Statistical Modeling of the Drug Load Distribution on Trastuzumab Emtansine (Kadcyla), a Lysine-Linked Antibody Drug Conjugate. *Bioconjugate Chem* **25**:1223–1232. doi:10.1021/bc5000109

Kim S, Poursine-Laurent J, Truscott SM, Lybarger L, Song Y-J, Yang L, French AR, Sunwoo JB, Lemieux S, Hansen TH, Yokoyama WM. 2005. Licensing of natural killer cells by host major histocompatibility complex class I molecules. *Nature* **436**:709–713. doi:10.1038/nature03847

Kim YJ, Borsig L, Varki NM, Varki A. 1998. P-selectin deficiency attenuates tumor growth and metastasis. *Proc Natl Acad Sci USA* **95**:9325–9330. doi:10.1073/pnas.95.16.9325

Kinzler KW, Nilbert MC, Su LK, Vogelstein B, Bryan TM, Levy DB, Smith KJ, Preisinger AC, Hedge P, McKechnie D. 1991. Identification of FAP locus genes from chromosome 5q21. *Science* **253**:661–665. doi:10.1126/science.1651562

Kinzler KW, Vogelstein B. 1996. Lessons from Hereditary Colorectal Cancer. *Cell* **87**:159–170. doi:10.1016/S0092-8674(00)81333-1

Kischkel FC, Hellbardt S, Behrmann I, Germer M, Pawlita M, Krammer PH, Peter ME. 1995. Cytotoxicity-dependent APO-1 (Fas/CD95)-associated proteins form a death-inducing signaling complex (DISC) with the receptor. *The EMBO Journal* **14**:5579–5588. doi:10.1002/j.1460-2075.1995.tb00245.x

Kissel K, Berber S, Nockher A, Santoso S, Bein G, Hackstein H. 2006. Human platelets target dendritic cell differentiation and production of proinflammatory cytokines. *Transfusion* **46**:818–827. doi:10.1111/j.1537-2995.2006.00802.x

Kisucka J, Butterfield CE, Duda DG, Eichenberger SC, Saffaripour S, Ware J, Ruggeri ZM, Jain RK, Folkman J, Wagner DD. 2006. Platelets and platelet adhesion support angiogenesis while preventing excessive hemorrhage. *Proc Natl Acad Sci USA* **103**:855–860. doi:10.1073/pnas.0510412103

Klemm F, Maas RR, Bowman RL, Kornete M, Soukup K, Nassiri S, Brouland J-P, Iacobuzio-Donahue CA, Brennan C, Tabar V, Gutin PH, Daniel RT, Hegi ME, Joyce JA. 2020. Interrogation of the Microenvironmental Landscape in Brain Tumors Reveals Disease-Specific Alterations of Immune Cells. *Cell* **181**:1643-1660.e17. doi:10.1016/j.cell.2020.05.007

Kopp H-G, Placke T, Salih HR. 2009. Platelet-Derived Transforming Growth Factor-β Down-Regulates NKG2D Thereby Inhibiting Natural Killer Cell Antitumor Reactivity. *Cancer Research* **69**:7775–7783. doi:10.1158/0008-5472.CAN-09-2123

Korsmeyer SJ. 1992. Chromosomal Translocations in Lymphoid Malignancies Reveal Novel Proto-Oncogenes. *Annu Rev Immunol* **10**:785–807. doi:10.1146/annurev.iy.10.040192.004033

Kostarelos K. 2008. The long and short of carbon nanotube toxicity. *Nat Biotechnol* **26**:774–776. doi:10.1038/nbt0708-774

Kowanetz M, Wu X, Lee J, Tan M, Hagenbeek T, Qu X, Yu L, Ross J, Korsisaari N, Cao T, Bou-Reslan H, Kallop D, Weimer R, Ludlam MJC, Kaminker JS, Modrusan Z, Van Bruggen N, Peale FV, Carano R, Meng YG, Ferrara N. 2010. Granulocyte-colony stimulating factor promotes lung metastasis through mobilization of Ly6G+Ly6C+ granulocytes. *Proc Natl Acad Sci USA* **107**:21248–21255. doi:10.1073/pnas.1015855107

Kramer RM, Shende VR, Motl N, Pace CN, Scholtz JM. 2012. Toward a Molecular Understanding of Protein Solubility: Increased Negative Surface Charge Correlates with Increased Solubility. *Biophysical Journal* **102**:1907–1915. doi:10.1016/j.bpj.2012.01.060

Kroto HW, Heath JR, O'Brien SC, Curl RF, Smalley RE. 1985. C60: Buckminsterfullerene. *Nature* **318**:162–163. doi:10.1038/318162a0

Krump NA, You J. 2018. Molecular mechanisms of viral oncogenesis in humans. *Nat Rev Microbiol* **16**:684–698. doi:10.1038/s41579-018-0064-6

Kuncic Z, Lacombe S. 2018. Nanoparticle radio-enhancement: principles, progress and application to cancer treatment. *Phys Med Biol* **63**:02TR01. doi:10.1088/1361-6560/aa99ce

Kuznetsov HS, Marsh T, Markens BA, Castaño Z, Greene-Colozzi A, Hay SA, Brown VE, Richardson AL, Signoretti S, Battinelli EM, McAllister SS. 2012. Identification of Luminal Breast Cancers That Establish a Tumor-Supportive Macroenvironment Defined by Proangiogenic Platelets and Bone Marrow–Derived Cells. *Cancer Discovery* **2**:1150–1165. doi:10.1158/2159-8290.CD-12-0216

L

Labelle M, Begum S, Hynes RO. 2014. Platelets guide the formation of early metastatic niches. *Proc Natl Acad Sci USA* **111**. doi:10.1073/pnas.1411082111

Labelle M, Begum S, Hynes RO. 2011. Direct Signaling between Platelets and Cancer Cells Induces an Epithelial-Mesenchymal-Like Transition and Promotes Metastasis. *Cancer Cell* **20**:576–590. doi:10.1016/j.ccr.2011.09.009

Lacerda L, Russier J, Pastorin G, Herrero MA, Venturelli E, Dumortier H, Al-Jamal KT, Prato M, Kostarelos K, Bianco A. 2012. Translocation mechanisms of chemically functionalised carbon nanotubes across plasma membranes. *Biomaterials* **33**:3334–3343. doi:10.1016/j.biomaterials.2012.01.024

Lainé A-L, Gravier J, Henry M, Sancey L, Béjaud J, Pancani E, Wiber M, Texier I, Coll J-L, Benoit J-P, Passirani C. 2014. Conventional versus stealth lipid nanoparticles: Formulation and in vivo fate prediction through FRET monitoring. *Journal of Controlled Release* **188**:1–8. doi:10.1016/j.jconrel.2014.05.042

Lane RS, Femel J, Breazeale AP, Loo CP, Thibault G, Kaempf A, Mori M, Tsujikawa T, Chang YH, Lund AW. 2018. IFNγ-activated dermal lymphatic vessels inhibit cytotoxic T cells in melanoma and inflamed skin. *Journal of Experimental Medicine* **215**:3057–3074. doi:10.1084/jem.20180654

Lanzavecchia A. 1998. Licence to kill. *Nature* **393**:413–414. doi:10.1038/30845

Läubli H, Spanaus K-S, Borsig L. 2009. Selectin-mediated activation of endothelial cells induces expression of CCL5 and promotes metastasis through recruitment of monocytes. *Blood* **114**:4583–4591. doi:10.1182/blood-2008-10-186585

Lavie D, Ben-Shmuel A, Erez N, Scherz-Shouval R. 2022. Cancer-associated fibroblasts in the single-cell era. *Nat Cancer* **3**:793–807. doi:10.1038/s43018-022-00411-z

Law RHP, Lukoyanova N, Voskoboinik I, Caradoc-Davies TT, Baran K, Dunstone MA, D'Angelo ME, Orlova EV, Coulibaly F, Verschoor S, Browne KA, Ciccone A, Kuiper MJ, Bird PI, Trapani JA, Saibil HR, Whisstock JC. 2010. The structural basis for membrane binding and pore formation by lymphocyte perforin. *Nature* **468**:447–451. doi:10.1038/nature09518

Lazetic S, Chang C, Houchins JP, Lanier LL, Phillips JH. 1996. Human natural killer cell receptors involved in MHC class I recognition are disulfide-linked heterodimers of CD94 and NKG2 subunits. *J Immunol* **157**:4741–4745.

Le Chapelain O, Jadoui S, Gros A, Barbaria S, Benmeziane K, Ollivier V, Dupont S, Solo Nomenjanahary M, Mavouna S, Rogozarski J, Mawhin M-A, Caligiuri G, Delbosc S, Porteu F, Nieswandt B, Mangin PH, Boulaftali Y, Ho-Tin-Noé B. 2024. The localization, origin, and impact of platelets in the tumor microenvironment are tumor type-dependent. *J Exp Clin Cancer Res* **43**:84. doi:10.1186/s13046-024-03001-2

Le Dréan E, Vély F, Olcese L, Cambiaggi A, Guia S, Krystal G, Gervois N, Moretta A, Jotereau F, Vivier E. 1998. Inhibition of antigen-induced T cell response and antibody-induced NK cell cytotoxicity by NKG2A: association of NKG2A with SHP-1 and SHP-2 protein-tyrosine phosphatases. *Eur J Immunol* **28**:264–276. doi:10.1002/(SICI)1521-4141(199801)28:01<264::AID-IMMU264>3.0.CO;2-O

Le Duc G, Miladi I, Alric C, Mowat P, Bräuer-Krisch E, Bouchet A, Khalil E, Billotey C, Janier M, Lux F, Epicier T, Perriat P, Roux S, Tillement O. 2011. Toward an Image-Guided Microbeam Radiation Therapy Using Gadolinium-Based Nanoparticles. *ACS Nano* **5**:9566–9574. doi:10.1021/nn202797h

Le Floc'h A, Tanaka Y, Bantilan NS, Voisinne G, Altan-Bonnet G, Fukui Y, Huse M. 2013. Annular PIP3 accumulation controls actin architecture and modulates cytotoxicity at the immunological synapse. *Journal of Experimental Medicine* **210**:2721–2737. doi:10.1084/jem.20131324

Leavell MD, Novak P, Behrens CR, Schoeniger JS, Kruppa GH. 2004. Strategy for selective chemical cross-linking of tyrosine and lysine residues. *J Am Soc Mass Spectrom* **15**:1604–1611. doi:10.1016/j.jasms.2004.07.018

Lebozec K, Jandrot-Perrus M, Avenard G, Favre-Bulle O, Billiald P. 2017. Design, development and characterization of ACT017, a humanized Fab that blocks platelet's glycoprotein VI function without causing bleeding risks. *mAbs* **9**:945–958. doi:10.1080/19420862.2017.1336592

Lee CZW, Ginhoux F. 2022. Biology of resident tissue macrophages. *Development* **149**:dev200270. doi:10.1242/dev.200270

Lee J-C, Lee K-M, Kim D-W, Heo DS. 2004. Elevated TGF-β1 Secretion and Down-Modulation of NKG2D Underlies Impaired NK Cytotoxicity in Cancer Patients. *The Journal of Immunology* **172**:7335–7340. doi:10.4049/jimmunol.172.12.7335

Lefrançais E, Ortiz-Muñoz G, Caudrillier A, Mallavia B, Liu F, Sayah DM, Thornton EE, Headley MB, David T, Coughlin SR, Krummel MF, Leavitt AD, Passegué E, Looney MR. 2017. The lung is a site of platelet biogenesis and a reservoir for haematopoietic progenitors. *Nature* **544**:105–109. doi:10.1038/nature21706

Lengauer C, Kinzler KW, Vogelstein B. 1998. Genetic instabilities in human cancers. *Nature* **396**:643–649. doi:10.1038/25292

Leu AJ, Berk DA, Lymboussaki A, Alitalo K, Jain RK. 2000. Absence of functional lymphatics within a murine sarcoma: a molecular and functional evaluation. *Cancer Res* **60**:4324–4327.

Levental KR, Yu H, Kass L, Lakins JN, Egeblad M, Erler JT, Fong SFT, Csiszar K, Giaccia A, Weninger W, Yamauchi M, Gasser DL, Weaver VM. 2009. Matrix Crosslinking Forces Tumor Progression by Enhancing Integrin Signaling. *Cell* **139**:891–906. doi:10.1016/j.cell.2009.10.027

Levin J. 1964. Thrombocytosis Associated With Malignant Disease. *Arch Intern Med* **114**:497. doi:10.1001/archinte.1964.03860100079008

Li J, Yap SQ, Chin CF, Tian Q, Yoong SL, Pastorin G, Ang WH. 2012. Platinum(iv) prodrugs entrapped within multiwalled carbon nanotubes: Selective release by chemical reduction and hydrophobicity reversal. *Chem Sci* **3**:2083. doi:10.1039/c2sc01086k

Li R, Ren M, Chen N, Luo M, Deng X, Xia J, Yu G, Liu J, He B, Zhang Xu, Zhang Z, Zhang Xiao, Ran B, Wu J. 2014. Presence of intratumoral platelets is associated with tumor vessel structure and metastasis. *BMC Cancer* **14**:167. doi:10.1186/1471-2407-14-167

Li X, Gruosso T, Zuo D, Omeroglu A, Meterissian S, Guiot M-C, Salazar A, Park M, Levine H. 2019. Infiltration of CD8 $^{+}$ T cells into tumor cell clusters in triple-negative breast cancer. *Proc Natl Acad Sci USA* **116**:3678–3687. doi:10.1073/pnas.1817652116

Lickert S, Kenny M, Selcuk K, Mehl JL, Bender M, Früh SM, Burkhardt MA, Studt J-D, Nieswandt B, Schoen I, Vogel V. 2022. Platelets drive fibronectin fibrillogenesis using integrin αIIbβ3. *Sci Adv* **8**:eabj8331. doi:10.1126/sciadv.abj8331

Lim L, Bui H, Farrelly O, Yang J, Li L, Enis D, Ma W, Chen M, Oliver G, Welsh JD, Kahn ML. 2019. Hemostasis stimulates lymphangiogenesis through release and activation of VEGFC. *Blood* **134**:1764–1775. doi:10.1182/blood.2019001736

Linsley PS, Greene JL, Brady W, Bajorath J, Ledbetter JA, Peach R. 1994. Human B7-1 (CD80) and B7-2 (CD86) bind with similar avidities but distinct kinetics to CD28 and CTLA-4 receptors. *Immunity* **1**:793–801. doi:10.1016/S1074-7613(94)80021-9

Liu F, Niko Y, Bouchaala R, Mercier L, Lefebvre O, Andreiuk B, Vandamme T, Goetz JG, Anton N, Klymchenko A. 2021. Drug-Sponge Lipid Nanocarrier for in Situ Cargo Loading and Release Using Dynamic Covalent Chemistry. *Angew Chem Int Ed* **60**:6573–6580. doi:10.1002/anie.202014259

Liu H, May K. 2012. Disulfide bond structures of IgG molecules: Structural variations, chemical modifications and possible impacts to stability and biological function. *mAbs* **4**:17–23. doi:10.4161/mabs.4.1.18347

Liu Xiaowei, Song J, Zhang Hao, Liu Xinyu, Zuo F, Zhao Yunuo, Zhao Yujie, Yin X, Guo X, Wu X, Zhang Hu, Xu J, Hu J, Jing J, Ma X, Shi H. 2023. Immune checkpoint HLA-E:CD94-NKG2A mediates evasion of circulating tumor cells from NK cell surveillance. *Cancer Cell* **41**:272-287.e9. doi:10.1016/j.ccell.2023.01.001

Liu Y, Jiang P, Capkova K, Xue D, Ye L, Sinha SC, Mackman N, Janda KD, Liu C. 2011. Tissue Factor–Activated Coagulation Cascade in the Tumor Microenvironment Is Critical for Tumor Progression and an Effective Target for Therapy. *Cancer Research* **71**:6492–6502. doi:10.1158/0008-5472.CAN-11-1145

Liu Y, Van Ginderachter JA, Brys L, De Baetselier P, Raes G, Geldhof AB. 2003. Nitric Oxide-Independent CTL Suppression during Tumor Progression: Association with Arginase-Producing (M2) Myeloid Cells. *The Journal of Immunology* **170**:5064–5074. doi:10.4049/jimmunol.170.10.5064

Loeb LA. 1991. Mutator phenotype may be required for multistage carcinogenesis. *Cancer Res* **51**:3075–3079.

Lonsdorf AS, Krämer BF, Fahrleitner M, Schönberger T, Gnerlich S, Ring S, Gehring S, Schneider SW, Kruhlak MJ, Meuth SG, Nieswandt B, Gawaz M, Enk AH, Langer HF. 2012. Engagement of αIIbβ3 (GPIIb/IIIa) with αvβ3 Integrin Mediates Interaction of Melanoma Cells with Platelets. *Journal of Biological Chemistry* **287**:2168–2178. doi:10.1074/jbc.M111.269811

Lu P, Weaver VM, Werb Z. 2012. The extracellular matrix: A dynamic niche in cancer progression. *Journal of Cell Biology* **196**:395–406. doi:10.1083/jcb.201102147

Lucotti S, Cerutti C, Soyer M, Gil-Bernabé AM, Gomes AL, Allen PD, Smart S, Markelc B, Watson K, Armstrong PC, Mitchell JA, Warner TD, Ridley AJ, Muschel RJ. 2019. Aspirin blocks formation of metastatic intravascular niches by inhibiting platelet-derived COX-1/thromboxane A2. *Journal of Clinical Investigation* **129**:1845–1862. doi:10.1172/JCI121985

Lutz MS, Klimovich B, Maurer S, Heitmann JS, Märklin M, Zekri L, Jung G, Salih HR, Hinterleitner C. 2022. Platelets subvert antitumor efficacy of T cell-recruiting bispecific antibodies. *J Immunother Cancer* **10**:e003655. doi:10.1136/jitc-2021-003655

Lux F, Mignot A, Mowat P, Louis C, Dufort S, Bernhard C, Denat F, Boschetti F, Brunet C, Antoine R, Dugourd P, Laurent S, Elst LV, Muller R, Sancey L, Josserand V, Coll J, Stupar V, Barbier E, Rémy C, Broisat A, Ghezzi C, Le Duc G, Roux S, Perriat P, Tillement O. 2011. Ultrasmall Rigid Particles as Multimodal Probes for Medical Applications. *Angew Chem Int Ed* **50**:12299–12303. doi:10.1002/anie.201104104

Luzzi KJ, MacDonald IC, Schmidt EE, Kerkvliet N, Morris VL, Chambers AF, Groom AC. 1998. Multistep Nature of Metastatic Inefficiency. *The American Journal of Pathology* **153**:865–873. doi:10.1016/S0002-9440(10)65628-3

Lyon RP, Setter JR, Bovee TD, Doronina SO, Hunter JH, Anderson ME, Balasubramanian CL, Duniho SM, Leiske CI, Li F, Senter PD. 2014. Self-hydrolyzing maleimides improve the stability and pharmacological properties of antibody-drug conjugates. *Nat Biotechnol* **32**:1059–1062. doi:10.1038/nbt.2968

M

Ma C, Fu Q, Diggs LP, McVey JC, McCallen J, Wabitsch S, Ruf B, Brown Z, Heinrich B, Zhang Q, Rosato U, Wang S, Cui L, Berzofsky JA, Kleiner DE, Bosco DB, Wu L-J, Lai CW, Rotman Y, Xie C, Korangy F, Greten TF. 2022. Platelets control liver tumor growth through P2Y12-dependent CD40L release in NAFLD. *Cancer Cell* **40**:986-998.e5. doi:10.1016/j.ccell.2022.08.004

Ma L, Perini R, McKnight W, Dicay M, Klein A, Hollenberg MD, Wallace JL. 2005. Proteinase-activated receptors 1 and 4 counter-regulate endostatin and VEGF release from human platelets. *Proc Natl Acad Sci USA* **102**:216–220. doi:10.1073/pnas.0406682102

Macatonia SE, Hosken NA, Litton M, Vieira P, Hsieh CS, Culpepper JA, Wysocka M, Trinchieri G, Murphy KM, O'Garra A. 1995. Dendritic cells produce IL-12 and direct the development of Th1 cells from naive CD4+ T cells. *J Immunol* **154**:5071–5079.

Bibliography

Machlus KR, Johnson KE, Kulenthirarajan R, Forward JA, Tippy MD, Soussou TS, El-Husayni SH, Wu SK, Wang S, Watnick RS, Italiano JE, Battinelli EM. 2016. CCL5 derived from platelets increases megakaryocyte proplatelet formation. *Blood* **127**:921–926. doi:10.1182/blood-2015-05-644583

Mädler S, Bich C, Touboul D, Zenobi R. 2009. Chemical cross-linking with NHS esters: a systematic study on amino acid reactivities. *J Mass Spectrom* **44**:694–706. doi:10.1002/jms.1544

Mammadova-Bach E, Gil-Pulido J, Sarukhanyan E, Burkard P, Shityakov S, Schonhart C, Stegner D, Remer K, Nurden P, Nurden AT, Dandekar T, Nehez L, Dank M, Braun A, Mezzano D, Abrams SI, Nieswandt B. 2020. Platelet glycoprotein VI promotes metastasis through interaction with cancer cell-derived Galectin-3. *Blood* blood.2019002649. doi:10.1182/blood.2019002649

Mammadova-Bach E, Zigrino P, Brucker C, Bourdon C, Freund M, De Arcangelis A, Abrams SI, Orend G, Gachet C, Mangin PH. 2016. Platelet integrin α6β1 controls lung metastasis through direct binding to cancer cell–derived ADAM9. *JCI Insight* **1**. doi:10.1172/jci.insight.88245

Manegold PC, Hutter J, Pahernik SA, Messmer K, Dellian M. 2003. Platelet-endothelial interaction in tumor angiogenesis and microcirculation. *Blood* **101**:1970–1976. doi:10.1182/blood.V101.5.1970

Manetti R, Parronchi P, Giudizi MG, Piccinni MP, Maggi E, Trinchieri G, Romagnani S. 1993. Natural killer cell stimulatory factor (interleukin 12 [IL-12]) induces T helper type 1 (Th1)-specific immune responses and inhibits the development of IL-4-producing Th cells. *The Journal of experimental medicine* **177**:1199–1204. doi:10.1084/jem.177.4.1199

Mantovani A, Marchesi F, Malesci A, Laghi L, Allavena P. 2017. Tumour-associated macrophages as treatment targets in oncology. *Nat Rev Clin Oncol* **14**:399–416. doi:10.1038/nrclinonc.2016.217

Martinet L, Ferrari De Andrade L, Guillerey C, Lee JS, Liu J, Souza-Fonseca-Guimaraes F, Hutchinson DS, Kolesnik TB, Nicholson SE, Huntington ND, Smyth MJ. 2015. DNAM-1 Expression Marks an Alternative Program of NK Cell Maturation. *Cell Reports* **11**:85–97. doi:10.1016/j.celrep.2015.03.006

Martínez-Jiménez F, Muiños F, Sentís I, Deu-Pons J, Reyes-Salazar I, Arnedo-Pac C, Mularoni L, Pich O, Bonet J, Kranas H, Gonzalez-Perez A, Lopez-Bigas N. 2020. A compendium of mutational cancer driver genes. *Nat Rev Cancer* **20**:555–572. doi:10.1038/s41568-020-0290-x

Martín-Granado V, Ortiz-Rivero S, Carmona R, Gutiérrez-Herrero S, Barrera M, San-Segundo L, Sequera C, Perdiguero P, Lozano F, Martín-Herrero F, González-Porras JR, Muñoz-Chápuli R, Porras A, Guerrero C. 2017. C3G promotes a selective release of angiogenic factors from activated mouse platelets to regulate angiogenesis and tumor metastasis. *Oncotarget* **8**:110994–111011. doi:10.18632/oncotarget.22339

Bibliography

Martins Castanheira N, Spanhofer AK, Wiener S, Bobe S, Schillers H. 2022. Uptake of platelets by cancer cells and recycling of the platelet protein CD42a. *Journal of Thrombosis and Haemostasis* **20**:170–181. doi:10.1111/jth.15543

Mascaux C, Angelova M, Vasaturo A, Beane J, Hijazi K, Anthoine G, Buttard B, Rothe F, Willard-Gallo K, Haller A, Ninane V, Burny A, Sculier J-P, Spira A, Galon J. 2019. Immune evasion before tumour invasion in early lung squamous carcinogenesis. *Nature* **571**:570–575. doi:10.1038/s41586-019-1330-0

Massagué J. 2008. TGFβ in Cancer. *Cell* **134**:215–230. doi:10.1016/j.cell.2008.07.001

Massberg S, Konrad I, Schürzinger K, Lorenz M, Schneider S, Zohlnhoefer D, Hoppe K, Schiemann M, Kennerknecht E, Sauer S, Schulz C, Kerstan S, Rudelius M, Seidl S, Sorge F, Langer H, Peluso M, Goyal P, Vestweber D, Emambokus NR, Busch DH, Frampton J, Gawaz M. 2006. Platelets secrete stromal cell–derived factor 1α and recruit bone marrow–derived progenitor cells to arterial thrombi in vivo. *The Journal of Experimental Medicine* **203**:1221–1233. doi:10.1084/jem.20051772

Mathieu C, Ghosh S, Draussin J, Gasser A, Jacquot G, Banerjee M, Gupta T, Schmutz M, Mirjolet C, Tillement O, Lux F, Klymchenko AS, Donzeau M, Pivot X, Harlepp S, Detappe A. 2024. Supramolecular Heterodimer Peptides Assembly for Nanoparticles Functionalization. *Adv Healthcare Materials* **13**:2304250. doi:10.1002/adhm.202304250

Matsumura Y, Maeda H. 1986. A new concept for macromolecular therapeutics in cancer chemotherapy: mechanism of tumoritropic accumulation of proteins and the antitumor agent smancs. *Cancer Res* **46**:6387–6392.

Matthews HK, Ganguli S, Plak K, Taubenberger AV, Win Z, Williamson M, Piel M, Guck J, Baum B. 2020. Oncogenic Signaling Alters Cell Shape and Mechanics to Facilitate Cell Division under Confinement. *Developmental Cell* **52**:563-573.e3. doi:10.1016/j.devcel.2020.01.004

Maurer S, Kropp KN, Klein G, Steinle A, Haen SP, Walz JS, Hinterleitner C, Märklin M, Kopp H-G, Salih HR. 2018. Platelet-mediated shedding of NKG2D ligands impairs NK cell immune-surveillance of tumor cells. *OncoImmunology* **7**:e1364827. doi:10.1080/2162402X.2017.1364827

Mazighi M, Köhrmann M, Lemmens R, Lyrer PA, Molina CA, Richard S, Toni D, Plétan Y, Sari A, Meilhoc A, Jandrot-Perrus M, Binay S, Avenard G, Comenducci A, Grouin J-M, Grotta JC, Albucher JF, Alonso A, Berrouschot J, Cordonnier C, De Raedt S, Desfontaines P, Doche E, Hemelsoet D, Macian-Montoro F, Masjuan J, Obadia M, Peeters A, Pelz J, Reiner P, Segura T, Serena J, Sibon I, Tembl JI, Vannier S, Zuber M. 2024. Safety and efficacy of platelet glycoprotein VI inhibition in acute ischaemic stroke (ACTIMIS): a randomised, double-blind, placebo-controlled, phase 1b/2a trial. *The Lancet Neurology* **23**:157–167. doi:10.1016/S1474-4422(23)00427-1

Mc Adam AJ, Schweitzer AN, Sharpe AH. 1998. The role of B7 co-stimulation in activation and differentiation ofCD4 $^{+}$ and CD8 $^{+}$ T cells. *Immunological Reviews* **165**:231–247. doi:10.1111/j.1600-065X.1998.tb01242.x

Bibliography

McCann FE, Vanherberghen B, Eleme K, Carlin LM, Newsam RJ, Goulding D, Davis DM. 2003. The Size of the Synaptic Cleft and Distinct Distributions of Filamentous Actin, Ezrin, CD43, and CD45 at Activating and Inhibitory Human NK Cell Immune Synapses. *The Journal of Immunology* **170**:2862–2870. doi:10.4049/jimmunol.170.6.2862

McCarron PA, Marouf WM, Quinn DJ, Fay F, Burden RE, Olwill SA, Scott CJ. 2008. Antibody Targeting of Camptothecin-Loaded PLGA Nanoparticles to Tumor Cells. *Bioconjugate Chem* **19**:1561–1569. doi:10.1021/bc800057g

McCarty OJ, Mousa SA, Bray PF, Konstantopoulos K. 2000. Immobilized platelets support human colon carcinoma cell tethering, rolling, and firm adhesion under dynamic flow conditions. *Blood* **96**:1789–1797.

McDevitt MR, Chattopadhyay D, Kappel BJ, Jaggi JS, Schiffman SR, Antczak C, Njardarson JT, Brentjens R, Scheinberg DA. 2007. Tumor Targeting with Antibody-Functionalized, Radiolabeled Carbon Nanotubes. *Journal of Nuclear Medicine* **48**:1180–1189. doi:10.2967/jnumed.106.039131

McEver RP, Beckstead JH, Moore KL, Marshall-Carlson L, Bainton DF. 1989. GMP-140, a platelet alpha-granule membrane protein, is also synthesized by vascular endothelial cells and is localized in Weibel-Palade bodies. *J Clin Invest* **84**:92–99. doi:10.1172/JCI114175

Medema JP, De Jong J, Peltenburg LTC, Verdegaal EME, Gorter A, Bres SA, Franken KLMC, Hahne M, Albar JP, Melief CJM, Offringa R. 2001. Blockade of the granzyme B/perforin pathway through overexpression of the serine protease inhibitor PI-9/SPI-6 constitutes a mechanism for immune escape by tumors. *Proc Natl Acad Sci USA* **98**:11515–11520. doi:10.1073/pnas.201398198

Medema JP, Toes REM, Scaffidi C, Zheng TS, Flavell RA, Melief CJM, Peter ME, Offringa R, Krammer PH. 1997. Cleavage of FLICE (caspase-8) by granzyme B during cytotoxic T lymphocyte-induced apoptosis. *Eur J Immunol* **27**:3492–3498. doi:10.1002/eji.1830271250

Messmer D, Yang H, Telusma G, Knoll F, Li J, Messmer B, Tracey KJ, Chiorazzi N. 2004. High Mobility Group Box Protein 1: An Endogenous Signal for Dendritic Cell Maturation and Th1 Polarization. *The Journal of Immunology* **173**:307–313. doi:10.4049/jimmunol.173.1.307

Metelli A, Wu BX, Riesenberg B, Guglietta S, Huck JD, Mills C, Li A, Rachidi S, Krieg C, Rubinstein MP, Gewirth DT, Sun S, Lilly MB, Wahlquist AH, Carbone DP, Yang Y, Liu B, Li Z. 2020. Thrombin contributes to cancer immune evasion via proteolysis of platelet-bound GARP to activate LTGF-β. *Sci Transl Med* **12**:eaay4860. doi:10.1126/scitranslmed.aay4860

Mezouar S, Darbousset R, Dignat-George F, Panicot-Dubois L, Dubois C. 2015. Inhibition of platelet activation prevents the P-selectin and integrin-dependent accumulation of cancer cell microparticles and reduces tumor growth and metastasis *in vivo*. *Int J Cancer* **136**:462–475. doi:10.1002/ijc.28997

Miao S, Lu M, Liu Y, Shu D, Zhu Y, Song W, Ma Y, Ma R, Zhang B, Fang C, Ming Z. 2020. Platelets are recruited to hepatocellular carcinoma tissues in a CX3CL1-CX3CR1 dependent manner and induce tumour cell apoptosis. *Molecular Oncology* **14**:2546–2559. doi:10.1002/1878-0261.12783

Miao S, Shu D, Zhu Y, Lu M, Zhang Q, Pei Y, He A-D, Ma R, Zhang B, Ming Z-Y. 2019. Cancer cell-derived immunoglobulin G activates platelets by binding to platelet FcγRIIa. *Cell Death Dis* **10**:87. doi:10.1038/s41419-019-1367-x

Michaloglou C, Vredeveld LCW, Soengas MS, Denoyelle C, Kuilman T, Van Der Horst CMAM, Majoor DM, Shay JW, Mooi WJ, Peeper DS. 2005. BRAFE600-associated senescence-like cell cycle arrest of human naevi. *Nature* **436**:720–724. doi:10.1038/nature03890

Mignot A, Truillet C, Lux F, Sancey L, Louis C, Denat F, Boschetti F, Bocher L, Gloter A, Stéphan O, Antoine R, Dugourd P, Luneau D, Novitchi G, Figueiredo LC, de Morais PC, Bonneviot L, Albela B, Ribot F, Van Lokeren L, Déchamps-Olivier I, Chuburu F, Lemercier G, Villiers C, Marche PN, Le Duc G, Roux S, Tillement O, Perriat P. 2013. A Top-Down Synthesis Route to Ultrasmall Multifunctional Gd-Based Silica Nanoparticles for Theranostic Applications. *Chemistry A European J* **19**:6122–6136. doi:10.1002/chem.201203003

Mitrugno A, Williams D, Kerrigan SW, Moran N. 2014. A novel and essential role for FcγRIIa in cancer cell–induced platelet activation. *Blood* **123**:249–260. doi:10.1182/blood-2013-03-492447

Mittelheisser V, Banerjee M, Pivot X, Charbonnière LJ, Goetz J, Detappe A. 2020. Leveraging Immunotherapy with Nanomedicine. *Advanced Therapeutics* **3**:2000134. doi:10.1002/adtp.202000134

Mittelheisser V, Coliat P, Moeglin E, Goepp L, Goetz JG, Charbonnière LJ, Pivot X, Detappe A. 2022. Optimal Physicochemical Properties of Antibody–Nanoparticle Conjugates for Improved Tumor Targeting. *Advanced Materials* **34**:2110305. doi:10.1002/adma.202110305

Mittelheisser V, Gensbittel V, Bonati L, Li W, Tang L, Goetz JG. 2024. Evidence and therapeutic implications of biomechanically regulated immunosurveillance in cancer and other diseases. *Nat Nanotechnol* **19**:281–297. doi:10.1038/s41565-023-01535-8

Miyashita T, Tajima H, Gabata R, Okazaki M, Shimbashi H, Ohbatake Y, Okamoto K, Nakanuma S, Sakai S, Makino I, Kinoshita J, Hayashi H, Nakamura K, Takamura H, Ninomiya I, Fushida S, Harmon JW, Ohta T. 2019. Impact of Extravasated Platelet Activation and Podoplanin-positive Cancer-associated Fibroblasts in Pancreatic Cancer Stroma. *Anticancer Res* **39**:5565–5572. doi:10.21873/anticanres.13750

Miyashita T, Tajima H, Makino I, Nakagawara H, Kitagawa H, Fushida S, Harmon JW, Ohta T. 2015. Metastasis-promoting role of extravasated platelet activation in tumor. *Journal of Surgical Research* **193**:289–294. doi:10.1016/j.jss.2014.07.037

Mo X, Zhang H, Preston S, Martin K, Zhou B, Vadalia N, Gamero AM, Soboloff J, Tempera I, Zaidi MR. 2018. Interferon-γ Signaling in Melanocytes and Melanoma Cells Regulates Expression of CTLA-4. *Cancer Research* **78**:436–450. doi:10.1158/0008-5472.CAN-17-1615

Mocikat R, Braumüller H, Gumy A, Egeter O, Ziegler H, Reusch U, Bubeck A, Louis J, Mailhammer R, Riethmüller G, Koszinowski U, Röcken M. 2003. Natural Killer Cells Activated by MHC Class ILow Targets Prime Dendritic Cells to Induce Protective CD8 T Cell Responses. *Immunity* **19**:561–569. doi:10.1016/S1074-7613(03)00264-4

Möhle R, Green D, Moore MAS, Nachman RL, Rafii S. 1997. Constitutive production and thrombin-induced release of vascular endothelial growth factor by human megakaryocytes and platelets. *Proc Natl Acad Sci USA* **94**:663–668. doi:10.1073/pnas.94.2.663

Monks CRF, Freiberg BA, Kupfer H, Sciaky N, Kupfer A. 1998. Three-dimensional segregation of supramolecular activation clusters in T cells. *Nature* **395**:82–86. doi:10.1038/25764

Morandi B, Mortara L, Carrega P, Cantoni C, Costa G, Accolla RS, Mingari MC, Ferrini S, Moretta L, Ferlazzo G. 2009. NK cells provide helper signal for CD8+ T cells by inducing the expression of membrane-bound IL-15 on DCs. *International Immunology* **21**:599–606. doi:10.1093/intimm/dxp029

Moretta A, Bottino C, Vitale M, Pende D, Cantoni C, Mingari MC, Biassoni R, Moretta L. 2001. Activating Receptors and Coreceptors Involved in Human Natural Killer Cell-Mediated Cytolysis. *Annu Rev Immunol* **19**:197–223. doi:10.1146/annurev.immunol.19.1.197

Motz GT, Santoro SP, Wang L-P, Garrabrant T, Lastra RR, Hagemann IS, Lal P, Feldman MD, Benencia F, Coukos G. 2014. Tumor endothelium FasL establishes a selective immune barrier promoting tolerance in tumors. *Nat Med* **20**:607–615. doi:10.1038/nm.3541

Munn DH, Sharma MD, Baban B, Harding HP, Zhang Y, Ron D, Mellor AL. 2005. GCN2 Kinase in T Cells Mediates Proliferative Arrest and Anergy Induction in Response to Indoleamine 2,3-Dioxygenase. *Immunity* **22**:633–642. doi:10.1016/j.immuni.2005.03.013

Muntasell A, Rojo F, Servitja S, Rubio-Perez C, Cabo M, Tamborero D, Costa-García M, Martínez-Garcia M, Menéndez S, Vazquez I, Lluch A, Gonzalez-Perez A, Rovira A, López-Botet M, Albanell J. 2019. NK Cell Infiltrates and HLA Class I Expression in Primary HER2+ Breast Cancer Predict and Uncouple Pathological Response and Disease-free Survival. *Clinical Cancer Research* **25**:1535–1545. doi:10.1158/1078-0432.CCR-18-2365

Murugesan S, Hong J, Yi J, Li D, Beach JR, Shao L, Meinhardt J, Madison G, Wu X, Betzig E, Hammer JA. 2016. Formin-generated actomyosin arcs propel T cell receptor microcluster movement at the immune synapse. *Journal of Cell Biology* **215**:383–399. doi:10.1083/jcb.201603080

Muzi L, Ménard-Moyon C, Russier J, Li J, Chin CF, Ang WH, Pastorin G, Risuleo G, Bianco A. 2015. Diameter-dependent release of a cisplatin pro-drug from small and large functionalized carbon nanotubes. *Nanoscale* **7**:5383–5394. doi:10.1039/C5NR00220F

Nakata M, Kawasaki A, Azuma M, Tsuji K, Matsuda H, Shinkai Y, Yagita H, Okumura K. 1992. Expression of perforin and cytolytic potential of human peripheral blood lymphocyte subpopulations. *Int Immunol* **4**:1049–1054. doi:10.1093/intimm/4.9.1049

N

Naumov GN, Folkman J, Straume O. 2009. Tumor dormancy due to failure of angiogenesis: role of the microenvironment. *Clin Exp Metastasis* **26**:51–60. doi:10.1007/s10585-008-9176-0

Ngo VN, Lucy Tang H, Cyster JG. 1998. Epstein-Barr Virus–induced Molecule 1 Ligand Chemokine Is Expressed by Dendritic Cells in Lymphoid Tissues and Strongly Attracts Naive T Cells and Activated B Cells. *The Journal of Experimental Medicine* **188**:181–191. doi:10.1084/jem.188.1.181

Nguyen LNM, Lin ZP, Sindhwani S, MacMillan P, Mladjenovic SM, Stordy B, Ngo W, Chan WCW. 2023. The exit of nanoparticles from solid tumours. *Nat Mater* **22**:1261–1272. doi:10.1038/s41563-023-01630-0

Nia HT, Liu H, Seano G, Datta M, Jones D, Rahbari N, Incio J, Chauhan VP, Jung K, Martin JD, Askoxylakis V, Padera TP, Fukumura D, Boucher Y, Hornicek FJ, Grodzinsky AJ, Baish JW, Munn LL, Jain RK. 2016. Solid stress and elastic energy as measures of tumour mechanopathology. *Nat Biomed Eng* **1**:0004. doi:10.1038/s41551-016-0004

Nielsen M, Thomsen J, Primdahl S, Dyreborg U, Andersen J. 1987. Breast cancer and atypia among young and middle-aged women: a study of 110 medicolegal autopsies. *Br J Cancer* **56**:814–819. doi:10.1038/bjc.1987.296

Nieswandt B, Hafner M, Echtenacher B, Männel DN. 1999. Lysis of tumor cells by natural killer cells in mice is impeded by platelets. *Cancer Res* **59**:1295–1300.

Ning Z, Liu K, Zhang H, Dong G, Wang X, Xiong H. 2024. Platelets induce CD39 expression in tumor cells to facilitate tumor metastasis. *Br J Cancer* **130**:1542–1551. doi:10.1038/s41416-024-02640-8

Nolz JC, Gomez TS, Zhu P, Li S, Medeiros RB, Shimizu Y, Burkhardt JK, Freedman BD, Billadeau DD. 2006. The WAVE2 Complex Regulates Actin Cytoskeletal Reorganization and CRAC-Mediated Calcium Entry during T Cell Activation. *Current Biology* **16**:24–34. doi:10.1016/j.cub.2005.11.036

Norian LA, Rodriguez PC, O'Mara LA, Zabaleta J, Ochoa AC, Cella M, Allen PM. 2009. Tumor-Infiltrating Regulatory Dendritic Cells Inhibit CD8+ T Cell Function via L-Arginine Metabolism. *Cancer Research* **69**:3086–3094. doi:10.1158/0008-5472.CAN-08-2826

Novák P, Kruppa GH. 2008. Intra-Molecular Cross-Linking of Acidic Residues for Protein Structure Studies. *Eur J Mass Spectrom (Chichester)* **14**:355–365. doi:10.1255/ejms.963

Novoselov KS, Geim AK, Morozov SV, Jiang D, Zhang Y, Dubonos SV, Grigorieva IV, Firsov AA. 2004. Electric Field Effect in Atomically Thin Carbon Films. *Science* **306**:666–669. doi:10.1126/science.1102896

Nowell PC. 1976. The Clonal Evolution of Tumor Cell Populations: Acquired genetic lability permits stepwise selection of variant sublines and underlies tumor progression. *Science* **194**:23–28. doi:10.1126/science.959840

O

Obeid M, Tesniere A, Ghiringhelli F, Fimia GM, Apetoh L, Perfettini J-L, Castedo M, Mignot G, Panaretakis T, Casares N, Métivier D, Larochette N, Van Endert P, Ciccosanti F, Piacentini M, Zitvogel L, Kroemer G. 2007. Calreticulin exposure dictates the immunogenicity of cancer cell death. *Nat Med* **13**:54–61. doi:10.1038/nm1523

O'Brien MER, Wigler N, Inbar M, Rosso R, Grischke E, Santoro A, Catane R, Kieback DG, Tomczak P, Ackland SP, Orlandi F, Mellars L, Alland L, Tendler C. 2004. Reduced cardiotoxicity and comparable efficacy in a phase IIItrial of pegylated liposomal doxorubicin HCl(CAELYX^{TM}/Doxil®) versus conventional doxorubicin forfirst-line treatment of metastatic breast cancer. *Annals of Oncology* **15**:440–449. doi:10.1093/annonc/mdh097

Orange JS, Harris KE, Andzelm MM, Valter MM, Geha RS, Strominger JL. 2003. The mature activating natural killer cell immunologic synapse is formed in distinct stages. *Proc Natl Acad Sci USA* **100**:14151–14156. doi:10.1073/pnas.1835830100

Osmani N, Follain G, García León MJ, Lefebvre O, Busnelli I, Larnicol A, Harlepp S, Goetz JG. 2019. Metastatic Tumor Cells Exploit Their Adhesion Repertoire to Counteract Shear Forces during Intravascular Arrest. *Cell Reports* **28**:2491-2500.e5. doi:10.1016/j.celrep.2019.07.102

P

Padera TP, Stoll BR, Tooredman JB, Capen D, Tomaso ED, Jain RK. 2004. Cancer cells compress intratumour vessels. *Nature* **427**:695–695. doi:10.1038/427695a

Pagès F, Kirilovsky A, Mlecnik B, Asslaber M, Tosolini M, Bindea G, Lagorce C, Wind P, Marliot F, Bruneval P, Zatloukal K, Trajanoski Z, Berger A, Fridman W-H, Galon J. 2009. In Situ Cytotoxic and Memory T Cells Predict Outcome in Patients With Early-Stage Colorectal Cancer. *JCO* **27**:5944–5951. doi:10.1200/JCO.2008.19.6147

Paget S. 1889. The distribution of secondary growths in cancer of the breast. *The Lancet* **133**:571–573. doi:10.1016/S0140-6736(00)49915-0

Palumbo JS, Talmage KE, Massari JV, La Jeunesse CM, Flick MJ, Kombrinck KW, Jirousková M, Degen JL. 2005. Platelets and fibrin(ogen) increase metastatic potential by impeding natural killer cell–mediated elimination of tumor cells. *Blood* **105**:178–185. doi:10.1182/blood-2004-06-2272

Pan J, Zhang M, Wang J, Wang Q, Xia D, Sun W, Zhang L, Yu H, Liu Y, Cao X. 2004. Interferon-γ is an autocrine mediator for dendritic cell maturation. *Immunology Letters* **94**:141–151. doi:10.1016/j.imlet.2004.05.003

Panczyk T, Jagusiak A, Pastorin G, Ang WH, Narkiewicz-Michalek J. 2013. Molecular Dynamics Study of Cisplatin Release from Carbon Nanotubes Capped by Magnetic Nanoparticles. *J Phys Chem C* **117**:17327–17336. doi:10.1021/jp405593u

Pasquier B, Pasquier D, N'golet A, Panh MH, Couderc P. 1980. Extraneural metastases of astrocytomas and glioblastomas clinicopathological study of two cases and review of literature. *Cancer* **45**:112–125. doi:10.1002/1097-0142(19800101)45:1<112::AID-CNCR2820450121>3.0.CO;2-9

Pastorin G, Wu W, Wieckowski S, Briand J-P, Kostarelos K, Prato M, Bianco A. 2006. Double functionalisation of carbon nanotubes for multimodal drug delivery. *Chem Commun* 1182. doi:10.1039/b516309a

Pathak AP, Artemov D, Neeman M, Bhujwalla ZM. 2006. Lymph Node Metastasis in Breast Cancer Xenografts Is Associated with Increased Regions of Extravascular Drain, Lymphatic Vessel Area, and Invasive Phenotype. *Cancer Research* **66**:5151–5158. doi:10.1158/0008-5472.CAN-05-1788

Patsoukis N, Bardhan K, Chatterjee P, Sari D, Liu B, Bell LN, Karoly ED, Freeman GJ, Petkova V, Seth P, Li L, Boussiotis VA. 2015. PD-1 alters T-cell metabolic reprogramming by inhibiting glycolysis and promoting lipolysis and fatty acid oxidation. *Nat Commun* **6**:6692. doi:10.1038/ncomms7692

Paul CD, Bishop K, Devine A, Paine EL, Staunton JR, Thomas SM, Thomas JR, Doyle AD, Miller Jenkins LM, Morgan NY, Sood R, Tanner K. 2019. Tissue Architectural Cues Drive Organ Targeting of Tumor Cells in Zebrafish. *Cell Systems* **9**:187-206.e16. doi:10.1016/j.cels.2019.07.005

Pedersen L, Milman N. 1996. Prognostic significance of thrombocytosis in patients with primary lung cancer. *Eur Respir J* **9**:1826–1830. doi:10.1183/09031936.96.09091826
Peigney A, Laurent Ch, Flahaut E, Bacsa RR, Rousset A. 2001. Specific surface area of carbon nanotubes and bundles of carbon nanotubes. *Carbon* **39**:507–514. doi:10.1016/S0008-6223(00)00155-X

Peinado H, Zhang H, Matei IR, Costa-Silva B, Hoshino A, Rodrigues G, Psaila B, Kaplan RN, Bromberg JF, Kang Y, Bissell MJ, Cox TR, Giaccia AJ, Erler JT, Hiratsuka S, Ghajar CM, Lyden D. 2017. Pre-metastatic niches: organ-specific homes for metastases. *Nat Rev Cancer* **17**:302–317. doi:10.1038/nrc.2017.6

Pende D, Parolini S, Pessino A, Sivori S, Augugliaro R, Morelli L, Marcenaro E, Accame L, Malaspina A, Biassoni R, Bottino C, Moretta L, Moretta A. 1999. Identification and Molecular Characterization of Nkp30, a Novel Triggering Receptor Involved in Natural Cytotoxicity Mediated by Human Natural Killer Cells. *The Journal of Experimental Medicine* **190**:1505–1516. doi:10.1084/jem.190.10.1505

Penn I. 1982. The occurrence of cancer in immune deficiencies. *Current Problems in Cancer* **6**:1–64. doi:10.1016/S0147-0272(82)80002-0

Pereira ER, Kedrin D, Seano G, Gautier O, Meijer EFJ, Jones D, Chin S-M, Kitahara S, Bouta EM, Chang J, Beech E, Jeong H-S, Carroll MC, Taghian AG, Padera TP. 2018. Lymph node metastases can invade local blood vessels, exit the node, and colonize distant organs in mice. *Science* **359**:1403–1407. doi:10.1126/science.aal3622

Perez OD, Mitchell D, Jager GC, Nolan GP. 2004. LFA-1 signaling through p44/42 is coupled to perforin degranulation in CD56+CD8+ natural killer cells. *Blood* **104**:1083–1093. doi:10.1182/blood-2003-08-2652

Petersen GH, Alzghari SK, Chee W, Sankari SS, La-Beck NM. 2016. Meta-analysis of clinical and preclinical studies comparing the anticancer efficacy of liposomal versus conventional non-liposomal doxorubicin. *Journal of Controlled Release* **232**:255–264. doi:10.1016/j.jconrel.2016.04.028

Philippe C, Philippe B, Fouqueray B, Perez J, Lebret M, Baud L. 1993. Protection from tumor necrosis factor-mediated cytolysis by platelets. *Am J Pathol* **143**:1713–1723.

Pietras K, Ostman A, Sjöquist M, Buchdunger E, Reed RK, Heldin CH, Rubin K. 2001. Inhibition of platelet-derived growth factor receptors reduces interstitial hypertension and increases transcapillary transport in tumors. *Cancer Res* **61**:2929–2934.

Pitti RM, Marsters SA, Lawrence DA, Roy M, Kischkel FC, Dowd P, Huang A, Donahue CJ, Sherwood SW, Baldwin DT, Godowski PJ, Wood WI, Gurney AL, Hillan KJ, Cohen RL, Goddard AD, Botstein D, Ashkenazi A. 1998. Genomic amplification of a decoy receptor for Fas ligand in lung and colon cancer. *Nature* **396**:699–703. doi:10.1038/25387

Placke T, Örgel M, Schaller M, Jung G, Rammensee H-G, Kopp H-G, Salih HR. 2012a. Platelet-Derived MHC Class I Confers a Pseudonormal Phenotype to Cancer Cells That Subverts the Antitumor Reactivity of Natural Killer Immune Cells. *Cancer Research* **72**:440–448. doi:10.1158/0008-5472.CAN-11-1872

Placke T, Salih HR, Kopp H-G. 2012b. GITR Ligand Provided by Thrombopoietic Cells Inhibits NK Cell Antitumor Activity. *The Journal of Immunology* **189**:154–160. doi:10.4049/jimmunol.1103194

Pogge Von Strandmann E, Simhadri VR, Von Tresckow B, Sasse S, Reiners KS, Hansen HP, Rothe A, Böll B, Simhadri VL, Borchmann P, McKinnon PJ, Hallek M, Engert A. 2007. Human Leukocyte Antigen-B-Associated Transcript 3 Is Released from Tumor Cells and Engages the NKp30 Receptor on Natural Killer Cells. *Immunity* **27**:965–974. doi:10.1016/j.immuni.2007.10.010

Polack FP, Thomas SJ, Kitchin N, Absalon J, Gurtman A, Lockhart S, Perez JL, Pérez Marc G, Moreira ED, Zerbini C, Bailey R, Swanson KA, Roychoudhury S, Koury K, Li P, Kalina WV, Cooper D, Frenck RW, Hammitt LL, Türeci Ö, Nell H, Schaefer A, Ünal S, Tresnan DB, Mather S, Dormitzer PR, Şahin U, Jansen KU, Gruber WC. 2020. Safety and Efficacy of the BNT162b2 mRNA Covid-19 Vaccine. *N Engl J Med* **383**:2603–2615. doi:10.1056/NEJMoa2034577

Prima V, Kaliberova LN, Kaliberov S, Curiel DT, Kusmartsev S. 2017. COX2/mPGES1/PGE $_2$ pathway regulates PD-L1 expression in tumor-associated macrophages and myeloid-derived suppressor cells. *Proc Natl Acad Sci USA* **114**:1117–1122. doi:10.1073/pnas.1612920114

Provenzano PP, Eliceiri KW, Campbell JM, Inman DR, White JG, Keely PJ. 2006. Collagen reorganization at the tumor-stromal interface facilitates local invasion. *BMC Med* **4**:38. doi:10.1186/1741-7015-4-38

Pucci F, Rickelt S, Newton AP, Garris C, Nunes E, Evavold C, Pfirschke C, Engblom C, Mino-Kenudson M, Hynes RO, Weissleder R, Pittet MJ. 2016. PF4 Promotes Platelet Production and Lung Cancer Growth. *Cell Reports* **17**:1764–1772. doi:10.1016/j.celrep.2016.10.031

Puram SV, Tirosh I, Parikh AS, Patel AP, Yizhak K, Gillespie S, Rodman C, Luo CL, Mroz EA, Emerick KS, Deschler DG, Varvares MA, Mylvaganam R, Rozenblatt-Rosen O, Rocco JW, Faquin WC, Lin DT, Regev A, Bernstein BE. 2017. Single-Cell Transcriptomic Analysis of Primary and Metastatic Tumor Ecosystems in Head and Neck Cancer. *Cell* **171**:1611-1624.e24. doi:10.1016/j.cell.2017.10.044

Pylaeva E, Korschunow G, Spyra I, Bordbari S, Siakaeva E, Ozel I, Domnich M, Squire A, Hasenberg A, Thangavelu K, Hussain T, Goetz M, Lang KS, Gunzer M, Hansen W, Buer J, Bankfalvi A, Lang S, Jablonska J. 2022. During early stages of cancer, neutrophils initiate anti-tumor immune responses in tumor-draining lymph nodes. *Cell Reports* **40**:111171. doi:10.1016/j.celrep.2022.111171

Q

Qi C, Li Jialin, Guo S, Li M, Li Y, Li Jiangchao, Zhang Q, Zheng L, He X, Zheng X, He Y, Wang L, Wei B. 2016. P-selectin-mediated LOX expression promotes insulinoma growth in Rip1-Tag2 mice by increasing tissue stiffness. *Int J Biol Sci* **12**:1289–1297. doi:10.7150/ijbs.16405

Qi C, Wei B, Zhou W, Yang Y, Li B, Guo S, Li Jialin, Ye J, Li Jiangchao, Zhang Q, Lan T, He X, Cao L, Zhou J, Geng J, Wang L. 2015. P-selectin-mediated platelet adhesion promotes tumor growth. *Oncotarget* **6**:6584–6596. doi:10.18632/oncotarget.3164

Qian B-Z, Li J, Zhang H, Kitamura T, Zhang J, Campion LR, Kaiser EA, Snyder LA, Pollard JW. 2011. CCL2 recruits inflammatory monocytes to facilitate breast-tumour metastasis. *Nature* **475**:222–225. doi:10.1038/nature10138

Qiu Y, Brown AC, Myers DR, Sakurai Y, Mannino RG, Tran R, Ahn B, Hardy ET, Kee MF, Kumar S, Bao G, Barker TH, Lam WA. 2014. Platelet mechanosensing of substrate stiffness during clot formation mediates adhesion, spreading, and activation. *Proc Natl Acad Sci USA* **111**:14430–14435. doi:10.1073/pnas.1322917111

Qureshi OS, Zheng Y, Nakamura K, Attridge K, Manzotti C, Schmidt EM, Baker J, Jeffery LE, Kaur S, Briggs Z, Hou TZ, Futter CE, Anderson G, Walker LSK, Sansom DM. 2011. Trans-Endocytosis of CD80 and CD86: A Molecular Basis for the Cell-Extrinsic Function of CTLA-4. *Science* **332**:600–603. doi:10.1126/science.1202947

R

Rachidi S, Metelli A, Riesenberg B, Wu BX, Nelson MH, Wallace C, Paulos CM, Rubinstein MP, Garrett-Mayer E, Hennig M, Bearden DW, Yang Y, Liu B, Li Z. 2017. Platelets subvert T cell immunity against cancer via GARP-TGFβ axis. *Sci Immunol* **2**:eaai7911. doi:10.1126/sciimmunol.aai7911

Rayes J, Watson SP, Nieswandt B. 2019. Functional significance of the platelet immune receptors GPVI and CLEC-2. *Journal of Clinical Investigation* **129**:12–23. doi:10.1172/JCI122955

Reddy ST, Van Der Vlies AJ, Simeoni E, Angeli V, Randolph GJ, O'Neil CP, Lee LK, Swartz MA, Hubbell JA. 2007. Exploiting lymphatic transport and complement activation in nanoparticle vaccines. *Nat Biotechnol* **25**:1159–1164. doi:10.1038/nbt1332

Ren J, He J, Zhang H, Xia Y, Hu Z, Loughran P, Billiar T, Huang H, Tsung A. 2021. Platelet TLR4-ERK5 Axis Facilitates NET-Mediated Capturing of Circulating Tumor Cells and Distant Metastasis after Surgical Stress. *Cancer Research* **81**:2373–2385. doi:10.1158/0008-5472.CAN-20-3222

Renaud L, Lebozec K, Voors-Pette C, Dogterom P, Billiald P, Jandrot Perrus M, Pletan Y, Machacek M. 2020. Population Pharmacokinetic/Pharmacodynamic Modeling of Glenzocimab (ACT017) a Glycoprotein VI Inhibitor of Collagen-Induced Platelet Aggregation. *The Journal of Clinical Pharma* **60**:1198–1208. doi:10.1002/jcph.1616

Restifo NP, Esquivel F, Kawakami Y, Yewdell JW, Mulé JJ, Rosenberg SA, Bennink JR. 1993. Identification of human cancers deficient in antigen processing. *The Journal of experimental medicine* **177**:265–272. doi:10.1084/jem.177.2.265

Reymond N, d'Água BB, Ridley AJ. 2013. Crossing the endothelial barrier during metastasis. *Nat Rev Cancer* **13**:858–870. doi:10.1038/nrc3628

Rhoden JJ, Wittrup KD. 2012. Dose Dependence of Intratumoral Perivascular Distribution of Monoclonal Antibodies. *Journal of Pharmaceutical Sciences* **101**:860–867. doi:10.1002/jps.22801

Ridge JP, Di Rosa F, Matzinger P. 1998. A conditioned dendritic cell can be a temporal bridge between a CD4+ T-helper and a T-killer cell. *Nature* **393**:474–478. doi:10.1038/30989

Riesenberg BP, Ansa-Addo EA, Gutierrez J, Timmers CD, Liu B, Li Z. 2019. Cutting Edge: Targeting Thrombocytes to Rewire Anticancer Immunity in the Tumor Microenvironment and Potentiate Efficacy of PD-1 Blockade. *The Journal of Immunology* **203**:1105–1110. doi:10.4049/jimmunol.1900594

Riess L. 1872. Zur pathologischen anatomie des blutes. *Arch Anat Physiol Wissensch Medical* **39**:237–240.

Riteau B, Barber DF, Long EO. 2003. Vav1 Phosphorylation Is Induced by β2 Integrin Engagement on Natural Killer Cells Upstream of Actin Cytoskeleton and Lipid Raft Reorganization. *The Journal of Experimental Medicine* **198**:469–474. doi:10.1084/jem.20021995

Roberts EW, Broz ML, Binnewies M, Headley MB, Nelson AE, Wolf DM, Kaisho T, Bogunovic D, Bhardwaj N, Krummel MF. 2016. Critical Role for CD103+/CD141+ Dendritic Cells Bearing CCR7 for Tumor Antigen Trafficking and Priming of T Cell Immunity in Melanoma. *Cancer Cell* **30**:324–336. doi:10.1016/j.ccell.2016.06.003

Rodig N, Ryan T, Allen JA, Pang H, Grabie N, Chernova T, Greenfield EA, Liang SC, Sharpe AH, Lichtman AH, Freeman GJ. 2003. Endothelial expression of PD-L1 and PD-L2 down-regulates CD8 $^{+}$ T cell activation and cytolysis. *Eur J Immunol* **33**:3117–3126. doi:10.1002/eji.200324270

Rodriguez-Martinez A, Simon-Saez I, Perales S, Garrido-Navas C, Russo A, De Miguel-Perez D, Puche-Sanz I, Alaminos C, Ceron J, Lorente JA, Molina MP, Gonzalez C, Cristofanilli M, Ortigosa-Palomo A, Real PJ, Rolfo C, Serrano MJ. 2022. Exchange of cellular components between platelets and tumor cells: impact on tumor cells behavior. *Theranostics* **12**:2150–2161. doi:10.7150/thno.64252

Rolfes V, Idel C, Pries R, Plötze-Martin K, Habermann J, Gemoll T, Bohnet S, Latz E, Ribbat-Idel J, Franklin BS, Wollenberg B. 2018. PD-L1 is expressed on human platelets and is affected by immune checkpoint therapy. *Oncotarget* **9**:27460–27470. doi:10.18632/oncotarget.25446

Rolli M, Fransvea E, Pilch J, Saven A, Felding-Habermann B. 2003. Activated integrin αvβ3 cooperates with metalloproteinase MMP-9 in regulating migration of metastatic breast cancer cells. *Proc Natl Acad Sci USA* **100**:9482–9487. doi:10.1073/pnas.1633689100

Rostovtsev VV, Green LG, Fokin VV, Sharpless KB. 2002. A Stepwise Huisgen Cycloaddition Process: Copper(I)-Catalyzed Regioselective “Ligation” of Azides and Terminal Alkynes. *Angew Chem Int Ed* **41**:2596–2599. doi:10.1002/1521-3773(20020715)41:14<2596::AID-ANIE2596>3.0.CO;2-4

Roweth HG, Malloy MW, Goreczny GJ, Becker IC, Guo Q, Mittendorf EA, Italiano JE, McAllister SS, Battinelli EM. 2022. Pro-inflammatory megakaryocyte gene expression in murine models of breast cancer. *Sci Adv* **8**:eabo5224. doi:10.1126/sciadv.abo5224

Rowland GF, O'Neill GJ, Davies DA. 1975. Suppression of tumour growth in mice by a drug-antibody conjugate using a novel approach to linkage. *Nature* **255**:487–488. doi:10.1038/255487a0

Rozenblatt-Rosen O, Regev A, Oberdoerffer P, Nawy T, Hupalowska A, Rood JE, Ashenberg O, Cerami E, Coffey RJ, Demir E, Ding L, Esplin ED, Ford JM, Goecks J, Ghosh S, Gray JW, Guinney J, Hanlon SE, Hughes SK, Hwang ES, Iacobuzio-Donahue CA, Jané-Valbuena J, Johnson Bruce E., Lau KS, Lively T, Mazzilli SA, Pe'er D, Santagata S, Shalek AK, Schapiro D, Snyder MP, Sorger PK, Spira AE, Srivastava S, Tan K, West RB, Williams EH, Aberle D, Achilefu SI, Ademuyiwa FO, Adey AC, Aft RL, Agarwal R, Aguilar RA, Alikarami F, Allaj V, Amos C, Anders RA, Angelo MR, Anton K, Ashenberg O, Aster JC, Babur O, Bahmani A, Balsubramani A, Barrett D, Beane J, Bender DE, Bernt K, Berry L, Betts CB, Bletz J, Blise K, Boire A, Boland G, Borowsky A, Bosse K, Bott M, Boyden E, Brooks J, Bueno R, Burlingame EA, Cai Q, Campbell J, Caravan W, Cerami E, Chaib H, Chan JM, Chang YH, Chatterjee D, Chaudhary O, Chen AA, Chen B, Chen Changya, Chen Chia-hui, Chen F, Chen Y-A, Chheda MG, Chin K, Chiu R, Chu S-K, Chuaqui R, Chun J, Cisneros L, Coffey RJ, Colditz GA, Cole K, Collins N, Contrepois K, Coussens LM, Creason AL, Crichton D, Curtis C, Davidsen T, Davies SR, De Bruijn I, Dellostritto L, De Marzo A, Demir E, DeNardo DG, Diep D, Ding L, Diskin S, Doan X, Drewes J, Dubinett S, Dyer M, Egger J, Eng J, Engelhardt B, Erwin G, Esplin ED, Esserman L, Felmeister A, Feiler HS, Fields RC, Fisher S, Flaherty K, Flournoy J, Ford JM, Fortunato A, Frangieh A, Frye JL, Fulton RS, Galipeau D, Gan S, Gao J, Gao L, Gao P, Gao VR, Geiger T, George A, Getz G, Ghosh S, Giannakis M, Gibbs DL, Gillanders WE, Goecks J, Goedegebuure SP, Gould A, Gowers K, Gray JW, Greenleaf W, Gresham J, Guerriero JL, Guha TK, Guimaraes AR, Guinney J, Gutman D, Hacohen N, Hanlon S, Hansen CR, Harismendy O, Harris KA, Hata A, Hayashi A, Heiser C, Helvie K, Herndon JM, Hirst G, Hodi F, Hollmann T, Horning A, Hsieh JJ, Hughes S, Huh WJ, Hunger S, Hwang SE, Iacobuzio-Donahue CA, Ijaz H, Izar B, Jacobson CA, Janes S, Jané-Valbuena J, Jayasinghe RG, Jiang L, Johnson Brett E., Johnson B, Ju T, Kadara H, Kaestner K, Kagan J, Kalinke L, Keith R, Khan A, Kibbe W, Kim AH, Kim E, Kim J, Kolodzie A, Kopytra M, Kotler E, Krueger R, Krysan K, Kundaje A, Ladabaum U, Lake BB, Lam H, Laquindanum R, Lau KS, Laughney AM, Lee H, Lenburg M, Leonard C, Leshchiner I, Levy R, Li J, Lian CG, Lim K-H, Lin J-R, Lin Y, Liu Q, Liu R, Lively T, Longabaugh WJR, Longacre T, Ma CX, Macedonia MC, Madison T, Maher CA, Maitra A, Makinen N, Makowski D, Maley C, Maliga Z, Mallo D, Maris J, Markham N, Marks J, Martinez D, Mashl RJ, Masilionais I, Mason J, Massagué J, Massion P, Mattar M, Mazurchuk R, Mazutis L, Mazzilli SA, McKinley ET, McMichael JF, Merrick D, Meyerson M, Miessner JR, Mills GB, Mills M, Mondal SB, Mori M, Mori Y, Moses E, Mosse Y, Muhlich JL, Murphy GF, Navin NE, Nawy T, Nederlof M, Ness R, Nevins S, Nikolov M, Nirmal AJ, Nolan G, Novikov E, Oberdoerffer P, O'Connell B, Offin M, Oh ST, Olson A, Ooms A, Ossandon M, Owzar K, Parmar S, Patel T, Patti GJ, Pe'er D, Pe'er I, Peng T, Persson D, Petty M, Pfister H, Polyak K, Pourfarhangi K, Puram SV, Qiu Q, Quintanal-Villalonga Á, Raj A, Ramirez-Solano M, Rashid R, Reeb AN, Regev A, Reid M, Resnick A, Reynolds SM, Riesterer JL, Rodig S, Roland JT, Rosenfield S, Rotem A, Roy S, Rozenblatt-Rosen O, Rudin CM, Ryser MD, Santagata S, Santi-Vicini M,

Sato K, Schapiro D, Schrag D, Schultz N, Sears CL, Sears RC, Sen S, Sen T, Shalek A, Sheng J, Sheng Q, Shoghi KI, Shrubsole MJ, Shyr Y, Sibley AB, Siex K, Simmons AJ, Singer DS, Sivagnanam S, Slyper M, Snyder MP, Sokolov A, Song S-K, Sorger PK, Southard-Smith A, Spira A, Srivastava S, Stein J, Storm P, Stover E, Strand SH, Su T, Sudar D, Sullivan R, Surrey L, Suvà M, Tan K, Terekhanova NV, Ternes L, Thammavong L, Thibault G, Thomas GV, Thorsson V, Todres E, Tran L, Tyler M, Uzun Y, Vachani A, Van Allen E, Vandekar S, Veis DJ, Vigneau S, Vossough A, Waanders A, Wagle N, Wang L-B, Wendl MC, West R, Williams EH, Wu C, Wu H, Wu H-Y, Wyczalkowski MA, Xie Y, Yang X, Yapp C, Yu W, Yuan Y, Zhang D, Zhang K, Zhang M, Zhang N, Zhang Y, Zhao Y, Zhou DC, Zhou Z, Zhu H, Zhu Q, Zhu X, Zhu Y, Zhuang X. 2020. The Human Tumor Atlas Network: Charting Tumor Transitions across Space and Time at Single-Cell Resolution. *Cell* **181**:236–249. doi:10.1016/j.cell.2020.03.053

Rubinstein N, Alvarez M, Zwirner NW, Toscano MA, Ilarregui JM, Bravo A, Mordoh J, Fainboim L, Podhajcer OL, Rabinovich GA. 2004. Targeted inhibition of galectin-1 gene expression in tumor cells results in heightened T cell-mediated rejection. *Cancer Cell* **5**:241–251. doi:10.1016/S1535-6108(04)00024-8

Ryu T, Nishimura S, Miura H, Yamada H, Morita H, Miyazaki H, Kitamura S, Miura Y, Saito T. 2003. Thrombopoietin-Producing Hepatocellular Carcinoma. *Intern Med* **42**:730–734. doi:10.2169/internalmedicine.42.730

S

Sabag B, Puthenveetil A, Levy M, Joseph N, Doniger T, Yaron O, Karako-Lampert S, Lazar I, Awwad F, Ashkenazi S, Barda-Saad M. 2024. Dysfunctional natural killer cells can be reprogrammed to regain anti-tumor activity. *EMBO J* **43**:2552–2581. doi:10.1038/s44318-024-00094-5

Sack GH, Levin J, Bell WR. 1977. Trousseau's syndrome and other manifestations of chronic disseminated coagulopathy in patients with neoplasms: clinical, pathophysiologic, and therapeutic features. *Medicine (Baltimore)* **56**:1–37.

Sahai E, Astsaturov I, Cukierman E, DeNardo DG, Egeblad M, Evans RM, Fearon D, Greten FR, Hingorani SR, Hunter T, Hynes RO, Jain RK, Janowitz T, Jorgensen C, Kimmelman AC, Kolonin MG, Maki RG, Powers RS, Puré E, Ramirez DC, Scherz-Shouval R, Sherman MH, Stewart S, Tlsty TD, Tuveson DA, Watt FM, Weaver V, Weeraratna AT, Werb Z. 2020. A framework for advancing our understanding of cancer-associated fibroblasts. *Nat Rev Cancer* **20**:174–186. doi:10.1038/s41568-019-0238-1

Saito R, Shoda K, Maruyama S, Yamamoto A, Takiguchi K, Furuya S, Hosomura N, Akaike H, Kawaguchi Y, Amemiya H, Kawaida H, Sudo M, Inoue S, Kono H, Suzuki-Inoue K, Ichikawa D. 2021. Platelets enhance malignant behaviours of gastric cancer cells via direct contacts. *Br J Cancer* **124**:570–573. doi:10.1038/s41416-020-01134-7

Salcedo TW, Azzoni L, Wolf SF, Perussia B. 1993. Modulation of perforin and granzyme messenger RNA expression in human natural killer cells. *J Immunol* **151**:2511–2520.

Salmon H, Franciszkiewicz K, Damotte D, Dieu-Nosjean M-C, Validire P, Trautmann A, Mami-Chouaib F, Donnadieu E. 2012. Matrix architecture defines the preferential localization and migration of T cells into the stroma of human lung tumors. *J Clin Invest* **122**:899–910. doi:10.1172/JCI45817

Salnikov AV, Bretz NP, Perne C, Hazin J, Keller S, Fogel M, Herr I, Schlange T, Moldenhauer G, Altevogt P. 2013. Antibody targeting of CD24 efficiently retards growth and influences cytokine milieu in experimental carcinomas. *Br J Cancer* **108**:1449–1459. doi:10.1038/bjc.2013.102

Salnikov AV, Iversen VV, Koisti M, Sundberg C, Johansson L, Stuhr LB, Sjöquist M, Ahlström H, Reed RK, Rubin K. 2003. Lowering of tumor interstitial fluid pressure specifically augments efficacy of chemotherapy. *FASEB j* **17**:1756–1758. doi:10.1096/fj.02-1201fje

Sancey L, Lux F, Kotb S, Roux S, Dufort S, Bianchi A, Crémillieux Y, Fries P, Coll J-L, Rodriguez-Lafrasse C, Janier M, Dutreix M, Barberi-Heyob M, Boschetti F, Denat F, Louis C, Porcel E, Lacombe S, Le Duc G, Deutsch E, Perfettini J-L, Detappe A, Verry C, Berbeco R, Butterworth KT, McMahon SJ, Prise KM, Perriat P, Tillement O. 2014. The use of theranostic gadolinium-based nanoprobes to improve radiotherapy efficacy. *BJR* **87**:20140134. doi:10.1259/bjr.20140134

Sanda MG, Restifo NP, Walsh JC, Kawakami Y, Nelson WG, Pardoll DM, Simons JW. 1995. Molecular Characterization of Defective Antigen Processing in Human Prostate Cancer. *JNCI Journal of the National Cancer Institute* **87**:280–285. doi:10.1093/jnci/87.4.280

Sasaki K, Kawai K, Tsuno NH, Sunami E, Kitayama J. 2012. Impact of Preoperative Thrombocytosis on the Survival of Patients with Primary Colorectal Cancer. *World j surg* **36**:192–200. doi:10.1007/s00268-011-1329-7

Scaffidi C. 1998. Two CD95 (APO-1/Fas) signaling pathways. *The EMBO Journal* **17**:1675–1687. doi:10.1093/emboj/17.6.1675

Schipper ML, Nakayama-Ratchford N, Davis CR, Kam NWS, Chu P, Liu Z, Sun X, Dai H, Gambhir SS. 2008. A pilot toxicology study of single-walled carbon nanotubes in a small sample of mice. *Nature Nanotech* **3**:216–221. doi:10.1038/nnano.2008.68

Schischlik F, Jäger R, Rosebrock F, Hug E, Schuster M, Holly R, Fuchs E, Milosevic Feenstra JD, Bogner E, Gisslinger B, Schalling M, Rumi E, Pietra D, Fischer G, Faé I, Vulliard L, Menche J, Haferlach T, Meggendorfer M, Stengel A, Bock C, Cazzola M, Gisslinger H, Kralovics R. 2019. Mutational landscape of the transcriptome offers putative targets for immunotherapy of myeloproliferative neoplasms. *Blood* **134**:199–210. doi:10.1182/blood.2019000519

Schneider MA, Heeb L, Beffinger MM, Pantelyushin S, Linecker M, Roth L, Lehmann K, Ungethüm U, Kobold S, Graf R, Van Den Broek M, Vom Berg J, Gupta A, Clavien P-A. 2021. Attenuation of peripheral serotonin inhibits tumor growth and enhances immune checkpoint blockade therapy in murine tumor models. *Sci Transl Med* **13**:eabc8188. doi:10.1126/scitranslmed.abc8188

Schoenberger SP, Toes REM, Van Der Voort EIH, Offringa R, Melief CJM. 1998. T-cell help for cytotoxic T lymphocytes is mediated by CD40–CD40L interactions. *Nature* **393**:480–483. doi:10.1038/31002

Schreiber RD, Old LJ, Smyth MJ. 2011. Cancer Immunoediting: Integrating Immunity's Roles in Cancer Suppression and Promotion. *Science* **331**:1565–1570. doi:10.1126/science.1203486

Schumacher D, Strilic B, Sivaraj KK, Wettschureck N, Offermanns S. 2013. Platelet-Derived Nucleotides Promote Tumor-Cell Transendothelial Migration and Metastasis via P2Y2 Receptor. *Cancer Cell* **24**:130–137. doi:10.1016/j.ccr.2013.05.008

Semeraro F, Ammollo CT, Morrissey JH, Dale GL, Friese P, Esmon NL, Esmon CT. 2011. Extracellular histones promote thrombin generation through platelet-dependent mechanisms: involvement of platelet TLR2 and TLR4. *Blood* **118**:1952–1961. doi:10.1182/blood-2011-03-343061

Serhan CN, Yang R, Martinod K, Kasuga K, Pillai PS, Porter TF, Oh SF, Spite M. 2009. Maresins: novel macrophage mediators with potent antiinflammatory and proresolving actions. *Journal of Experimental Medicine* **206**:15–23. doi:10.1084/jem.20081880

Serrano M, Lin AW, McCurrach ME, Beach D, Lowe SW. 1997. Oncogenic ras Provokes Premature Cell Senescence Associated with Accumulation of p53 and p16INK4a. *Cell* **88**:593–602. doi:10.1016/S0092-8674(00)81902-9

Shankaran V, Ikeda H, Bruce AT, White JM, Swanson PE, Old LJ, Schreiber RD. 2001. IFNγ and lymphocytes prevent primary tumour development and shape tumour immunogenicity. *Nature* **410**:1107–1111. doi:10.1038/35074122

Sharma S, Stolina M, Lin Y, Gardner B, Miller PW, Kronenberg M, Dubinett SM. 1999. T Cell-Derived IL-10 Promotes Lung Cancer Growth by Suppressing Both T Cell and APC Function. *The Journal of Immunology* **163**:5020–5028. doi:10.4049/jimmunol.163.9.5020

Shay JW, Bacchetti S. 1997. A survey of telomerase activity in human cancer. *European Journal of Cancer* **33**:787–791. doi:10.1016/S0959-8049(97)00062-2

Shen B-Q, Xu K, Liu L, Raab H, Bhakta S, Kenrick M, Parsons-Reponte KL, Tien J, Yu S-F, Mai E, Li D, Tibbitts J, Baudys J, Saad OM, Scales SJ, McDonald PJ, Hass PE, Eigenbrot C, Nguyen T, Solis WA, Fuji RN, Flagella KM, Patel D, Spencer SD, Khawli LA, Ebens A, Wong WL, Vandlen R, Kaur S, Sliwkowski MX, Scheller RH, Polakis P, Junutula JR. 2012. Conjugation site modulates the in vivo stability and therapeutic activity of antibody-drug conjugates. *Nat Biotechnol* **30**:184–189. doi:10.1038/nbt.2108

Shin MS, Kim HS, Lee SH, Park WS, Kim SY, Park JY, Lee JH, Lee SK, Lee SN, Jung SS, Han JY, Kim H, Lee JY, Yoo NJ. 2001. Mutations of tumor necrosis factor-related apoptosis-inducing ligand receptor 1 (TRAIL-R1) and receptor 2 (TRAIL-R2) genes in metastatic breast cancers. *Cancer Res* **61**:4942–4946.

Shojaei F, Wu X, Zhong C, Yu L, Liang X-H, Yao J, Blanchard D, Bais C, Peale FV, Van Bruggen N, Ho C, Ross J, Tan M, Carano RAD, Meng YG, Ferrara N. 2007. Bv8 regulates myeloid-cell-dependent tumour angiogenesis. *Nature* **450**:825–831. doi:10.1038/nature06348

Sindhwani S, Syed AM, Ngai J, Kingston BR, Maiorino L, Rothschild J, MacMillan P, Zhang Y, Rajesh NU, Hoang T, Wu JLY, Wilhelm S, Zilman A, Gadde S, Sulaiman A, Ouyang B, Lin Z, Wang L, Egeblad M, Chan WCW. 2020. The entry of nanoparticles into solid tumours. *Nat Mater* **19**:566–575. doi:10.1038/s41563-019-0566-2

Singh AP, Guo L, Verma A, Wong GG-L, Thurber GM, Shah DK. 2020. Antibody Coadministration as a Strategy to Overcome Binding-Site Barrier for ADCs: a Quantitative Investigation. *AAPS J* **22**:28. doi:10.1208/s12248-019-0387-x

Singh LP, Bhattacharyya SK, Kumar R, Mishra G, Sharma U, Singh G, Ahalawat S. 2014. Sol-Gel processing of silica nanoparticles and their applications. *Advances in Colloid and Interface Science* **214**:17–37. doi:10.1016/j.cis.2014.10.007

Singh MV, Suwunnakorn S, Simpson SR, Weber EA, Singh VB, Kalinski P, Maggirwar SB. 2021. Monocytes complexed to platelets differentiate into functionally deficient dendritic cells. *Journal of Leukocyte Biology* **109**:807–820. doi:10.1002/JLB.3A0620-460RR

Singh Y, Meher JG, Raval K, Khan FA, Chaurasia M, Jain NK, Chourasia MK. 2017. Nanoemulsion: Concepts, development and applications in drug delivery. *Journal of Controlled Release* **252**:28–49. doi:10.1016/j.jconrel.2017.03.008

Sivori S, Vitale M, Morelli L, Sanseverino L, Augugliaro R, Bottino C, Moretta L, Moretta A. 1997. p46, a Novel Natural Killer Cell–specific Surface Molecule That Mediates Cell Activation. *The Journal of Experimental Medicine* **186**:1129–1136. doi:10.1084/jem.186.7.1129

Slamon DJ, Clark GM, Wong SG, Levin WJ, Ullrich A, McGuire WL. 1987. Human Breast Cancer: Correlation of Relapse and Survival with Amplification of the HER-2/*neu* Oncogene. *Science* **235**:177–182. doi:10.1126/science.3798106

Slamon DJ, Leyland-Jones B, Shak S, Fuchs H, Paton V, Bajamonde A, Fleming T, Eiermann W, Wolter J, Pegram M, Baselga J, Norton L. 2001. Use of Chemotherapy plus a Monoclonal Antibody against HER2 for Metastatic Breast Cancer That Overexpresses HER2. *N Engl J Med* **344**:783–792. doi:10.1056/NEJM200103153441101

Sletten EM, Bertozzi CR. 2009. Bioorthogonal Chemistry: Fishing for Selectivity in a Sea of Functionality. *Angew Chem Int Ed* **48**:6974–6998. doi:10.1002/anie.200900942

Smyth MJ, Cretney E, Takeda K, Wiltrout RH, Sedger LM, Kayagaki N, Yagita H, Okumura K. 2001. Tumor Necrosis Factor–Related Apoptosis-Inducing Ligand (Trail) Contributes to Interferon γ–Dependent Natural Killer Cell Protection from Tumor Metastasis. *The Journal of Experimental Medicine* **193**:661–670. doi:10.1084/jem.193.6.661

Smyth MJ, Thia KYT, Street SEA, MacGregor D, Godfrey DI, Trapani JA. 2000. Perforin-Mediated Cytotoxicity Is Critical for Surveillance of Spontaneous Lymphoma. *The Journal of Experimental Medicine* **192**:755–760. doi:10.1084/jem.192.5.755

Sofias AM, Combes F, Koschmieder S, Storm G, Lammers T. 2021. A paradigm shift in cancer nanomedicine: from traditional tumor targeting to leveraging the immune system. *Drug Discovery Today* **26**:1482–1489. doi:10.1016/j.drudis.2021.02.017

Sojka DK, Bruniquel D, Schwartz RH, Singh NJ. 2004. IL-2 Secretion by CD4+ T Cells In Vivo Is Rapid, Transient, and Influenced by TCR-Specific Competition. *The Journal of Immunology* **172**:6136–6143. doi:10.4049/jimmunol.172.10.6136

Sostres C, Lanas A. 2011. Gastrointestinal effects of aspirin. *Nat Rev Gastroenterol Hepatol* **8**:385–394. doi:10.1038/nrgastro.2011.97

Spiegel A, Brooks MW, Houshyar S, Reinhardt F, Ardolino M, Fessler E, Chen MB, Krall JA, DeCock J, Zervantonakis IK, Iannello A, Iwamoto Y, Cortez-Retamozo V, Kamm RD, Pittet MJ, Raulet DH, Weinberg RA. 2016. Neutrophils Suppress Intraluminal NK Cell–Mediated Tumor Cell Clearance and Enhance Extravasation of Disseminated Carcinoma Cells. *Cancer Discovery* **6**:630–649. doi:10.1158/2159-8290.CD-15-1157

Sprick MR, Weigand MA, Rieser E, Rauch CT, Juo P, Blenis J, Krammer PH, Walczak H. 2000. FADD/MORT1 and Caspase-8 Are Recruited to TRAIL Receptors 1 and 2 and Are Essential for Apoptosis Mediated by TRAIL Receptor 2. *Immunity* **12**:599–609. doi:10.1016/S1074-7613(00)80211-3

Steeg PS. 2006. Tumor metastasis: mechanistic insights and clinical challenges. *Nat Med* **12**:895–904. doi:10.1038/nm1469

Stellos K, Langer H, Daub K, Schoenberger T, Gauss A, Geisler T, Bigalke B, Mueller I, Schumm M, Schaefer I, Seizer P, Kraemer BF, Siegel-Axel D, May AE, Lindemann S, Gawaz M. 2008. Platelet-Derived Stromal Cell–Derived Factor-1 Regulates Adhesion and Promotes Differentiation of Human CD34 $^{+}$ Cells to Endothelial Progenitor Cells. *Circulation* **117**:206–215. doi:10.1161/CIRCULATIONAHA.107.714691

Stinchcombe JC, Salio M, Cerundolo V, Pende D, Arico M, Griffiths GM. 2011. Centriole polarisation to the immunological synapse directs secretion from cytolytic cells of both the innate and adaptive immune systems. *BMC Biol* **9**:45. doi:10.1186/1741-7007-9-45

Stoll S, Jonuleit H, Schmitt E, Müller G, Yamauchi H, Kurimoto M, Knop J, Enk AH. 1998. Production of functional IL-18 by different subtypes of murine and human dendritic cells (DC): DC-derived IL-18 enhances IL-12-dependent Th1 development. *Eur J Immunol* **28**:3231–3239. doi:10.1002/(SICI)1521-4141(199810)28:10<3231::AID-IMMU3231>3.0.CO;2-Q

Stone RL, Nick AM, McNeish IA, Balkwill F, Han HD, Bottsford-Miller J, Rupaimoole R, Armaiz-Pena GN, Pecot CV, Coward J, Deavers MT, Vasquez HG, Urbauer D, Landen CN, Hu W, Gershenson H, Matsuo K, Shahzad MMK, King ER, Tekedereli I, Ozpolat B, Ahn EH, Bond VK, Wang R, Drew AF, Gushiken F, Lamkin D, Collins K, DeGeest K, Lutgendorf SK, Chiu W, Lopez-Berestein G, Afshar-Kharghan V, Sood AK. 2012. Paraneoplastic Thrombocytosis in Ovarian Cancer. *N Engl J Med* **366**:610–618. doi:10.1056/NEJMoa1110352

Strand S, Hofmann WJ, Hug H, Müller M, Otto G, Strand D, Mariani SM, Stremmel W, Krammer PH, Galle PR. 1996. Lymphocyte apoptosis induced by CD95 (APO–1/Fas) ligand–expressing tumor cells — A mechanism of immune evasion? *Nat Med* **2**:1361–1366. doi:10.1038/nm1296-1361

Street SEA, Cretney E, Smyth MJ. 2001. Perforin and interferon-γ activities independently control tumor initiation, growth, and metastasis. *Blood* **97**:192–197. doi:10.1182/blood.V97.1.192

Strilic B, Offermanns S. 2017. Intravascular Survival and Extravasation of Tumor Cells. *Cancer Cell* **32**:282–293. doi:10.1016/j.ccell.2017.07.001

Stylianopoulos T, Martin JD, Chauhan VP, Jain SR, Diop-Frimpong B, Bardeesy N, Smith BL, Ferrone CR, Hornicek FJ, Boucher Y, Munn LL, Jain RK. 2012. Causes, consequences, and remedies for growth-induced solid stress in murine and human tumors. *Proc Natl Acad Sci USA* **109**:15101–15108. doi:10.1073/pnas.1213353109

Sutmuller RPM, Van Duivenvoorde LM, Van Elsas A, Schumacher TNM, Wildenberg ME, Allison JP, Toes REM, Offringa R, Melief CJM. 2001. Synergism of Cytotoxic T Lymphocyte–Associated Antigen 4 Blockade and Depletion of Cd25+ Regulatory T Cells in Antitumor Therapy Reveals Alternative Pathways for Suppression of Autoreactive Cytotoxic T Lymphocyte Responses. *The Journal of Experimental Medicine* **194**:823–832. doi:10.1084/jem.194.6.823

Suzuki A, Takahashi T, Nakamura K, Tsuyuoka R, Okuno Y, Enomoto T, Fukumoto M, Imura H. 1992. Thrombocytosis in patients with tumors producing colony-stimulating factor. *Blood* **80**:2052–2059.

Suzuki-Inoue K, Kato Y, Inoue O, Kaneko MK, Mishima K, Yatomi Y, Yamazaki Y, Narimatsu H, Ozaki Y. 2007. Involvement of the Snake Toxin Receptor CLEC-2, in Podoplanin-mediated Platelet Activation, by Cancer Cells. *Journal of Biological Chemistry* **282**:25993–26001. doi:10.1074/jbc.M702327200

Swaminathan V, Mythreye K, O'Brien ET, Berchuck A, Blobe GC, Superfine R. 2011. Mechanical Stiffness Grades Metastatic Potential in Patient Tumor Cells and in Cancer Cell Lines. *Cancer Research* **71**:5075–5080. doi:10.1158/0008-5472.CAN-11-0247

Swerdlow SH, Campo E, Harris NL, Jaffe ES, Pileri SA, Stein H, Thiele J, editors. 2017. WHO classification of tumours of haematopoietic and lymphoid tissues, Revised 4th edition. ed, World Health Organization classification of tumours. Lyon: International Agency for Research on Cancer.

Symonds H, Krall L, Remington L, Saenz-Robles M, Lowe S, Jacks T, Van Dyke T. 1994. p53-Dependent apoptosis suppresses tumor growth and progression in vivo. *Cell* **78**:703–711. doi:10.1016/0092-8674(94)90534-7

Szczeklik A, Stevenson DD. 1999. Aspirin-induced asthma: Advances in pathogenesis and management. *Journal of Allergy and Clinical Immunology* **104**:5–13. doi:10.1016/S0091-6749(99)70106-5

Szczerba BM, Castro-Giner F, Vetter M, Krol I, Gkountela S, Landin J, Scheidmann MC, Donato C, Scherrer R, Singer J, Beisel C, Kurzeder C, Heinzelmann-Schwarz V, Rochlitz C, Weber WP, Beerenwinkel N, Aceto N. 2019. Neutrophils escort circulating tumour cells to enable cell cycle progression. *Nature* **566**:553–557. doi:10.1038/s41586-019-0915-y

Szebeni J. 2014. Complement activation-related pseudoallergy: A stress reaction in blood triggered by nanomedicines and biologicals. *Molecular Immunology* **61**:163–173. doi:10.1016/j.molimm.2014.06.038

Szebeni J. 2005. Complement activation-related pseudoallergy: A new class of drug-induced acute immune toxicity. *Toxicology* **216**:106–121. doi:10.1016/j.tox.2005.07.023

Takanami I, Takeuchi K, Giga M. 2001. The prognostic value of natural killer cell infiltration in resected pulmonary adenocarcinoma. *The Journal of Thoracic and Cardiovascular Surgery* **121**:1058–1063. doi:10.1067/mtc.2001.113026

Tanaka K, Okugawa Y, Toiyama Y, Inoue Y, Saigusa S, Kawamura M, Araki T, Uchida K, Mohri Y, Kusunoki M. 2014. Brain-Derived Neurotrophic Factor (BDNF)-Induced Tropomyosin-Related Kinase B (Trk B) Signaling Is a Potential Therapeutic Target for Peritoneal Carcinomatosis Arising from Colorectal Cancer. *PLoS ONE* **9**:e96410. doi:10.1371/journal.pone.0096410

T

Tanaka N, Kanatani S, Tomer R, Sahlgren C, Kronqvist P, Kaczynska D, Louhivuori L, Kis L, Lindh C, Mitura P, Stepulak A, Corvigno S, Hartman J, Micke P, Mezheyeuski A, Strell C, Carlson JW, Fernández Moro C, Dahlstrand H, Östman A, Matsumoto K, Wiklund P, Oya M, Miyakawa A, Deisseroth K, Uhlén P. 2017. Whole-tissue biopsy phenotyping of three-dimensional tumours reveals patterns of cancer heterogeneity. *Nat Biomed Eng* **1**:796–806. doi:10.1038/s41551-017-0139-0

Tasis D, Tagmatarchis N, Bianco A, Prato M. 2006. Chemistry of Carbon Nanotubes. *Chem Rev* **106**:1105–1136. doi:10.1021/cr050569o

Tau GZ, Cowan SN, Weisburg J, Braunstein NS, Rothman PB. 2001. Regulation of IFN-γ Signaling Is Essential for the Cytotoxic Activity of CD8+ T Cells. *The Journal of Immunology* **167**:5574–5582. doi:10.4049/jimmunol.167.10.5574

Taucher S, Salat A, Gnant M, Kwasny W, Mlineritsch B, Menzel R-C, Schmid M, Smola MG, Stierer M, Tausch C, Galid A, Steger G, Jakesz R, Austrian Breast and Colorectal Cancer Study Group. 2003. Impact of pretreatment thrombocytosis on survival in primary breast cancer. *Thromb Haemost* **89**:1098–1106.

Tepper CG, Seldin MF. 1999. Modulation of caspase-8 and FLICE-inhibitory protein expression as a potential mechanism of Epstein-Barr virus tumorigenesis in Burkitt's lymphoma. *Blood* **94**:1727–1737.

Thivat E, Casile M, Moreau J, Molnar I, Dufort S, Seddik K, Le Duc G, De Beaumont O, Loeffler M, Durando X, Biau J. 2023. Phase I/II study testing the combination of AGuIX nanoparticles with radiochemotherapy and concomitant temozolomide in patients with newly diagnosed glioblastoma (NANO-GBM trial protocol). *BMC Cancer* **23**:344. doi:10.1186/s12885-023-10829-y

Thomas L. 1959. Discussion inCellular and Humoral Aspects of the Hypersensitive States: A Symposium Held at the New York Academy of Medicine, Symposia No. 9. P.B. Hoeber.

Thurber GM, Wittrup KD. 2008. Quantitative Spatiotemporal Analysis of Antibody Fragment Diffusion and Endocytic Consumption in Tumor Spheroids. *Cancer Research* **68**:3334–3341. doi:10.1158/0008-5472.CAN-07-3018

Thurber GM, Zajic SC, Wittrup KD. 2007. Theoretic Criteria for Antibody Penetration into Solid Tumors and Micrometastases. *Journal of Nuclear Medicine* **48**:995–999. doi:10.2967/jnumed.106.037069

Totaro KA, Liao X, Bhattacharya K, Finneman JI, Sperry JB, Massa MA, Thorn J, Ho SV, Pentelute BL. 2016. Systematic Investigation of EDC/sNHS-Mediated Bioconjugation Reactions for Carboxylated Peptide Substrates. *Bioconjugate Chem* **27**:994–1004. doi:10.1021/acs.bioconjchem.6b00043

Trainor K, Broom A, Meiering EM. 2017. Exploring the relationships between protein sequence, structure and solubility. *Current Opinion in Structural Biology* **42**:136–146. doi:10.1016/j.sbi.2017.01.004

Traut RR, Bollen A, Sun T-T, Hershey JWB, Sundberg J, Pierce LR. 1973. Methyl 4-mercaptobutyrimidate as a cleavable crosslinking reagent and its application to the Escherichia coli 30S ribosome. *Biochemistry* **12**:3266–3273. doi:10.1021/bi00741a019

Trousseau A. 1872. Clinique Medicale de l'Hotel-Dieu de Paris (Lectures on Clinical Medicine at the Hotel-Dieu, Paris).

Tse JM, Cheng G, Tyrrell JA, Wilcox-Adelman SA, Boucher Y, Jain RK, Munn LL. 2012. Mechanical compression drives cancer cells toward invasive phenotype. *Proc Natl Acad Sci USA* **109**:911–916. doi:10.1073/pnas.1118910109

Tumey LN, Charati M, He T, Sousa E, Ma D, Han X, Clark T, Casavant J, Loganzo F, Barletta F, Lucas J, Graziani EI. 2014. Mild Method for Succinimide Hydrolysis on ADCs: Impact on ADC Potency, Stability, Exposure, and Efficacy. *Bioconjugate Chem* **25**:1871–1880. doi:10.1021/bc500357n

Turajlic S, Litchfield K, Xu H, Rosenthal R, McGranahan N, Reading JL, Wong YNS, Rowan A, Kanu N, Al Bakir M, Chambers T, Salgado R, Savas P, Loi S, Birkbak NJ, Sansregret L, Gore M, Larkin J, Quezada SA, Swanton C. 2017. Insertion-and-deletion-derived tumour-specific neoantigens and the immunogenic phenotype: a pan-cancer analysis. *The Lancet Oncology* **18**:1009–1021. doi:10.1016/S1470-2045(17)30516-8

Turley SJ, Inaba K, Garrett WS, Ebersold M, Unternaehrer J, Steinman RM, Mellman I. 2000. Transport of Peptide-MHC Class II Complexes in Developing Dendritic Cells. *Science* **288**:522–527. doi:10.1126/science.288.5465.522

U

Ugurel S, Rappl G, Tilgen W, Reinhold U. 2001. Increased soluble CD95 (sFas/CD95) serum level correlates with poor prognosis in melanoma patients. *Clin Cancer Res* **7**:1282–1286.

Urlaub D, Höfer K, Müller M-L, Watzl C. 2017. LFA-1 Activation in NK Cells and Their Subsets: Influence of Receptors, Maturation, and Cytokine Stimulation. *The Journal of Immunology* **198**:1944–1951. doi:10.4049/jimmunol.1601004

Uyttenhove C, Pilotte L, Théate I, Stroobant V, Colau D, Parmentier N, Boon T, Van Den Eynde BJ. 2003. Evidence for a tumoral immune resistance mechanism based on tryptophan degradation by indoleamine 2,3-dioxygenase. *Nat Med* **9**:1269–1274. doi:10.1038/nm934

V

Valastyan S, Weinberg RA. 2011. Tumor Metastasis: Molecular Insights and Evolving Paradigms. *Cell* **147**:275–292. doi:10.1016/j.cell.2011.09.024

Valcourt DM, Dang MN, Scully MA, Day ES. 2020. Nanoparticle-Mediated Co-Delivery of Notch-1 Antibodies and ABT-737 as a Potent Treatment Strategy for Triple-Negative Breast Cancer. *ACS Nano* **14**:3378–3388. doi:10.1021/acsnano.9b09263

Van Den Broek ME, Kägi D, Ossendorp F, Toes R, Vamvakas S, Lutz WK, Melief CJ, Zinkernagel RM, Hengartner H. 1996. Decreased tumor surveillance in perforin-deficient mice. *The Journal of experimental medicine* **184**:1781–1790. doi:10.1084/jem.184.5.1781

Van Geel R, Wijdeven MA, Heesbeen R, Verkade JMM, Wasiel AA, Van Berkel SS, Van Delft FL. 2015. Chemoenzymatic Conjugation of Toxic Payloads to the Globally Conserved N-Glycan of Native mAbs Provides Homogeneous and Highly Efficacious Antibody–Drug Conjugates. *Bioconjugate Chem* **26**:2233–2242. doi:10.1021/acs.bioconjchem.5b00224

Venturelli E, Fabbro C, Chaloin O, Ménard-Moyon C, Smulski CR, Da Ros T, Kostarelos K, Prato M, Bianco A. 2011. Antibody Covalent Immobilization on Carbon Nanotubes and Assessment of Antigen Binding. *Small* **7**:2179–2187. doi:10.1002/smll.201100137

Verheul HMW, Jorna AS, Hoekman K, Broxterman HJ, Gebbink MFBG, Pinedo HM. 2000. Vascular endothelial growth factor–stimulated endothelial cells promote adhesion and activation of platelets. *Blood* **96**:4216–4221. doi:10.1182/blood.V96.13.4216

Vey E, Rodger C, Booth J, Claybourn M, Miller AF, Saiani A. 2011. Degradation kinetics of poly(lactic-co-glycolic) acid block copolymer cast films in phosphate buffer solution as revealed by infrared and Raman spectroscopies. *Polymer Degradation and Stability* **96**:1882–1889. doi:10.1016/j.polymdegradstab.2011.07.011

Villa CH, McDevitt MR, Escorcia FE, Rey DA, Bergkvist M, Batt CA, Scheinberg DA. 2008. Synthesis and Biodistribution of Oligonucleotide-Functionalized, Tumor-Targetable Carbon Nanotubes. *Nano Lett* **8**:4221–4228. doi:10.1021/nl801878d

Vitale M, Bottino C, Sivori S, Sanseverino L, Castriconi R, Marcenaro E, Augugliaro R, Moretta L, Moretta A. 1998. NKp44, a Novel Triggering Surface Molecule Specifically Expressed by Activated Natural Killer Cells, Is Involved in Non–Major Histocompatibility Complex–restricted Tumor Cell Lysis. *The Journal of Experimental Medicine* **187**:2065–2072. doi:10.1084/jem.187.12.2065

Vitale M, Falco M, Castriconi R, Parolini S, Zambello R, Semenzato G, Biassoni R, Bottino C, Moretta L, Moretta A. 2001. Identification of NKp80, a novel triggering molecule expressed by human NK cells. *Eur J Immunol* **31**:233–242. doi:10.1002/1521-4141(200101)31:1<233::AID-IMMU233>3.0.CO;2-4

Vivier E, Raulet DH, Moretta A, Caligiuri MA, Zitvogel L, Lanier LL, Yokoyama WM, Ugolini S. 2011. Innate or Adaptive Immunity? The Example of Natural Killer Cells. *Science* **331**:44–49. doi:10.1126/science.1198687

Vlodavsky I, Eldor A, Haimovitz-Friedman A, Matzner Y, Ishai-Michaeli R, Lider O, Naparstek Y, Cohen IR, Fuks Z. 1992. Expression of heparanase by platelets and circulating cells of the immune system: possible involvement in diapedesis and extravasation. *Invasion Metastasis* **12**:112–127.

Vogel CL, Cobleigh MA, Tripathy D, Gutheil JC, Harris LN, Fehrenbacher L, Slamon DJ, Murphy M, Novotny WF, Burchmore M, Shak S, Stewart SJ, Press M. 2002. Efficacy and Safety of Trastuzumab as a Single Agent in First-Line Treatment of *HER2* -Overexpressing Metastatic Breast Cancer. *JCO* **20**:719–726. doi:10.1200/JCO.2002.20.3.719

Vogelstein B, Papadopoulos N, Velculescu VE, Zhou S, Diaz LA, Kinzler KW. 2013. Cancer Genome Landscapes. *Science* **339**:1546–1558. doi:10.1126/science.1235122

Volpert OV, Dameron KM, Bouck N. 1997. Sequential development of an angiogenic phenotype by human fibroblasts progressing to tumorigenicity. *Oncogene* **14**:1495–1502. doi:10.1038/sj.onc.1200977

Volz J, Mammadova-Bach E, Gil-Pulido J, Nandigama R, Remer K, Sorokin L, Zernecke A, Abrams SI, Ergün S, Henke E, Nieswandt B. 2019. Inhibition of platelet GPVI induces intratumor hemorrhage and increases efficacy of chemotherapy in mice. *Blood* **133**:2696–2706. doi:10.1182/blood.2018877043

Von Hoff DD, Mita MM, Ramanathan RK, Weiss GJ, Mita AC, LoRusso PM, Burris HA, Hart LL, Low SC, Parsons DM, Zale SE, Summa JM, Youssoufian H, Sachdev JC. 2016. Phase I Study of PSMA-Targeted Docetaxel-Containing Nanoparticle BIND-014 in Patients with Advanced Solid Tumors. *Clinical Cancer Research* **22**:3157–3163. doi:10.1158/1078-0432.CCR-15-2548

Vyas YM, Mehta KM, Morgan M, Maniar H, Butros L, Jung S, Burkhardt JK, Dupont B. 2001. Spatial Organization of Signal Transduction Molecules in the NK Cell Immune Synapses During MHC Class I-Regulated Noncytolytic and Cytolytic Interactions. *The Journal of Immunology* **167**:4358–4367. doi:10.4049/jimmunol.167.8.4358

W

Walzer T, Dalod M, Robbins SH, Zitvogel L, Vivier E. 2005. Natural-killer cells and dendritic cells: “l’union fait la force.” *Blood* **106**:2252–2258. doi:10.1182/blood-2005-03-1154

Wang R, Stone RL, Kaelber JT, Rochat RH, Nick AM, Vijayan KV, Afshar-Kharghan V, Schmid MF, Dong J-F, Sood AK, Chiu W. 2015. Electron cryotomography reveals ultrastructure alterations in platelets from patients with ovarian cancer. *Proc Natl Acad Sci USA* **112**:14266–14271. doi:10.1073/pnas.1518628112

Wang T, Niu G, Kortylewski M, Burdelya L, Shain K, Zhang S, Bhattacharya R, Gabrilovich D, Heller R, Coppola D, Dalton W, Jove R, Pardoll D, Yu H. 2004. Regulation of the innate and adaptive immune responses by Stat-3 signaling in tumor cells. *Nat Med* **10**:48–54. doi:10.1038/nm976

Wang W, Guo H, Geng J, Zheng X, Wei H, Sun R, Tian Z. 2014. Tumor-released Galectin-3, a Soluble Inhibitory Ligand of Human NKp30, Plays an Important Role in Tumor Escape from NK Cell Attack. *Journal of Biological Chemistry* **289**:33311–33319. doi:10.1074/jbc.M114.603464

Wang X, Liu S, Sun Y, Yu X, Lee SM, Cheng Q, Wei T, Gong J, Robinson J, Zhang D, Lian X, Basak P, Siegwart DJ. 2023. Preparation of selective organ-targeting (SORT) lipid nanoparticles (LNPs) using multiple technical methods for tissue-specific mRNA delivery. *Nat Protoc* **18**:265–291. doi:10.1038/s41596-022-00755-x

Ward Y, Lake R, Faraji F, Sperger J, Martin P, Gilliard C, Ku KP, Rodems T, Niles D, Tillman H, Yin J, Hunter K, Sowalsky AG, Lang J, Kelly K. 2018. Platelets Promote Metastasis via Binding Tumor CD97 Leading to Bidirectional Signaling that Coordinates Transendothelial Migration. *Cell Reports* **23**:808–822. doi:10.1016/j.celrep.2018.03.092

Warren HS, Altin JG, Waldron JC, Kinnear BF, Parish CR. 1996. A carbohydrate structure associated with CD15 (Lewis x) on myeloid cells is a novel ligand for human CD2. *J Immunol* **156**:2866–2873.

Wei SC, Fattet L, Tsai JH, Guo Y, Pai VH, Majeski HE, Chen AC, Sah RL, Taylor SS, Engler AJ, Yang J. 2015. Matrix stiffness drives epithelial–mesenchymal transition and tumour metastasis through a TWIST1–G3BP2 mechanotransduction pathway. *Nat Cell Biol* **17**:678–688. doi:10.1038/ncb3157

Weigel C, Bellaci J, Spiegel S. 2023. Sphingosine-1-phosphate and its receptors in vascular endothelial and lymphatic barrier function. *Journal of Biological Chemistry* **299**:104775. doi:10.1016/j.jbc.2023.104775

Weinberg RA. 1995. The retinoblastoma protein and cell cycle control. *Cell* **81**:323–330. doi:10.1016/0092-8674(95)90385-2

Welte S, Kuttruff S, Waldhauer I, Steinle A. 2006. Mutual activation of natural killer cells and monocytes mediated by NKp80-AICL interaction. *Nat Immunol* **7**:1334–1342. doi:10.1038/ni1402

Wilhelm S, Tavares AJ, Dai Q, Ohta S, Audet J, Dvorak HF, Chan WCW. 2016. Analysis of nanoparticle delivery to tumours. *Nat Rev Mater* **1**:16014. doi:10.1038/natrevmats.2016.14

Winkelhake JL. 1977. Effects of chemical modification of antibodies on their clearance from the circulation. Addition of simple aliphatic compounds by reductive alkylation and carbodiimide-promoted amide formation. *J Biol Chem* **252**:1865–1868.

Wong JL, Berk E, Edwards RP, Kalinski P. 2013. IL-18–Primed Helper NK Cells Collaborate with Dendritic Cells to Promote Recruitment of Effector CD8+ T Cells to the Tumor Microenvironment. *Cancer Research* **73**:4653–4662. doi:10.1158/0008-5472.CAN-12-4366

Wong SY, Hynes RO. 2006. Lymphatic or Hematogenous Dissemination: How Does a Metastatic Tumor Cell Decide? *Cell Cycle* **5**:812–817. doi:10.4161/cc.5.8.2646

Woodward RB, Olofson RA, Mayer H. 1961. A NEW SYNTHESIS OF PEPTIDES. *J Am Chem Soc* **83**:1010–1012. doi:10.1021/ja01465a072

Wright WE, Pereira-Smith OM, Shay JW. 1989. Reversible Cellular Senescence: Implications for Immortalization of Normal Human Diploid Fibroblasts. *Molecular and Cellular Biology* **9**:3088–3092. doi:10.1128/mcb.9.7.3088-3092.1989

Wu S, Wu F, Chen X. 2022. Antibody-Incorporated Nanomedicines for Cancer Therapy. *Advanced Materials* **34**:2109210. doi:10.1002/adma.202109210

Wu W, Wieckowski S, Pastorin G, Benincasa M, Klumpp C, Briand J, Gennaro R, Prato M, Bianco A. 2005. Targeted Delivery of Amphotericin B to Cells by Using Functionalized Carbon Nanotubes. *Angew Chem Int Ed* **44**:6358–6362. doi:10.1002/anie.200501613

Wülfing C, Davis MM. 1998. A Receptor/Cytoskeletal Movement Triggered by Costimulation During T Cell Activation. *Science* **282**:2266–2269. doi:10.1126/science.282.5397.2266

X

Xiong G, Chen J, Zhang G, Wang S, Kawasaki K, Zhu J, Zhang Y, Nagata K, Li Z, Zhou BP, Xu R. 2020. Hsp47 promotes cancer metastasis by enhancing collagen-dependent cancer cell-platelet interaction. *Proc Natl Acad Sci USA* **117**:3748–3758. doi:10.1073/pnas.1911951117

Y

Yap ML, McFadyen JD, Wang X, Zia NA, Hohmann JD, Ziegler M, Yao Y, Pham A, Harris M, Donnelly PS, Hogarth PM, Pietersz GA, Lim B, Peter K. 2017. Targeting Activated Platelets: A Unique and Potentially Universal Approach for Cancer Imaging. *Theranostics* **7**:2565–2574. doi:10.7150/thno.19900

Yarchoan M, Hopkins A, Jaffee EM. 2017. Tumor Mutational Burden and Response Rate to PD-1 Inhibition. *N Engl J Med* **377**:2500–2501. doi:10.1056/NEJMc1713444

Ye Q-N, Zhu L, Liang J, Zhao D-K, Tian T-Y, Fan Y-N, Ye S-Y, Liu H, Huang X-Y, Cao Z-T, Shen S, Wang J. 2024. Orchestrating NK and T cells via tri-specific nano-antibodies for synergistic antitumor immunity. *Nat Commun* **15**:6211. doi:10.1038/s41467-024-50474-y

Yokosuka T, Takamatsu M, Kobayashi-Imanishi W, Hashimoto-Tane A, Azuma M, Saito T. 2012. Programmed cell death 1 forms negative costimulatory microclusters that directly inhibit T cell receptor signaling by recruiting phosphatase SHP2. *Journal of Experimental Medicine* **209**:1201–1217. doi:10.1084/jem.20112741

Yoshida K, Gowers KHC, Lee-Six H, Chandrasekharan DP, Coorens T, Maughan EF, Beal K, Menzies A, Millar FR, Anderson E, Clarke SE, Pennycuick A, Thakrar RM, Butler CR, Kakiuchi N, Hirano T, Hynds RE, Stratton MR, Martincorena I, Janes SM, Campbell PJ. 2020. Tobacco smoking and somatic mutations in human bronchial epithelium. *Nature* **578**:266–272. doi:10.1038/s41586-020-1961-1

Yoshimatsu K, Golijanin D, Paty PB, Soslow RA, Jakobsson PJ, DeLellis RA, Subbaramaiah K, Dannenberg AJ. 2001. Inducible microsomal prostaglandin E synthase is overexpressed in colorectal adenomas and cancer. *Clin Cancer Res* **7**:3971–3976.

Yu L-X, Yan L, Yang W, Wu F-Q, Ling Y, Chen S-Z, Tang L, Tan Y-X, Cao D, Wu M-C, Yan H-X, Wang H-Y. 2014. Platelets promote tumour metastasis via interaction between TLR4 and tumour cell-released high-mobility group box1 protein. *Nat Commun* **5**:5256. doi:10.1038/ncomms6256

Yu M, Bardia A, Wittner BS, Stott SL, Smas ME, Ting DT, Isakoff SJ, Ciciliano JC, Wells MN, Shah AM, Concannon KF, Donaldson MC, Sequist LV, Brachtel E, Sgroi D, Baselga J, Ramaswamy S, Toner M, Haber DA, Maheswaran S. 2013. Circulating Breast Tumor Cells Exhibit Dynamic Changes in Epithelial and Mesenchymal Composition. *Science* **339**:580–584. doi:10.1126/science.1228522

Z

Zamora C, Cantó E, Nieto JC, Bardina J, Diaz-Torné C, Moya P, Magallares B, Ortiz MA, Julià G, Juarez C, Llobet JM, Vidal S. 2017. Binding of Platelets to Lymphocytes: A Potential Anti-Inflammatory Therapy in Rheumatoid Arthritis. *The Journal of Immunology* **198**:3099–3108. doi:10.4049/jimmunol.1601708

Zaslavsky AB, Gloeckner-Kalousek A, Adams M, Putluri N, Venghatakrishnan H, Li H, Morgan TM, Feng FY, Tewari M, Sreekumar A, Palapattu GS. 2015. Platelet-Synthesized Testosterone in Men with Prostate Cancer Induces Androgen Receptor Signaling. *Neoplasia* **17**:490–496. doi:10.1016/j.neo.2015.05.003

Zelenay S, van der Veen AG, Böttcher JP, Snelgrove KJ, Rogers N, Acton SE, Chakravarty P, Girotti MR, Marais R, Quezada SA, Sahai E, Reis e Sousa C. 2015. Cyclooxygenase-Dependent Tumor Growth through Evasion of Immunity. *Cell* **162**:1257–1270. doi:10.1016/j.cell.2015.08.015

Zhang AL, Colmenero P, Purath U, Teixeira De Matos C, Hueber W, Klareskog L, Tarner IH, Engleman EG, Söderström K. 2007. Natural killer cells trigger differentiation of monocytes into dendritic cells. *Blood* **110**:2484–2493. doi:10.1182/blood-2007-02-076364

Zhang G, Han J, Welch EJ, Ye RD, Voyno-Yasenetskaya TA, Malik AB, Du X, Li Z. 2009. Lipopolysaccharide Stimulates Platelet Secretion and Potentiates Platelet Aggregation via TLR4/MyD88 and the cGMP-Dependent Protein Kinase Pathway. *The Journal of Immunology* **182**:7997–8004. doi:10.4049/jimmunol.0802884

Zhang W, Zhou H, Li H, Mou H, Yinwang E, Xue Y, Wang S, Zhang Y, Wang Z, Chen T, Sun H, Wang F, Zhang J, Chai X, Chen S, Li B, Zhang C, Gao J, Ye Z. 2023. Cancer cells reprogram to metastatic state through the acquisition of platelet mitochondria. *Cell Reports* **42**:113147. doi:10.1016/j.celrep.2023.113147

Zhang Y, Cedervall J, Hamidi A, Herre M, Viitaniemi K, D'Amico G, Miao Z, Unnithan RVM, Vaccaro A, Van Hooren L, Georganaki M, Thulin Å, Qiao Q, Andrae J, Siegbahn A, Heldin C-H, Alitalo K, Betsholtz C, Dimberg A, Olsson A-K. 2020. Platelet-Specific PDGFB Ablation Impairs Tumor Vessel Integrity and Promotes Metastasis. *Cancer Research* **80**:3345–3358. doi:10.1158/0008-5472.CAN-19-3533

Zhang Y, Manouchehri Doulabi E, Herre M, Cedervall J, Qiao Q, Miao Z, Hamidi A, Hellman L, Kamali-Moghaddam M, Olsson A-K. 2022. Platelet-Derived PDGFB Promotes Recruitment of Cancer-Associated Fibroblasts, Deposition of Extracellular Matrix and Tgfβ Signaling in the Tumor Microenvironment. *Cancers* **14**:1947. doi:10.3390/cancers14081947

Bibliography

Zhang Y, Unnithan RVM, Hamidi A, Caja L, Saupe F, Moustakas A, Cedervall J, Olsson A-K. 2019. TANK-binding kinase 1 is a mediator of platelet-induced EMT in mammary carcinoma cells. *FASEB j* **33**:7822–7832. doi:10.1096/fj.201801936RRR

Zhou L, Wu D, Zhou Y, Wang D, Fu H, Huang Q, Qin G, Chen J, Lv J, Lai S, Zhang H, Tang K, Ma J, Fiskesund R, Zhang Y, Zhang X, Huang B. 2023. Tumor cell-released kynurenine biases MEP differentiation into megakaryocytes in individuals with cancer by activating AhR–RUNX1. *Nat Immunol* **24**:2042–2052. doi:10.1038/s41590-023-01662-3

Zhou M, Feng Y, Zhang X, Chen J, Yao N, Fu S, Ni T, Chen Y, Xie F, Roy S, Liu J, Yang Y, He Y, Zhao Y, Yang N. 2024. Platelet-derived microparticles adoptively transfer integrin β3 to promote antitumor effect of tumor-infiltrating T cells. *OncoImmunology* **13**:2304963. doi:10.1080/2162402X.2024.2304963

Zhou Y, Drummond DC, Zou H, Hayes ME, Adams GP, Kirpotin DB, Marks JD. 2007. Impact of Single-chain Fv Antibody Fragment Affinity on Nanoparticle Targeting of Epidermal Growth Factor Receptor-expressing Tumor Cells. *Journal of Molecular Biology* **371**:934–947. doi:10.1016/j.jmb.2007.05.011

Zhu C, Anderson AC, Schubart A, Xiong H, Imitola J, Khoury SJ, Zheng XX, Strom TB, Kuchroo VK. 2005. The Tim-3 ligand galectin-9 negatively regulates T helper type 1 immunity. *Nat Immunol* **6**:1245–1252. doi:10.1038/ni1271

Zhu J, Xiong G, Fu H, Evers BM, Zhou BP, Xu R. 2015. Chaperone Hsp47 Drives Malignant Growth and Invasion by Modulating an ECM Gene Network. *Cancer Research* **75**:1580–1591. doi:10.1158/0008-5472.CAN-14-1027

Zulueta-Coarasa T, Fadul J, Ahmed M, Rosenblatt J. 2022. Physical confinement promotes mesenchymal trans-differentiation of invading transformed cells in vivo. *iScience* **25**:105330. doi:10.1016/j.isci.2022.105330

Zuo X, Yang Y, Zhang Y, Zhang Z, Wang X, Shi Y. 2019. Platelets promote breast cancer cell MCF-7 metastasis by direct interaction: surface integrin α2β1-contacting-mediated activation of Wnt-β-catenin pathway. *Cell Commun Signal* **17**:142. doi:10.1186/s12964-019-0464-x

ANNEXES

Annex 1 – Platelets: tailoring metastasis treatment.

This invited review in *Trends in Cancer* aims to summarize recent understanding of how platelets shape metastasis with a particular focus on platelet-mediated immunomodulation. This review also discusses platelet-borne molecular targets that could represent new avenues for therapeutically targeting platelets contribution to metastasis. I wrote this review based on the Chapter I of my PhD manuscript in collaboration with the laboratory of Pierre Mangin (INSERM UMR_S1255, Etablissement Français du Sang-Alsace).

Annex 2 – Depletion of all platelet integrins impacts hemostasis, thrombosis and tumor metastasis.

This project in collaboration with the laboratory of Pierre Mangin (INSERM UMR_S1255, Etablissement Français du Sang-Alsace) aims to decipher the additive effect of β1/β3 integrins in platelet-mediated cancer progression. For this study, I performed platelets binding to TCs and tumor-infiltrating lymphocytes immunophenotyping.

Annex 3 – Anti-BCMA immuno-nanoPET radiotracers for improved detection of multiple myeloma.

This project aims to improve sensitivity of immuno-nanoPET radiotracers to detect tumor cells by conjugating BCMA-targeted silica-based gadolinium NPs with NODAGA chelators for ^{64}Cu labeling. For this study, I performed revision experiments to assess anti-BCMA antibody binding capacities post-conjugation on the NPs.

Annex 4 – Reinforced polymer–nanoparticle hydrogels for subcutaneous and sustained delivery of trastuzumab.

This project in collaboration with the laboratory of Mark Tibbitt (Macromolecular Engineering Laboratory, Department of Mechanical and Process Engineering, ETH Zurich) aims to develop reinforced polymer-nanoparticle hydrogels for subcutaneous prolonged release of trastuzumab to improve patient's quality of life. For this study, I followed trastuzumab bioactivity upon release for the hydrogel.

1. Platelets: tailoring metastasis treatment

Platelets: tailoring metastasis treatment

Vincent Mittelheisser[1-5,*], Cristina Liboni[1-5,*], Silvia Maria Grazia Trivigno[3,6,*], Olivier Lefebvre[1-5], Pierre H. Mangin[3,6,§], and Jacky G. Goetz[1-5,§]

[1]Tumor Biomechanics lab

[2]INSERM UMR_S1109, Strasbourg, France.

[3] Université de Strasbourg, Strasbourg, France.

[4] Fédération de Médecine Translationnelle de Strasbourg (FMTS), Strasbourg, France.

[5] Equipe Labellisée Ligue Contre le Cancer.

[6] UMR_S1255, INSERM, Etablissement Français du Sang-Alsace.

*** Equal contribution:**

VM, CL and SMGT and have contributed equally.

§ Correspondence:

Pierre Mangin, Pierre.Mangin@efs.sante.fr

UMR-S1255, INSERM, Etablissement Français du Sang-Alsace, Université de Strasbourg, F-67000, France.

Jacky G. Goetz, jacky.goetz@inserm.fr

INSERM UMR_S1109, Tumor Biomechanics Lab, Centre de Recherche en Biomédecine de Strasbourg (CRBS), , 67000 Strasbourg, France.

Web: www.goetzlab.fr

Abstract

The dreadful liaison between platelets and tumor cells has been discovered half a century ago. Since then, a plethora of studies have characterized the contribution of platelets to primary tumor development, survival of circulating tumor cells in the bloodstream, and metastatic seeding and outgrowth. Yet, while these provided a deep understanding of how platelets shape cancer progression, the field suffers from a lack of additional knowledge required to design efficient therapeutic strategies. Here, we aim to summarize recent discoveries that identify new ways by which platelets shape metastasis beyond their initial intravascular role. Doing so, we will further discuss platelet-borne molecular targets that could represent new avenues for therapeutically targeting platelets contribution to metastasis.

Keywords

Platelets, tumor, metastasis, therapy

Introduction

Successful tumor progression is a complex journey which requires tumor cells (TCs) to indoctrinate the tumor microenvironment (TME) and body fluids components by recruiting and reprogramming non-malignant cells. Among them, platelets have been one of the first non-tumoral component whose relevance in cancer pathology was highlighted. Back in 1968, Gasic and collaborators [1] reported that a reduction in platelet count decreases the colonization of TCs to the lungs. From that time on, many reports have described the contribution of platelets to the intravascular phase of the metastatic cascade. Indeed, platelets react quickly to TCs intravasation and are vital to maintain their survival by protecting circulating TCs (CTCs) from the deleterious effects of shear stress and by avoiding their recognition and destruction by innate immune cells, particularly NK cells [2]. Despite their well-recognized role in the bloodstream, platelets additionally contribute to cancer progression also in extra vascular compartments. Indeed, platelets were described to populate primary and metastatic tumor sites where they promote TCs' fitness and finely tune the TME both through cell-cell contact mechanisms and the secretion of soluble factors [2]. Overall, improving our understanding of how and where platelets shape the TME would help to identify specific druggable targets, exploitable from a pharmacological point-of-view, to counteract cancer progression. Here, we will discuss recent studies examining the role of platelets in the primary and metastatic tumor microenvironment, focusing on their contributions to TCs outgrowth, their ability to reshape the TME, and the identification of useful targets for tailoring future therapies.

Platelets populate primary and secondary tumor sites

Platelets are small non-nucleated cells which represent the most abundant blood component after erythrocytes. Hundreds of billions of platelets are produced daily from bone marrow megakaryocytes [3] in order to fulfill their role as guardians against spontaneous bleeding, and to arrest bleeding in case of a vascular breach. Interestingly, TCs can hijack platelet production through a paracrine circuit of thrombopoietic factors released from the primary tumor. As a matter of fact, primary tumors may enhance thrombopoiesis in a thrombopoietin (TPO)-dependent or independent manner (via CCL5, GM-CSF, PF4 or kynurenine) thereby causing

paraneoplastic thrombocytosis, which can be an indicator of overt or occult malignancies [2], [4].

Once produced, platelets circulate in the bloodstream in a quiescent state, mainly locating close to the vessel wall (platelet margination), without adhering to it or being activated since the intact endothelium is a non-thrombogenic surface [5]. Platelet activation is triggered by thrombogenic signals transduced by a plethora of receptors. Such inputs are often physiological but may additionally derive from several pathological contexts including thrombosis, inflammation, and cancer. In fact, once solid tumors reach a critical size, they require increased vascularization to meet their oxygen and nutrient requirements. To that end, TCs release pro-angiogenic factors, such as the VEGF, that activate endothelial cells which in turn upregulate, among the others, the expression of von Willebrand Factor (vWF), P-selectin, integrin $\alpha_V\beta_3$ and tissue factor (TF), thus triggering the local recruitment of platelets at the tumor site [5]. Remarkably, intravital microscopy (IVM) experiments show that platelets roll along the endothelium and adhere to the endothelial surface of peritumoral and intratumoral aberrant vessels [6]. Platelet interactions with the endothelial wall engage integrin activation and initiate extravasation from adjacent vessels and subsequent infiltration within the primary TME, notably via pathways mediated by the focal adhesion kinase (FAK), the CX3C chemokine receptor 1 (CX3CR1) or the G protein-coupled receptors (GPCRs) Gαi and Gα13 [7], [8].

Newly formed tumor vessels are also a way for TCs to access the systemic circulation. Interestingly, it was shown that, at the tumor site, platelets promote this process by directly binding and supporting TCs epithelial-to-mesenchymal transition (EMT) [7]. Once in the bloodstream, circulating platelets interact with CTCs, supporting their survival and dissemination to secondary sites, as extensively studied in the past. Nevertheless, whether the interaction between platelets and TCs is equal (in terms of number of interacting platelets) and stable among TC types and patients has never been investigated before. Only recently it was shown that platelets binding is heterogenous among metastatic TCs [9] and thus likely among CTCs within a single individual. This inter-individual heterogeneity in platelet binding was further highlighted in a recent study showing that a high-fat diet and elevated body mass index reinforce platelet-TC interactions and subsequent TCs homing and metastasis by inducing fibronectin overexpression in both platelets and endothelial cells [10]. While high-

platelet binding TCs heavily rely on platelets for their metastatic dissemination, low-platelet binding TCs benefit of their contribution once metastases are already formed. Indeed, platelets efficiently colonize metastatic foci, in both murine and human samples and favor the outgrowth of established metastases [9].

While more work is needed to fully understand platelets' role into primary and secondary lesions (*i.e.*, how platelets populate metastatic foci), their contribution throughout all stages of the metastatic cascade is pivotal to sustain TCs growth, CTCs dissemination and metastatic outgrowth.

Platelets engage an intricated crosstalk within the TME

At the molecular level, platelets are activated within both primary and metastatic TME through direct contact with TCs via galectin-3-glycoprotein VI (GPVI), ADAM9-integrin $\alpha_6\beta_1$, and podoplanin (PDPN)-CLEC-2 interactions [11], [12], [13]. Additionally, TC-secreted platelet agonists (*e.g.*, ADP, IgG or HMGB1) and extracellular vesicles (EVs) also contribute to this process in a paracrine manner [2], [14], [15]. While fundamental mechanisms of platelet binding to TC are well understood, the molecular determinants controlling the efficiency of binding of platelets to TCs has remained unclear. In this regard, building on the observation that the binding of platelets varies between TCs [9], CD24 was identified as a new molecular rheostat of platelet binding to tumor cells and their subsequent pro-metastatic function. CD24 is known to bind platelet P-selectin, among multiple other functions [16].

Upon activation during interactions with TCs, platelets release α-granules-stored factors (*e.g.*, EGF, VEGF or TGFβ) that stimulate TCs growth and EMT (**Figure 1**). Furthermore, activated platelets are also able to release platelet-EVs (PEVs) containing mitochondria, microRNAs, cytokines and proteins [17], [18], [19], [20]. These components could subsequently be transferred to TCs, endowing their proliferation, metabolic fitness, resistance to chemotherapies and metastasis. PEVs can also functionally reprogram hematopoietic cells and foster megakaryopoiesis [21]. Beyond promoting tumor progression in a paracrine manner through their releasates, several studies show that platelets also significantly impact TCs behavior by direct interacting with them. Amongst, platelets $\beta1$ ($\alpha_2\beta_1$, $\alpha_5\beta_1$ and $\alpha_6\beta_1$) and $\beta3$ ($\alpha_{IIb}\beta_3$ and $\alpha_v\beta_3$) integrins attend direct interaction between TCs and platelets, thus regulating

platelet-dependent support of tumor development [22]. In accordance, another study shows that platelets binding via integrin $\alpha_2\beta_1$ activates downstream Wnt/β-catenin pathway, endowing TCs EMT phenotype [23]. Furthermore, direct platelet-TC interactions also stimulate the secretion of matrix metalloproteinases (MMPs) from TCs, enabling their escape from the primary site and invasion into the peripheral blood circulation [24] (**Figure 1**). Strikingly, other reports reveal that TCs can internalize platelets or platelet-derived organelles through direct contact, facilitating the transfer of RNA, proteins or lipids [24], [25], [26], [27]. In this context, platelet-derived mitochondria enhance TCs metabolic fitness by increasing cellular respiration and decreasing oxidative stress [25]. Moreover, platelets uptake also allow TCs to access to the complete and undiluted platelet proteome, transcriptome, and secretome [27]. This mechanism is of pivotal importance during the hematogenous phase of metastasis when platelets' receptors recycled at TCs surface facilitate adhesion to the endothelium at secondary sites, potentially enhancing their metastatic abilities [26].

Reciprocally, platelets are also modified by their interaction with TCs, in a feed-forward exchange. Interestingly, this systemic effect can affect the megakaryocytic lineage at the level of the bone marrow, with cancer-induced alterations that can be inherited onto their platelet progeny [28] [29], [30]. Consequently, platelets undergo qualitative changes, displaying elevated levels of pro-inflammatory mRNA and proteins (*e.g.*, Ctsg, Lcn2, S100a8, S100a9) [28] and expressing immune checkpoints like GITRL, RANKL PD-1/PD-L1 and CD155, which, in feedback, promote tumor metastasis [29], [30], [31], [32]. Additionally, TC-secreted factors such as EVs are also taken up by circulating platelets resulting in altered platelet mRNA profiles including the transfer of tumoral mRNA markers to platelets [33], [34]. Building on these findings, several prospective clinical trials highlight the potential of platelets mRNA sequencing as a diagnostic tool, demonstrating its ability to distinguish cancer patients from healthy individuals with >90% specificity [35], [36], [37], [38]. Interestingly, the normalization of the platelet transcriptome following surgical tumor resection underlines the potential of platelets mRNA sequencing to not only diagnose cancer but also monitor the effectiveness of treatment and detect disease recurrence [33].

Primary solid tumors are composed not only of TCs but also of a myriad of supportive cells collectively defined as the TME. This comprises a rich diversity of immune cells, cancer-associated fibroblasts (CAFs) and endothelial cells. Given their

multifaced functions within the TME, it is not surprising that platelets can also interact with non-neoplastic cells, thereby further promoting tumor outgrowth. Notably, platelets critically influence the cancer angiogenesis nexus. By releasing α-granules-stored VEGF and PDGF, platelets stimulate alternative pro-angiogenic signaling and promote the proliferation of endothelial cells [39] (**Figure 1**) as well as the recruitment of pericytes [40] and endothelial precursors [41]. In addition of fostering tumor neo-vascularization and preserving vascular integrity, platelets have been implicated in resistance to anti-angiogenic therapies, including such as the anti-VEGF antibody bevacizumab and the VEGFR/PDGFR tyrosine kinase inhibitor sunitinib. Yet, the precise mechanisms by which platelets contribute to this resistance remain only sparsely explored. Potentially, such resistance may be mediated by the substantial repertoire of factors secreted or receptors expressed by platelets. For instance, platelet-derived VEGF and PDGFR might function as sink for bevacizumab and sunitinib, thereby reducing their bioavailability [42], [43], [44]. Furthermore, α-granules-stored bFGF may act as an alternative pro-angiogenic driver [45], bypassing VEGF signaling inhibition by bevacizumab. Beyond angiogenesis, platelets can interact with PDPN-expressing CAFs via CLEC-2 [46], [47], [48]. This interaction induces platelets activation, aggregation and α-granules-stored PDGFB secretion [47], [48]. In turn, secreted PDGFB recruit CAFs and enhance ECM molecules fibronectin and collagen I deposition, hence restricting immune cell infiltration [48] (**Figure 1**). Another study reports that platelets also induce mesothelial cells activation in human cancer settings thereby inducing ECM molecules deposition [49]. Besides, platelets are capable of direct ECM reorganization by driving fibronectin fibrillogenesis *in vitro* via integrin $\alpha_{IIb}\beta_3$ [50] and are thus likely to shape structural elements of the TME.

While the contribution of platelets within the TME is wide and involves several non-tumoral components, many aspects of platelets role within the TME remain to be elucidated, including a precise definition of how the platelets' transcriptome and proteome tumor-driven evolution sustain TCs fitness.

Platelets compromise anti-tumor immune response

Following their recruitment into the TME, platelets can modulate the immune response by impacting already infiltrated or co-infiltrating immune cells. In this line, it

was recently demonstrated, through bulk RNA sequencing of a metastatic TME, that platelets GPVI profoundly shapes the immune TME by enhancing the expression of immune checkpoints and by suppressing immune cells infiltration [9]. Interestingly, intravascular interaction between platelets and CTCs already tunes the immune TME of subsequently formed metastases. Indeed, two independent works have demonstrated that platelet-TC interactions, through CD24, can affect accumulation of neutrophils and T and B cells in metastasis foci formed [16], [51].

Platelets play a pivotal role in modulating various components of the tumor immune microenvironment, interacting with the immune responses at multiple levels. Activated platelets secrete several immunosuppressive factors such as TGFβ, lactate and platelet factor 4 (PF4 or CXCL4), which constrain the function of cytotoxic T cells and spoil bispecific antibodies-mediated T cell anti-tumor responses [52], [53], [54] (**Figure 1**). A recent study highlighted that platelet-secreted thromboxane A_2 (TxA_2) suppresses anti-metastatic immune responses by restricting T cell activation and proliferation in response to T cell receptor (TCR) signaling through a T cell-intrinsic immunosuppressive pathway dependent on the guanine exchange factor ARHGEF1 [55]. Platelet releasates further amplify the differentiation of $CD4^+$ T cells towards a regulatory phenotype [56]. During their activation by TCs, platelets also release PEVs that reduce T cells migration and potentiate their calcium-induced apoptosis [57]. Activated platelets secretome also impair NK cells cytotoxic functions against their prototypical K562 leukemic target [56]. In addition to influencing immune responses through soluble factors, platelets can directly interact with T cells via P-selectin, integrin $\alpha_{IIb}\beta_3$, TREM-like transcript 1 protein (TLT-1), or CD40L [58], [59], leading to suppression of $CD8^+$ T cell responses [59], [60] and instructing regulatory T cells to release immunosuppressive mediators [61]. Platelets not only weaken T cell responses within the primary immune TME but also affect the myeloid compartment. Activated platelets secretome and PEVs drive the generation of myeloid-derived suppressor cells (MDSCs) [62], [63] and promote the polarization of macrophages towards an M2 immunosuppressive/pro-fibrotic phenotype [61], [64], [65], [66] (**Figure 1**). Altogether, platelet-modulated immunosuppressive myeloid cells ultimately subvert T cells functions within the TME. Additionally, platelets also directly bind to myeloid cells, with functional outcomes varying depending on cell type. On one hand, platelets binding to monocytes suppresses their development in functional dendritic cells (DCs)

[67], [68], or promote the induction of tolerogenic DCs via the secretion of Dickkopf-1(DKK1) [69]. On the other hand, TC-activated platelets are crucial for recruiting and activating neutrophils at the early metastatic nice [70]. Platelet-triggered neutrophil activation induces the formation of neutrophil extracellular traps (NETs) [58], which are well-established promoters of cancer progression [59]. Interestingly, when forming aggregates with platelets, neutrophils display a distinct transcriptomic profile marked by enhanced activation and chemotaxis, which has been linked to a poor prognosis in patients [73]. A recent study further emphasizes the key role of platelets in the establishment of the early metastatic nice. Specifically, during lung metastasis formation, TC-reprogrammed interstitial macrophages secrete integrin $\alpha_X\beta_2$-bearing EVs that activate platelets through their GPIb receptor [74]. This interaction contributes to the formation of a pro-thrombotic niche and promotes metastasis formation, likely by facilitating TC arrest within the lung vasculature. Altogether, this suggests that the interaction of platelets with immune cells might trigger distinct changes which might be worth exploring for prognostic and diagnostic purposes.

Platelets also influence anti-tumoral responses by modulating the immune checkpoint landscape within the TME, as a result of complex interactions between platelets and TCs. Platelets promote immune checkpoint expression in TCs by releasing their α- and δ-granules contents [75], [76], [77] while TCs educate platelets by enhancing immune checkpoint expression (*e.g.*, PD-L1, RANKL and GITRL) during platelet production [6], [29], [30]. TCs can also directly transfer PD-L1 proteins to platelets in a fibronectin-integrin $\alpha_5\beta_1$-GPIbα-dependent manner within the TME [78], [79]. Platelet-expressed immune checkpoints contribute to global immunosuppression in the TME, fostering pro-tumorigenic myeloid immune responses and inhibiting cytotoxic $CD8^+$ T cells activity [6], [30], [78], [79], [80] (**Figure 1**). Interestingly, platelet PD-L1 expression has been shown to outperform standard histological PD-L1 quantification in predicting responses to immune checkpoint inhibitors in non-small cell lung cancer [79], [81], [82] and colorectal cancer [78]. Clinical reports further support this notion by showing a reduction in platelet PD-L1 expression following immune checkpoint blockade (ICB) therapy. In contrast, other clinical reports highlight that intra-tumoral megakaryocytes infiltration predicts unfavorable prognosis in clear cell renal cell carcinoma [83] and non-small cell lung cancer [84]. More recent studies suggest that intra-tumoral megakaryocytes impair the adaptive immune response by

suppressing DC activation and promoting T cell exhaustion [31], [85]. Taken together, megakaryocytes and platelets show promise as biomarkers for monitoring responses to immunotherapy [86]. Beyond serving as biomarkers, platelets were also successfully weaponized to deliver anti-PD-L1 antibodies or chemotherapeutic drugs directly to the TME (**Text Box 1**), thus offering novel avenues to enhance the precision and efficacy of cancer immunotherapies.

It is worth mentioning that most of the reports underpinning the immunosuppressive functions of platelets focus on breast and lung cancers. In different contexts (such as hepatocellular carcinomas), it was reported that platelets suppress liver tumor growth via activating $CD8^+$ T cells through $P2Y_{12}$-dependent CD40L release or β3 integrins transfer to T cells [87], [88]. Additional work further validates differences in platelet-driven immune response modulation between triple negative breast cancer (TNBC) and melanoma [89]. Similarly, while *in vivo* interactions between platelets and myeloid cells induce tolerogenic DCs, their *in vitro* interactions promote cross-presentating DCs through platelet P-selectin engagement of monocyte PSGL-1 [90], [91]. This suggests that platelets' impact on the immune TME, and its subsequent functions, might be cancer type- as well as microenvironment-dependent and warrants further case-by-case investigation.

Antiplatelet agents in cancer therapy

Given the broad implications of platelets at each step of the cancer dissemination and during later metastatic outgrowth, the use of anti-platelet strategies to hamper cancer progression seems a highly appealing approach. Notably, anti-platelet drugs not only reduce the metastatic potential of TCs but also significantly enhance responses to chemotherapy [92], [93], ICB therapies [78], [94], [95], and adoptive cell transfer efficacy [52]. In support of this, preliminary pre-clinical studies on the repurposing of clinically available anti-platelet agents such as cyclooxygenase (COX) inhibitors (*i.e.*, aspirin) [96], purinergic $P2Y_{12}$ receptor antagonists (*e.g.*, clopidogrel or ticagrelor) [97], phosphodiesterase (PDE) inhibitors (*e.g.*, cilostazol or dipyridamole) [98], or integrin $\alpha_{IIb}\beta_3$ antagonists (*e.g.*, abciximab or eptifibatide) [99] have shown promising results in preventing cancer progression in mouse tumor models (**Figure 2**). The recent additional demonstration that aspirin-mediated COX

inhibition reinvigorates anti-metastatic adaptive immune response by alleviating TxA_2-mediated T cell suppression paves the way for more effective anti-metastatic immunotherapies. Related meta-analyses reveal that patients taking daily aspirin for vascular event prevention present a reduced incidence of multisite metastasis [100] in particular when the TCs express HLA class I antigens [101]. Building on these observations and on the role of platelets in modulating the immune system, ongoing clinical trials (NCT06554535, NCT04188119) are evaluating whether antiplatelet agents can prime towards a better response to ICB therapies. Encouragingly, completed clinical trials on small patient cohorts testing antiplatelet agents alongside immune checkpoint inhibitors resulted in improved therapeutic responses in head and neck squamous cell carcinoma (NCT03245489), in melanoma [102] and in colorectal cancer [78].

While associating anti-platelet agents to ICB therapies gave promising results, currently on-going clinical trials primarily focus on high-dose aspirin (>300 mg/day). This dosage irreversibly inactivates COX-2 in nucleated cells, leading to an on-target, off-platelet effect [103]. As a result, COX-2 inhibition reduces PGE_2 levels in the TME, thereby mitigating immunosuppression [94]. This effect, however, may introduce a confounding factor when evaluating the synergy between aspirin treatment and ICB therapies. Additionally, a recent single-center retrospective study found that anti-platelet drugs, such as aspirin, may increase the risk of checkpoint inhibitor-related pneumonitis in advanced cancer patients [104]. Furthermore, epidemiological studies have identified a dose-dependent relationship between aspirin use and the incidence of adverse events, including gastrointestinal toxicity, an increased risk of subarachnoid hemorrhage, and renal dysfunction [103], [105]. These risks limit the routine use of anti-platelet agents in oncologic care. Consequently, identifying specific platelet receptors that can be targeted without adverse or off-platelet effects could open new therapeutic avenues (**Figure 2**) [106].

Among them, P-selectin has been regarded as a prominent druggable target, due to its ability to bind to several tumor receptors (namely CD24, CD44, PSGL-1). Indeed, inhibiting P-selectin by heparin damps platelet-TC interactions, thereby attenuating metastasis. In this regard, innovative heparin-like molecules for antimetastatic therapy are being developed with little impact on bleeding. Low anticoagulant heparin (LA-hep) and propylene glycol alginate sodium sulfate (PSS)

showed a remarkable capacity to inhibit primary tumor growth and metastatic dissemination *in vivo*, with only mild effects on bleeding [107], [108] (**Figure 2**). Within the same receptor family, CLEC-2 binding to PDPN-expressing TCs promote melanoma pulmonary metastasis [13]. Some agents have been found to be effective in inhibiting the PDPN-CLEC-2 axis and metastasis formation *in vivo*, such as the 5-nitrobenzoate (2CP), the recombinant rhodocytin, and the cobalt hematoporphyrin (co-HP) (**Figure 2**) [109], [110], [111]. While P-selectin and CLEC-2 are promising antimetastatic therapy targets, they are not exclusively expressed by platelets, impinging that the observed efficacy may not be solely due to their targeting.

To better understand the impact of platelet targeting on therapeutic outcomes, several studies have focused on receptors selectively expressed on platelet surfaces, such as glycoproteins Ibα (GPIbα) and VI (GPVI). While the role of GPIbα in cancer progression remains debated, the novel anti-human GPIbα monoclonal antibody YQ3 has been shown to reduce metastasis formation by targeting the vWF-GPIbα axis, without significantly affecting platelet count or causing severe bleeding complications [112], [113] (**Figure 2**). As another key target, GPVI is one of the most promising platelet-related candidates for cancer treatment due to its role in promoting cancer progression [9], [12] and its minimal involvement in hemostasis, making its targeting less likely to disrupt platelet count or cause severe bleeding complications [114], [115]. Therefore, anti-GPVI therapies offer a potentially safe therapeutic option, particularly for late-stage malignancies, where GPVI-dependent mechanisms contribute to chemoresistance and support metastatic growth [9], [12], [92]. Among the developed anti-GPVI therapies, glenzocimab (ACT017) stands out as one of the most exciting compounds [116]. This humanized anti-GPVI antibody Fab fragment, developed by Acticor Biotech (Paris, France), has been evaluated in clinical trials for acute ischemic stroke (NCT05559398, NCT06437431) in more than 800 patients, with no bleeding events reported, thereby highlighting its favorable safety profile [92], [116], [117] (**Figure 2**). Glenzocimab was recently investigated in preclinical studies, demonstrating its therapeutic potential in impairing melanoma metastatic outgrowth in the lungs without inducing collateral hemostatic perturbations [9]. Interestingly, GPVI pharmacological blockade also promotes intratumoral lymphocyte accumulation and reduces immune checkpoint expression [6]. We observe similar effects of GPVI in immune regulation using a GPVI knock-out mouse model [9]. While glenzocimab

shows great potential, its very short half-life (≈ 10 hours) makes its use as an anti-metastatic strategy impractical [118]. Given this pharmacokinetic limitation, there is a clear need for additional drugs. One could speculate that anti-GPVI antibody Fab fragment EMA601 [119] and the anti-GPVI nanobody Nb2 [117] would have very similar pharmacokinetic issues than glenzocimab, and that increasing anti-GPVI agents half-life to allow a chronic treatment might represent a very promising pharmacological strategy to hamper tumor metastasis. Interestingly, GPVI-blocking agents also exhibit effects beyond platelet-TC interactions. In mouse models of prostate and breast cancer, pharmacological blocking of GPVI caused severe intratumoral hemorrhage by disrupting vessel integrity, thereby enhancing chemotherapeutic drug accumulation in tumors [92]. In conclusion, targeting GPVI holds significant promise as a therapeutic strategy for cancer treatment by reducing metastatic outgrowth, modulating immune responses and improving chemotherapy accumulation. The development and clinical testing of anti-GPVI compounds alone or in combination therapy could offer a safe and effective means to combat metastasis without disrupting normal hemostasis, advancing the field of cancer therapeutics.

Despite their potential effectiveness in cancer treatment, the identification of novel antiplatelet druggable targets is currently on hold. While more studies in this field are highly needed, additional drug screening platforms might also contribute to this campaign. In this line, a recent study developed an ultra-high throughput screening platform to compare inhibitors of platelets' activation [120]. By following platelet Ca^{2+} responses induced by 16,635 chemically diverse small molecules, the authors validate 3 hit compounds hence demonstrating the ability of this ultra-high throughput-based screening to identify anti-platelets drugs [120].

Concluding remarks and future perspectives

Platelets contribution to tumor progression has been widely addressed in the past decades. Historically, platelets have been recognized for their ability to bind to CTCs, while only recently it was demonstrated that not all tumor cells equally interact with platelets in the bloodstream [9]. In addition, it was shown that platelets are able to populate primary [2] and metastatic sites [9]. More work is needed to determine the exact mechanisms by which platelets infiltrate these sites and their origin (see

outstanding questions **– Text Box 2**). This can be achieved by tracing the temporal dynamics of multi-step platelet recruitment owning to the recently developed *in vivo* platelets pulse-labeling technique [121].

Within the TME, platelets foster TCs fitness and proliferation both via cell-cell contact, or the secretion of soluble factors (including PEVs) [2]. Moreover, platelets also affect non-tumor cells (as CAFs) [2] and profoundly rewire the immune microenvironment both via direct and indirect mechanism [46], [49], [50]. Whereas these effects have been described in the primary TME, the characterization of platelets role in the metastatic TME still remains poorly defined and further studies will be highly needed to fill this gap (see outstanding questions **– Text Box 2**). Although murine models have been instrumental in characterizing the global role of platelets in cancer, significant translational gaps remain. Notably, species-specific differences in platelet biology challenge the direct extrapolation of murine observations to human cancers and hinder the identification of novel druggable interactions between platelets and TCs, underscoring the necessity of validating murine findings within relevant human contexts. Yet, the available humanized mouse models do not fully recapitulate human platelet biology and the TME remains largely murine, thus affecting the interactions between TCs and platelets. Recently developed complex *ex vivo* models, such as organs-on-a-chip, OoC [122]; patient's derived organoids, PDOs [123] and human fresh tissue slices [124], [125] hold great promise for bridging this translational gap by discerning specific pathways involved in platelet pro-tumoral processes, while retaining the complexity of *in vivo* interactions. These cutting-edge systems have already been successfully used to explore the platelets-cancer nexus by assessing platelet extravasation within the tumor bed [126], their subsequent interactions with the TME [93] and impacts on angiogenesis [127] and their role on early metastatic dissemination [128]. While these results are encouraging for advancing our understanding of the role of platelets in tumor progression, further studies should also focus on the therapeutic perspective and identify additional platelets-specific druggable targets (see outstanding questions **– Text Box 2**) since, currently, most of anti-platelets agents still present many side effects (as increased bleeding risk). The combination of complex *ex vivo* models, and advanced omics techniques may provide useful data in this regard. As the complex *ex vivo* systems have a high-throughput nature, they are well-suited for drug screening purposes. Composed of human-derived cells and retaining a high-

similarity to the original tumor, they have already demonstrated their high-relevance as platforms to assess response to treatment in pre-clinical trials [93], [128] and for identifying potential new therapeutic targets [32]. Moreover, novel digital analysis methods (*e.g.*, image processing, bioinformatics, machine learning and AI-based technology) [129] will enable the generation of comprehensive multi-omics data on platelets-cancer interactions.

Albeit significant advances have been made in elucidating the multifaceted roles of platelets in cancer progression, many questions remain. Future studies should address the timing of platelet recruitment to primary and metastatic tumor sites, the nature of their contributions within these niches, and the molecular determinants underpinning these processes. This will be of utmost importance not only for defining the full extent of platelet involvement in tumor progression but also for identifying new therapeutic strategies to target the platelet-cancer axis. Bridging the gap between pre-clinical models and human systems, and leveraging innovative *ex vivo* platforms and multi-omics approaches, will be essential to uncover actionable targets and refine therapeutic interventions.

Text Box 1 – Platelets: new weapon for tumor drug delivery.

Fascinatingly, platelets abilities to populate primary and secondary tumor sites can be harnessed to achieve potent drug delivery in the tumor bed. *Ex vivo* engineering of platelets has led to the development of platelets decorated with anti-PD-L1 antibodies [130], [131] or loaded with chemotherapeutic drugs [132], [133]. These engineered platelets retain their inherent ability to accumulate in tumors and activate in response to TCs stimuli. Upon activation, they release their chemotherapeutic payload within the TME, promoting TC apoptosis [132], [133] or release anti-PD-L1-bearing PEVs that act as decoys, blocking PD-L1 on TCs [130], [131]. Of note, drug-free platelet decoys have also been shown to impair TCs hematogenous dissemination by disrupting CTCs clusters [134] and reducing TCs extravasation [135]. PEV-mediated ICB therapies reverses T cells exhaustion, promoting a robust anti-tumor immune response and inhibiting tumor recurrence in mouse models of melanoma and triple-negative breast cancer [130], [131]. Building on these preclinical findings, combination treatment strategies using platelets carrying anti-PD-1/anti-PD-L1 antibodies and loaded with chemotherapeutic or immunomodulatory drugs have been developed, successfully enhancing therapeutic effects [136], [137], [138], [139]. Similarly, co-administration of CAR-T cells with platelets bearing anti-PD-L1 antibodies significantly enhances CAR-T cells functions and persistence [140]. Moreover, the accumulation of activated platelets within the TME generates new targets for cancer detection and therapy. Targeting activated platelets with a single-chain variable fragment (scFv) antibody against integrin $\alpha_{IIb}\beta_3$ successfully enables molecular imaging and localization of breast cancers and lymphoma [141]. Additionally, the same scFv antibody, conjugated to a chemotherapeutic drug, demonstrates anti-tumoral efficacy in a murine model of triple-negative breast cancer [142]. This highlights a potential strategy for targeting platelets with antibody-drug conjugates for therapy and antibody-based imaging in cases where tumor cell-specific epitopes are absent.

Text Box 2 – Outstanding questions.

1. Do platelets seed metastases solely through their interaction with TCs (used as trojan horses) in circulation or do they rely on active and independent extravasation?
2. What is the origin of tumor-infiltrating platelets? Are they recruited from the circulation or are they generated from extramedullary megakaryopoiesis [84], [143]?
3. Do platelets impact the immune TME within the metastatic foci through direct interactions with immune cells or via soluble factors?
4. How platelets transcriptome and proteome evolve within the TME and contribute to tumor progression?
5. Are platelets likely to sensitize some tumors to ICB treatments?
6. How can one identify a reliable platelet-dependent druggable target, with no collateral damage, for oncology purposes?

Figures

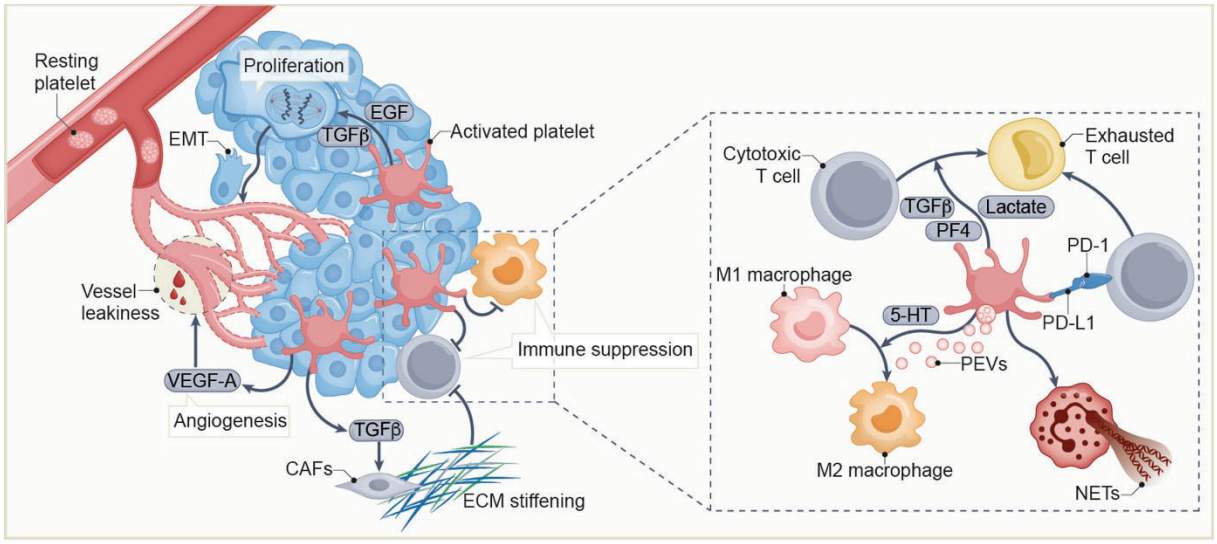

Figure 1 – Platelets functions within tumor bed.

Within the primary tumor, platelets sustain TCs proliferation and pro-invasive EMT phenotype through the secretion of growth factors such as EGF or TGFβ. They also promote angiogenesis through VEGF-A secretion. Besides, platelet-derived TGFβ recruits cancer-associated fibroblasts, promotes excessive deposition of ECM by CAFs, which can impede the intratumoral infiltration of immune cells. Furthermore, platelet-derived factors contribute to an immunosuppressive microenvironment by respectively hindering T cells function, promoting the transition of M1 macrophages to the M2 phenotype and triggering neutrophils NETosis.

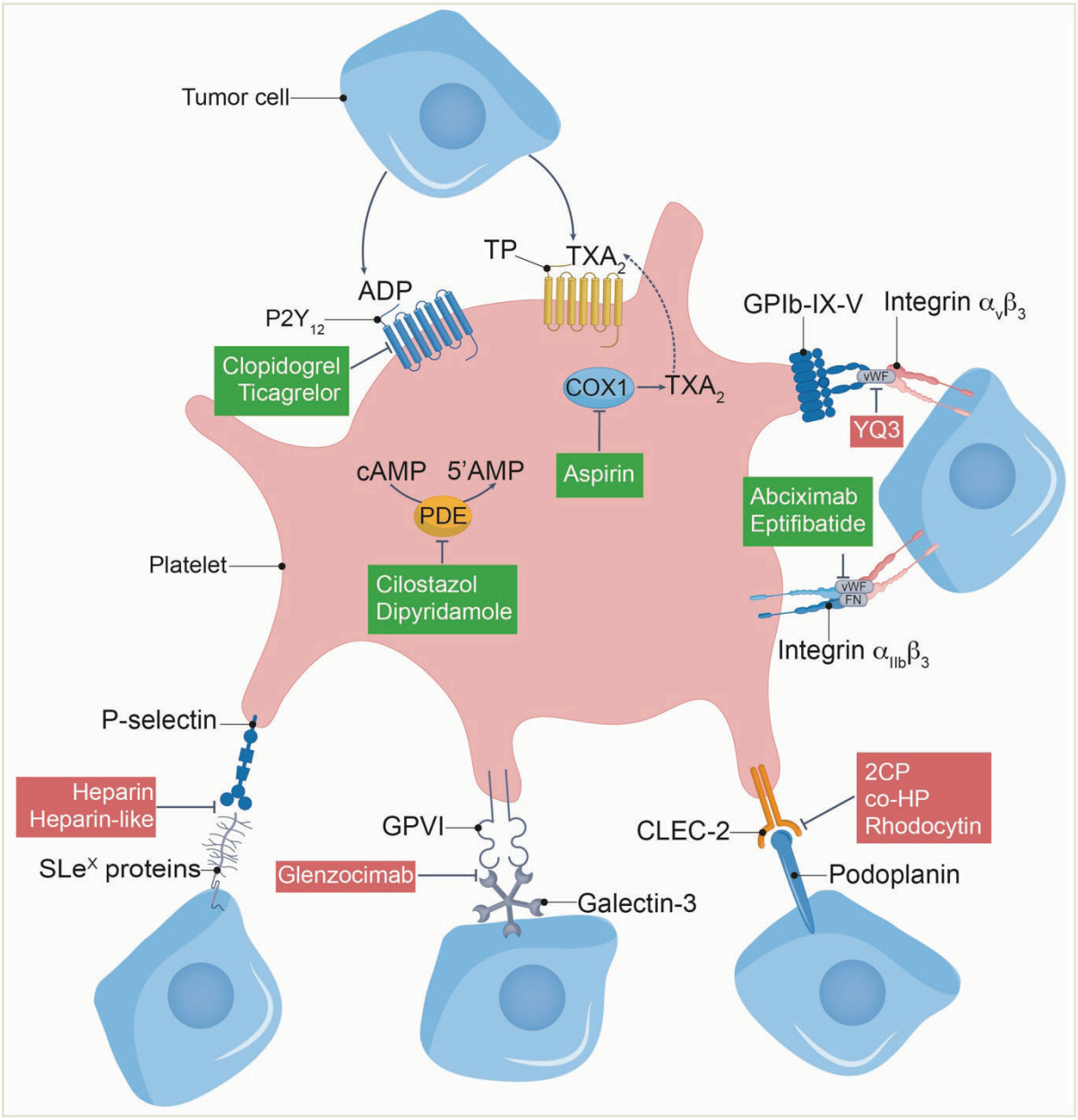

Figure 2 – Mechanisms of action of anti-platelet agents.

Several anti-platelet agents are being investigated in the clinical oncological practice (green panels) or under development (red panels) to tackle platelets interaction with tumor cells. ADP: adenosine diphosphate; cAMP: cyclic adenosine monophosphate; 2CP: 5-nitrobenzoate; co-HP: cobalt hematoporphyrin; COX-1: cyclooxygenase-1; GP: glycoprotein; PDE: phosphodiesterase; FN: Fibronectin; SLe^X: Sialyl-Lewis^X proteins (*e.g.*, CD24, CD44, PSGL-1); TP: TxA2 receptor; TxA_2: thromboxane A_2; vWF: von Willebrand Factor.

References

[1] G. J. Gasic, T. B. Gasic, and C. C. Stewart, “Antimetastatic effects associated with platelet reduction.,” *Proceedings of the National Academy of Sciences*, vol. 61, no. 1, pp. 46–52, Sep. 1968, doi: 10.1073/pnas.61.1.46.

[2] S. Li *et al.*, “The dynamic role of platelets in cancer progression and their therapeutic implications,” *Nat Rev Cancer*, pp. 1–16, Dec. 2023, doi: 10.1038/s41568-023-00639-6.

[3] K. R. Machlus and J. E. Italiano, “The incredible journey: From megakaryocyte development to platelet formation,” *J Cell Biol*, vol. 201, no. 6, pp. 785–796, Jun. 2013, doi: 10.1083/jcb.201304054.

[4] L. Zhou *et al.*, “Tumor cell-released kynurenine biases MEP differentiation into megakaryocytes in individuals with cancer by activating AhR–RUNX1,” *Nat Immunol*, vol. 24, no. 12, pp. 2042–2052, Dec. 2023, doi: 10.1038/s41590-023-01662-3.

[5] F. Gaertner and S. Massberg, “Patrolling the vascular borders: platelets in immunity to infection and cancer,” *Nat Rev Immunol*, vol. 19, no. 12, Art. no. 12, Dec. 2019, doi: 10.1038/s41577-019-0202-z.

[6] J. B. Schaubaecher *et al.*, “Procoagulant platelets promote immune evasion in triple-negative breast cancer,” *Blood*, vol. 144, no. 2, pp. 216–226, Jul. 2024, doi: 10.1182/blood.2023022928.

[7] M. Haemmerle *et al.*, “FAK regulates platelet extravasation and tumor growth after antiangiogenic therapy withdrawal,” *J Clin Invest*, vol. 126, no. 5, pp. 1885–1896, May 2016, doi: 10.1172/JCI85086.

[8] S. Miao *et al.*, “Platelets are recruited to hepatocellular carcinoma tissues in a CX3CL1-CX3CR1 dependent manner and induce tumour cell apoptosis,” *Molecular Oncology*, vol. 14, no. 10, pp. 2546–2559, 2020, doi: 10.1002/1878-0261.12783.

[9] M. J. Garcia-Leon *et al.*, “Platelets favor the outgrowth of established metastases,” *Nat Commun*, vol. 15, no. 1, p. 3297, May 2024, doi: 10.1038/s41467-024-47516-w.

[10] M. Hergueta-Redondo *et al.*, “The impact of a high fat diet and platelet activation on pre-metastatic niche formation,” *Nat Commun*, vol. 16, no. 1, p. 2897, Apr. 2025, doi: 10.1038/s41467-025-57938-9.

[11] E. Mammadova-Bach *et al.*, “Platelet integrin **α**6**β**1 controls lung metastasis through direct binding to cancer cell–derived ADAM9,” *JCI Insight*, vol. 1, no. 14, Sep. 2016, doi: 10.1172/jci.insight.88245.

[12] E. Mammadova-Bach *et al.*, “Platelet glycoprotein VI promotes metastasis through interaction with cancer cell–derived galectin-3,” *Blood*, vol. 135, no. 14, pp. 1146–1160, Apr. 2020, doi: 10.1182/blood.2019002649.

[13] M. Sheng, R. Sun, J. Fu, and G. Lu, “The podoplanin-CLEC-2 interaction promotes platelet-mediated melanoma pulmonary metastasis,” *BMC Cancer*, vol. 24, no. 1, p. 399, Apr. 2024, doi: 10.1186/s12885-024-12194-w.

[14] T. Dudiki *et al.*, “Mechanism of Tumor-Platelet Communications in Cancer,” *Circulation Research*, vol. 132, no. 11, pp. 1447–1461, May 2023, doi: 10.1161/CIRCRESAHA.122.321861.

[15] T. Sasano *et al.*, “Podoplanin promotes tumor growth, platelet aggregation, and venous thrombosis in murine models of ovarian cancer,” *J Thromb Haemost*, vol. 20, no. 1, pp. 104–114, Jan. 2022, doi: 10.1111/jth.15544.

[16] V. Mittelheisser *et al.*, “Tumoral CD24 tunes platelets binding and pro-metastatic functions,” Apr. 15, 2025, *bioRxiv*. doi: 10.1101/2025.04.09.648049.

[17] L. Cereceda, J. C. Cardenas, M. Khoury, E. Silva-Pavez, and Y. Hidalgo, “Impact of platelet-derived mitochondria transfer in the metabolic profiling and progression of metastatic MDA-MB-231 human triple-negative breast cancer cells,” *Front Cell Dev Biol*, vol. 11, p. 1324158, 2023, doi: 10.3389/fcell.2023.1324158.

[18] D. Cacic, H. Reikvam, O. Nordgård, P. Meyer, and T. Hervig, “Platelet Microparticles Protect Acute Myelogenous Leukemia Cells against Daunorubicin-Induced Apoptosis,” *Cancers*, vol. 13, no. 8, Art. no. 8, Jan. 2021, doi: 10.3390/cancers13081870.

[19] F. Li *et al.*, “Platelet-derived extracellular vesicles inhibit ferroptosis and promote distant metastasis of nasopharyngeal carcinoma by upregulating ITGB3,” *Int J Biol Sci*, vol. 18, no. 15, pp. 5858–5872, 2022, doi: 10.7150/ijbs.76162.

[20] E. Gharib, V. Veilleux, L. H. Boudreau, N. Pichaud, and G. A. Robichaud, “Platelet-derived microparticles provoke chronic lymphocytic leukemia malignancy through metabolic reprogramming,” *Front Immunol*, vol. 14, p. 1207631, 2023, doi: 10.3389/fimmu.2023.1207631.

[21] S. L. French *et al.*, “Platelet-derived extracellular vesicles infiltrate and modify the bone marrow during inflammation,” *Blood Advances*, vol. 4, no. 13, pp. 3011–3023, Jul. 2020, doi: 10.1182/bloodadvances.2020001758.

[22] E. Janus-Bell *et al.*, “Depletion of all platelet integrins impacts hemostasis, thrombosis and tumor metastasis,” Nov. 22, 2024, *bioRxiv*. doi: 10.1101/2024.11.22.624871.

[23] X. Zuo, Y. Yang, Y. Zhang, Z. Zhang, X. Wang, and Y. Shi, “Platelets promote breast cancer cell MCF-7 metastasis by direct interaction: surface integrin α2β1-contacting-mediated activation of Wnt-β-catenin pathway,” *Cell Communication and Signaling*, vol. 17, no. 1, p. 142, Nov. 2019, doi: 10.1186/s12964-019-0464-x.

[24] R. Saito *et al.*, “Platelets enhance malignant behaviours of gastric cancer cells via direct contacts,” *Br J Cancer*, vol. 124, no. 3, pp. 570–573, Feb. 2021, doi: 10.1038/s41416-020-01134-7.

[25] W. Zhang *et al.*, “Cancer cells reprogram to metastatic state through the acquisition of platelet mitochondria,” *Cell Reports*, vol. 42, no. 9, p. 113147, Sep. 2023, doi: 10.1016/j.celrep.2023.113147.

[26] N. Martins Castanheira, A. K. Spanhofer, S. Wiener, S. Bobe, and H. Schillers, “Uptake of platelets by cancer cells and recycling of the platelet protein CD42a,” *Journal of Thrombosis and Haemostasis*, vol. 20, no. 1, pp. 170–181, 2022, doi: 10.1111/jth.15543.

[27] A. Rodriguez-Martinez *et al.*, “Exchange of cellular components between platelets and tumor cells: impact on tumor cells behavior,” *Theranostics*, vol. 12, no. 5, pp. 2150–2161, 2022, doi: 10.7150/thno.64252.

[28] H. G. Roweth *et al.*, “Pro-inflammatory megakaryocyte gene expression in murine models of breast cancer,” *Science Advances*, vol. 8, no. 41, p. eabo5224, Oct. 2022, doi: 10.1126/sciadv.abo5224.

[29] K. L. Clar, C. Hinterleitner, P. Schneider, H. R. Salih, and S. Maurer, “Inhibition of NK Reactivity Against Solid Tumors by Platelet-Derived RANKL,” *Cancers*, vol. 11, no. 3, Art. no. 3, Mar. 2019, doi: 10.3390/cancers11030277.

[30] Y. Zhou *et al.*, “Platelet-expressed immune checkpoint regulator GITRL in breast cancer,” *Cancer Immunol Immunother*, vol. 70, no. 9, pp. 2483–2496, Sep. 2021, doi: 10.1007/s00262-021-02866-y.

[31] Z. Zhang *et al.*, “Targeting Erbin-mitochondria axis in platelets/megakaryocytes promotes B cell-mediated antitumor immunity,” *Cell Metab*, vol. 36, no. 3, pp. 541-556.e9, Mar. 2024, doi: 10.1016/j.cmet.2023.12.020.
[32] Y. Sun *et al.*, “Platelet-mediated circulating tumor cell evasion from natural killer cell killing through immune checkpoint CD155-TIGIT,” *Hepatology*, vol. 81, no. 3, p. 791, Mar. 2025, doi: 10.1097/HEP.0000000000000934.
[33] L. Yang *et al.*, “An Immuno-Cardiac Model for Macrophage-Mediated Inflammation in COVID-19 Hearts,” *Circ Res*, vol. 129, no. 1, pp. 33–46, Jun. 2021, doi: 10.1161/CIRCRESAHA.121.319060.
[34] Z. Eslami-S *et al.*, “In vitro cross-talk between metastasis-competent circulating tumor cells and platelets in colon cancer: a malicious association during the harsh journey in the blood,” *Front. Cell Dev. Biol.*, vol. 11, Aug. 2023, doi: 10.3389/fcell.2023.1209846.
[35] Y. Hu *et al.*, “TRIM27 revealing by tumor educated platelet RNA-sequencing, as a potential biomarker for malignant ground-glass opacities diagnosis mediates glycolysis of non-small cell lung cancer cells partially through HOXM1,” *Translational Lung Cancer Research*, vol. 13, no. 9, Sep. 2024, doi: 10.21037/tlcr-24-157.
[36] F. I. Mulder *et al.*, “Platelet RNA sequencing for cancer screening in patients with unprovoked venous thromboembolism: a prospective cohort study,” *J Thromb Haemost*, vol. 21, no. 4, pp. 905–916, Apr. 2023, doi: 10.1016/j.jtha.2023.01.003.
[37] L. Xu *et al.*, “RNA profiling of blood platelets noninvasively differentiates colorectal cancer from healthy donors and noncancerous intestinal diseases: a retrospective cohort study,” *Genome Medicine*, vol. 14, no. 1, p. 26, Mar. 2022, doi: 10.1186/s13073-022-01033-x.
[38] S. G. J. G. In ’t Veld *et al.*, “Detection and localization of early- and late-stage cancers using platelet RNA,” *Cancer Cell*, vol. 40, no. 9, pp. 999-1009.e6, Sep. 2022, doi: 10.1016/j.ccell.2022.08.006.
[39] L. Jiang *et al.*, “Platelet releasate promotes breast cancer growth and angiogenesis via VEGF–integrin cooperative signalling,” *Br J Cancer*, vol. 117, no. 5, pp. 695–703, Aug. 2017, doi: 10.1038/bjc.2017.214.
[40] Y. Zhang *et al.*, “Platelet-Specific PDGFB Ablation Impairs Tumor Vessel Integrity and Promotes Metastasis,” *Cancer Res*, vol. 80, no. 16, pp. 3345–3358, Aug. 2020, doi: 10.1158/0008-5472.CAN-19-3533.
[41] W. Feng, M. Madajka, B. A. Kerr, G. H. Mahabeleshwar, S. W. Whiteheart, and T. V. Byzova, “A novel role for platelet secretion in angiogenesis: mediating bone marrow-derived cell mobilization and homing,” *Blood*, vol. 117, no. 14, pp. 3893–3902, Apr. 2011, doi: 10.1182/blood-2010-08-304808.
[42] B. Sobolewska *et al.*, “Human Platelets Take up Anti-VEGF Agents,” *J Ophthalmol*, vol. 2021, p. 8811672, Jun. 2021, doi: 10.1155/2021/8811672.
[43] S. Sabrkhany *et al.*, “Sunitinib uptake inhibits platelet function in cancer patients,” *Eur J Cancer*, vol. 66, pp. 47–54, Oct. 2016, doi: 10.1016/j.ejca.2016.07.016.
[44] H. M. W. Verheul *et al.*, “Platelets take up the monoclonal antibody bevacizumab,” *Clin Cancer Res*, vol. 13, no. 18 Pt 1, pp. 5341–5347, Sep. 2007, doi: 10.1158/1078-0432.CCR-07-0847.
[45] J. A. Ware and M. Simons, “Angiogenesis in ischemic heart disease,” *Nat Med*, vol. 3, no. 2, pp. 158–164, Feb. 1997, doi: 10.1038/nm0297-158.
[46] T. Miyashita *et al.*, “Impact of Extravasated Platelet Activation and Podoplanin-positive Cancer-associated Fibroblasts in Pancreatic Cancer Stroma,”

Anticancer Res, vol. 39, no. 10, pp. 5565–5572, Oct. 2019, doi: 10.21873/anticanres.13750.

[47] T. Shirai *et al.*, “Cancer-associated fibroblasts promote venous thrombosis through podoplanin/CLEC-2 interaction in podoplanin-negative lung cancer mouse model,” *J Thromb Haemost*, vol. 21, no. 11, pp. 3153–3165, Nov. 2023, doi: 10.1016/j.jtha.2023.07.005.

[48] Y. Zhang *et al.*, “Platelet-Derived PDGFB Promotes Recruitment of Cancer-Associated Fibroblasts, Deposition of Extracellular Matrix and Tgfβ Signaling in the Tumor Microenvironment,” *Cancers (Basel)*, vol. 14, no. 8, p. 1947, Apr. 2022, doi: 10.3390/cancers14081947.

[49] B. Malacrida *et al.*, “A human multi-cellular model shows how platelets drive production of diseased extracellular matrix and tissue invasion,” *iScience*, vol. 24, no. 6, p. 102676, Jun. 2021, doi: 10.1016/j.isci.2021.102676.

[50] S. Lickert *et al.*, “Platelets drive fibronectin fibrillogenesis using integrin αIIbβ3,” *Science Advances*, vol. 8, no. 10, p. eabj8331, Mar. 2022, doi: 10.1126/sciadv.abj8331.

[51] S.-H. Chan, H.-J. Tseng, and L.-H. Wang, “CD24a knockout transforms the tumor microenvironment from cold to hot by promoting tumor-killing immune cell infiltration in a murine triple-negative breast cancer model,” Jul. 17, 2024, *bioRxiv*. doi: 10.1101/2024.07.15.603489.

[52] S. Rachidi *et al.*, “Platelets subvert T cell immunity against cancer via GARP-TGFβ axis,” *Sci Immunol*, vol. 2, no. 11, p. eaai7911, May 2017, doi: 10.1126/sciimmunol.aai7911.

[53] M. S. Lutz *et al.*, “Platelets subvert antitumor efficacy of T cell-recruiting bispecific antibodies,” *J Immunother Cancer*, vol. 10, no. 2, p. e003655, Feb. 2022, doi: 10.1136/jitc-2021-003655.

[54] M. Mulet *et al.*, “Platelet factor 4 regulates T cell effector functions in malignant pleural effusions,” *Cancer Lett*, vol. 491, pp. 78–86, Oct. 2020, doi: 10.1016/j.canlet.2020.06.014.

[55] J. Yang *et al.*, “Aspirin prevents metastasis by limiting platelet TXA2 suppression of T cell immunity,” *Nature*, vol. 640, no. 8060, pp. 1052–1061, Apr. 2025, doi: 10.1038/s41586-025-08626-7.

[56] L. M. Gockel, K. Nekipelov, V. Ferro, G. Bendas, and M. Schlesinger, “Tumour cell-activated platelets modulate the immunological activity of CD4+, CD8+, and NK cells, which is efficiently antagonized by heparin,” *Cancer Immunol Immunother*, vol. 71, no. 10, pp. 2523–2533, Oct. 2022, doi: 10.1007/s00262-022-03186-5.

[57] M. Vismara *et al.*, “Proteomic and functional profiling of platelet-derived extracellular vesicles released under physiological or tumor-associated conditions,” *Cell Death Discov.*, vol. 8, no. 1, pp. 1–8, Nov. 2022, doi: 10.1038/s41420-022-01263-3.

[58] C. K. Meikle *et al.*, “Platelet-T cell aggregates in lung cancer patients: Implications for thrombosis,” *PLOS ONE*, vol. 15, no. 8, p. e0236966, août 2020, doi: 10.1371/journal.pone.0236966.

[59] C. Polasky, F. Wendt, R. Pries, and B. Wollenberg, “Platelet Induced Functional Alteration of CD4+ and CD8+ T Cells in HNSCC,” *International Journal of Molecular Sciences*, vol. 21, no. 20, Art. no. 20, Jan. 2020, doi: 10.3390/ijms21207507.

[60] T. Tyagi *et al.*, “Platelet-derived TLT-1 promotes tumor progression by suppressing CD8+ T cells,” *J Exp Med*, vol. 220, no. 1, p. e20212218, Jan. 2023, doi: 10.1084/jem.20212218.
[61] J. Rossaint *et al.*, “Platelets orchestrate the resolution of pulmonary inflammation in mice by T reg cell repositioning and macrophage education,” *J Exp Med*, vol. 218, no. 7, p. e20201353, Jul. 2021, doi: 10.1084/jem.20201353.
[62] R. Joseph *et al.*, “CD8+ T cells inhibit metastasis and CXCL4 regulates its function,” *Br J Cancer*, vol. 125, no. 2, pp. 176–189, Jul. 2021, doi: 10.1038/s41416-021-01338-5.
[63] L. Wang *et al.*, “Platelet-derived TGF-β1 induces functional reprogramming of myeloid-derived suppressor cells in immune thrombocytopenia,” *Blood*, vol. 144, no. 1, pp. 99–112, Jul. 2024, doi: 10.1182/blood.2023022738.
[64] J. Qian *et al.*, “Platelet-rich plasma-derived exosomes attenuate intervertebral disc degeneration by promoting NLRP3 autophagic degradation in macrophages,” *Int Immunopharmacol*, vol. 110, p. 108962, Sep. 2022, doi: 10.1016/j.intimp.2022.108962.
[65] K. Hoeft *et al.*, “Platelet-instructed SPP1+ macrophages drive myofibroblast activation in fibrosis in a CXCL4-dependent manner,” *Cell Rep*, vol. 42, no. 2, p. 112131, Feb. 2023, doi: 10.1016/j.celrep.2023.112131.
[66] M. Palviainen *et al.*, “Beyond basic characterization and omics: Immunomodulatory roles of platelet-derived extracellular vesicles unveiled by functional testing,” *J Extracell Vesicles*, vol. 13, no. 10, p. e12513, Oct. 2024, doi: 10.1002/jev2.12513.
[67] M. V. Singh *et al.*, “Monocytes complexed to platelets differentiate into functionally deficient dendritic cells,” *J Leukoc Biol*, vol. 109, no. 4, pp. 807–820, Apr. 2021, doi: 10.1002/JLB.3A0620-460RR.
[68] A. Saris *et al.*, “Inhibition of Dendritic Cell Activation and Modulation of T Cell Polarization by the Platelet Secretome,” *Front. Immunol.*, vol. 12, Feb. 2021, doi: 10.3389/fimmu.2021.631285.
[69] O. C. Ihedioha, A. Sivakoses, H. Q. Marcarian, M. Sajeev, D. McMahon-Pratt, and A. L. M. Bothwell, “Platelet DKK1 promotes tolerogenic dendritic cells and non-healing responses in cutaneous leishmaniasis,” May 31, 2025, *bioRxiv*. doi: 10.1101/2025.05.27.656395.
[70] M. Labelle, S. Begum, and R. O. Hynes, “Platelets guide the formation of early metastatic niches,” *Proceedings of the National Academy of Sciences*, vol. 111, no. 30, pp. E3053–E3061, Jul. 2014, doi: 10.1073/pnas.1411082111.
[71] A. Constantinescu-Bercu, L. Grassi, M. Frontini, I. I. Salles-Crawley, K. Woollard, and J. T. Crawley, “Activated αIIbβ3 on platelets mediates flow-dependent NETosis via SLC44A2,” *eLife*, vol. 9, p. e53353, Apr. 2020, doi: 10.7554/eLife.53353.
[72] J. M. Adrover, S. A. C. McDowell, X.-Y. He, D. F. Quail, and M. Egeblad, “NETworking with cancer: The bidirectional interplay between cancer and neutrophil extracellular traps,” *Cancer Cell*, vol. 41, no. 3, pp. 505–526, Mar. 2023, doi: 10.1016/j.ccell.2023.02.001.
[73] P. Lecot *et al.*, “Gene signature of circulating platelet-bound neutrophils is associated with poor prognosis in cancer patients,” *Int J Cancer*, vol. 151, no. 1, pp. 138–152, Jul. 2022, doi: 10.1002/ijc.33991.
[74] S. Lucotti *et al.*, “Extracellular vesicles from the lung pro-thrombotic niche drive cancer-associated thrombosis and metastasis via integrin beta 2,” *Cell*, vol. 188, no. 6, pp. 1642-1661.e24, Mar. 2025, doi: 10.1016/j.cell.2025.01.025.

[75] Q. Guo, M. W. Malloy, H. G. Roweth, S. S. McAllister, J. E. Italiano, and E. M. Battinelli, “Platelets upregulate tumor cell programmed death ligand 1 in an epidermal growth factor receptor-dependent manner in vitro,” *Blood Adv*, vol. 6, no. 20, pp. 5668–5675, Oct. 2022, doi: 10.1182/bloodadvances.2021006120.

[76] M. A. Schneider *et al.*, “Attenuation of peripheral serotonin inhibits tumor growth and enhances immune checkpoint blockade therapy in murine tumor models,” *Sci Transl Med*, vol. 13, no. 611, p. eabc8188, Sep. 2021, doi: 10.1126/scitranslmed.abc8188.

[77] A. Asgari *et al.*, “Platelets stimulate programmed death-ligand 1 expression by cancer cells: Inhibition by anti-platelet drugs,” *J Thromb Haemost*, vol. 19, no. 11, pp. 2862–2872, Nov. 2021, doi: 10.1111/jth.15478.

[78] J. Li *et al.*, “PD-L1 positive platelets mediate resistance to immune checkpoint inhibitors in patients with colorectal cancer,” *Cell Commun Signal*, vol. 23, no. 1, p. 29, Jan. 2025, doi: 10.1186/s12964-025-02034-0.

[79] C. Hinterleitner *et al.*, “Platelet PD-L1 reflects collective intratumoral PD-L1 expression and predicts immunotherapy response in non-small cell lung cancer,” *Nat Commun*, vol. 12, no. 1, Art. no. 1, Dec. 2021, doi: 10.1038/s41467-021-27303-7.

[80] A. B. Zaslavsky *et al.*, “Platelet PD-L1 suppresses anti-cancer immune cell activity in PD-L1 negative tumors,” *Sci Rep*, vol. 10, no. 1, p. 19296, Nov. 2020, doi: 10.1038/s41598-020-76351-4.

[81] Z. Hu *et al.*, “PD-L1 mRNA derived from tumor-educated platelets as a potential immunotherapy biomarker in non-small cell lung cancer,” *Translational Lung Cancer Research*, vol. 13, no. 2, Feb. 2024, doi: 10.21037/tlcr-24-29.

[82] C. Colarusso *et al.*, “High levels of PD-L1 on platelets of NSCLC patients contributes to the pharmacological activity of Atezolizumab,” *Biomed Pharmacother*, vol. 168, p. 115709, Dec. 2023, doi: 10.1016/j.biopha.2023.115709.

[83] S. R. Williamson, K. J. Mast, L. Cheng, and M. T. Idrees, “Clear cell renal cell carcinoma with intratumoral and nodal extramedullary megakaryopoiesis: a potential diagnostic pitfall,” *Hum Pathol*, vol. 45, no. 6, pp. 1306–1309, Jun. 2014, doi: 10.1016/j.humpath.2014.01.011.

[84] W. Huang *et al.*, “Presence of intra-tumoral CD61+ megakaryocytes predicts poor prognosis in non-small cell lung cancer,” *Transl Lung Cancer Res*, vol. 8, no. 4, pp. 323–331, Aug. 2019, doi: 10.21037/tlcr.2019.08.23.

[85] Y. Wang *et al.*, “Intratumoral erythroblastic islands restrain anti-tumor immunity in hepatoblastoma,” *Cell Rep Med*, vol. 4, no. 5, p. 101044, May 2023, doi: 10.1016/j.xcrm.2023.101044.

[86] V. Rolfes *et al.*, “PD-L1 is expressed on human platelets and is affected by immune checkpoint therapy,” *Oncotarget*, vol. 9, no. 44, pp. 27460–27470, Jun. 2018, doi: 10.18632/oncotarget.25446.

[87] M. Zhou *et al.*, “Platelet-derived microparticles adoptively transfer integrin β3 to promote antitumor effect of tumor-infiltrating T cells,” *Oncoimmunology*, vol. 13, no. 1, p. 2304963, 2024, doi: 10.1080/2162402X.2024.2304963.

[88] C. Ma *et al.*, “Platelets control liver tumor growth through P2Y12-dependent CD40L release in NAFLD,” *Cancer Cell*, vol. 40, no. 9, pp. 986-998.e5, Sep. 2022, doi: 10.1016/j.ccell.2022.08.004.

[89] O. Le Chapelain *et al.*, “The localization, origin, and impact of platelets in the tumor microenvironment are tumor type-dependent,” *Journal of Experimental &*

Clinical Cancer Research, vol. 43, no. 1, p. 84, Mar. 2024, doi: 10.1186/s13046-024-03001-2.

[90] P. Han *et al.*, “Platelet P-selectin initiates cross-presentation and dendritic cell differentiation in blood monocytes,” *Science Advances*, vol. 6, no. 11, p. eaaz1580, Mar. 2020, doi: 10.1126/sciadv.aaz1580.

[91] “An anti-cancer cell therapy platform utilizing ex vivo physiologic dendritic cells expressing mRNA-encoded antigens and immune checkpoint blockers,” Sciety. Accessed: Jun. 10, 2025. [Online]. Available: https://sciety.org/articles/activity/10.21203/rs.3.rs-6480245/v1

[92] J. Volz *et al.*, “Inhibition of platelet GPVI induces intratumor hemorrhage and increases efficacy of chemotherapy in mice,” *Blood*, vol. 133, no. 25, pp. 2696–2706, Jun. 2019, doi: 10.1182/blood.2018877043.

[93] B. Saha *et al.*, “Human tumor microenvironment chip evaluates the consequences of platelet extravasation and combinatorial antitumor-antiplatelet therapy in ovarian cancer,” *Science Advances*, vol. 7, no. 30, p. eabg5283, Jul. 2021, doi: 10.1126/sciadv.abg5283.

[94] S. Zelenay *et al.*, “Cyclooxygenase-Dependent Tumor Growth through Evasion of Immunity,” *Cell*, vol. 162, no. 6, pp. 1257–1270, Sep. 2015, doi: 10.1016/j.cell.2015.08.015.

[95] B. P. Riesenberg, E. A. Ansa-Addo, J. Gutierrez, C. D. Timmers, B. Liu, and Z. Li, “Cutting Edge: Targeting Thrombocytes to Rewire Anticancer Immunity in the Tumor Microenvironment and Potentiate Efficacy of PD-1 Blockade,” *J Immunol*, vol. 203, no. 5, pp. 1105–1110, Sep. 2019, doi: 10.4049/jimmunol.1900594.

[96] S. Lucotti *et al.*, “Aspirin blocks formation of metastatic intravascular niches by inhibiting platelet-derived COX-1/thromboxane A_2,” *J Clin Invest*, vol. 129, no. 5, pp. 1845–1862, May 2019, doi: 10.1172/JCI121985.

[97] A. J. Gareau, C. Brien, S. Gebremeskel, R. S. Liwski, B. Johnston, and M. Bezuhly, “Ticagrelor inhibits platelet–tumor cell interactions and metastasis in human and murine breast cancer,” *Clin Exp Metastasis*, vol. 35, no. 1, pp. 25–35, Feb. 2018, doi: 10.1007/s10585-018-9874-1.

[98] D. Spano *et al.*, “Dipyridamole prevents triple-negative breast-cancer progression,” *Clin Exp Metastasis*, vol. 30, no. 1, pp. 47–68, Jan. 2013, doi: 10.1007/s10585-012-9506-0.

[99] J. A. Varner, M. T. Nakada, R. E. Jordan, and B. S. Coller, “Inhibition of angiogenesis and tumor growth by murine 7E3, the parent antibody of c7E3 Fab (abciximab; ReoPro),” *Angiogenesis*, vol. 3, no. 1, pp. 53–60, 1999, doi: 10.1023/a:1009019223744.

[100] P. M. Rothwell, M. Wilson, J. F. Price, J. F. F. Belch, T. W. Meade, and Z. Mehta, “Effect of daily aspirin on risk of cancer metastasis: a study of incident cancers during randomised controlled trials,” *Lancet*, vol. 379, no. 9826, pp. 1591–1601, Apr. 2012, doi: 10.1016/S0140-6736(12)60209-8.

[101] M. S. Reimers *et al.*, “Expression of HLA class I antigen, aspirin use, and survival after a diagnosis of colon cancer,” *JAMA Intern Med*, vol. 174, no. 5, pp. 732–739, May 2014, doi: 10.1001/jamainternmed.2014.511.

[102] Z. Quandt *et al.*, “Phase II trial of pembrolizumab, ipilimumab, and aspirin in melanoma: clinical outcomes and translational predictors of response,” *BJC Rep*, vol. 2, no. 1, pp. 1–10, Jun. 2024, doi: 10.1038/s44276-024-00057-7.

[103] C. Patrono, C. Baigent, J. Hirsh, and G. Roth, “Antiplatelet drugs: American College of Chest Physicians Evidence-Based Clinical Practice Guidelines (8th

Edition)," *Chest*, vol. 133, no. 6 Suppl, pp. 199S-233S, Jun. 2008, doi: 10.1378/chest.08-0672.
[104] T. Araki *et al.*, "Antiplatelet drugs may increase the risk for checkpoint inhibitor-related pneumonitis in advanced cancer patients," *ESMO Open*, vol. 8, no. 6, p. 102030, Dec. 2023, doi: 10.1016/j.esmoop.2023.102030.
[105] T. Juhlin, B. A. G. Jönsson, and P. Höglund, "Renal effects of aspirin are clearly dose-dependent and are of clinical importance from a dose of 160 mg," *European Journal of Heart Failure*, vol. 10, no. 9, pp. 892–898, 2008, doi: 10.1016/j.ejheart.2008.06.014.
[106] N. Mackman, W. Bergmeier, G. A. Stouffer, and J. I. Weitz, "Therapeutic strategies for thrombosis: new targets and approaches," *Nat Rev Drug Discov*, vol. 19, no. 5, pp. 333–352, May 2020, doi: 10.1038/s41573-020-0061-0.
[107] J. M. Motta *et al.*, "A low-anticoagulant heparin suppresses metastatic dissemination through the inhibition of tumor cell-platelets association," *Biomed Pharmacother*, vol. 171, p. 116108, Feb. 2024, doi: 10.1016/j.biopha.2023.116108.
[108] H. Xu *et al.*, "Propylene glycol alginate sodium sulfate suppressed lung metastasis by blocking P-selectin to recruit CD4 regulatory T cells," *International Journal of Biological Macromolecules*, vol. 279, p. 134976, Nov. 2024, doi: 10.1016/j.ijbiomac.2024.134976.
[109] Y.-W. Chang *et al.*, "Identification of a novel platelet antagonist that binds to CLEC-2 and suppresses podoplanin-induced platelet aggregation and cancer metastasis," *Oncotarget*, vol. 6, no. 40, pp. 42733–42748, Oct. 2015, doi: 10.18632/oncotarget.5811.
[110] T. Sasaki *et al.*, "Functional characterization of recombinant snake venom rhodocytin: rhodocytin mutant blocks CLEC-2/podoplanin-dependent platelet aggregation and lung metastasis," *J Thromb Haemost*, vol. 16, no. 5, pp. 960–972, May 2018, doi: 10.1111/jth.13987.
[111] N. Tsukiji *et al.*, "Cobalt hematoporphyrin inhibits CLEC-2–podoplanin interaction, tumor metastasis, and arterial/venous thrombosis in mice," *Blood Advances*, vol. 2, no. 17, pp. 2214–2225, Sep. 2018, doi: 10.1182/bloodadvances.2018016261.
[112] Y. Qi *et al.*, "Novel antibodies against GPIbα inhibit pulmonary metastasis by affecting vWF-GPIbα interaction," *Journal of Hematology & Oncology*, vol. 11, no. 1, p. 117, Sep. 2018, doi: 10.1186/s13045-018-0659-4.
[113] Q. Wang *et al.*, "von Willebrand factor promotes platelet-induced metastasis of osteosarcoma through activation of the VWF-GPIb axis," *J Bone Oncol*, vol. 25, p. 100325, Dec. 2020, doi: 10.1016/j.jbo.2020.100325.
[114] K. Mayer *et al.*, "Efficacy and Safety of Revacept, a Novel Lesion-Directed Competitive Antagonist to Platelet Glycoprotein VI, in Patients Undergoing Elective Percutaneous Coronary Intervention for Stable Ischemic Heart Disease: The Randomized, Double-blind, Placebo-Controlled ISAR-PLASTER Phase 2 Trial," *JAMA Cardiol*, vol. 6, no. 7, pp. 753–761, Jul. 2021, doi: 10.1001/jamacardio.2021.0475.
[115] M. Mazighi *et al.*, "Safety and efficacy of platelet glycoprotein VI inhibition in acute ischaemic stroke (ACTIMIS): a randomised, double-blind, placebo-controlled, phase 1b/2a trial," *Lancet Neurol*, vol. 23, no. 2, pp. 157–167, Feb. 2024, doi: 10.1016/S1474-4422(23)00427-1.

[116] P. Billiald *et al.*, “Targeting platelet GPVI with glenzocimab: a novel mechanism for inhibition,” *Blood Advances*, vol. 7, no. 7, pp. 1258–1268, Mar. 2023, doi: 10.1182/bloodadvances.2022007863.
[117] N. J. Jooss *et al.*, “Anti-GPVI nanobody blocks collagen- and atherosclerotic plaque-induced GPVI clustering, signaling, and thrombus formation,” *J Thromb Haemost*, vol. 20, no. 11, pp. 2617–2631, Nov. 2022, doi: 10.1111/jth.15836.
[118] L. Renaud *et al.*, “Population Pharmacokinetic/Pharmacodynamic Modeling of Glenzocimab (ACT017) a Glycoprotein VI Inhibitor of Collagen-Induced Platelet Aggregation,” *The Journal of Clinical Pharmacology*, vol. 60, no. 9, pp. 1198–1208, 2020, doi: 10.1002/jcph.1616.
[119] S. Navarro *et al.*, “The humanized platelet glycoprotein VI Fab inhibitor EMA601 protects from arterial thrombosis and ischaemic stroke in mice,” *European Heart Journal*, vol. 45, no. 43, pp. 4582–4597, Nov. 2024, doi: 10.1093/eurheartj/ehae482.
[120] D. I. Fernández *et al.*, “Ultra-high throughput-based screening for the discovery of antiplatelet drugs affecting receptor dependent calcium signaling dynamics,” *Sci Rep*, vol. 14, no. 1, p. 6229, Mar. 2024, doi: 10.1038/s41598-024-56799-4.
[121] A. Anjum *et al.*, “Aging platelets shift their hemostatic properties to inflammatory functions,” *Blood*, vol. 145, no. 14, pp. 1568–1582, Apr. 2025, doi: 10.1182/blood.2024024901.
[122] L. D. Ghosh and A. Jain, “The prospects of microphysiological systems in modeling platelet pathophysiology in cancer,” *Platelets*, vol. 34, no. 1, p. 2247489, Dec. 2023, doi: 10.1080/09537104.2023.2247489.
[123] S.-Y. Kim, M. van de Wetering, H. Clevers, and K. Sanders, “The future of tumor organoids in precision therapy,” *Trends in Cancer*, Apr. 2025, doi: 10.1016/j.trecan.2025.03.005.
[124] E. Donnadieu, Y. Michel, and M.-L. Hansmann, “Live Imaging of Resident T-Cell Migration in Human Lymphoid Tissue Slices Using Confocal Microscopy,” *Methods Mol Biol*, vol. 1930, pp. 75–82, 2019, doi: 10.1007/978-1-4939-9036-8_10.
[125] M. Vierhout *et al.*, “A novel ex vivo approach for investigating profibrotic macrophage polarization using murine precision-cut lung slices,” *Biochem Biophys Res Commun*, vol. 741, p. 151038, Dec. 2024, doi: 10.1016/j.bbrc.2024.151038.
[126] B. Saha *et al.*, “OvCa-Chip microsystem recreates vascular endothelium–mediated platelet extravasation in ovarian cancer,” *Blood Advances*, vol. 4, no. 14, pp. 3329–3342, Jul. 2020, doi: 10.1182/bloodadvances.2020001632.
[127] L. D. Ghosh *et al.*, “Angiogenesis-Enabled Human Ovarian Tumor Microenvironment-Chip Evaluates Pathophysiology of Platelets in Microcirculation,” *Advanced Healthcare Materials*, vol. 13, no. 19, p. 2304263, 2024, doi: 10.1002/adhm.202304263.
[128] M. Crippa *et al.*, “A microphysiological early metastatic niche on a chip reveals how heterotypic cell interactions and inhibition of integrin subunit β3 impact breast cancer cell extravasation,” *Lab Chip*, vol. 21, no. 6, pp. 1061–1072, Mar. 2021, doi: 10.1039/D0LC01011A.
[129] Q. Yang, M. Li, Z. Xiao, Y. Feng, L. Lei, and S. Li, “A New Perspective on Precision Medicine: The Power of Digital Organoids,” *Biomaterials Research*, vol. 29, p. 0171, Mar. 2025, doi: 10.34133/bmr.0171.

[130] C. Wang, W. Sun, Y. Ye, Q. Hu, H. N. Bomba, and Z. Gu, “In situ activation of platelets with checkpoint inhibitors for post-surgical cancer immunotherapy,” *Nat Biomed Eng*, vol. 1, no. 2, pp. 1–10, Jan. 2017, doi: 10.1038/s41551-016-0011.
[131] X. Han *et al.*, “Platelets as platforms for inhibition of tumor recurrence post-physical therapy by delivery of anti-PD-L1 checkpoint antibody,” *Journal of Controlled Release*, vol. 304, pp. 233–241, Jun. 2019, doi: 10.1016/j.jconrel.2019.05.008.
[132] Z. Zhao *et al.*, “Platelet-Drug Conjugates Engineered via One-step Fusion Approach for Metastatic and Postoperative Cancer Treatment,” *Angewandte Chemie International Edition*, vol. 63, no. 37, p. e202403541, 2024, doi: 10.1002/anie.202403541.
[133] P. Xu *et al.*, “Doxorubicin-loaded platelets as a smart drug delivery system: An improved therapy for lymphoma,” *Sci Rep*, vol. 7, no. 1, p. 42632, Feb. 2017, doi: 10.1038/srep42632.
[134] B. Schnoor, K. Morris, R. K. Kottana, R. Muldoon, J. Barron, and A.-L. Papa, “Fibrinolytic Platelet Decoys Reduce Cancer Metastasis by Dissociating Circulating Tumor Cell Clusters,” *Advanced Healthcare Materials*, vol. 13, no. 26, p. 2304374, 2024, doi: 10.1002/adhm.202304374.
[135] A.-L. Papa *et al.*, “Platelet decoys inhibit thrombosis and prevent metastatic tumor formation in preclinical models,” *Sci Transl Med*, vol. 11, no. 479, p. eaau5898, Feb. 2019, doi: 10.1126/scitranslmed.aau5898.
[136] Y. Wang *et al.*, “Active recruitment of anti–PD-1–conjugated platelets through tumor-selective thrombosis for enhanced anticancer immunotherapy,” *Science Advances*, vol. 9, no. 13, p. eadf6854, Mar. 2023, doi: 10.1126/sciadv.adf6854.
[137] Q. Lu *et al.*, “Bioengineered Platelets Combining Chemotherapy and Immunotherapy for Postsurgical Melanoma Treatment: Internal Core-Loaded Doxorubicin and External Surface-Anchored Anti-PD-L1 Antibody Backpacks,” *Nano Lett*, vol. 22, no. 7, pp. 3141–3150, Apr. 2022, doi: 10.1021/acs.nanolett.2c00907.
[138] H. Li *et al.*, “Disrupting tumour vasculature and recruitment of aPDL1-loaded platelets control tumour metastasis,” *Nat Commun*, vol. 12, no. 1, Art. no. 1, May 2021, doi: 10.1038/s41467-021-22674-3.
[139] X. Zhang *et al.*, “Engineering PD-1-Presenting Platelets for Cancer Immunotherapy,” *Nano Lett.*, vol. 18, no. 9, pp. 5716–5725, Sep. 2018, doi: 10.1021/acs.nanolett.8b02321.
[140] Q. Hu *et al.*, “Inhibition of post-surgery tumour recurrence via a hydrogel releasing CAR-T cells and anti-PDL1-conjugated platelets,” *Nat Biomed Eng*, vol. 5, no. 9, pp. 1038–1047, Sep. 2021, doi: 10.1038/s41551-021-00712-1.
[141] M. L. Yap *et al.*, “Targeting Activated Platelets: A Unique and Potentially Universal Approach for Cancer Imaging,” *Theranostics*, vol. 7, no. 10, pp. 2565–2574, Jun. 2017, doi: 10.7150/thno.19900.
[142] M. L. Yap *et al.*, “Activated platelets in the tumor microenvironment for targeting of antibody-drug conjugates to tumors and metastases,” *Theranostics*, vol. 9, no. 4, pp. 1154–1169, Feb. 2019, doi: 10.7150/thno.29146.
[143] E. Lefrançais *et al.*, “The lung is a site of platelet biogenesis and a reservoir for haematopoietic progenitors,” *Nature*, vol. 544, no. 7648, pp. 105–109, Apr. 2017, doi: 10.1038/nature21706.

2. Depletion of all platelet integrins impacts hemostasis, thrombosis and tumor metastasis

bioRxiv preprint doi: https://doi.org/10.1101/2024.11.22.624871; this version posted November 22, 2024. The copyright holder for this preprint (which was not certified by peer review) is the author/funder. All rights reserved. No reuse allowed without permission.

Depletion of all platelet integrins impacts hemostasis, thrombosis and tumor metastasis

Emily Janus-Bell[1*], Cristina Liboni[2-5*], Alexandra Yakusheva[1], Vincent Mittelheisser[2-5], Clarisse Mouriaux[1], Catherine Bourdon[1], Louis Bochler[2-5], Vincent Hyenne[2-6], Maria Garcia-Leon[2-5,7], Olivier Lefebvre[2-5], Jacky G. Goetz[2-5¥], Pierre H. Mangin[1¥]

[1]Université de Strasbourg, INSERM, EFS Grand Est, BPPS UMR-S1255, FMTS, F-67065 Strasbourg, France; [2]Tumor Biomechanics, INSERM UMR_S1109, Strasbourg, France; [3]Université de Strasbourg, Strasbourg, France; [4]Fédération de Médecine Translationnelle de Strasbourg (FMTS), Strasbourg, France ; [5]Equipe Labellisée Ligue Contre le Cancer; [6]CNRS, SNC5055, Strasbourg, France; [7]Present address: Domain therapeutics, Parc d'Innovation − 220 Boulevard Gonthier D'Andernach, 67400 Strasbourg – Illkirch, France.

*co-first authors/[¥]co-last authors

Corresponding author: Emily Janus-Bell, Université de Strasbourg, INSERM, EFS Grand-Est, BPPS UMR-S1255, FMTS, 10 rue Spielmann, F-67065 Strasbourg, France; Phone: (+33) 3 88 21 25 25; Fax: (+33) 3 88 21 25 21; E-mail: emily.janus-bell@efs.sante.fr

Abstract word count: 140

Text character count: 20,053

Number of figures: 3

Supplementary file: 1

Short running title: Platelet integrins in hemostasis, thrombosis and tumor metastasis

bioRxiv preprint doi: https://doi.org/10.1101/2024.11.22.624871; this version posted November 22, 2024. The copyright holder for this preprint (which was not certified by peer review) is the author/funder. All rights reserved. No reuse allowed without permission.

40-word summary: Depletion of all platelet integrins in PF4Cre-β1$^{-/-}$/β3$^{-/-}$ mice leads to increased bleeding time and inhibits *in vivo* arterial thrombosis. Integrin-null platelets reduce tumor growth and metastatic burden in orthotopic and experimental metastasis models. Platelet integrins control hemostasis, thrombosis and metastasis.

bioRxiv preprint doi: https://doi.org/10.1101/2024.11.22.624871; this version posted November 22, 2024. The copyright holder for this preprint (which was not certified by peer review) is the author/funder. All rights reserved. No reuse allowed without permission.

ABSTRACT

Platelet integrins, in addition to other platelet receptors, are known to control hemostasis, thrombosis but also metastatic progression. Yet, their exclusive but combined deficiency has never been tested in these processes. Taking advantage of PF4Cre-$\beta1^{-/-}/\beta3^{-/-}$ mouse strain, we show that platelets are exclusively depleted for all integrins. While they displayed impaired binding to fibrinogen and annexin-V, P-selectin exposure was normal. Platelet adhesion was abrogated on immobilized fibrinogen and fibrillar fibronectin under shear flow. PF4Cre-$\beta1^{-/-}/\beta3^{-/-}$ mice presented an increased bleeding time and a profound defect in experimental models of arterial thrombosis. Platelet adhesion to tumor cells was also reduced, with a profound impact on tumor growth and metastatic burden in a model of triple negative breast cancer. Overall, these results confirm the central role of platelet integrins in hemostasis and thrombosis, and define their role in tumor growth and metastasis formation.

bioRxiv preprint doi: https://doi.org/10.1101/2024.11.22.624871; this version posted November 22, 2024. The copyright holder for this preprint (which was not certified by peer review) is the author/funder. All rights reserved. No reuse allowed without permission.

INTRODUCTION

Platelets are small anucleated circulating blood cells, which play a central role in hemostasis. At site of vessel injury, they adhere, activate and aggregate to form a platelet plug that stops bleeding. Platelet adhesion at site of injury is molecularly initiated through GPIb-IX-V complex interaction with subendothelial von Willebrand factor (vWF) (Savage et al., 1996, 1998). GPIb-vWF bond formation is crucial for platelet attachment under elevated wall shear rates. Under lower shear conditions, platelet β1 and β3 integrins ensure the recruitment of circulating platelets by themselves (Savage et al., 1996, 1998). In addition, platelet integrins are particularly important for securing their stable adhesion to extracellular matrix (ECM) proteins. Once stably adhered, platelet activation is mostly initiated through GPVI – collagen interaction (Nieswandt et al., 2001; Nieswandt and Watson, 2003). This induces the conformational change of integrin αIIbβ3 towards a high affinity state for circulating fibrinogen (Takagi et al., 2002), inducing platelet aggregation and the formation of a platelet plug sealing the breach (Versteeg et al., 2013). Platelets are also key players in arterial thrombosis, which is initiated upon rupture of an atherosclerotic plaque in a diseased artery. This pathological process leads to the formation of a thrombus that results in life-threatening ischemic pathologies such as myocardial infarction or ischemic stroke (Jackson, 2011).

Integrins are heterodimer transmembrane receptors composed of an α and a β chain. Platelets express at their surface three β1 integrins, α2β1, α5β1 and α6β1 interacting with collagen, fibronectin and laminins, respectively (Beumer et al., 1994; Hindriks et al., 1992; Saelman et al., 1994; Sonnenberg et al., 1988); and two β3 integrins, αvβ3 and αIIbβ3 interacting with vitronectin and fibrinogen (Marguerie et al., 1979; Paul et al., 2003). The role of β1 integrins is limited to platelet adhesion and activation on ECM proteins, with no major role in hemostasis as evidence by a normal tail bleeding time in platelet α2, α5 and α6 deficient mice (Habart et al., 2013; Janus-Bell et al., 2021; Schaff et al., 2013). Furthermore, while no patient with a

bioRxiv preprint doi: https://doi.org/10.1101/2024.11.22.624871; this version posted November 22, 2024. The copyright holder for this preprint (which was not certified by peer review) is the author/funder. All rights reserved. No reuse allowed without permission.

deficiency in one of the platelet β1 integrins has been identified, a patient with a depletion in α2 presented mild bleeding during childhood but then the risk of bleeding decreased in adulthood (Nieuwenhuis et al., 1986). Integrins α2β1 and α6β1, but not α5β1, are implicated in experimental thrombosis since their genetic depletion in mice lead to thrombosis reduction in several experimental models (He et al., 2003; Kuijpers et al., 2003; Schaff et al., 2013; Janus-Bell et al., 2021). Concerning platelet β3 integrins, the most abundant is αIIbβ3 bearing a central role in platelet aggregation through its interaction with circulating fibrinogen. αIIbβ3 role in hemostasis is evidence by Glanzmann thrombasthenia, an hemorrhagic disease caused by its absence or non-functionality (Solh et al., 2015). αIIbβ3 also plays a key role in arterial thrombosis as evidenced by currently used antithrombotic drugs targeting αIIbβ3 (van den Kerkhof et al., 2021).

Besides their key role in hemostasis and arterial thrombosis, platelets are also implicated in non-hemostatic functions such as embryonic and fetal development (Finney et al., 2012; Osada et al., 2012) or immunity (Tang et al., 2002; Yeaman, 2014). There is solid experimental evidence that platelets contribute to tumor metastasis: tumor cells (TCs) colonized much less efficiently the lungs in mice in the context of severe thrombocytopenia (Gasic et al., 1968). Since, the importance of platelets in tumor growth and metastasis has been confirmed in several experimental models (Nieswandt et al., 1999; Camerer et al., 2004; Coupland et al., 2012; Garcia-Leon et al., 2024; Mammadova-Bach et al., 2016). Platelets actively populate the tumor microenvironment where they modulate TCs proliferation, angiogenesis, immune cell infiltration and function (Li et al., 2024). Circulating platelets interact with TCs in the bloodstream, which protects them from shear forces (Egan et al., 2014) and immune attacks (Nieswandt et al., 1999) notably through inhibition of natural killer cells activity (Kopp et al., 2009) and the transfer of major histocompatibility complex class I to TCs (Placke et al., 2012). At distant sites, platelets favor TCs adhesion to the endothelium (Dardik et al., 1997; Pilch et

bioRxiv preprint doi: https://doi.org/10.1101/2024.11.22.624871; this version posted November 22, 2024. The copyright holder for this preprint (which was not certified by peer review) is the author/funder. All rights reserved. No reuse allowed without permission.

al., 2002; Anvari et al., 2021; Garcia-Leon et al., 2024) and facilitate the extravasation process (Schumacher et al., 2013; Labelle et al., 2011; Garcia-Leon et al., 2024), which favors metastatic colonization. Post-extravasation metastatic foci have been shown to be populated with platelets where they further support metastatic outgrowth through immune modulation (Garcia-Leon et al., 2024). The action of platelets at distant sites is mediated by several receptors, including the GPIb-IX-V complex (Jain et al., 2007; Qi et al., 2018; Erpenbeck et al., 2010), CLEC-2 (Shirai et al., 2017; Ichikawa et al., 2020; Chang et al., 2015; Tsukiji et al., 2018; Sasaki et al., 2018) and GPVI (Jain et al., 2009; Mammadova-Bach et al., 2020; Garcia-Leon et al., 2024).

Platelet β1 and β3 integrins were reported to contribute to tumor metastasis. We previously reported that mice lacking all platelet β1 integrins developed less lung metastasis in both an experimental metastasis model and an orthotopic model, with α6β1 playing a primary role (Mammadova-Bach et al., 2016). Its implication could be dependent on its interaction with ADAM-9 expressed on TCs in the bloodstream (Mammadova-Bach et al., 2016), shielding them from shear stress and immune surveillance. Interestingly, the interaction of platelet α2β1 with MCF-7 breast cancer cells induces transforming growth factor β1 secretion, a cytokine known to promote epithelial-mesenchymal transition, likely suggesting this integrin to fuel in this way TCs invasive properties (Labelle et al., 2011; Zuo et al., 2019). In addition, αIIbβ3 has been reported to be implicated in tumor metastasis as αIIbβ3 inhibitors or its deficiency decrease experimental metastasis (Amirkhosravi et al., 1999, 2003; Bakewell et al., 2003; Honn et al., 1992; Zhang et al., 2012). In fact, αIIbβ3 is able to interact with TCs *via* bridging with fibrinogen or vWF (interacting on the other side with αvβ3 expressed on TCs surface), therefore contributing to the formation of a shield around TCs.

In this study, we characterize a mouse strain specifically deficient for all five platelet integrins (PF4Cre-$\beta1^{-/-}/\beta3^{-/-}$) which allows to distinguish integrin-based adhesion from other known

bioRxiv preprint doi: https://doi.org/10.1101/2024.11.22.624871; this version posted November 22, 2024. The copyright holder for this preprint (which was not certified by peer review) is the author/funder. All rights reserved. No reuse allowed without permission.

receptors and to study the full contribution of platelet integrins by overcoming potential redundancies, that we know are important for platelet integrins (Janus-Bell et al., 2024). We ensured that depletion of integrins did not perturb expression levels of known platelet receptors and assessed the combined role of platelet integrins in the function on platelets, using flow cytometry and flow-based *in vitro* assays. Doing so, we confirmed the already known prominent contribution to hemostasis and arterial thrombosis using bleeding time assays and arterial thrombosis mouse models. We further demonstrate for the first time that they actively participate to tumor growth and confirmed their role in metastasis using orthotopic and experimental models of metastasis.

bioRxiv preprint doi: https://doi.org/10.1101/2024.11.22.624871; this version posted November 22, 2024. The copyright holder for this preprint (which was not certified by peer review) is the author/funder. All rights reserved. No reuse allowed without permission.

MATERIALS AND METHODS

Materials

U46619, PAR-4 peptide, Polydimethylsiloxane (PDMS) (Sylgrad 184 Silicone elastomer base and curing agent), cellular fibronectin, fatty acid free human serum albumin (HSA), Bovine Serum Albumin (BSA), Tween20, $MgCl_2$, NH_4Cl, $KHCO_3$ and Citrate buffer pH 6.0, Antigen Retriever were from Sigma-Aldrich. Alexa Fluor 488-coupled fibrinogen (Cat. F-13191) and $DIOC_6$ (3,3′-dihexyloxacarbocyanine iodide) were from Molecular Probes. Ethylenediaminetetraacetic acid (EDTA), iFluor 488-Phalloidin (1:1000), APC-Cy7-Viability Zombie NIR (1:1000), Annexin V-Alexa Fluor488 (used at 1 µg/mL) and eBioscience™ FOXP3/Transcription factor staining buffer set (Cat.00-5523-00) were from Invitrogen. Phosphate-buffered saline (PBS) was from ThermoFisher Scientific (DPBS 1X) and recombinant hirudin from Transgene. Alexa Fluor 488-annexin V was from Life Technologies (Cat. A13201) and paraformaldehyde (PFA) and Eukitt mounting medium (Cat.15320) were from Electron microscopy sciences. Adenosine diphosphate (ADP) was from Mast group. Convulxin was from Cryoprep. Fibrinogen was from Intertransfusion, vWF A3 binding peptide vA3-III-23 was from Cambcol and collagen was from Takeda (Kollagenreagens Horm). Ferric chloride ($FeCl_3$) was from Prolabo. RPMI1640 and Fetal Bovine Serum (FBS) were from Dutscher. Penicillin/Streptomycin and puromycin were from Gibco. Luciferin was from Euromedex. Harris Hematoxylin Acidified (ref.6765003), Eosin Y alcoholic (ref.6766007) and Superfrost slides (Cat.J1800AMNZ) were from Epredia. Avidin/biotin blocking kit (Cat.SP-2001) was from Vector Laboratories and Fluoromount-G™ with DAPI (Fischer Scientific, Cat. 00-4959-52). Masson Trichrome kit, light green variation (Cat.361350-0000) was from CellaVision-RalDiagnostics, 12 well chambers (Cat. 81201) were from Ibidi and Tumor Dissociation kit-mouse (Cat. 130-096-730) from Miltenyi.

Antibodies

bioRxiv preprint doi: https://doi.org/10.1101/2024.11.22.624871; this version posted November 22, 2024. The copyright holder for this preprint (which was not certified by peer review) is the author/funder. All rights reserved. No reuse allowed without permission.

For platelet glycoprotein expression: FITC-conjugated anti-αIIbβ3 (clone Leo.F2, Cat. M025-1, 1:20), anti-GPIbα (clone Xia.G7, Cat. M042-1, 1:20), anti-GPV (clone Gon.G6, Cat. M061-1, 1:20), anti-GPIX (clone Xia.B4, Cat. M051-1, 1:20) and anti-GPVI antibodies (clone Jaq.1, Cat. M011-1, 1:100) and anti-β3 (clone Luc.H11, Cat. M031-1, 1:20), were from Emfret Analytics. PE-conjugated anti-α2 (clone HMα2, Cat. 103506, used: 1 µg/mL), anti-α5 (clone 5H10-27, Cat. 103805, used: 2 µg/mL), anti-α6 (clone GOH3, Cat. 313612, used: 1 µg/mL), and Alexa Fluor 488-conjugated anti-β1 antibodies (clone HMβ1-1, Cat. 102211, used: 1 µg/mL), were from BioLegend.

For P-selectin exposure: FITC-coupled anti-P-selectin antibody (clone RB40.34, Cat. 561923, used: 2.5 µg/mL) was from BD Pharmingen.

For *ex vivo* tumor multiparametric flow cytometry: PE/Dazzle594 anti-CD103 (clone 2E7, Cat.121430, 1:100), PerCP/Cy5 anti-CD11b (clone M1/70, Cat. 101211, 1:500), PE anti-CD11c (clone N418, Cat. 117308, 1:200), APC anti-CD138 (clone, 281-2, Cat. 558626, 1:200), BV711 anit-CD19 (clone 6D5, Cat. 115554, 1:800), BV421 anti-CD25 (clone A18246A, Cat. 113705, 1:100), PerCP/Cy5 anti-CD3 (clone 17A2, Cat.100218, 1:50), Alexa Fluor 700 anti-CD4 (clone RM4-5, Cat. 100536, 1:1000), BV510 anti-CD45 (clone 30-F11, Cat.103138, 1:200), BV605 anti-CD8 (clone 53-6.7, Cat.100744, 1:200), PE anti-CTLA4/CD152 (clone UC10-4B9, Cat. 106306, 1:20), PE/Cy7 anti-F4/80 (clone BM8, Cat.123114, 1:100), PE/Cy7 anti-IgD (clone 11-26c.2a, Cat. 405720, 1:100), Alexa Fluor 488 anti-Ly6C (clone HK1.4, Cat. 128022, 1:1000), BV711 anti-Ly6G (clone 1A8, Cat. 127643, 1:200), Alexa Fluor 700 anti-MHCII (clone M5/114.15.2, Cat. 107622, 1:200), BV421 anti-NK1.1 (clone PK136, Cat. 108731, 1:100), PE/Dazzle594 anti-PD-1/CD279 (clone 29F.1A12, Cat. 135228, 1:200) and TruStain FcX™ (anti CD32/16 antibody, 1:50) were from BioLegend. PE anti-CD38 (clone 90/CD38, Cat. 553764, 1:300), PE anti-CD44 (clone IM7, Cat. 553134, 1:400), PE/Dazzle594 anti-CD80 (clone 16-10A1, Cat. 562504, 1:200), Alexa Fluor 647 anti-TCF-1 (clone S33-966,

bioRxiv preprint doi: https://doi.org/10.1101/2024.11.22.624871; this version posted November 22, 2024. The copyright holder for this preprint (which was not certified by peer review) is the author/funder. All rights reserved. No reuse allowed without permission.

Cat. 566693, 1:300) were from BD Pharmingen. FITC anti-FoxP3 (clone FJK-16S, Cat. 53-5773-82, 1:50), PE/Cy7 anti-TIM-3/CD366 (clone RMT3-23, Cat. 25-5870-82, 1:200) were from eBioscience.

For tumor immunofluorescence: primary: anti-mouse CD45 biotinylated (clone#30-F11, Cat.103103, 1:100), secondary: Streptavidin-AF647 (Cat.405237, 1:200) were from BioLegend.

For immunofluorescence of platelets-TCs interactions: Alexa Fluor 647 coupled anti-RAM.1 (used 2 µg/mL) was produced in-house (EFS).

Mice

We used C57BL/6J mice lacking platelet β1 and β3 integrins (PF4Cre-$\beta1^{-/-}/\beta3^{-/-}$) (Janus-Bell et al., 2024). PF4-Cre^{+} (called PF4Cre) mice served as controls. Male and female mice were used except for tumor models with murine triple negative breast cancer cell line where only females were used. All procedures for animal experiments were approved by the regional ethical committee for animal experimentation and the French government (animal facility authorization: G67-482-10 and APAFIS 27659-2020101308518816, C67-482-33 and APAFIS 37433-2022052016445806).

Platelet count evaluation

After severing the tail of anesthetized mice, whole blood was collected into EDTA (6 mM). Platelet count was analyzed in an automatic cell counter (Element HT5, Heska).

Platelet glycoprotein expression

After severing the tail of anesthetized mice, whole blood was collected into EDTA (6 mM). Blood was diluted with PBS to obtain 100,000 platelets/µL. Labeled murine antibodies were incubated with diluted blood for 30 min at room temperature. After incubation, blood was

bioRxiv preprint doi: https://doi.org/10.1101/2024.11.22.624871; this version posted November 22, 2024. The copyright holder for this preprint (which was not certified by peer review) is the author/funder. All rights reserved. No reuse allowed without permission.

diluted with 500 µL of PBS and surface glycoprotein expression of 10,000 platelet events was determined by flow cytometry (Gallios, Beckman Coulter).

Measurement of platelet soluble fibrinogen binding, P-selectin exposure and annexin V binding

Blood was drawn into hirudin anticoagulant (100 U/mL final concentration) from the abdominal aorta of anesthetized mice. For soluble fibrinogen binding and P-selectin exposure, whole blood was diluted into 0.35% tyrode albumin buffer containing hirudin (100 U/mL), incubated with 488-fibrinogen (20 µg/mL) or FITC-coupled anti-P-selectin antibody and stimulated with agonists (ADP 2 µmol/L, U46619 2 µmol/L or PAR-4 peptide 1 mmol/L) for 10 min. Samples were fixed by adding 50 µL of 4% PFA for 20 min and then diluted with 600 µL of PBS. For phosphatidylserine exposure, whole blood was diluted into 0.35% tyrode albumin buffer containing hirudin (100 U/mL), stimulated with agonists (convulxin 15 nmol/L or collagen-related peptide 1 µg/mL and PAR4 1 mmol/L) for 10 min and then incubated with Alexa Fluor 488-annexin V (1 µg/mL) for 20 min in the presence of hirudin. Fluorescence was determined on 10,000 platelet events by flow cytometry (Gallios, Beckman Coulter).

***In vitro* flow based assay**

Flow experiments were performed as previously described (Schaff et al., 2013). PDMS flow chambers (0.1 x 1 mm) were coated with fibrinogen (100 µg/mL), cellular fibronectin (300 µg/mL), vWF A3 binding peptide vA3-III-23 (100 µg/mL) or collagen (200 µg/mL) overnight at 4°C. Mechanical stretching of cellular fibronectin was performed by connecting 2 silicon tubes to vacuum pumps switched on at 100 mbar. Silicon tubes were clamp and, after 1 min, connected to the inlet and outlet of the flow chamber. The clamps were then opened to apply a tensile force to the surface and allow cellular fibronectin to multimerize through mechanical stretching. Flow channels were blocked with PBS containing HSA (10 mg/mL) for 30 min at

bioRxiv preprint doi: https://doi.org/10.1101/2024.11.22.624871; this version posted November 22, 2024. The copyright holder for this preprint (which was not certified by peer review) is the author/funder. All rights reserved. No reuse allowed without permission.

room temperature to limit unspecific platelet adhesion. Hirudinated (100 U/mL) whole blood was drawn from the abdominal aorta of anesthetized mice and perfused through the channels with a programmable syringe pump (Harvard Apparatus, PHD 2000) at 300 s^{-1} (over fibrinogen, fibronectin and collagen) or at 1,500 s^{-1} (over vWF A3 binding peptide). Platelet adhesion or thrombus formation were monitored by differential interference contrast (DIC) (Leica DMI4000B) using a 63x or a 40x objective and a Hammamatsu ORCA Flash 4L.T camera (Hammatsu Photonics). The number of platelet adhering or the area of thrombus was quantified using Fiji.

Bleeding time

Tail bleeding time was determined by severing 3 mm at the tip of the tail of anesthetized mice. The tail was immersed in 0.9% saline at 37°C and the time needed for the bleeding to stop was recorded. Tubes containing blood were spun for 5 min, the pellet were homogenized in lysis buffer (NH_4Cl 150 mM, $KHCO_3$ 1 mM, EDTA 0.1 mM, pH 7.2) and used for blood lost quantification as compared to a standard curve optical density at 540 nm. Standard curve was based on 50 µL of blood diluted in 450 µL of lysis buffer. Bleeding time was also determined by 25G needle puncture of the carotid artery of anesthetized mice. The time to cessation of bleeding after injury was determined using fluorescent macroscope (Leica Microsystems) coupled to a charge-coupled device (CCD) camera (ORCA-Fusion C14440-20UP, Hamamatsu). Image acquisition was performed with Metamorph software (Molecular Devices) and analysis with Fiji.

***In vivo* thrombosis models**

Mice received $DIOC_6$ injection to label platelets. For the ferric chloride model, after exposition of the left common carotid artery, a vascular injury was induced by applying laterally to the carotid a 3x3 mm Whatman filter paper saturated with 7.5% $FeCl_3$ for 2.5 min. For the pinching

bioRxiv preprint doi: https://doi.org/10.1101/2024.11.22.624871; this version posted November 22, 2024. The copyright holder for this preprint (which was not certified by peer review) is the author/funder. All rights reserved. No reuse allowed without permission.

model, a mechanical injury was induced by pinching the abdominal aorta with forceps for 15 s. Thrombus formation was monitored for 20 min with a fluorescent macroscope (Leica Microsystems) coupled to a CCD camera (ORCA-Fusion C14440-20UP, Hamamatsu). Image acquisition was performed with Metamorph software (Molecular Devices) and analysis of the thrombus size with Fiji.

Tumor cells

We decided to exploit a murine triple negative breast cancer cell line (AT3) which was previously established in the laboratory (Garcia-Leon et al., 2024). Cells were cultured at 37°C 5% CO_2 in RPMI1640 supplemented with 10% Fetal Bovine Serum-FBS (Dutscher) and 1% Penicillin/Streptomycin under puromycin selection (1 µg/mL). At confluency, cells were trypsinized and sub-cultured for further passing.

Platelets-tumor cells interaction (immunofluorescence)

For platelets-TCs interaction, 6,000 AT3-RedLuc-L2 (AT3) cells were seeded per well on a 12 well chamber and left to adhere overnight in complete medium. The following day, platelets (citrated platelet rich plasma prepared as in Garcia-Leon et al., 2024) were added to each well at the concentration of 500 platelets per cell and let to interact for 30 minutes at 37°C 5% CO_2 in Tyrode's buffer without $MgCl_2$. After three PBS washes, cells were fixed in PFA 0.5% in PBS for 20 minutes at room temperature. After three PBS washes, cells were stained with Alexa Fluor 647 coupled anti-RAM.1 (2 µg/mL) and Phalloidin-iFluor 488 (1:1.000) for 1 hour at room temperature. Slides were then washed and mounted in Fluoromount-G™ with DAPI. Images were acquired with 60x/water objective at Olympus Spinning disk confocal microscope. Analysis was performed with Fiji. The number of cells interacting platelets was manually counted and data were then post-processed in Excel 6.0 and GraphPad Prism 9.0 for statistical analysis.

bioRxiv preprint doi: https://doi.org/10.1101/2024.11.22.624871; this version posted November 22, 2024. The copyright holder for this preprint (which was not certified by peer review) is the author/funder. All rights reserved. No reuse allowed without permission.

Syngeneic orthotopic tumor model

Two-hundred fifty-thousand AT3 syngeneic triple negative breast cancer cells were intraductally injected in PF4Cre-$\beta1^{-/-}/\beta3^{-/-}$ and control (PF4Cre). Tumor dimensions were measured longitudinally up to 18 days post-injection (dpi) through Caliper and tumor volume was calculated as in the following formula (volume = $width^2$ x length). At the sacrifice, tumors were excised, weighted and processed for *ex-vivo* flow-cytometry immunophenotyping or immunofluorescence/Masson staining. Together, lungs were harvested and processed for subsequent staining.

Syngeneic experimental metastasis model

One-hundred-fifty-thousand AT3 cells syngeneic triple negative breast cancer cells were tail-vein injected in PF4Cre-$\beta1^{-/-}/\beta3^{-/-}$ and control (PF4Cre). Metastatic outgrowth was longitudinally followed *in vivo* by intraperitoneal injection of luciferin (5 µg/kg) and imaging with IVIS Lumina III (PerkinElmer) (Garcia-Leon et al., 2024). Fourteen dpi, mice were sacrificed. IVIS results were analysed with Living Image®, Excel 6.0 and GraphPad Prism 9.0 graphing the ratio of photon emission compared to D0 (Garcia-Leon et al., 2024).

Mouse organs processing

Tumors and lungs were harvested and fixed in PFA 4%/PBS overnight and processed for paraffin inclusion as previously described (Garcia-Leon et al., 2024). Briefly, following two subsequent washes in PBS and ethanol 50%, tumors were dehydrated overnight in 70% ethanol. Later, tissues were included in an automated Leica inclusion machine according to this scheme: ethanol baths (2x at 70%, 1x at 80%, 1x at 95% and 2x at 100%) 1 hour each, 2 xylene baths (1 hour each) and 2 paraffin embedding baths (1 hour each).

Hematoxylin and Eosin staining

bioRxiv preprint doi: https://doi.org/10.1101/2024.11.22.624871; this version posted November 22, 2024. The copyright holder for this preprint (which was not certified by peer review) is the author/funder. All rights reserved. No reuse allowed without permission.

Lung 10 µm slices were dewaxed and rehydrated with a decreasing alcohol scale until ethanol 70%. Slides were finally rinsed under a continuous stream of tap water for 5 minutes. Hematoxylin staining was carried out in Harris Hematoxylin Acidified for 3 minutes and then washed under a continuous stream of tap water for 5 minutes. Staining was differentiated with a quick wash in acid alcohol (1% HCl + 70% ethanol) and washed again under a continuous stream of water for 5 minutes. Counterstaining was carried out in Eosin for 15 seconds and washed again under a continuous stream of water for 5 minutes. Slides were then dehydrated in an increasing alcohol scale until a final bath in xylene and then mounted in Eukitt mounting medium. Images were acquired with Slide Scanner VS200 microscope (Olympus) with a 20x/air objective. Analysis was performed with QuPath 0.5.0 (Bankhead et al., 2017). Metastastic areas were manually annotated as the hematoxylin-dense areas. Total percentage of metastatic areas was calculated over the tissue area (automatically annotated *via* eosin signal thresholding).

Immunofluorescence staining and analysis

Ten-µm slices from paraffin-embedded tumors were obtained with a Leica microtome on Superfrost slides. Slices were dewaxed and rehydrated with a decreasing alcohol scale and antigen was de-masked after boiling in Citrate buffer pH 6.0, Antigen Retriever (Garcia-Leon et al., 2024). Primary antibody (1:100) was incubated overnight at 4°C after background minimization in blocking solution (3% bovine serum albumin-BSA, 20 mM $MgCl_2$, 0.3% Tween 20, 5% FBS in PBS) and endogenous avidin/biotin blockade. The following day, slides were incubated in Streptavidin-AF647 diluted 1:200 in BSA 5% (Sigma) for 1h at room temperature. Slides were mounted in Fluoromount-G™ with DAPI. Images were acquired with 40x/oil objective at Zeiss LSM800 confocal microscope. Analysis was performed with Fiji (Schindelin et al., 2012). Number of nuclei was automatically measured using "analyse particles" plug-in after background subtraction and thresholding on slides. The number of

bioRxiv preprint doi: https://doi.org/10.1101/2024.11.22.624871; this version posted November 22, 2024. The copyright holder for this preprint (which was not certified by peer review) is the author/funder. All rights reserved. No reuse allowed without permission.

$CD45^+$ positive cells was manually annotated on processed images. The percentage of $CD45^+$ cells on the number of nuclei was expressed in Excel 6.0, while graph and statistical analysis were carried out in GraphPad Prism 9.0.

Masson Trichrome staining and analysis

Paraffin-embedded tumors were cut in 5 µm slices with a Leica microtome on Superfrost slides. Following dewaxing in a degrading alcohol scale and hydratation, tissue slides were stained with Masson Trichrome kit, light green variation following manufacturer's instruction modified with 5 min mordant and 10 min staining incubation. At the end, slides were dehydrated in a growing alcohol scale with two final baths in xylene and then mounted in Eukitt mounting medium. Images were acquired with Slide Scanner VS200 microscope (Olympus) with a 20x/air objective. Analysis was performed with QuPath 0.5.0 (Bankhead et al., 2017). Tissue area was thresholded and automatically annotated in the blue channel at high resolution (1.10 µm/px), while Masson positive area was thresholded and automatically annotated in the residual channel at very high resolution (0.55 µm/px). The analysis was manually corrected to remove tissue artifacts. Percentage of Masson positive area was calculated over the total tissue area in Excel 6.0 and statistical analysis was performed in GraphPad 9.0.

***Ex-vivo* multiparametric flow-cytometry tumor immunophenotyping**

A single cell suspension was obtained from freshly harvested tumors as in (Garcia-Leon et al., 2024). Briefly, 2 mm^3 tumor pieces were cut in pieces before to be enzymatically digested using the Tumor Dissociation kit, mouse diluted in RPMI1640 according to manufacturer's instruction. The digestion was carried out for 42 minutes at 37°C using the gentleMACS Octo Dissociator (Miltenyi, 130-096-427). Prior to antibody staining, the cell suspension was filtered through a 50 µm nylon mesh and red blood cells were lysed in ACK Buffer (150 mM NH_4Cl, 10 mM $KHCO_3$, 0.1 mM Na_2EDTA). Gating of only viable cells was ensured with Viability

bioRxiv preprint doi: https://doi.org/10.1101/2024.11.22.624871; this version posted November 22, 2024. The copyright holder for this preprint (which was not certified by peer review) is the author/funder. All rights reserved. No reuse allowed without permission.

Dye staining (Zombie NIR) for 15 minutes at room temperature in the dark, while antibodies' aspecific binding was lowered thanks to the blockade of CD32/CD16 receptor for 20 minutes at 4°C. Next, cells were stained with primary conjugated antibodies (see antibodies section) for 15 minutes at 4°C. For intracellular staining, cellular suspensions were further fixed and permeabilized using the FOXP3/Transcription factor staining buffer set according to manufacturer's instructions. Antibodies targeting intracellular antigens (FOXP3, TCF-1) were incubated for 15 minutes at 4°C. After washing, samples were acquired at Attune NxT (Invitrogen) flow cytometer and data were analyzed using FlowJo™ v10 Software (ThreeStar). Excel 6.0 and Prism GraphPad 9.0 were used for data post-processing.

Statistical analyses

Statistical analyses were performed with GraphPad Prism software 9.5.0. Shapiro-Wilk normality test was applied before statistical test. Based on the Gaussian or non-Gaussian distribution of the data, unpaired t-test or Mann-Whitney test (in case of 2 groups comparison) was used. Welch correction (2 groups) was applied. In case of longitudinal analysis, Two-way ANOVA with Original FDR method of Benjamini and Hochberg was applied. Mantel-Cox test was applied for bleeding time. p- or q-values together with the number of replicates and independent experiments are indicated in figure legends.

bioRxiv preprint doi: https://doi.org/10.1101/2024.11.22.624871; this version posted November 22, 2024. The copyright holder for this preprint (which was not certified by peer review) is the author/funder. All rights reserved. No reuse allowed without permission.

RESULTS AND DISCUSSION

The central role of integrins in platelet function.

To characterize the impact of all platelet integrins depletion, we took advantage of a mouse strain specifically deficient for platelet integrins (PF4Cre-$\beta1^{-/-}/\beta3^{-/-}$) (Janus-Bell et al., 2024). PF4Cre-$\beta1^{-/-}/\beta3^{-/-}$ mice are viable and fertile, but present reduced breeding, linked to an increased mortality during parturition. They have a 50% reduction in platelet count as compared to controls (PF4Cre: 10.7 x 10^5 platelets/µL; PF4Cre-$\beta1^{-/-}/\beta3^{-/-}$ 4.58 x 10^5 platelets/µL) (**Figure 1A**). The platelet surface expression of GPIbα, GPV, GPIX and GPVI was normal while, as expected, the levels of every integrin subunit was profoundly reduced (**Figure 1B**). Using flow cytometry, we observed that PF4Cre-$\beta1^{-/-}/\beta3^{-/-}$ platelets were unable to bind detectable levels of soluble fibrinogen in response to ADP or the PAR-4 peptide, due to the absence of αIIbβ3 (**Figure 1C**). In contrast, P-selectin exposure in response to the TxA2 analog U46619 or to the PAR-4 peptide, was completely normal, indicating no major role of platelet integrin in the secretion of the granule content **(Figure 1D)**. Concerning annexin-V binding, we observed that it was markedly impaired in PF4Cre-$\beta1^{-/-}/\beta3^{-/-}$ mice compared to controls (**Figure 1E**). This result appears in contrast with the work of other groups demonstrating no impact or increase procoagulant platelet formation in Glanzmann patients (Aliotta et al., 2020), or with αIIbβ3 antagonists treatment (Hamilton et al., 2004) and it could result from the combined deficiency in all platelet integrins. Next, we evaluated the ability of integrins to support platelet adhesion to different surfaces under flow condition. Perfusing PF4Cre-$\beta1^{-/-}/\beta3^{-/-}$ mouse blood through microfluidic chips, we observed a complete inhibition of platelet adhesion over fibrinogen or fibrillar fibronectin at an arterial wall shear rate of 300 s^{-1} (fibrinogen, PF4Cre: 4.69 ± 0.96 x 10^4 platelets/mm^2; PF4Cre-$\beta1^{-/-}/\beta3^{-/-}$: 0.03 ± 0.02 x 10^4 platelets/mm^2; fibrillar fibronectin, PF4Cre: 1.30 ± 0.61 x 10^4 platelets/mm^2; PF4Cre-$\beta1^{-/-}/\beta3^{-/-}$: 0.07 ± 0.03 x 10^4 platelets/mm^2) (**Figure 1F-H**), indicating that β1 and β3 integrins are fundamental for platelets attachment and

bioRxiv preprint doi: https://doi.org/10.1101/2024.11.22.624871; this version posted November 22, 2024. The copyright holder for this preprint (which was not certified by peer review) is the author/funder. All rights reserved. No reuse allowed without permission.

stable adhesion under relatively low shear flow. In sharp contrast, platelet adhesion to plasma vWF at 1,500 s^{-1} was normal (PF4Cre: 3.10 ± 0.24 x 10^4 platelets/mm^2; PF4Cre-$\beta1^{-/-}/\beta3^{-/-}$: 2.54 ± 0.18 x 10^4 platelets/mm^2) (**Figure 1I**), confirming the modest contribution of integrins to the transient adhesion of platelets to immobilized vWF under high shear rate (Savage et al., 1996). Overall, $\beta1^{-/-}/\beta3^{-/-}$ platelets are unable to bind to fibrinogen or fibrillar fibronectin under flow conditions.

PF4Cre-$\beta1^{-/-}/\beta3^{-/-}$ mice exhibit a major defect in hemostasis and experimental thrombosis.

As the combined role of platelet integrins in thrombus formation was never characterized before, we assess their involvement in this process. Hence, anticoagulated whole blood of PF4Cre-$\beta1^{-/-}/\beta3^{-/-}$ mice was perfused through a microfluidic chip coated with immobilized type-I collagen at 300 s^{-1}. Aggregation was abolished with PF4Cre-$\beta1^{-/-}/\beta3^{-/-}$ blood, where only single platelet adhesion to the surface was observed (area of thrombus, PF4Cre: 2.9 ± 1.0 x 10^4 μm^2; PF4Cre-$\beta1^{-/-}/\beta3^{-/-}$: 0.0 ± 0.0 x 10^4 μm^2) (**Figure 2A, B**). This result highlights the instrumental role of platelet integrins in thrombus formation under flow condition, but also questions the mechanism by which platelets are able to stably adhere over collagen in absence of α2β1, the most known platelet adhesion receptor to collagen. We speculate that the combined role of the GPIb-IX-V complex, binding to collagen-bound vWF, coupled to GPVI binding to collagen, might explains the residual PF4Cre-$\beta1^{-/-}/\beta3^{-/-}$ platelet attachment to the surface. Considering this major defect in thrombus formation, we then move to assess the bleeding time. Using a well-characterized mouse tail bleeding time model, we observed that PF4Cre-$\beta1^{-/-}/\beta3^{-/-}$ mice present a very marked increase in bleeding time, forcing us to stop the experiment at 600 s by cauterizing the injury to avoid the mice to bleed to death (**Figure 2C**). In addition, the volume of blood loss was markedly augmented in PF4Cre-$\beta1^{-/-}/\beta3^{-/-}$ mice as compared to controls (PF4Cre: 17.0 ± 9.74 µL; PF4Cre-$\beta1^{-/-}/\beta3^{-/-}$: 344 ± 34.3 µL) (**Figure 2D**). These findings were confirmed in a second hemostasis model consisting in a needle puncture of the

bioRxiv preprint doi: https://doi.org/10.1101/2024.11.22.624871; this version posted November 22, 2024. The copyright holder for this preprint (which was not certified by peer review) is the author/funder. All rights reserved. No reuse allowed without permission.

carotid artery, which is much more severe than the classical tail-bleeding assay (**Figure 2E**). This increase in bleeding time is not explained by the 50% reduction in platelet count, as thrombocytopenic mice only present an increased bleeding time when the platelet count is below 100,000 platelet/µL (Morowski et al., 2013). These results confirmed the expected major role of platelet integrins in hemostasis in mice, especially the one of αIIbβ3 which is evidenced by the severe bleeding phenotype observed in Glanzmann thrombasthenia patients (Solh et al., 2015).

As we only observed single platelet adhesion and no aggregation when perfusing PF4Cre-$\beta1^{-/-}/\beta3^{-/-}$ blood over collagen *in vitro*, we next evaluated the combined role of all platelet integrins in two mouse models of arterial thrombosis: a ferric chloride injury of the carotid artery and a mechanical injury of the abdominal aorta. We observed a very profound inhibition of *in vivo* thrombus formation in PF4Cre-$\beta1^{-/-}/\beta3^{-/-}$ mice with barely any sign of platelet adhesion at site of lesion (area under the curve for ferric chloride model, PF4Cre: 1.65 ± 0.51 x 10^6 µm^2; PF4Cre-$\beta1^{-/-}/\beta3^{-/-}$: 0.005 ± 0.005 x 10^6 µm^2; for mechanical injury: PF4Cre: 3.46 ± 0.44 x 10^7 µm^2; PF4Cre-$\beta1^{-/-}/\beta3^{-/-}$: 0.01 ± 0.01 x 10^7 µm^2) (**Figure 1F-K**), highlighting the instrumental role of mouse platelet integrins in thrombus formation also *in vivo*. Similarly to the bleeding time, these results are not explained by the 50% reduction in platelet count, as mice with a platelet count above 300,000 platelets/µL in a model of mechanical injury and 200,000 platelets/µL in a model of ferric-chloride injury, present normal experimental thrombosis (Morowski et al., 2013). In summary, these results demonstrate that integrins are central to hemostasis and arterial thrombosis as they finely control platelet adhesion and aggregation at the site of vascular injury.

PF4Cre-$\beta1^{-/-}/\beta3^{-/-}$ mice present a reduced primary tumor and metastatic growth.

We next aimed at testing whether combined integrin deficiency would alter platelet-dependent tumor phenotypes. Interestingly, adhesion of integrin-deficient platelets to triple-negative

bioRxiv preprint doi: https://doi.org/10.1101/2024.11.22.624871; this version posted November 22, 2024. The copyright holder for this preprint (which was not certified by peer review) is the author/funder. All rights reserved. No reuse allowed without permission.

breast cancer cells (AT3 cells) was strongly reduced (PF4Cre-β1$^{-/-}$/β3$^{-/-}$: 0-3 platelets/cell; PF4Cre: 0-12 platelets/cell) **(Figure 3A)** prompting us to assess whether it could impact tumor progression. Platelets are a component of the tumor microenvironment and support primary tumor growth (Le Chapelain et al., 2024; Le Chapelain and Ho-Tin-Noé, 2022; Li et al., 2024). We first decided to investigate whether combined platelet β1 and β3 integrins deficiency might alter primary tumor growth using a syngeneic orthotopic model (AT3 cells) in PF4Cre-β1$^{-/-}$/β3$^{-/-}$ and PF4Cre mice (**Figure 3B**). Mammary tumor volume and weight were significantly reduced in PF4Cre-β1$^{-/-}$/β3$^{-/-}$ when compared to control mice (**Figure 3C**). Interestingly, lung metastasis were similarly perturbed in PF4Cre-β1$^{-/-}$/β3$^{-/-}$ mice, yet only mildly, suggesting that integrin deficiency is likely to impact multiple steps of metastatic progression (**Figure 3D**). Tumors of mice lacking platelet integrins had a tendency towards increased collagen deposition (**Figure 3E**). This suggests that absence of integrins in platelets impact their ability to organize the tumor-associated stroma, as seen in the light of the known role of platelets in ECM deposition (Malacrida et al., 2021) and integrin αIIbβ3 recognition as a driver of fibronectin fibrillogenesis *in vitro* (Lickert et al., 2022). In addition to these structural components, the stroma also comprises tumor-associated stromal cells including immune cells. Considering the well-established feedforward communication between platelets and the tumor immune microenvironment (Li et al., 2024), we further investigated this compartment by tumor immunofluorescence and observed a trend towards reduced infiltration of CD45^{+} cells in PF4Cre-β1$^{-/-}$/β3$^{-/-}$ derived tumors (**Figure 3F**). Additional analysis using *ex vivo* multiparametric flow-cytometry analysis of the tumor immune microenvironment initially confirmed that PF4Cre-β1$^{-/-}$/β3$^{-/-}$ tumors present a trend towards reduced number of CD45^{+} cells (**Figure 3G**). Within the myeloid panel, only neutrophils displayed an accumulation in PF4Cre-β1$^{-/-}$/β3$^{-/-}$ mice (**Figure S1**). With regards to the lymphoid lineage, while no variance in total T cells was observed, both CD4^{+} and CD8^{+} relative amount were slightly reduced in PF4Cre-β1^{-}

bioRxiv preprint doi: https://doi.org/10.1101/2024.11.22.624871; this version posted November 22, 2024. The copyright holder for this preprint (which was not certified by peer review) is the author/funder. All rights reserved. No reuse allowed without permission.

$^{-/-}$/β3$^{-/-}$ tumors (**Figure 3G**). While a decrease in PD1- TIM3- compartment was observed both in CD4^{+} and in CD8^{+} cells (**Figure 3G**), PD1^{+} TIM3^{-} interferon producing effector/exhausted cells (Sakuishi et al., 2010; Fourcade et al., 2009) were exclusively increased in CD4^{+} subgroup (**Figure 3G**). In addition, T regulatory cells resulted increased in PF4Cre-β1$^{-/-}$/β3$^{-/-}$ mice (**Figure 3G**). While these data further question platelets' role in immune cells recruitment at the tumor site (Schaubaecher et al., 2024), they demonstrate a non-negligible contribution of platelet integrins, as suggested by previous studies showing that platelets could promote anti-tumor T cells function *via* microparticle adoptive transfer of β3 integrin in a hepatocellular carcinoma model (Zhou et al., 2024). Alternatively, platelet integrins might alter the surface expression of immune checkpoint molecules hence remodeling T cell response (Schaubaecher et al., 2024). Overall, our data point towards a key involvement of combined platelet β1 and β3 integrins deficiency in impairing primary tumor growth, ECM deposition and immune cells recruitment and function.

While understanding how platelets mechanistically control the recruitment of immune components requires additional investigation (Schaubaecher et al., 2024), they are known to bind to circulating TCs in the bloodstream where they foster metastasis (Labelle et al., 2014; Garcia-Leon et al., 2024). Since orthotopically-implanted tumors of PF4Cre-β1$^{-/-}$/β3$^{-/-}$ mice displayed a reduced, yet non-significant, metastatic potential (**Figure 3D**) and provide that adhesion of β1$^{-/-}$/β3$^{-/-}$ platelets to TCs was significantly reduced (**Figure 3A**), we set up an experimental metastasis model aiming at directly testing the contribution of platelet integrins to the hematogenous phase of metastasis (**Figure 3H**). As expected, metastatic outgrowth of AT3 cells was significantly reduced in PF4Cre-β1$^{-/-}$/β3$^{-/-}$ mice at 14 dpi (**Figure 3I**). This reduction in metastatic outgrowth is unlikely to be due to the 50% reduction of the platelet count as it has been described that 30% of the normal platelet count still allow a normal metastatic development (Coupland et al., 2012). While this result further recapitulates what was previously

bioRxiv preprint doi: https://doi.org/10.1101/2024.11.22.624871; this version posted November 22, 2024. The copyright holder for this preprint (which was not certified by peer review) is the author/funder. All rights reserved. No reuse allowed without permission.

observed with platelet β1 deficiency (Mammadova-Bach et al., 2016) and β3 deficiency (Amirkhosravi et al., 1999; Bakewell et al., 2003; Honn et al., 1992; Zhang et al., 2012) or platelet integrins pharmacological blockade (Amirkhosravi et al., 1999, 2003; Bakewell et al., 2003; Honn et al., 1992; Zhang et al., 2012), it reinforces the central role of both platelet β1 and β3 integrins in mediating platelets-TCs interaction and subsequent metastatic progression.

In conclusion, this study characterizes PF4Cre-β1$^{-/-}$/β3$^{-/-}$ mice assessing the effect of all platelets integrins depletion on hemostasis, thrombosis and tumor growth. While integrins' surface expression was completely abrogated, PF4Cre-β1$^{-/-}$/β3$^{-/-}$ platelets presented a normal glycoprotein surface expression and P-selectin exposure, indicating no major role of platelet integrins in granule content secretion. We provide evidence for a key role of integrins in many platelets' function including platelet procoagulant activity and platelet attachment and stable adhesion at relatively low shear. In addition, aggregation over collagen under flow condition was completely blunted in the absence of platelet integrins, a notion which was confirmed *in vivo* by a complete prevention of thrombosis in two distinct models of arterial thrombosis. PF4Cre-β1$^{-/-}$/β3$^{-/-}$ mice presented severely increased bleeding in two distinct models of bleeding time, probably due to the absence of αIIbβ3, which reflects the severe phenotype observe in Glanzmann patients. Moreover, we showed that platelet integrins participate in platelets-TCs interaction. Their deficiency reduced primary tumor growth and, to some extent, pulmonary metastatic dissemination in a syngeneic AT3 model, impacting ECM deposition and immune cells accumulation and functionality at the tumor site. Furthermore, PF4Cre-β1$^{-/-}$/β3$^{-/-}$ mice presented diminished metastatic outgrowth in an AT3 experimental metastasis model. Overall, our study shed light on the irreplaceable functions of platelet integrins in dictating hemostasis and arterial thrombosis. In addition, we demonstrated their non-negligible participation in shaping primary and metastatic tumor growth.

bioRxiv preprint doi: https://doi.org/10.1101/2024.11.22.624871; this version posted November 22, 2024. The copyright holder for this preprint (which was not certified by peer review) is the author/funder. All rights reserved. No reuse allowed without permission.

ACKNOWLEDGEMENTS

This work was supported by INSERM, EFS and ARMESA. We would like to acknowledge the PICSTRA imaging Platform for the technical support during imaging acquisition and Marina Peralta for Fiji analysis pipeline design. This work has been supported by funds from the French National Cancer Institute to P.M. and J.G.G. (PLBIO2023-173), which covers the financial support to C.L. V.M. is supported by a fellowship from the French Ministry of Science (MESRI) and a fourth-year thesis fellowship from the Fondation ARC pour la recherche sur le cancer. L.B. is supported by a PhD scholarship from FRM-Foundation pour la Recherche Medicale. Parts of the figures were created using material from Servier Medical Art. Servier Medical Art by Servier is licensed under a Creative Commons Attribution 3.0 Unported License (https://creativecommons.org/licenses/by/4.0/).

AUTHORSHIP CONTRIBUTIONS

E.J.B. and C.L. acquired, analyzed, interpreted the data and wrote the manuscript; A.Y., V.M and O.L. acquired, analyzed, interpreted the data and contributed to the writing of the manuscript; C.M, C.B., L.B. and M.G.L. acquired, analyzed and interpreted the data; V.H. provided technical support; P.H.M. and J.G.G. conceived and designed the research, interpreted the data, wrote the manuscript and handled funding and supervision.

DISCLOSURE OF CONFLICTS OF INTEREST

The authors declare that no conflicts of interest exist.

bioRxiv preprint doi: https://doi.org/10.1101/2024.11.22.624871; this version posted November 22, 2024. The copyright holder for this preprint (which was not certified by peer review) is the author/funder. All rights reserved. No reuse allowed without permission.

Correspondence: Emily Janus-Bell, Université de Strasbourg, INSERM, EFS Grand-Est, BPPS UMR-S1255, FMTS, F-67065 Strasbourg, France, e-mail: emily.janus-bell@efs.sante.fr

bioRxiv preprint doi: https://doi.org/10.1101/2024.11.22.624871; this version posted November 22, 2024. The copyright holder for this preprint (which was not certified by peer review) is the author/funder. All rights reserved. No reuse allowed without permission.

REFERENCES

Aliotta, A., M. Krüsi, D. Bertaggia Calderara, M.G. Zermatten, F.J. Gomez, A.P. Batista Mesquita Sauvage, and L. Alberio. 2020. Characterization of Procoagulant COAT Platelets in Patients with Glanzmann Thrombasthenia. *Int J Mol Sci*. 21:9515. doi:10.3390/ijms21249515.

Amirkhosravi, A., M. Amaya, F. Siddiqui, J.P. Biggerstaff, T.V. Meyer, and J.L. Francis. 1999. Blockade of GpIIb/IIIa inhibits the release of vascular endothelial growth factor (VEGF) from tumor cell-activated platelets and experimental metastasis. *Platelets*. 10:285–292. doi:10.1080/09537109975915.

Amirkhosravi, A., S.A. Mousa, M. Amaya, S. Blaydes, H. Desai, T. Meyer, and J.L. Francis. 2003. Inhibition of tumor cell-induced platelet aggregation and lung metastasis by the oral GpIIb/IIIa antagonist XV454. *Thromb Haemost*. 90:549–554. doi:10.1160/TH03-02-0102.

Anvari, S., E. Osei, and N. Maftoon. 2021. Interactions of platelets with circulating tumor cells contribute to cancer metastasis. *Sci Rep*. 11:15477. doi:10.1038/s41598-021-94735-y.

Bakewell, S.J., P. Nestor, S. Prasad, M.H. Tomasson, N. Dowland, M. Mehrotra, R. Scarborough, J. Kanter, K. Abe, D. Phillips, and K.N. Weilbaecher. 2003. Platelet and osteoclast beta3 integrins are critical for bone metastasis. *Proc Natl Acad Sci U S A*. 100:14205–14210. doi:10.1073/pnas.2234372100.

Bankhead, P., M.B. Loughrey, J.A. Fernández, Y. Dombrowski, D.G. McArt, P.D. Dunne, S. McQuaid, R.T. Gray, L.J. Murray, H.G. Coleman, J.A. James, M. Salto-Tellez, and P.W. Hamilton. 2017. QuPath: Open source software for digital pathology image analysis. *Sci Rep*. 7:16878. doi:10.1038/s41598-017-17204-5.

Beumer, S., M.J. IJsseldijk, P.G. de Groot, and J.J. Sixma. 1994. Platelet adhesion to fibronectin in flow: dependence on surface concentration and shear rate, role of platelet membrane glycoproteins GP IIb/IIIa and VLA-5, and inhibition by heparin. *Blood*. 84:3724–3733.

Camerer, E., A.A. Qazi, D.N. Duong, I. Cornelissen, R. Advincula, and S.R. Coughlin. 2004. Platelets, protease-activated receptors, and fibrinogen in hematogenous metastasis. *Blood*. 104:397–401. doi:10.1182/blood-2004-02-0434.

Chang, Y.-W., P.-W. Hsieh, Y.-T. Chang, M.-H. Lu, T.-F. Huang, K.-Y. Chong, H.-R. Liao, J.-C. Cheng, and C.-P. Tseng. 2015. Identification of a novel platelet antagonist that binds to CLEC-2 and suppresses podoplanin-induced platelet aggregation and cancer metastasis. *Oncotarget*. 6:42733–42748. doi:10.18632/oncotarget.5811.

Coupland, L.A., B.H. Chong, and C.R. Parish. 2012. Platelets and P-selectin control tumor cell metastasis in an organ-specific manner and independently of NK cells. *Cancer Res.* 72:4662–4671. doi:10.1158/0008-5472.CAN-11-4010.

Dardik, R., Y. Kaufmann, N. Savion, N. Rosenberg, B. Shenkman, and D. Varon. 1997. Platelets mediate tumor cell adhesion to the subendothelium under flow conditions: involvement of platelet GPIIb-IIIa and tumor cell alpha(v) integrins. *Int J Cancer*. 70:201–207. doi:10.1002/(sici)1097-0215(19970117)70:2<201::aid-ijc11>3.0.co;2-l.

Egan, K., N. Cooke, and D. Kenny. 2014. Living in shear: platelets protect cancer cells from shear induced damage. *Clin. Exp. Metastasis*. 31:697–704. doi:10.1007/s10585-014-9660-7.

bioRxiv preprint doi: https://doi.org/10.1101/2024.11.22.624871; this version posted November 22, 2024. The copyright holder for this preprint (which was not certified by peer review) is the author/funder. All rights reserved. No reuse allowed without permission.

Erpenbeck, L., B. Nieswandt, M. Schön, M. Pozgajova, and M.P. Schön. 2010. Inhibition of platelet GPIb alpha and promotion of melanoma metastasis. *J Invest Dermatol*. 130:576–586. doi:10.1038/jid.2009.278.

Finney, B.A., E. Schweighoffer, L. Navarro-Núñez, C. Bénézech, F. Barone, C.E. Hughes, S.A. Langan, K.L. Lowe, A.Y. Pollitt, D. Mourao-Sa, S. Sheardown, G.B. Nash, N. Smithers, C. Reis e Sousa, V.L.J. Tybulewicz, and S.P. Watson. 2012. CLEC-2 and Syk in the megakaryocytic/platelet lineage are essential for development. *Blood*. 119:1747–1756. doi:10.1182/blood-2011-09-380709.

Fourcade, J., P. Kudela, Z. Sun, H. Shen, S.R. Land, D. Lenzner, P. Guillaume, I.F. Luescher, C. Sander, S. Ferrone, J.M. Kirkwood, and H.M. Zarour. 2009. PD-1 Is a Regulator of NY-ESO-1-Specific CD8+ T Cell Expansion in Melanoma Patients. *The Journal of Immunology*. 182:5240–5249. doi:10.4049/jimmunol.0803245.

Garcia-Leon, M.J., C. Liboni, V. Mittelheisser, L. Bochler, G. Follain, C. Mouriaux, I. Busnelli, A. Larnicol, F. Colin, M. Peralta, N. Osmani, V. Gensbittel, C. Bourdon, R. Samaniego, A. Pichot, N. Paul, A. Molitor, R. Carapito, M. Jandrot-Perrus, O. Lefebvre, P.H. Mangin, and J.G. Goetz. 2024. Platelets favor the outgrowth of established metastases. *Nat Commun*. 15:3297. doi:10.1038/s41467-024-47516-w.

Gasic, G.J., T.B. Gasic, and C.C. Stewart. 1968. Antimetastatic effects associated with platelet reduction. *Proc. Natl. Acad. Sci. U.S.A.* 61:46–52.

Habart, D., Y. Cheli, D.J. Nugent, Z.M. Ruggeri, and T.J. Kunicki. 2013. Conditional knockout of integrin α2β1 in murine megakaryocytes leads to reduced mean platelet volume. *PLoS ONE*. 8:e55094. doi:10.1371/journal.pone.0055094.

Hamilton, S.F., M.W. Miller, C.A. Thompson, and G.L. Dale. 2004. Glycoprotein IIb/IIIa inhibitors increase COAT-platelet production in vitro. *J Lab Clin Med*. 143:320–326. doi:10.1016/j.lab.2004.02.001.

He, L., L.K. Pappan, D.G. Grenache, Z. Li, D.M. Tollefsen, S.A. Santoro, and M.M. Zutter. 2003. The contributions of the alpha 2 beta 1 integrin to vascular thrombosis in vivo. *Blood*. 102:3652–3657. doi:10.1182/blood-2003-04-1323.

Hindriks, G., M.J. Ijsseldijk, A. Sonnenberg, J.J. Sixma, and P.G. de Groot. 1992. Platelet adhesion to laminin: role of Ca2+ and Mg2+ ions, shear rate, and platelet membrane glycoproteins. *Blood*. 79:928–935.

Honn, K.V., Y.Q. Chen, J. Timar, J.M. Onoda, J.S. Hatfield, S.E. Fligiel, B.W. Steinert, C.A. Diglio, I.M. Grossi, and K.K. Nelson. 1992. Alpha IIb beta 3 integrin expression and function in subpopulations of murine tumors. *Exp Cell Res*. 201:23–32. doi:10.1016/0014-4827(92)90344-8.

Ichikawa, J., T. Ando, T. Kawasaki, T. Sasaki, T. Shirai, N. Tsukiji, Y. Kimura, K. Aoki, K. Hayakawa, K. Suzuki-Inoue, M. Saitoh, and H. Haro. 2020. Role of Platelet C-Type Lectin-Like Receptor 2 in Promoting Lung Metastasis in Osteosarcoma. *J Bone Miner Res*. 35:1738–1750. doi:10.1002/jbmr.4045.

Jackson, S.P. 2011. Arterial thrombosis--insidious, unpredictable and deadly. *Nat. Med.* 17:1423–1436. doi:10.1038/nm.2515.

bioRxiv preprint doi: https://doi.org/10.1101/2024.11.22.624871; this version posted November 22, 2024. The copyright holder for this preprint (which was not certified by peer review) is the author/funder. All rights reserved. No reuse allowed without permission.

Jain, S., S. Russell, and J. Ware. 2009. Platelet glycoprotein VI facilitates experimental lung metastasis in syngenic mouse models. *J. Thromb. Haemost.* 7:1713–1717. doi:10.1111/j.1538-7836.2009.03559.x.

Jain, S., M. Zuka, J. Liu, S. Russell, J. Dent, J.A. Guerrero, J. Forsyth, B. Maruszak, T.K. Gartner, B. Felding-Habermann, and J. Ware. 2007. Platelet glycoprotein Ib alpha supports experimental lung metastasis. *Proc. Natl. Acad. Sci. U.S.A.* 104:9024–9028. doi:10.1073/pnas.0700625104.

Janus-Bell, E., N. Receveur, L. Mercier, C. Mouriaux, S. Magnenat, J. Reiser, F. Lanza, B. Hechler, B. Ho-Tin-Noé, and P.H. Mangin. 2024. Cooperation Between Platelet β1 and β3 Integrins in the Arrest of Bleeding Under Inflammatory Conditions in Mice. *Arterioscler Thromb Vasc Biol*. doi:10.1161/ATVBAHA.124.321104.

Janus-Bell, E., A. Yakusheva, C. Scandola, N. Receveur, U.M. Ahmed, C. Mouriaux, C. Bourdon, C. Loubière, A. Eckly, Y.A. Senis, M.A. Panteleev, C. Gachet, and P.H. Mangin. 2021. Characterization of the Role of Integrin α5β1 in Platelet Function, Hemostasis, and Experimental Thrombosis. *Thromb Haemost*. doi:10.1055/a-1659-6214.

van den Kerkhof, D.L., P.E.J. van der Meijden, T.M. Hackeng, and I. Dijkgraaf. 2021. Exogenous Integrin αIIbβ3 Inhibitors Revisited: Past, Present and Future Applications. *Int J Mol Sci*. 22:3366. doi:10.3390/ijms22073366.

Kopp, H.-G., T. Placke, and H.R. Salih. 2009. Platelet-derived transforming growth factor-beta down-regulates NKG2D thereby inhibiting natural killer cell antitumor reactivity. *Cancer Res*. 69:7775–7783. doi:10.1158/0008-5472.CAN-09-2123.

Kuijpers, M.J.E., V. Schulte, W. Bergmeier, T. Lindhout, C. Brakebusch, S. Offermanns, R. Fässler, J.W.M. Heemskerk, and B. Nieswandt. 2003. Complementary roles of glycoprotein VI and alpha2beta1 integrin in collagen-induced thrombus formation in flowing whole blood ex vivo. *FASEB J.* 17:685–687. doi:10.1096/fj.02-0381fje.

Labelle, M., S. Begum, and R.O. Hynes. 2011. Direct signaling between platelets and cancer cells induces an epithelial-mesenchymal-like transition and promotes metastasis. *Cancer Cell*. 20:576–590. doi:10.1016/j.ccr.2011.09.009.

Labelle, M., S. Begum, and R.O. Hynes. 2014. Platelets guide the formation of early metastatic niches. *Proc. Natl. Acad. Sci. U.S.A.* 111:E3053-3061. doi:10.1073/pnas.1411082111.

Le Chapelain, O., and B. Ho-Tin-Noé. 2022. Intratumoral Platelets: Harmful or Incidental Bystanders of the Tumor Microenvironment? *Cancers*. 14:2192. doi:10.3390/cancers14092192.

Le Chapelain, O., S. Jadoui, A. Gros, S. Barbaria, K. Benmeziane, V. Ollivier, S. Dupont, M. Solo Nomenjanahary, S. Mavouna, J. Rogozarski, M.-A. Mawhin, G. Caligiuri, S. Delbosc, F. Porteu, B. Nieswandt, P.H. Mangin, Y. Boulaftali, and B. Ho-Tin-Noé. 2024. The localization, origin, and impact of platelets in the tumor microenvironment are tumor type-dependent. *J Exp Clin Cancer Res*. 43:84. doi:10.1186/s13046-024-03001-2.

Li, S., Z. Lu, S. Wu, T. Chu, B. Li, F. Qi, Y. Zhao, and G. Nie. 2024. The dynamic role of platelets in cancer progression and their therapeutic implications. *Nat Rev Cancer*. 24:72–87. doi:10.1038/s41568-023-00639-6.

bioRxiv preprint doi: https://doi.org/10.1101/2024.11.22.624871; this version posted November 22, 2024. The copyright holder for this preprint (which was not certified by peer review) is the author/funder. All rights reserved. No reuse allowed without permission.

Lickert, S., M. Kenny, K. Selcuk, J.L. Mehl, M. Bender, S.M. Früh, M.A. Burkhardt, J.-D. Studt, B. Nieswandt, I. Schoen, and V. Vogel. 2022. Platelets drive fibronectin fibrillogenesis using integrin αIIbβ3. *Sci Adv*. 8:eabj8331. doi:10.1126/sciadv.abj8331.

Malacrida, B., S. Nichols, E. Maniati, R. Jones, R. Delanie-Smith, R. Roozitalab, E.J. Tyler, M. Thomas, G. Boot, J. Mackerodt, M. Lockley, M.M. Knight, F.R. Balkwill, and O.M.T. Pearce. 2021. A human multi-cellular model shows how platelets drive production of diseased extracellular matrix and tissue invasion. *iScience*. 24:102676. doi:10.1016/j.isci.2021.102676.

Mammadova-Bach, E., J. Gil-Pulido, E. Sarukhanyan, P. Burkard, S. Shityakov, C. Schonhart, D. Stegner, K. Remer, P. Nurden, A.T. Nurden, T. Dandekar, L. Nehez, M. Dank, A. Braun, D. Mezzano, S.I. Abrams, and B. Nieswandt. 2020. Platelet glycoprotein VI promotes metastasis through interaction with cancer cell-derived galectin-3. *Blood*. 135:1146–1160. doi:10.1182/blood.2019002649.

Mammadova-Bach, E., P. Zigrino, C. Brucker, C. Bourdon, M. Freund, A. De Arcangelis, S.I. Abrams, G. Orend, C. Gachet, and P.H. Mangin. 2016. Platelet integrin α6β1 controls lung metastasis through direct binding to cancer cell-derived ADAM9. *JCI Insight*. 1:e88245. doi:10.1172/jci.insight.88245.

Marguerie, G.A., E.F. Plow, and T.S. Edgington. 1979. Human platelets possess an inducible and saturable receptor specific for fibrinogen. *J Biol Chem*. 254:5357–5363.

Morowski, M., T. Vögtle, P. Kraft, C. Kleinschnitz, G. Stoll, and B. Nieswandt. 2013. Only severe thrombocytopenia results in bleeding and defective thrombus formation in mice. *Blood*. 121:4938–4947. doi:10.1182/blood-2012-10-461459.

Nieswandt, B., C. Brakebusch, W. Bergmeier, V. Schulte, D. Bouvard, R. Mokhtari-Nejad, T. Lindhout, J.W. Heemskerk, H. Zirngibl, and R. Fässler. 2001. Glycoprotein VI but not alpha2beta1 integrin is essential for platelet interaction with collagen. *EMBO J.* 20:2120–2130. doi:10.1093/emboj/20.9.2120.

Nieswandt, B., M. Hafner, B. Echtenacher, and D.N. Männel. 1999. Lysis of tumor cells by natural killer cells in mice is impeded by platelets. *Cancer Res*. 59:1295–1300.

Nieswandt, B., and S.P. Watson. 2003. Platelet-collagen interaction: is GPVI the central receptor? *Blood*. 102:449–461. doi:10.1182/blood-2002-12-3882.

Nieuwenhuis, H.K., K.S. Sakariassen, W.P. Houdijk, P.F. Nievelstein, and J.J. Sixma. 1986. Deficiency of platelet membrane glycoprotein Ia associated with a decreased platelet adhesion to subendothelium: a defect in platelet spreading. *Blood*. 68:692–695.

Osada, M., O. Inoue, G. Ding, T. Shirai, H. Ichise, K. Hirayama, K. Takano, Y. Yatomi, M. Hirashima, H. Fujii, K. Suzuki-Inoue, and Y. Ozaki. 2012. Platelet activation receptor CLEC-2 regulates blood/lymphatic vessel separation by inhibiting proliferation, migration, and tube formation of lymphatic endothelial cells. *J Biol Chem*. 287:22241–22252. doi:10.1074/jbc.M111.329987.

Paul, B.Z.S., G. Vilaire, S.P. Kunapuli, and J.S. Bennett. 2003. Concurrent signaling from Galphaq- and Galphai-coupled pathways is essential for agonist-induced alphavbeta3 activation on human platelets. *J Thromb Haemost*. 1:814–820. doi:10.1046/j.1538-7836.2003.00099.x.

bioRxiv preprint doi: https://doi.org/10.1101/2024.11.22.624871; this version posted November 22, 2024. The copyright holder for this preprint (which was not certified by peer review) is the author/funder. All rights reserved. No reuse allowed without permission.

Pilch, J., R. Habermann, and B. Felding-Habermann. 2002. Unique ability of integrin alpha(v)beta 3 to support tumor cell arrest under dynamic flow conditions. *J Biol Chem*. 277:21930–21938. doi:10.1074/jbc.M201630200.

Placke, T., M. Örgel, M. Schaller, G. Jung, H.-G. Rammensee, H.-G. Kopp, and H.R. Salih. 2012. Platelet-derived MHC class I confers a pseudonormal phenotype to cancer cells that subverts the antitumor reactivity of natural killer immune cells. *Cancer Res.* 72:440–448. doi:10.1158/0008-5472.CAN-11-1872.

Qi, Y., W. Chen, X. Liang, K. Xu, X. Gu, F. Wu, X. Fan, S. Ren, J. Liu, J. Zhang, R. Li, J. Liu, and X. Liang. 2018. Novel antibodies against GPIbα inhibit pulmonary metastasis by affecting vWF-GPIbα interaction. *J Hematol Oncol*. 11:117. doi:10.1186/s13045-018-0659-4.

Saelman, E.U., H.K. Nieuwenhuis, K.M. Hese, P.G. de Groot, H.F. Heijnen, E.H. Sage, S. Williams, L. McKeown, H.R. Gralnick, and J.J. Sixma. 1994. Platelet adhesion to collagen types I through VIII under conditions of stasis and flow is mediated by GPIa/IIa (alpha 2 beta 1-integrin). *Blood*. 83:1244–1250.

Sakuishi, K., L. Apetoh, J.M. Sullivan, B.R. Blazar, V.K. Kuchroo, and A.C. Anderson. 2010. Targeting Tim-3 and PD-1 pathways to reverse T cell exhaustion and restore anti-tumor immunity. *Journal of Experimental Medicine*. 207:2187–2194. doi:10.1084/jem.20100643.

Sasaki, T., T. Shirai, N. Tsukiji, S. Otake, S. Tamura, J. Ichikawa, M. Osada, K. Satoh, Y. Ozaki, and K. Suzuki-Inoue. 2018. Functional characterization of recombinant snake venom rhodocytin: rhodocytin mutant blocks CLEC-2/podoplanin-dependent platelet aggregation and lung metastasis. *J Thromb Haemost*. 16:960–972. doi:10.1111/jth.13987.

Savage, B., F. Almus-Jacobs, and Z.M. Ruggeri. 1998. Specific synergy of multiple substrate-receptor interactions in platelet thrombus formation under flow. *Cell*. 94:657–666. doi:10.1016/s0092-8674(00)81607-4.

Savage, B., E. Saldívar, and Z.M. Ruggeri. 1996. Initiation of platelet adhesion by arrest onto fibrinogen or translocation on von Willebrand factor. *Cell*. 84:289–297.

Schaff, M., C. Tang, E. Maurer, C. Bourdon, N. Receveur, A. Eckly, B. Hechler, C. Arnold, A. de Arcangelis, B. Nieswandt, C.V. Denis, O. Lefebvre, E. Georges-Labouesse, C. Gachet, F. Lanza, and P.H. Mangin. 2013. Integrin α6β1 is the main receptor for vascular laminins and plays a role in platelet adhesion, activation, and arterial thrombosis. *Circulation*. 128:541–552. doi:10.1161/CIRCULATIONAHA.112.000799.

Schaubaecher, J.B., B. Smiljanov, F. Haring, K. Steiger, Z. Wu, A. Ugurluoglu, J. Luft, S. Ballke, S. Mahameed, V. Schneewind, J. Hildinger, M. Canis, L.A. Mittmann, C. Braun, G. Zuchtriegel, R. Kaiser, L. Nicolai, M. Mack, W. Weichert, K. Lauber, B. Uhl, and C.A. Reichel. 2024. Procoagulant platelets promote immune evasion in triple-negative breast cancer. *Blood*. 144:216–226. doi:10.1182/blood.2023022928.

Schindelin, J., I. Arganda-Carreras, E. Frise, V. Kaynig, M. Longair, T. Pietzsch, S. Preibisch, C. Rueden, S. Saalfeld, B. Schmid, J.-Y. Tinevez, D.J. White, V. Hartenstein, K. Eliceiri, P. Tomancak, and A. Cardona. 2012. Fiji: an open-source platform for biological-image analysis. *Nat Methods*. 9:676–682. doi:10.1038/nmeth.2019.

bioRxiv preprint doi: https://doi.org/10.1101/2024.11.22.624871; this version posted November 22, 2024. The copyright holder for this preprint (which was not certified by peer review) is the author/funder. All rights reserved. No reuse allowed without permission.

Schumacher, D., B. Strilic, K.K. Sivaraj, N. Wettschureck, and S. Offermanns. 2013. Platelet-derived nucleotides promote tumor-cell transendothelial migration and metastasis via P2Y2 receptor. *Cancer Cell*. 24:130–137. doi:10.1016/j.ccr.2013.05.008.

Shirai, T., O. Inoue, S. Tamura, N. Tsukiji, T. Sasaki, H. Endo, K. Satoh, M. Osada, H. Sato-Uchida, H. Fujii, Y. Ozaki, and K. Suzuki-Inoue. 2017. C-type lectin-like receptor 2 promotes hematogenous tumor metastasis and prothrombotic state in tumor-bearing mice. *J Thromb Haemost*. 15:513–525. doi:10.1111/jth.13604.

Solh, T., A. Botsford, and M. Solh. 2015. Glanzmann's thrombasthenia: pathogenesis, diagnosis, and current and emerging treatment options. *J Blood Med*. 6:219–227. doi:10.2147/JBM.S71319.

Sonnenberg, A., P.W. Modderman, and F. Hogervorst. 1988. Laminin receptor on platelets is the integrin VLA-6. *Nature*. 336:487–489. doi:10.1038/336487a0.

Takagi, J., B.M. Petre, T. Walz, and T.A. Springer. 2002. Global conformational rearrangements in integrin extracellular domains in outside-in and inside-out signaling. *Cell*. 110:599–511. doi:10.1016/s0092-8674(02)00935-2.

Tang, Y.-Q., M.R. Yeaman, and M.E. Selsted. 2002. Antimicrobial peptides from human platelets. *Infect Immun*. 70:6524–6533. doi:10.1128/iai.70.12.6524-6533.2002.

Tsukiji, N., M. Osada, T. Sasaki, T. Shirai, K. Satoh, O. Inoue, N. Umetani, C. Mochizuki, T. Saito, S. Kojima, H. Shinmori, Y. Ozaki, and K. Suzuki-Inoue. 2018. Cobalt hematoporphyrin inhibits CLEC-2-podoplanin interaction, tumor metastasis, and arterial/venous thrombosis in mice. *Blood Adv*. 2:2214–2225. doi:10.1182/bloodadvances.2018016261.

Versteeg, H.H., J.W.M. Heemskerk, M. Levi, and P.H. Reitsma. 2013. New fundamentals in hemostasis. *Physiol. Rev.* 93:327–358. doi:10.1152/physrev.00016.2011.

Yeaman, M.R. 2014. Platelets: at the nexus of antimicrobial defence. *Nat Rev Microbiol*. 12:426–437. doi:10.1038/nrmicro3269.

Zhang, W., S. Dang, T. Hong, J. Tang, J. Fan, D. Bu, Y. Sun, Z. Wang, and T. Wisniewski. 2012. A humanized single-chain antibody against beta 3 integrin inhibits pulmonary metastasis by preferentially fragmenting activated platelets in the tumor microenvironment. *Blood*. 120:2889–2898. doi:10.1182/blood-2012-04-425207.

Zhou, M., Y. Feng, X. Zhang, J. Chen, N. Yao, S. Fu, T. Ni, Y. Chen, F. Xie, S. Roy, J. Liu, Y. Yang, Y. He, Y. Zhao, and N. Yang. 2024. Platelet-derived microparticles adoptively transfer integrin β3 to promote antitumor effect of tumor-infiltrating T cells. *OncoImmunology*. 13:2304963. doi:10.1080/2162402X.2024.2304963.

Zuo, X.-X., Y. Yang, Y. Zhang, Z.-G. Zhang, X.-F. Wang, and Y.-G. Shi. 2019. Platelets promote breast cancer cell MCF-7 metastasis by direct interaction: surface integrin α2β1-contacting-mediated activation of Wnt-β-catenin pathway. *Cell Commun Signal*. 17:142. doi:10.1186/s12964-019-0464-x.

bioRxiv preprint doi: https://doi.org/10.1101/2024.11.22.624871; this version posted November 22, 2024. The copyright holder for this preprint (which was not certified by peer review) is the author/funder. All rights reserved. No reuse allowed without permission.

FIGURE LEGENDS

Figure 1: PF4Cre-β1$^{-/-}$/β3$^{-/-}$ mice platelet count, expression of major surface glycoproteins and platelet function. A. Platelet count. Platelet count from PF4Cre (n = 30) and PF4Cre-β1$^{-/-}$/β3$^{-/-}$ mice (n = 30) was evaluated. Data are from 6 independent experiments and unpaired t-test was applied. **B.** Glycoproteins surface expression. Surface expression of various glycoproteins on platelets in whole blood from PF4Cre (n = 3 or 6) and PF4Cre-β1$^{-/-}$/β3$^{-/-}$ mice (n = 3 or 6) was evaluated using selective antibodies and flow cytometry. Data are from 2 independent experiments and unpaired t-test or Mann-Whitney test were applied. **C.** Fibrinogen binding. Whole blood from PF4Cre (n = 6 or 9) and PF4Cre-β1$^{-/-}$/β3$^{-/-}$ mice (n = 6 or 9) was stimulated for 10 min with ADP (2 µmol/L) or protease-activated receptor 4 peptide (PAR-4 peptide) (1 mmol/L) and the binding of fluorescein isothiocyanate (FITC)-fibrinogen was detected by flow cytometry. Data are from 3 independent experiments and Mann-Whitney test was applied. **D**. P-selectin exposure. Whole blood from PF4Cre (n = 6 or 9) and PF4Cre-β1$^{-/-}$/β3$^{-/-}$ mice (n = 6 or 9) was stimulated for 10 min with U46619 (2 µmol/L) or PAR-4 peptide (1 mmol/L) and a FITC-conjugated anti-P-selectin antibody was detected by flow cytometry. Data are from 3 independent experiments and unpaired t-test or Mann-Whitney were applied. **E.** Annexin V binding. Whole blood from PF4Cre (n = 6 to 9) and PF4Cre-β1$^{-/-}$/β3$^{-/-}$ mice (n = 6 to 9) was stimulated with convulxin (15 nmol/L) or collagen related peptide (CRP) (1 µg/mL) + PAR-4 peptide (1 mmol/L) for 10 min, incubated with Alexa Fluor 488-annexin V for 20 min and analyzed by flow cytometry. The forward light scatter and fluorescence intensity of 10,000 cells were collected with a logarithmic gain and the percentage of annexin V-positive platelets was determined in the upper quadrant of the plot. Data are from 6 independent experiments and unpaired t-test or Mann-Whitney were applied. **F to I.** *In vitro* flow assays. Whole blood from PF4Cre (n = 4-5) and PF4Cre-β1$^{-/-}$/β3$^{-/-}$ mice (n = 3-5) was perfused through PDMS flow chambers coated with fibrinogen (100

bioRxiv preprint doi: https://doi.org/10.1101/2024.11.22.624871; this version posted November 22, 2024. The copyright holder for this preprint (which was not certified by peer review) is the author/funder. All rights reserved. No reuse allowed without permission.

µg/mL) at 300 s^{-1} for 5 min (F and G) or with fibrillar cellular fibronectin (300 µg/mL) at 300 s^{-1} for 8 min (H) or with vWF A3 binding peptide vA3-III-23 (100 µg/mL) at 1,500 s^{-1} for 2 min (I). Platelet adhesion was visualized in random fields by DIC microscopy, scale bar 50 µm (F), and the number of adherent platelets was quantified (G, H and I). Data are from 2 or 3 independent experiments and unpaired t-test (I) or Mann-Whitney (G and H) were applied. Results are expressed as the mean ± standard error of the mean (SEM); ns $p > 0.05$; * $p < 0.05$; ** $p < 0.01$; *** $p < 0.001$; **** $p < 0.0001$.

Figure 2: PF4Cre-β1$^{-/-}$/β3$^{-/-}$ mice are not able to form thrombosis and present an increased bleeding time. A and B. Thrombus formation *in vitro*. Whole blood from PF4Cre (n = 4) and PF4Cre-β1$^{-/-}$/β3$^{-/-}$ mice (n = 4) was perfused at 300 s^{-1} through PDMS flow chambers coated with collagen (200 µg/mL) for 8 min. Platelet aggregation was visualized in random fields by DIC microscopy, scale bar 50 µm (A). The area of the thrombi was quantified (B). Data are from 2 independent experiments and Mann-Whitney was applied. **C and D.** Tail bleeding time. The tail of PF4Cre (n = 5) and PF4Cre-β1$^{-/-}$/β3$^{-/-}$ mice (n = 5) was sectioned. The time required for the bleeding to stop was recorded (C) and the volume of blood lost (D) was measured. Data are from 1 experiment and Mantel-Cox test (C) or Mann-Whitney test (D) were applied. **E.** Carotid bleeding time. The carotid artery of PF4Cre (n = 4) and PF4Cre-β1$^{-/-}$/β3$^{-/-}$ mice (n = 4) was punctured and the time required for the bleeding to stop was measured. Data are from 1 experiment and Mantel-Cox test was applied. **F to H.** $FeCl_3$ thrombosis of the carotid artery. Thrombosis was triggered in PF4Cre (n = 4) and PF4Cre-β1$^{-/-}$/β3$^{-/-}$ mice (n = 3) by application of a filter paper saturated with 7.5% $FeCl_3$ to the common carotid artery. Representative fluorescence images of the thrombus (green) at the indicated time points after injury, scale bar 500 µm (F). The area of the thrombi was quantified (G) and area under the curves (AUC) are used to compare data (H). Data are from

bioRxiv preprint doi: https://doi.org/10.1101/2024.11.22.624871; this version posted November 22, 2024. The copyright holder for this preprint (which was not certified by peer review) is the author/funder. All rights reserved. No reuse allowed without permission.

1 experiment and Mann-Whitney test was applied. **I to K.** Pinching-induced thrombosis of the abdominal aorta. Thrombosis was triggered in PF4Cre (n = 3) and PF4Cre-$\beta1^{-/-}/\beta3^{-/-}$ mice (n = 3) by compression of the abdominal aorta with forceps. Representative fluorescence images of the thrombus (green) at the indicated time points after injury, scale bar 500 µm (I). The area of the thrombi was quantified (J) and AUC are used to compare data (K). Data are from 1 experiment and Mann-Whitney test was applied. The symbols correspond to individual mice. Results are expressed as the mean ± standard error of the mean (SEM); * $p < 0.05$; ** $p < 0.01$; *** $p < 0.001$; **** $p < 0.0001$.

Figure 3. PF4Cre-$\beta1^{-/-}/\beta3^{-/-}$ platelets promotes a reduced binding to tumor cells, primary tumor growth and metastatic outgrowth. A. Platelets-Tumor cells *in vitro* interaction. Left: Experiment infographics. Middle: Representative confocal microscopy images (scale bar 10 µm). Right: graph representing the number of interacting platelets per single tumor cell for PF4Cre (356 cells) and PF4Cre-$\beta1^{-/-}/\beta3^{-/-}$ (288 cells). Data are from 1 experiment and Mann-Whitney test was applied. **B.** Orthotopic tumor model. Left: Infographics of the experimental scheme of the *in vivo* orthotopic tumor model. Right: Representative images of PF4Cre and PF4Cre-$\beta1^{-/-}/\beta3^{-/-}$ tumors at the sacrifice. Scale bar 1 cm. **C.** Orthotopic tumor model results. Left: Longitudinal tumor model measurement *in vivo* (measured *via* caliper) from PF4Cre (n = 13) and PF4Cre-$\beta1^{-/-}/\beta3^{-/-}$ mice (n = 12) during the course of the experiment. Mean ± range is represented (dotted lines). Data are from 2 independent experiments and Two-way ANOVA was applied. On the upper left, classification of number of mice with different tumor volume. The classification method is indicated in the figure. Right: *Ex-vivo* tumor weight measurement in PF4Cre (n=13) and PF4Cre-$\beta1^{-/-}/\beta3^{-/-}$ (n=12). Mean, quartiles and data distribution are represented. Data are from 2 independent experiments and Mann-Whitney test was applied. **D**. Hematoxylin and Eosin staining on paraffin-embedded lungs from orthotopic tumor model.

bioRxiv preprint doi: https://doi.org/10.1101/2024.11.22.624871; this version posted November 22, 2024. The copyright holder for this preprint (which was not certified by peer review) is the author/funder. All rights reserved. No reuse allowed without permission.

Left: Representative images (scale bar 200 µm). Right: Quantification of the percentage of metastatic area on the total tissue area from PF4Cre (24 images from 6 mice) and PF4Cre-$\beta1^{-/-}$ /$\beta3^{-/-}$ (20 images from 5 mice). Each dot represents a single mouse. Mean ± SD per experimental group is represented. Data are from 1 experiment. **E.** Masson Trichrome staining. Upper: representative images (scale bar 100 µm). Bottom: quantification of the percentage of Masson positive area from PF4Cre (6 images from 2 mice) and PF4Cre-$\beta1^{-/-}$/$\beta3^{-/-}$ (6 images from 3 mice). Each bigger point represents the mean value of a single mouse; littler points are representative of the mean of distinct images. Mean per experimental group is represented. Data are from 1 experiment and Mann-Whitney test was applied. **F.** Tumor Immunofluorescence on paraffin slides (IF) for $CD45^{+}$ cells. Upper: representative images (scale bar 20 µm). Bottom: quantification of the percentage of $CD45^{+}$ cells on the number of nuclei from PF4Cre (55 images from 6 mice) and PF4Cre-$\beta1^{-/-}$/$\beta3^{-/-}$ (52 images from 6 mice). Each bigger point represents the mean value of a single mice; littler points are representative of the mean of distinct images. Mean per experimental group is represented. Data are from 1 experiment and Mann-Whitney test was applied. **G.** *Ex-vivo* tumor immunophenotyping by flow-cytometry. Percentages of immune cell populations within the defined gating are represented for PF4Cre (n=5) and PF4Cre-$\beta1^{-/-}$/$\beta3^{-/-}$ (n=6). Data are from 1 experiment and Mann-Whitney test was applied. **H.** Left: Infographics of the experimental scheme of the *in vivo* experimental metastasis model. Right: Representative images at day 0 and day 14. **I.** Body Luminescence Index (BLI) from the experimental metastasis experiment. Relative photon flux (p/s) compared to day 0 is represented for PF4Cre (n=8) and PF4Cre-$\beta1^{-/-}$/$\beta3^{-/-}$ (n=6). Mean ± range is represented. Data are from 1 experiment and Two-way ANOVA was applied.

bioRxiv preprint doi: https://doi.org/10.1101/2024.11.22.624871; this version posted November 22, 2024. The copyright holder for this preprint (which was not certified by peer review) is the author/funder. All rights reserved. No reuse allowed without permission.

Figure 1

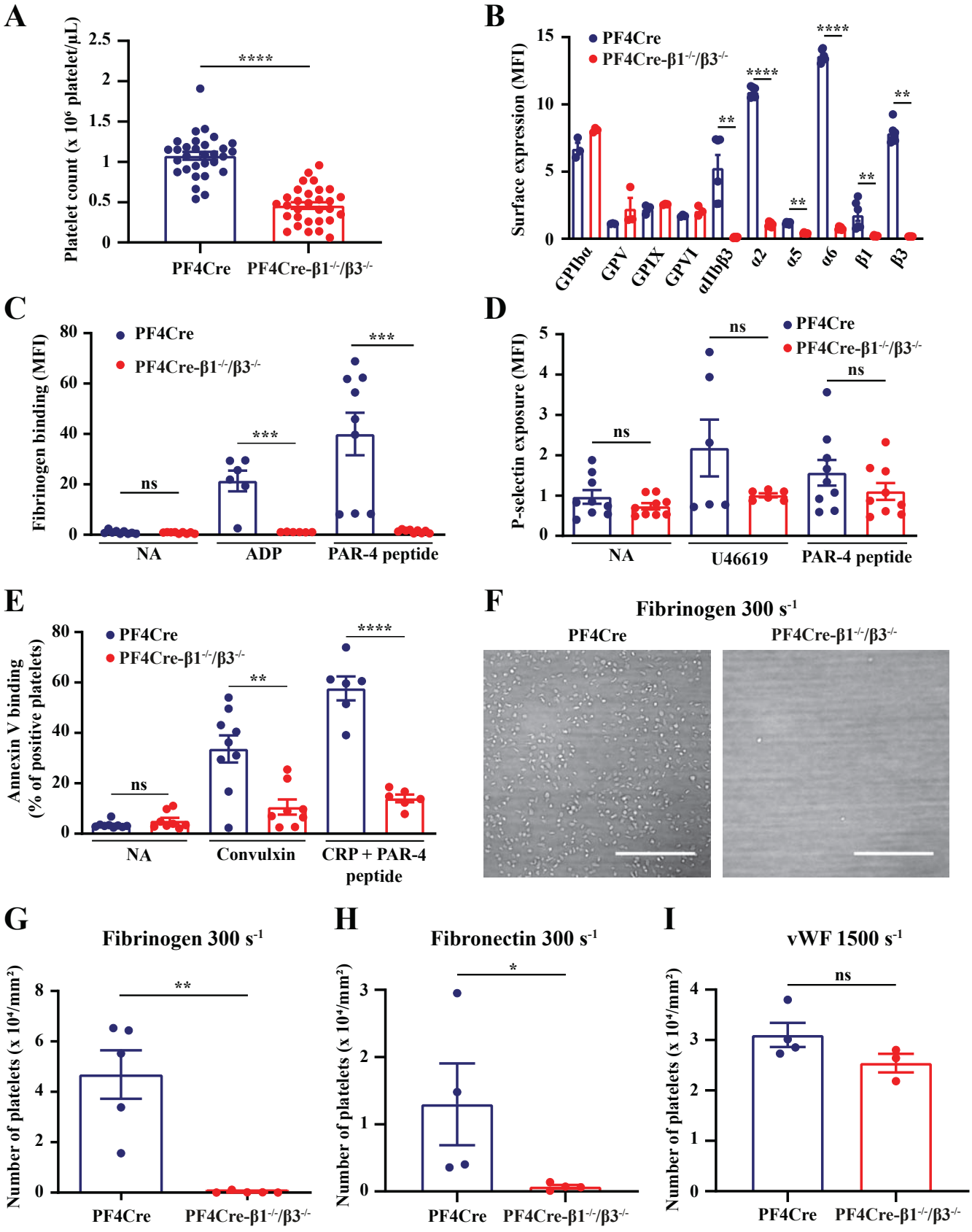

Figure 2

bioRxiv preprint doi: https://doi.org/10.1101/2024.11.22.624871; this version posted November 22, 2024. The copyright holder for this preprint (which was not certified by peer review) is the author/funder. All rights reserved. No reuse allowed without permission.

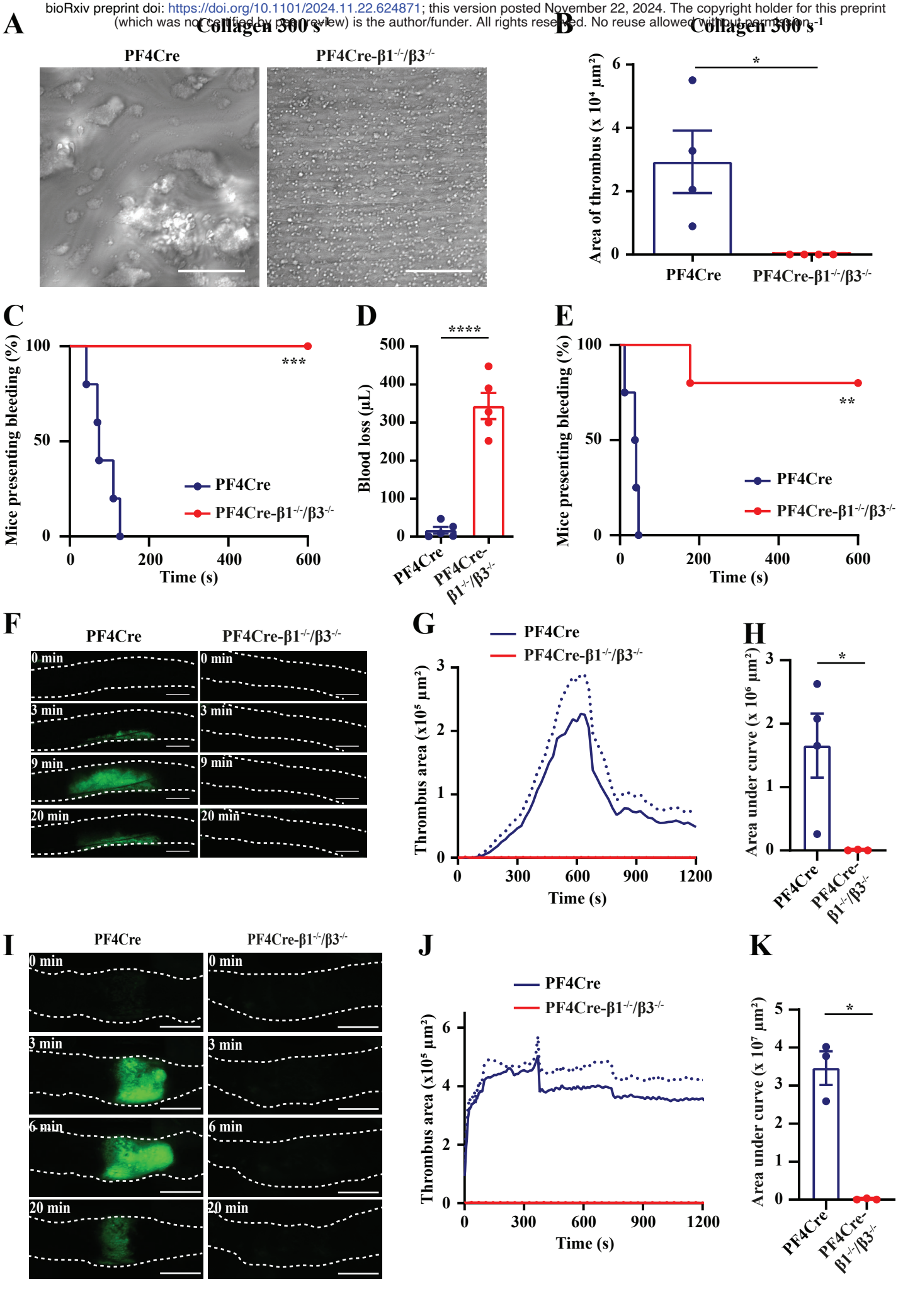

Figure 3

bioRxiv preprint d https://doi.org/10.1101/2024.11.22.624871; this version posted November 22, 2024. The copyright holder for this preprint (which was not certified by peer review) is the author/funder. All rights reserved. No reuse allowed without permission.

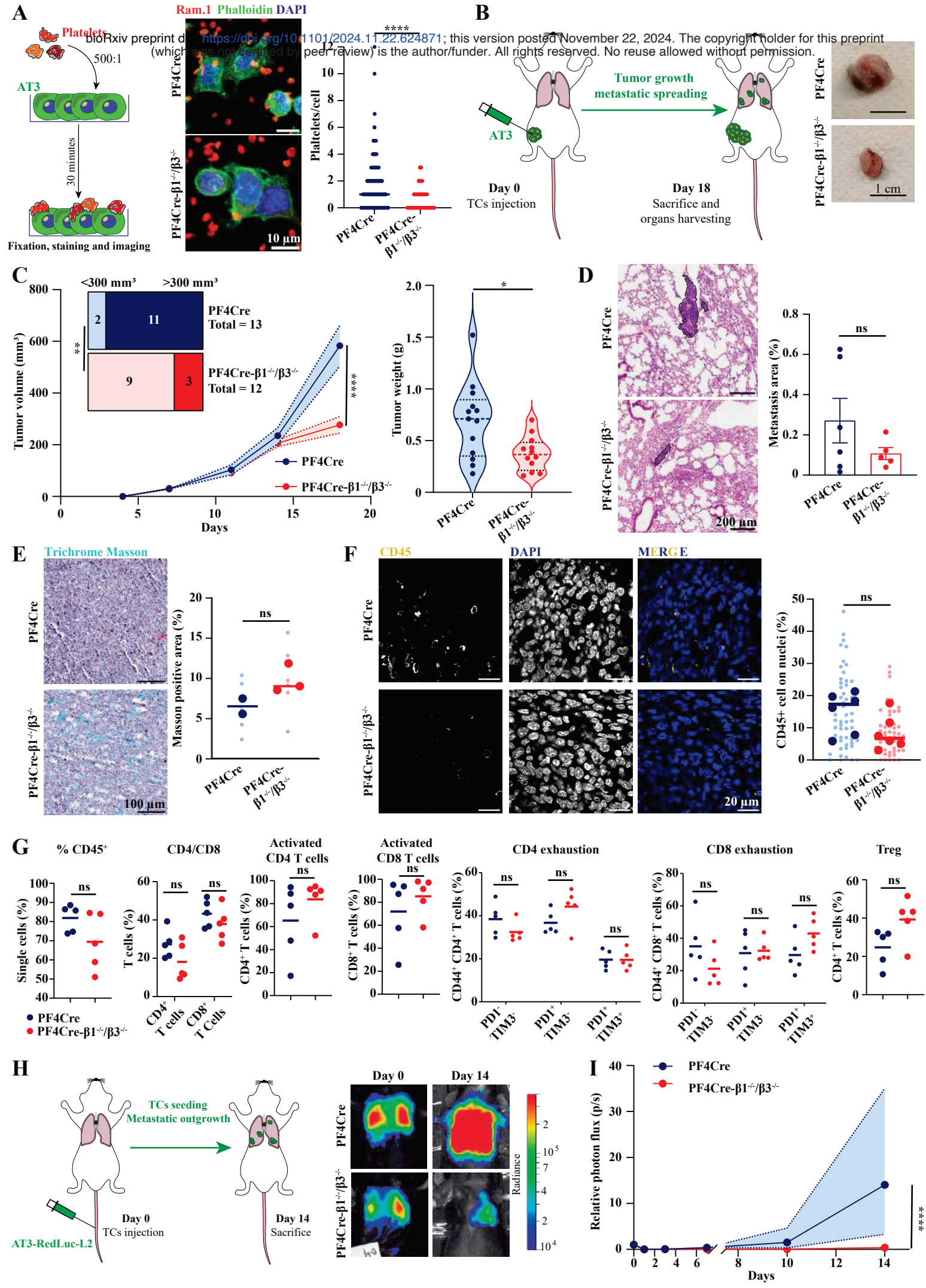

3. Anti-BCMA immuno-nanoPET radiotracers for improved detection of multiple myeloma.

Check for updates

RESEARCH ARTICLE

ADVANCED HEALTHCARE MATERIALS
www.advhealthmat.de

Anti-BCMA Immuno-NanoPET Radiotracers for Improved Detection of Multiple Myeloma

Eloise Thomas, Clélia Mathieu, Patricia Moreno-Gaona, Vincent Mittelheisser, François Lux, Olivier Tillement, Xavier Pivot, Paiman Peter Ghoroghchian, and Alexandre Detappe**

Current clinical imaging modalities for the sensitive and specific detection of multiple myeloma (MM) rely on nonspecific imaging contrast agents based on gadolinium chelates for magnetic resonance imaging (MRI) or for ^{18}F-FDG-directed and combined positron emission tomography (PET) and computed tomography (CT) scans. These tracers are not, however, able to detect minute plasma cell populations in the tumor niche, leading to false negative results. Here, a novel PET-based anti-BCMA nanoplatform labeled with ^{64}Cu is developed to improve the monitoring of these cells in both the spine and femur and to compare its sensitivity and specificity to more conventional immunoPET (^{64}Cu labeled anti-BCMA antibody) and passively targeted PET radiotracers ($^{64}CuCl_2$ and ^{18}F-FDG). This proof-of-concept preclinical study confirmed that by conjugating up to four times more radioisotopes per antibody with the immuno-nanoPET platform, an improvement in the sensitivity and in the specificity of PET to detect tumor cells in an orthotopic model of MM is observed when compared to the traditional immunoPET approach. It is anticipated that when combined with tumor biopsy, this immuno-nanoPET platform may improve the management of patients with MM.

1. Introduction

Imaging modalities for the early detection and longitudinal tracking of multiple myeloma (MM) have been significantly improved due to the optimization of novel magnetic resonance imaging (MRI) acquisition protocols and positron emission tomography (PET) tracers.[1–4] While MRI and PET tracers are routinely used to diagnose and monitor the progression of MM, these tracers are far from optimal due to their nonspecific binding to tumor cells. MRI tracers accumulate in tumor environments based on the enhanced permeability and retention (EPR) effect,[5] while PET radiotracers, and more specifically the ^{18}F-FDG tracer, function by imaging the tumor based on its glucose uptake, which, at low density, remains nonspecific[6,7] and can lead to false negative results in the context of cellular inactivity.[8]

Recently, immunoPET radiotracers have been translated into the clinic due to the specificity of selected antibodies and the high sensitivity of PET imaging[9,10]. Preclinical studies involving immunoPET radiotracers (using antibodies or nanobodies)[11–13] and antibody-conjugated MRI tracers[14] have demonstrated the possibility of significantly improving longitudinal monitoring of MM. The development of novel immunoPET radiotracers is of keen interest due to their better signal-to-noise ratios (SNRs) over MRI-based methods and their ability to detect small

E. Thomas
LAGEPP Université Claude Bernard Lyon 1
CNRS UMR5007
Villeurbanne France

C. Mathieu
Université Paris-Saclay
CNRS UMR 8612
Institut Galien Paris-Saclay
France

P. Moreno-Gaona, V. Mittelheisser, X. Pivot, A. Detappe
Institut de Cancérologie Strasbourg Europe (ICANS)
Strasbourg France
E-mail: a.detappe@icans.eu

The ORCID identification number(s) for the author(s) of this article can be found under https://doi.org/10.1002/adhm.202101565

DOI: 10.1002/adhm.202101565

F. Lux, O. Tillement
Institut Lumière-Matière
Université Claude Bernard Lyon 1
CNRS UMR5306
Villeurbanne France

F. Lux
Institut Universitaire de France (IUF)
Paris France

P. P. Ghoroghchian
David H Koch Institute for Integrative Cancer Research
MIT, Cambridge, MA USA
E-mail: ppg@mit.edu

P. P. Ghoroghchian
Dana Farber Cancer Institute
Boston, MA USA

A. Detappe
Strasbourg Drug Discovery and Development Institute (IMS)
Strasbourg France

 © 2021 Wiley-VCH GmbH

clusters of cells, potentially enabling the identification of minimal residual disease (MRD), which is currently difficult with passive contrast agents for PET imaging.[3] Importantly, recent preclinical and clinical studies have demonstrated promising results with the development of novel immunoPET radiotracers based on the use of anti-CD38 (mAb) and anti-CD138 monoclonal antibodies (mAbs) conjugated with DOTA-^{64}Cu or DOTA-^{89}Zr to monitor MM cells.[11,12] The results of the first clinical trials in MM patients using these tracers[12] demonstrated that the use of CD38-immunoPET radiotracers improved both the sensitivity and specificity of MM detection in comparison to fluorodeoxyglucose (^{18}F) (^{18}F-FDG)-based PET imaging.

Leveraging these promising results, we designed an innovative approach that targets the B-cell maturation antigen (BCMA) that is widely used as a therapeutic target in MM and that is highly expressed at all stages of the disease; notably, this approach differs from traditional methods that have instead targeted CD38, which is a transmembrane glycoprotein that is almost exclusively expressed on MM cells.[14] BCMA is a known target for chimeric antigen receptor (CAR) T-cell[15] and bispecific antibody therapy;[16] but, it has yet to be adopted for MM imaging.[17] While we previously successfully demonstrated that targeting BCMA for preclinical MRI-based imaging of MM is a relevant approach,[14] here, we hypothesized that the use of a immuno-nanoPET radiotracer would enable a decrease in the amount of mAb needed for injection in comparison to the amounts of immunoPET radiotracer required to improve the sensitivity of PET imaging. To develop this platform, we conjugated polysiloxane-based ultrasmall (<5 nm) nanoparticles (NPs) with NODAGA chelators for efficient ^{64}Cu labeling. Then, further functionalization between the NP-NODAGA and the anti-BCMA mAb was performed to generate the anti-BCMA/NP conjugate. We selected the radioisotope ^{64}Cu instead of ^{89}Zr because of its shorter half-life (12.7 h vs. 3.3 days, respectively), enabling longitudinal injections in a clinically relevant workflow.

The functionalization of the polysiloxane matrix to NODAGA chelators was performed on a polysiloxane matrix presenting already chelated gadolinium atoms in DOTAGA chelates.[18,19] This grafting approach is similar to the previously described protocol performed to conjugate a second metal to the surface of the same NP.[20] Additionally, we previously described that such NPs are safe and nontoxic after conjugation to various antibodies, including an anti-BCMA mAb.[14,21] However, we did not use the intrinsic gadolinium MRI properties for bimodal imaging in this study as we focused only on evaluating PET imaging sensitivity and specificity in comparison to conventional PET contrast agents

The motivation to functionalize anti-BCMA mAbs with NPs was based on two reasons: i) we previously demonstrated that the anti-BCMA mAb could be loaded with up to 4 NPs on its structure without affecting its targeting specificity in vitro or in vivo and that this conjugation effectively reduced the half-life and improved the clearance of the mAb from the body;[14] ii) while the synthesis of the currently used immunoPET tracers is limited to approximately 2 to 4 radioisotopes per antibody,[11,12] immuno-nanoPET tracers allow optimization of the number of molecules per mAb (i.e., the drug-to-antibody ratio (DAR)) up to of 4[14] and enable an increase amount of radiotracer per mAb (as each NP can carry several radionuclides).[22] In this study, we functionalized an anti-BCMA mAb with ultrasmall NPs bearing a NODAGA chelator filled with the radioisotope ^{64}Cu (i.e., anti-BCMA/NP@^{64}Cu). We compared its sensitivity and specificity to detect MM cells in an orthotopic MM mouse model and to results obtained with anti-BCMA immunoPET (anti-BCMA@^{64}Cu), untargeted NP@^{64}Cu, $^{64}CuCl_2$, and ^{18}F-FDG radiotracers (**Figure 1**A–C).

2. Results and Discussion

The synthesis of the immune-nanoPET radiotracer was performed in three steps. First, ultrasmall NPs of approximately 3.6 nm in diameter were synthesized; their surfaces were functionalized with NODAGA chelators, leading to small particles with diameters of 4.3 nm.[22] The addition of approximately 4 NODAGA chelators to the particle surface was confirmed with several complementary techniques, including zetametry, infrared spectroscopy, and titrations with europium and copper ions (see Materials and Methods and Figure S1, Supporting Information). In the second step, NP/NODAGA was grafted onto the mAb, using a previously reported transcyclooctene (TCO)-tetrazin (Tz) click chemistry approach[21] and leading to approximately 3 NPs per antibody. Finally, the anti-BCMA/NPs were successfully labeled with ^{64}Cu and purified to give 100% radiochemical purity. In comparison to classical immunoPET tracers, the NP-based immunoPET strategy has an advantage in its ease of loading for an increased number of radioisotopes per mAb; and, with up to 3 NPs per antibody and 4 NODAGA chelators per NP, we were able to conjugate up to 12 radioisotopes per mAb instead of the typical 2 to 4 radioisotopes obtained through standard immunoPET approaches. Importantly, the conjugation of an average of 3 NPs per anti-BCMA mAb does not interfere with its binding affinity (Figure S2, Supporting Information).

An in vivo evaluation of the developed immuno-nanoPET tracer was then performed on an orthotopic xenograft MM mouse model. The conjugation of the ultrasmall NPs to monoclonal antibodies (mAbs) significantly decreased the circulation time of the mAbs (31.4 min for anti-BCMA/NP@^{64}Cu vs. 25.4 h for anti-BCMA@^{64}Cu) in comparison to the anti-BCMA@^{64}Cu immunoPET tracer (Figure 1D–F). The pharmacokinetic (PK) results showed significantly different biodistribution profiles for anti-BCMA@^{64}Cu in comparison to NP@^{64}Cu and anti-BCMA/NP@^{64}Cu (Figure 1G–I). While anti-BCMA@^{64}Cu seems to be equivalently represented in the majority of organs from 15 min to 48 h after intravenous (IV) administration in healthy mice, rapid washout through the kidneys was observed for both the untargeted and targeted NP platforms, which was in line with results from previous studies.[14]

A comparative study was performed by determining the optimal SNR based on the diverging BD profiles of the biomarkers (Figure 1A). No signs of macroscopic toxicity were observed after IV injection of the different tracers as evidenced from stable body weights during monitoring (Figure S3, Supporting Information) and on previously conducted in-depth blood and tissue analyses after hematoxylin and eosin staining.[14] The biodistribution profile of anti-BCMA/NP@^{64}Cu is similar to that from the previously described anti-BCMA/NP@Gd^{3+} compound.[14] We first validated the specificity of the anti-BCMA/NP@^{64}Cu to target BCMA+ cells in vivo by performing a blocking study in an orthotopic mouse model. MM.1$S_{GFP+}/_{Luc+}$ cells were injected

© 2021 Wiley-VCH GmbH

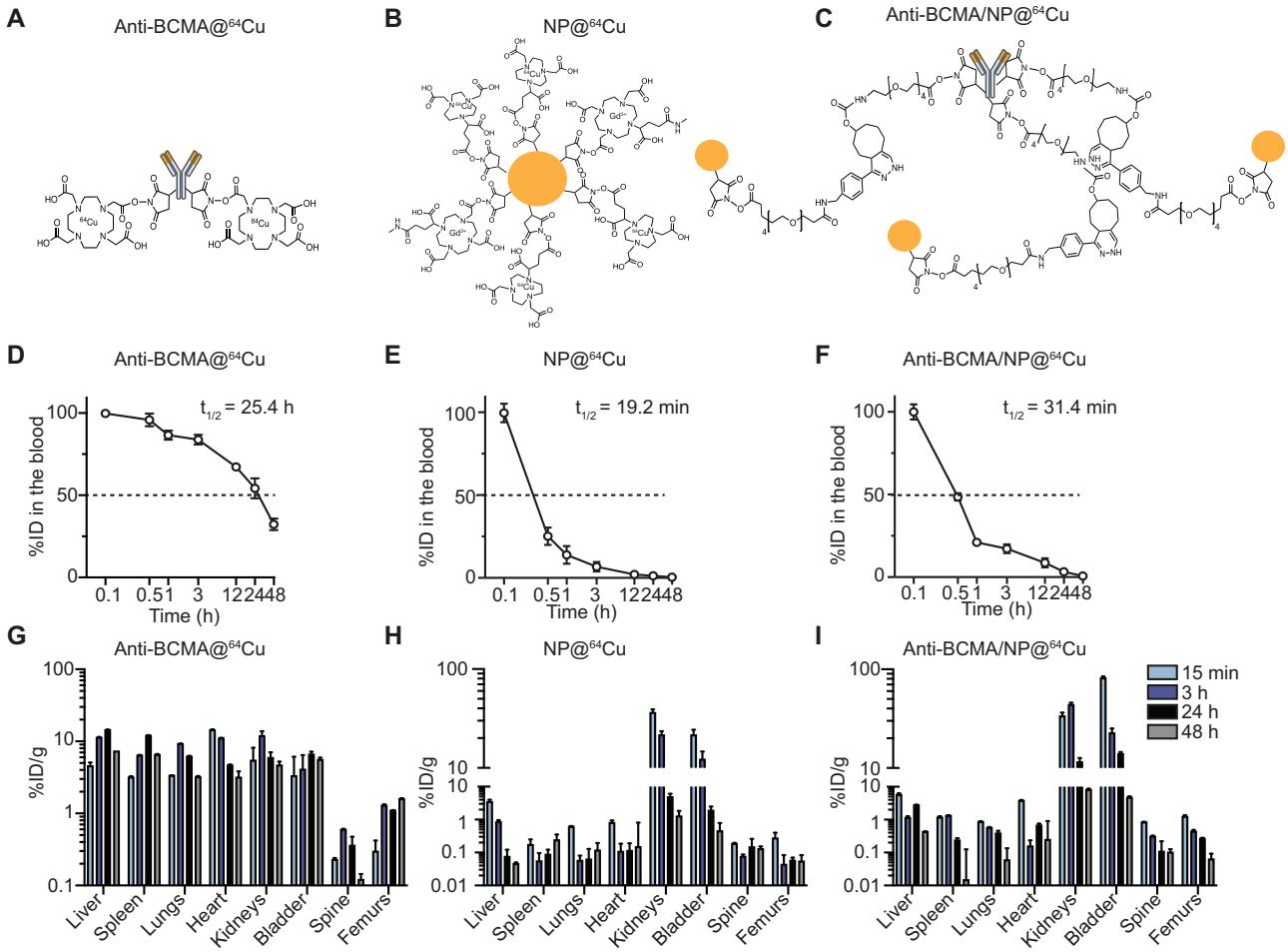

Figure 1. Design and pharmacokinetic profiles of the radioisotopes. A) Structures of the anti-BCMA@^{64}Cu immunoPET, B) untargeted NP@^{64}Cu, and C) anti-BCMA/NP@^{64}Cu immuno-nanoPET radiotracers. D) Pharmacokinetic profiles of anti-BCMA@^{64}Cu, E) NP@^{64}Cu, and F) anti-BCMA/NP@^{64}Cu in healthy BALB/c mice (n = 5/time point). **G**. Biodistribution data in the major organs over time in anti-BCMA@^{64}Cu, H. NP@^{64}Cu, and I) anti-BCMA/NP@^{64}Cu healthy BALB/c mice (n = 5/time point). All measurements were decay-corrected.

(IV) and allowed to grow for 15 days before a positive bioluminescence signal was observed in the spine and femur. For the blocking study, we pretreated a group of mice with unlabeled anti-BCMA mAbs 24 h before IV injection (Figure S4, Supporting Information) and subsequently confirmed the specificity of the anti-BCMA immuno-nanoPET tracer to specifically target tumor cells in unblocked mice rather than to penetrate the tumor by passive internalization in both groups, which matched previously reported findings.[14]

To demonstrate the rationale of developing the anti-BCMA PET nanoplatform, we next sought to compare the specificity of the anti-BCMA immuno-nanoPET tracer to conventional PET tracers in the same orthotopic model of MM (i.e., MM.1S$_{GFP+/Luc+}$ cells implanted and allowed to grow for 15 days with positive bioluminescence signal confirmed in the spine and femur). We performed a quantification study based on equivalent quantities of radioisotope after IV administration (10 MBq). Each study group was imaged at their respective optimal time points: 5 min for ^{18}F-FDG, 15 min for ^{64}CuCl$_2$ and NP@^{64}Cu, 2 h for anti-BCMA/NP@^{64}Cu, and 6 h for anti-BCMA@^{64}Cu (**Figure 2** and Figure S5, Supporting Information). We observed a significantly brighter signal in the spines (Figure 2A,B) and femurs (Figure 2C,D) of mice administered with the anti-BCMA/NP@^{64}Cu radiotracer, which can be explained by the greater numbers of radiotracer in these organs (8.2 ± 2.1%ID/g and 1.3 ± 0.4%ID g^{-1}, respectively) in comparison to the anti-BCMA@^{64}Cu immunoPET tracer (3.8 ± 1.4%ID g^{-1}, $p < 0.01$ and 0.6 ± 0.2%ID g^{-1}, $p < 0.001$, respectively) as well as the passive control groups, consisting of NP@^{64}Cu (spine: 2.1 ± 0.3%ID g^{-1}, $p < 0.001$; femur: 0.4 ± 0.4%ID g^{-1}, $p < 0.001$) and the ^{64}CuCl$_2$ radiotracer.

Each agent that is currently used in clinical settings provided a very low signal in the two observed tumor sites (spine: 1.6 ± 0.2%ID g^{-1}, $p < 0.001$; femur: 0.001 ± 2.001, $p < 0.001$). Signals from ^{18}F-FDG were mostly observed in the spine at significantly lower levels than the signals observed with the immuno-nanoPET and immunoPET approaches. In addition, almost no signal was observed in the mouse femurs (Figure 2C,D). These results confirmed the need to design novel targeted PET imaging agents that are more specific than conventional ^{18}F-FDG and other untargeted radioisotopes. The lack of specificity of ^{18}F-FDG in these mice can be attributed to the low number of tumor cell clusters, which decreases the detection ability of

 © 2021 Wiley-VCH GmbH

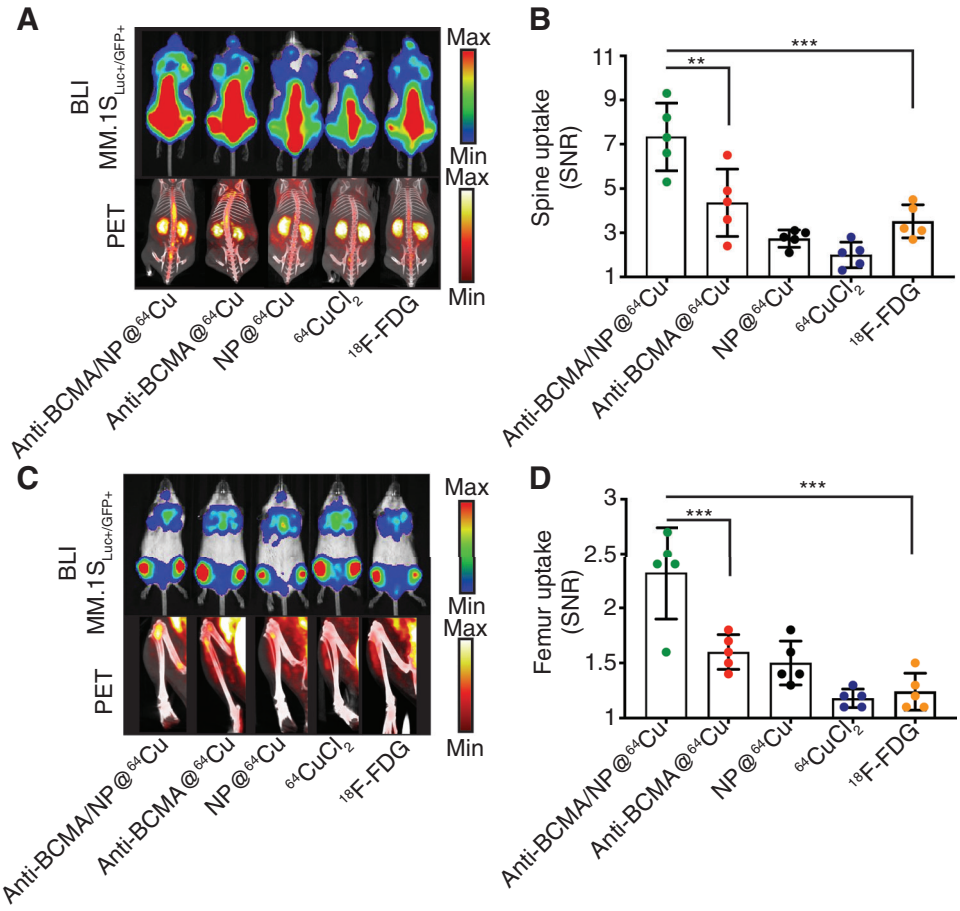

Figure 2. Anti-BCMA immuno-nanoPET radiotracers enhance the specificity of multiple myeloma detection. A) Bioluminescence imaging (BLI) of the dissemination of humanized myeloma cells (MM.1S) in SCID/beige mice confirmed the radiotracer presence in the spine of the animals. In parallel, mice were administered (IV) 10 MBq of radiotracers to evaluate their specificity to reach the tumor site located in the spine by whole-body PET-CT. Acquisitions were performed at $t = 2$ h for anti-BCMA/NP@^{64}Cu, $t = 6$ h for anti-BCMA@^{64}Cu, $t = 15$ min for NP@^{64}Cu and $^{64}CuCl_2$, and $t = 5$ min for ^{18}F-FDG. B) Quantification of the signal-to-noise ratios (SNRs) was based on the PET signal emitted from the spine of the animals after imaging ($n = 5$/group). C) Qualitative imaging confirms the presence of tumor cells in the femurs by BLI and the uptake of the PET radiotracers. D) SNR quantification in the femurs of each mouse. All experiments were performed with $n = 5$ /group. The Mann-Whitney test was performed for statistical analysis. $^{**}p < 0.01$; $^{***}p < 0.005$.

^{18}F-FDG and which is consistent with previous observations.[14] The stronger signals in the spines and femurs of animals in the anti-BCMA/NP@^{64}Cu group when compared to those in the anti-BCMA@^{64}Cu group were attributed to the differences in the amounts of mAb injected (1.12 mg kg^{-1} vs 4.5 mg kg^{-1}, respectively), which lead to lower off-target effects and, hence, better overall uptake at the tumor sites.

Finally, we sought to compare the sensitivity of anti-BCMA/NP@^{64}Cu to anti-BCMA@^{64}Cu. For this purpose, we injected groups of mice with the respective agents at the same doses based on anti-BCMA mAb (4.5 mg kg^{-1}) (**Figure 3**). It appeared that immuno-nanoPET tracers significantly improved the SNR compared to the anti-BCMA immunoPET tracers. With a signal intensity increase of approximately five-fold ($p < 0.001$, two-way ANOVA) in the spine (Figure 3A,B) and approximately three-fold in the femur (Figure 3C,D); the anti-BCMA immuno-nanoPET radiotracers allowed for improved sensitivity with potentially lower risks of antibody-associated toxicity when compared to the immunoPET radiotracer. These improvements were attributed to the increased amount (12x) of radioisotope per mAb when comparing anti-BCMA/NP@^{64}Cu with anti-BCMA@^{64}Cu.

3. Conclusion

We demonstrate that ultrasmall targeted NPs may outperform conventional PET tracers for MM detection. Attributable to the superior amounts of PET tracer per mAb that may be achieved in the immune-nanoPET platform, an anti-BCMA/NP@^{64}Cu radiotracer was developed and demonstrated to enable improvements in imaging sensitivity and specificity when compared with immunoPET and passively targeted PET radiotracers, including $^{64}CuCl_2$, ^{18}F-FDG, and untargeted NPs@^{64}Cu over the time course studies in this study. The use of anti-BCMA/NP@^{64}Cu allowed maximal contrast as quickly as 30 min after injection, potentially enabling its translation into a clinical workflow. In addition, its short half-life in the body affords an optimal diagnostic tool that can be readministered frequently in the context of longitudinal monitoring. We observed rapid renal clearance

© 2021 Wiley-VCH GmbH

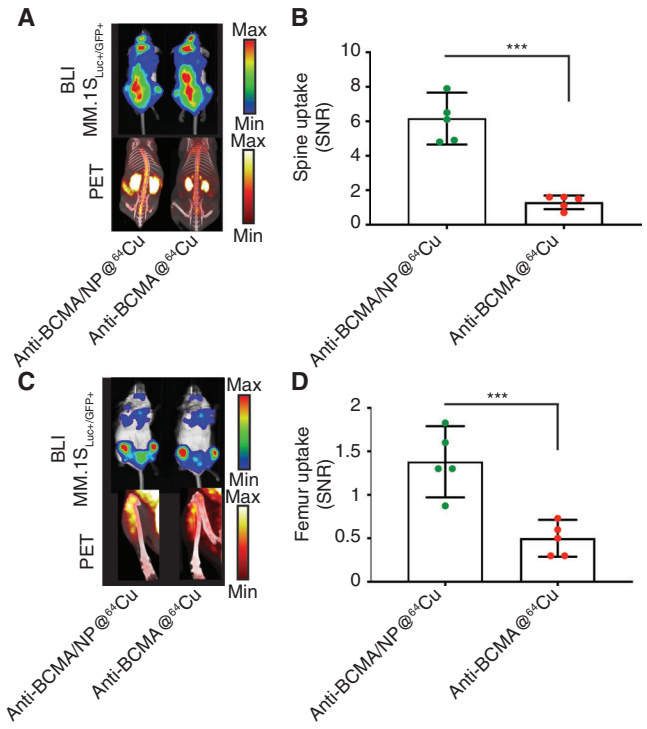

Figure 3. Anti-BCMA immuno-nanoPET radiotracers improve the sensitivity of multiple myeloma detection. A) Bioluminescence imaging (BLI) of the dissemination of humanized myeloma cells (MM.1S) in SCID/beige mice confirmed radiotracer presence in the spines of the animals. Anti-BCMA/NP@^{64}Cu and anti-BCMA@^{64}Cu were IV injected at a dose of 4.5 mg kg^{-1} mAb. B) Quantification of the PET radiotracers confirmed the improved sensitivity of the anti-BCMA immuno-nanoPET over anti-BCMA immunoPET. C) Similarly, imaging of the femurs and D) quantitative analysis of the SNR demonstrated the improved sensitivity of anti-BCMA/NP@^{64}Cu to detect MM cells. All experiments were performed with $n = 5$/group. The Mann-Whitney test was performed for statistical analysis. ***$p < 0.005$.

of the complex after intravenous injection; but, the DLS measurements did not show any degradation of the complex in the urine of the animals, which is similar to previously reported results.[14] Moreover, we did not observe higher uptake of this new agent into the liver than observed with the previous anti-BCMA immunoPET tracers. While our results suggest significant improvements from our previous generations of anti-BCMA ultrasmall NPs made with Gd^{3+} chelates for MRI-based detection, it is important to note that further studies are necessary to understand the full elimination of antibody-targeted ultrasmall immuno-nanoPET tracers.

Finally, this targeted immuno-nanoPET platform introduces potential clinical innovations that could circumvent the sensitivity limitations of analogous immuno-MRI contrast agents. The enhanced sensitivity afforded for the detection of heterogeneous disease foci, as evidenced in the femurs of study mice, could promote clinical detection of disease missed by bone marrow biopsy or by am MR imaging technique that could be based on the previously designed anti-BCMA targeted MRI contrast agent.[14] Therefore, the current study could pave a path towards clinical translation of this innovative immuno-nanoPET platform in MM patients and open the door for future therapeutic approaches where the radioisotope ^{64}Cu may be replaced by ^{67}Cu.

4. Experimental Section

Synthesis of the Nanoparticles: Polysiloxane-based NPs (obtained from NH TherAguix) were synthesized by previously described methods.[23] Briefly, a gadolinium oxide (Gd_2O_3) core was synthesized in DEG (diethylene glycol) and encapsulated in a polysiloxane shell comprised of TEOS (tetraethyl orthosilicate) and APTES (amino-propyltriethoxysilane). The surfaces of the NPs were functionalized by DOTAGA chelators (1,4,7,10-tetra-azacyclododecane-1-glutaric anhydride-4,7,10-triacetic acid) via the formation of a covalent amide bond between the primary amino group of APTES and the anhydride of the chelates. The nanoconstructs were then transferred from DEG to water, leading to Gd_2O_3 core dissolution and the complexation of Gd^{3+} ions by DOTAGA. Because of this dissolution, the polysiloxane hollow matrix collapsed and fragmented, leading to ultrasmall NPs that presented a hydrodynamic diameter less than 5 nm (3.6 ± 0.8 nm) and were composed of a polysiloxane core surrounded by approximately ten DOTAGA-Gd^{3+} chelates. The number of free chelates (not complexing Gd^{3+}) available at the surface of the NPs was found to be low (≈1%).[22] Additionally, amino groups remained on the surface and could be used for further functionalization.

Synthesis of the NODAGA-Nanoparticles: NP@NODAGA was synthesized via the formation of a covalent amide bond between the abovementioned NPs, presenting free amino groups and NODAGA-NHS chelates (2,2'-(7-(1-carboxy-4-((2,5-dioxopyrrolidin-1-yl)oxy)-4-oxobutyl)-1,4,7-triazonane-1,4-diyl)diacetic acid) as previously described.[22] First, the NPs were incubated with NODAGA-NHS in water at neutral pH and at RT for 5.5 h. They were then purified by tangential filtration over a 5 kDa cutoff membrane under acidic conditions to remove the nongrafted chelates. Purification by HPLC followed (Figure S1, Supporting Information). The obtained nanostructure presented a hydrodynamic diameter of less than 5 nm (4.3 ± 0.9 nm), which is known to be favorable for renal elimination. The addition of NODAGA at the particle surface was confirmed by the decrease in the isoelectric point (from 7.6 mV for NP to 5.2 mV for NP/NODAGA). This evolution is consistent with the exchange of the amino groups at the surface for carboxylic acid moieties. In addition, the infrared spectrum of NP/NODAGA showed the appearance of a vibration band at 1720 cm^{-1}, corresponding to the elongation vibration of the C=O bonds of the carboxylic acids of NODAGA (Figure S1, Supporting Information). The numbers of NODAGA chelators added to the particle surface was quantified using two different techniques: titration with europium ions (Eu^{3+}) as previously described[22] and titration with copper ions (Cu^{2+}) followed by HPLC (see Supporting Information). Both techniques gave consistent results of approximately 4 NODAGA chelators per particle. In addition, the determinations of the Gd, Si, C, and N content of the particles were carried out with ICP-MS; and, the following formula was proposed: $Gd_{10}APTES^*_{33}TEOS^*_{41}DOTAGA^*_{10\text{-}2}NODAGA^*_{4.1}$ where APTES*, TEOS*, DOTAGA* and NODAGA* refer to the corresponding molecules that reacted and that are actually present within each NP. This conjugation method allowed an average of 4 NODAGA loaded per NP.

Anti-BCMA Radiolabeling: The anti-BCMA immunoconjugates were radiolabeled with ^{64}Cu, using a freeze-dried kit based on an established protocol[24] that contains 4 mg of anti-BCMA monoclonal antibody (mAb) (BioLegend Inc. San Diego, CA, USA – Cat. No. 357502). DOTA-NHS-ester was purchased from Macrocyclics (Plano, Tx, USA). Briefly, 10 mg ml^{-1} anti-BCMA mAbs were incubated with DTPA (40 mM; 4 °C for 30 min), loaded on a PD-10 column (Sephadex G25, GE Healthcare) and eluted with phosphate buffer (0.05 M; pH 7.0). The concentration of mAb was determined by the Bradford assay prior to mAb incubation with a 100-fold molar excess of DOTA-NHS-ester (4 °C for 24 h). The reaction mixture was transferred to an ammonium acetate buffer (0.5 M; pH 5.5) to remove excess unbound DOTA. The final concentration of mAb was assessed by the Bradford assay. For the radiolabeling process, mAbs in ammonium acetate

© 2021 Wiley-VCH GmbH

buffer (0.3 M; pH 7.0) were incubated with 500 MBq of $^{64}CuCl_2$ dissolved in a 250 µl solution of HCl (0.1 N; 1.5 h and at 40 °C). The labeling purity was assessed by instant thin layer chromatography (iTLC-SG) in citrate buffer (pH 4.5; 0.1 M) and was determined to be 86%.

NODAGA-NPs were conjugated to the mAbs by using a previously reported transcyclooctene-tetrazin click chemistry approach.[21] Briefly, NPs@NODAGA (50 mM) was mixed in a 1:10 molar ratio with NHS-PEG4-Tz linker for 30 min at RT. Non-bound NHS-Tz was removed by tangential ultracentrifugation, using a Vivaspin device (MWCO = 3 kDa). In parallel, anti-BCMA mAb was co-incubated with NHS-PEG4-TCO linkers at RT for 3 h followed by centrifugation filtration (15 000 rcf), using a 50 kDa molecular weight cutoff membrane (Millipore), before resuspension in PBS. This process was performed in triplicate to remove all unbound NPs. These surface-modified NPs were subsequently mixed at a 100:1 molar ratio with the anti-BCMA mAb and stirred at RT for 1 h. Centrifugation filtration (15 000 rcf) was performed by using a 50 kDa molecular weight cutoff membrane (Millipore) before resuspension in PBS. This process was performed in triplicate to remove all unbound NPs. Labeling of NP@^{64}Cu and anti-BCMA/NP@^{64}Cu was performed by using the same protocol as employed for labeling of the immunoconjugate mAb. The final concentration of NPs was assessed by ICP-MS; and, the final concentration of mAb was assessed by the Bradford assay. We observed an average of 3 NPs per mAb, and hence an average of 12 NODAGA chelators per mAb for the anti-BCM/NP constructs.

Cell Lines: The MM.1S cell line was purchased from ATCC (Manassas, VA, USA). Cells were transduced using the pGC-GFP/Luc vector and authenticated by short tandem repeat DNA profiling. MM.1S cells were cultivated in RPMI medium containing 10% fetal bovine serum, 1% penicillin/streptavidin, and 1% glutamine.

Animals: All mouse work was performed in accordance with the IACUC of the Dana-Farber Cancer Institute (protocol 14-001). A total of 5×10^6 MM.1S$_{GFP+/Luc+}$ cells were injected (IV) into SCID/beige mice (n = 5/group) for dissemination in the bone marrow and femurs, establishing the orthotopic xenograft MM mouse model. The same 5 mice/group underwent the bioluminescence and PET-CT imaging study.

Bioluminescence Imaging (BLI): To monitor tumor dissemination, mice were injected (I.P.) with luciferin (100 µl) and placed under anesthesia with 5% isoflurane. Animals were then randomly assigned to each study group and tumor dissemination was tracked by the BLI signal, using the IVIS system (Perkin Elmer).

PET-CT imaging: PET-CT scans were obtained on a Inveon multimodality system (Siemens Medical Solutions USA Inc.). The CT scans were performed using low-dose radiation based on preliminarily established protocols[14,21] (80 kVp, 0.5 mA, 220degree rotation, 600 ms per degree exposure time, 80 µm reconstruction pixel time) for both anatomical reference and delineation of the region and volume of interest (ROI/VOI). PET acquisitions were performed after IV injection of the radiotracers. For ^{18}F-FDG imaging, mice that were fastered for 12 h prior to image acquisition, anesthetized with 5% isoflurane, and administered (IV) 10 MBq of radiotracer (200 µl). For $^{64}CuCl_2$ acquisitions, similar procedures were performed but without requisite animal fasting. Similarly, PET imaging with anti-BCMA@^{64}Cu, NP@^{64}Cu, and anti-BCMA/NP@^{64}Cu was performed after injection (IV) based on equivalent amounts of radiotracer (10 MBq) for specificity comparisons or of antibody (4.5 mg kg^{-1}) for sensitivity comparisons. The VOIs were drawn manually by using the Inveon Research Workplace software and were converted to the percentage of the injected radioactive dose per g of tissue (%ID g^{-1}) by assuming a 1 g ml^{-1} tissue density. Correlations of the radiation decay were performed to compare biodistribution data. The SNR was calculated as the intensity/noise ratio, where the noise was the signal intensity emitted in the muscle of the analyzed mouse.

Biodistribution and Pharmacokinetic Study: A total of n = 5/time point/group (different from the imaging studies) were used for biodistribution and pharmacokinetic studies. Blood and major organs, including bone marrow (from the spine and femurs), liver, kidney, lung, muscle, spleen, brain, and heart, were dissected, weighed, and counted on a calibrated and normalized gamma counter.

Statistical Analysis: Statistical analyses were performed using GraphPad Prism software V.9.0. Sensitivity and specificity differences were assessed by the Mann-Whitney test. A p-value < 0.05 was considered significant.

Supporting Information

Supporting Information is available from the Wiley Online Library or from the author.

Acknowledgements

P.P.G acknowledges the generous support of the Kathryn Fox Samway Foundation and of the Charles W. and Jennifer C. Johnson Clinical Investigator Fund. A.D. acknowledges support from the Foundation Française pour la Recherche Contre le Myélome et Les Gammapathies Monoclonales (FFRMG), the Multiple Myeloma Research Foundation (MMRF), and the International Myeloma Foundation (IMF). This project has also received funding from the European Research Council (ERC) under the European Union's Horizon 2020 research and innovation programme (ERC Starting Grant TheranoImmuno, grant agreement No. 950101).

Conflict of Interest

F.L. and O.T., who are inventors of WO2011/135 101 that protects the based NPs described in this publication, are employees of NH TherAguix. F.L., O.T., A.D. are shareholders of NH TherAguix, which is developing the base NP technology for commercial purposes.

Data Availability Statement

Research data are not shared.

Keywords

diagnostics, multiple myeloma, positron emission tomography, targeted-nanoparticles

Received: August 1, 2021
Revised: October 9, 2021
Published online:

[1] C. P. Shortt, T. G. Gleeson, K. A. Breen, J. McHugh, M. J. O'Connell, P. J. O'Gorman, S. J. Eustace, *AJR Am. J. Roentgenol.* **2009**, *192*, 980.
[2] A. G. Ormond Filho, B. C. Carneiro, D. Pastore, I. P. Silva, S. R. Yamashita, F. D. Consolo, V. T. M. Hungria, A. F. Sandes, E. G. Rizzatti, M. A. C. Nico, *Radiographics* **2019**, *39*, 1077.
[3] C. Nanni, *Cancers* **2020**, *12*, 1030.
[4] S. Mule, E. Reizine, P. Blanc-Durand, L. Baranes, P. Zerbib, R. Burns, R. Nouri, E. Itti, A. Luciani, *Cancers* **2020**, *12*, 3155.
[5] H. Maeda, J. Wu, T. Sawa, Y. Matsumura, K. Hori, *J. Controlled Release* **2000**, *65*, 271.
[6] Y. Shou, J. Lu, T. Chen, D. Ma, L. Tong, *J. Cancer Res. Ther.* **2012**, *8*, 96.
[7] J. R. Bading, A. F. Shields, *J. Nucl. Med.* **2008**, *49*, 64S.
[8] Y. Abe, S. Ikeda, A. Kitadate, K. Narita, H. Kobayashi, D. Miura, M. Takeuchi, E. O'Uchi, T. O'Uchi, K. Matsue, *Eur. J. Nucl. Med. Mol. Imaging* **2019**, *46*, 1345.

 © 2021 Wiley-VCH GmbH

[9] W. Wei, Z. T. Rosenkrans, J. Liu, G. Huang, Q. Y. Luo, W. Cai, *Chem. Rev.* **2020**, *120*, 3787.
[10] C. Bailly, S. Gouard, F. Guerard, B. Chalopin, T. Carlier, A. Faivre-Chauvet, P. Remaud-Le Saec, M. Bourgeois, N. Chouin, L. Rbah-Vidal, R. Tripier, F. Haddad, F. Kraeber-Bodere, C. Bodet-Milin, M. Cherel, *Int. J. Mol. Sci.* **2019**, *20*, 2564.
[11] C. Bailly, S. Gouard, M. Lacombe, P. Remaud-Le Saec, B. Chalopin, M. Bourgeois, N. Chouin, R. Tripier, Z. Halime, F. Haddad, A. Faivre-Chauvet, F. Kraeber-Bodere, M. Cherel, C. Bodet-Milin, *Oncotargets* **2018**, *9*, 9061.
[12] G. A. Ulaner, N. B. Sobol, J. A. O'Donoghue, A. S. Kirov, C. C. Riedl, R. Min, E. Smith, L. M. Carter, S. K. Lyashchenko, J. S. Lewis, C. O. Landgren, *Radiology* **2020**, *295*, 606.
[13] C. Wang, Y. Chen, Y. N. Hou, Q. Liu, D. Zhang, H. Zhao, Y. Zhang, S. An, L. Li, J. Hou, G. Huang, J. Liu, Y. J. Zhao, W. Wei, *Eur. J. Nucl. Med. Mol. Imaging* **2021**, *48*, 2749.
[14] A. Detappe, M. Reidy, Y. Yu, C. Mathieu, H. V. Nguyen, T. P. Coroller, F. Lam, P. Jarolim, P. Harvey, A. Protti, Q. D. Nguyen, J. A. Johnson, Y. Cremillieux, O. Tillement, I. M. Ghobrial, P. P. Ghoroghchian, *Nanoscale* **2019**, *11*, 20485.
[15] N. Raje, J. Berdeja, Y. Lin, D. Siegel, S. Jagannath, D. Madduri, M. Liedtke, J. Rosenblatt, M. V. Maus, A. Turka, L. P. Lam, R. A. Morgan, K. Friedman, M. Massaro, J. Wang, G. Russotti, Z. Yang, T. Campbell, K. Hege, F. Petrocca, M. T. Quigley, N. Munshi, J. N. Kochenderfer, *N. Engl. J. Med.* **2019**, *380*, 1726.
[16] S. Hipp, Y. T. Tai, D. Blanset, P. Deegen, J. Wahl, O. Thomas, B. Rattel, P. J. Adam, K. C. Anderson, M. Friedrich, *Leukemia* **2017**, *31*, 1743.
[17] S. F. Cho, L. Lin, L. Xing, Y. Li, T. Yu, K. C. Anderson, Y. T. Tai, *Cancers* **2020**, *12*, 1473.
[18] A. Detappe, S. Kunjachan, P. Drane, S. Kotb, M. Myronakis, D. E. Biancur, T. Ireland, M. Wagar, F. Lux, O. Tillement, R. Berbeco, *Sci. Rep.* **2016**, *6*, 34040.
[19] A. Detappe, S. Kunjachan, L. Sancey, V. Motto-Ros, D. Biancur, P. Drane, R. Guieze, G. M. Makrigiorgos, O. Tillement, R. Langer, R. Berbeco, *J. Controlled Release* **2016**, *238*, 103.
[20] A. Detappe, E. Thomas, M. W. Tibbitt, S. Kunjachan, O. Zavidij, N. Parnandi, E. Reznichenko, F. Lux, O. Tillement, R. Berbeco, *Nano Lett.* **2017**, *17*, 1733.
[21] A. Detappe, C. Mathieu, C. Jin, M. P. Agius, M. C. Diringer, V. L. Tran, X. Pivot, F. Lux, O. Tillement, D. Kufe, P. P. Ghoroghchian, *Int. J. Radiat. Oncol., Biol., Phys.* **2020**, *108*, 1380.
[22] P. Bouziotis, D. Stellas, E. Thomas, C. Truillet, C. Tsoukalas, F. Lux, T. Tsotakos, S. Xanthopoulos, M. Paravatou-Petsotas, A. Gaitanis, L. A. Moulopoulos, V. Koutoulidis, C. D. Anagnostopoulos, O. Tillement, *Nanomedicine* **2017**, *12*, 1561.
[23] G. L.e Duc, S. Roux, A. Paruta-Tuarez, S. Dufort, E. Brauer, A. Marais, C. Truillet, L. Sancey, P. Perriat, F. Lux, O. Tillement, *Cancer Nanotechnol.* **2014**, *5*, 4.
[24] W. Wojdowska, U. Karczmarczyk, M. Maurin, P. Garnuszek, R. Mikolajczak, *Curr. Radiopharm.* **2015**, *8*, 62.

© 2021 Wiley-VCH GmbH

4. Reinforced polymer-NPs hydrogels for subcutaneous and sustained delivery of trastuzumab

Check for updates

RESEARCH ARTICLE

ADVANCED HEALTHCARE MATERIALS
www.advhealthmat.de

Reinforced Polymer–Nanoparticle Hydrogels for Subcutaneous and Sustained Delivery of Trastuzumab

Giovanni Bovone, Stéphane Bernhard, Guillaume Jacquot, Vincent Mittelheisser, Céline Mirjolet, Elia A. Guzzi, Lorenza Garau Paganella, Luca Liebi, Julien Draussin, Pedro Lopez Navarro, Elsa Barbé, Olivier Lefebvre, Jacky G. Goetz, Loic J. Charbonnière, Xavier Pivot, Sébastien Harlepp, Mark W. Tibbitt, and Alexandre Detappe**

In oncology, the advent of monoclonal antibody (mAb) therapeutics represents a breakthrough in various cancer diseases. However, these therapies often necessitate iterative hospital visits for intravenous infusion that alter patient quality of life and contribute to the chronic saturation of hospitals. Subcutaneous formulations of mAbs offer a promising alternative facilitating faster administration compared with traditional intravenous methods, while still maintaining the same dosing schedule and providing time-saving advantages. Here, an injectable mAb delivery platform using α-cyclodextrin (αCD)-reinforced polymer–nanoparticle hydrogels to perform subcutaneous mAb depots and delay their release is developed. By leveraging mAb–polymer electrostatic complexation, hyaluronic acid- and alginate-based injectable drug depots are formulated by simply mixing components that are generally regarded as safe. Trastuzumab is included as a clinically relevant therapeutic antibody. These formulations delayed mAb release both in vitro and in vivo mice models, with a similar pharmacokinetic performance to the clinically approved Herceptin SC (Roche) formulation composed of trastuzumab with recombinant human hyaluronidase (rHuPH20).

1. Introduction

Monoclonal antibodies (mAbs) have emerged as a groundbreaking advancement in the field of oncology, revolutionizing cancer treatments. These mAbs represent a paradigm shift in precision medicine, offering a targeted and tailored approach to cancer therapy that have improved patient prognosis and survival rates for various cancers. Biotherapies, such as trastuzumab for HER2-positive breast cancer, are a prime example of how mAbs have transformed the therapeutic landscape. Typically, trastuzumab administration requires regular out-patient visits, either every week or every three weeks, to maintain the therapeutic concentration of the pharmacological active agent over one year or more, depending on the disease stage. These iterative injections have a detrimental impact on patient quality of

G. Bovone, S. Bernhard, E. A. Guzzi, L. G. Paganella, L. Liebi, M. W. Tibbitt
Macromolecular Engineering Laboratory
Department of Mechanical and Process Engineering
ETH Zurich
Zurich 8092, Switzerland
E-mail: mtibbitt@ethz.ch

G. Jacquot, V. Mittelheisser, J. Draussin, P. Lopez Navarro, E. Barbé, X. Pivot, S. Harlepp, A. Detappe
Nanomedicine laboratory
Institut de Cancérologie Strasbourg Europe
Strasbourg 67000, France
E-mail: a.detappe@icans.eu

The ORCID identification number(s) for the author(s) of this article can be found under https://doi.org/10.1002/adhm.202404660

© 2025 The Author(s). Advanced Healthcare Materials published by Wiley-VCH GmbH. This is an open access article under the terms of the Creative Commons Attribution-NonCommercial License, which permits use, distribution and reproduction in any medium, provided the original work is properly cited and is not used for commercial purposes.

DOI: 10.1002/adhm.202404660

G. Jacquot, V. Mittelheisser, J. Draussin, P. Lopez Navarro, E. Barbé, X. Pivot, S. Harlepp, A. Detappe
Strasbourg Drug Discovery and Development Institute (IMS)
University of Strasbourg
Strasbourg 67000, France

G. Jacquot, V. Mittelheisser, J. Draussin, P. Lopez Navarro, E. Barbé, O. Lefebvre, J. G. Goetz, X. Pivot, S. Harlepp, A. Detappe
Equipe labellisée Ligue contre le cancer

V. Mittelheisser, O. Lefebvre, J. G. Goetz
Tumour Biomechanics lab
INSERM UMR_S1109, University of Strasbourg
Strasbourg 67000, France

C. Mirjolet
Radiation Oncology Department
Georges François Leclerc Cancer Center
Unicancer
Dijon 21000, France

C. Mirjolet
INSERM 1231
Cadir Team, Faculté de Médecine
Dijon 27877, France

life. In this context, the subcutaneous (SC) formulation of trastuzumab presents a notable advancement, offering significant time-saving benefits in the clinic compared with traditional intravenous (IV) administration. Exploring extended intervals between treatments could further alleviate the negative impact of frequent injections, ultimately improving patient well-being.

The SC route offers benefits but introduces complexities. The skin consists of three layers: the epidermis, dermis, and hypodermis (or SC tissue).[1] The hypodermis is a loose connective tissue containing fat cells, fibroblasts, and immune cells in a vascular extracellular matrix (ECM) made of collagen and glycosaminoglycans like hyaluronic acid (HA).[2] This negatively-charged HA influences drug transport and stability, particularly for biotherapeutics like proteins and antibodies.[3]

Although SC administration benefits from low proteolytic activity and a network of blood and lymphatic capillaries, it has limitations. Drugs administered SC lead to a slower onset as the drug needs to diffuse into the bloodstream.[4] SC injections are also limited in volume (typically 2–3 mL), as larger amounts can cause pain, tissue damage, or leakage.[5] The dense ECM structure, especially the HA, further restricts drug transport, leading to slower absorption and variable bioavailability, ranging from 9% to 90%, typically approx. 50% to 80%.[6,7] The SC space is a complex and dense ECM that influences how nanoscale drug delivery systems are dispersed and absorbed into the bloodstream leading to a higher variability in patient outcomes compared with direct IV injections.

To address the challenge posed by the ECM barrier and enable the administration of larger volumes, various strategies utilizing enzymatic combinations have been explored. Among these, only one has achieved clinical approval, the recombinant human hyaluronidase (rHuPH20) from Halozyme, registered in 2005. This enzyme facilitates SC delivery by depolymerizing HA within the ECM, creating local space for up to 20 mL and thereby enhancing the absorption of the injected mAbs. Nevertheless, these innovations have not provided controlled or sustained release of the mAbs for long-lasting delivery. To address this gap, several injectable biomaterials have been developed to form long-lasting and/or local depots for the sustained release of mAbs, and in particular trastuzumab.[8–12] Vitamin E-functionalized block copolymers assembled to create micellar hydrogel networks that released trastuzumab in a murine model.[8,9] HA-based scaffolds exhibited a delayed trastuzumab release, which was hypothesized to be due to the formation of polyanion–antibody complexes between the negatively-charged HA and the positively-charged trastuzumab.[10–12] For many of the systems mentioned, complicated processing steps, such as enzymatic or photo-cross-linking chemistries and microfluidic handling, were required for hydrogel formation. Generally, materials assembled from unmodified components that are approved by the US Federal Drug Administration (FDA) or generally regarded as safe (GRAS) have improved chances of being translated clinically.

L. J. Charbonnière
Equipe de Synthèse Pour l'Analyse (SynPA), Institut Pluridisciplinaire Hubert Curien (IPHC)
UMR 7178, CNRS, Université de Strasbourg, ECPM
Strasbourg 67087 Cedex, France

Polymer–nanoparticle (PNP) hydrogels comprise a class of injectable biomaterials that form via intermolecular interactions between GRAS-listed polymers and biodegradable nanoparticles (NPs).[13] PNP hydrogels are injectable through narrow gauge syringes and catheters as they can flow upon applied stress (shear-thin) and reform a stable network (self-heal) when the stresses are removed.[14,15] They have been applied as drug delivery systems for several applications, including immune cell recruitment, to release COVID-19 vaccines, to deliver immunostimulatory antibodies, and to supply CAR-T cells.[15–18] PNP hydrogels have also been implemented for the subcutaneous delivery of mAbs against SARS-Cov-2 as well as immunostimulatory CD40 agonist mAbs.[18,19] Recently, the addition α-cyclodextrin (αCD) to PNP formulations improved the mechanical properties and enabled the utilization of diverse building blocks, both polymers and NPs, for hydrogel formation.[20]

In this work, we explore the use of αCD-reinforced PNP (CD–PNP) hydrogels to provide alternatives to currently available trastuzumab formulations, to test the tolerance of CD–PNP formulations in vivo, and to use them as a platform to investigate electrostatic complexation as a mean to delay mAbs release. We designed one formulation based on HA and the other on alginate (Alg). We validated the in vitro release profiles of trastuzumab for both formulations and assessed the stability of trastuzumab post-release from the hydrogel to ensure its integrity. Furthermore, we performed pharmacokinetic studies in mice where both formulations were administered subcutaneously and compared with both the IV and SC clinically approved formulations of trastuzumab.

2. Results and Discussion

2.1. Design of CD–PNP Hydrogels for Trastuzumab Delivery

Trastuzumab is a first-in-class mAb for the treatment of HER2-positive breast cancer.[21] However, multiple SC or IV injections are needed to maintain therapeutic mAb levels in the body. This results in frequent hospital visits, which impacts life quality. A sustained release system for trastuzumab, and potentially other therapeutic mAbs, is needed to improve clinical application of these powerful therapeutics. To address this need, we prepared trastuzumab-loaded CD–PNP hydrogels by mixing PEGylated NPs, αCD, a biopolymer, and trastuzumab (**Figure 1**).[20] Given the target of in vivo application, we assembled trastuzumab-loaded CD–PNP hydrogels using GRAS building blocks: PEG-*block*-poly(*D,L*-lactide) (PEG-*b*-PLA) NPs, αCD, and pharma-grade alginate or HA (Figure 1a). At the molecular scale, the threading of αCD onto the PEG chains of NPs and the subsequent formation of polypseudorotaxanes enhanced the interactions between NPs, improving the mechanical properties of the injectable biomaterials.[22] To ensure biocompatibility, we used HA as the structural polymer given its natural presence in connective, epithelial, and neural tissues. Since HA cannot undergo cross-linking without chemical modification, we selected alginate as an alternative structural polymer to enable an optional post-stabilization by cross-linking with divalent cations (Ca^{2+}). Detailed information on the hydrogel platform can be found in a previous publication by our group.[20]

© 2025 The Author(s). Advanced Healthcare Materials published by Wiley-VCH GmbH

21922659, 0, Downloaded from https://advanced.onlinelibrary.wiley.com/doi/10.1002/adhm.202404660 by Cochrane France, Wiley Online Library on [09/06/2025]. See the Terms and Conditions (https://onlinelibrary.wiley.com/terms-and-conditions) on Wiley Online Library for rules of use; OA articles are governed by the applicable Creative Commons License

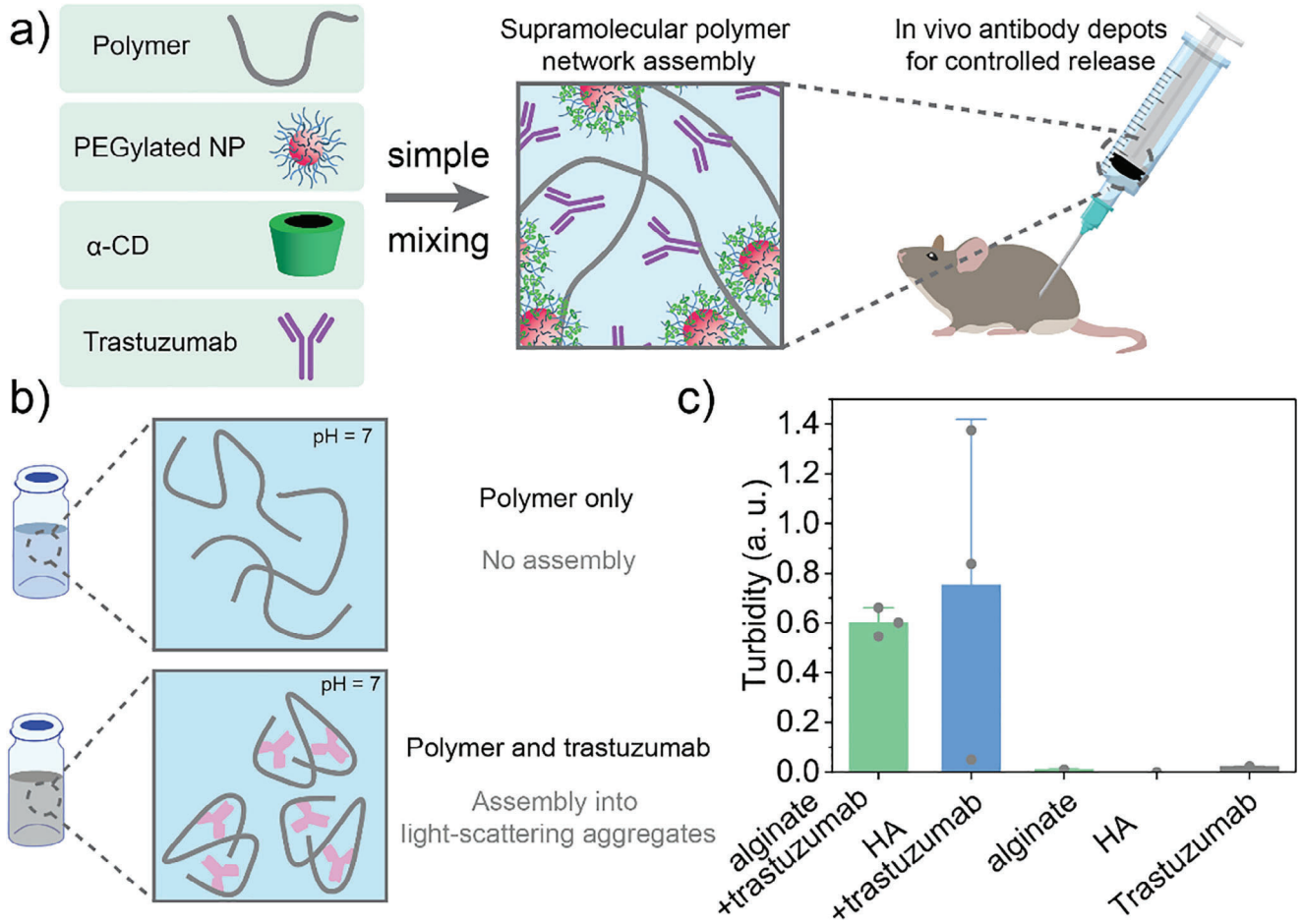

Figure 1. CD–PNP hydrogels for the controlled release of trastuzumab in vivo. a) Trastuzumab-encapsulating CD–PNP hydrogels were formed by simply mixing α-cyclodextrin (αCD), PEGylated nanoparticles (NPs), alginate or hyaluronic acid (HA), and trastuzumab. Network formation was promoted by threading of αCD onto NP PEG chains and subsequent polypseudorotaxane formation. The designed formulations were used for in vivo controlled release of trastuzumab. b) At physiological pH, alginate and HA are negatively-charged, whereas trastuzumab is positively-charged.[10] This is advantageous as it allows the complexation of the trastuzumab with the support polymers during gel preparation, providing a mechanism for sustained release.[12] c) Turbidity measured at 450 nm indicated that aggregates formed upon mixing HA or alginate with trastuzumab. Data shown as mean ± SD, $n = 3$ for alginate or HA + trastuzumab, and $n = 1$ for alginate, HA, and trastuzumab.

Trastuzumab was encapsulated into CD–PNP hydrogels via incorporation within the hydrogel precursors. Given that the isoelectric points are $pI \approx 9.2$ for trastuzumab, ≈5.4 for alginate, and ≈2.5 for HA,[23–25] trastuzumab is positively-charged at physiological pH (≈7.4) whereas alginate and HA are negatively-charged. This facilitates the formation of polymer–trastuzumab complexes that can prolong the release of mAbs for both formulations (Figure 1b): HA CD–PNP (2 wt.% HA, 5 wt.% NPs, 10 wt.% αCD) and Alg CD–PNP (2 wt.% alginate, 5 wt.% NPs, 10 wt.% αCD).[10–12] To investigate for electrostatic interactions between HA and alginate with trastuzumab, we have performed turbidity experiments. At physiological pH, HA or alginate were mixed with trastuzumab and an increase in turbidity was indicative of the formation of light-scattering aggregates likely due to electrostatic complexation (Figure 1c). The turbidity values of the biopolymers or trastuzumab alone were similar to the phosphate-buffered saline (PBS) control. This suggested assembly of trastuzumab with the structural polymers used in our formulations.[12]

2.2. CD–PNP Hydrogels were Moldable and Allowed Post-Fabrication Stabilization

The rheological properties of CD–PNP hydrogels were characterized via shear rheometry (**Figure 2**). The frequency-dependent behavior of HA CD–PNP and Alg CD–PNP formulations was described with oscillatory frequency sweeps in the linear viscoelastic region ($\gamma = 0.1\%$; Figure S1a, Supporting Information). We first characterized CD–PNP formulations that were assembled via non-covalent interactions between the polymers, αCD, and the NPs. Both HA CD–PNP and Alg CD–PNP hydrogels had storage moduli, G', between 0.1 and 1 kPa and solid-like properties ($G' > G''$) over the entire frequency spectrum tested ($\omega = 0.1$–100 rad s^{-1}, Figure 2a). The moduli increased with increasing frequency, consistent with the presence of entangled polymers. The self-healing (elastic recovery) behavior of CD–PNP formulations was studied by alternating high oscillatory shear strain intervals ($\gamma = 200\%$ or 10%, $\omega = 10$ rad s^{-1}) and low oscillatory shear strain intervals ($\gamma = 0.1\%$, $\omega = 10$ rad^{-1}; Figure 2b; Figure S1b, Sup-

© 2025 The Author(s). Advanced Healthcare Materials published by Wiley-VCH GmbH

21922659, 0, Downloaded from https://advanced.onlinelibrary.wiley.com/doi/10.1002/adhm.202404660 by Cochrane France, Wiley Online Library on [09/06/2025]. See the Terms and Conditions (https://onlinelibrary.wiley.com/terms-and-conditions) on Wiley Online Library for rules of use; OA articles are governed by the applicable Creative Commons License

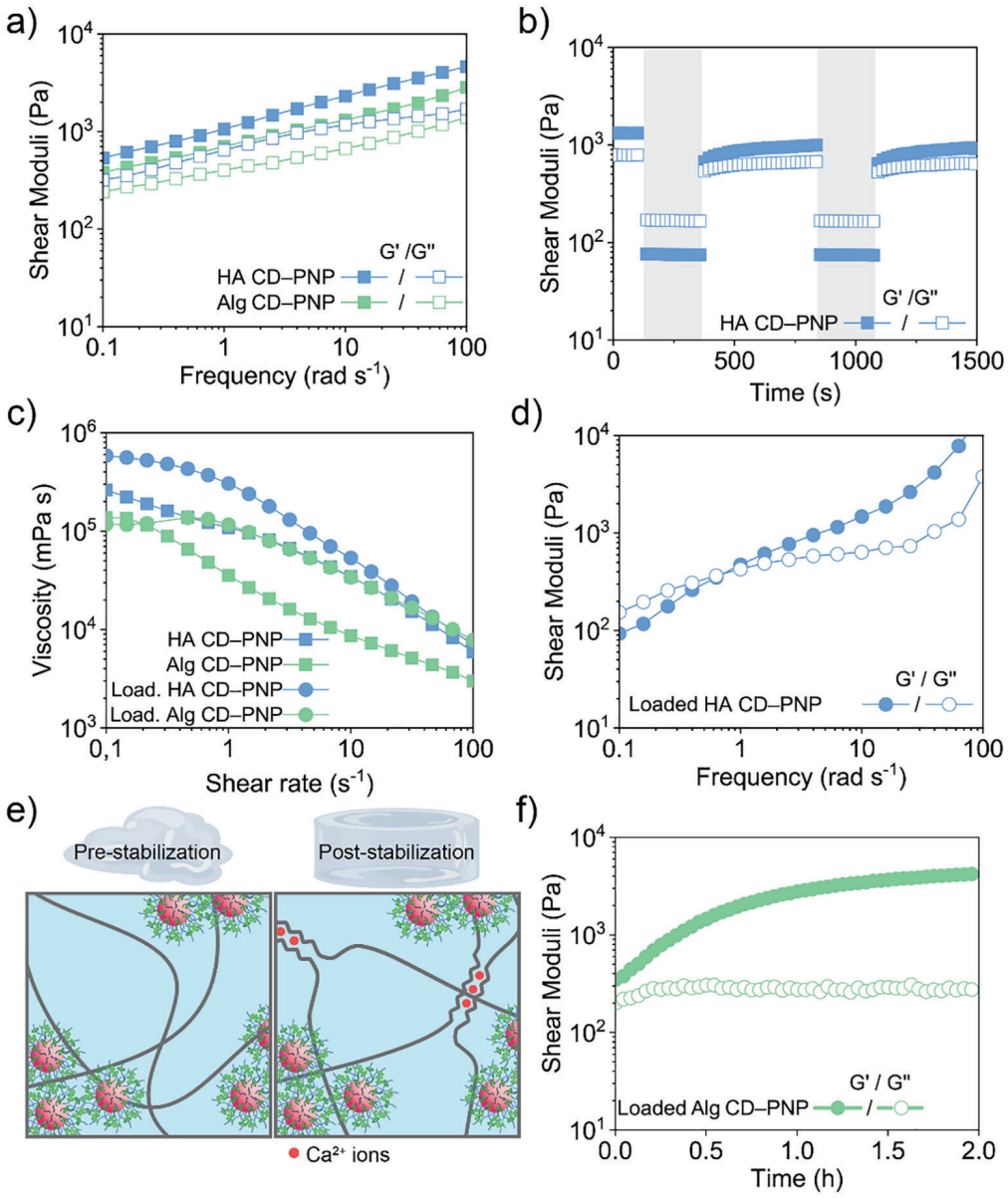

Figure 2. HA and alginate CD–PNP hydrogels are suitable scaffolds to make antibody depots. a) Oscillatory frequency sweeps of HA CD–PNP and Alg CD–PNP hydrogels ($\gamma = 0.1\%$). Both formulations formed solid-like viscoelastic hydrogels over the whole frequency range ($G' > G''$). b) HA CD–PNP hydrogels were subjected to periods of high oscillatory shear strains ($\gamma = 200\%$; $\omega = 10$ rad s^{-1}) alternated to periods of low oscillatory shear strains ($\gamma = 0.1\%$; $\omega = 10$ rad s^{-1}) to simulate syringe extrusion. At high shear strains, the hydrogel network was broken ($G' < G''$) and partially recovered during low strain periods ($G' > G''$). c) Rotational shear rate ramp experiments of trastuzumab-loaded and non-loaded CD–PNP formulations confirmed their shear-thinning behavior. d) Oscillatory frequency sweep of HA CD–PNP loaded with 12 wt.% mAb trastuzumab ($\gamma = 0.1\%$). The data suggested an acceleration of polymer dynamics upon mAb loading. e) Alg CD–PNP hydrogels allowed post-fabrication stabilization via ionic Ca^{2+} cross-linking. f) Time sweeps of trastuzumab-loaded Alg CD–PNP showed that Ca^{2+}-induced post-stabilization occurred within ≈2 h ($\gamma = 0.1\%$; $\omega = 10$ rad s^{-1}). $n = 3$, data shows one representative replicate.

porting Information). At high shear, the hydrogel network was broken ($G' < G''$) and at low shear, the solid-like properties were partially recovered ($G' > G''$). The hysteresis in recovery shown by the strain recovery experiments is in accordance with previous literature.[20]

We next characterized how loading clinically relevant amounts of trastuzumab (120 mg mL^{-1}) impacted the hydrogel rheological properties. Rotational shear rate ramp experiments showed that all non-loaded and loaded HA CD–PNP and alginate CD–PNP hydrogels were shear-thinning (Figure 2c). We fitted the viscosity versus shear rate data between 1 and 100 s^{-1} to a power law model, $\eta = K\,\dot{\gamma}^{n-1}$; all hydrogels had $n < 0.5$ confirming their shear-thinning behavior. Frequency sweeps of HA CD–PNP hydrogels loaded with trastuzumab preserved their solid-like behavior for $\omega > 1$ rad s^{-1} (Figure 2d). The yield strains of non-loaded hydrogels were ≈5% for Alg CD–PNP and

© 2025 The Author(s). Advanced Healthcare Materials published by Wiley-VCH GmbH

21922659, 0, Downloaded from https://advanced.onlinelibrary.wiley.com/doi/10.1002/adhm.202404660 by Cochrane France, Wiley Online Library on [09/06/2025]. See the Terms and Conditions (https://onlinelibrary.wiley.com/terms-and-conditions) on Wiley Online Library for rules of use; OA articles are governed by the applicable Creative Commons License

≈10% for HA CD–PNP (Figure S1a, Supporting Information). After trastuzumab loading, the yield strain increased to approx. 100% for HA CD–PNP (Figure S1c, Supporting Information) and decreased to <1% for Alg CD–PNP (Figure S1d, Supporting Information). Since mAb loading affected the stability of the hydrogel network (Figure S1e, Supporting Information), we further investigated scaffold post-stabilization strategies by further cross-linking alginate with Ca^{2+} ions (Figure 2e,f; Figure S1f, Supporting Information). This data is an interesting addition to previous reports on polymer–NP hydrogels where it is reported that mAb loading did not impact the mechanical properties.[18,19] The reason for this discrepancy is that, in this work, we are loading a clinically-relevant fraction of trastuzumab that was ten-fold higher than previous studies. Since CD–PNP hydrogels comprise an overall polymer content of solely 2 wt.% alginate or HA and 5% PEG–*b*–PLA NPs, it is reasonable that the addition of 12 wt.% trastuzumab affects the mechanical properties of the hydrogel.

We included solid $CaCO_3$ and glucono-*delta*-lactone (GDL; a cyclic ester) into the formulation. The slow hydrolysis of GDL reduces the local pH of the solution, which promotes a gradual dissolution of $CaCO_3$ releasing the Ca^{2+} ions necessary for post-cross-linking of the network.[26] In Alg CD–PNP hydrogels, released Ca^{2+} ions progressively cross-linked and stabilized the network (Figure 2f). Time-sweeps of trastuzumab-loaded alginate CD–PNP hydrogels indicated that the final storage modulus was reached within hours ($G' \approx 1.4$ kPa; $\gamma = 0.1\%$; $\omega = 10$ rad s^{-1}).

2.3. CD–PNP Depots Delayed the Release of Trastuzumab In Vitro

Having established that mAb-loaded CD–PNP hydrogels formed injectable biomaterials, we then investigated the ability of CD–PNP hydrogels to delay the release of trastuzumab by including a clinically relevant loading of mAb within the hydrogel formulation. In the commercially available SC formulation, the dosage for humans is 600 mg of trastuzumab dissolved into 5 mL of physiological solution (≈12 wt.%).[27] We prepared samples with an equivalent loading of trastuzumab in HA CD–PNP and post-stabilized Alg CD–PNP hydrogels and studied the in vitro drug release in PBS (**Figure 3**). As an uncharged control, we made CD–PNP formulations using methyl cellulose (MC).

We report the data as a cumulative fraction of trastuzumab released M_t/M_∞, where M_t is the mass released up to a specific timepoint, t, and M_∞ is the total dose loaded (Figure 3a). Trastuzumab loaded in uncharged MC CD–PNP hydrogels was released rapidly over the course of 2 days with a burst release of $M_{1d}/M_\infty \approx 0.87$ (Figure 3b). Negatively charged HA CD–PNP hydrogels exhibited an initial burst release of $M_{1d}/M_\infty \approx 0.26$, followed by a constant release of trastuzumab up to day 7. Post-stabilized alginate CD–PNP hydrogels had a burst release of $M_{1d}/M_\infty \approx 0.40$ and did not fully release their payload over the experimental period of 9 days. The in vitro half-life, $t_{1/2}$, was defined as the length of time required for a substance to decrease to half of the initial dose. The half-life of trastuzumab in HA CD–PNP and Alg CD–PNP were $t_{1/2} \approx 2.65$ and ≈1.4 days respectively. In contrast, trastuzumab loaded in uncharged MC CD–PNP exhibited $t_{1/2} \approx 0.25$. For HA CD–PNP and post-stabilized Alg CD–PNP, we fitted the first fraction to the Ritger–Peppas model, which describes the Fickian and non-Fickian release behavior of hydrogels,[29,30] to determine the release exponent, n, which is 0.5 for Fickian diffusion, $0.5 < n < 1$ for non-Fickian transport, and $n \approx 1$ for zero-order release (Figure S2, Supporting Information). For HA CD–PNP, $n \approx 0.85$ indicating an erosion-like release mechanism, whereas for Alg CD–PNP, $n \approx 0.66$ suggesting a diffusion-like release mechanism (Figure 3c). Trastuzumab diluted in sodium chloride solutions is chemically and physically stable for up to 6 months.[31] To assess whether hydrogel encapsulation had a detrimental effect on the bioactivity of trastuzumab, we measured the ability of the antibody to bind cellular HER2 and performed cell-based potency assays. We examined the capacity of mAbs released on days 1 and 3 to bind HER2. Cy5.5-labeled trastuzumab was loaded in HA or post-stabilized alginate CD–PNP hydrogels (Figure 3d; Figure S3, Supporting Information). Upon incubation of the release supernatants with HER2-overexpressing breast cancer cells (SK-BR-3) flow cytometry and confocal microscopy demonstrated that ≈80% of the cells were Cy5.5 positive irrespective of the day of release (Figure S4, Supporting Information). The same supernatants had negligible binding when incubated with HER2-negative breast cancer cells (MDA-MB-231). Bevacizumab used as an isotype mAb control, exhibited negligible binding with both HER2-positive and negative cells. Equivalent concentrations of fresh trastuzumab in PBS showed ≈95% binding to $HER2^+$ cells (Figure S5, Supporting Information).

Overall, both HA and Alg CD–PNP hydrogels delayed the release of trastuzumab. Since trastuzumab loaded in uncharged CD–PNP hydrogels was released extremely rapidly over the course of 2 days, it is reasonable to conclude that polymer–mAb complexation immobilized the mAb to the hydrogel scaffold and delayed its release. Fitting to the Ritger–Peppas model suggested that the main elements governing trastuzumab release were an interplay between scaffold erosion and diffusion of non-bound mAbs, where scaffold erosion dominated in HA CD–PNP hydrogels and diffusion of unbound mAbs was more prominent in Alg CD–PNP hydrogels. We hypothesized that the initial burst release in the first day could be caused by the *pI* differences of trastuzumab with HA ($\Delta pI \approx 6.7$, $M_{1d}/M_\infty \approx 0.26$) and alginate ($\Delta pI \approx 3.8$, $M_{1d}/M_\infty \approx 0.4$); however, to prove this point additional experiments would be necessary.[28] Release differences could also be attributed, in part, to mechanically weaker hydrogel networks resulting from weaker electrostatic interactions between polymer and mAb. The released trastuzumab maintained the ability to bind $HER2^+$ human cancer cells with high specificity. When compared to fresh trastuzumab in PBS, the released trastuzumab showed a 20% decrease of Cy5.5-labeled SK-BR-3 cells; however, this difference was not affected by the distinct release time points. The data suggest that the released trastuzumab maintained their binding capacity to $HER2^+$ cells and we speculate that this difference could be caused by the presence of hydrogel debris in the release supernatant. Since the scaffolds were entirely composed of GRAS materials, they were suitable mAb release depots to be tested in vivo.

© 2025 The Author(s). Advanced Healthcare Materials published by Wiley-VCH GmbH

21922659, 0, Downloaded from https://advanced.onlinelibrary.wiley.com/doi/10.1002/adhm.202404660 by Cochrane France, Wiley Online Library on [09/06/2025]. See the Terms and Conditions (https://onlinelibrary.wiley.com/terms-and-conditions) on Wiley Online Library for rules of use; OA articles are governed by the applicable Creative Commons License

21922659, 0, Downloaded from https://advanced.onlinelibrary.wiley.com/doi/10.1002/adhm.202404660 by Cochrane France, Wiley Online Library on [09/06/2025]. See the Terms and Conditions (https://onlinelibrary.wiley.com/terms-and-conditions) on Wiley Online Library for rules of use; OA articles are governed by the applicable Creative Commons License

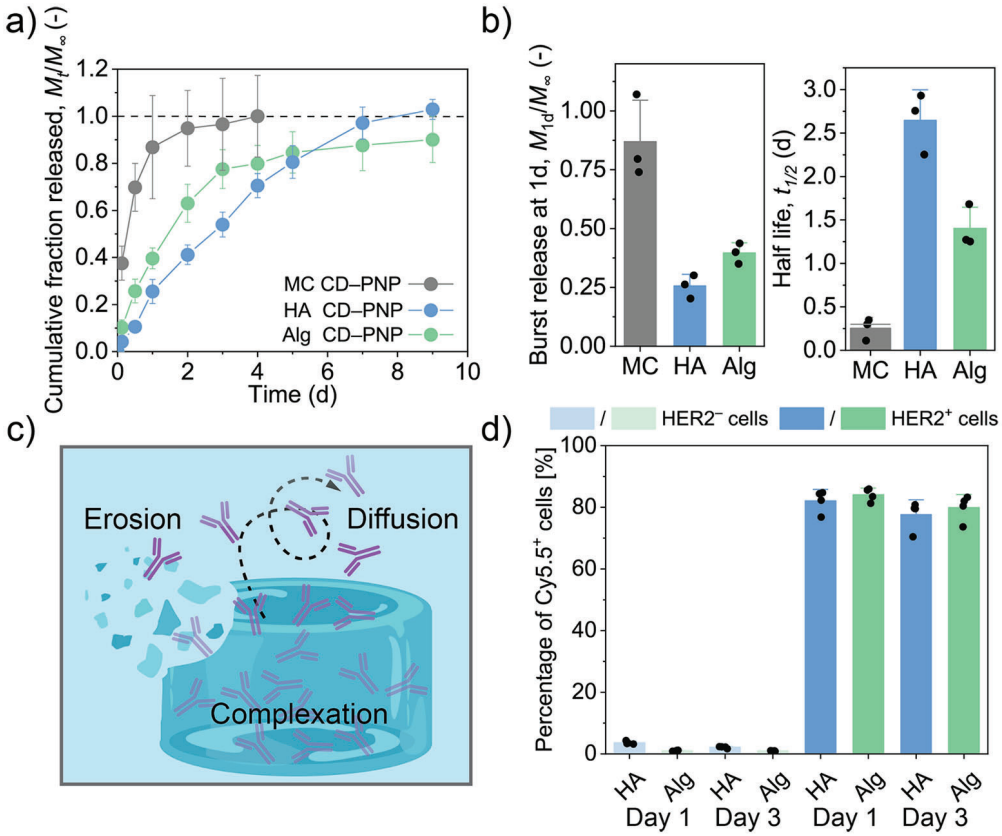

Figure 3. CD–PNP hydrogels delayed the release of trastuzumab in vitro. Trastuzumab (120 mg mL^{-1}) was loaded in CD–PNP hydrogels and the amount released in a PBS solution was quantified over time. a) M_t/M_∞ represents the cumulative fraction of trastuzumab released up to the timepoint t for methyl cellulose (MC) CD–PNP hydrogels (2 wt.% MC, 5 wt.% NPs, 10 wt.% αCD), HA CD–PNP hydrogels (2 wt.% HA, 5 wt.% NPs, 10 wt.% αCD) and post-stabilized Alg CD–PNP hydrogels (2 wt.% alginate, 5 wt.% NPs, 10 wt.% αCD; cross-linked with $CaCO_3$ and GDL for 1 h). b) Burst release after 24 h, M_{1d}/M_∞, and half-life, $t_{1/2}$, of trastuzumab.[28] c) Fitting to the Ritger–Peppas model (Figure S2, Supporting Information) suggested that HA CD–PNP released trastuzumab via an erosion-based mechanism ($n \approx 0.85$) and Alg CD–PNP via mostly diffusive mechanism ($n \approx 0.66$).[29,30] d) Cy5.5-labeled trastuzumab was released from CD–PNP hydrogels on day 1 and day 3. The supernatants were incubated with HER2-overexpressing (SK-BR-3 cells) or HER2-negative (MDA-MB-231) human breast cancer cells. Flow cytometry analysis demonstrated that the antibody bound solely to HER2$^+$ cells, indicating preserved bioactivity and specificity after release. Data plotted as mean ± SD, $n = 3$.

2.4. CD–PNP Hydrogels Effectively and Safely Localized Antibodies In Vivo and Delayed the Release of Trastuzumab

Having assessed the delayed antibody release of CD–PNP hydrogels in vitro, we tested if CD–PNP hydrogels were safe and effective in vivo (**Figure 4**). As a demonstration of the biocompatibility of CD–PNP hydrogels, CD–PNP hydrogels were SC administered in female Balb/c mice and compared with control PBS injections. Qualitatively, while the PBS bolus quickly dissipated, the post-stabilized Alg CD–PNP scaffolds remained intact for the entire duration of the experiment (6 days). The injected hydrogels were harvested and the tissues at the injection site were stained for hematoxylin and eosin (Figure 4a).

Lymphocytes concentrated at the interface between the tissue and the scaffold, but no evidence of fibrosis or damage in adjacent muscle tissues was visible over the course of the experiment. No cell infiltration into the scaffolds was visible, suggesting limited remodeling of alginate on this time scale.[33] We next injected the scaffold SC and followed the mouse weight for 20 days. The weight of all mice fluctuated between ±5% (Figure 4b), suggesting no macroscopic adverse effects of the injections.

Given that SC CD–PNP injections were not locally immunogenic, we further assessed whether CD–PNP hydrogels could serve as in vivo antibody depots. We SC injected CD–PNP hydrogels loaded with 120 mg mL^{-1} trastuzumab and 1.25 mg mL^{-1} (≈9 μM) of Cy5.5-labeled trastuzumab. In vivo, fluorescence imaging corroborated the hypothesis that the mAbs remained localized near the site of injection (Figure S6, Supporting Information). The total fluorescence decayed over time suggesting a sustained release of trastuzumab.

We next evaluated the pharmacokinetics of trastuzumab following SC administration using both the HA CD–PNP and post-stabilized Alg CD–PNP formulations (Figure 4c). As controls, we administered the mAb as a liquid solution via IV with PBS as a carrier solution and compared with a prior SC dataset containing trastuzumab and rHuPH20.[32] The relevant pharmacokinetic parameters—maximum concentration in the plasma (C_{max}), time when C_{max} was reached (t_{max}), half-life ($t_{1/2}$), and area under the curve (AUC_{0-20d}; **Table 1**, Figure S7, Supporting Information)

© 2025 The Author(s). Advanced Healthcare Materials published by Wiley-VCH GmbH

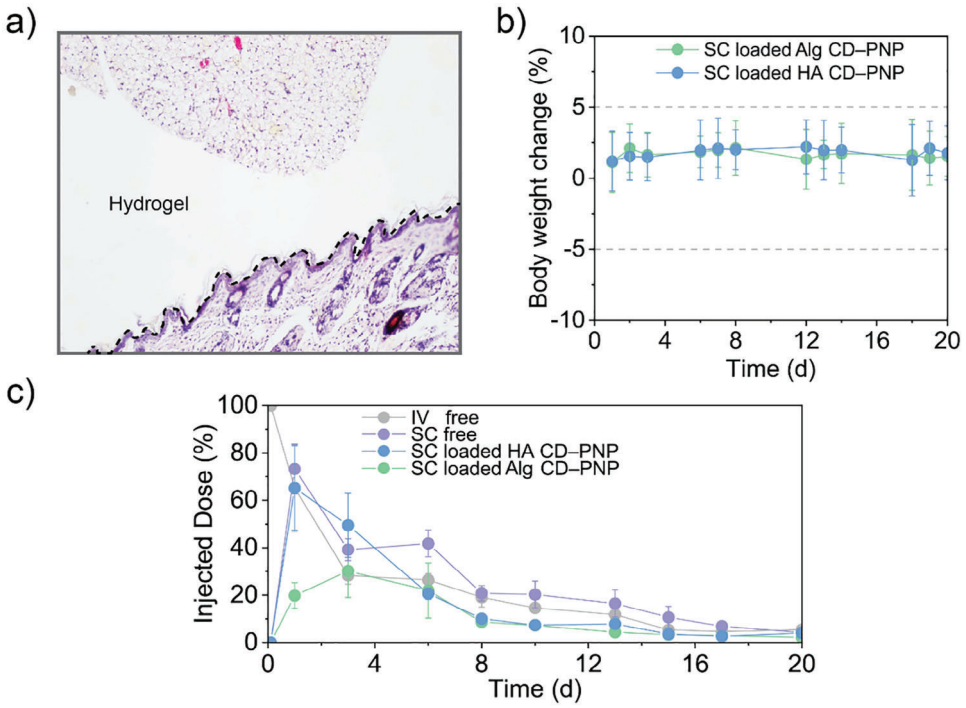

Figure 4. In vivo trastuzumab hydrogel depots for controlled release. a) Hematoxylin and eosin staining of mouse injection tissues. The interface between the post-stabilized Alg CD–PNP hydrogel and tissues is marked with a dashed black line. Lymphocytes were present at the interface. No major adverse effects such as fibrosis or damage in adjacent tissues are evident. Cells did not infiltrate into the post-stabilized Alg CD–PNP hydrogel scaffold, indicating limited scaffold biodegradation. $n = 3$, the image shows one representative replicate. b) The mouse weights remained within ±5%, indicating no macroscopic adverse effects. c) TR-FLISA measurements for trastuzumab concentration determination in the blood plasma expressed as a percentage of the injected dose (27.6 mg). Relevant pharmacokinetic parameters are presented in Table 1. When compared with free trastuzumab injections, CD–PNP hydrogels delayed the time to reach C_{max} concentration by ≈3 days. SC data was retrieved from a dataset containing trastuzumab and rHuPH20.[32] For (b) and (c), data shown as mean ± SD, $n = 3$.

were quantified. The release from CD–PNP hydrogels exhibited a prolonged release profile.

The C_{max} was lower for each SC formulation (C_{max} ≈ 2.92–7.33 mg mL^{-1}) as compared with the IV injection (C_{max} ≈ 10 mg mL^{-1}). SC injections delayed t_{max} by ≈1 day[32] and post-stabilized Alg CD–PNP gels further delayed t_{max} to 3 days. While the half-life of trastuzumab in blood sera, $t_{1/2}$, for free liquid trastuzumab was 6.04 days, post-stabilized Alg CD–PNP delayed $t_{1/2}$ to 7.34 days demonstrating controlled release. The $AUC_{0–20d}$ of both subcutaneously-injected CD–PNP formulations decreased by 50% as compared with IV and SC injections of liquid trastuzumab solutions. It is likely that this difference was related to antibody retention inside the hydrogels.

Overall, our data demonstrated for the first time that the CD–PNP formulations tested in this study were well-tolerated and formed trastuzumab depots for sustained release. CD–PNP hydrogel is made by simply mixing FDA-approved or GRAS components, such as α-cyclodextrin, hyaluronic acid, alginate, and PEG-PLA nanoparticles, ensuring that the system is readily scalable, biocompatible, and avoids reliance on complex or clinically challenging fabrication techniques. Unlike many hydrogel-based antibody delivery systems tested at low experimental loadings (<5 wt.%), our formulations incorporated trastuzumab

Table 1. Calculated pharmacokinetic parameters for the different formulations.

Route of administration	Intravenous	Subcutaneous[32]	Subcutaneous	Subcutaneous
Carrier	PBS	rHuPH20	HA CD–PNP	Alg CD–PNP
C_{max}	10 mg mL^{-1}	7.33 ± 1 mg mL^{-1}	5.87 ± 2 mg mL^{-1}	2.92 ± 0.4 mg mL^{-1}
t_{max}	0 days	1 ± 0.1 days	1 ± 0.28 days	3 ± 0.6 days
$t_{1/2}$	1.56 ± 0.6 days	6.04 ± 0.1 days	4.4 ± 0.1 days	7.34 ± 1.3 days
$AUC_{0–20d}$	41.8 ± 0.2 mg mL^{-1} day	49.1 ± 2.1 mg mL^{-1} day	31.6 ± 5.8 mg mL^{-1} day	21.6 ± 0.9 mg mL^{-1} days

C_{max} is the maximum blood serum concentration of trastuzumab; t_{max} is the time when C_{max} was observed; $t_{1/2}$ is the half-life; and AUC_{0-20d} is the area under the concentration curve. SC data was retrieved from a dataset containing trastuzumab and rHuPH20.[32] In Figure S7 (Supporting Information) the data is reported as ratio to rHuPH20. Data is displayed as mean ± SD, $n = 3$.

© 2025 The Author(s). Advanced Healthcare Materials published by Wiley-VCH GmbH

21922659, 0, Downloaded from https://advanced.onlinelibrary.wiley.com/doi/10.1002/adhm.202404660 by Cochrane France, Wiley Online Library on [09/06/2025]. See the Terms and Conditions (https://onlinelibrary.wiley.com/terms-and-conditions) on Wiley Online Library for rules of use; OA articles are governed by the applicable Creative Commons License

21922659, 0, Downloaded from https://advanced.onlinelibrary.wiley.com/doi/10.1002/adhm.202404660 by Cochrane France, Wiley Online Library on [09/06/2025]. See the Terms and Conditions (https://onlinelibrary.wiley.com/terms-and-conditions) on Wiley Online Library for rules of use; OA articles are governed by the applicable Creative Commons License

at ≈12 wt.%, matching clinical concentrations used in marketed Herceptin SC, thereby enhancing the translational relevance of our findings. When compared with IV injections of trastuzumab formulations, our data confirmed previous literature findings where SC administrations attenuated C_{max} and prolonged $t_{1/2}$.[27] In vitro, both CD–PNP formulations successfully delayed the release of trastuzumab, whereas in vivo, only alginate CD–PNP prolonged antibody release when compared with IV and SC administration of rHUPH20-trastuzumab. The general decrease of the AUC_{0-20d} for CD–PNP hydrogels suggests that some of the mAbs were retained in the hydrogel.[12] In the literature, while many studies related to engineering materials for the controlled release of trastuzumab directly focus on tumor-bearing mice experiments, only a few investigate antibody pharmacokinetics.[8,11,12] Among them, Kurisawa and coworkers developed an HA–tyramine hydrogel for the sustained release of trastuzumab with t_{max} and a $t_{1/2}$ comparable to those observed in our research.[10] The therapeutic efficacy of trastuzumab, at least in clinical settings, is not reliant on C_{max} but is instead influenced by AUC, with an effective biotherapeutic concentration estimated at 20 µg mL^{-1}.[34] In the in vivo therapeutic study, the minimal level of activity is >1% of the administered trastuzumab dose (27 mg). Clinically, patients receive treatment every 21 days. The goal of this study was to demonstrate that our formulation could sustain drug release over this timeframe. It is well-established that systemic exposure to trastuzumab correlates with increased survival in HER2$^+$ tumor-bearing models. Our study conducted in healthy non-tumor-bearing mice provides foundational insights into antibody release kinetics, which are critical parameters for optimizing future delivery strategies. Moving forward, we recommend exploring strategies to accelerate hydrogel degradation, thus increasing the AUC and facilitating the release of complexed antibodies. This could be achieved by utilizing lower molecular weight or fast-degrading polymers and incorporating enzymes to degrade the hydrogel matrix more efficiently. While electrostatic mAb complexation has already been explored to delay the release from soft and inorganic materials, our study applies this concept to supramolecular hydrogels and confirms the potential of polymer–antibody complexation to engineer depots that release antibodies in vivo.[12,32,35] It provides a comprehensive evaluation of CD–PNP hydrogels for monoclonal antibody delivery, integrating turbidity analysis, rheology, in vitro release, mathematical modeling, flow cytometry, confocal imaging, in vivo pharmacokinetics, IVIS imaging, and histological analysis—offering valuable and translationally relevant data. Having this extensive data on different formulation strategies and validation of previously proposed concepts in clinically relevant contexts is critically important to both academic research and industrial translation at a time when the development of complex biologics such as antibody–drug conjugates and multispecific antibodies is rapidly accelerating.[36–38]

3. Conclusion

We designed two locally-injectable CD–PNP hydrogels aimed at delaying the release of mAbs and we studied as lead candidate the sustained release of trastuzumab. At physiological pH, we leveraged electrostatic interactions between positively charged trastuzumab and negatively charged structural biopolymers, namely HA and alginate, to delay the release of the antibody. Rheological characterization demonstrated that both CD–PNP hydrogel formulations exhibited shear-thinning and self-healing properties. Additionally, the Alg CD–PNP hydrogels allowed post-stabilization of the network by cross-linking with divalent cations. HA and Alg CD–PNP delayed the release of trastuzumab by 3 to 7 days in vitro. Trastuzumab loaded in uncharged MC CD–PNP hydrogels was released over 2 days suggesting that polymer–antibody complexation plays a relevant role in delaying antibody release. Histology and in vivo fluorescence showed that CD–PNP hydrogels do not cause toxicity and could localize trastuzumab in SC depots. In vivo, when compared with free IV and SC tratuzumab injections, Alg CD–PNP delayed the release of trastuzumab to ≈7.34 days. Their pharmacokinetic profiles were comparable to SC trastuzumab with rHuPH20.[32] Overall, our study demonstrated that CD–PNP hydrogels are potential candidates for delivering antibodies in cancer therapies and providing tunable delayed release might allow us to revisit the schedule of iterative administration. Future efforts should be directed at liberating the quantity of residual antibodies that remain electrostatically complexed to the hydrogel scaffold.

4. Experimental Section

Materials: Water was deionized, dH_2O, using a milliQ purification system and a BioPak filter. For in vitro experiments, αCD (Ref. C0776) was purchased from TCI Chemicals (Tokyo, Japan). For in vivo experiments, US pharma-grade αCD (Ref. 235 027) was purchased from US Biological Life Sciences (Salem, USA). Pharma-grade sodium hyaluronate (M_w ≈ 620–1200 kDa) and sterile ultrapure alginate Pronova SLG100 (M_w ≈ 120–250 kDa) were purchased from Novamatrix (Sandvika, Norway). Acetone was purchased from Thommen–Furler AG (Rüti b. Büren, Switzerland). Poly(ethylene glycol) methyl ether (PEG; M_n ≈ 5 kDa; Ref. 81323), 3,6-dimethyl-1,4-dioxane-2,5-dione (lactide; Ref. 303 143), tin(II)-2-ethylhexanoate ($SnOct_2$; Ref. S3252), diethyl ether (Ref. 32 203), calcium carbonate ($CaCO_3$; Ref. 21 069), δ-gluconic acid lactone (GDL, Ref. G4750) and ethyl acetate (Ref. 34 858) were purchased from Sigma-Aldrich (Buchs, Switzerland). PBS was purchased from Thermo Fisher Scientific and endotoxin-free water was used for in vivo experiments (Thermo Fisher Scientific). Trazimera (Pfizer, USA) 420 mg and Herceptin SC (Roche) was provided by the pharmacy of the Institut de Cancérologie Strasbourg Europe.

Methods–PEG-b-PLA Synthesis: PEG-*b*-PLA was synthesized according to a previously-published protocol.[39] All flasks used were flame-dried and the glass condenser was dried at 105 °C. PEG (3.5 g; 0.7 mmol; 1 eq.) and lactide (11.2 g; 77.5 mol; 111 eq.) were dried overnight under vacuum by heating at 50 °C and gentle stirring. Toluene (30 mL) was dried with freeze–pump–thaw cycles under an argon atmosphere and added to the flask containing the reactants. Upon dissolution of lactide and PEG at 100 °C, $SnOct_2$ (317 µL; 1 mmol; 1.4 eq.) was added to the reaction mixture, the temperature was raised to 140 °C, and the reaction was left under reflux for ≈6 h. The block copolymer was precipitated in ice-cold diethyl ether, filtered, and redissolved in DCM a total of three times. The resulting white solid was dried under a vacuum. ^{1}H-NMR spectra were acquired on a Bruker Avance III 400 (Bruker BioSpin GmbH) and the chemical shifts were reported relative to the solvent peak of $CDCl_3$: $\delta = 7.26$ ppm. ^{1}H-NMR (400 MHz, CDCL3): δ = 5.29–5.05 (m, 237H), 4.39–4.21 (m, 3H), 3.76–3.52 (m, 555H), 3.37 (s, 3H), 1.64–1.41 (m, 725H). Molecular weight by ^{1}H-NMR: PEG ≈6 kDa, PLA ≈ 18 kDa. GPC (poly(styrene)-*co*-divinylbenzene calibration): M_n = 34 kDa, M_w = 41 kDa, $Đ$ = 1.23.

Nanoparticle Synthesis: NPs were formed via batch nanoprecipitation whereby 140 mg of PEG-*b*-PLA were dissolved in 2.5 mL of acetone and added dropwise to 10 mL of dH_2O under stirring. The residual acetone was evaporated under ambient conditions overnight. The NPs were puri-

© 2025 The Author(s). Advanced Healthcare Materials published by Wiley-VCH GmbH

fied and concentrated via ultrafiltration using Amicon Ultra centrifugation filters (MWCO: 30 kDa, 4500 rcf, 30 min) and washed with 9 mL of sterile PBS. This step was repeated a second time and the NPs were concentrated again via ultrafiltration at 4500 rcf for 50 min and resuspended to a final concentration of 20 wt.%.

CD–PNP Hydrogel Formation: The whole study was performed with two hydrogel formulations: HA CD–PNP (2 wt.% HA, 5 wt.% NPs, 10 wt.% αCD) and Alg CD–PNP (2 wt.% alginate, 5 wt.% NPs, 10 wt.% αCD). For convenience, the formation of 1000 mg CD–PNP hydrogels was described but this volume can be scaled up or down depending on the need. For HA CD–PNP hydrogels, 100 mg of αCD and 20 mg of HA were dissolved in 394 µL PBS (pH 7.4) within a plastic syringe. The syringe was sealed and allowed to equilibrate overnight. 250 mg of 20 wt.% NPs and 236 µL PBS were prepared in a separate plastic syringe. The NP and polymer syringes were connected with a female-to-female luer-lock adapter (Cellink, Sweden), gently mixed for 5 min, allowed to equilibrate overnight at room temperature, and stored at 4 °C until further use. For trastuzumab-loaded formulation, the antibody was added instead of PBS to the NP-containing syringe. Alg CD–PNP hydrogels were prepared analogously as explained above, replacing HA with alginate.

For post-stabilization of the scaffold, 2.8 mg of solid $CaCO_3$ and 10 mg of solid GDL were added to a syringe. About half of the PBS that would be used to dissolve alginate (394 µL) was used to form the calcium carbonate slurry. This meant that if 200 µL PBS were added to the syringe containing alginate, then the remaining 194 µL PBS were used in a separate syringe to form a suspension containing $CaCO_3$ and GDL. To make the calcium-cross-linked hydrogels, supramolecular Alg CD–PNP hydrogels were formed and let equilibrate overnight, and right before injection, PBS was added to the syringe containing solid $CaCO_3$ and GDL. The Alg CD–PNP and the calcium carbonate slurry syringes were connected with a female-to-female luer-lock adapter, mixed for 20 s, and used.[18] Trastuzumab was loaded in the hydrogels using the FDA-approved pharmaceutical equivalent Trastuzumab by entrapping the antibody into the hydrogel network during formation. Trastuzumab was dissolved overnight in the NP suspension and subsequently mixed with the remaining components as described above. To prepare quantities lower than 300 mg, the same sequential mixing process was performed in Eppendorf tubes and, to ensure a correct ratio of components, the Ca^{2+} slurry was sometimes prepared on larger scales, well mixed, and only a fraction was pipetted into the syringe.

Rheology: The rheological characterization of the hydrogels was performed on a shear rheometer (MCR 502; Anton Paar; Zofingen, Switzerland) equipped with a Peltier stage and a covering hood. Hydrogels were tested at 25 °C using a parallel plate geometry with a diameter of 20 mm and a gap size of 0.5 mm. After loading the sample, an oscillatory interval (ω = 0.1 rad s^{-1}, γ = 0.01%, t = 30 min) was performed to reduce the loading history of the sample. The linear viscoelastic region was determined with dynamic oscillatory strain amplitude sweep measurements with constant angular frequency (ω = 10 rad s^{-1}). The hydrogel response to different frequencies was probed with dynamic oscillator frequency sweep measurements conducted with constant strain amplitude (γ = 0.1%) and a decreasing angular frequency (from 100 to 0.1 rad s^{-1}). The ability of the CD–PNP formulations to flow and recover was characterized with dynamic oscillatory time sweep measurements with alternating low (γ_{low} = 0.1%) and high (γ_{high} = 10 or 200%) strain intervals at constant frequency (ω = 10 rad s^{-1}). The shear-thinning properties of CD–PNP hydrogels were tested with rotational shear rate measurements. The shear rate, $\delta\gamma/\delta t$ was increased from 0.01 to 100 s^{-1}. The data was fitted to the following power-law model

$$\eta = K\dot{\gamma}^{n-1} \quad (1)$$

where $n \approx 1$ for Newtonian, $n > 1$ for shear-thickening, and $n < 1$ for shear-thinning fluids.

Turbidity Measurements: Polymer–trastuzumab complexation was confirmed via turbidity measurements. Solutions containing 2 wt.% of polymer (HA or alginate) with or without trastuzumab (3 wt.%) were formed in a 96-well plate. The solutions were left to equilibrate for 2 days on a shaking plate. Afterward, the absorbance of the mixture as well as of pure PBS and PBS with 3 wt.% trastuzumab was measured at 450 nm.

In Vitro Release of Trastuzumab: To study the in vitro release properties of trastuzumab from CD–PNP formulations, ≈100 mg of hydrogel containing 12 wt.% trastuzumab was placed at the bottom of a 2 mL microcentrifuge tube. The experiment was started by gently adding 0.75 mL of 1× PBS and incubating the samples at 37 °C. At each timepoint, the supernatant was gently mixed once by aspirating and releasing 300 µL of supernatant. Subsequently, 300 µL was collected and replaced with fresh PBS. Quantification of released antibodies was accomplished through bicinchoninic acid assay (Pierce BCA Protein Assay Kits, Thermo Fisher Scientific) following manufacturer instructions. The absorbance of the supernatant was measured at 562 nm using a Hidex Sense and compared with calibration curves. The release data for MC CD–PNP hydrogels were normalized to the final time point.

Drug Release Modeling: The Ritger–Peppas equation was used to analyze the early release kinetics to distinguish between an erosion- or a diffusion-based release.[29,30] This equation described both Fickian and non-Fickian release from the hydrogel, and was expressed as follows:

$$M_t/M_\infty = k \cdot t^n \quad (2)$$

where, M_t and M_∞ represent the released mass at time t and infinite time, respectively. k is a constant, and n is the power governing the release activity. In brief, a value of n between 0.42 and 0.5 indicates a purely diffusive system, while $n > 0.5$ suggests an anomalous release, often associated with gel degradation.

In Vitro Binding Assays: The trastuzumab integrity post-release was assessed by flow cytometry toward $HER2^+$ SK-BR-3 and $HER2^-$ MDA-MB-231 breast cancer cell lines. First, trastuzumab was labeled with Cy5.5 prior to loading in the hydrogel formulation. After the in vitro release, supernatant was collected to assess the specificity of the trastuzumab. 1–2 × 10^5 cells per condition were incubated with 100 µL of supernatant for 5 min at room temperature. The cells were washed three times with PBS and centrifuged at 300 rcf for 5 min for each wash. MACSQuant Analyzer 10 Flow Cytometer (Miltenyi) allowed data acquisition, and subsequent analysis was performed using FlowJoTM software (V. 10.8.2) or FCS express (V. 7.22.0031).

In Vitro Microscopy Analysis of Trastuzumab Activity: Trastuzumab activity post-release was evaluated using confocal microscopy in the $HER2^+$ SK-BR-3 cell line. Following in vitro release, 1–2 × 10^5 cells per condition were incubated with 100 µL of supernatant for 5 min at room temperature. Cells were then washed three times with phosphate-buffered saline (PBS) and centrifuged at 300 rcf for 5 min per wash. Fixation was performed using 4% paraformaldehyde in 0.1 M PBS (pH 7.4) (Electron Microscopy Sciences, #15735-85) for 15 min, followed by three additional PBS washes. Slides were prepared using Fluoromount-G mounting medium with DAPI (Invitrogen, #00-4959-52) for nuclear staining.

Dosage of Trastuzumab in Mouse Serum: The quantification of plasma/serum levels of trastuzumab was conducted utilizing time resolved-fluorescence linked immunosorbent assay (TR-FLISA) kits designed for mice, procured from Poly-Dtech (Strasbourg, France). Experimental procedures were conducted in accordance with the manufacturer's guidelines. Briefly, microtiter plates were subjected to three washes with washing buffer, followed by the addition of 100 µL of standards and samples in duplicate. A standard curve for each mAb of interest was employed, utilizing dilution buffer as the zero standard (0 ng mL^{-1}) and plasma collected from mice prior to administration as a negative control. Various plasma dilutions were examined for all mouse samples to establish the experimental setup. Subsequently, the plates were incubated with gentle shaking for 1 h at 37 °C, followed by three washes. Next, 100 µL of the detection antibody, diluted in assay buffer, was added to each well and incubated with shaking for 1 h at 37 °C. A final wash comprised six cycles (5 min incubation with shaking per wash) to minimize background interference. Following this, 200 µL of washing buffer was added to each well, and fluorescence readings were recorded at 535 nm (excitation at 340 nm) utilizing the time-resolved fluorescence (TRF) read mode of a SpectraMax ID5 (Molecular Devices), adhering to the TRF plate reader settings as out-

© 2025 The Author(s). Advanced Healthcare Materials published by Wiley-VCH GmbH

21922659, 0, Downloaded from https://advanced.onlinelibrary.wiley.com/doi/10.1002/adhm.202404660 by Cochrane France, Wiley Online Library on [09/06/2025]. See the Terms and Conditions (https://onlinelibrary.wiley.com/terms-and-conditions) on Wiley Online Library for rules of use; OA articles are governed by the applicable Creative Commons License

lined in the manufacturer's instructions. Raw data were processed using the corresponding SoftMax Pro software, employing a 5-parameter logistic curve for analysis.

Pharmacokinetic Parameters Quantification: To extract the parameters for the pharmacokinetic profile, an extravascular route of drug administration was employed, characterized by a differential equation describing the drug concentration in blood over time, incorporating absorption and elimination rates

$$dX/dt = K_a \cdot X_a - K \cdot X. \quad (3)$$

here, dX/dt represents the rate of change of drug concentration in blood, X signifies the amount of drug in the blood at time t, X_a denotes the amount of absorbable drug at the absorption site at time t, and K_a and K represent the first-order absorption and elimination rate constants, respectively. The pharmacokinetic parameters were derived from the solution of this equation. The half-life ($t_{1/2}$) was determined using the formula $t_{1/2} = \ln(2)/K_a$. C_{Max}, representing the maximum drug concentration, was obtained from the adjusted curve. The area under the curve (AUC) was calculated using the AreaXY function, integrating the curve with respect to elapsed time and the amount of drug in the blood. The entire analysis was conducted utilizing IGOR Pro (V.9.0, Wavemetrix).

In Vivo Tracking of Hydrogel-Loaded Trastuzumab: The HA CD–PNP hydrogel was loaded with Cy5.5-labelled Trastuzumab. The hydrogel was subcutaneously injected in a 4-months old Balb/c female mouse under isoflurane anesthesia. Sequential fluorescent images were acquired using an Illumina LT device system (Perkin–Elmer) from day 0 to day 26. Animal procedures were performed in accordance with institutional guidelines and approval under APAFIS number #37434-2022052016466198.

Supporting Information

Supporting Information is available from the Wiley Online Library or from the author.

Acknowledgements

This work was supported by the Swiss National Science Foundation (200021_184697; M.W.T.) and the Ligue contre le cancer (A.D.). This research was also funded, in part, by the European Research Council (ERC) Proof-of-Concept Grant Sub-NK, grant agreement No. 101138078 (A.D.). A.D. also acknowledges the Strasbourg Drug Discovery and Development Institute (IMS) for funding part of this study, as part of the Interdisciplinary Thematic Institute (ITI) 2021-2028 program of the University of Strasbourg, CNRS and Inserm, IdEx Unistra (ANR-10-IDEX-0002), and by the SFRI-STRAT US project (ANR-20-SFRI-0012) under the framework of the French Investments for the Future Program. V.M. was supported by a fellowship from the French Ministry of Science (MESRI) and a fourth-year thesis fellowship from the Foundation ARC (Association pour la Recherche sur le Cancer). The authors thank Chloé Guilbaud-Chereau for contributing to the initial discussions. Figures were drawn using elements of the Adobe Stock library.

Conflict of Interest

The authors declare no conflict of interest.

Author Contributions

A.D. and M.W.T. conceived the project. G.B., S.B., E.A.G., and M.W.T. designed the hydrogel formulation with support from L.G.P. and L.L. on the ionic cross-linking design. G.B. carried out the hydrogel rheological characterization and the in vitro trastuzumab delivery experiments. V.M. supported hydrogel formulation selection and preliminary in vitro antibody release experiments. V.M. and J.D. labeled trastuzumab with fluorophores, V.M. and P.L. performed in vitro antibody binding experiments, and E.B. performed confocal microscopy. G.B., A.D., C.M., and M.W.T. planned the in vivo pharmacokinetic experiments. G.B. and E.A.G. prepared the hydrogels for the in vivo experiments. G.B., C.M., S.H, G.J., and V.M. carried out the in vivo pharmacokinetic experiments, the histological analysis, and quantified the blood plasma concentrations of trastuzumab. O.L. and J.G.G. carried out the in vivo fluorescence analysis. L.J.C. and X.P. provided support and guidance on the experimental design. G.B., M.W.T., and A.D. wrote the manuscript with input from all authors.

Data Availability Statement

The data that support the findings of this study are available from the corresponding author upon reasonable request.

Keywords

controlled release, immunotherapy, In vivo drug delivery, injectable biomaterials, supramolecular biomaterials

Received: November 21, 2024
Revised: May 12, 2025
Published online:

[1] R. R. Driskell, B. M. Lichtenberger, E. Hoste, K. Kretzschmar, B. D. Simons, M. Charalambous, S. R. Ferron, Y. Herault, G. Pavlovic, A. C. Ferguson-Smith, F. M. Watt, *Nature* **2013**, *504*, 277.
[2] R. Wong, S. Geyer, W. Weninger, J.-C. Guimberteau, J. K. Wong, *Exp. Dermatol.* **2016**, *25*, 92.
[3] A. Datta-Mannan, S. Estwick, C. Zhou, H. Choi, N. E. Douglass, D. R. Witcher, J. Lu, C. Beidler, R. Millican, *mAbs* **2020**, *12*, 1770028.
[4] N. Varkhede, L. Forrest, *J. Pharm. Pharm. Sci.* **2018**, *21*, 130s.
[5] G. Jacquot, P. Lopez Navarro, C. Grange, L. Boudali, S. Harlepp, X. Pivot, A. Detappe, *Adv. Mater.* **2024**, *36*, 2406604.
[6] M. R. Turner, S. V. Balu-Iyer, *J. Pharm. Sci.* **2018**, *107*, 1247.
[7] R. Deng, Y. G. Meng, K. Hoyte, J. Lutman, Y. Lu, S. Iyer, L. E. DeForge, F.-P. Theil, P. J. Fielder, S. Prabhu, *mAbs* **2012**, *4*, 101.
[8] C. Yang, A. Lee, S. Gao, S. Liu, J. L. Hedrick, Y. Y. Yang, *J. Controlled Release* **2019**, *293*, 193.
[9] A. L. Z. Lee, V. W. L. Ng, S. Gao, J. L. Hedrick, Y. Y. Yang, *Adv. Funct. Mater.* **2014**, *24*, 1538.
[10] K. Xu, F. Lee, S. Gao, M.-H. Tan, M. Kurisawa, *J. Controlled Release* **2015**, *216*, 47.
[11] J. Chen, K. Huang, Q. Chen, C. Deng, J. Zhang, Z. Zhong, *ACS Appl. Mater. Interfaces* **2018**, *10*, 3929.
[12] D. Schweizer, K. Schönhammer, M. Jahn, A. Göpferich, *Biomacromolecules* **2013**, *14*, 75.
[13] E. A. Appel, M. W. Tibbitt, M. J. Webber, B. A. Mattix, O. Veiseh, R. Langer, *Nat. Commun.* **2015**, *6*, 6295.
[14] A. N. Steele, L. M. Stapleton, J. M. Farry, H. J. Lucian, M. J. Paulsen, A. Eskandari, C. E. Hironaka, A. D. Thakore, H. Wang, A. C. Yu, D. Chan, E. A. Appel, Y. J. A. B Woo, *Adv. Healthcare Mater.* **2019**, *8*, 1801147.
[15] O. S. Fenton, M. W. Tibbitt, E. A. Appel, S. Jhunjhunwala, M. J. Webber, R. Langer, *Biomacromolecules* **2019**, *20*, 4430.
[16] E. C. Gale, A. E. Powell, G. A. Roth, E. L. Meany, J. Yan, B. S. Ou, A. K. Grosskopf, J. Adamska, V. C. T. M. Picece, A. I. Dâ Aquino, B. Pulendran, P. S. Kim, E. A. Appel, *Adv. Mater.* **2021**, *33*, 2104362.
[17] A. K. Grosskopf, L. Labanieh, D. D. Klysz, G. A. Roth, P. Xu, O. Adebowale, E. C. Gale, C. K. Jons, J. H. Klich, J. Yan, C. L. Maikawa, S. Correa, B. S. Ou, A. I. Aquinod', J. R. Cochran, O. Chaudhuri, C. L. Mackall, E. A. Appel, *Sci. Adv.* **2022**, *8*, abn8264.

© 2025 The Author(s). Advanced Healthcare Materials published by Wiley-VCH GmbH

21922659, 0, Downloaded from https://advanced.onlinelibrary.wiley.com/doi/10.1002/adhm.202404660 by Cochrane France, Wiley Online Library on [09/06/2025]. See the Terms and Conditions (https://onlinelibrary.wiley.com/terms-and-conditions) on Wiley Online Library for rules of use; OA articles are governed by the applicable Creative Commons License

[18] S. Correa, E. L. Meany, E. C. Gale, J. H. Klich, O. M. Saouaf, A. T. Mayer, Z. Xiao, C. S. Liong, R. A. Brown, C. L. Maikawa, A. K. Grosskopf, J. L. Mann, J. Idoyaga, E. A. Appel, *Adv. Sci.* **2022**, *9*, 2103677.
[19] C. M. Kasse, A. C. Yu, A. E. Powell, G. A. Roth, C. S. Liong, C. K. Jons, A. Buahin, C. L. Maikawa, X. Zhou, S. Youssef, J. E. Glanville, E. A. Appel, *Biomater. Sci.* **2023**, *11*, 2065.
[20] G. Bovone, E. A. Guzzi, S. Bernhard, T. Weber, D. Dranseikiene, M. W. Tibbitt, *Adv. Mater.* **2022**, *34*, 2106941.
[21] D. Slamon, W. Eiermann, N. Robert, T. Pienkowski, M. Martin, M. Press, J. Mackey, J. Glaspy, A. Chan, M. Pawlicki, T. Pinter, V. Valero, M.-C. Liu, G. Sauter, G. von Minckwitz, F. Visco, V. Bee, M. Buyse, B. Bendahmane, I. Tabah-Fisch, M.-A. Lindsay, A. Riva, J. Crown, *N. Engl. J. Med.* **2011**, *365*, 1273.
[22] A. Harada, J. Li, M. Kamachi, *Nature* **1992**, *356*, 325.
[23] H. Wiig, C. C. Gyenge, O. Tenstad, *J. Physiol.* **2005**, *567*, 557.
[24] H. H. Paradies, D. Wagner, W. R. Fischer, *Ber. Bunsenges. Phys. Chem.* **1996**, *100*, 1299.
[25] I. Gatej, M. Popa, M. Rinaudo, *Biomacromolecules* **2005**, *6*, 61.
[26] C. K. Kuo, P. X. Ma, *Biomaterials* **2001**, *22*, 511.
[27] X. Pivot, J. Gligorov, V. Müller, P. Barrett-Lee, S. Verma, A. Knoop, G. Curigliano, V. Semiglazov, G. López-Vivanco, V. Jenkins, N. Scotto, S. Osborne, L. Fallowfield, *Lancet Oncol.* **2013**, *14*, 962.
[28] J. Li, D. J. Mooney, *Nat. Rev. Mater.* **2016**, *1*, 16071.
[29] P. L. Ritger, N. A. Peppas, *J. Controlled Release* **1987**, *5*, 23.
[30] P. L. Ritger, N. A. Peppas, *J. Controlled Release* **1987**, *5*, 37.
[31] M. Paul, V. Vieillard, R. Da Silva Lemos, L. Escalup, A. Astier, *Int. J. Pharm.* **2013**, *448*, 101.
[32] T. Gréa, G. Jacquot, A. Durand, C. Mathieu, A. Gasser, C. Zhu, M. Banerjee, E. Hucteau, J. Mallard, P. Lopez Navarro, B. V. Popescu, E. Thomas, D. Kryza, J. Sidi-Boumedine, G. Ferrauto, E. Gianolio, G. Fleith, J. Combet, S. Brun, S. Erb, S. Cianferani, L. J. Charbonnière, L. Fellmann, C. Mirjolet, L. David, O. Tillement, F. Lux, S. Harlepp, X. Pivot, A. Detappe, *Adv. Mater.* **2024**, *36*, 2308738.
[33] A. Al-Shamkhani, R. Duncan, *J. Bioact. Compat. Polym.* **1995**, *10*, 4.
[34] M. Pegram, S. Hsu, G. Lewis, R. Pietras, M. Beryt, M. Sliwkowski, D. Coombs, D. Baly, F. Kabbinavar, D. Slamon, *Oncogene* **1999**, *18*, 2241.
[35] J. S. Andrew, E. J. Anglin, E. C. Wu, M. Y. Chen, L. Cheng, W. R. Freeman, M. J. Sailor, *Adv. Funct. Mater.* **2010**, *20*, 4168.
[36] L. Carretero-Iglesia, O. J. Hall, J. Berret, D. Pais, C. Estoppey, M. Chimen, T. Monney, J. Loyau, C. Dreyfus, J. Macoin, C. Perez, V. Menon, I. Gruber, A. Laurendon, L. N. Caro, G. S. Gudi, T. Matsuura, P. H. van der Graaf, S. Blein, M. L. Mbow, R. Croasdale-Wood, A. Srivastava, M. R. Dyson, T. Matthes, Z. Kaya, C. M. Edwards, J. R. Edwards, S. Maiga, C. Pellat-Deceunynck, C. Touzeau, et al., *Nat. Cancer* **2024**, *5*, 1494.
[37] C. H. Chau, P. S. Steeg, W. D. Figg, *Lancet* **2019**, *394*, 793.
[38] C. Klein, U. Brinkmann, J. M. Reichert, R. E. Kontermann, *Nat. Rev. Drug Discovery* **2024**, *23*, 301.
[39] E. A. Guzzi, R. Bischof, D. Dranseikiene, D. V. Deshmukh, A. Wahlsten, G. Bovone, S. Bernhard, M. W. Tibbitt, *Biofabrication* **2021**, *13*, 044105.

© 2025 The Author(s). Advanced Healthcare Materials published by Wiley-VCH GmbH

21922659, 0, Downloaded from https://advanced.onlinelibrary.wiley.com/doi/10.1002/adhm.202404660 by Cochrane France, Wiley Online Library on [09/06/2025]. See the Terms and Conditions (https://onlinelibrary.wiley.com/terms-and-conditions) on Wiley Online Library for rules of use; OA articles are governed by the applicable Creative Commons License

Université de Strasbourg

Vincent MITTELHEISSER

École Doctorale des Sciences de la Vie et de la Santé STRASBOURG

Understanding the tumor immune microenvironment: bridging fundamental research and nanomedicine innovations

La progression métastatique des cellules cancéreuses est à l'origine de plus de 90 % des décès liés au cancer. Il est donc nécessaire de mieux comprendre les métastases du cancer afin de faire progresser les stratégies thérapeutiques et d'améliorer les résultats cliniques. Dans ces projets, nous avons décrypté les rôles pro-métastatiques des plaquettes dans la dissémination précoce et tardive des cellules tumorales. Nous démontrons notamment que l'aptitude métastatique des cellules tumorales est médiée par leur expression de CD24. De plus, nous avons mis en évidence pour la première fois que les plaquettes favorisent la croissance des métastases établies en induisant un microenvironnement immunosuppresseur. Plusieurs approches thérapeutiques ont été développées pour lutter contre l'immunosuppression intra-tumorale, mais elles sont associées à des effets indésirables sévères. Dans la deuxième partie de ma thèse, nous visons à contourner ces limitations en nous appuyant sur les approches de la nanomédecine. Pour ce faire, nous étudions les capacités de nanomatériaux à réactiver *ex vivo* des cellules immunitaires humaines cultivées dans un environnement immunosuppresseur. Nous avons identifié les nanoparticules de PLGA comme des candidats appropriés et prometteurs pour d'autres approches de ciblage visant à réactiver le système immunitaire des patients atteints de cancer. Nos résultats suggèrent que l'impact intrinsèque des matériaux PLGA NPs pourrait être en synergie avec des agents immuno-activateurs pour cibler et moduler efficacement le système immunitaire.

Metastasis is a multistep process characterized by the spread of malignant cells to distant organs. Metastatic disease accounts for over 90% of cancer-related deaths. Therefore, there is a need to gain a deeper understanding of cancer metastasis in order to advance therapeutic strategies and improve clinical outcomes. In these projects we unravel platelets pro-metastatic roles in the early and late tumor cells dissemination. We notably demonstrate that tumor cells early metastatic fitness is mediated by their expression of CD24. We highlight for the first time that platelets favor the outgrowth of established metastasis by inducing an immunosuppressive microenvironment. Several therapeutic approaches were developed to tackle intra-tumoral immunosuppression, yet they are associated with severe adverse events. In a second part of my thesis work, we aim to circumvent these limitations by building on nanomedicine approaches. To do so, we investigate in a bench to bed side approach, the abilities of drug-free nanomaterials to reactivate *ex vivo* human immune cells cultured in an immunosuppressive environment. We identify drug-free PLGAs NPs as suitable and promising candidates for further targeting approaches aiming to reactivate the immune system of cancer patients. Our results suggest that intrinsic PLGAs NPs materials impact could synergize with immuno-activating agents to efficiently target and modulate the immune system.